

**ISOLATION, IDENTIFICATION AND PHARMACOLOGICAL
EVALUATION OF THE UTERINE ACTIVES OF *FICUS EXASPERATA*
VAHL (MORACEAE)**

AND

**THE DEVELOPMENT AND APPLICATION OF METABOLOMIC
TECHNIQUES IN DRUG DISCOVERY**

A THESIS PRESENTED FOR THE DEGREE OF DOCTOR OF PHILOSOPHY IN
THE FACULTY OF SCIENCE
STRATHCLYDE INSTITUTE OF PHARMACY AND BIOMEDICAL SCIENCES
UNIVERSITY OF STRATHCLYDE

BY

ENITOME E. BAFOR

B.Pharm., M.Sc.

Strathclyde Institute of Pharmacy and Biomedical Sciences
University of Strathclyde,
161 Cathedral Street,
Glasgow,
G4 0RE
United Kingdom.

OCTOBER 2014

This thesis is the result of the author's original research. It has been composed by the author and has not been previously submitted for examination which has led to the award of a degree.

The copyright of this thesis belongs to the author under the terms of the United Kingdom Copyright Acts as qualified by University of Strathclyde Regulation 3.50. Due acknowledgement must always be made of the use of any material contained in, or derived from, this thesis.

Signed:

Date:

DEDICATION

This work is dedicated to God Almighty!! Thank you Lord.

ACKNOWLEDGEMENTS

I am utterly and deeply thankful to God Almighty for His favour and mercies for the entire duration of my PhD programme. It was rough and tough but He was there for me every step of the way. Thank you, Lord!

I would like to thank my principal supervisor Dr. RuAngelie Edrada-Ebel, who afforded me the opportunity to carry out this research. Dr. RuAn was very supportive and extended a deep measure of understanding to my situation. I have learned and acquired substantial knowledge from working with her especially in the field of metabolomics and cutting edge research in general. She provided advice, ideas and encouragement to me when needed. Her dedication to her students and research is worth emulating. I would also like to thank my second supervisor, Dr. Edward G. Rowan in whose laboratory I performed all pharmacology experiments. He was very supportive, and provided much needed encouragement and advice whenever approached. I am also grateful to Prof. Alexander Gray in whose laboratory I performed my first Soxhlet extraction procedure. He would occasionally drop by to observe my progress and give advice and support.

I would like to thank each and every one of my family members because without their love, care and support I would have been unable to complete my programme. I would like to thank my wonderful and extremely supportive husband Dr. Anire Bafor (you're the best! I thank God every day for bringing you into my life) and my lovely brave kids Mimi, Omare and Dida (you kids are truly blessings!). My parents, Dr. and Mrs. J. A.O. Efeturi and my parents –in laws Prof. and Dr. (Mrs) B.E Bafor, who were all very instrumental in my securing a position in the PhD

programme financially, as well as in providing continued monetary support for our living expenses, not to mention prayers, advice, encouragement and support thank you all so much. I want to especially thank my mum who ensured she visited regularly to care for my kids and assist in every way possible so I could concentrate on my studies - I love you mum! To my brothers Dr. K. Efeturi and family, Mr. Oreva Efeturi and family, Mr. Ifo Efeturi and family and especially Mr. Ofego Efeturi for their prayers and support during my PhD studies, thank you so much. My brother Ofego, has been of immense assistance to me especially during my analyses and even my write-up, thank you so much! To my brother-in law Mr. Gbugbemi Bafor and family, my sisters-in law Mrs. Jolomi Wilbert and family and Ms. T. Bafor, thank you all for everything.

I am grateful to my research group members and friends, Christina Viegelmann (Chiara), Nurkhalida Kamal (Halida), Ahmed Tawfike, Noor wini (Wini) Binti Mazlan, Dr. Lynsey Macintyre, Cheng Cheng, and Weqas Alotaibi, thank you all so much for everything. They stood by me and they went out of their way to be of assistance whenever they could. I would like to specially thank Chiara who from the first day we met has been of immense assistance in every possible way, thanks Chiara!

I would not forget Scott and Sandra Isaac and their wonderful family who were also very supportive and of immense assistance throughout my stay in Scotland. I am grateful to Dr. John Igoli of the Phytochemistry laboratory who was also supportive. He assisted me in the early phase of my research and was always willing to be of assistance. I am grateful to Dr. Valerie Ferro for her kindness and advice over the course of my programme and in particular for her assistance in the

application for a project license. I am also grateful to Dr. Tong Zhang for his immense assistance during all my HRESI-MS measurements. I would also like to thank Dr. John Dempster who assisted me with some of the statistical analysis and Ms. Chiew Vien who assisted with some of the fractionation experiments. I would also like to appreciate Prof. Susan Wray of the Institute of Translational Medicine, University of Liverpool, UK who provided me with very helpful suggestions at certain stages of my research.

I wouldn't fail to thank Prof. E.K.I Omogbai, Prof. R.I.Ozolua, Dr. Z.A.M Nworgu, Dr. S. Okpo, Dr. O. Owolabi, Pharm. F. Amaechina, Dr. I. Igbe and Ms. L. Iniaghe of the Department of Pharmacology and Toxicology, University of Benin, Nigeria, for their assistance, throughout the period of my PhD programme.

Lastly, I would like to thank the Education Trust Fund Organisation, Nigeria for providing financial support for my PhD program.

CONTENTS

Contents Pages	vi
Abstract	xv
Graphic Abstracts	xviii
Abbreviations	xx
List of Figures	xxvi
List of Tables	xxxvii
Publications	xl

Table of Contents

CHAPTER ONE.....	1
GENERAL INTRODUCTION AND SIGNIFICANCE OF STUDY	1
1.0 Introduction	2
1.1 Ethnopharmacological Background	2
1.2 Study Plant (<i>Ficus exasperata</i>)	2
1.2.1 The Moraceae Family	3
1.2.2 An Overview and Brief Description of the Genus <i>Ficus</i>	3
1.2.3 Phytochemistry and Medicinal Uses of Some <i>Ficus</i> Species	4
1.3 <i>Ficus Exasperata</i>	6
1.3.1 Description.....	6

1.3.2. Some Medicinal Uses of <i>F. exasperata</i>	8
1.3.3 Toxicity Review on <i>F. exasperata</i>	9
1.3.4 Phytochemistry of <i>F. exasperata</i>	10
1.4. The Uterus.....	11
1.4.1. Anatomy and Physiology of the Human and Rodent Uterus	11
1.4.2. The Non - Pregnant Uterus	16
1.4.2.1 Spontaneous Uterine Contractions.....	17
1.4.2.2. Uterine Relaxation	23
1.4.2.3. Lipid Rafts and Uterine Signalling.....	25
1.4.2.4. Uterine Contractions in Dysmenorrhoea	28
1.4.3. The Pregnant Uterus.....	29
1.4.3.1. Pre - term Labour	30
1.4.4. Biochemistry of the Uterus.....	35
1.4.4.1. pH Changes in the Myometrium	35
1.4.4.2. pH and dysfunctional labour	35
1.5. Pharmacological Effect of Drugs on the Uterus	37
1.5.1. Oxytocics.....	37
1.5.2. Tocolytics	37
1.6. Secondary Plant Metabolites	37
1.7 Summary	38
1.8 Hypothesis of Research	39
1.9 Aim of Present Research.....	39

1.10 Specific Objectives/Experimental Plan	39
CHAPTER TWO: PHYTOCHEMICAL AND PHARMACOLOGICAL CHARACTERIZATION OF THE LEAVES OF <i>FICUS EXASPERATA</i>	41
2.1 Introduction	42
2.2 Extraction Methods	43
2.3 Solvent Extraction	43
2.3.1 Extraction Solvents and Specific Phytochemical Groups.....	45
2.4 Analytical Techniques	46
2.4.1 Qualitative/Analytical Thin Layer Chromatography	46
2.4.2 Nuclear Magnetic Resonance Spectroscopy.....	48
2.4.3 Mass Spectrometry	49
2.5 Functional Uterine Pharmacological Assay	51
2.6 Materials and Method	54
2.6.1 Plant Material.....	54
2.6.2 Phytochemical and Pharmacological Analysis of the Crude Leaf Extracts of <i>F. exasperata</i>	54
2.6.2.1 Plant Material.....	54
2.6.2.2 Extraction using the Soxhlet Apparatus	55
2.6.2.3 Extraction via Maceration.....	55
2.6.2.4 Preliminary Identification of Extracts	57
2.6.3 Pharmacological Screening of Extracts	61

2.6.3.1 Animals	61
2.6.3.2 Uterine Tissue Isolation and Mounting.....	61
2.6.3.3 Evaluation of the Effects of Extracts on Uterine Smooth Muscle Activity	62
2.6.4 Isolation of Chemical Constituents.....	63
2.6.4.1 Medium-Pressure Liquid Column Chromatography Experiments	63
2.6.4.2 Fractionation of E1 and E2	64
2.6.4.3 Fractionation of M1	64
2.6.4.4 TLC Analysis of Extracts	67
2.6.4.5 Identification and Structural Characterization of Compounds	67
2.6.4.6 HPLC-ICP-MS.....	68
2.6.5 In Vitro Uterine Assay of the Fractions and Compounds of <i>F. exasperata</i> ...	68
2.6.5.1 Uterine Tissue Set-up.....	68
2.6.5.2 Study on Spontaneous Uterine Contractions.....	69
2.6.5.3 Studies on Oxytocin-induced Uterine Contractions.....	69
2.6.5.4 Studies on KCl-pre-contracted Uterus.....	69
2.6.6 Drugs and Chemicals.....	70
2.6.7 Curve Fitting and Statistical Analysis.....	70
2.7 Results.....	71
2.7.1 Yields of Extracts and Fractions.....	71
2.7.2 TLC Analysis of Extracts	72
2.7.3 Qualitative Flavonoid Analysis of Extracts of <i>F. exasperata</i>	76

2.7.4 ¹ H-NMR OF EXTRACTS	78
2.7.5 LC-MS Analysis of Extracts of <i>F. exasperata</i>	87
2.7.6 Effects of Extracts on Uterine Contractility	88
2.7.7 Identification of Chemical Constituents.....	97
2.7.7.1 Fatty Acids, Glycerol Esters and Glycerol Derivatives	97
2.7.7.2 Pheophorbide and Pheophytin Derivatives	108
2.7.7.3 Flavonoid Derivatives	124
2.7.7.4 N-Methyl Pyrimidine and Salt isolated from <i>F. exasperata</i>	133
2.7.7.4.1 Compound 15	137
2.7.7.5 Summary of the Compounds Isolated from the Leaves of <i>F. exasperata</i>	139
2.7.8 Pharmacological Effects of Identified Compounds on Uterine Contractility	142
2.7.8.1 Effect on Spontaneous Uterine Contractility.....	153
2.7.8.2 Effect on Oxytocin-induced Uterine Contractions.....	160
2.7.8.3 Effect on KCl-induced Uterine Contractions	165
2.8 Discussion	166
2.8.1 Plant Extraction	166
2.8.2 TLC Analysis of Extracts	167
2.8.3 ¹ H-NMR Analysis of Extracts of <i>F. exasperata</i>	168
2.8.4 LC-ESIMS Analysis of Extracts of <i>F. exasperata</i>	169
2.8.5 Uterine Contractility Effect of Extracts.....	170
2.8.6 Fatty Acids Isolated from <i>F. exasperata</i>	171

2.8.7 Pheophorbides and Pheophytins.....	173
2.8.8 Flavonoids.....	175
2.8.9 Pyrimidines.....	176
2.8.10 Compound 15.....	177
2.9 Conclusion.....	177
 CHAPTER THREE: DEVELOPMENT OF A METABOLOMIC MODEL FOR THE DETERMINATION OF MYOMETRIAL FUNCTION.....	
3.0 Introduction.....	180
3.1 Systematic Application/Interpretation of the Metabolomic Results	183
3.2 Uterine Metabolomic Profiling.....	184
3.3 Aim and Objectives of Study.....	185
3.4 Materials and Methods.....	186
3.4.1 Animals.....	186
3.4.2. Contractility Experiments.....	187
3.4.3 Concentration-Response Studies.....	187
3.5 Sampling.....	188
3.5.1 Tissue Metabolite Extraction.....	188
3.5.2 Bath Fluid Metabolite Extraction.....	189
3.6 HPLC-HRFTMS Data Acquisition.....	189
3.7 ¹ H-NMR Data Acquisition.....	190
3.8 Data Processing and Analysis.....	191
3.8.1 HPLC-HRFTMS Profiles.....	191

3.8.2 Preprocessing of HPLC-HRFTMS Data.....	192
3.8.3 HPLC-HRFTMS Data Analysis	192
3.8.4 Bioinformatic Analysis of HPLC-HRFTMS Data.....	194
3.8.5 NMR Pre-processing and Analysis	194
3.9 Results.....	198
3.9.1 Effect of Drugs on Spontaneous Uterine Contractions.....	198
3.9.2 Metabolomic Analyses of the Effect of Drugs on the Mouse Uterus	201
3.9.3 Bioinformatics	210
3.9.4 Comparison of ¹ H-NMR Metabolic Profiles of Uterine Tissues and Bath Fluids.....	218
3.9.5 Comparison of ¹ H-NMR Metabolic Profiles of Oxytocin Treated Uterine Tissues and Bath Fluids with Controls	222
3.10 Discussion	229
3.11 Conclusion	234
CHAPTER FOUR: ELUCIDATION OF THE MECHANISM OF ACTION OF THE EXTRACTS OF <i>F. EXASPERATA</i> ON UTERINE CONTRACTION USING METABOLOMIC MODELS	236
4.1 INTRODUCTION	237
4.2 Metabolomics in Systems Biology	239
4.3 Metabolomics in the Determination of Mode of Action of Herbal Medicines.....	241
4.4 Aim of Current Study	242

4.5 Materials and Methods	243
4.6 Pharmacological Studies	243
4.7 HR-FTLCMS Results.....	243
4.7.1 HPLC-HRFTMS of E1	244
4.7.2 HR-FTLCMS of F14.....	254
4.7.3 HPLC-HRFTMS of F4-31	266
4.7.4. HPLC-HRFTMS of F6.17	279
4.7.5 HPLC-HRFTMS of F28	294
4.8 ¹H-NMR Results	307
4.8.1 ¹H-NMR Multivariate Analysis of the fractions of <i>F. exasperata</i>	314
4.9 DISCUSSION.....	345
4.9.1 Pharmaco-Metabolomic Analysis of Extract and Fractions	345
4.9.2 The Phospholipids and their involvement in this Study	355
4.9.2.1 Physiological Role of Phosphatidylserine.....	356
4.9.2.2 Phosphatidylethnaolamine (PE) and Ananadamide (AEA).....	357
4.9.2.4 Physiological Role of Phosphatidylinositol (PI).....	359
4.9.3 CONCLUSION	361
CHAPTER FIVE: SUMMARY, FUTURE RESEARCH AND CONCLUDING	
REMARKS	363
5.1 Isolation and Identification of Uterine Active Phytochemical Constituents	
of <i>F. exasperata</i>	365

5.2 Development of a Metabolomic Model for the Investigation of Drug Action	366
5.3 Application of Pharmacology coupled with Metabolomics in the	
Evaluation of the Mechanism of Action of the Fractions	367
5.4 Future Research	368
5.5 Conclusion	369
6.0 REFERENCES	370
APPENDIX	442
APPENDIX 1	442
APPENDIX 2	444
APPENDIX 3	448
APPENDIX 4	464

ABSTRACT

In the search for new, safe and efficacious uterine active agents, the plant *Ficus exasperata* was subjected to phytochemical screening and pharmacological analysis. Ethyl acetate and methanolic leaf extracts of *F. exasperata* were fractionated and purified by a series of chromatographic techniques. The isolation process was guided by in vitro functional uterine assays involving the use of C57Bl/6 female mice. Identification of the active chemical constituents was performed by several spectroscopic techniques which included 1D and 2D nuclear magnetic resonance (NMR) and high resolution mass spectrometry (HRMS). The uterine effects of these compounds were investigated on lidocaine-induced, spontaneous, oxytocin-induced and high KCl-induced contractions using isolated uterine segments of non-pregnant female mice. The activity of different compounds on the amplitude (maximum tension above basal force) and frequency of uterine contractions were simultaneously measured and then statistically analysed. The structure-activity relationships were also examined where possible.

These studies led to the identification of some new phytochemical derivatives. Pharmacological assays revealed the presence of both uterine stimulatory and inhibitory constituents. The new pheophytin/pheophorbide derivatives, flavonoids, fatty acids and glycerol derivatives significantly reduced the frequency and amplitude of uterine contraction, while KCl salt, pyrimidine and pheophorbide-b derivatives significantly augmented both spontaneous and agonist-induced contractions.

This study has demonstrated that *F. exasperata* generates secondary metabolites which have proven effective in the significant inhibition of uterine contractions and thus a potential source of new tocolytic agents. Additionally, uterine stimulatory constituents were also generated some of which may be potential drugs for contraception and/or labour facilitation. Lead compounds generated from this study are the pheophytin/pheophorbide derivatives, pyrimidine derivatives and flavonoid derivatives.

The rather low yield of compounds frequently experienced in the course of bioassay-guided phytochemical screening has made it almost impossible to investigate the possible mechanism(s) of action of active fractions and/or compounds. This necessitated study into the development of high throughput analytical tools combining metabolomics and pharmacology in the investigation of the function of drugs. This study involved the application of liquid chromatography coupled to high resolution Fourier transform mass spectrometry (LC-HRFTMS) and proton NMR ($^1\text{H-NMR}$) as analytical platforms in the determination of myometrial function. An initial study was performed to determine the success of the method and this was achieved by assessment of mouse myometrial metabolites altered in response to oxytocin and ritodrine. The myometrial tissues and bath fluids were extracted at the peak of activity and subjected to LC-HRFTMS analysis. The use of the bath fluids in this study was an innovative approach in sampling. The resulting data were preprocessed and analyzed via a pair-wise chemometric comparison model. Pathway analyses following metabolite identification confirmed previously known mechanism(s) thus validating the method while revealing new insights and creating knowledge-driven hypotheses for future research. This study therefore

enabled the development of a technique which combines metabolomics with in vitro pharmacology for the rapid detection of compelling myometrial metabolites in drug function and was successfully applied in the determination of possible mechanism(s) of the active constituents of *F. exasperata*.

GRAPHIC ABSTRACTS

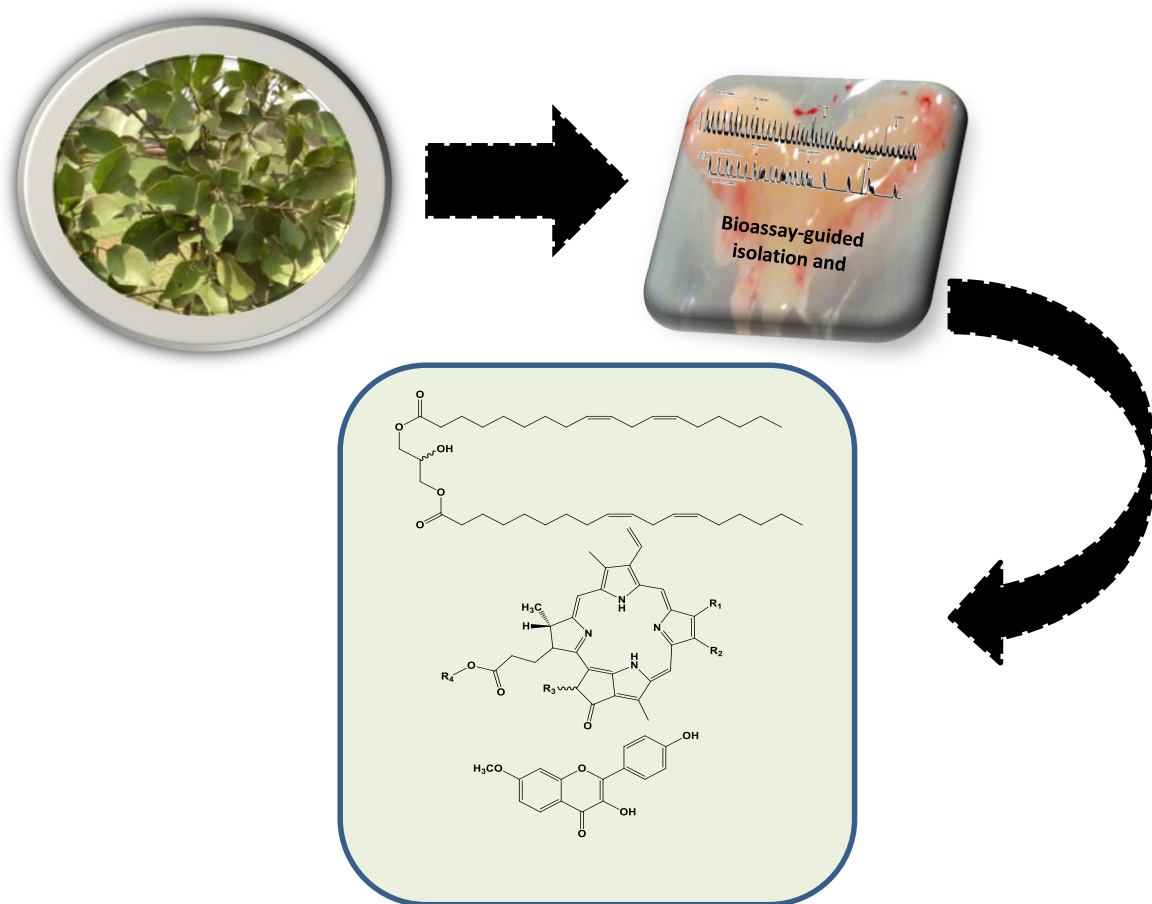


Figure A. Graphic abstract of first phase of this study involving the bioassay-guided fractionation and isolation of uterine active constituents of the leaves of *F. exasperata*.

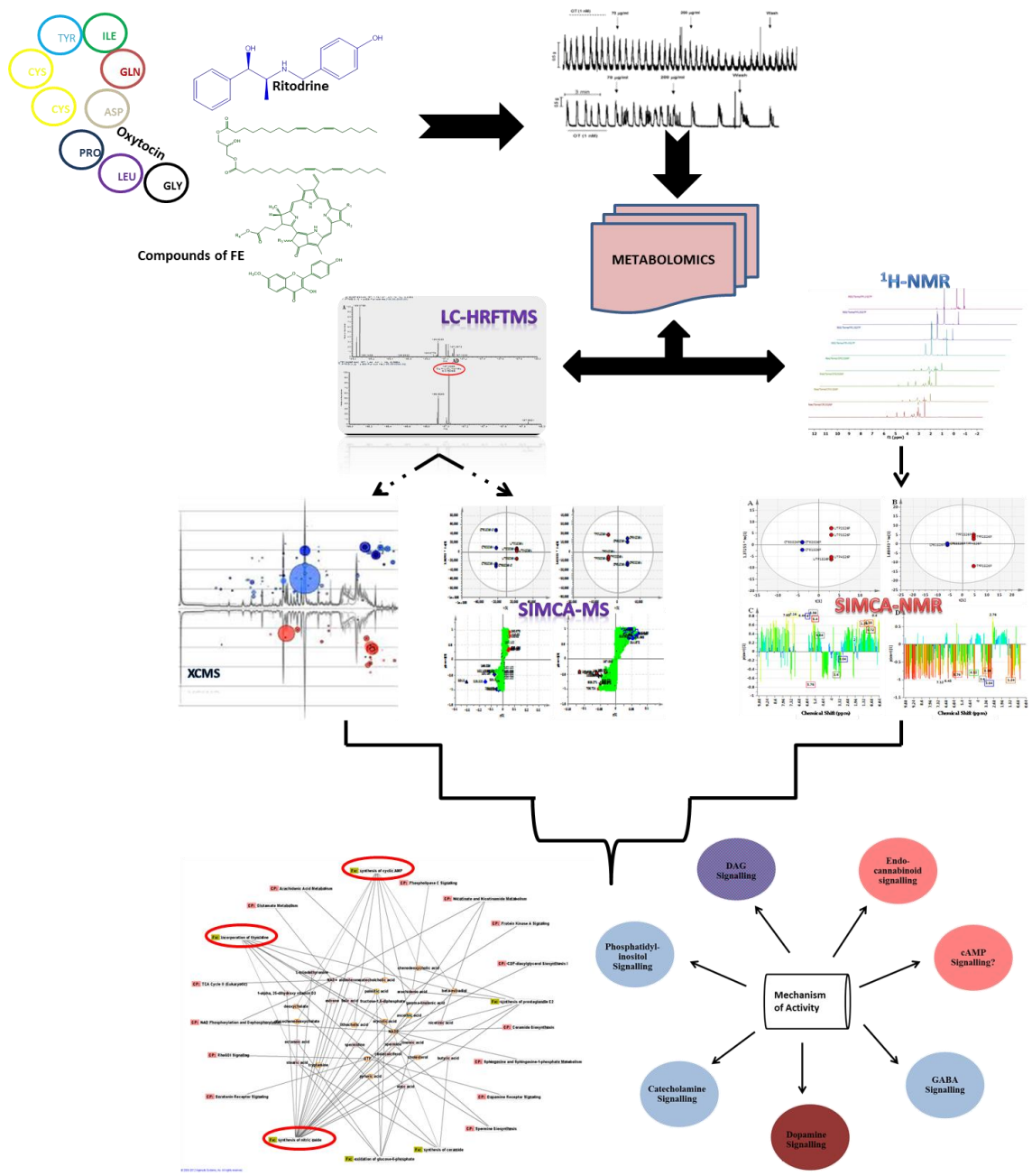


Figure B. Graphic abstract summarizing the second phase of this study involving development and application of metabolomic techniques for the determination of function of drugs.

LIST OF ABBREVIATIONS

1D	One dimensional
¹H-NMR	Proton nuclear magnetic resonance
2D	Two dimensional
ASC	Ascorbic Acid
ACN	Acetonitrile
ADP	Adenosine diphosphate
AEA	Anandamide (N-arachidonyl amine)
Akt or PKB	Protein kinase B
Al₂O₃	Aluminium
aa	Amino Acid
AMP	Adenosine monophosphate
ANOVA	Analysis of variance
AA	Arachidonic acid
ATP	Adenosine triphosphate
ATPase	Adenosine triphosphatase
AUC	Area under the curve
B2	Butanol extract
BGMF	Bioassay-guided MPLC Fractionation
BK	Big Potassium or Maxi-K ion channels
BKCa	Large conductance Ca ²⁺ -activated K ⁺ channels
BKg CPS	Background count per second
C57Bl/6	C57 Black 6 strain of mice
Ca²⁺	Calcium ion
CaCl₂	Calcium chloride
CAD	Caldesmon
cAMP	Cyclic adenosine monophosphate
CAPs	Contraction associated proteins
CB₁	Cannabinoid receptor subtype 1
CB₂	Cannabinoid receptor subtype 2
CB₃	Cannabinoid receptor subtype 3
CBR	Cannabinoid receptor
CCL₄	Carbon tetrachloride
CDc42	Cell division control protein 42
CDCl₃	Deuterated chloroform
CDP	Cytidine diphosphate
CDP-DAG	Cytidine diphosphate diacylglycerol
CDPM	Cysteinyl dopamine
CER	Ceramide
cGMP	Cyclicguanosine monophosphate
CHO	Aldehyde group
CLA	Conjugated linoleic acid
CMP	Cytidine monophosphate
CO₂	Carbon (iv) oxide
CoA	Coenzyme A
COOCH₃	Carboxylic acid
COSY	Correlation spectroscopy

COX-1	Cyclooxygenase 1
COX-2	Cyclooxygenase-2
CP1-17	A protein kinase C substrate
DAD	Diode array detection
DAG	Diacylglycerol
DCM	Dichloromethane
DHA	Docosahexaenoic acid
DHQ	Dihydroquercetin
DMSO	Dimethyl sulfoxide
DMSO-D₆	Deuterated dimethyl sulfoxide
E1	Ethylacetate extract1
E2	Ethylacetate extract2
EC50	Effective concentration producing 50% of maximal responses
ECs	Endocannabinoids
EFA	Essential Fatty acid
EP₂	Prostaglandin E receptor subtype 2
ER	Endoplasmic reticulum
ERK	extracellular signal regulated kinase
ESI	Electron spray ionization
ESIMS	Electron spray ionisation mass spectrometry
EtoAC	Ethylacetate
FA	Fatty acids
FAF	Fatty acid (F14) treated fluids
FAT	Fatty acid (F14) treated tissues
FC	Fold change
FDA	Food and Drug Administration
FE	<i>Ficus exasperata</i>
FLF	Flavonoid (F28) treated fluids
FLT	Flavonoid (F28) treated tissues
GABA	Gamma amino butyric acid
GABA_BR	gamma amino butyric acid receptor subtype B
GPC	Glycerophosphocholine
GPR55	G protein coupled receptor 55
GTP	Guanosine triphosphate
H1	Hexane extract
H₂O	Water
H₂SO₄	Sulfuric acid
HB	Hydroxybutyric acid
HCA	Hierarchical analysis
HCl	Hydrochloric acid
hERG	human Ether-à-go-go-Related Gene
HMBC	Heteronuclear multiple bond correlation
HMQC	Heteronuclear multiple quantum correlation
HPLC	High pressure liquid chromatography
HPLC-MS	High pressure liquid chromatography-mass spectrometry
HRESI-MS	High resolution Electron spray ionization mass

	spectrometry
ICP-MS	Inductively coupled plasma-mass spectrometry
ICRAC	Store operated calcium channels
IL-1	Interleukin 1
IL-6	Interleukin-6
INDO	Indomethacin
IP₃	Inositol triphosphate
IP₄	Inositol 1, 3, 4, 5 tetrakisphosphate
IPA	Ingenuity pathway analysis
IQ	Intelligent quotient
J	Coupling constant
K⁺	Potassium ion
K_{ATP}	Adenosine triphosphate activated potassium channels
K_{Ca}	Calcium activated potassium channels
KCNK	Potassium channel subfamily K
KH₂PO₄	Monopotassium phosphate
Kv	Voltage-gated potassium channels
LA n-6	Linoleic acid
LC-ESIMS	Liquid chromatography-Electron spray ionisation mass spectrometry
LC-HRFTMS	Liquid chromatography-high resolution fourier transform mass spectrometry
LC-MS	Liquid chromatography-mass spectrometry
LG	Light green
LID	Lidocaine
LnA	Linolenic acid
LOX	Lipoxygenase
m/z	mass to charge ratio
M1	Methanol extract
MAM	Mitochondria associated membranes
MANOVA	Multiple analysis of variance
MAPK	Mitogen activated protein kinases
MCD	Methyl cyclodextrin
MDG	Millennium development goal
MeOH	Methanol
MgSO₄	Magnesium Sulphate
MI	Myoinositol
MLCK	Myosin light chain kinase
MLCP	Myosin light chain phosphatase
MPLC	Medium pressure liquid chromatography
MS	Mass spectrometry
mTOR	mammalian target of rapamycin
MVA	Multivariate analysis
MVDA	Multivariate data analysis
n.d.	Not detectable
NA	Nucleic acid
Na⁺	Sodium ion

NAA	N-acetylaspartate
NaCl	Sodium chloride
NAD	Nicotinic acid adenine
NADA	N-arachidonyl dopamine
NADP	Nicotinic acid adenine dinucleotide phosphate
NAE	N-arachidonyl amine (anandamide)
NaHCO₃	Sodium bicarbonate
NAPE	N-acylPhosphatidylethanolamine
NAPE-PLD	NAPE-hydrolyzing phospholipase D
NCX	Na ⁺ -Ca ²⁺ exchanger
NH₄⁺	Ammonium ion
NMR	Nuclear magnetic resonance
NO	Nitric oxide
NOESY	Nuclear Overhauser Enhancement Spectroscopy
NP	Natural Product
O₂	Oxygen
OPLS	Orthogonal partial least square
OPLS-DA	Orthogonal partial least square-discriminant analysis
OT	Oxytocin
OTF	Oxytocin-treated fluids
OTFNP	Oxytocin-treated fluids non-polar
OTFP	Oxytocin-treated fluid polar
OTR	Oxytocin receptor
OTT	Oxytocin-treated tissues
OTTNP	Oxytocin-treated tissues non polar
OTTP	Oxytocin-treated tissues polar
PA	Phosphatidic acid
PACs	Phosphofurin acidic cluster sorting protein
PAF	Pheophytin A (F6_17) treated tissues
PAT	Pheophytin A (F6_17) treated tissues
PC	Phosphatidylcholine
PCA	Principal component analysis
P(corr)	Correlation Loading
PCr	Phosphocreatine
P(ctr)	Absolute value of correlation loading
PE	Phosphatidylethanolamine
PG	Glycerophosphate
PGE	Prostaglandin E
PGF	Prostaglandin F
PHE	Phenylalanine
pHi	Internal pH
pHo	External pH
Pi	Inorganic phosphate
PI	Phosphatidylinositol
PI3K	Phosphatidylinositol 3-kinase
PKB or Akt	Protein kinase B
PLS	Partial least squares

PLS-DA	Partial least square-discriminant analysis
PMCA	Plasma membrane Ca ²⁺ -ATPase
PPARα	Peroxisome proliferator-activated receptor- α
Ppm	parts per million
PS	Phosphatidylserine
PS I	Phosphatidylserine synthase I
PS II	Phosphatidylserine synthase II
PV	P value
PYRF	Pyropheophytin (F4_31) treated fluids
PYRT	Pyropheophytin (F4_31) treated tissues
Q	Quercetin
Q²Y	Model quality parameter
QTOFMS	Quadruple time of flight mass spectrometry
R²Y	Predictability parameter
Rac	Subfamily of the Rho GTPase
Ras	Rat sarcoma family of g proteins
Rb	Rubidium
RDBE	Ring and double bond equivalents
R_f	Retention Factor
Rho	Ras homolog gene
RhoA	Ras homolog gene family-member A
RIC	Resurrected ion chromatogram
RIT	Ritodrine
RITF	Ritodrine-treated fluids
RITFNP	Ritodrine-treated fluids non-polar
RITFP	Ritodrine-treated fluids polar
RITT	Ritodrine-treated tissues
RITTNP	Ritodrine-treated tissues non polar
RITTP	Ritodrine-treated tissues polar
RMP	Resting membrane potential
RNA	Ribonucleic acid
ROK	Rho-associated kinase
ROS	Reactive oxygen species
Rt	Retention time
RT-PCR	Real time-polymerase chain reaction
RyR	Ryanodine receptor
S.E.M.	Standard Error of Mean
SD	Standard deviation
SDK	Stretch dependent potassium channels
SERCA	Sarco/endoplasmic reticulum Ca ²⁺ -ATPase
SIMCA	Soft Independent Method of Class Analogy
SIPBS	Strathclyde Institute of Pharmacy and Biomedical Sciences
SR	Sarcoplasmic reticulum
STOCSY	Statistical total correlation spectroscopy
TCA	Tricarboxylic acid
TCM	Traditional Chinese medicine
TEA	Tetraethylammonium

TG	Triacylglycerol
TIC	Total ion chromatogram
TLC	Thin Layer Chromatography
TNFα	Tumour necrosis factor alpha
TREK	Stretch-dependent potassium channels
TRPV1	Transient receptor potential vanilloid 1
UDPLAra4O	Uridine 5'-diphospho -beta-L-threo-pentapyranos-4-ulose
UPLC	Ultra performance liquid chromatography
UPLC-MS	Ultra performance liquid chromatography-mass spectrometry
UPLC-QTOFms	Ultra performance liquid chromatography-Quadruple time-of-flight mass spectrometry
UV	Ultra violet
VDCs	Voltage-dependent calcium channels
VGSCs	Voltage gated sodium channels
W2	Water extract
XIC	Extracted ion chromatogram

LIST OF FIGURES

Figure 1.1	Photographs of <i>F. exasperata</i>	7
Figure 1.2	Photograph of the dissected mouse uterus	11
Figure 2.0	Schematic diagram showing the first phase extraction of the leaves of <i>F. exasperata</i>	57
Figure 2.1	Schematic diagram summarizing the bioassay-guided fractionation procedure for E1	66
Figure 2.2	TLC plates of H1 , E1 and E2 developed in hexane:EtoAc (80:20)	73
Figure 2.3	TLC plates of M1 , W2 and B2	74
Figure 2.4	TLC plates under UV wavelength of M1 , B2 , W2 and H1 , E1 and E2	76
Figure 2.5	¹ H-NMR spectrum at 400 MHz in CDCl ₃ of H1	79
Figure 2.6	¹ H-NMR spectrum at 400 MHz in CDCl ₃ of E1	80
Figure 2.7	¹ H-NMR spectrum at 400 MHz in CDCl ₃ of E2	81
Figure 2.8	¹ H-NMR spectrum at 400 MHz in DMSO-D ₆ of M1	82
Figure 2.9	¹ H-NMR spectrum at 400 MHz in DMSO-D ₆ of B2	83
Figure 2.10	¹ H-NMR spectrum at 400 MHz in DMSO-D ₆ of W2	84
Figure 2.11a	Stacked ¹ H-NMR spectra of H1 , E1 , E2 , M1 , W2	85
Figure 2.11b	Expanded stacked ¹ H-NMR spectra of H1 , E1 , E2 , M1 , B2 and W2	86
Figure 2.12	Stacked Base Peak Chromatograms of H1 , E1 and E2	87
Figure 2.13	Stacked Base Peak Chromatograms of M1 (A), B2 (B) and W2 (C)	88
Figure 2.14	Representative tracing of H1 on lidocaine-induced contractions of the isolated mouse uterus	89
Figure 2.15	Representative tracing of E1 on lidocaine-induced contractions of the isolated mouse uterus	90
Figure 2.16	Representative tracing of E2 on lidocaine-induced contractions of the isolated mouse uterus	91

Figure 2.17	Representative tracing of M1 on lidocaine-induced contractions of the isolated mouse uterus	91
Figure 2.18	Representative tracing of W2 on lidocaine-induced contractions of the isolated mouse uterus	92
Figure 2.19	Representative tracing of B2 on lidocaine-induced contractions of the isolated mouse uterus	93
Figure 2.20	HRESI-MS showing the relative abundance and the m/z of hexadecanoic acid	98
Figure 2.21	HRESI-MS showing the relative abundance and the m/z of gammalinolenic acid	99
Figure 2.22	1D ¹ H-NMR spectrum of gammalinolenic acid	100
Figure 2.23	HRESI-MS showing the relative abundance and the m/z of compound 1 .	101
Figure 2.24	The 1D ¹ H-NMR spectrum of Fr. 4-14Ea in CDCl ₃	102
Figure 2.25	2D COSY ¹ H-NMR spectra of Fr.4-14Ea in CDCl ₃	103
Figure 2.26	HMQC spectrum of compound 1 in CDCl ₃	104
Figure 2.27	HRESI-MS showing the relative abundance and the m/z of compound 2	105
Figure 2.28	The 1D ¹ H-NMR spectrum of compound 2 in CDCl ₃	106
Figure 2.29	An expanded portion of the COSY ¹ H-NMR spectrum of compound 2 in CDCl ₃	107
Figure 2.30	HRESI-MS chromatogram showing the relative abundance and the m/z of compound 3	112
Figure 2.31	HRESI-MS chromatogram showing the relative abundance and the m/z of compound 4	113
Figure 2.32	HRESI-MS chromatogram showing the relative abundance and the m/z of compound 5	114
Figure 2.33	HRESI-MS chromatogram showing the relative abundance and the m/z of compound 6	115
Figure 2.34	¹ H-NMR spectrum of pheophytin-a derivatives measured	116

	in CDCl ₃ at 400MHz	
Figure 2.35	HMBC spectrum of pheophytin a derivatives in CDCl ₃ at 400 MHz	117
Figure 2.36	HRESI-MS chromatogram showing the relative abundance and the m/z of compound 7	118
Figure 2.37	HRESI-MS chromatogram showing the relative abundance and the m/z of compound 8	119
Figure 2.38	HRESI-MS chromatogram showing the relative abundance and the m/z of compound 9	120
Figure 2.39	1D ¹ H-NMR spectrum in CDCl ₃ at 400 MHz of pheophorbide b derivatives with compound 7 as the major compound	121
Figure 2.40	1D ¹ H-NMR spectrum in CDCl ₃ at 400 MHz of pheophorbide b, (compound 8) and pheophytin b, compound 9	122
Figure 2.41	HMQC spectrum of Fr.10-22Ea (compounds 7 , 8 and 9).	123
Figure 2.42	Positive (A) and negative (B) HRESI-MS chromatograms showing the relative abundance and the m/z of compound 10	125
Figure 2.43	1D ¹ H-NMR in CDCl ₃ measured at 400 MHz	126
Figure 2.44	1D Nuclear Overhauser Enhancement Spectroscopy (NOESY) spectrum of compound 10 in CDCl ₃ measured at 400 MHz	127
Figure 2.45	2D COSY spectrum of compound 10 in CDCl ₃ measured at 400 MHz	128
Figure 2.46	Positive and negative HRESI-MS chromatograms showing the relative abundance and the m/z of compound 11	129
Figure 2.47	1D ¹ H-NMR spectrum of compound 11 in CDCl ₃ measured at 400 MHz	130
Figure 2.48	Positive and negative HRESI-MS chromatograms showing the relative abundance and the m/z of compound 13	131

Figure 2.49	1D ¹ H-NMR spectrum in CDCl ₃ measured at 400MHz	132
Figure 2.50	Positive and negative HRESI-MS chromatograms showing the relative abundance and the m/z of compound 14	134
Figure 2.51	1D ¹ H-NMR spectrum of compound 14 in CDCl ₃	135
Figure 2.52	2D COSY spectra compound 14 in CDCl ₃ measured at 400 MHz	136
Figure 2.53	The ¹ H-NMR spectrum of the salt in DMSO-d ₆ from the leaves of <i>F. exasperata</i>	137
Figure 2.54a	Compounds 1 and 2 isolated from the leaves of <i>F. exasperata</i>	139
Figure 2.54b	Compounds 3-10 isolated from the leaves of <i>F. exasperata</i>	140
Figure 2.54c	Compounds 11-14 isolated from the leaves of <i>F. exasperata</i>	141
Figure 2.55	Representative tracings showing the effect of increasing concentrations of compound 1	142
Figure 2.56	Representative recordings of increasing concentrations (10 – 200 µg/ml) of compound 2 on spontaneous uterine contractions	143
Figure 2.57	Original recordings showing increasing concentrations of Fr. 28Ea	144
Figure 2.58	Representative tracings showing increasing concentrations of Fr. 6.17Ea (10 – 200 µg/ml) on spontaneous uterine contractions	145
Figure 2.59	Original recordings of different concentrations of compound 6 on spontaneous uterine contractions	146
Figure 2.60	Representative recordings showing increasing concentrations of compound 7 (10 -200 µg/ml) on spontaneous uterine contractions	147
Figure 2.61	Representative recordings showing the effect of trilinolein on uterine smooth muscle.	147

Figure 2.62	Representative recordings showing the effect of pyrimidine on uterine smooth muscle	148
Figure 2.63	Representative tracing showing the effect of compound 14 on the non-stimulated uterus	148
Figure 2.64	Representative tracing of the effects of KCl (isolated from the leaves of <i>F. exasperata</i>)	149
Figure 2.65	The effects of compounds from the leaves of <i>F. exasperata</i> on the frequency of spontaneous uterine contractions	154
Figure 2.66	The effects of compounds from the leaves of <i>F. exasperata</i> on the amplitude of spontaneous uterine contractions	155
Figure 2.67	The effect of trilinolein and pyrimidine on the frequency and amplitude of spontaneous contractions	156
Figure 2.68	Concentration-response curves showing the effect of increasing concentrations of compound 15 (KCl isolated from the leaves of <i>F. exasperata</i>) on spontaneously contracting uterine tissue	157
Figure 2.69	Bar graphs of the effect of compound 14 on uterine contractions	159
Figure 2.70	Original recording showing the effect of compound 1 on OT-induced uterine contractions	161
Figure 2.71	Original recording of compound 2 on OT-induced uterine contractions	161
Figure 2.72	Original tracings of Fr. 28Ea on OT-induced uterine contractions	162
Figure 2.73	Original tracings of Fr. 6.17Ea on OT-induced uterine contractions	162
Figure 2.74	Representative tracing of compound 9 on OT-induced uterine contractions	163
Figure 2.75	Representative tracing of compound 10 on OT-induced uterine contractions	163

Figure 2.76	Original recording of the effect of pyrimidine on OT-induced contractions	164
Figure 2.77	The effects of compounds from the leaves of <i>F. exasperata</i> on the frequency of OT-induced uterine contractions	164
Figure 2.78	The effects of compounds from the leaves of <i>F. exasperata</i> on the amplitude of OT-induced uterine contractions	165
Figure 3.1	Flow chart showing the steps involved in the pharmacometabolomic analysis	197
Figure 3.2	A recording of the representative effect of oxytocin (OT (1 nM)) on spontaneously contracting mouse uterine tissues	198
Figure 3.3	A recording of the representative effect of ritodrine (RIT (0.1 nM)) on spontaneously contracting uterine tissues	198
Figure 3.4	Mean responses (\pm S.E.M) of the isolated uterus to OT calculated within a 5 min time range	199
Figure 3.5	Mean responses (\pm S.E.M) of the isolated uterus to RIT calculated within a 5 min time range	200
Figure 3.6	OPLS-DA scatter score plots of differential metabolites observed on treatment of the isolated uterus with OT as determined by HR-FTLCMS	202
Figure 3.7	OPLS-DA scatter score plots of differential metabolites observed on treatment of the isolated uterus with RIT as determined by HR-FTLCMS	203
Figure 3.8	S-Plots of differentially expressed metabolites with OT treatment of the isolated uterine tissues, and the surrounding bath fluids as determined by HR-FTLCMS	204
Figure 3.9	S-Plots of differentially expressed metabolites with RIT treatment of the isolated uterine tissues, and the surrounding bath fluids as determined	205

by HR-FTLCMS

Figure 3.10	Top functions extracted by IPA software that have been perturbed on treatment of the isolated uterus with oxytocin	210
Figure 3.11	Top canonical pathways for OT extracted by IPA bioinformatics software	211
Figure 3.12	Top functions associated with the effect of RIT on uterine contraction.	212
Figure 3.13	Top canonical pathways extracted by IPA bioinformatics software for the effect of RIT on uterine contractions	213
Figure 3.14	IPA network of top functions and signalling pathways detected on analysis of OT- treated uterine tissues	214
Figure 3.15	IPA network of top functions and signalling pathways detected on analysis of bath fluids in which OT- treated uterine tissues were immersed	215
Figure 3.16	IPA network of top functions and signalling pathways detected on analysis of RIT- treated uterine tissues	216
Figure 3.17	IPA network of top functions and signalling pathways detected on analysis of bath fluids in which RIT- treated uterine tissues were immersed	217
Figure 3.18	Biplots of OT- and RIT-treated uterine tissues and surrounding bath fluids	220
Figure 3.19	Differentially Expressed Metabolites with OT and RIT as determined by NMR	221
Figure 3.20	Pair matched 1D ¹ H-NMR spectra showing polar extracts of control versus OT-treated uterine tissues	222
Figure 3.21	Pair matched 1D ¹ H-NMR spectra showing non-polar extracts of control versus OT-treated uterine tissues	223
Figure 3.22	Representative pair matched 1D ¹ H-NMR spectra showing polar extracts of control versus OT-treated bath fluids	224
Figure 3.23	Representative pair matched 1D ¹ H-NMR spectra showing	

	non-polar extracts of control versus OT-treated bath fluids	225
Figure 3.24	Representative pair matched 1D ¹ H-NMR spectra showing polar extracts of control versus RIT-treated tissues	226
Figure 3.25	Representative pair matched 1D ¹ H-NMR spectra showing non-polar extracts of control versus RIT-treated tissue	227
Figure 3.26	Representative pair matched 1D ¹ H-NMR spectra showing polar extracts of control versus RIT-treated bath fluids	228
Figure 3.27	Representative pair matched 1D ¹ H-NMR spectra showing non-polar extracts of control versus ritodrine-treated bath fluids	229
Figure 4.1	OPLSDA score plots of polar E1 treated groups	245
Figure 4.2	OPLSDA S plots of polar E1 treated groups	246
Figure 4.3	OPLSDA score plots of non-polar E1 treated groups	247
Figure 4.4	OPLSDA S plots of polar E1 treated groups	248
Figure 4.5	Predicted significantly regulated pathways of E1 on uterine contraction	253
Figure 4.6	OPLSDA score plots of polar F14 treated groups	255
Figure 4.7	OPLSDA S plots of polar F14 treated groups	256
Figure 4.8	OPLSDA score plots of non-polar F14 treated groups	257
Figure 4.9	OPLSDA S plots of non-polar F14 treated groups	258
Figure 4.10a	Bar charts displaying top functions and canonical pathways extracted by IPA software for F14 treated uterine tissues	264
Figure 4.10b	IPA-generated bar charts displaying top functions and canonical pathways for bath fluids in which the F14 treated uterine tissues were immersed	265
Figure 4.11	OPLSDA score plots of polar F4-31 treated groups	267
Figure 4.12	OPLSDA S plots of polar F4-31 treated groups	268
Figure 4.13	OPLSDA score plots of non-polar F4-31 treated groups	269
Figure 4.14	OPLSDA S plots of non-polar F4-31 treated groups.	270
Figure 4.15a	Bar charts displaying top functions (A) and canonical	277

	pathways (B) extracted by IPA software for F4-31 treated uterine tissues	
Figure 4.15b	IPA-generated bar charts displaying top functions (C) and canonical pathways (D) for bath fluids in which the F14 treated uterine tissues were immersed	278
Figure 4.16	OPLSDA score plots (A and B) of polar F6.17 treated groups	280
Figure 4.17	OPLSDA S plots of polar F6.17 treated groups	281
Figure 4.18	OPLSDA score plots of non-polar F6.17 treated groups	282
Figure 4.19	OPLSDA S plots of non-polar F6.17 treated groups	283
Figure 4.20a	Bar charts displaying top functions (A) and canonical pathways (B) extracted by IPA software for F6.17 treated uterine tissues	292
Figure 4.20b	IPA-generated bar charts displaying top functions (C) and canonical pathways (D) for bath fluids in which the F6.17 treated uterine tissues were immersed	293
Figure 4.21	OPLSDA score plots of polar F28 treated groups	295
Figure 4.22	OPLSDA S plots of polar F28 treated groups	296
Figure 4.23	OPLSDA score plots of non-polar F28 treated groups	297
Figure 4.24	OPLSDA S plots of non-polar F28 treated groups	298
Figure 4.25a	Bar charts displaying top functions (A) and canonical pathways (B) extracted by IPA software for F28 treated uterine tissues	304
Figure 4.25b	IPA-generated bar charts displaying top functions (C) and canonical pathways (D) for bath fluids in which the F28 treated uterine tissues were immersed	305
Figure 4.26	OPLSDA scatter plots showing ¹ H-NMR analysis of polar E1 -treated uterine tissues and bath fluids in which the uterine tissues were immersed	318
Figure 4.27	Correlation coefficient plots showing the distribution of metabolites in the NMR spectra of the polar E1 -treated	319

	groups	
Figure 4.28	OPLSDA scatter plots showing ¹ H-NMR analysis of non-polar E1 -treated uterine tissues (A) and bath fluids in which the uterine tissues were immersed	320
Figure 4.29	Correlation coefficient plots showing the distribution of metabolites in the NMR spectra of the non-polar E1 -treated groups	321
Figure 4.30	OPLSDA score plots showing ¹ H-NMR analysis of polar F14 treated uterine tissues (A) and bath fluids in which the uterine tissues were immersed (B).	322
Figure 4.31	Correlation coefficient plots showing the distribution of metabolites in the NMR spectra of the polar F14 -treated groups	323
Figure 4.32	OPLSDA score plots showing ¹ H-NMR analysis of non-polar F14 treated uterine tissues and bath fluids in which the uterine tissues were immersed.	324
Figure 4.33	Correlation coefficient plots showing the distribution of metabolites in the NMR spectra of the non-polar F14 -treated groups	325
Figure 4.34	OPLSDA score plots showing ¹ H-NMR analysis of polar F4-31 treated uterine tissues and bath fluids in which the uterine tissues were immersed	326
Figure 4.35	Correlation coefficient plots showing the distribution of metabolites in the NMR spectra of the polar F4-31 -treated groups	327
Figure 4.36	OPLSDA score plots showing ¹ H-NMR analysis of non-polar F4-31 treated uterine tissues and bath fluids in which the uterine tissues were immersed	328
Figure 4.37	Correlation coefficient plots showing the distribution of metabolites in the NMR spectra of the non-polar F4-31 -treated groups	329

Figure 4.38	OPLSDA score plots showing ¹ H-NMR analysis of polar F6.17 treated uterine tissues and fluids	330
Figure 4.39	Correlation coefficient plots showing the distribution of metabolites in the NMR spectra of the polar F4-31 -treated groups	331
Figure 4.40	OPLSDA score plots showing ¹ H-NMR analysis of non-polar F6.17 treated uterine tissues (A) and bath fluids in which the uterine tissues were immersed	332
Figure 4.41	Correlation coefficient plots showing the distribution of metabolites in the NMR spectra of the non-polar F6.17 treated groups	333
Figure 4.42	OPLSDA score plots showing ¹ H-NMR analysis of polar F28 treated uterine tissues (A) and bath fluids in which the uterine tissues were immersed	334
Figure 4.43	Correlation coefficient plots showing the distribution of metabolites in the NMR spectra of the polar F28 -treated groups	335
Figure 4.44	OPLSDA score plots showing ¹ H-NMR analysis of non-polar F28 treated uterine tissues (A) and bath fluids in which the uterine tissues were immersed	336
Figure 4.45	Correlation coefficient plots showing the distribution of metabolites in the NMR spectra of the non-polar F28 -treated groups	337
Figure 4.46	Typical ¹ H-NMR spectra showing polar extracts of uterine tissues (A-E) and bath fluids in which the uterine tissues were immersed	338
Figure 4.47	Typical ¹ H-NMR spectra showing non-polar extracts of uterine tissues (A-E) and bath fluids in which the uterine tissues were immersed	339
Figure 4.48	Structure of Phospholipids showing the different functional groups	356

LIST OF TABLES

Table 2.0	Solvents and Respective Extracted Phytochemical Groups	45
Table 2.1	Extract Colours and Respective R _f values after spraying with anisaldehyde	75
Table 2.2	Qualitative Flavonoid Test for H1 , E1 and E2	77
Table 2.3	Qualitative Flavonoid Test for M1 , W2 and B2	78
Table 2.4	Effect of Extracts on the Frequency of Uterine Contraction	94
Table 2.5	Effect of Extracts on the Amplitude of Uterine Contraction	95
Table 2.6	Effect of Extracts on the AUC of Uterine Contraction	96
Table 2.7	¹ H NMR (400 MHz) data of compounds 3-9 in CDCl ₃	110
Table 2.8	¹³ C NMR (400 MHz) data of compounds 3 - 8 in CDCl ₃	111
Table 2.9	¹ H-NMR, ¹³ C NMR, COSY and HMBC (400 MHz) of N-methyl pyrimidine (14) in CDCl ₃	137
Table 2.10	Semi Quantitative Table showing ICP-MS analysis of the salt	138
Table 2.11	Effect of E1a Fractions on the Contraction Frequency (cycles/5 min) of the Uterus	150
Table 2.12	Effect of E1a Fractions on the Contraction Amplitude (g) of the Uterus.	151
Table 2.13	Effect of E1a Fractions on the AUC (g. s) of the Uterus	152
Table 2.14	Contractility Parameters for Inhibitory Compounds on Spontaneous Contractions of the Isolated Non-Pregnant Mouse Uterus	158
Table 2.15	Summary Table for Active Compounds Isolated from the Leaves of <i>Ficus exasperata</i>	166
Table 3.1A	Summary of OPLS-DA Parameters for the MS Data on Tissues	206
Table 3.1B	Summary of OPLS-DA Parameters for the MS Data on Fluids	206
Table 3.2A	Summary of Parameters for the OPLS-DA NMR Study	

	Models on Tissues.	207
Table 3.2B	Summary of Parameters for the OPLS-DA NMR Study	
	Models on Fluids	207
Table 3.3	Summary of Differentially Regulated Metabolites/Pathways Detected on Treatment of the Isolated Uterus with Oxytocin and Ritodrine	208
Table 3.4	Chemical Shift Assignment of Uterine Metabolites	218
Table 4.1	Pathways and Metabolites detected by HR-FTLCMS on Treatment of the Uterus with E1	249
Table 4.2	Pathways and Metabolites detected by HR-FTLCMS on Effect of F14 on Uterine Contractility	259
Table 4.3	Pathways and Metabolites detected by HR-FTLCMS on Effect of F4-31 on Uterine Contractility	271
Table 4.4	Pathways and Metabolites detected by HR-FTLCMS on Effect of F6.17 on Uterine Contractility	284
Table 4.5	Pathways and Metabolites detected by HR-FTLCMS on Effect of F28 on Uterine Contractility	299
Table 4.6	Summary of Pathways and Metabolites detected by HR- FTLCMS on Effect of Fractions of <i>F. exasperata</i> on Uterine Contractility	306
Table 4.7	Summarised table showing significant metabolites and pathways detected by ¹ H-NMR analysis to be involved in the action of Ficus fractions on uterine contraction	308
Table 4.8a	Summary of the Proposed Mechanism(s) of Action of crude extract E1 of <i>Ficus exasperata</i> leaves Determined from Pharmaco-metabolomic Analysis	340
Table 4.8b	Summary of the Proposed Mechanism(s) of Action of F14 of <i>Ficus exasperata</i> leaves Determined from Pharmaco- metabolomic Analysis	341
Table 4.8c	Summary of the Proposed Mechanism(s) of Action of F4-31 of <i>Ficus exasperata</i> leaves Determined from Pharmaco-	342

	metabolomic Analysis	
Table 4.8d	Summary of the Proposed Mechanism(s) of Action of F6.17 of <i>Ficus exasperata</i> leaves Determined from Pharmacometabolomic Analysis	343
Table 4.8e	Summary of the Proposed Mechanism(s) of Action of F28 of <i>Ficus exasperata</i> leaves Determined from Pharmacometabolomic Analysis	344
Table 4.9	Signal Transduction Pathways in the Uterus Activated by Endocannabinoids on Binding to Different Receptors	360

PUBLICATION FROM THESIS

Bafor E.E., Lim C.V., Rowan E.G., Edrada-Ebel R., (2010). The leaves of *Ficus exasperata* Vahl (Moraceae) generate uterine active chemical constituents. *Journal of Ethnopharmacology* **145**(3): 803-812

CHAPTER ONE

GENERAL INTRODUCTION AND SIGNIFICANCE OF STUDY

1.0 Introduction

1.1 Ethnopharmacological Background

Over half of the world's population use plant medicines as their first line of therapy (Cordell and Colvard, 2005). A number of the medicines used in ancient times were plant materials and a number of drugs in existence today were derived from plant materials (Gurib-Fakim, 2006). Plants are well known for the medicinal benefits and therapeutic effects provided and this necessitated their use in the past centuries and in several countries around the world today (Houghton and Raman, 1998). Herbs/plants are thus referred to as 'man's oldest companions' as they not only can be used in building homes but also to provide food and medicines (Gilani and Rahman, 2005). In Nigeria, West Africa for instance, the traditional healing method plays a significant part in health care and a significant number of the population are reported to still depend on traditional health care which employs the use of plant materials (Akah *et al.*, 1998).

1.2 Study Plant (*Ficus exasperata*)

One of the many plants employed in Nigerian traditional medicine is *Ficus exasperata* Vahl which belongs to the family Moraceae (Mulberry family). Though there are several studies on *F. exasperata* (Abotsi *et al.*, 2010; Adewole *et al.*, 2011; Akah *et al.*, 1997; Akah *et al.*, 1998; Anowi *et al.*, 2012; Ayinde *et al.*, 2007; Bafor and Igbinuwen, 2009; Bafor *et al.*, 2009b; Bafor *et al.*, 2010; Bafor *et al.*, 2009a; Bafor *et al.*, 2011; Dongfack *et al.*, 2011; Irene and Iheanacho, 2007; Macfoy and Cline, 1990; Odunbaku *et al.*, 2008; Ogunleye *et al.*, 2005; Okafor *et al.*, 2001;

Oladosu *et al.*, 2009; Taiwo and Aderogba, 2007; Woode *et al.*, 2011; Woode *et al.*, 2009) detailed investigation into the phytochemical constituents responsible for the uterine activity of the plant are lacking.

1.2.1 The Moraceae Family

The Moraceae family consists of about 40 genera and about 1100 species (Datwyler and Weiblen, 2004). Species of the *Ficus* genera have been reported to contain phytochemical constituents such as furanocoumarins (a plant phototoxin) and flavonoids (Joseph and Raj, 2010), alkaloids, anthraquinones, saponins and tannins have also been reported (Ahmad *et al.*, 2011; Sandabe *et al.*, 2006; Usman *et al.*, 2009). Antioxidants from figs of the moraceae family have also been reported (Joseph and Raj, 2010).

1.2.2 An Overview and Brief Description of the Genus *Ficus*

Ficus, also referred to as the fig genus, is a member of the mulberry (Moraceae) family in addition to about 40 other genera (Woodland, 1997). The fig species reported to be of principal significance based on frequency of reports and records are *Ficus carica* L. (common fig), *Ficus religiosa* L. (Bo tree), *Ficus elastica* R. (the rubber tree), *Ficus benghalensis* L. (the banyan) and *Ficus racemosa* L. (the great cluster tree) (Lansky *et al.*, 2008).

Members of the *Ficus* genus contain a sappy substance inside their vascular walls (Niangadouma, 2010), which most plants utilize for protection and is often exuded after tissue injury (Dussourd and Eisner, 1987). The fruits or figs originate

from an inflorescence with a unique arrangement (Lansky *et al.*, 2008). It also consists of a soft exocarp and the mesocarp varies in colour among the fig species. The fruit is also quite juicy and sweet to taste when fully ripe (Lansky *et al.*, 2008). The presence of specific compounds which are volatile in nature are utilized by the *Ficus* species for pollination by specific female wasps (Grison-Pige *et al.*, 2002).

1.2.3 Phytochemistry and Medicinal Uses of Some *Ficus* Species

A broad range of compounds have been isolated to date from several parts of the *Ficus* species. A few examples of the phytochemical constituents of *Ficus* spp and their biological activities are given below.

A mixture of sitosterol compounds which inhibited tumor cell proliferation was isolated from the sap of *F. carica* (Rubnov *et al.*, 2001). Using a supercritical CO₂ extraction technique; Wang and Ma have reported that extracts of fig residues have significant cytotoxic activity in some cancer cell lines both in vitro and in vivo (Wang and Ma, 2005). A dichloromethane extract of *F. citrifolia* augmented the action of daunomycin in leukemic cell lines and also augmented the anticancer action of vinblastine on MESSA and Dx5 cell lines (Simon *et al.*, 2001). Flavonoids isolated from the stem bark of *F. formosana* Maxim have been reported to exhibit anticancer activities in several cancer cell lines (Sheu *et al.*, 2005). Some triterpenoid and some alkaloids isolated from *F. elastica* also exhibited cytotoxic effects (Lansky *et al.*, 2008). Lectins and polysaccharide complexes have been isolated from fig seeds (Ray *et al.*, 1993) which promote white blood cell cohesion in leukemic patients (Agrawal and Agarwal, 1990).

Extracts of *F. racemosa* demonstrated significant antidiarrhoeal activity (Mandal *et al.*, 1997). Tannins in the leaves of *F. hispida* were reported to be responsible for its antidiarrhoeal activity (Mandal and Kumar, 2002).

Antifungal and antibacterial activities have also been reported for extracts of the leaves of *F. hispida* (Deraniyagala *et al.*, 1998; Mandal *et al.*, 2000).

The methanolic extract of the stem bark of *F. racemosa* has been reported to induce hypothermia in both normothermic and pyrexia albino rats. The stem bark was shown to decrease urinary Na⁺ level, and also to increase the osmolarity of urine (Ratnasooriya *et al.*, 2003).

A furan compound isolated from *F. racemosa* was reported to inhibit cyclooxygenase-1 (COX-1) and 5-lipoxygenase (5-LOX) activity in vitro (Li *et al.*, 2004). A dose-dependent analgesic effect of the ethanolic leaf and bark extract has also been reported (Malairajan *et al.*, 2006). The aqueous and ethanol extracts also displayed effective antioxidant activity (Veerapur *et al.*, 2009).

The ethanol extract of the leaves of *F. racemosa* and β -sistosterol from the stem bark was shown to cause hypoglycemia in alloxan-diabetic rats (Joseph and Raj, 2010). The fruits decreased cholesterol levels and also suppressed KBrO₃-mediated nephrotoxicity in rats. The methanolic extract of the stem bark produced significant hepatoprotective effect against CCl₄-induced hepatotoxicity in rats (Ahmed and Urooj, 2010).

A glycoside known as benghalenoside, isolated from *F. benghalensis* was reported to reduce hyperglycemia in normal and alloxan-induced diabetic rabbits (Augusti, 1975). A dimethoxy ether compound derived from leucopelargonidin rhamnoside (Augusti, 1975) and a dimethoxy compound obtained from a

leucocyanidin cellobioside were isolated from the bark of *F. bengalensis* and shown to reduce blood sugar concentration in streptozotocin-induced diabetic animals and cause an increase in serum concentrations of insulin in normal and diabetic rats (Achrekar *et al.*, 1991; Kumar and Augusti, 1989). The aqueous extract of the bark of *F. benghalensis* produced antioxidant effects in hypercholesterolemic rabbits (Shukla *et al.*, 2004). The extracts of the aerial roots also produced similar blood glucose lowering activity in rats (Singh *et al.*, 2009).

Aqueous extracts of *F. asperifolia* were reported to increase the implantation sites in female rats and produce uterotrophic-like activities in female rats (Watcho *et al.*, 2009). The extracts of the fruits of *F. asperifolia* were reported to produce a concentration-dependent increase in rat uterine contractions, an effect which might be related to the release of prostaglandins and stimulation of other uterine contractility receptors (Watcho *et al.*, 2011).

More than 100 phytochemical compounds have been identified in *Ficus* species (Lansky *et al.*, 2008). *Ficus* species were found to compose largely of phenanthroindolizidine alkaloids; other compounds included the coumarins, flavonoids and triterpenoid compounds. Several triacylglycerols have also been identified (Lansky *et al.*, 2008). Simple terpenoids and other small aliphatics have also been reported (Grison-Pige *et al.*, 2002).

1.3 *Ficus Exasperata*

1.3.1 Description

Ficus exasperata Vahl, belongs to the mulberry family (Moraceae) (Odunbaku *et al.*, 2008).

It is classified as a terrestrial Afro-tropical plant that can grow up to about 20 m in height and is occasionally found in evergreen and secondary forest areas (Abotsi *et al.*, 2010). One of the plant's prominent features is the presence of rough surfaced leaves and as a consequence it is commonly known as 'the sand paper tree' (Ijeh and Ukwani, 2007). The mature leaves are usually dark green in colour (Figure 1.1) while the tender leaves are a lighter green colour (Ijeh and Ukwani, 2007).



Figure 1.1 Photographs of *F. exasperata*

(A) A photograph of *F. exasperata* tree taken in Benin City, Nigeria. (B) A photograph of the leaves of *F. exasperata* taken in Benin City, Nigeria. These photographs were taken on the 19th of December, 2007 at the premises of the University of Benin, Benin City, Edo State, Nigeria.

1.3.2. Some Medicinal Uses of *F. exasperata*

Medicinally, several parts of the plant are reported to be used for a variety of diseases and ailments. In South Western Nigeria where it is called *Eepin*, a decoction of the roots is used in the management of diabetes (Abo *et al.*, 2008). The glutinous sap is used for the management of eye ailments and stomach pains in the Ivory Coast (Kerharo and Bouquet, 1950). In Ghana, the sap is also used to manage haemorrhage (Ijeh and Ukwani, 2007). The extracts of the stem bark of *F. exasperata* have been reported to be useful in the management of leprosy sores (Ijeh and Ukwani, 2007).

The traditional use of *F. exasperata* in Nigeria for peptic ulcer management has been investigated (Akah *et al.*, 1998). Their findings revealed that *F. exasperata* protected rats with aspirin-induced ulcer. A reduction in gastrointestinal transit time was also observed alongside a significant pH increase and volume of gastric secretions (Akah *et al.*, 1998). The leaves of *F. exasperata* have been reported to reduce triacyl-glycerol concentrations and β -hydroxyl butyrate levels in plasma of alloxan-induced diabetic rats (Nimenibo-Uadia, 2003). Other research investigated the blood pressure lowering effect of the plant (Ayinde *et al.*, 2007). Their studies showed that the aqueous leaf extract of *F. exasperata* produced a dose-dependent reduction in the mean arterial blood pressures in rabbits. This hypotensive effect was attributed to the possible interaction with muscarinic receptors in the cardiovascular system or the release of histamine into the circulatory system (Ayinde *et al.*, 2007). The anti-inflammatory, anti-pyretic and antinociceptive effects of the ethanol extracts of *F. exasperata* were investigated and results of the study indicated that the extract showed a dose-dependent anti-inflammatory activity of carrageenan-induced oedema in chicks and a dose-dependent antinociceptive effect in mice (Woode *et al.*,

2009). A weak antipyretic effect on baker's yeast-induced pyrexia in mice was reported (Woode *et al.*, 2009). Bafor and colleagues also investigated the antipyretic effects of *F. exasperata* using three different solvents of extraction. Their results revealed that the extracts of *F. exasperata* produced a time-dependent antipyretic effect within the 3 h period of study (Bafor *et al.*, 2010b).

In Nigeria, the plant is used by traditional medicine healers to counter preterm labour contractions and in certain regions of Nigeria, it is used typically in hastening labour in both humans and animals (personal communication with some traditional healers in Edo State, Nigeria). These seeming dual activities have however been supported by reports from several countries of Africa. In Togo, the aqueous macerated leaves are used in the management of dysmenorrhea (Adjanohoun *et al.*, 1986). The use of the plant as an oxytocic has also been described and there are reports of the plant being used to hasten ejection of the placenta in cows following the birth of a calf (Ijeh and Agbo, 2006). The aqueous extract of the leaves were reported to facilitate rat uterine contraction *in vitro* via histamine H₁-receptor activation and adrenergic receptor activation, calcium channel regulation and the synthesis of prostaglandins *in utero* (Bafor *et al.*, 2010a). Additionally, the aqueous extract of the leaves of *F. exasperata* was reported to inhibit oxytocin-induced uterine contraction in rats *in vitro*, at concentrations lower than those reported to cause uterine contraction (Bafor *et al.*, 2011).

1.3.3 Toxicity Review on *F. exasperata*

The leaves of *F. exasperata* are fed to goats, sheep (Carew *et al.*, 1980), and chimpanzees (Tweheyo and Lye, 2007) as a source of nourishment. This may suggest that the leaves of *F. exasperata* are relatively benign. One study has reported

that high doses of extracts of the leaves could result in impaired renal function (Ijeh and Agbo, 2006). Studies on the acute toxic effects of the leaves of *F. exasperata* on body temperature and haematological parameters such as haemoglobin concentration, haematocrit ratios, red blood cell count, and body weight revealed that a single administration may not lead to changes in any of the observed parameters however, daily administration for up to a period of 14 days might slightly alter body temperature and some haematological parameters (Bafor and Igbinuwen, 2009).

1.3.4 Phytochemistry of *F. exasperata*

Preliminary phytochemical investigations reported the presence of cardiac glycosides, saponins, and tannins in the root bark (Gill, 1992) and alkaloids, tannins, saponins, flavonoids and cyanogenic glycosides in the leaves and the bark (Bafor *et al.*, 2009; Ijeh and Ukwani, 2007).

1.4. The Uterus

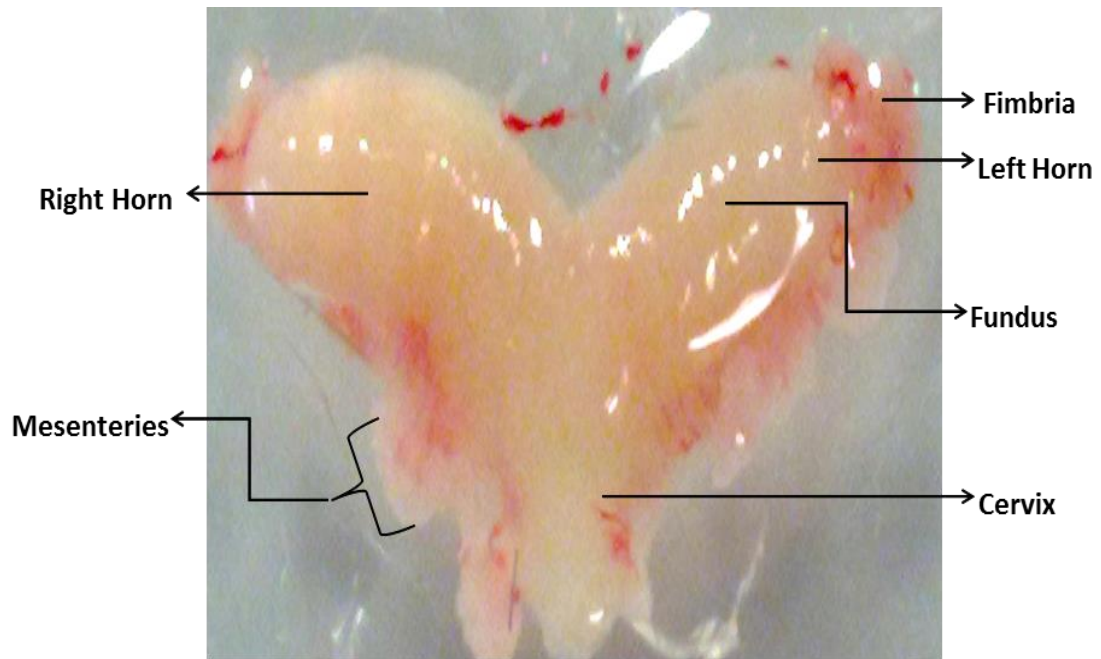


Figure 1.2 The Dissected Mouse Uterus.

Figure 1.2 Photograph of the dissected mouse uterus. The uterine horns were dissected out while in a pro-oestrous state from a virgin mouse and placed in a petri dish containing Krebs' physiological solution.

1.4.1. Anatomy and Physiology of the Human and Rodent Uterus

The uterus of humans and some mammals occurs usually as a thick pear-shaped muscular organ (Gruber and O'Brien, 2011) while that of rodents is shaped like a 'V' expressing two horns (Fig. 1.2) often described as a long duplex structure and these horns are associated with dual cervices (Branham *et al.*, 1985; Spencer *et al.*, 2012; Cooke *et al.*, 2013). The uteri of both non-primates and primates have three distinct parts: the fundus, the body or corpus and the cervix. The uterine wall consists of three layers, the outer layer of connective tissues also known as the

perimetrium or serosa; the middle layer of smooth muscle also known as the myometrium; and the inner epithelial mucous layer also known as the endometrium. The lumen of the uterus is lined by the endometrium. The endometrium is a stratified squamous, non-keratinized epithelium that consists of a *stratum basale* and a *stratum functionale*. During the cycle period, the stratum functionale cyclically grows thicker and this is a direct result of the effect of oestrogen and progesterone stimulation. It is eventually shed at menstruation (Branham *et al.*, 1985; Cunha, 1976; Cunha *et al.*, 1985; Fox, 2002). The uterus varies in size and weight and during pregnancy the capacity of the uterus is greater. The functions of the myometrium and the endometrium include nidation, protection and evacuation (Garfield and Yallampali, 1994). The myometrium is the thickest layer of the uterine wall with a heterogeneous composition. In non-primate species, the myometrium is made up of the outer longitudinal muscle layer and the inner circular layer (Aguilar and Mitchell, 2010). The human myometrium on the other hand is composed of three layers which are the stratum subvasculare next to the endometrium and it has principally a circular arrangement of muscular fibres, there is also a longitudinal arrangement of muscular fibres which is the subserosal stratum supravasculare and in the middle is the stratum vasculare which consists of a three-dimensional network of short muscular bundles and this makes up the bulk of the uterine muscular wall in the adult female (Noe *et al.*, 1999). The outer longitudinal muscle layer consists of a network of smooth muscle cell bundles that are aligned in the long axis of the uterus; these interconnect to form a lattice over and across the uterine surface. Arranged concentrically around the longitudinal axis of the uterus are the circular muscle cells which exhibit a more diffuse arrangement (Garfield and Yallampali, 1994). Smooth muscle cells of the

myometrium are generally believed to be long and spindle shaped but the shape may be irregular. There is considerable variation in size of the muscle between species. The muscle cells of the human uterus are considerably larger than those of the mouse for instance (Garfield and Yallampali, 1994). The fundus has the highest distribution of the myometrium but lesser amounts exist in the lateral walls than in the anterior and posterior walls. At the endometrial-myometrial surface the distribution is greater than that where the myometrium and the serosa meet (Ramsey, 1994). There is a gradual decrease in the amount of smooth muscle along the caudal part of the uterine wall and about 10% of muscle tissue is found in the cervix, the remainder consists of fibrous connective tissue (Ramsey, 1994). During pregnancy, there is a significant increase in the size of the myometrium, this is a result of an increase in the number of muscle cells (hyperplasia) accompanied by an increase in size (hypertrophy) to a lesser degree (Ramsey, 1994). The endometrium is also not idle during these processes of adjustments of the uterus. During the reproductive cycle in the non-pregnant uterus, the activities of the endometrium are regulated by the ovarian hormones which are under the control of the pituitary. The aorta is the main source of the uterine blood which passes through the uterine and the iliac arteries, however there is also a slight contribution from the ovaries (Ramsey, 1994).

Non-primate female mammals (e.g. rats, mice, guinea pigs, cats, dogs) usually undergo reproductive cycles (known as the oestrous cycle), that can be divided into four phases- pro-oestrus, oestrus, metoestrus and dioestrus and in some cases, anoestrus. The reproductive cycle usually lasts for a period of 4-5 days in mice and rats (Wray and Noble, 2008). Pro-oestrous typically lasts 12–14 h, oestrous 25–27 h, metoestrous is the shortest (lasting 6–8 h) and dioestrous phase can last

between 55–57 h (Wray and Noble, 2008). The oestrus phase is usually under regulation by gonadotropic hormones (specifically 17β -oestradiol and progesterone) and ovarian follicles mature about this period (Caligioni, 2009; Bronson *et al.*, 1966). The animal on the other hand, exhibits a sexually receptive behaviour, which may be indicated by observable physiologic changes. A primary trait of oestrus is the lordosis reflex in which the animal spontaneously raises her hindquarters. In some species, the vulva may be reddened (Pfaff *et al.*, 1974; Pfaff and Sakuma, 1979). Ovulation may occur spontaneously in some species (e.g. cow) (Lauderdale, 2009; Wiltbank and Pursley, 2014); while in others it is induced by copulation (e.g. cat) (Conway, 1971; Jochle, 1975 and Bakker and Baum, 2000). Following the absence of copulation in an induced ovulator, oestrus may continue for a couple of days, followed by interoestrus, and a subsequently a return into the oestrus phase. This process continues until ovulation and copulation occurs (Wray and Noble, 2008). The oestrus is the same as the late follicular phase and ovulation in humans (Velardo, 1959). It is therefore expected that similar endocrine conditions would occur. The endometrial proliferative phase is initiated while the ovary is in the follicular phase. Proliferation of the endometrial stratum functionale is stimulated by increasing amounts of oestradiol secreted by the developing follicles. Prior to ovulation, an increase in the rate of oestradiol secretion occurs which stimulates a surge of luteinizing hormone and subsequent rupture of the Graafian follicle (Sarkar *et al.*, 1976; Freeman, 1994; Fox, 2002). Oestrus is sometimes induced in animals during experiments in order to synchronize the hormonal state which minimizes fluctuations of results (Day *et al.*, 2000; Macmillan *et al.*, 1995; Macmillan and Burke, 1996). Another reason for induction of oestrus during experiments would be to create an

environment of increased uterine sensitivity and an imitation of the factors that occur during labour (Roberts *et al.*, 1989), as it has been reported that circulating factors do play a major role in increasing uterine activity at parturition and at oestrus (Sigger *et al.*, 1984). Oestrogens have profound effects on the uterus. At peak oestradiol concentrations, the wet weight of the rat uterus is maximal and this occurs during the pro-oestrous phase. The pro-oestrous uterus appears congested and oedematous with a thickened endometrium. The number and type of cells in the vaginal epithelium has been observed to change throughout the oestrous cycle (Walmer *et al.*, 1992; Parkening *et al.*, 1982; Solberg, 2004). During the oestrus phase, the vaginal cells are observed to consist nearly entirely of keratinized superficial cells that form groups as oestrus progresses and by the end of this stage of the cycle large flakes are formed (Walmer *et al.*, 1992; Parkening *et al.*, 1982; Solberg, 2004). The degree to which neutrophils, nucleated, and keratinized epithelial cells are detected in the vaginal cytology can be employed in the determination of the stage of the oestrous cycle (Wray and Noble, 2008; Caligioni, 2009).

Uterine physiology varies widely in different species as does the response of the uterus to drugs. A major characteristic of the uterus is the cyclical changes it undergoes which modulates the function (Schild, 1983). The uterus contracts both in situ and when excised, contraction could be regular or irregular. These contractions promote cyclic shedding of the endometrial lining and also functions to expel the foetus at birth. The uterine movements originate myogenically and exist even after separation of the uterine nerves (Schild, 1983). The complex hormonal control and the conditions of the menstrual cycle which modulates uterine function produces varied differences in the frequency and force of uterine (Schild, 1983). The electrical

activity within the uterus also plays a role in the contractions of the uterus. The action potential discharge, the action potentials train within each muscle cell, and the total number of cells together active have been considered as major determining factors of the frequency, duration, and magnitude of uterine contractions (Garfield and Yallampali, 1994). The propagation therefore of action potentials originating from pacemaker regions or from areas acted upon by stimulatory agents which maybe either next to or distant to the myometrium, are of vital importance to the events controlling excitability and contractility. It has also been observed that gap junctions appear between myometrial cells during the onset and progression of labour (Garfield and Yallampali, 1994), and these play vital and important roles.

1.4.2. The Non - Pregnant Uterus

The hormonal cycle in the non-pregnant uterus occurs in a specific manner. The proliferative phase is dominated by oestrogen secretion and in the secretory phase, oestrogen and increasing quantities of progesterone are secreted until some days before menstruation at which time the production of the hormones decline (Schild, 1983). Throughout the menstrual cycle contractility of the non-pregnant uterus has been described to exhibit 3 distinct patterns: the late follicular phase (de Ziegler *et al.*, 2001), the luteal phase (i.e. after ovulation) (Cabral *et al.*, 1994), and the luteo-follicular transition (i.e. during menses) (Bulletti *et al.*, 2001; Martinez-Gaudio *et al.*, 1973). The different layers of the myometrium participate in the contractile process of the non-pregnant uterus which is necessary for the expulsion of the uterine content (seen as menstrual blood). At this time of the cycle, uterine contractions are

frequently and commonly observed by women, oftentimes resulting in a condition called dysmenorrhea (de Ziegler *et al.*, 2001).

1.4.2.1 Spontaneous Uterine Contractions

Prostaglandins of the E and F series are reported to be involved in the functioning of the uterus and are released upon uterine distension (Poyser, 1984). Reports have shown that the isolated uteri release prostaglandins into the bathing fluid and exhibit spontaneous contractions. Both the release of prostaglandins and the subsequent uterine contractions were observed to be abolished by indomethacin, suggesting that local prostaglandin production is significant to the maintenance of the intrinsic smooth muscle activity (Vane and Williams, 1973). Myometrial contraction is dependent on ion distribution across the plasma membrane and it is such that sodium and calcium ions are higher outside the cell than inside while potassium ions are higher inside. The resting membrane potential (RMP) (difference between inside and outside) is approximately -45 mV (range -40 to -60 mV) but can vary depending on hormonal state (Garfield and Yallampali, 1994). The gradients produced when the ions are distributed across the membranes promote response of the muscle cells to small changes in permeability (Garfield and Yallampali, 1994). Therefore when there is a change in the membrane permeability, excitation occurs due to movement of ions down their electrochemical gradients. This again suggests that the source of uterine contractions is connected to the electrical and chemical variations that occur within the muscle cells. Phasic contractile activity is a consequence of the underlying electrical activity of the muscle cells (Garfield and Maner, 2007). The succession of contraction and relaxation is a result of the

depolarization (inward current of Ca^{2+} and Na^{+}) and repolarization (outward current of K^{+}) of the muscle cell which occurs in the form of action potentials, and the presence of pacemaker regions in the myometrium are believed to produce the force that drives propagated action potentials. The frequency and intensity of uterine contractions are directly related and in proportion to the degree of regularity and duration of action potentials in each uterine muscle cell and total number of active cells (Garfield and Maner, 2007).

The concentration of free intracellular ionized calcium drives the contraction of smooth muscles in general through activation of the contractile elements. Therefore a reduction in free intracellular calcium (either as a result of efflux or re-uptake) terminates uterine contraction. The free calcium (or activator calcium) is determined by the influx and efflux of calcium and release and reuptake into the sarcoplasmic reticulum (Matthew *et al.*, 2004). Uterine smooth muscle cells have an extensive system of the sarcoplasmic reticulum (SR) consisting of a network of tubules and sacs within the cytoplasm (Cheng *et al.*, 1993). The SR functions primarily for storage of activator calcium and for protein synthesis. Inhibition of the SR Ca^{2+} pumps therefore results in an increase of Ca^{2+} and consequently an increase in force. This is probably due to the link between SR Ca^{2+} releases and Ca^{2+} - activated K^{+} (BK) channels. Local SR Ca^{2+} releases can also result from the opening of the ryanodine receptor (RyR) which causes what is known as sparks (Cheng *et al.*, 1993). It has also been proposed that culmination of these local Ca^{2+} releases may result in the production of an overall Ca^{2+} waves in blood vessels and an increase in tone, but there is more evidence for their association in vasodilatation via activation of BK channels (Miriel *et al.*, 1999; Nelson *et al.*, 1995). The local Ca^{2+} sparks are

thought to cause an increase in Ca^{2+} around BK channels in sufficient amounts to cause activation. A side by side arrangement between the SR and plasma membrane have been reported to facilitate this mechanism (Blaustein *et al.*, 2002). The opening of BK channels is also associated with small hyperpolarizations, which decreases the opening of L-type Ca^{2+} channels, a fall of Ca^{2+} and hence relaxation (Burdyga and Wray, 2005). Therefore, if Ca^{2+} sparks or BK channels were inhibited, an increase in Ca^{2+} transients and force would be predicted to occur, as was observed in the myometrium. Such a mechanism in vascular smooth muscles and a spark–BK mechanism for the control of excitability using effects on the refractory period in ureteric smooth muscle has been described (Burdyga and Wray, 2005). Gestation has been shown to regulate the expression and distribution of BK channels in the uterus (Khan *et al.*, 2001) and it has been suggested that this could be an important mechanism for maintaining uterine quiescence before term. Both inositol triphosphate (IP_3) and RyR receptors have been identified on the SR. It has however been suggested that the Ca^{2+} released from these receptors may offer little contribution to the activation of contraction. This suggestion was drawn from experiments in a variety of species, which showed an increase in both Ca^{2+} transients and contractions upon disabling the SR (Kupittayanant *et al.*, 2002; Noble and Wray, 2002; Taggart and Wray, 1998) with the use of drugs such as cyclopiazonic acid which inhibit the sarcoendoplasmic reticulum Ca^{2+} -ATPase (SERCA) required to transport Ca^{2+} into the SR. The SR may however be involved in calcium buffering (Shmygol *et al.*, 1999). It has also been reported that such data may not support the augmentation of contraction by SR Ca^{2+} release (Shmygol and Wray, 2004). In addition, even under agonist stimulation and IP_3 production, hormones such as

oxytocin are unable to produce force in the uterus if Ca^{2+} entry is inhibited, i.e. due to rapid depletion of SR Ca^{2+} release (Kupittayanant *et al.*, 2002). While the stimulatory actions of oxytocin on the myometrium are often attributed to SR Ca^{2+} release, there is also the stimulation of Ca^{2+} entry and a decrease of Ca^{2+} efflux (Soloff and Sweet, 1982). Both of these actions will increase and/or prolong Ca^{2+} transients. Oxytocin can significantly increase uterine contractions in the human myometrium even when the SR is inhibited, an effect that has been proposed to occur through L-type Ca^{2+} channels. It has also been observed that even with a functional SR, blockade of Ca^{2+} entry inhibits oxytocin-induced uterine contractions (Wray, 2007). SR Ca^{2+} stores may therefore play a modulatory role, a mechanism which may underlie the stimulatory actions of hormones such as oxytocin (Berridge, 2008).

An essential link between SR, RyR and BK channel activation in the uterus is yet to be made (Burdyga *et al.*, 2007). Despite studies on single myocytes and intact uterine strips under conditions in which they are apparent, Ca^{2+} sparks were not recorded in the uterus (Burdyga *et al.*, 2007). Some factors have been proposed as being responsible for the lack of the sparks–BK mechanism in the uterus and these have been based on the following studies: (1) caffeine, an RyR agonist, failed to increase Ca^{2+} in intact tissues instead relaxation was observed (Dabertrand *et al.*, 2006); This is however contradicted by a previous study by Izumi *et al.* (1994) which showed an increase in uterine contractions upon caffeine stimulation of the pregnant myometrium (Izumi *et al.*, 1994); and (2) antagonism of RyR has been proposed to either have little or no effect on Ca^{2+} (the effect being an increase in uterine contractility) (Dabertrand *et al.*, 2006). It has been suggested that splice variations of RyRs in the uterus may render it unable to produce Ca^{2+} sparks (Dabertrand *et al.*,

2006). Alternatively, there may be sparks but they may either be too small or rather short lived to be detected. It is clear, however, that a comprehensive study into the role of the SR in the uterus requires further investigation.

Also worth mentioning is the emerging modulatory roles of the mitochondria in pacemaking and contractile activities (Gravina *et al.*, 2010). There is also the role played by voltage-dependent calcium channels (VDCs). It has so far been seen that spontaneous movement of uterine smooth muscle is considered myogenic in origin and tightly regulated by cycles of depolarization resulting in a rapid influx of calcium through VDCs (Matthew *et al.*, 2004). The VDCs allow influx of calcium which contributes to further depolarization of the plasmalemma and promotes interaction with the contractile elements. Perhaps the most crucial occurrence in the control of uterine contractility is the influx of calcium from the extracellular space, therefore if an agent that increases the open probability of the VDCs acts on the myometrium, increased myogenic contractions occur (Kupittayanant *et al.*, 2002). Smith *et al.*, (2007) reported that voltage-gated potassium channels (K_v) similarly contribute to the regulation of spontaneous uterine contractility in the myometrium (Smith *et al.*, 2007). Aaronson *et al.*, (2006) had also earlier noted that K_v channels make a significant contribution to the control of basal myometrial contractility (Aaronson *et al.*, 2006). Electrophysiological studies have identified at least four types of K^+ currents or channels in the human myometrium. These include the large conductance Ca^{2+} -activated K^+ channels (BK_{Ca}) and three different types of K_v currents. In addition, biochemical and pharmacological evidence for myometrial ATP-activated K^+ (K_{ATP}) channels have also been presented (Aaronson *et al.*, 2006). Aaronson and colleagues also stated that BK_{Ca} channels serve important regulatory myometrial

functions and these channels have been shown to be activated by a variety of agents, which inhibit myometrial contractility; these include β -adrenoceptor agonists, relaxin, human chorionic gonadotrophin and nitric oxide. Previously, it had been demonstrated that the BK_{Ca} channel inhibitors iberiotoxin and tetraethylammonium (TEA) increased the frequency of spontaneous myometrial contractions in myometrial strips from oestrogen-primed rats, and also initiated spontaneous contractions in quiescent myometrial strips from term-pregnant women (Anwer *et al.*, 1993).

Studies have shown that spontaneous and periodic baseline contractions by the myometrium, from both pregnant and non-pregnant mice, indicate the presence of an endogenous pacemaker within the uterine tissue. An increase in cellular communication due to gap junction assembly may contribute to the rise in contraction amplitude (Mackler *et al.*, 1999). Gap junctions have been described as intercellular channels that promote the movement of low molecular weight molecules and ions, thereby enabling cellular communication. It is also suggested that gap junctions provide low resistance channels or pathways which spreads the depolarizing signals and eventually coordinates the myometrial contractions. Myometrial gap junctions therefore improve coordination and increase the force of uterine contraction (e.g. during parturition), whereas inhibition of gap junction intercellular communication in the myometrium is associated with decreased uterine contractility (Loch-Caruso *et al.*, 2003). Some myometrial cell cultures have shown the presence of connexin₄₃, the gap junction protein reported to dominate the pregnant uterus during parturition (Loch-Caruso *et al.*, 1992).

It is noteworthy that despite the overall importance and contribution of Ca^{2+} to myometrial contraction, the Ca^{2+} -calmodulin-myosin light chain kinase (MLCK) pathway is also considered to be vital for uterine contraction, this is because if the enzyme MLCK is inhibited but Ca^{2+} release occurs, there will be no contraction (Wray, 2007). If there must be significant interaction between the contractile elements, myosin and actin in the uterine smooth muscle or any other smooth muscle, the amino acid serine 19 positioned on the regulatory light chains of myosin must be phosphorylated (Wray *et al.*, 2003; Wray *et al.*, 2001). MLCK has so far remained the primary enzyme responsible for this activity (Moore and Lopez Bernal, 2003). Binding of Ca^{2+} to calmodulin, activates MLCK an action which results in the phosphorylation and subsequent cross-bridging. The VDCs and/or release from the SR have been proposed to be responsible for the increase in activator Ca^{2+} entry as earlier mentioned. In phasic smooth muscles, such as the uterus, where action potentials occur, opening of L-type Ca^{2+} channels is considered the major source of Ca^{2+} for contraction (Matthew *et al.*, 2004). There is some evidence however, that T-type Ca^{2+} channels may contribute to Ca^{2+} entry in the human myometrium (Young *et al.*, 1993).

1.4.2.2. Uterine Relaxation

Biochemically, the myometrium relaxes following a reversal occurring in the Ca^{2+} -calmodulin-MLCK pathway (Wray *et al.*, 2003). Thus, as the L-type Ca^{2+} channels closes and the mechanisms regulating the Ca^{2+} efflux mechanisms are activated, dephosphorylation of the myosin light chains occurs alongside a decrease in Ca^{2+} . Subsequently Ca^{2+} dissociates from calmodulin and MLCK is inactivated (Haeberle

et al., 1985). The plasma membrane Ca^{2+} -ATPase (PMCA) and the Na^{+} - Ca^{2+} exchanger (NCX) regulate Ca^{2+} efflux in the uterus (Kosterin *et al.*, 1994). The NCX is considered a high capacity mechanism but it has a low affinity for Ca^{2+} . The ion concentration in the subplasmalemmal space and Ca^{2+} from bulk cytoplasm may vary (Blaustein *et al.*, 2002) this however facilitates activation of the exchanger under conditions of high Ca^{2+} and the simultaneous elimination of Ca^{2+} from the cell. The function and activity of the NCX is determined by the gradient of transplasmalemmal Na^{+} which also depends on the $\text{Na}^{+}/\text{K}^{+}$ -ATPase. Experimentally, when external Na^{+} is lowered or eliminated, a reversal of the exchanger and Ca^{2+} entry occurs which is able to activate SR Ca^{2+} release in cardiac muscle (Ritter *et al.*, 2003). However, since the uterus has been proposed to lack Ca^{2+} sparks, the mechanism described above may not occur in the myometrium. The PMCA maintains resting Ca^{2+} levels and is described as a high-affinity/capacity system which functions to keep the levels of Ca^{2+} low (Matthew *et al.*, 2004). It has been proposed that NCX and PMCA releases 30% and 70% of Ca^{2+} respectively and blockade of these pathways would prevent efflux completely (Shmigol *et al.*, 1998; Shmigol *et al.*, 1999). The SR takes up Ca^{2+} and in this way acts as a Ca^{2+} sink, from where it is released to the two transporters with a corresponding increase in activity, but SERCA alone does not lower Ca^{2+} in uterine myocytes (Shmigol *et al.*, 1999). Mechanisms that regulate uterine relaxation can be targeted by agonists, an example is oxytocin which inhibits the efflux of Ca^{2+} from uterine cells thereby stimulating contraction (Soloff and Sweet, 1982). Uterine relaxants work through several signalling pathways such as the nitric oxide (NO)-cyclic guanosine monophosphate (cGMP) signalling pathway. One target in NO-cGMP pathway is the myosin phosphatase (MLCP). Cyclic GMP

stimulates the activity of MLCP accelerating the separation of phosphate from myosin light chain which eventually results in the inhibition of contraction/force (Sanborn *et al.*, 2005). This process is referred to as Ca^{2+} desensitization (Sanborn *et al.*, 2005). In some instances force production can be promoted by Ca^{2+} -sensitizing agonists, many of which work through the inhibition of MLCP (Stull *et al.*, 1990). Activation of rho-associated kinase (ROK) which occurs when MLCP subunits are phosphorylated by the ras homolog gene (Rho) has been described as one of the principal processes/mechanisms affecting contractility (Kupittayanant *et al.*, 2001). Processes such as this play principally dominant roles in tonic smooth muscles which may be because Ca^{2+} fluxes and shorter contractions are controlled by excitability in phasic muscles. It has also been shown that the effect of phosphorylation of MLCP by ROK produces a rather small force production in the uterus (Kupittayanant *et al.*, 2001). It has also been suggested that CP1-17, an MLCP inhibitor, might produce some effect in the myometrium through a protein kinase pathway (Sakamoto *et al.*, 2003). Ca^{2+} sensitization also plays a role in the effect of oxytocin in the myometrium (McKillen *et al.*, 1999). Generation of phasic activity in the uterus depends on Ca^{2+} entry and myosin light chain phosphorylation for the production of action potentials. Removal of Ca^{2+} by NCX and Ca^{2+} -ATPase abolishes phasic contractions. The contribution of the SR to these pathways is not clear, as is the production of Ca^{2+} sparks, and Ca^{2+} desensitization appears to play a minor role.

1.4.2.3. Lipid Rafts and Uterine Signalling

Lipid rafts are special microdomains located in the plasma membrane. They are associated with some of the Ca^{2+} signalling elements in the uterine smooth muscle as

well as other smooth muscles (Brown and London, 1998b). These lipid rafts are rich in cholesterol and sphingolipids, and are also considered detergent-insoluble regions of the plasma membrane. The high cholesterol reduces movement and fluidity in the bilayer of the plasma membrane as such the term 'rafts' has been coined to describe that they float in the more fluid non-raft regions (Brown and London, 1998b). Certain signalling pathway components are included in these rafts through a dynamic process involving the switching on or off or alteration of the selected pathways (Pawson and Scott, 1997). Communication with annexins which are cytoskeletal proteins have been suggested to play a role in the regulation of these rafts (Babiyshuk *et al.*, 2002; Draeger *et al.*, 2005). Caveolae (which are Ω -shaped invaginations created when the protein caveolin-1 interacts with the rafts in the plasma membrane surface) are significantly present in the plasma membranes of smooth muscles and it has been suggested to play a role in the smooth muscle raft signalling mechanisms (Taggart, 2001). Manipulation of the cholesterol content within the plasma membrane enables modification of rafts or caveolae and can also promote sequestration of cholesterol into hydrophobic pockets (Smith *et al.*, 2005). Methyl cyclodextrin (MCD), can be employed for such sequestration process leading to an interference of rafts and caveolae mechanisms. Such treatments have been shown to significantly decrease the number of caveolae in the uterus and to decrease membrane cholesterol (Smith *et al.*, 2005). MCD has been shown to stimulate spontaneous and agonist-induced Ca^{2+} -contractions by reduction of cholesterol content however, the increase in contractions produced were reversed when MCD-cholesterol was applied (Kendrick *et al.*, 2004; Smith *et al.*, 2005). Similar results were obtained upon reduction of cholesterol by the bacterial enzyme cholesterol

oxidase (Smith *et al.*, 2005). It has been suggested that this occurrence is due to the addition of cholesterol to myometrial preparations which decreases Ca^{2+} transients and contractions (Kendrick *et al.*, 2004). It is also suggested that myometrial rafts, functions to decrease Ca^{2+} signals and promote repolarization of the membrane by K^+ currents thus limiting Ca^{2+} entry, an effect that has been proposed to be optimal when localized by caveolae (Smith *et al.*, 2005). Studies have also shown associations of the K^+ channel subunit with myometrial rafts (Babiychuk *et al.*, 2002; Brainard *et al.*, 2005). Again a possible association of BK channels located in caveolae where the α -subunit is connected with the membrane detergent-resistant fraction in sucrose density gradient experiments has been reported (Smith *et al.*, 2005). It is also suggested that interference or disruption of rafts destroys the connection with the α -subunit which can also lead to a loss in function. Studies in isolated myocytes have suggested also that MCD is aimed at BK channels (Shmygol *et al.*, 2007; Wray and Shmygol, 2007) and the observation that MCD does not result in further reduction of outward current, suggests a reduction in the capacitance of the myocytes by MCD (Wray and Shmygol, 2007). It is also suggested that currents elicited by activation of BK channels are decreased by MCD possibly through internalization of the BK channel subunits, which culminates in excitation of the myometrium and an increase in Ca^{2+} signalling. Since the influence of BK channels on uterine contractility in intact tissue is rather small the authors suggests that other pathways may also play a role (Noble *et al.*, 2006).

Oxytocin signalling is another pathway suggested to be affected by lipid rafts. The high-affinity oxytocin receptor has been reported to be localized in lipid rafts (Klein *et al.*, 1995). The oestrogen receptor has also been suggested to be localized in

rafts but inhibited in the raft environment. Disruption therefore of this raft-inhibitory mechanism has been reported as a key factor in 17β - oestradiol-stimulated mammary tumourigenesis (Zhang *et al.*, 2005). It would therefore appear that oestrogen can promote downregulation of the quantities of caveolae and the protein caveolin-1 in the uterus. Conflicting reports on the expression of caveolae at term exists. A significant increase in caveolae close to term has been reported (Turi *et al.*, 2001), however the opposite effect has also been reported (Ciray *et al.*, 1995). The contributions of cholesterol manipulation or alterations in membrane fluidity should also be considered (Noble *et al.*, 2006),

In summary, the uterus utilizes caveolae and rafts as important loci for signalling pathways. An active regulatory mechanism that includes or excludes signalling components to rafts may also be involved which would influence the effect of rafts and caveolae on contractility especially as studies have shown that outward current from BK channels is particularly affected by the lipid environment and that this can explain why cholesterol reduction is associated with increased contractility. Since an increase in cholesterol impairs contractility it has been suggested that this may a likely cause of uterine dysfunction in many pregnant obese women exposing them to an increased risk of caesarean birth (Wray, 2007).

1.4.2.4. Uterine Contractions in Dysmenorrhoea

Dysmenorrhea has been described as a major alteration to uterine contractility at the time of menstruation (Wang *et al.*, 2004). It is a clinical condition characterized by painful, uterine cramps which occur just before, or during the time of menstruation. It is also considered the most common gynaecological disorder among women of

reproductive age (Wang *et al.*, 2004). There are two types of dysmenorrhoea: primary and secondary. Primary dysmenorrhoea has been described as painful menstruation unassociated with any detectable disease or pathology and commonly occurs in adolescent females and the etiology remains to be clearly elucidated (Marjoribanks *et al.*, 2003). On the other hand, secondary dysmenorrhoea has also been described as painful menstruation but commonly associated with pelvic pathology (Jones, 2004). An increase in the concentration of prostaglandins has been suggested to contribute to the pain (Dawood, 1993). It is also suggested that TNF α production due to ischaemic re-perfusion (Okazaki *et al.*, 2005) might play a role in dysmenorrhoea since the excessive production of prostaglandins leads to vasoconstriction (Sales and Jabbour, 2003). Therefore, successful treatment of dysmenorrhoea with drugs capable of reducing the uterine smooth muscle contractility leading to an increase in uterine blood flow will counteract dysmenorrhea (Dawood, 1988).

1.4.3. The Pregnant Uterus

During pregnancy, the uterus is quiet and oftentimes will not respond to stimulants and should contractions occur, they are usually poorly coordinated. However, at term, the uterus generates strong, frequent contractions which are highly coordinated. The uterus at this stage also responds effectively to contraction stimulatory agents (such as oxytocin and certain prostaglandins) (Challis and Lye, 1994). It has been reported that this change which occurs in the uterus at term consists of an increase in the expression of certain proteins termed "contraction-associated" proteins (CAPs) (Challis and Lye, 1994). It would therefore seem that

the onset of labour requires activation of these CAPs. The oxytocin receptor (OTR) has been described as an example of CAPs (Challis and Lye, 1994). A raised concentration of the oestrogen: progesterone ratio has been proposed as being primarily responsible for the onset of labour. This increased concentration of the reproductive hormones in the maternal circulation is induced in most species upon activation of the foetal hypothalamic-pituitary-adrenal axis (Challis and Lye, 1994). The highly coordinated contractions produced at term results in powerful propulsive movements which is necessary for expelling the foetus. These uterine contractions are known to be stimulated, primarily, by:

1) **Oxytocin** – a polypeptide produced in the hypothalamus and released by the posterior pituitary (and also produced within the uterus); and

2) **Prostaglandins** - a class of cyclic fatty acids with paracrine functions produced within the uterus. The particular prostaglandins involved are $\text{PGF}_{2\alpha}$ and PGE_2 . In certain situations, labour is induced by administration of injections of oxytocin or by prostaglandin insertion as a suppository (Fox, 2002). Several theories exist regarding the initiation of labour.

1.4.3.1. Pre - term Labour

About 3.6 million infants are reported to die in the first 1-4 weeks of life annually (neonatal period) however a huge uncounted mortality rate has been reported to occur at home (Lawn *et al.*, 2010; Heron *et al.*, 2010). The World Health Organization (WHO) defines a pre-term delivery as birth of more than 20 but less than 37 weeks gestational age. Pre-term labour can be defined as regular purposeful contractions associated with changes to the cervix which occurs at less than 37 weeks

gestational age (Goldenberg, 2002) The origin and development of pre-term labour is not well understood, and could be a result of an early activation of the processes that regulate labour itself or secondary to a disease or other pathology. Premature birth is considered one of the significant causes of neonatal morbidity and mortality (Cirrilo *et al.*, 2003). This is because it is reported as one of the major causes of infant mortality and is responsible for over 80% of neonatal deaths around the world and is also responsible for perinatal and maternal morbidity and mortality (Goldenberg *et al.*, 2008; Lawn *et al.*, 2010). Translating to ‘an infant mortality rate of 6.7 deaths per 1000 live births, a stillbirth rate of 6.2 per 1000 deliveries, and preterm births comprising 12.8% of live births’ (Lawn *et al.*, 2010). This represents a significant global burden and has led to the development of the Millennium Development Goals (MDG) 4 and 5 for child and maternal survival respectively which is aimed at decreasing the rate and incidence of neonatal and maternal morbidity and mortality in the world. While there has been some progress in reducing the incidence of neonatal tetanus and neonatal infections, the incidence and mortality rates from pre-term birth and intrapartum-related neonatal deaths remain quite high (Lawn *et al.*, 2010). In 2005, the World Health Organizations estimated a 12.9 million incidence of pre-term birth worldwide (Beck *et al.*, 2010). This estimated figure has increased steadily since then as observed from the literatures despite the implementation of several measures related to public health as well as several medical interventions (Zhou *et al.*, 2010). This has staged pre-term birth as an enormous global health burden however it still lacks widespread acknowledgement and investment/funding proportionate to the burden (Lawn *et al.*, 2010). Some long-term health issues have been associated with pre-term birth. For instance neurodevelopmental, respiratory

and gastrointestinal complications are on the rise (Saigal and Doyle, 2008), resulting in significant medical costs. Infants who survive pre-term labour and birth may develop several health problems during early childhood which could range from respiratory issues such as asthma to motor delay, cerebral palsy, lower IQs and behavioural problems (McCormick *et al.*, 2011). Some reports have suggested a potential development of hypertension in pre-term birth survivors (Coelli *et al.*, 2011). Neonatal deaths contribute a significant proportion of all pre-term birth related deaths in children less than 5 years of age worldwide and a significant number (more than two-thirds) of these neonatal deaths have been reported to be dominant in African and Asian countries (Lawn *et al.*, 2005). There appears to be a disproportionate distribution in the rates and incidence of pre-term births in low and middle-income countries where about 99% of the neonatal deaths occur in these regions (Lawn *et al.*, 2005; Rajaratnam *et al.*, 2010). It has been reported that of the 10 countries worldwide where pre-term mortality dominates, Nigeria is 1 of 5 of these countries that together account for over 2 million new-born mortalities (representative of more than one-half the total) whereas 10 countries alone account for two-thirds of all deaths, this has been considered a significant disparity in the incidence. In figures, Nigeria accounts for 298,000 neonatal deaths annually, a maternal mortality ratio of 836 per 100,000 live births and an estimated total of 50,000 maternal deaths annually (Lawn *et al.*, 2010).

More than half of pre-term deliveries appear to be spontaneous and have been associated with several risk factors (Goldenberg *et al.*, 2008). About 30 % of pre-term labour cases are associated with infection or chorioamnionitis (Gibbs *et al.*, 1992). This is supported by reports of increased levels of prostaglandins and

inflammatory cytokines in both humans and mice, (e.g., interleukin-1 (IL-1), IL-6, and tumour necrosis factor α) (Mussalli *et al.*, 1999). The observed increase of all prostaglandins in the amniotic fluids also supports a role for prostaglandins in the initiation of both pre-term and term labour (Casey *et al.*, 1988). Uterine malformations (such as a bicornuate or unicorn uterus), uterine fibroids (particularly submucosal and subplacental fibroids) and cervical incompetence are also reported to contribute to pre-term labour (Goldenberg *et al.*, 2008). It would therefore seem that the search for new agents for the prevention of pre-term birth and pre-term labour is a global health challenge not just for Nigeria alone but for the world at large. It is of utmost importance therefore to develop more effective tocolytic treatments which would have significant benefits for mothers and babies at risk of early birth.

Preventing pre-term labour is considered one of the primary processes for the reduction of pre-term birth (Lawn *et al.*, 2010) and contractility of the uterus is the most frequent and common symptom of pre-term labour, therefore it has been suggested that the development and use of effective tocolytic agents with the aim of prolonging pregnancy through inhibition of uterine contractility should be utilized for the treatment of preterm labour (Conde-Agudelo *et al.*, 2011). The frequency of contractions of the uterus are mostly employed in the detection and assessment of labour, however measurement of the frequency alone provides no information about synchrony or force of the contraction (Garfield and Yallampali, 1994). It may therefore be necessary to include other measurements that give a complete picture of the uterine contractile process. Tocolytic agents can be employed for acute or maintenance tocolysis (Conde-Agudelo *et al.*, 2011). Interventions such as progesterone therapy appears to contribute about less than 3-4% reduction of global

pre-term birth rates, an estimate that highlights the need for continued research into efficacious interventions to prevent pre-term birth (Simmons *et al.*, 2010). Therefore, development of new safe and effective tocolytic agents is considered a global need and a vital research area (Shih *et al.*, 2009).

Several uterine contraction inhibitors are currently in use but each one is encumbered with various limitations. The β_2 -adrenergic-receptor agonists for instance are reported to reduce the incidence of pre-term delivery within 48 hours of treatment (Anotayanonth *et al.*, 2004). The observed reduction however, in incidence does not suggest improvement in neonatal outcomes and maternal side effects still remain a problem (Anotayanonth *et al.*, 2004); magnesium sulphate though employed as a tocolytic agent, its effectiveness as a tocolytic agent remains to be verified, and its use has been associated with an increase in neonatal mortality rates (Crowther *et al.*, 2003); inhibitors of prostaglandin synthesis are also used to treat or prevent pre-term birth but their effectiveness still requires further investigation and their use is associated with significant risk to mother and foetus (King *et al.*, 2005); While oxytocin antagonists have also been employed in pre-term birth and improvement in maternal expectancy have been observed, risks associated with neonates remains a possibility (Romero *et al.*, 2002). The use of nitric oxide donors and calcium channel blockers as tocolytic agents have also been suggested but more studies are required to investigate their efficacy in relation to other tocolytic agents in clinical use (Smith *et al.*, 2010).

1.4.4. Biochemistry of the Uterus

1.4.4.1. pH Changes in the Myometrium

Dawson and Wray first measured *in vitro* uterine intracellular pH (pHi) in rats with the use of ^{31}P NMR spectroscopy and the pHi showed a value of about 7.1 (Dawson and Wray, 1985). Further studies showed a decrease in the external pH (pHo) on pHi in the uterus; a 1 pH unit change in pHo would result in a 0.3 pH unit change in pHi (Wray, 1988). These experiments were confirmed with the use of pH-sensitive fluorescent indicators, e.g. carboxy-SNARF, for the measurement of uterine pHi (Taggart and Wray, 1993). Measurements performed on the human myometrium showed similarities to the measurements obtained in rats, where a pHi of 7.1–7.2 was observed (Parratt *et al.*, 1994). The first NMR spectroscopy measurements of *in vivo* myometrial pHi were performed on rats' myometrium where a value of 7.25 was obtained (Larcombe-McDouall *et al.*, 1998). Again, fluorescent indicators were used in these studies and pHi values showed an improved temporal resolution and also showed that each phasic contraction was associated with small pH transients (0.04 pH unit) (Taggart and Wray, 1993). Not much is known however of the function and consequences of these pH changes.

1.4.4.2. pH and dysfunctional labour

In dysfunctional labour, myometrial contractions that result are often irregular and too weak to elicit dilatation of the cervix and expulsion of the foetus. The underlying mechanism of dysfunctional labour is generally unknown and intriguingly the original labour may be normal (Wray, 2007). It is reported as the most common

reason for emergency caesarean sections and is therefore considered a significant global health and economic issue (Thomas *et al.*, 2000). Oxytocin is currently the major treatment for dysfunctional labour and it remains difficult to predict which group of women will respond to oxytocin treatment and which group will not undergo caesarean section (Blanch *et al.*, 1998). Hypoxia frequently occurs in the human myometrium. In vitro and in vivo studies show a fall in pHi during periods of hypoxia which may result in a decrease in intracellular Ca^{2+} and an eventual decrease in contractions (Earley and Wray, 1993; Larcombe-McDouall *et al.*, 1999; Pierce *et al.*, 2003) and may play a role in the occurrence of dysfunctional labour. It was recently proposed that acidification in the myometrium may be a primary cause of dysfunctional labour (Quenby *et al.*, 2004). Acidosis was observed in blood samples from women having dysfunctional labour and there was high level of lactate but decreased partial oxygen pressure and increased lactate in the blood samples. This led to the conclusion that a more acidic myometrium occurs in women with dysfunctional labour (Wray, 2007). The increased lactate and decreased oxygen suggests a role for myometrial hypoxia in the acidification that occurs in dysfunctional labours (Wray, 2007). Isoforms of lactate dehydrogenase (1–5) have been observed to change as term approaches and this has been proposed to be a result of readiness of the uterus for the hypoxic conditions which occurs during labour (Wynn, 1977).

1.5. Pharmacological Effect of Drugs on the Uterus

1.5.1. Oxytocics

These are drugs that stimulate contraction of the myometrium. They are used clinically to induce or augment labour at term, to prevent or treat postpartum haemorrhage and to manage haemorrhage from abortion. However, they may also be used alone or in combination with other drugs for therapeutic abortions (abortifacients). Oxytocics include the neurohypophyseal hormone, oxytocin, certain prostaglandins and the ergot alkaloids (Rang *et al.*, 2007). Following delivery of the baby, oxytocics are needed to maintain the muscle tone of the myometrium and also to reduce haemorrhaging from the uterine arteries (Fox, 2002).

1.5.2. Tocolytics

These agents promote uterine quiescence. Clinically, they are used to prevent premature delivery and control pregnancy (Wilson *et al.*, 1990). Examples include the β -adrenoceptor agonists e.g. ritodrine, calcium channel blockers e.g. nifedipine, oxytocin receptor antagonists e.g. atosiban, magnesium sulphate and prostaglandin synthesis inhibitors e.g. indomethacin.

1.6. Secondary Plant Metabolites

Natural product-based secondary metabolites are defined as small molecules with formed by living systems and usually have molecular weights of about 1500 amu or less. These micromolecules or secondary metabolites constitute a very broad group with diverse chemical structure, a factor which also governs the choice of extraction methods (Cannell, 1998). Common structural classes of natural products include:

polyketides, non-ribosomal peptides, terpenes, and alkaloids. Classification of natural products is occasionally performed based on shared basic skeleton, which is a reflection of the manner in which the structures are assembled and the pathways of biosynthesis (Cannell, 1998; Clardy and Walsh, 2004). Natural products have been used to interpret various processes of biosynthesis and have also served as templates for drug discovery and development (Clardy and Walsh, 2004). It has been reported that between the years 1981 and 2002, 1,031 new compounds were approved for use as drugs by the US Food and Drug Administration (FDA). Of this newly approved drugs, natural products constituted 5%, while 23% constituted natural-product-derived molecules (Newman *et al.*, 2003b). This therefore implies that natural products still serve as significant sources for the development of novel drugs. Certain limitations, however exist in the development of drugs from natural products for example, the scope required for chemical modification in order to optimize their activity might be limited due to the complex nature of these products. Also it can be tedious and difficult to constantly obtain active compounds from natural products (Newman *et al.*, 2003b).

1.7 Summary

The isolation of secondary metabolites from natural products and the discoveries and elucidation of new structures and functions is ongoing though there appears to be less investment in the area of natural-products research in recent years, this has probably arisen due to the difficulty associated with isolation of active compounds from natural products and possibly the minimal results achieved despite immense input in this area. It is however hoped that recent advances in technology as is seen in the

high throughput methods used today for the isolation and identification of active agents may overcome this hurdle (Clardy and Walsh, 2004). Some of these high throughput technologies have been applied in this study in the isolation of uterine-active compounds from *F. exasperata*. The plant *F. exasperata* has shown potential of having significant phytochemical and medicinal values. *F. exasperata* has also been shown to have significant effect on the isolated uterus amongst several other tissues. The possible compound(s)/secondary metabolites responsible for these activities are however yet to be investigated and identified.

1.8 Hypothesis of Research

The leaves of *F. exasperata* contain different novel biologically active phytochemical constituents. Some of these constituents inhibit the uterine smooth muscle contractility while others stimulate uterine contractility.

1.9 Aim of Present Research

The current research involved the investigation of the phytochemical analysis of the plant with a concurrent stepwise bioassay-guided fractionation, isolation, purification and characterization. In vitro pharmacological/biological analysis and metabolomic profiling of the effects of the plant at various stages on uterine action will also be performed.

1.10 Specific Objectives/Experimental Plan

- Phytochemical studies to detect the presence of selected secondary metabolites of leaf extracts of *F. exasperata*;

- Isolation and identification of uterine active compounds from the leaves of *F. exasperata* utilizing spectroscopy techniques such as Nuclear Magnetic Resonance, and Mass Spectroscopy (MS);
- Pharmacological and metabolomic analysis of the activities of *F. exasperata* on uterine contraction using a combination of pharmacological techniques and high throughput metabolomic assays and multivariate analysis.

CHAPTER TWO

**PHYTOCHEMICAL AND PHARMACOLOGICAL CHARACTERIZATION
OF THE LEAVES OF *FICUS EXASPERATA***

2.1 Introduction

This chapter deals with the identification and isolation of the myometrial stimulant and relaxant compounds *F. exasperata* via a stepwise integration of bioassay-guided approach using recent metabolite detection methods. In this study, *F. exasperata* was selected based on its use in traditional medicine in facilitating birth ([Ijeh and Agbo, 2006](#)) and also in preterm labour (personal communication with Mr. Sunday Nweke, herbal plants specialist, Edo State Nigeria). The specific aim was to identify potential efficacious tocolytic agents which may be used in their original isolated structure or with slight modifications of the chemical structure.

Most of the earliest pharmaceuticals were plant-based materials and consumption of plant products is widely associated with numerous health benefits (Houghton and Raman, 1998; Cragg and Newman, 2013). Over the past century natural products have been used as starting materials for a wide range of chemical products and this has led to significant advances in pharmaceutical discovery (Mishra and Tiwari, 2011). Increased knowledge on the specific composition and activity of secondary metabolites has promoted structural modifications and this has been made possible through advances in synthetic chemistry (Gullo *et al.*, 2006).

Several secondary metabolites in living organisms, plants inclusive, are tightly held together intracellularly in complex mixtures. Separation of these tightly held metabolites requires prior detachment from the intracellular mixture and may involve several separation processes before assay and/or structure determination can be performed (Cragg and Newman, 2013; Houghton and Raman, 1998). This initial step where a part is detached or separated from a complete unit is termed extraction and several methods exist for this purpose (Houghton and Raman, 1998). It is

important that the reason for the extraction is considered at the initial stage as it may determine the extraction method of choice as well as solvents to be used. According to the traditional healers in Nigeria, the leaves of the plant are either boiled then consumed as tea or they are simply washed using tap water at room temperature and then consumed.

2.2 Extraction Methods

Plant materials are occasionally powdered and dried in order to remove moisture prior to extraction. Several extraction methods exist some of which include solvent extraction, steam distillation, the advanced phytonic process, enfleurage, expression, sublimation, pervaporation, and microwave treatment. For the purpose of this study only the solvent extraction method will be briefly discussed.

2.3 Solvent Extraction

The extraction solvent is poured over the plant material to be extracted and left in contact for a specified time period. At the expiration of the specified time period, the solution is filtered and the residue is separated. The following are the processes involved as earlier described by Houghton and Raman, (1998) and Cannell, (1998):

- a) **The Percolation Method:** In this method, the material is packed into a column which has a fitted tap at the bottom. Some of the columns may also contain an intermediary filter which helps to prevent loss of material. When the material is suitably packed in the column, the selected extraction solvent is poured down the top of the column and the tap is opened. The solvent is

allowed to flow down through the material in the column and the effluent is collected.

- b) **The Infusion Method:** In this method, the plant material is soaked in selected solvents at room temperature for a defined period of time and may be followed by intermittent shaking. At the expiration of the time period the solution is separated from the residue by filtration or decanting. Controlled heat may be applied in this method and heating mantles or water baths can be used in cases where flammable solvents are used.
- c) **Hot Continuous Extraction:** A Soxhlet extractor may be employed in order to achieve exhaustive extraction. Here, the material is placed in a central compartment called a thimble. The thimble is usually made of cellulose or cloth. To the side of the thimble is attached a siphoning device and an arm connected to the lower part of the compartment. A reflux condenser is usually attached above the thimble. At the bottom of the thimble, the solvent is contained in a round bottomed flask which is heated to boiling. The vapour from the heated solvent flows through the side arm to the reflux condenser. In the reflux condenser the vapour turns to liquid and flows into the thimble where the plant material is contained. The hot liquid solvent then perfuses through the material and the extract solution collects in the thimble. As the level of the extract solution rises to the top of the siphon, the entire liquid flows through the siphon and then back into the lower solvent container, and the process is repeated severally till the collected extract in the round bottom flask becomes concentrated. The soxhlet process is useful for: exhaustive

extraction of a plant material with a particular solvent where a high percentage yield is expected.

2.3.1 Extraction Solvents and Specific Phytochemical Groups

The main groups of phytochemical compounds usually considered during extraction are fixed oils, fats, volatile oils, carotenoids, alkaloids, glycosides, aglycones, phenolic compounds, polysaccharides as well as proteins. Table 2.0 gives a general outline of the classes of compounds and solvents appropriate for selective extraction.

Table 2.0 Solvents and Respective Extracted Phytochemical Groups

Polarity	Solvent	Polarity Index*	Phytochemical Group
High	Aqueous alkali	**	Sugars, Amino acids Acids
	Aqueous acid	**	Sugars, Amino acids Bases
	Water	9.0	Sugars, Amino acids Glycosides
Medium	Dichloromethane	3.1	Alkaloids, Aglycones Volatile oils
	Diethylether	2.8	Alkaloids Aglycones
	Ethylacetate	4.4	Alkaloids, Aglycones Glycosides
	Acetone	5.1	Alkaloids, Aglycones Glycosides
	Ethanol	5.2	Glycosides
	Methanol	5.1	Sugars, Amino acids Glycosides
	Low	Light petroleum	0.1
Hexane		0.1	Waxes, Fats Fixed oils
Cyclohexane		0.2	Waxes, Fats Fixed oils
Toluene		2.4	Alkaloids, Fats Fixed oils Volatile oils
Chloroform		4.1	Alkaloids, Aglycones Volatile oils

Modified from Houghton and Raman, (1998). * = measure of the relative polarity of a solvent which is useful for the identification of suitable mobile phase solvents. It increases as polarity increases; **= variable and is dependent on the strength.

2.4 Analytical Techniques

2.4.1 Qualitative/Analytical Thin Layer Chromatography

Thin layer chromatography (TLC) is a form of planar chromatography that involves the separation of mixtures on thin layer adsorbents usually coated on glass, plastics or aluminum sheets (Gibbons and Gray, 1998). Use of TLC requires spotting the extract onto a sorbent material that has been applied to a backing plate and marking out the solvent front (distance run from origin) (Stahl, 1988), the most commonly available analytical TLC plates are the silica gel plates, which may be plastic or aluminum backed Kieselgel 60 F₂₅₄ with about 0.2 mm thickness of silica sorbent (Gibbons and Gray, 1998). Analytical TLC has found application in compound detection and monitoring. If the compound is known, qualitative as well as quantitative information can be obtained from the TLC. It has also found application in chemical classification of organisms based on their chemical constituents. Tracking of natural products can also be achieved via analytical TLC. It is important that qualitative TLC screening of extracts is routinely performed as certain compounds can be detected at an early stage. Some organic compounds are coloured and can be easily visualized on the TLC plates, however others are colourless. In most cases, the observation of separated spots by ultraviolet (UV) light works well (Stahl, 1975). TLC plates normally contain a fluorescent indicator which makes the TLC plate emit green light under UV wavelength of 254 nm (Stahl, 1975). Compounds that absorb UV light will quench the green fluorescence yielding dark purple or bluish spots on the plate. Under long UV light (366 nm), some indicators will give a purple light and are normally used for compounds that fluoresce. Some compounds such as the furocoumarins give out blue or yellow fluorescence under

long UV while compounds like the chlorophylls give out red, blue, orange or yellow colours. Unfortunately compounds that do not absorb UV light will remain invisible (Jork *et al.*, 1990). Another useful visualizing technique is an iodine chamber (Houghton and Raman, 1998). In some cases, the class of compounds can be identified by the use of spray reagents which gives particular colour reactions representative of a particular chemical class (Houghton and Raman, 1998). Spray detection employs the use of colour reactions between the compound and the spray reagent (Houghton and Raman, 1998). The most commonly used reagents include anisaldehyde/sulfuric acid used for the detection of many compounds especially terpenes, sugars, phenols, and steroids; vanillin/sulfuric acid, phosphomolybdic acid, ammonium molybdate (IV), antimony (III) chloride and tin (IV) chloride which colours terpenes red and blue (Jork *et al.*, 1990); dragendorff's reagent which does not necessarily require heat is used for alkaloid detection where an orange-red colouration is produced, however some non-alkaloids such as some iridoids or flavonoids may also give a positive reaction; 2,4 dinitro-phenyl hydrazine gives a yellow-to-red coloration with aldehydes and ketones; perchloric acid, though a universal spray is especially useful for steroids and triterpenes; bortrager reagent is employed for the detection of coumarins and anthraquinones (Jork *et al.*, 1990); Naturstoff /polyethylene glycol reagent is used for the detection of flavonoids and the plates are observed under UV (365 nm) and the following compounds with respective colours can be observed; flavonones give an orange color, naringenin gives a green color, DHQ gives a yellowish color, and flavones give a blue color (Conde *et al.*, 1992).

2.4.2 Nuclear Magnetic Resonance Spectroscopy

NMR spectroscopy is a technique that involves the application of a magnetic field in the measurement of atomic nuclei resonance (Madsen *et al.*, 2010). It measures characteristic resonance frequencies of nuclei that are magnetically active and this provides information that is directly related to the molecular structure (Cavanagh *et al.*, 2007; Claridge, 1999) and dynamics of the compound(s) (Aubin *et al.*, 2014). It is a highly reproducible, non-destructive technique useful in determining the fingerprints of compounds that contain the following atoms: ^1H , ^{13}C , ^{15}N , ^{19}F , ^{23}Na and ^{31}P . The nuclei of these atoms are of biological interest as they have stable isotopes with spin $\frac{1}{2}$, natural abundance written in parenthesis: ^1H (99%); ^{13}C (1.1%); ^{15}N (0.37%), ^{19}F (100%); ^{23}Na (100%), and ^{31}P (100%) respectively. It is however not very sensitive especially when compared with the mass spectrometric technique as the magnetization detected comes from approximately 80 nuclei per million of the sample under detection at room temperature (Madsen *et al.*, 2010; Aubin *et al.*, 2014). In NMR spectroscopy, the active nuclei of samples behave similarly to small magnets which are detected by a coil of conductive wire (Cavanagh *et al.*, 2007; Claridge, 1999; Evans, 1995). Hardware routinely required for measurement of NMR frequencies include: a strong magnet for the generation of bulk magnetization, an appropriate electronic apparatus which tilts and measures the frequency of the processing magnetization, and a computer system which assists in the control of the radiofrequency console and in the storage of data (Cavanagh *et al.*, 2007; Claridge, 1999; Evans, 1995). NMR is routinely employed in drug discovery and natural product research and can be used to identify metabolites in extracts. It

can also be employed in small molecule drug therapeutic analysis as well as in protein biopharmaceuticals (Aubin *et al.*, 2014).

2.4.3 Mass Spectrometry

Mass spectrometry (MS) is a technique used in the detection of metabolites in a mixture. Unlike chromatographic techniques which separates compounds based on their physical and chemical characteristics, MS measures and identifies gas phase ions based on their mass-to-charge ratio (m/z) (Yuan *et al.*, 2014) It is a highly sensitive analytical technique and can be used together with NMR spectroscopy providing a more complete picture of the compound(s) under analysis (Viant, 2007). Unlike NMR however, it is a destructive technique and depending on the metabolites being analyzed, ionization may not always be achieved. It is frequently employed in conjunction with other separation techniques such as gas chromatography (GC) or liquid chromatography (LC) (Tolstikov *et al.*, 2007). This enables separation of the metabolites in the mixture being analyzed while individual spectra of their masses are simultaneously obtained. Coupling of MS to chromatographic techniques have been frequently employed to confirm drugs in forensic toxicology, routine drug testing in workplaces, clinical toxicology, control of doping as well as in pain management (Maurer, 1999). MS-based methods often used include, liquid chromatography-tandem MS (LC-MS/MS) and gas chromatography-MS (GC-MS). While the most prevailing MS analyzer in use is the quadrupole mass spectrometer (QMS) that allows the selection of ions with specific m/z and can be operated in the scan mode (allows scanning across a user-defined m/z range) or in the selected ion monitoring (SIM) mode (which only monitors specific ions) (Versace *et al.*, 2012;

Yuan *et al.*, 2014). The carrier for target analytes in GC is usually an inert gas such as helium, which transports the analytes through a capillary column immersed in a liquid stationary phase, which usually has a temperature gradient (Fraser *et al.*, 2001). This enables compounds with different physico-chemical properties to elute at different rates, and exit the GC at different times. As the effluent enters the MS ion source, the eluted analytes are then ionized either by electron ionization (EI) or by chemical ionization (CI) (Yuan *et al.*, 2014). Ionization and fragmentation occur at the same time in EI with an ionization energy of 70 eV, while in CI, ionization of the molecules is achieved with less fragmentation (Versace *et al.*, 2012). The resulting ionized molecules are then measured based on their m/z by an MS analyzer which could either be a QMS or an ion trap (Versace *et al.*, 2012). Measured parameters include the chromatographic retention times, m/z , and signal intensity, all of which are measured and recorded for identification and quantification (Yuan *et al.*, 2014). The LC functions similarly to the GC, with the exception that LC utilizes a liquid mobile phase and a solid stationary phase. In LC-MS/MS, separated compounds are then ionized by atmospheric pressure ionization (API) techniques (e.g. electrospray ionization [ESI] and atmospheric pressure chemical ionization [APCI]) (Hoja *et al.*, 1997). Subsequent MS/MS analysis proceeds with the use of triple quadrupole MS instruments which is usually operated in the multiple reaction monitoring (MRM) mode (Seger, 2012). MRM allows compounds of interest to be selected in the first QMS, fragmented in a collision cell, resulting in fragmented ions which are monitored in the second QMS (Seger, 2012). Compared to the GC-MS, the LC-MS/MS requires simpler sample preparation (Marquet, 2002) and can be used to measure hydrophilic, heat-unstable, and nonvolatile compounds without prior

derivatization (Peters, 2011). The MS spectrum produced from a scan can then be searched using pre-established spectral libraries and identification is achieved by spectrum matching (Peters, 2011).

2.5 Functional Uterine Pharmacological Assay

Research on uterine contractility is a rather broad subject and quite complex. Studies on myometrial contraction provide basic knowledge which may be applied to clinical situations such as the prevention of premature labour (Rizzo *et al.*, 1994). Pharmacological and physiological evaluations of the uterus range from *in vitro* to *in vivo* assays which may include isolated tissue segments or strips, cell cultures to intrauterine measurements and whole animal assessments. Prior to the development of any uterine assessment model, a proper and thorough understanding of the uterine anatomy and physiology is required and most importantly the factors which govern contraction. Critical to the evaluation of potential therapeutics for myometrial function is the reproducibility of these pharmacological assessments and consideration of the limitations in the *in vitro* technique should also be considered in the experimental protocol.

A brief discussion on *in vitro* assay involving the isometric-force measurement of smooth muscles will be provided. In order to obtain accurate measurements of force produced by smooth muscles *in vitro* it is important that factors such as surgical dissection, the use of an accurate force recording equipment, and adequate muscle perfusion procedure should be properly performed (Lynch *et al.*, 2001).

Measurement of uterine activity has posed a challenge to researchers. Some of the problems creating these challenges include: (1) occurrence of differences among species; (2) complexity of the uterus due to the presence of different functional cell types; (3) differences in uterine behavior and responses due to hormonal status and pregnancy; and (4) development of spontaneous contractile activity that can make study and analysis of drug-induced effect difficult (Crankshaw, 2001). Pharmacological measurement of myometrial activity can either be descriptive or quantitative (Crankshaw, 2001). In the descriptive experiment, the responsiveness of the uterus to an agent is analysed while in the quantitative experiment numerical descriptors such as potency, medial and maximum responses are analysed (Crankshaw, 2001). It is also important that equilibrium conditions are attained and maintained for the entire duration of the experiment. For this to be achieved it is necessary to (1) choose and maintain a specie for the experiment; (2) select a desired hormonal state; (3) choose and maintain the use of specific parts of the uterus or the whole uterus; (4) decide what muscle layer to investigate (Crankshaw, 2001). Muscle strips, rings or segments can be attached by wire, silk suture, thread or other attachment to a force transducer, and is usually pre-stretched. In the present study, uterine muscle segments were used and attached to the force transducer by threads. Whatever the attachment used it is necessary that it is in line with the transducer and not come in contact with the bath wall. Force generated by the muscle is transmitted as an electrical signal and recorded. Transmission of the force is made possible by the transducer. As much as possible, the tissue should be positioned in a manner that the aerating bubble stream does not generate artifacts during recording (Barton *et al.*, 2005). Isometric or isotonic measurements can be

made with appropriate transducers. Measurements of isometric force in units such as grams, Newtons and in some cases centimeters are more commonly used in pharmacological experiments. Occasionally the output range of the transducer can be adjusted to improve the signal to noise ratio. The frequency response of the transducer can also be adjusted to reduce the contribution of external vibrations and artifacts but care must be taken so that these adjustments do not reduce the ability to detect rapid changes in force. Generally, isometric measurement of the uterine tissue is most commonly performed (Crankshaw, 2001).

Upon tissue mounting, a period of tissue acclimatization or stabilization generally referred to as the equilibration period is required in order for the tissue to adjust to the post dissection injury, handling, washing out of metabolites, anaesthetics and other products used or produced during tissue preparation and mounting. This period can vary from 15 min to several hours (Crankshaw and Morrison, 2011). Factors such as tissue sample, tissue excision, experimental procedures and storage govern the duration of the acclimatization period. During the acclimatization period, the tissue may be gradually stretched or undergo pretreatment with selected agonists or antagonists (to limit or increase physiologic and pharmacological responses) (Crankshaw and Morrison, 2011).

The use of series of controls which may be positive or negative is also an important consideration in isometric force measurements. These controls can give an idea of the performance of the tissue set up and may be mechanical, pharmacological or physiological. For example, oxytocin (a standard uterotonic agent) has been used to contract isolated myometrial preparations to determine the function (Bafor *et al.*, 2010a; Kaingu *et al.*, 2012; Lourenço *et al.*, 2012). The effect of oxytocin on

parameters such as the stability of the baseline activity, the response of the tissue preparation to agonists, the response in the presence and absence of antagonists, the range of the effective dose response, onset of the response, the effect of stretching, oxygen consumption and carbon dioxide production can be utilized to examine the performance of the smooth muscle preparation and how it compares to another preparation. These controls may be performed at the start, middle and conclusion of the experiment. Quality control and trouble shooting of the set up can also be monitored with the use of standard controls as reviewed by Crankshaw, (2001).

2.6 Materials and Method

2.6.1 Plant Material

The matured leaves of *Ficus exasperata* were collected between July and August, 2010 in the City of Benin, Edo State of Nigeria. The leaves were previously authenticated by Mr Felix Usang of the Forest Research Institute of Nigeria, Ibadan, where a voucher specimen has been stored (Bafor and Igbinuwen, 2009).

2.6.2 Phytochemical and Pharmacological Analysis of the Crude Leaf Extracts of *F. exasperata*

2.6.2.1 Plant Material

The leaves were shade-dried and pulverised into loose powder with the use of a grinding machine. Traditionally, the leaves are collected and prepared either by boiling or by simply washing in room temperature water and drunk. Based on this the

plant material were extracted using heat and also extracted at room temperature. Five hundred grams (500 g) each of the powdered leaves was subjected to exhaustive hot extraction (using a Soxhlet apparatus) and also subjected to maceration at room temperature. Both extraction processes involved the use of different solvents. These procedures were performed according to methods described by Cannell, (1998) and Houghton and Raman, (1998).

2.6.2.2 Extraction using the Soxhlet Apparatus

The dried powdered leaves were subjected to exhaustive extraction with 7.5 L of hexane using the soxhlet extractor. The heating mantle was set at 40°C and extraction was started with hexane and performed for 3 days. The same procedure was repeated using ethylacetate (EtoAc) and methanol (MeOH) solvents for extraction in successive sessions. Each solvent-extract was concentrated using a rotavapor (R-3 Büchi Labortechnik AG/Sigma Aldrich U.K.) set at 40°C to give the hexane extract (**H1**) with a yield of 3.85% (19.23 g), the ethylacetate extract (**E1**) with a yield of 2.89% (14.49 g) and the methanol extract (**M1**) with a yield of 5.55% (27.75 g) (Fig. 2.0).

2.6.2.3 Extraction via Maceration

a) Acetone-Methanol Extraction

For the cold extraction, the powdered leaves were first macerated in 500 ml acetone for 24 h 3x and continuously stirred using a magnetic stirrer. Acetone was used to break up the cells and since it absorbs water, it is expected to simultaneously extract some polar substances. The combined acetone extracts were macerated in 600 ml of

MeOH (sufficient to cover the extract) for another 24 h 3x. The acetone extract was combined with that of the MeOH extract for the next phase of extraction.

b) Solvent-Solvent Phase Extraction

The dried total Acetone-MeOH extract, was reconstituted and suspended in 100 ml of water which was transferred to a 250 ml separatory funnel. EtoAc (3 to 4 x 100 ml) was added to the funnel and shaken gently. It was then left to stand for about 10 min to form two solvent phases. Exhaustive partitioning with EtoAc was performed until the organic phase was relatively clear. The combined organic extract was dried under vacuo resulting in a yield of (3.15%) 15.74 g of the cold EtoAc extract (**E2**). The aqueous fraction obtained from the partitioning process was subjected to further exhaustive partitioning using saturated butanol to give a yield of 0.04% (0.2 g) of the butanol extract (**B2**) and a yield of 0.09% (0.46 g) of water extract (**W2**). At the termination of the extraction procedures, 6 extracts were obtained viz **H1**, **E1**, **M1**, **E2**, **B2** and **W2**. These extracts were stored at -20°C until required for further processing

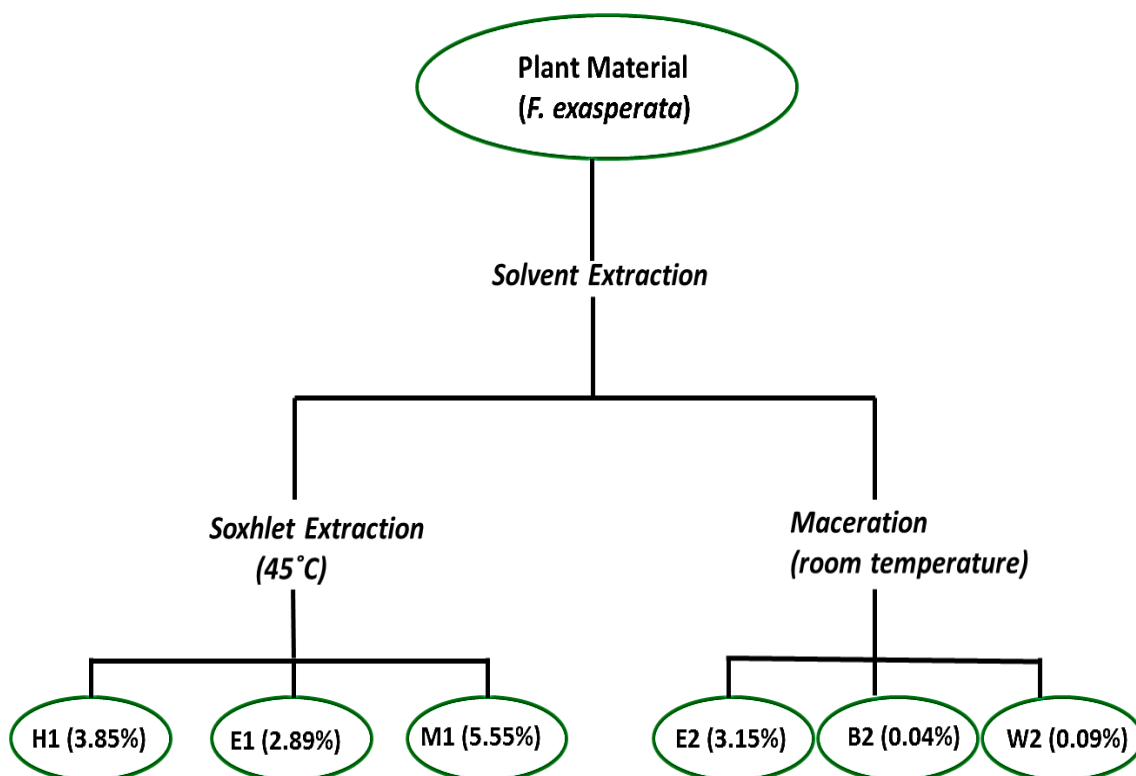


Figure 2.0 Schematic diagram showing the first phase extraction of the leaves of *F. exasperata*. Numbers in bracket represent the percentage yield following each phase of extraction. **H1**= hexane extract from soxhlet extraction, **E1**= ethylacetate extract from soxhlet extraction, **M1**= methanol extract from soxhlet extraction, **E2**= ethylacetate extract from maceration, **B2**= Butanol extract from maceration, **W2**= water extract from maceration.

2.6.2.4 Preliminary Identification of Extracts

Preliminary identification of the extracts was performed using nuclear magnetic resonance (NMR), mass spectrometry (MS) and TLC. The NMR phenomenon is based on the fact that nuclei of atoms have magnetic properties that can be utilized to

yield chemical information. NMR spectroscopy is an important technique used in the determination of structures of organic compounds.

a) NMR Analysis of Extracts

The extracts were weighed 10 mg each, and reconstituted in the appropriate deuterated solvents. **E1**, **E2** and **H1** were constituted in 750 μl of deuterated chloroform (CDCl_3) while **M1**, **W2** and **B2** were constituted in 750 μl of deuterated dimethyl sulphoxide (DMSO-D_6), with a Hamilton syringe (Alltech, Nevada). The reconstituted samples were subsequently transferred to labelled 5 mm NMR glass tubes and the proton (^1H) NMR for each extract was obtained using either an AS-400 JEOL NMR Instrument fitted with a 40TH5AT/FG broadband high sensitivity Pulse Field Gradient AutotuneTM 5 mm probe located in the Strathclyde Institute of Pharmacy and Biomedical Sciences (SIPBS) or a Bruker 400 and 500 MHz instruments at the Department of Chemistry, University of Strathclyde, UK as stated in the appropriate sections. The spectra were processed using MestReNova V8.1 and residual solvent signals were used as internal standards (reference signal). Chemical shifts (δ) of the processed spectra were obtained in parts per million (ppm) and coupling constants (J) were processed in Hertz (Hz).

a) LC-MS Analysis of Extracts

Liquid chromatography mass spectrometry (LC-MS) assays provides a robust platform for the analysis of the elemental composition of several important biological molecules and for elucidation of chemical structures. The MS principle operates by converting analytes to ionized forms which is followed by the analysis and measurement of the mass-to-charge ratio (m/z) of these ions or fragment ions (Fenn

et al., 1989). The LCQ Deca Ion Trap Mass Spectrometer (Thermo Finnigan, USA), which has a built-in electron spray ionization (ESI) source and functions in both the negative and positive ion modes, was employed in the ESI mass spectra analysis of the extracts. The ESI operation mode was developed by Fenn and colleagues in 1989 (Fenn *et al.*, 1989) for which they won the Nobel Prize in 2002 (The Nobel Prize in Chemistry, 2002). The liquid samples are pumped through a capillary to produce a fine spray of charged molecules which streams into the ion source where it intersects with an electron beam. The capillary is usually positioned orthogonally to the beam to reduce contamination (Fenn *et al.*, 1989). The interaction between the electrons and the neutral molecules generates positively charged molecular ions. The electrospray ionization mass spectrometry (ESIMS) was the alternative ionization procedure to LC-ESIMS for the natural products lacking chromophore (e.g. triterpenes) and for compounds which do not produce molecular ions or produced a low intensity under ESI conditions (Fenn *et al.*, 1989).

The MS column used in this study was the silica type ACE HPLC Column (Hichrom Limited, UK) 7.5 cm in length and 3.0 mm in diameter. The particle size of the silica was 5 μm , pore size 100 \AA with a pore volume of 1.0 ml/g and a 300 m^2/g surface area. The column was maintained at a temperature of 22 $^{\circ}\text{C}$ with an approximate pressure of 37 bar and a flow rate of 0.4 ml/min. About 1 mg of the extract was dissolved in HPLC grade MeOH and solutions containing insoluble materials were filtered to prevent blockade of the sample introduction line. The samples were transferred to 1.5 ml glass HPLC auto sampler vials from which the Agilent 1100 autosampler withdrew samples that were set at 200 $\mu\text{l}/\text{min}$ ejection speeds, one wash cycle and 20 wash strokes. The aqueous and organic eluents were

also prepared in 1L volumes, 0.1% formic acid in water (A) and 0.1% formic acid in acetonitrile (B) respectively. A multi-step linear gradient was applied for the Agilent 1100 Quaternary Pump: from 10% B to 90% B in 30 min, then 90% B to 10% B in 1 min and 10% B to 10% B in 4 min. The flow rate was 0.4 ml/min. The UV-vis spectra were recorded via the Agilent 1100 DAD between 200 and 400 nm with scan step of 2. The LC-ESIMS measurements were performed in SIPBS.

2.6.2.5 TLC Analysis of Extracts

Approximately 2 mg each of the dried extracts were reconstituted and spotted, a centimetre apart on aluminium TLC plates (silica gel sheets 60 F₂₅₄ from Merck, Germany). The plates were then developed in a solvent-equilibrated rectangular chamber at room temperature (Stahl, 1956; Garcia *et al.*, 1993). Various solvent system combinations were employed viz: dichloromethane: methanol and hexane: ethyl acetate (95:5, 90:10, 80:20, 70:30, 60:40 and 50:50). Spotting of the extracts was achieved using a fine capillary tube which was rinsed in acetone before each spot was made. Each developed chromatogram sheet was air-dried, observed with both short and long wavelength ultraviolet light (254 and 366 nm respectively) and bands carefully marked with a pencil. The plates were subsequently sprayed, within the fume hood, with anisaldehyde/H₂SO₄ reagent (0.5 ml anisaldehyde, 10 ml glacial acetic acid, 85 ml methanol and 5 ml concentrated sulphuric acid) (Circosta *et al.*, 2007) and heated to 105°C (Houghton and Raman, 1998). The solvent system combination which gave the best separation of compounds within each extract, based

on the retention factor (R_f), was selected for subsequent column fractionation and purification procedures (Cannell, 1998).

2.6.3 Pharmacological Screening of Extracts

Pharmacological analyses were performed on the extracts at this stage. This was necessary in order to assess the individual activity of the extracts on uterine contraction and subsequently determine and prioritize those with significant effects on uterine contraction.

2.6.3.1 Animals

Laboratory female mice (20-30 g) of the C57Bl/6 strain at different stages of the oestrus cycle were employed. The animals were bred at the Biological Procedures Unit of the University of Strathclyde, Glasgow, UK and were maintained under standard conditions according to Guidelines set for use of laboratory animals in the Animal Health and Welfare (Scotland) Act 2006. The animals were fed *ad libitum* and had free access to water.

2.6.3.2 Uterine Tissue Isolation and Mounting

Studies were conducted on non-gravid animals. The animals were euthanized by CO₂ asphyxiation followed by cervical dislocation and the uterine horns were carefully dissected out and surrounding mesenteries, fat and other adherent non-myometrial tissues were trimmed off. Longitudinal uterine horns about 1-1.5 cm in length were

subsequently mounted in 10 ml organ baths containing warmed (37°C), aerated (O₂/CO₂ 95 : 5) Krebs-Henseleit solution of the following composition: 118.4 NaCl, 25 NaHCO₃, 11.1 Glucose, 4.69 KCl, 2.41 MgSO₄, 1.18 KH₂PO₄, 2.5 CaCl₂ (mM) under a resting tension of 0.5 g.. Adequate care was taken throughout the whole procedure to avoid unnecessary stretching of the tissue. The tissue was allowed to equilibrate for 30 min before subsequent drug/sample additions. The activity of each uterine tissue segment was recorded via Grass (FT 03) isometric force transducers (range 0 – 25 g) connected to a bridge amplifier, which in turn was connected to a PowerLab data acquisition system made up of a recording unit coupled to a LabChart software (ADInstruments, UK).

2.6.3.3 Evaluation of the Effects of Extracts on Uterine Smooth Muscle Activity

At the end of the equilibration period, 0.2 mM lidocaine was added into the baths for 5 min. Lidocaine was used in this experiment to sustain and regularize rhythmic uterine phasic contractions. Each sample concentration was cumulatively added every 5 min. Numerical descriptors which included the integral (area under the time-response curve), amplitude of contraction (maximum tension above basal force) and frequency of uterine contractions were measured during the 5 min period following each addition. Prior to data analysis each 5 min period were highlighted and under the unit conversion window in the LabChart reader, the decimal place was increased to 3, and units set at grams for all data. All data were imported into the data pad and each column was modified to measure frequency, amplitude and integral. General height was selected for detection settings and adjusted to 0.2 g for minimum peak height.

2.6.4 Isolation of Chemical Constituents

Based on the results of uterine functional assays, **E1**, **E2** and **M1** extracts were selected for further purification since these extracts showed better activity profiles compared to the other extracts. Chromatographic procedures are the most widely used procedures in the fractionation of extracts. TLC was used routinely in monitoring complexities and fraction purities.

2.6.4.1 Medium-Pressure Liquid Column Chromatography Experiments

The medium-pressure liquid column chromatographic (MPLC) procedure was employed for the fractionation process. It applies the same principle as the open column chromatography, but differs in the additional use of pressure to drive the solvent through the stationary phase which enables a rapid separation of compounds with correspondingly higher resolution. Active extracts identified through the bioassay-guided pharmacological investigation were selected for further separation and purification. Choice of the column size and solvent system was dependent on the amount of the sample and pattern of compounds elution on the TLC plate. The solvent system allowed an R_f value of between 0.15 - 0.20 for the compounds of interest. Selected chromatographic columns used in this study were silica gel columns (Buchi Oldham, UK and Grace Deerfield, US).

The extracts were dissolved in suitable solvent, 7 g of **E1** and 10 g of **E2** dissolved in EtoAc and 10 g of **M1** in dichloromethane respectively. Each solution was incorporated with diatomaceous earth or kieselgur (Celite®) to serve as a sample carrier for dry loading. The homogenous mixture was subsequently dried. The extracts were then subjected to chromatographic separation on a silica gel column

(20-45 μm , C18 VersaPak cartridge, Bellefonte, U.S.A) connected to a Büchi Pump Manager C-615 coupled to binary pumps (Büchi Modules C-601) labelled A and B.

2.6.4.2 Fractionation of E1 and E2

A linear gradient system with hexane (A) and EtOAc (B) at a flow rate of 100 ml/min was employed for the elution of **E1 and E2**: 100% A was held for 5 min followed by 100% A to 100% B for the next 40 min and a reverse of starting conditions, 100 % B for a further 5 min giving a total run of 45 min. The column was subsequently flushed with 500 ml of 100% EtOAc and 500 ml of 50:50 acetone/MeOH each for 5 min. The eluent was collected in fractions of 100 ml for **E1**, 50 ml for **E2** and fractions with similar TLC profiles were pooled to yield a total of 44 and 23 fractions for **E1** and **E2** respectively. These fractions were labelled **E1a** or **E2a** fractions while the eluent from the wash were labelled **E1b or E2b** and **E1c or E2c** (respectively).

Fraction series **E1a**, **E1b**, and **E1c** were subjected to further analysis and screening. Bioactive fractions were subjected to further purification. For the purification procedures about 200-400 mg of each sample was dissolved in 2 ml hexane and EtOAc at a ratio of 9:1. The sample solution was then injected into a silica gel cartridge (23 x 53 mm²). MPLC isocratic elution was performed using hexane and EtOAc (90:10) at a flow rate of 10 ml/min for 30 min.

2.6.4.3 Fractionation of M1

A step-wise gradient system was employed in which a two solvent-system combination in each run was performed for the elution of **M1** at a flow rate of 100 ml/min viz: 10 g of **M1** was separated on 200 g of silica gel 60 (Merck, Germany) using flash column chromatography with step gradient elution of the following

composition: step 1: hexane–EtoAC (100% A for 5 min); step 2: hexane–EtoAc (100 A-0% B increasing to 0%A-100% B in 40 min); step 3: hexane–EtoAC (100% B for a further 5 min); step 4: DCM-MeOH (100% A for 5 min); step 5: DCM-MeOH (100-80% A and 0-20% B for 20 min); step 6: DCM-MeOH (80%A - 20%B held for 5 min); The column was flushed with acetone-MeOH (50:50) for 5 min at 100 ml/min. The eluent was collected in fractions of 100 ml. Fractions obtained from the hexane-EtoAc solvent system combination were labelled using the suffix **Ma** while fractions obtained from the DCM-MeOH solvent system combination were labelled using the suffix **Mb**, while the eluent from the flush was labelled using the suffix **Mc**. Fractions with the same TLC and NMR profiles were then combined to yield a total of 15, 6 and 2 combined fractions for **Ma, Mb and MC** respectively. A diagram showing the fractions and procedures is shown in figure 2.1.

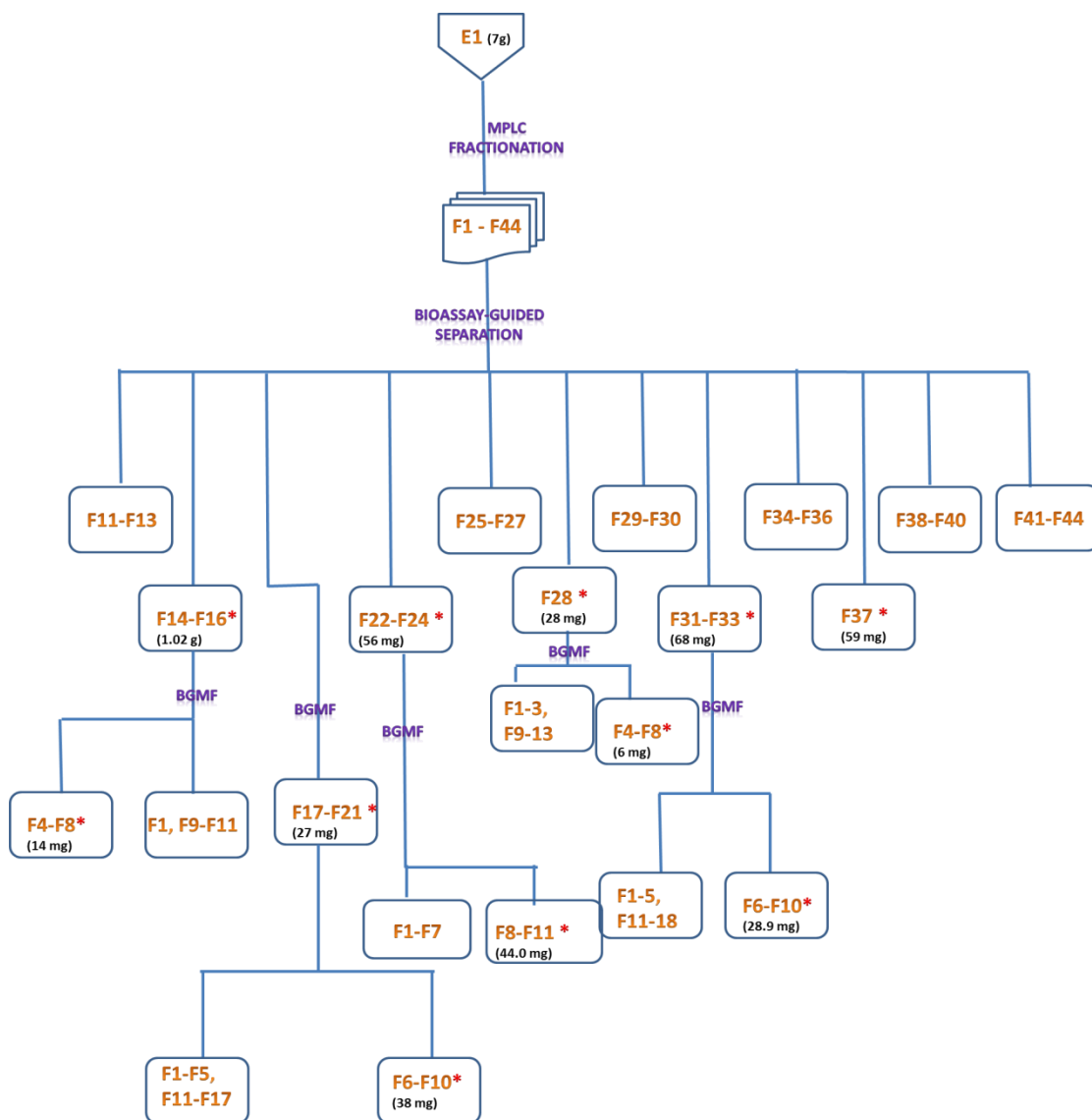


Figure 2.1 Schematic diagram summarizing the bioassay-guided fractionation procedure for **E1**. * = significantly active fractions; BGMF = Bioassay-guided MPLC Fractionation.

2.6.4.4 TLC Analysis of Extracts

The TLC procedure for the extracts (2.6.2.5) was repeated for the fractions.

2.6.4.5 Identification and Structural Characterization of Compounds

One- and two-dimensional NMR experiments were acquired at 400 MHz on an AS-400 JEOL NMR Instrument operating on an eclipse-400 spectrometer at 23°C equipped with a 40TH5AT/FG broadband high sensitivity Pulse Field Gradient 'Autotune™' 5 mm probe. **E1** and **E2** samples were dissolved in deuterated chloroform (CDCl₃) and the chemical shifts were recorded while **M1** samples were constituted in deuterated dimethyl sulphoxide (DMSO-D₆). 1D-NMR spectra were obtained using the following parameters; 16-32k data points, spectral width of 7199 and pulse width of 5.4750 Hz respectively, an acquisition time of 1.14 min and a relaxation delay of about 2.0 s. Sequential MS was also carried out to identify compounds in the fractions obtained using LC-HRFTMS analysis with a Dionex UltiMate® 3000 HPLC system (Thermo Fisher Scientific Inc., Hemel Hempstead, UK) employing a silica type 75.0 x 3.0 mm C18 ACE HPLC column (Hichrom Limited, UK), particle size of the silica was 5 µm, pore size 100Å with a pore volume of 1.0 ml/g and a surface area of 300 m²/g which was maintained at a temperature of 22°C and an approximate pressure of 37 bar. The column was eluted with a linear gradient of 90% A (0.1% v/v formic acid in water) and 10% B (0.1% v/v formic acid in acetonitrile) mobile phases with a flow rate of 0.3 ml/min over 0-35 min then to 100% B for a further 5-min isocratic elution, and a return to starting conditions at 40 min for re-equilibration for the last 5 min, using up a total of 45 min for the run. MS identification and analysis were carried out using a ThermoScientific Exactive (Thermo Fisher Scientific Inc, Hemel Hempstead, UK) with a 10 µl

injection volume and the mass spectrometer was operated with UV detection at 254 nm using both positive and negative ions modes. Approximately 1 mg of the extracts was dissolved in 1 ml HPLC grade methanol and solutions containing insoluble materials were filtered to avert blockade of the sample introduction line. The samples were transferred to 1.5 ml glass HPLC auto sampler vials from which the Agilent 1100 auto sampler withdrew samples that were set at 200 $\mu\text{l}/\text{min}$ ejection speeds, one wash cycle and 20 wash strokes.

2.6.4.6 HPLC-ICP-MS

A size exclusion column, Superdex 75 (10/300GL, Tricorn, Sweden), and HPLC system with quaternary pump, degasser, manual injector (50 μL loop) coupled to an Agilent ICP-MS (Model 7500 X, Agilent, Tokyo, Japan) were used for salt identification. Pump speed was set at 0.70 mlmin^{-1} , and 0.02 $\text{mol}^{\text{l}^{-1}}$ Tris-HCl pH 7.4 was used as the mobile phase. HPLC-ICP-MS has been shown to be a valuable tool in detecting trace elements (Prange and Schaumloffel, 2002).

2.6.5 In Vitro Uterine Assay of the Fractions and Compounds of *F. exasperata*

Virgin female mice (weighing 20-30 g) of the C57Bl/6 strain were employed. Care and use of animals were as previously described (2.6.3.1 and 2.6.3.2).

2.6.5.1 Uterine Tissue Set-up

Studies were conducted on non-gravid animals. Experiments were as previously described (2.6.3.3). The contractions obtained during the last 3 min of the stable

spontaneous or the agonist-induced contractions before the addition of the plant extracts, fractions or standard drugs were taken as the control. The effects of each concentration of the extracts or standard drugs on uterine contraction during the last 3-min incubation period were expressed as a percentage of the control. Data from animals in the pro-oestrous to oestrous stages were employed for this study.

2.6.5.2 Study on Spontaneous Uterine Contractions

At the end of a 30 min equilibration period, the consistent spontaneous contractions were measured for 10 min and the plant extracts or fractions were added into the bathing solution in a cumulative manner. In a parallel control experiment, the effect of dimethylsulphoxide (DMSO) solvent vehicle on the contraction of the uterus was also tested.

2.6.5.3 Studies on Oxytocin-induced Uterine Contractions

In another set of experiments, uterine segments were treated with a submaximal concentration of oxytocin (1 nM), in order to determine the longevity of the response. As oxytocin-induced contraction was sustained for over 1 h it was determined that this protocol allowed the evaluation of the plant extracts, fractions or standard drugs via cumulative additions every 5 min. The amplitude of contraction (maximum tension above basal force) and frequency of uterine contractions were obtained during the 5 min period following each sample addition where necessary.

2.6.5.4 Studies on KCl-pre-contracted Uterus

KCl (80 mM) was used to pre-contract the uterine segments and after achievement of stable responses, the fractions found to inhibit contractions in other experiments,

were added to the bath in increasing cumulative concentrations (70 - 200 µg/ml) at 2 min intervals. The concentration of KCl used was chosen from preliminary experiments where it was observed that lower concentrations failed to produce a reasonable reproducible force of contraction in the mouse uterus.

2.6.6 Drugs and Chemicals

The drugs used were oxytocin (Sigma Aldrich, UK) which was constituted in distilled water. The plant extracts and fractions were constituted in DMSO to give a final concentration of 200 or 100 mg/ml respectively and kept as a stock solution at a temperature of -20°C until use. The final concentration of DMSO in the organ bath was calculated to be less than 0.5%.

2.6.7 Curve Fitting and Statistical Analysis

Responses of the uterus to the different concentration of the extracts were expressed as mean ± S.E.M (standard error of the mean) of the frequency (cycles/5 min), amplitude (g) and area under the curve (AUC). In each case n represented the number of experiments. Comparisons were made using one-way ANOVA with Dunnett's Multiple Comparison Test for the activity of the extracts and Bonferroni's correction for multiple comparisons for the activity of the fractions via the GraphPad Prism (v4.0; U.S.A). $P < 0.05$ indicated statistical significance in all cases. In cases with sufficient data points concentration-response curves were constructed from the data obtained and fitted to the equation:

$$Y = \text{Bottom} + (\text{Top}-\text{Bottom})/(1+10^{((\text{LogEC50}-X)*\text{Hill Slope}))}.$$

Where Y = response which starts at the Bottom and goes to the Top in sigmoid shape; X = logarithm of concentration and EC_{50} is the concentration that produces half the maximal responses. The EC_{50} and E_{max} for frequency and amplitude of contractions were calculated and compared after curve fitting where possible.

In the study on oxytocin-induced contractions, data points were considered too few for curve fitting.

2.7 Results

2.7.1 Yields of Extracts and Fractions

Extraction of the leaves via soxhlet extractor resulted in the hexane extract (**H1**), ethylacetate extract (**E1**) and methanol extract (**M1**) with yields of 19.23 g (3.84%), 14.49 g (2.89%) and 27.75 g (5.55%) respectively. The maceration procedure produced extracts **E2** with a yield of 15.74 g (3.15%), **B2** with a yield of 200 mg (0.04%) and **W2** with a yield of 459 mg (0.09%).

With respect to physical characteristics, **W2** and **B2** extracts displayed a brownish-golden colour with a characteristic pungent smell. These characteristics distinguished **W2** and **B2** from the other extracts which were mostly green in colour and sweet smelling, however **H1** had a much darker almost black colour which glistened indicating the presence of fats and oils.

2.7.2 TLC Analysis of Extracts

TLC was mainly used in this study for qualitative analysis. Different solvent systems involving several combinations of hexane, EtoAc and MeOH were employed but during the course of this research it was observed that a solvent system combination of hexane:EtoAc:MeOH worked best for the separation of compounds from the leaves of *F. exasperata*. The TLC was also a means of determining an appropriate solvent system for MPLC fractionation. However, since the MPLC set up was controlled by a binary pump the use of the three solvent system combination was not carried out. **E1** and **E2** showed good separations at mobile phase combinations of hexane:EtoAc (80:20) while **M1**, **W2** and **B2** showed good separations at mobile phase combinations of DCM:MeOH (95:5).

H1 and **E2** displayed the most number of compounds (estimated from the number of bands observed before and after spraying) this was followed closely by **E1**, and then **M1**, **B2** and lastly **W2** (Fig. 2.2 and Fig. 2.3). Violet and pink bands were observed in **H1**, **E1**, and **E2** upon spraying with anisaldehyde reagent but these coloured bands were more intense in **H1** and **E2**, while **E1** was mostly green. **M1** was characterized by more green bands, while **W1** and **B2** exhibited dark brown bands with anisaldehyde spray. **W2** and **B2**, in particular had a patch of white band at an R_f of 0.72 in DCM: MeOH 95:5, which did not absorb or reflect any colour when sprayed with anisaldehyde reagent. This band was more intense in **W2** when viewed under long UV (Table 2.1).

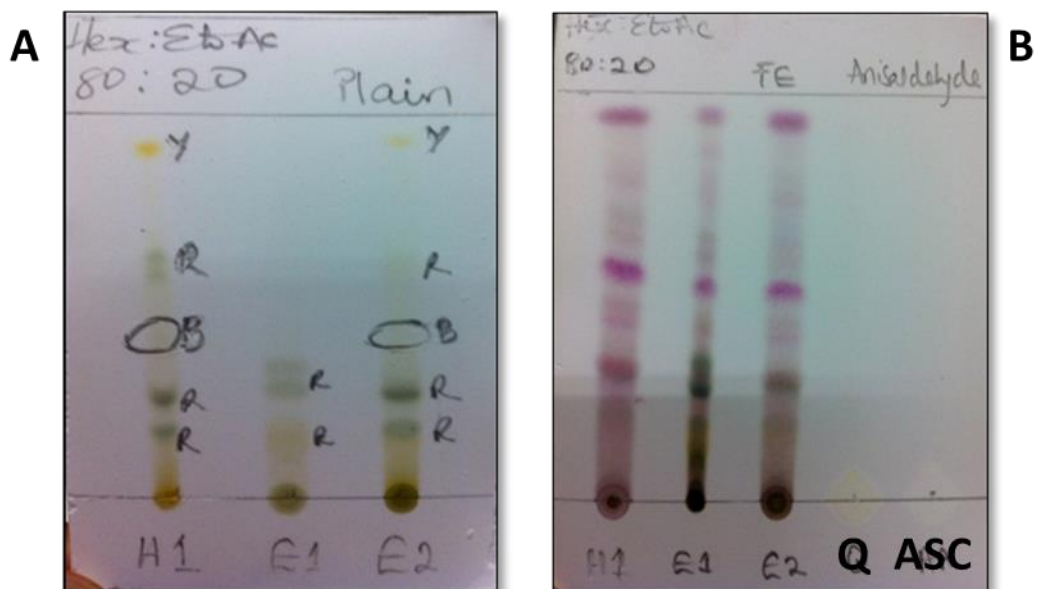


Figure 2.2 TLC plates of **H1**, **E1** and **E2** developed in hexane:EtoAc (80:20). Plate **A** indicates thin layer chromatogram with no spray reagent applied and Plate **B** indicates a photograph of thin layer chromatogram plate sprayed with anisaldehyde reagent and observed under UV at wavelength of 354 nm. Y=yellow; R=red; B=blue. Q= quercetin; ASC = ascorbic acid

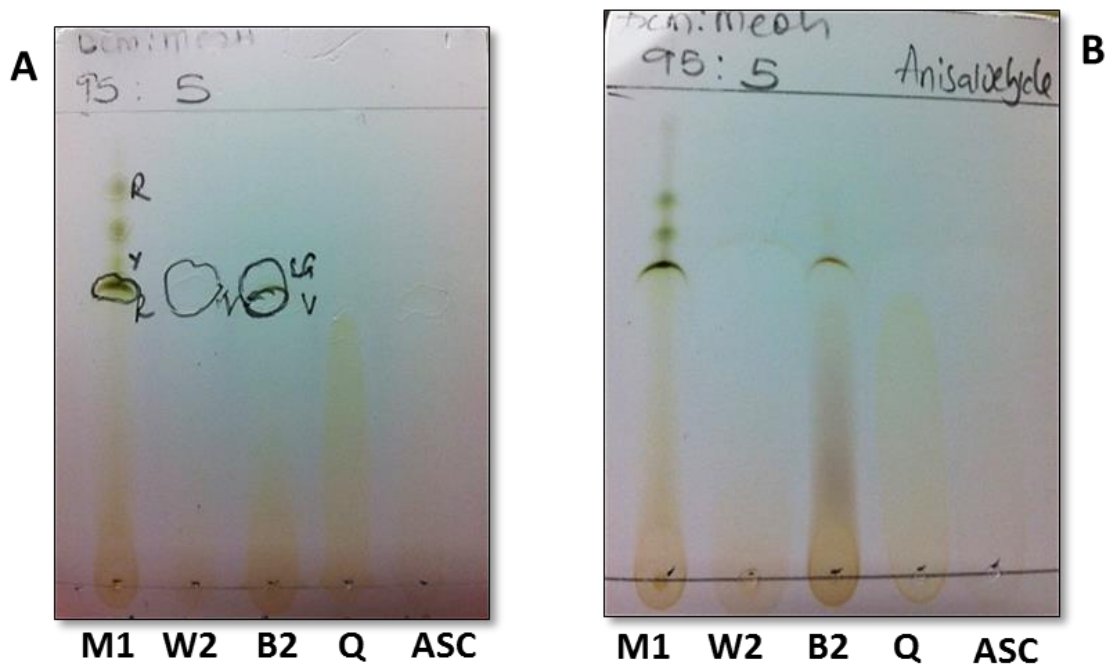






















Figure 2.3 TLC plates of **M1**, **W2** and **B2**. A photograph of a thin layer chromatogram plate with no spray reagent applied (A) and Plate **B** indicates a photograph of a thin layer chromatogram plate sprayed with anisaldehyde reagent observed under UV at wavelength of 254 nm. Both plates were developed in DCM:MeOH (95:5). Y=yellow; R=red; B= blue. Q= quercetin; ASC = ascorbic acid.

Table 2.1 Extract Colours and Respective R_f values after spraying with anisaldehyde

Extract	Colours and Respective R_f Values			
H1	 0.35, 0.5,0.96	 0.44, 0.48, 0.64	 0.06, 0.28, 0.6, 0.84	 0.06, 0.24, 0.68
E1	 0.5, 0.96	 0.62	 0.0, 0.06, 0.12, 0.2, 0.28, 0.36, 0.84	 0.44, 0.68
E2	 0.35, 0.5	 0.44, 0.48, 0.64	 0.0, 0.06, 0.2, 0.28, 0.84	 0.68
M1	 0.10	 0.63	 0.70, 0.77	
W2	 0.08	 0.66		
B2	 0.08	 0.66	 0.62	

Colour bands and corresponding R_f values after spraying with anisaldehyde observed within each extract during TLC analysis.

2.7.3 Qualitative Flavonoid Analysis of Extracts of *F. exasperata*

On spraying with Naturstoff reagent, colour changes were observed within each extract (Fig. 2.4, Table 2.2 and 2.3). **H1**, **E1** and **E2** displayed similar zones of colour changes with each other (Table 2.2). **M1** and **B2** showed green fluorescence at the origin and greenish yellow fluorescence at 0.1. **W2** displayed a yellowish green fluorescence at 0.08 (Table 2.3).

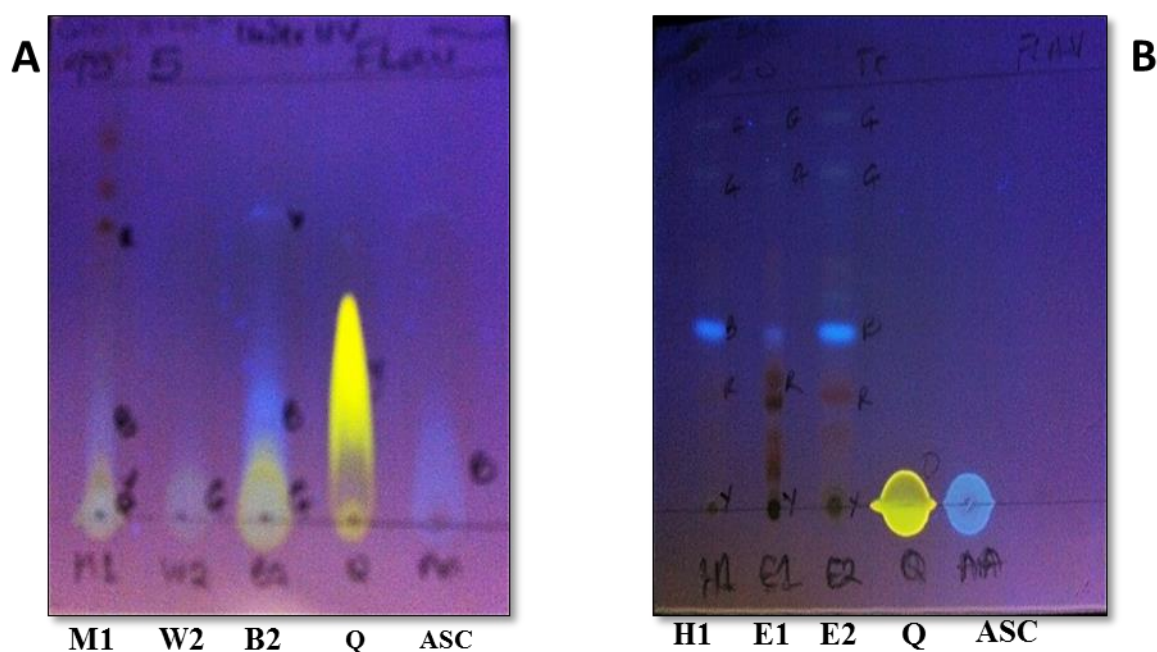


Figure 2.4 TLC plates under UV wavelength of 365 nm of **M1**, **B2**, **W2** extracts (A) and **H1**, **E1** and **E2** extracts (B) in DCM : MeOH (95:5) and hexane : EtoAc (80:20) respectively after spraying with Naturstoff reagent A and B. Q= quercetin and ASC = ascorbic acid.

Table 2.2 Qualitative Flavonoid Test for **H1, E1** and **E2**

Colour changes in **H1, E1** and **E2** after spraying with Naturstoff reagent and viewed under UV wavelength of 356 nm. The R_f values with respect to colour changes were similar across all three extracts. The value 0.0 indicates that the compounds specified remained at the origin. Q = quercetin; ASC = ascorbic acid































Band	R_f	Before	After
H1, E1 and E2	0.08		 yellow
	0.28		 yellow
	0.5		 orange
	0.64		 yellow-green
	0.96		 yellow-green
Q	0.0		 Bright yellow
ASC	0.0		 light blue

Table 2.3 Qualitative Flavonoid Test for **M1, W2 and B2**

Table showing the colour changes in **M1, W2 and B2** after spraying TLC spotted plates with Naturstoff reagent and viewed under UV wavelength of 365 nm. Q= quercetin; ASC = ascorbic acid

Extracts/Standards	Band	R _f	Before spraying	After spraying
M1	1	0.10		 yellow-green
	2	0.08		 light green
	3	0.26		 light blue
W2	1	0.08		 yellow-green
B2	1	0.08		 yellow green
	2	0.10		 blue
Q	Q	0.0		 yellow
ASC	ASC	0.0		 light blue

2.7.4 ¹H-NMR OF EXTRACTS

H1 showed peaks at aliphatic (0 - 3.5 ppm), olefinic (3.5 – 5.0 ppm) and aromatic (6.5 - 9.75 ppm) regions with the peaks at the aliphatic region being more intense (Fig. 2.5). Peaks in **E2** similarly occurred within the aliphatic, olefinic and aromatic regions up to 9.75 ppm but the peaks within both the aliphatic and olefinic regions were the most intense (Fig. 2.7). **E1** displayed peaks up to 11.5 ppm. Also more peaks were observed in **E1** at 4 - 5 ppm (Fig. 2.6). **M1, B2 and W2** displayed peaks from 0 - 9.5 ppm (Fig. 2.8, 2.9 and 2.10).

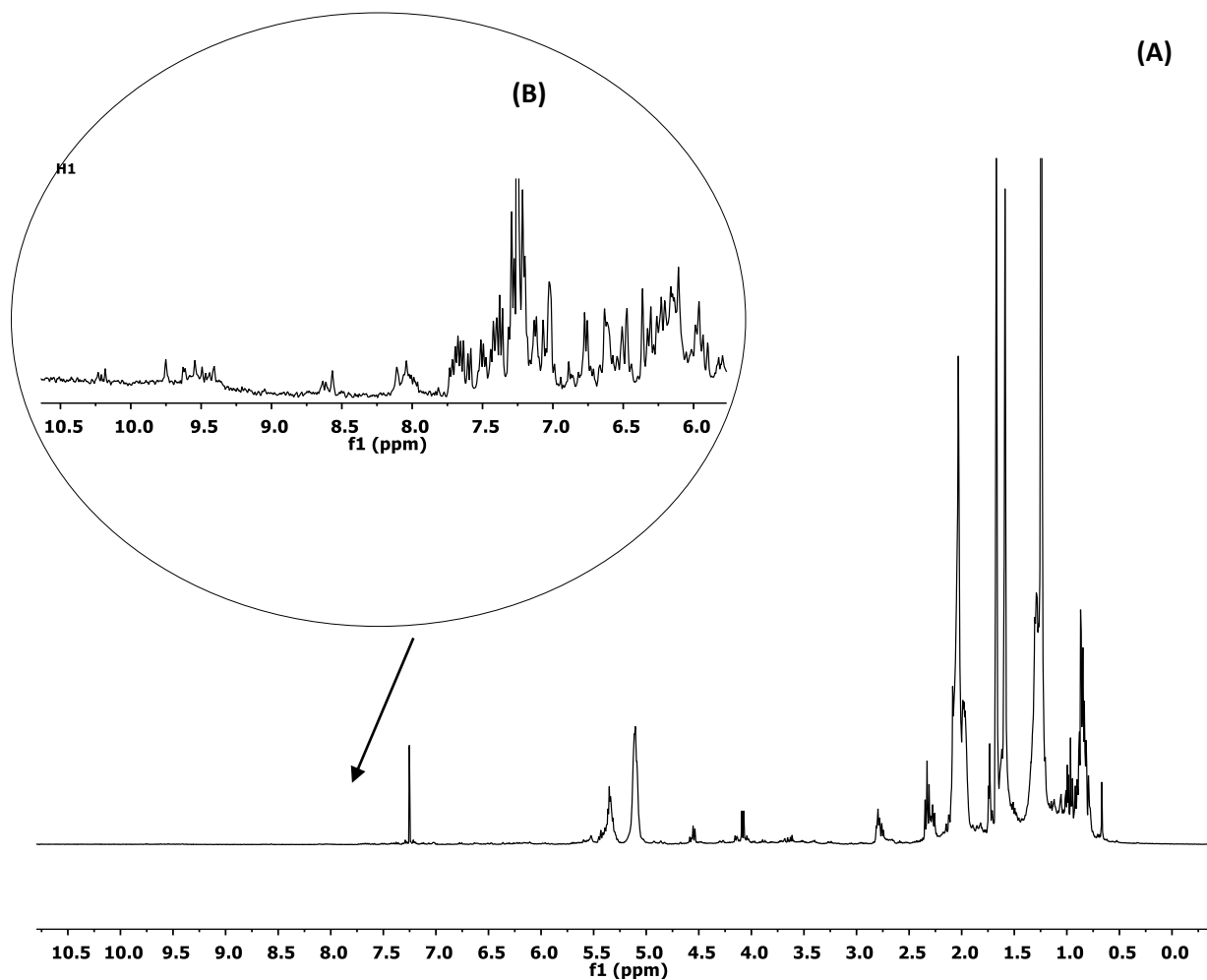


Figure 2.5 $^1\text{H-NMR}$ spectrum at 400 MHz in CDCl_3 of **H1** (Apodization: Gaussian 3.00; Baseline correction: Bernstein Polynomial Fit) showing the range of proton signals from the aliphatic to the aromatic region (0.5 -10.5 ppm). Less intense peaks at the aromatic region of 6.5 - 9.75 ppm are shown in B above.

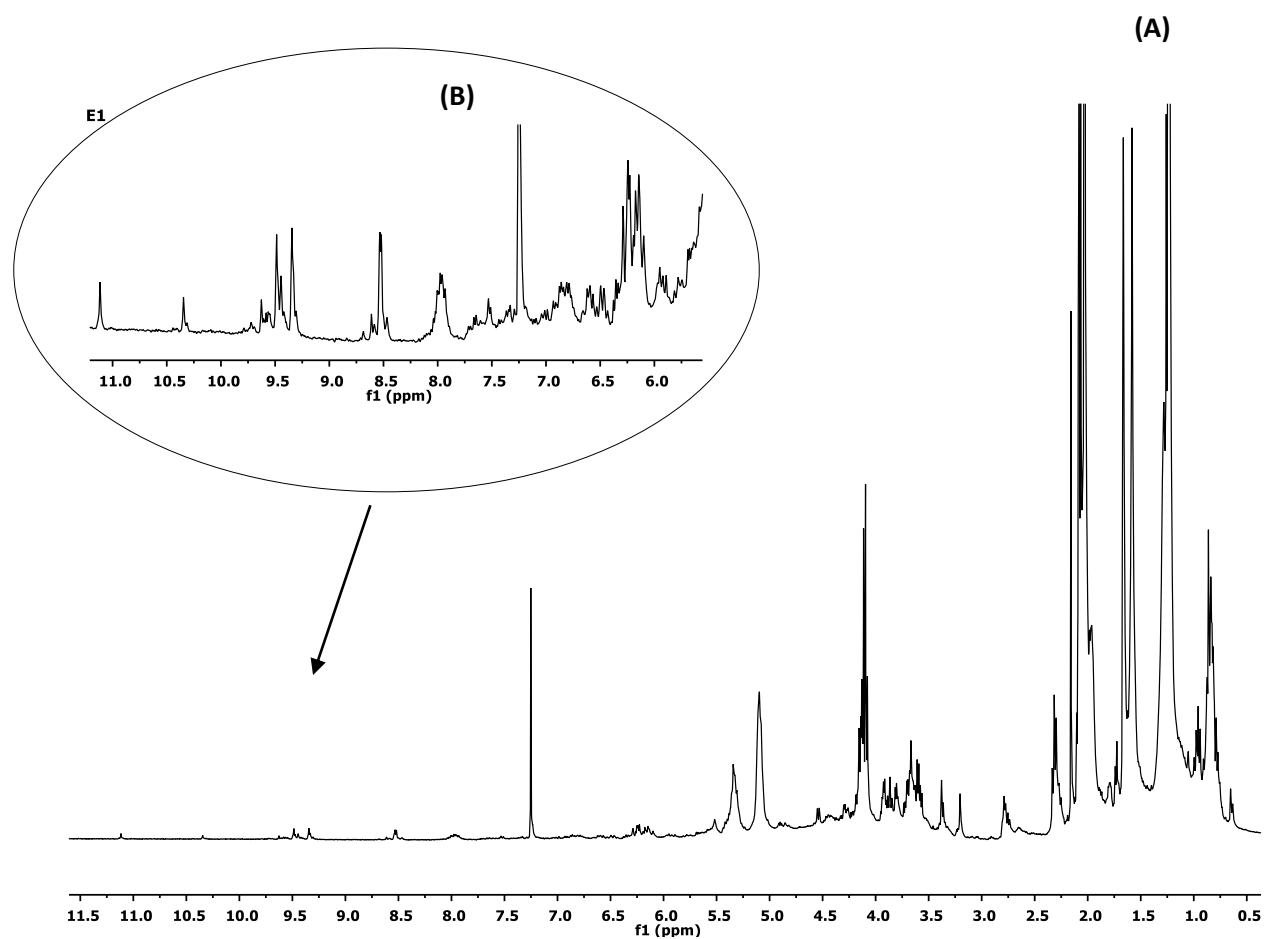


Figure 2.6 ¹H-NMR spectrum at 400 MHz in CDCl₃ of **E1** (Apodization: Gaussian 3.00; Baseline correction: Bernstein Polynomial Fit) showing the range of proton signals from the aliphatic to the aromatic region (0.5 -11.5 ppm). Less intense peaks at the aromatic region of 6.0 - 11.5 ppm are shown in B above.

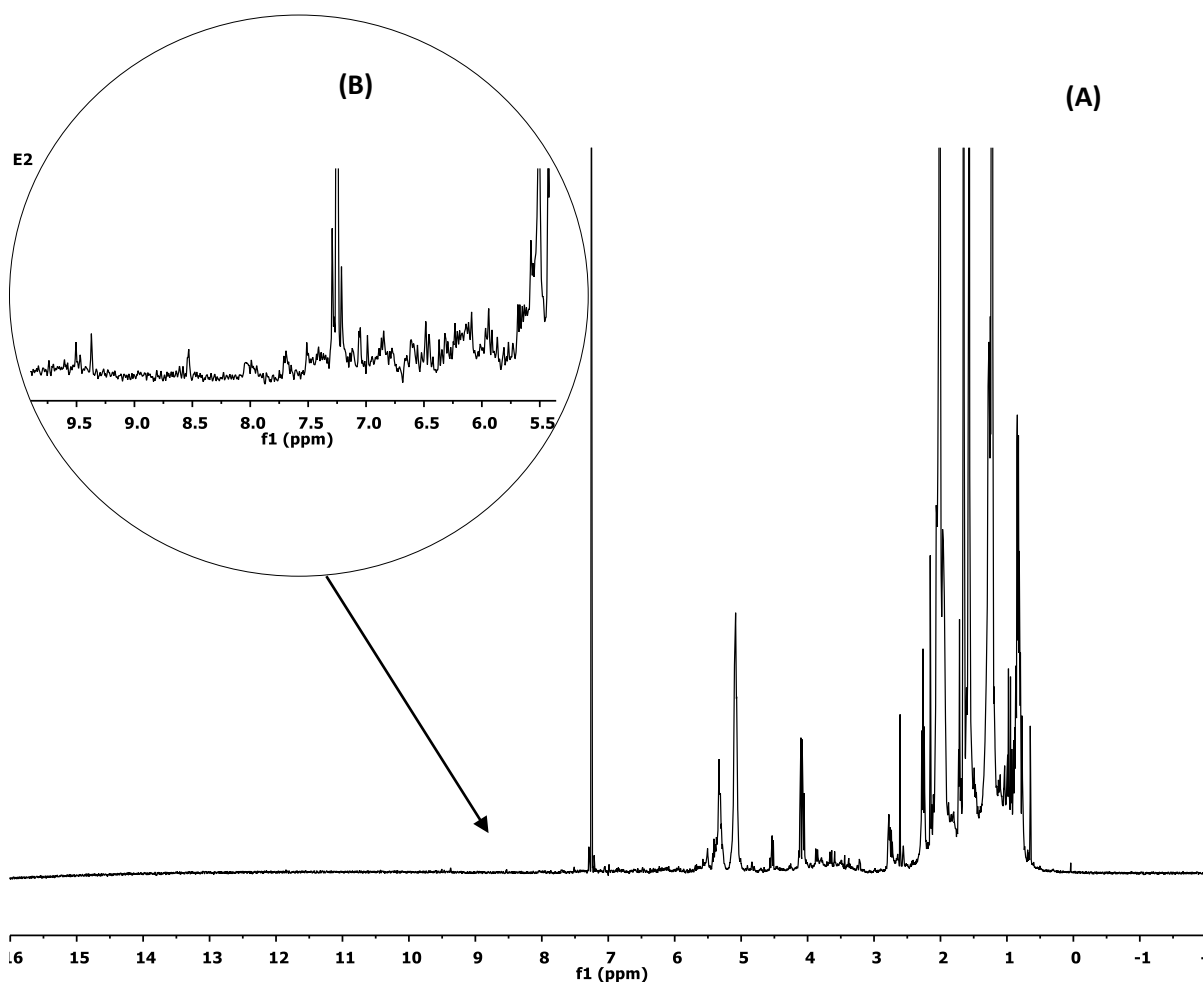


Figure 2.7 ¹H-NMR Spectrum at 400 MHz in CDCl₃ of **E2** (Apodization: Gaussian 3.00; Baseline correction: Bernstein Polynomial Fit) showing the range of proton signals from the aliphatic to the aromatic region (0.5 -10.0 ppm). Less intense peaks at the aromatic region of 6.0 - 9.5 ppm are shown in B above.

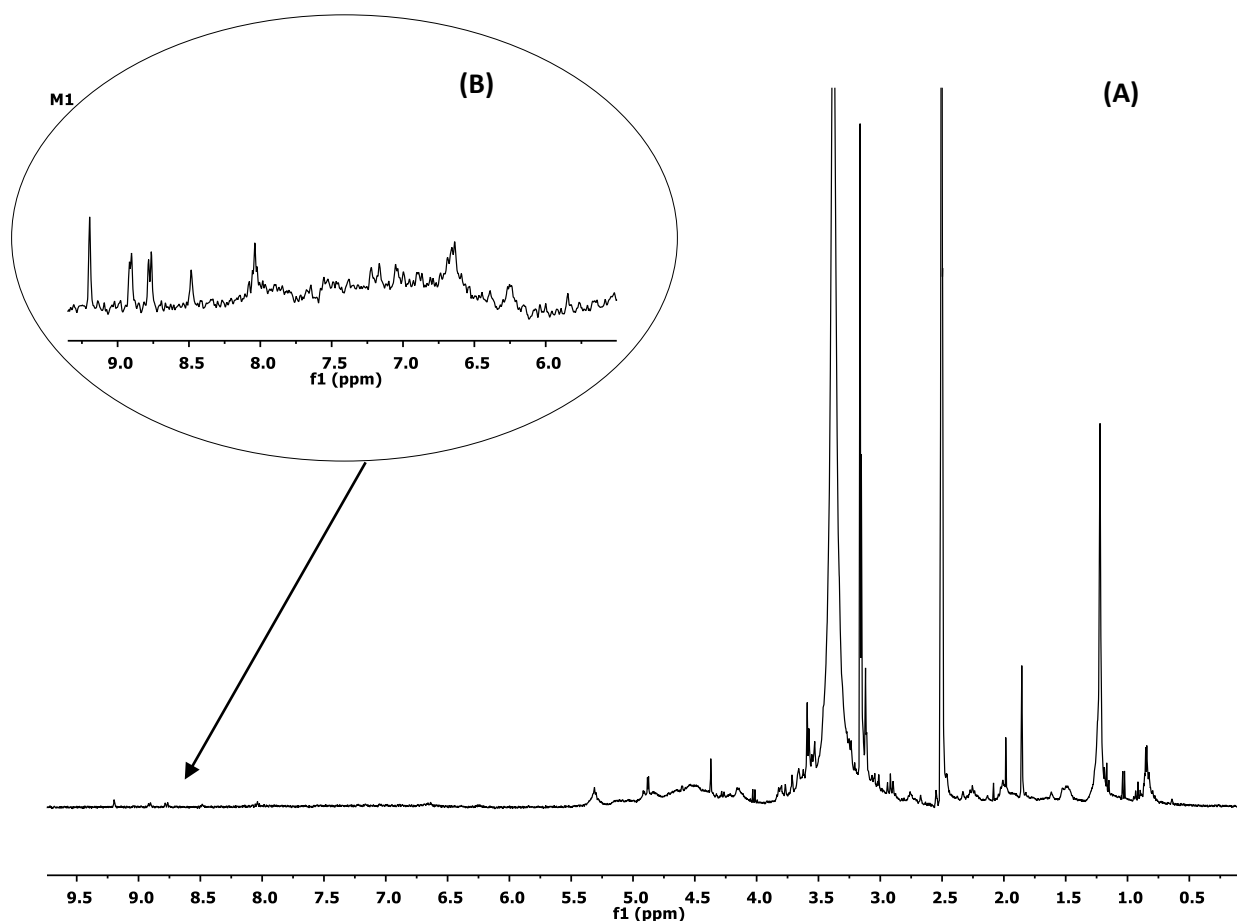


Figure 2.8 $^1\text{H-NMR}$ spectrum at 400 MHz in DMSO-D_6 of **M1** (Apodization: Gaussian 3.00; Baseline correction: Bernstein Polynomial Fit) showing the range of proton signals from the aliphatic to the aromatic region (0.5 - 9.5 ppm). Less intense peaks at the aromatic region of 6.0 – 9.0 ppm are shown in B above.

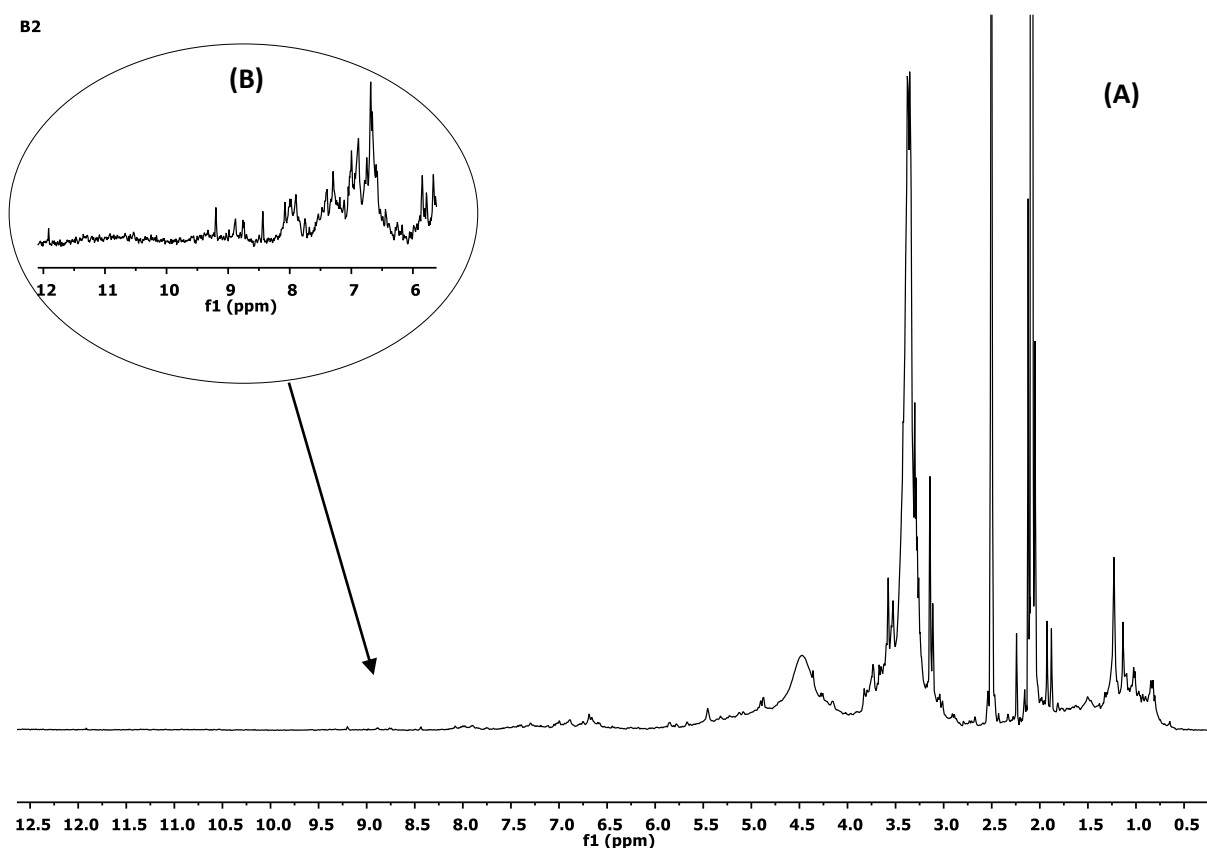


Figure 2.9 $^1\text{H-NMR}$ spectrum at 400 MHz in DMSO-D_6 of **B2** (Apodization: Gaussian 3.00; Baseline correction: Bernstein Polynomial Fit) showing the range of proton signals from the aliphatic to the aromatic region (0.5 – 12.0 ppm). Less intense peaks at the aromatic region of 6.0 – 12.0 ppm are shown in B above.

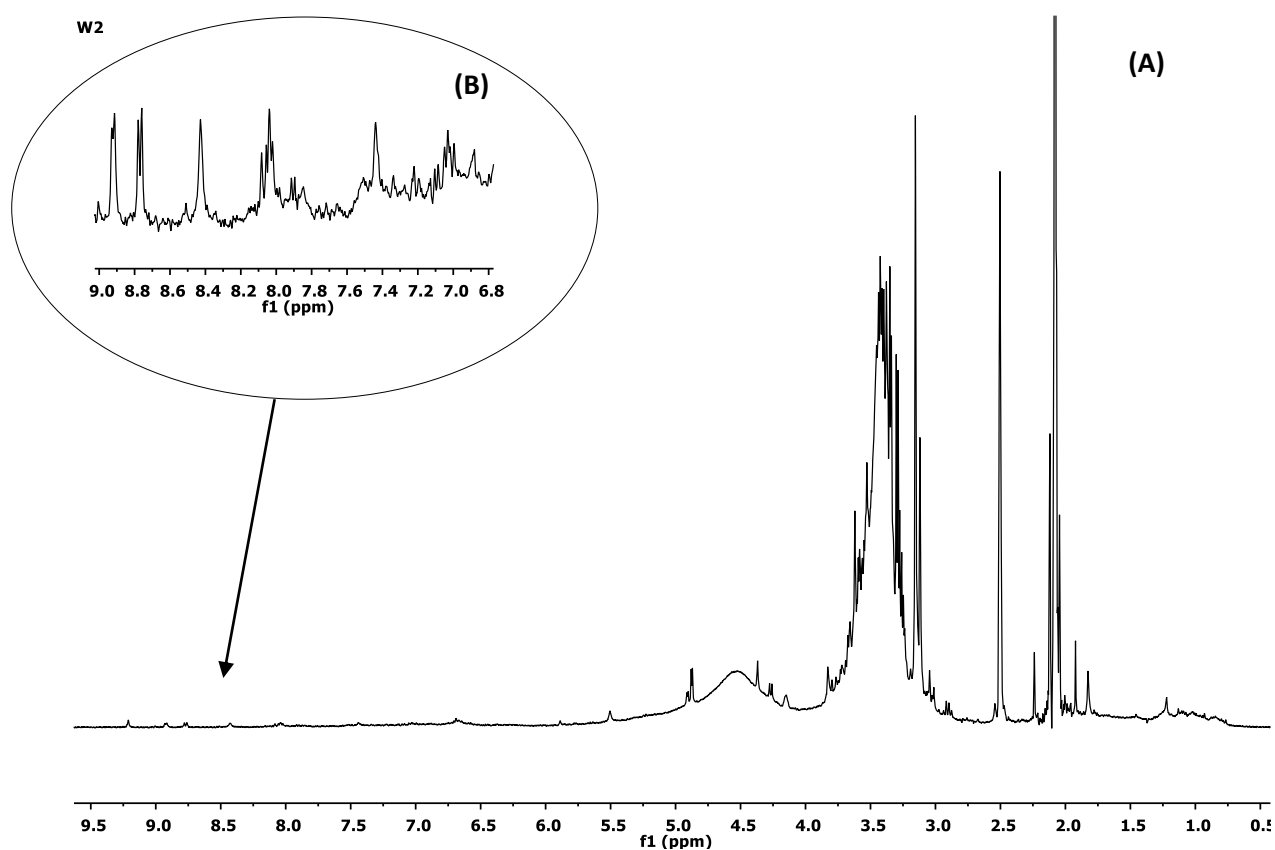


Figure 2.10 ¹H-NMR spectrum at 400 MHz in DMSO-D₆ of **W2** (Apodization: Gaussian 3.00; Baseline correction: Bernstein Polynomial Fit) showing the range of proton signals from the aliphatic to the aromatic region (0.5 - 9.5 ppm). Less intense peaks at the aromatic region of 6.8 – 9.0 ppm are shown in B above.

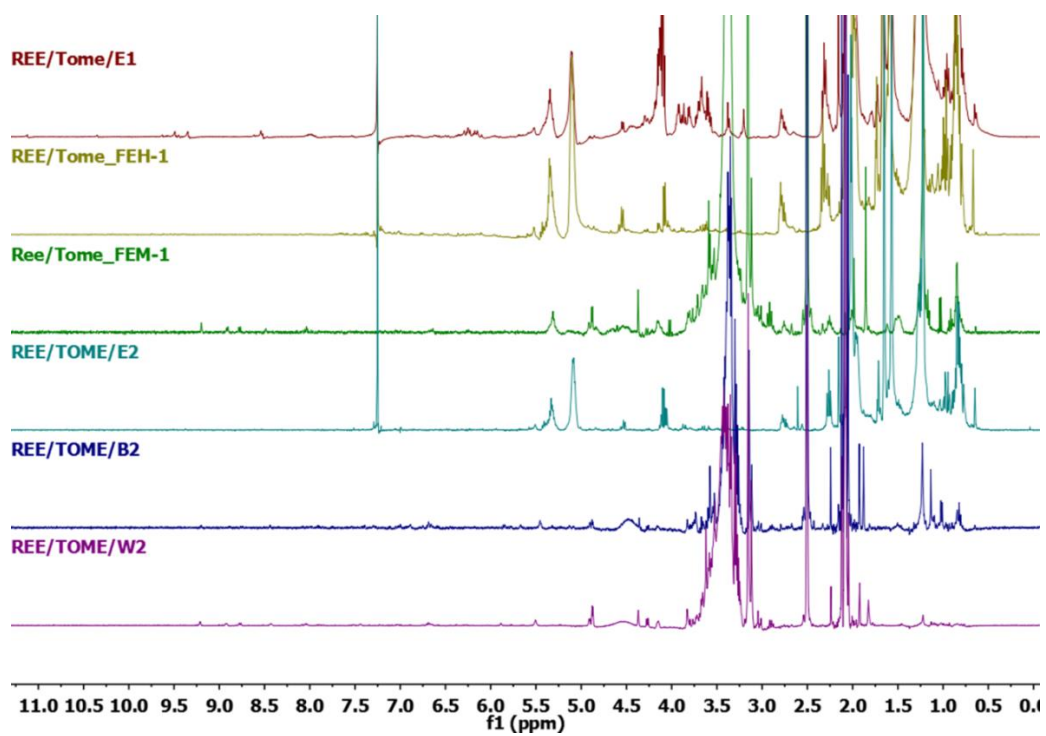


Figure 2.11a Stacked ¹H-NMR spectra of **H1**, **E1**, **E2**, **M1**, **W2**. **E2**, **M1** and **B2** have common peaks between 0.6 -1.2 ppm, while **W2** and **B2** share common peaks between 1.85-2.25 ppm, all three extracts have common peaks between 3.1- 5.3 ppm.

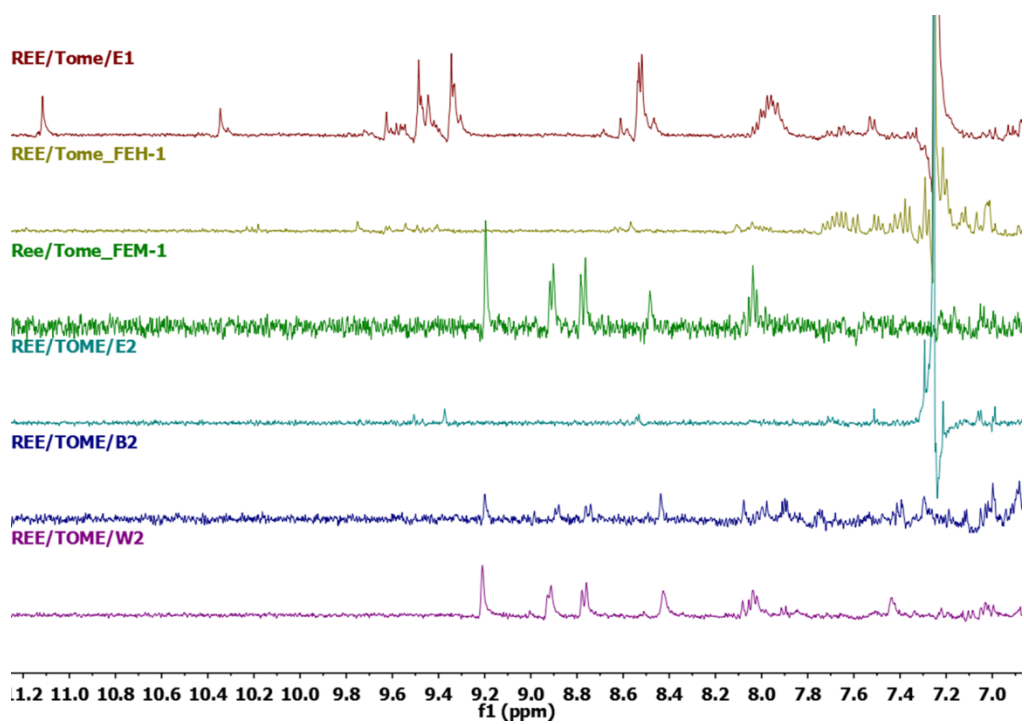


Figure 2.11 b Expanded stacked ¹H-NMR spectra of **H1**, **E1**, **E2**, **M1**, **W2** and **B2** between 7.3–11.1 ppm. Signals in the aromatic region were similar between **E1** and **E2** while similar aromatic signals occurred in **M1**, **B2** and **W2**.

2.7.5 LC-MS Analysis of Extracts of *F. exasperata*

A peak at retention time (Rt) of 10.00 min was common to **H1**, **E1** and **E2**. **E2** and **E1** differed from **H1** by the possession of peaks at retention time ± 42 min (Fig. 2.12). **M1** and **W2** exhibited similar peaks and same retention times and **B2** exhibited some peaks at Rt of 6.9-8.3 min (Fig. 2.13).

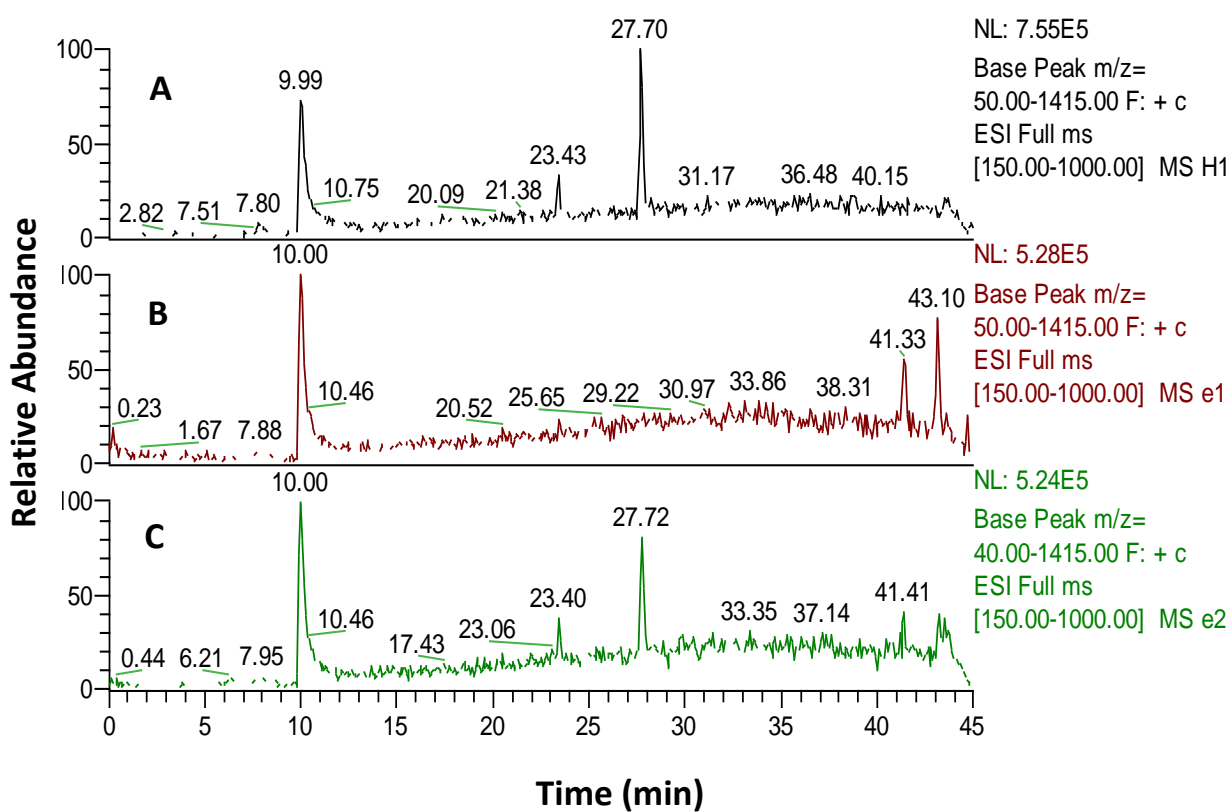


Figure 2.12 Stacked Base Peak Chromatograms of **H1** (A), **E1** (B) and **E2** (C) in the positive full MS mode.

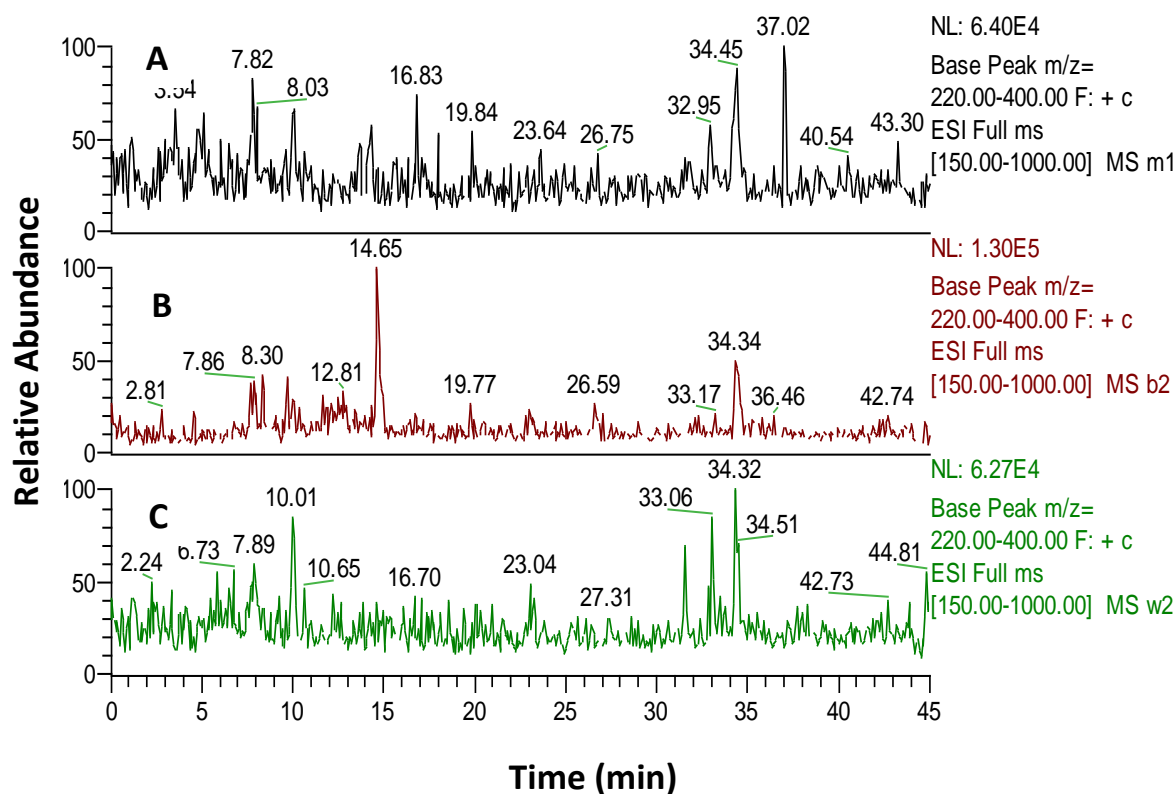


Figure 2.13 Stacked Base Peak Chromatograms of **M1** (A), **B2** (B) and **W2** (C) in the positive full MS mode.

2.7.6 Effects of Extracts on Uterine Contractility

E1, **E2** and **W2** reduced the frequency of lidocaine-induced uterine contractions (Fig. 2.15, Fig. 2.16 and Fig. 2.18 respectively) while **H1**, **M1** and **B2** displayed mostly uterotonic effects (Fig. 2.14, 2.17 and Fig. 2.19). The word “mostly” has been coined into the description of activity as some degree of inhibition of the frequency of contractions occurred (considered statistically insignificant). The inhibitory activity of **E1** seemed to begin at a concentration of 400 µg/ml and at 800 µg/ml **E1** caused an almost complete blockade of contractions which were not easily reversed on washout (Fig. 2.15). **E2** displayed an increase in the frequency of contractions at 200

$\mu\text{g/ml}$ but beyond this concentration there seemed to be a decrease in amplitude accompanied by irregular contractions (Fig. 2.16). A similar effect was observed with **M1** (Fig. 2.17).

Total contractile force generated by each uterine segment in response to the extract was additionally estimated by calculating the area under the contraction force curve over time which is a summative estimate of a change in the contraction frequency and amplitude. **H1**, **E1**, **E2**, **B2** and **W2** significantly decreased the basal contractility of uterine contractions as measured from the area under the curve. **H1**, **E1**, **E2**, **M1** and **B2**, all exhibited activity from $200 \mu\text{g/ml}$ (Table 2.6).

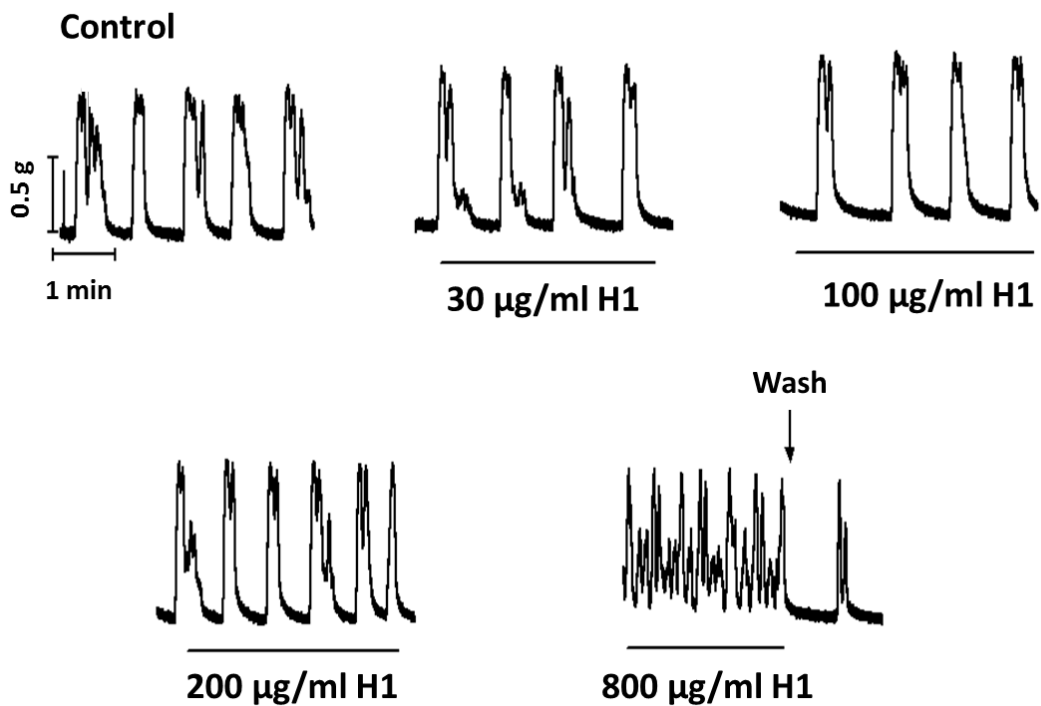


Figure 2.14 Representative tracing illustrating the effect of increasing cumulative concentrations of **H1** on lidocaine-induced contractions of the isolated mouse uterus.

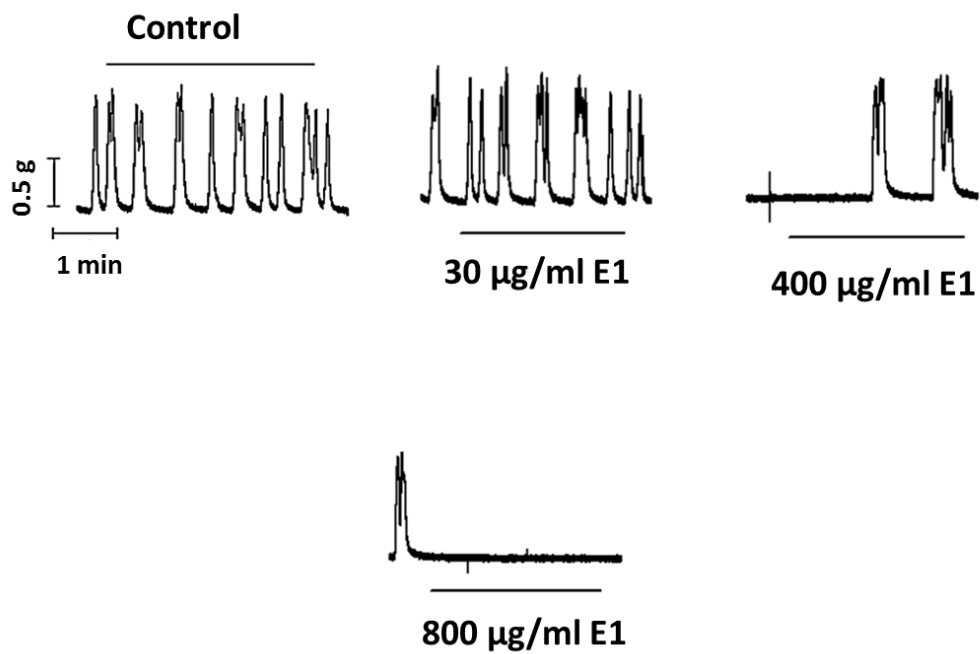


Figure 2.15 Representative tracing illustrating the effect of increasing cumulative concentrations of **E1** on lidocaine-induced contractions of the isolated mouse uterus.

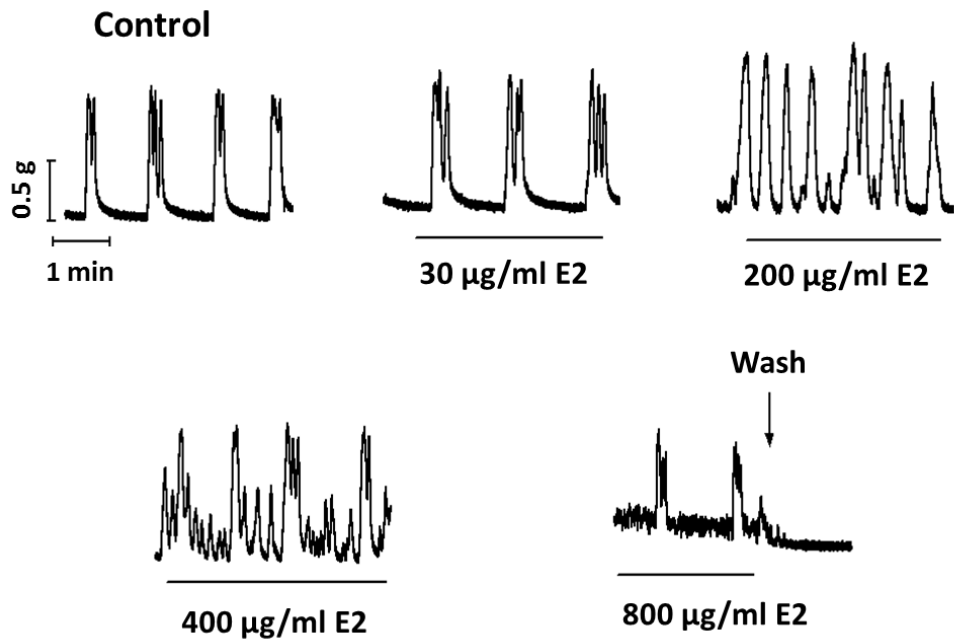


Figure 2.16 Representative tracing illustrating the effect of increasing cumulative concentrations of **E2** on lidocaine-induced contractions of the isolated mouse uterus.

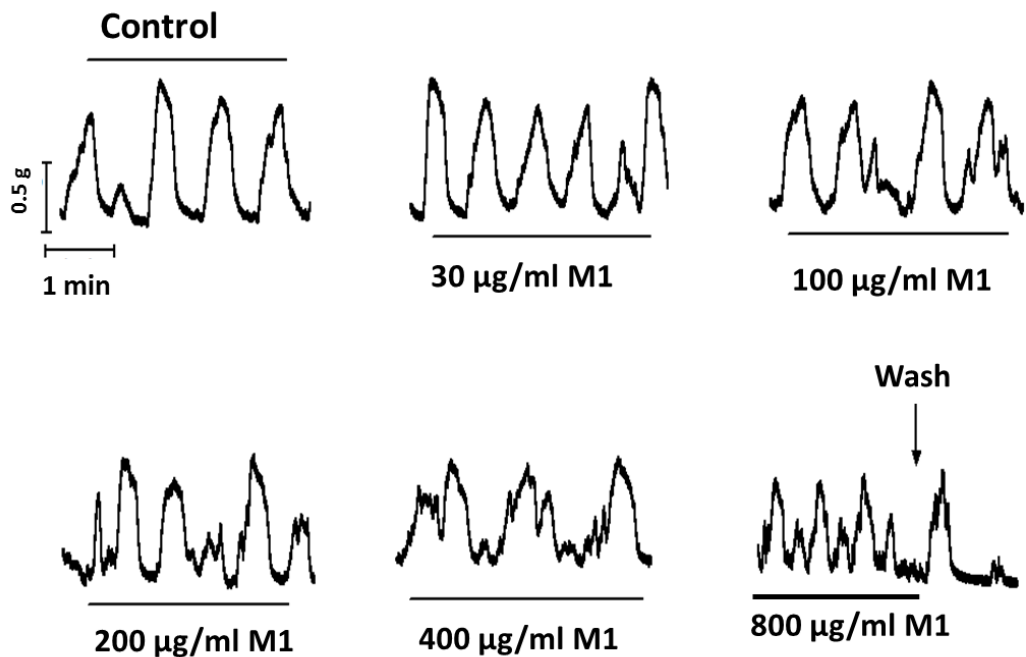


Figure 2.17 Representative tracing illustrating the effect of increasing cumulative concentrations of **M1** on lidocaine-induced contractions of the isolated mouse uterus.

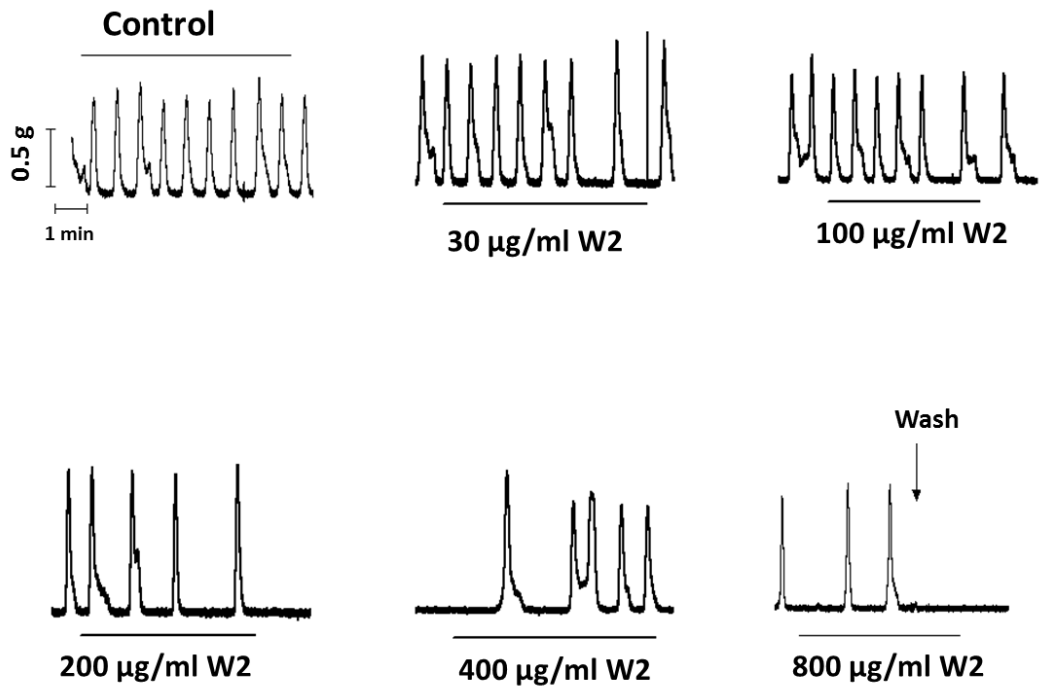


Figure 2.18 Representative tracing illustrating the effect of increasing cumulative concentrations of **W2** on lidocaine-induced contractions of the isolated mouse uterus.

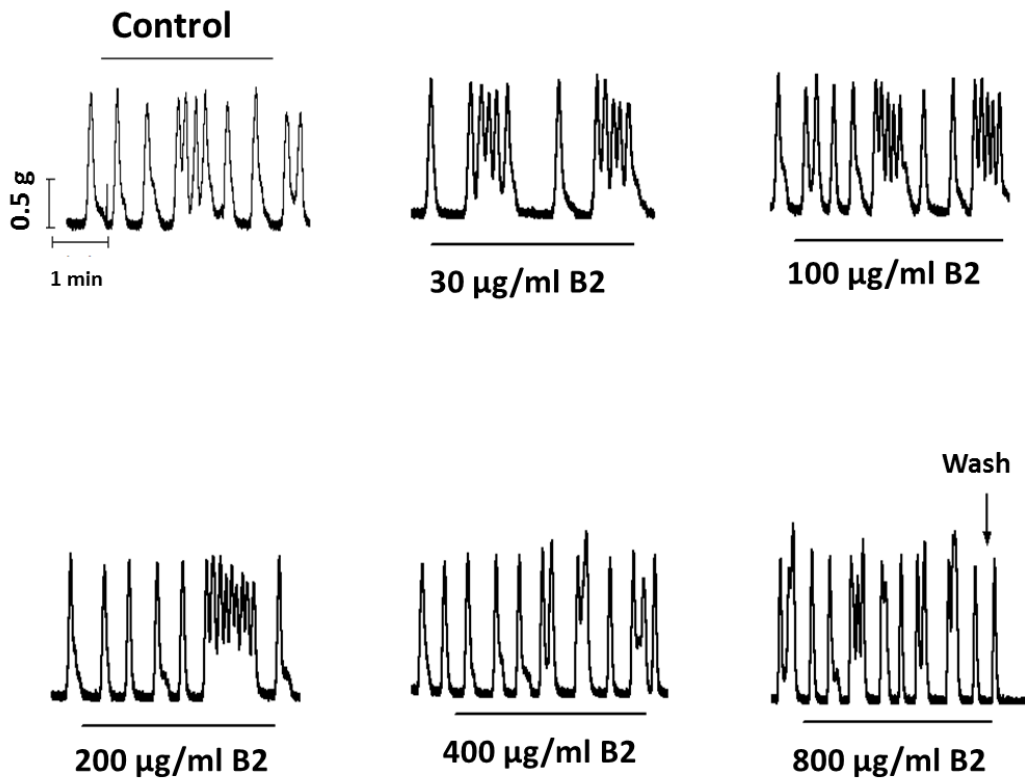


Figure 2.19 Representative tracing illustrating the effect of increasing cumulative concentrations of **B2** on lidocaine-induced contractions of the isolated mouse uterus.

Table 2.4 Effect of Extracts on the Frequency of Uterine Contraction (cycles/5 min)

Extracts	Concentration ($\mu\text{g/ml}$)					
	0	30	100	200	400	800
H1	12.75 \pm 0.85	12.5 \pm 0.28	12.5 \pm 0.47	13.25 \pm 0.47	17.25 \pm 0.47	20.5 \pm 0.50 [#]
E1	12.0 \pm 1.08	8.75 \pm 0.62*	8.75 \pm 1.25*	6.25 \pm 0.47**	5.25 \pm 0.47**	0.75 \pm 0.47 **
E2	12.4 \pm 1.54	12.6 \pm 1.29	11.4 \pm 1.36	14.2 \pm 1.16	18.4 \pm 2.04*	18.0 \pm 1.56*
M1	10.5 \pm 0.22	15.5 \pm 0.22*	19.5 \pm 0.67**	21.0 \pm 0.23**	29.0 \pm 1.56**	31.5 \pm 2.46**
B2	7.75 \pm 0.25	8.25 \pm 0.45	10.25 \pm 0.63*	10.5 \pm 0.64**	8.75 \pm 0.63	7.75 \pm 0.63
W2	6.6 \pm 0.92	8.2 \pm 0.73	9.0 \pm 1.26	10.8 \pm 0.86*	7.6 \pm 0.92	6.8 \pm 0.58

A table of the activity of *F. exasperata* (FE) extracts on the contraction frequency of the isolated mouse uterus at different concentrations. # represents 2 experiments; * $p < 0.05$; ** $p < 0.01$; n=5-6 experiments.

Table 2.5 Effect of Extracts on the Amplitude of Uterine Contraction (g)

Extracts	Concentrations (µg/ml)					
	0	30	100	200	400	800
H1	1.15 ± 0.14	0.99 ± 0.16	0.95 ± 0.13	0.87 ± 0.10	0.74 ± 0.09*	0.88 ± 0.10 [#]
E1	0.87 ± 0.07	0.64 ± 0.06*	0.57 ± 0.06**	0.52 ± 0.04**	0.44 ± 0.06**	0.07 ± 0.40**
E2	1.38 ± 0.17	1.30 ± 0.23	1.21 ± 0.25	1.15 ± 0.29	1.01 ± 0.32*	0.92 ± 0.16*
M1	0.88 ± 0.82	0.81 ± 0.52	0.75 ± 0.20*	0.59 ± 0.34**	0.42 ± 0.31**	0.38 ± 0.22**
B2	0.56 ± 0.11	0.64 ± 0.13	0.79 ± 0.13	0.55 ± 0.17	0.48 ± 0.27	0.49 ± 0.19
W2	0.79 ± 0.13	0.81 ± 0.15	0.87 ± 0.14	1.33 ± 0.11*	0.97 ± 0.29	0.87 ± 0.11

A table of the activity of **FE** extracts on the contraction amplitude of the isolated mouse uterus at different concentrations. # represents 2 experiments; * $p < 0.05$; ** $p < 0.01$; n=5-6 experiments.

Table 2.6 Effect of Extracts on the AUC of Uterine Contraction (g.s)

Extract	Concentrations ($\mu\text{g/ml}$)					
	0	30	100	200	400	800
H1	356.6 \pm 10.38	346.21 \pm 14.0	329.4 \pm 9.47	313.8 \pm 5.62*	386.4 \pm 4.60**	238.05 \pm 32.2#
E1	279.4 \pm 2.54	272.6 \pm 1.05	245.8 \pm 1.15	224.0 \pm 4.7*	194.3 \pm 5.24**	47.5 \pm 2.5**
E2	219.3 \pm 5.66	200.0 \pm 4.23	143.5 \pm 2.91*	144.3 \pm 4.9**	187.9 \pm 10.67**	146.8 \pm 3.35**
M1	297.1 \pm 5.99	310.9 \pm 6.72	309.2 \pm 6.36	320.8 \pm 7.54*	323.5 \pm 6.59*	325.2 \pm 5.08*
B2	228.7 \pm 5.25	188.5 \pm 8.9	154.7 \pm 3.69*	151.6 \pm 13.0**	141.0 \pm 15.08**	129.9 \pm 14.15**
W2	260.7 \pm 4.75	254.7 \pm 2.13	259.3 \pm 5.02	250.3 \pm 3.51	237.0 \pm 3.53**	211.1 \pm 3.97**

A table of the activity of **FE** extracts on the isolated uterus at different concentrations, calculated as integrals. # represents 2 experiments; * $p < 0.05$; ** $p < 0.01$; n=5-6 experiments.

2.7.7 Identification of Chemical Constituents

Several phytochemical classes of secondary metabolites were identified. Some of the compounds were isolated as mixtures and due to the low yield in some cases, further purification and/or pharmacological characterization was not possible.

2.7.7.1 Fatty Acids, Glycerol Esters and Glycerol Derivatives

Fractions 11-13Ea and Fr. 14-16 Ea, were identified as containing compounds from the fatty acid class of secondary plant metabolites. Fractions 11-13Ea yielded brownish-yellow oil which was solid on standing (1.14 g). It was identified via LC-HRESI-MS to contain a mixture of hexadecanoic acid ($[M+1]^+$ peak at m/z 257.2578, corresponding to a molecular formula of $C_{16}H_{33}O_2$) (Fig. 2.20) and gamma linolenic acid ($[M+1]^+$ peak at m/z 279.2324, corresponding to a molecular formula of $C_{18}H_{31}O_2$) (Fig. 2.21). The 1H -NMR is shown in figure 2.22. The compounds were also identified by comparing the spectral data with the literature (Joshi *et al.*, 2009).

Fractions 14-16Ea were pooled, given the broad name 14Ea and identified as consisting of glycerol 1,3 dilinolein (**1**) ($[M+1]^+$ peak at m/z 617.5139, corresponding to a molecular formula of $C_{39}H_{69}O_5$) (Fig. 2.23). 1H -NMR (400 MHz, CHLOROFORM-D) δ 5.44 – 5.25 (m, 4H), 4.13 (dd, $J = 14.4, 7.1$ Hz, 1H), 2.78 (dt, $J = 14.5, 6.4$ Hz, 2H), 2.64 (s, OH), 2.33 (t, $J = 7.4$ Hz, 2H), 2.16 (s, OH), 2.09 – 1.97 (m, 4H), 1.63 (dd, $J = 14.9, 7.7$ Hz, 1H), 1.24 (s, 24H), 0.96 (t, $J = 7.7$ Hz, 3H) (Fig. 2.24, 2.25 and 2.26). It was also identified by comparing the spectral data with the literatures (Cai *et al.*, 2013; Wang *et al.*, 2001).

The compound 3-O-glycerolacetate (**2**) was isolated and identified from Fraction 37Ea. The compound exhibited an $[M+1]^+$ peak at m/z 135.0652 corresponding to the molecular formula $C_5H_{11}O_4$ (Fig. 2.27). 1H NMR (400 MHz, CHLOROFORM-D) δ 4.17 (dd, $J = 12.0, 4.0$ Hz, 1H), 4.14 (d, $J = 12.0, 4.0$ Hz, 1H), 3.93 (m, 1H), 3.69 (dd, $J = 12.0, 4.0$ Hz, 1H), 3.59 (dd, $J = 12.0, 4.0$ Hz, 1H), 2.09 (s, 3H) (Fig. 2.28, 2.29). To our knowledge this is the first report of the isolation of 3-O-glycerolacetate in plants.

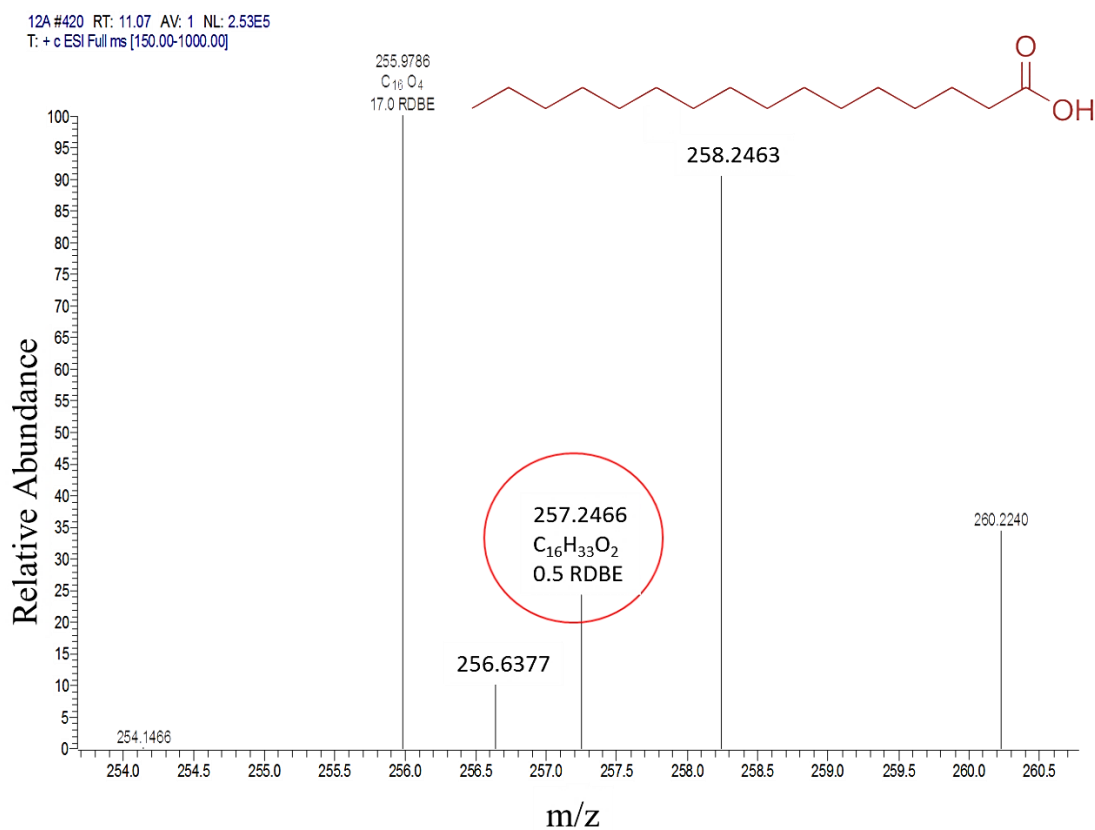


Figure 2.20 HRESI-MS showing the relative abundance (y-axis) and the m/z (x-axis) of hexadecanoic acid. The corresponding molecular structure is embedded at the top.

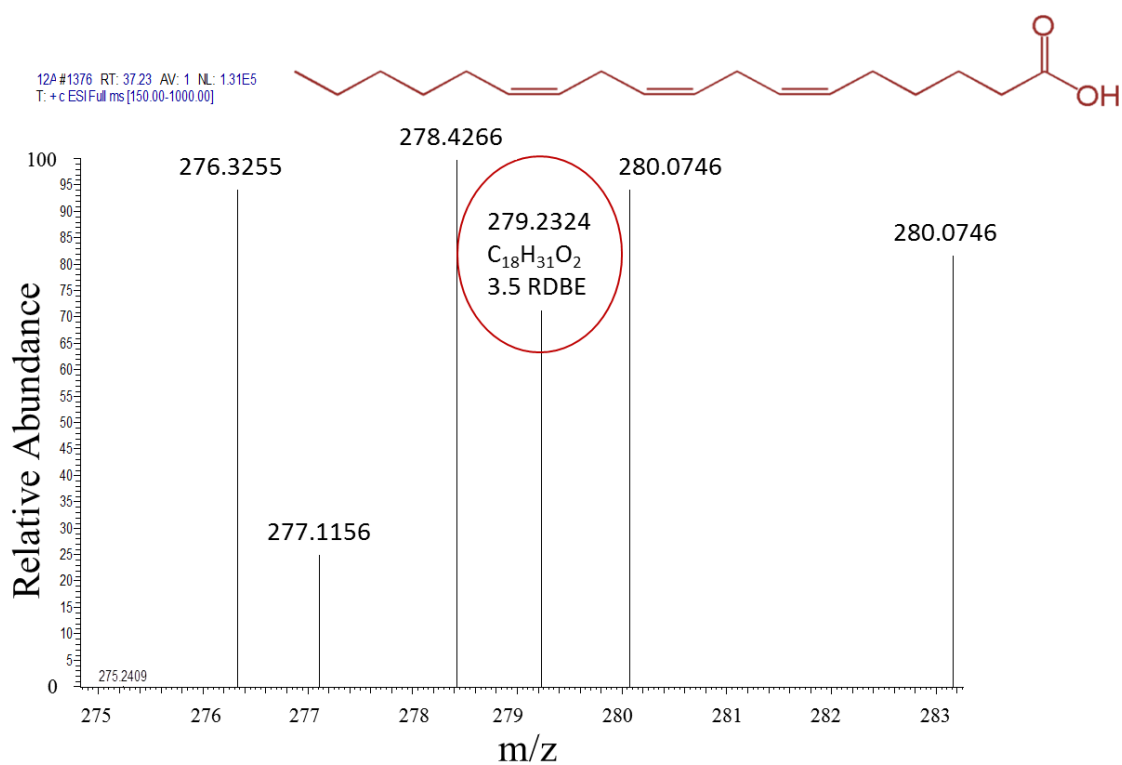


Figure 2.21 HRESI-MS showing the relative abundance (y-axis) and the m/z (x-axis) of gammalinolenic acid. The corresponding molecular structure is embedded at the top of the figure.

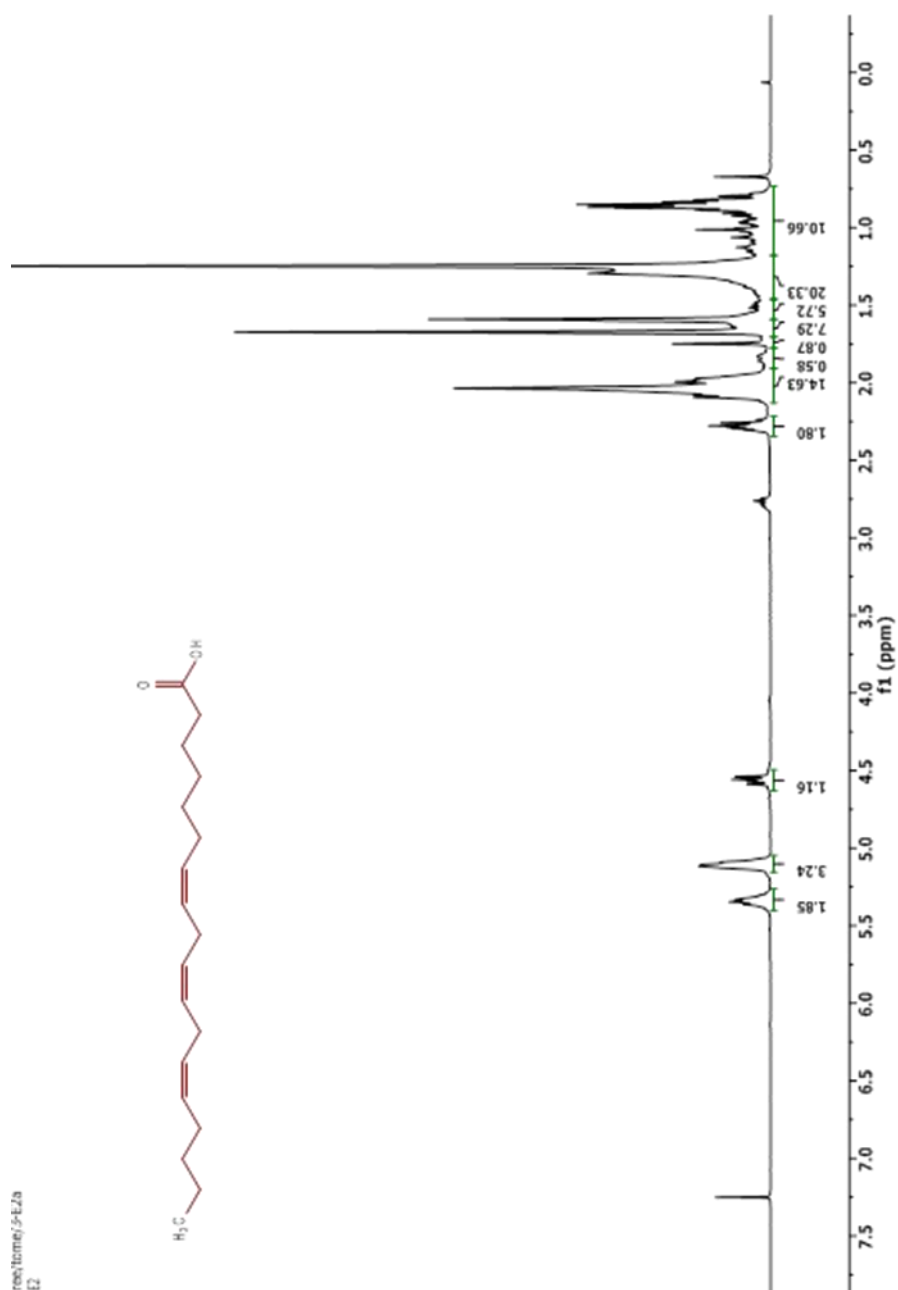


Figure 2.22 The 1D ¹H-NMR spectrum of gamma-linolenic acid which is observed as the major compound in this fraction and occurs between 0.0 – 2.5 ppm, the presence of the minor compounds can be observed, the peak at 4.5 ppm belonging to linoleic acid and the peaks at 5.10 and 5.34 ppm belonging to octadecadienoic acid.

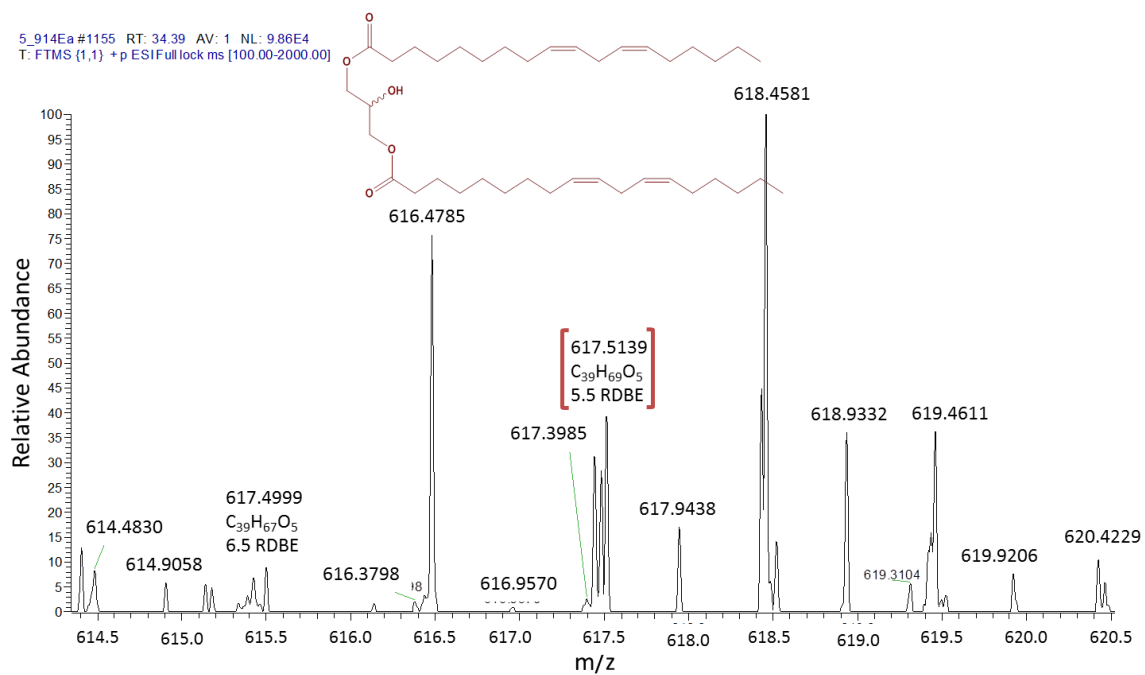


Figure 2.23 HRESI-MS showing the relative abundance (y-axis) and the m/z (x-axis) of compound **1** (molecular formula and m/z in red brackets). The corresponding molecular structure is embedded at the top of the figure.

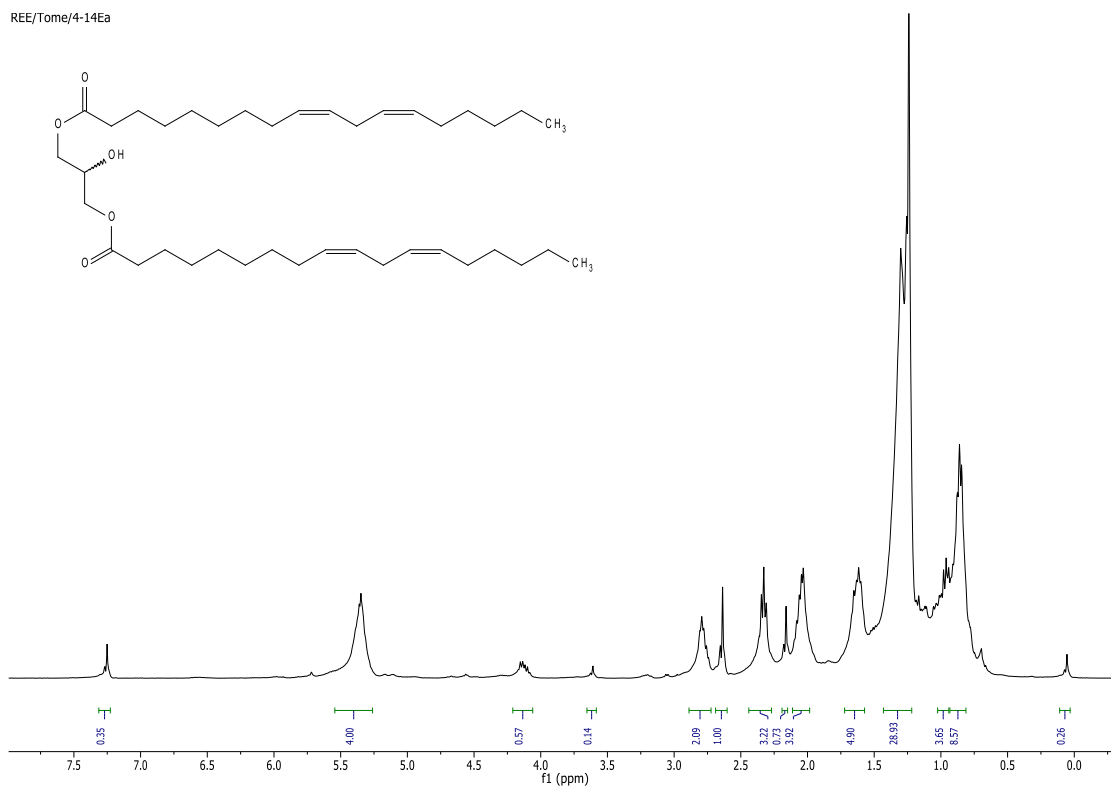


Figure 2.24 The 1D ¹H-NMR spectrum of **Fr. 4-14Ea** in CDCl₃ showing the presence of dilinolein (compound **1**).

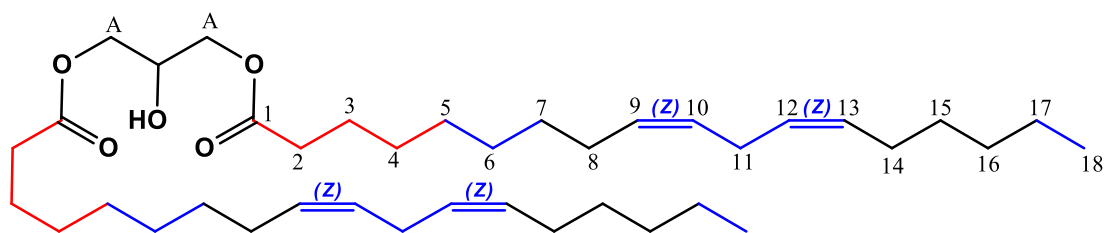
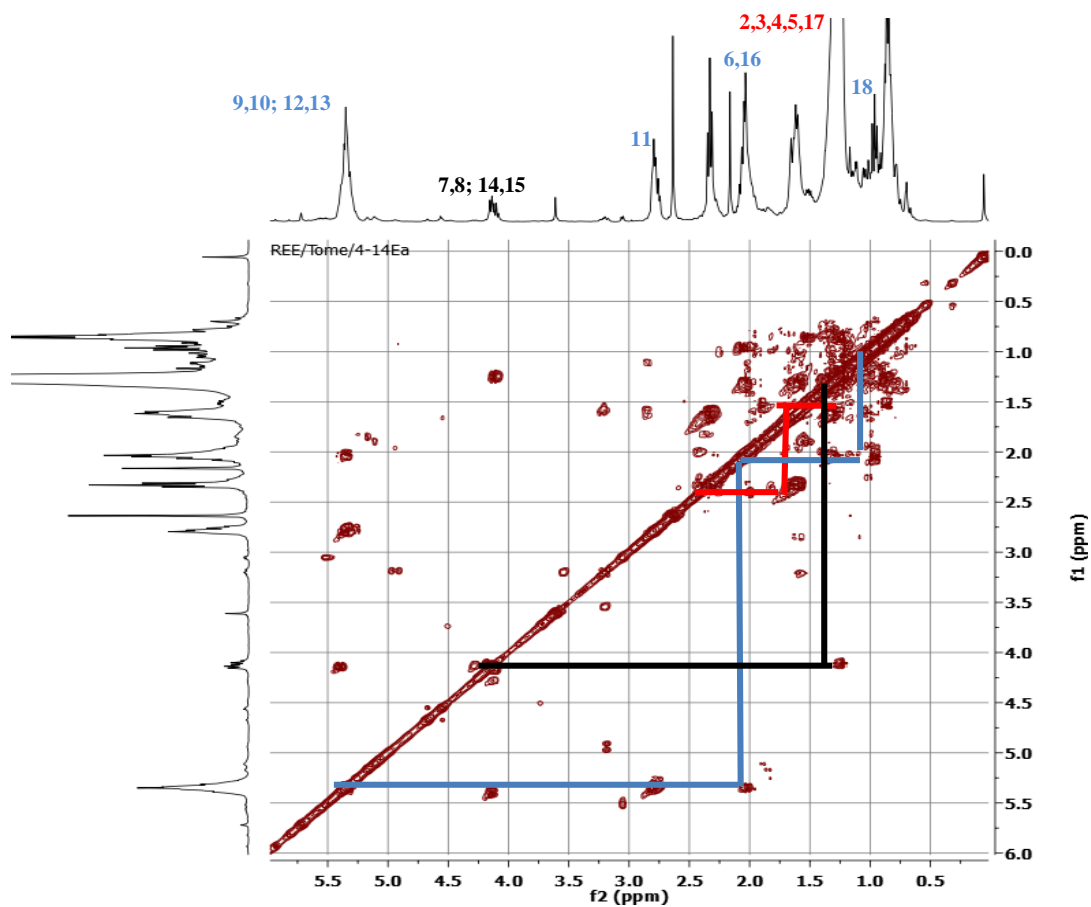


Figure 2.25 2D COSY ^1H -NMR spectra of **Fr.4-14Ea** in CDCl_3 showing the bond correlations within dilinolein (compound **1**). The coloured lines indicate the spin systems within the structure and each colour represents a different spin system.

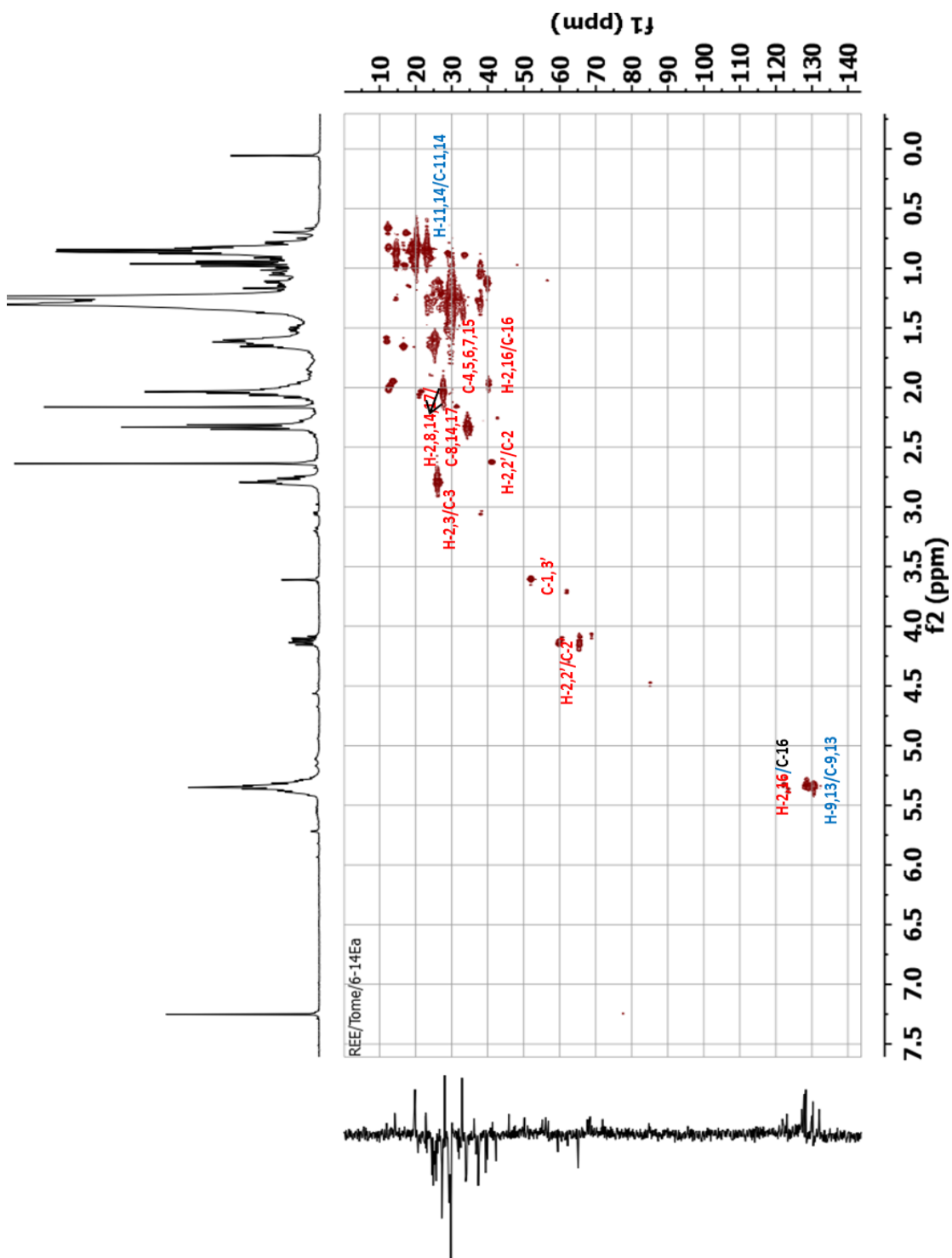


Figure 2.26 HMQC spectrum of compound **1** in CDCl_3

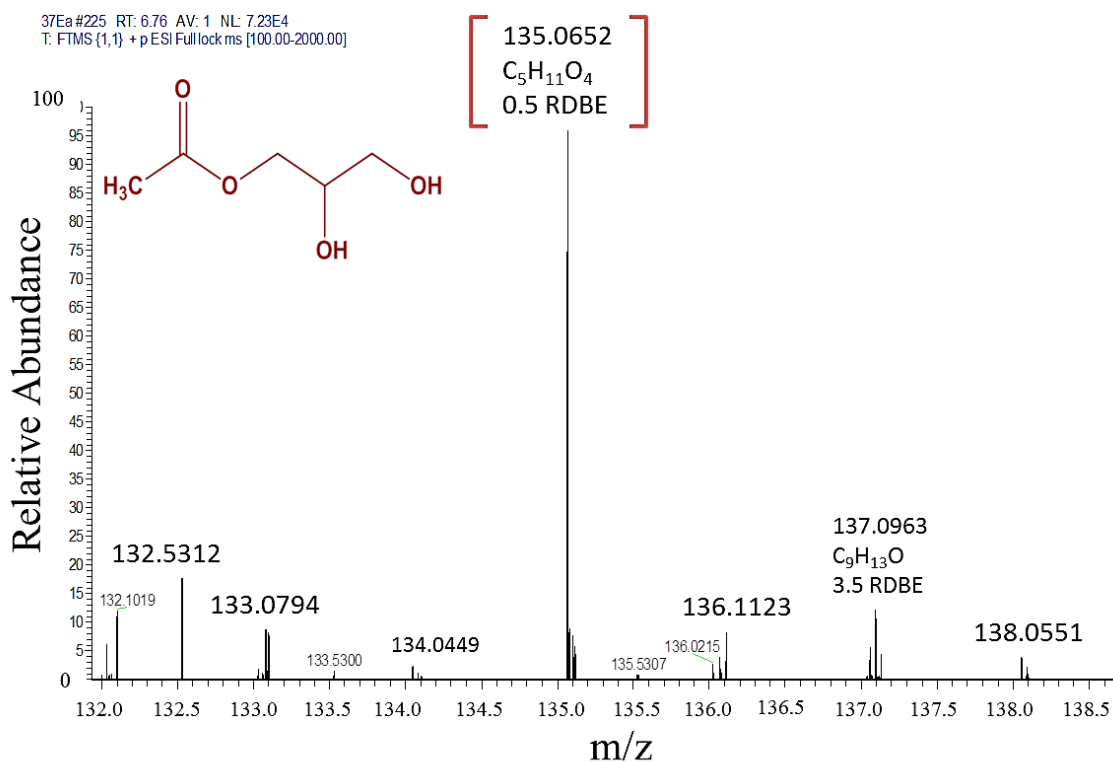


Figure 2.27 HRESI-MS showing the relative abundance (y-axis) and the m/z (x-axis) of compound **2** (chemical formula and m/z in red brackets). The corresponding molecular structure is embedded at the top left corner.

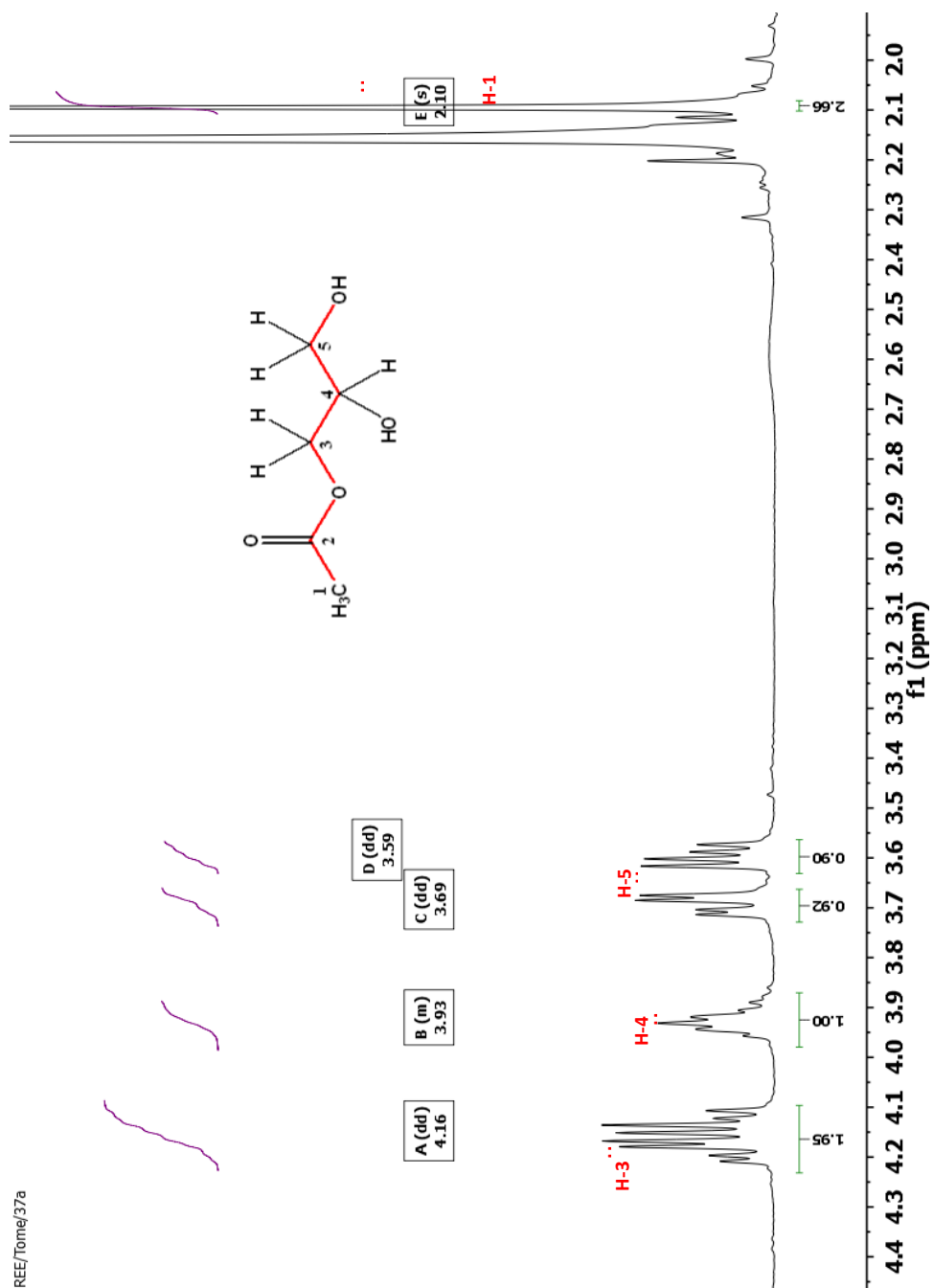


Figure 2.28 The 1D ^1H -NMR spectrum of compound **2** in CDCl_3 . Red lines in the structure corresponds with the protons designated in red fonts in the figure.

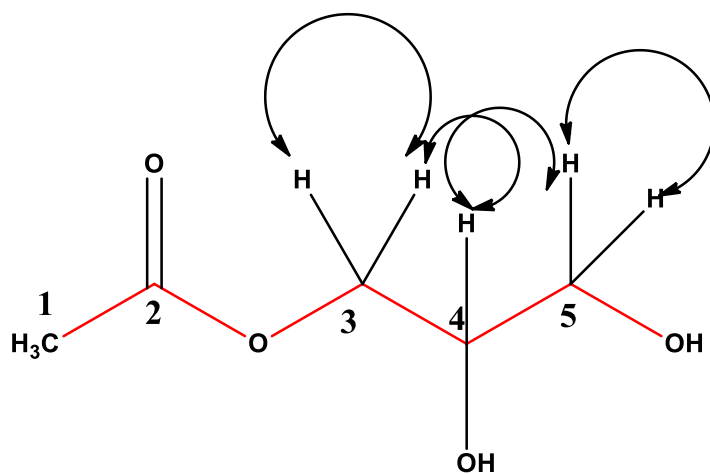
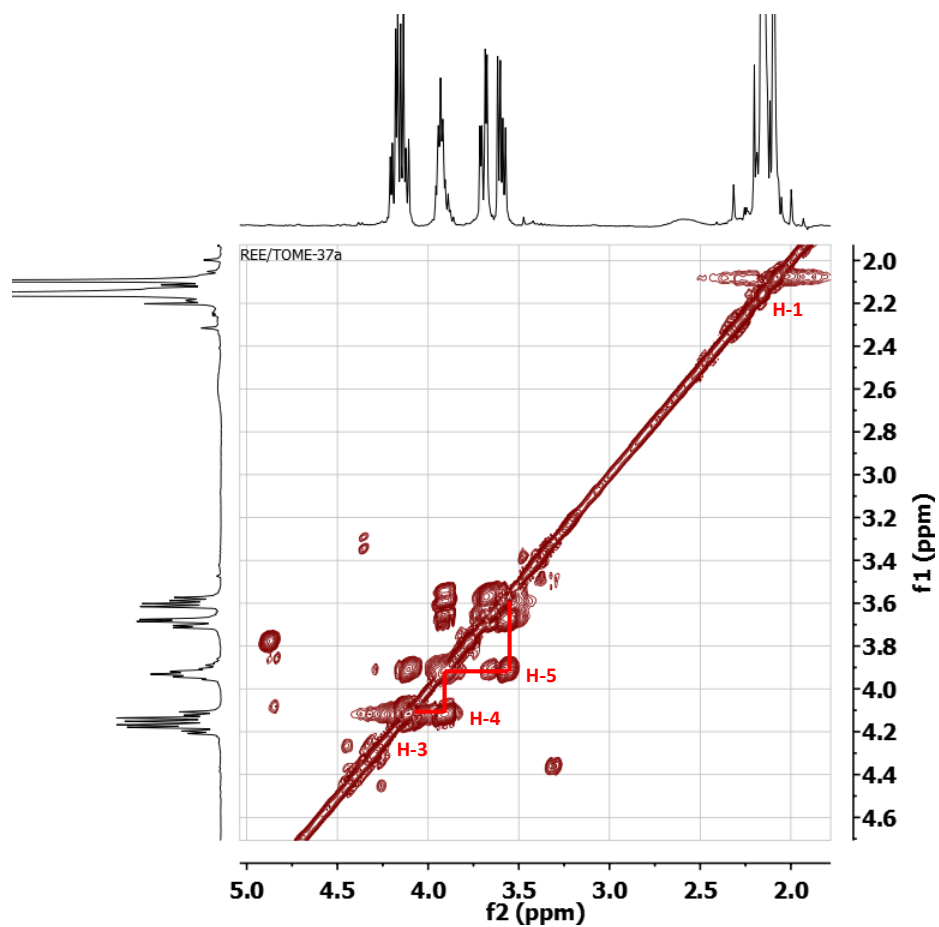


Figure 2.29 An expanded portion of the COSY ^1H -NMR spectrum of compound **2** in CDCl_3 showing the bond correlations within the structure indicated by the red lines.

2.7.7.2 Pheophorbide and Pheophytin Derivatives

New pheophorbides of the a-derivative (**3** and **4**) as well as pheophorbide-a (**5**) and b derivatives (listed below) were identified from fractions 17-24 of **E1a** and fractions 13-19 of **E2a**. Pyropheophorbide a (**6**) was isolated as a greenish black solid. The new pheophorbide-b derivatives (compounds **7**, **8** and **9**) were isolated and identified as dark brown solids. The ¹H-NMR spectrum of the pheophorbide compounds showed characteristic signals of a porphyrin skeleton, which includes: the three methyl groups directly connected to the conjugated ring system at δ 3 – 4 ppm, a vinyl group (δ 6-8 ppm), and three meso-olefinic singlets at δ 8.5-9.9 ppm (Kamarulzaman *et al.*, 2011). The HRESIMS of compound **3** exhibited a [M+H]⁺ peak at *m/z* 869.5582 corresponding to a molecular formula of C₅₅H₇₃N₄O₅ (Fig. 2.30), compound **4** exhibited a [M+H]⁺ peak at *m/z* 607.2917 corresponding to a molecular formula of C₃₆H₃₉N₄O₅ (Fig. 2.31) and compound **5** exhibited a [M+H]⁺ peak at *m/z* 593.2754 corresponding to a molecular formula of C₃₅H₃₇N₄O₅ (Fig. 2.32). Compound **6** exhibited a [M+H]⁺ peak at *m/z* 535.2704 corresponding to a molecular formula of C₃₃H₃₅N₄O₃ (Fig. 2.33). The primary differences between compounds **3** and **4** were due to the presence of a phytol group (C₂₂H₄₂) on position R₄ in **3** and a methyl group (CH₃) on position R₄ in **4**. While the primary modification between these and pheophorbide-a occurred in the 13² position due to the presence of the COOCH₃ group in pheophorbide-a and its absence in **3** and **4**. The ¹H NMR spectra of **3**, **4**, **5** and **6** showed three aromatic singlet protons and an aromatic doublet of doublets (dd) at δ 7-10, consistent with those of the methyl and methane groups of pheophorbide a derivatives (Fig. 2.34, 2.35). Compounds **7**, **8** and **9** were eluted as a mixture and proved difficult to separate despite several MPLC and

silica open column chromatographic procedures using hexane and ethyl acetate as eluents. The HRESI-MS data of **7** exhibited a peak at m/z $[M+H]^+$ 635.2863 consistent with the molecular formula of $C_{37}H_{39}N_4O_6$ (Fig. 2.36) while that of compound **8** was at m/z $[M+H]^+$ 885.5511 consistent with the molecular formula of $C_{55}H_{73}N_4O_6$ (Fig. 2.37). Compound **9** exhibited a peak at m/z $[M+H]^+$ 607.2554 corresponding to the molecular formula of $C_{35}H_{35}N_4O_6$ (Fig. 2.38). 1H -NMR of **7**, **8** and **9** showed the distinguishing signals of pheophorbide-b derivatives at ca. δ_H 11.0 (s) corresponding to δ_C 187.8, assignable to a CHO group at position C-7¹ (Fig 2.39 and Fig. 2.40) and as previously described in the literature (Kamarulzaman *et al.*, 2011). Further assignments of 1H and ^{13}C NMR are outlined in Table 2.7 and Table 2.8. The main differences between all three compounds stemmed from composition of the phytyl chain at position 17¹. Compound **7** possessed a propylene group at position 17¹; compound **8** possessed a long chain carbonyl group at the same position while compound **9** possessed a methylene group at that position. These differences were obtained from mass spectrometric analysis and screening. The close similarities in their structures may have been responsible for the difficulty experienced in separating them into singular compounds.

Generally, the distinguishing features of the new analogues of pheophorbides in comparison with previously identified pheophorbide derivatives are the ethyl group in position 8¹ replaced by a methyl group; and the presence of a carboxyl group at position 13² instead of a carboxylic ester or a proton.

Table 2.7 ¹H NMR (400 MHz) data of compounds **3-9** in CDCl₃.

Position	3	4	5	6	7	8	9
2¹	3.20 (s)	3.22 (s)	3.22 (s)	3.38 (s)	3.36 (s)	3.38 (s)	3.38 (s)
3¹	7.96 (dd)	7.96 (dd)	7.96 (dd)	7.96 (dd)	7.97 (dd)	8.02 (dd)	8.02 (dd)
3^{2a}	6.16 (d)	6.16 (d)	6.17 (d)	6.14 (d)	6.30 (dd)	6.30 (dd)	6.30 (dd)
3^{2b}	6.27 (d)	6.27 (d)	6.31 (d)	6.25 (d)	6.55 (dd)	6.55 (dd)	6.55 (dd)
5	9.36 (s)	9.37 (s)	9.38 (s)	9.32 (s)	10.30 (s)	10.23 (s)	10.23 (s)
7¹	3.39 (s)	3.37 (s)	3.39 (s)	3.19 (s)	11.08 (s)	11.03 (s)	11.03 (s)
8¹	3.89 (s)	3.81 (s)	3.71 (q)	3.63 (q)	3.86 (s)	3.95 (s)	3.95 (s)
8²	-	-	1.65 (m)	1.66 (t)	-	-	-
10	9.49 (s)	9.51 (s)	9.51 (s)	9.43 (s)	9.44 (s)	9.50 (s)	9.50 (s)
12¹	3.67 (s)	3.65 (s)	3.68 (s)	3.61 (s)	3.64 (s)	3.65 (s)	3.65 (s)
13²	-	-	6.25 (s)	-	5.15 (m)	5.15 (m)	5.15 (m)
13² a (B)	-	-	-	5.08 (d)	-	-	-
13² b (α)	-	-	-	5.28 (d)	-	-	-
17	4.21 (br d)	4.21 (br d)	4.28 (br d)	4.28 (br d)	4.28 (br d)	4.11 (br d)	4.11 (br d)
17^{1a}	2.35 (m)	2.35 (m)	2.35 (m)	2.20 (m)	2.36 (t)	2.36 (t)	2.36 (t)
17^{2a}	2.17 (m)	2.17 (m)	2.17 (m)	2.29 (m)	2.19 (s)	2.19 (s)	2.19 (s)
17^{2b}	2.45 (m)	2.45 (m)	-	2.56 (m)	2.06 (s)	2.06 (s)	2.06 (s)
17³	5.35 (m)	-	5.35 (m)	-	5.39 (m)	5.39 (m)	5.39 (m)
17⁴	0.99-1.24 (m)	-	-	-	-	0.99-1.24 (m)	-
18	4.47 (m)	4.47 (m)	4.44 (m)	4.47 (q)	4.44-4.48 (m)	4.44-4.48 (m)	4.44-4.48 (m)
18¹	1.80 (d)	1.80 (d)	1.73 (d)	1.80 (d)	1.86 (d)	1.86 (d)	1.86 (d)
20	8.55 (s)	8.55 (s)	8.54 (s)	8.53 (s)	8.53 (s)	8.55 (s)	8.55 (s)
NH	-1.65 (br s)	-1.46 (br s)	-1.64 (s)	0.06 (s)	-1.69 (br s)	-1.46 (br s)	-1.46 (br s)

Table 2.8 ^{13}C NMR (400 MHz) data of compounds **3** - **8** in CDCl_3 .*

Position	3	4	5	6	7	8
1	144.1	144.07	144.1	144.5	144.5	144.5
2	136.7	136.2	136.2	132.7	132.7	132.7
2¹	11.9	11.9	12.6	12.0	12.0	12.0
3	138.7	138.7	138.7	138.6	138.6	138.6
3¹	129.5	129.5	129.5	129.0	129.0	129.0
3²	123.3	123.3	123.3	138.5	138.5	138.5
4	136.6	136.6	136.6	151.7	151.7	151.7
5	98.0	98.0	98.0	138.7	138.7	138.7
6	136.4	136.4	136.4	133.4	133.4	133.4
7	138.0	138.0	138.0	132.5	132.5	132.2
7¹	11.6	11.6	11.6	187.8	187.8	187.8
8	142.4	142.4	142.4	158.1	158.1	158.1
8¹	17.9	17.9	17.9	20.0	20.0	20.0
9	147.4	147.4	147.4	148.0	148.0	148.0
10	104.9	104.9	104.9	107.4	107.1	107.1
11	136.1	136.1	136.1	137.6	137.6	137.6
12	148.6	148.6	148.6	139.8	139.8	139.8
12¹	12.6	12.6	12.6	12.7	12.7	12.8
13	132.7	132.7	132.7	130.5	130.5	130.5
13¹	190.3	190.3	190.3	-	-	-
13²	64.7	65.0	65.9	66.3	65.2	65.0
13²-R₃	170.2	170.2	170.1	65.1	-	-
15	105.0	105.0	105.6	106.1	105.0	102.0
16	167.5	167.5	167.5	161.5	160.5	160.5
17	52.0	52.0	52.0	52.0	52.0	52.0
17¹	41.7	41.7	41.7	30.4	30.4	31.9
17²	41.7	41.7	41.7	32.7	32.7	32.7
17³	172.5	172.53	172.5	-	-	-
17⁴	15.0-30.0	50.4	50.4	50.3	50.4	15.0-30.0
18	50.3	50.3	50.3	50.3	50.4	51.8
18¹	126.7	126.7	118.1	23.6	23.6	23.5
19	-	-	-	-	-	-
20	93.6	93.6	93.6	93.8	93.8	93.8

*Chemical shifts determined by HMBC and HMQC

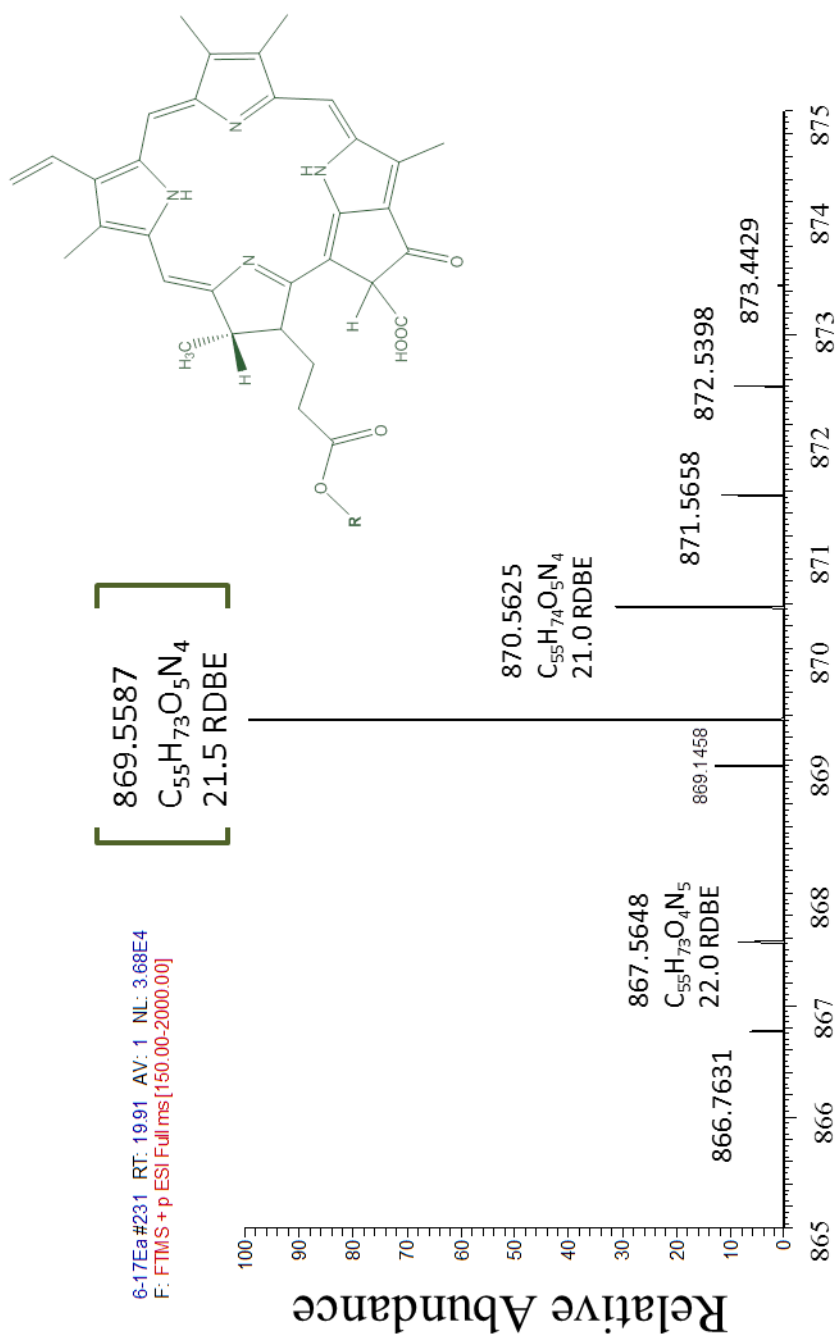


Figure 2.30 HRESI-MS chromatogram showing the relative abundance (y-axis) and the m/z (x-axis) of compound **3** (chemical formula and m/z indicated in green brackets). The corresponding molecular structure is embedded at the top right corner. R = C₂₂H₄₂.

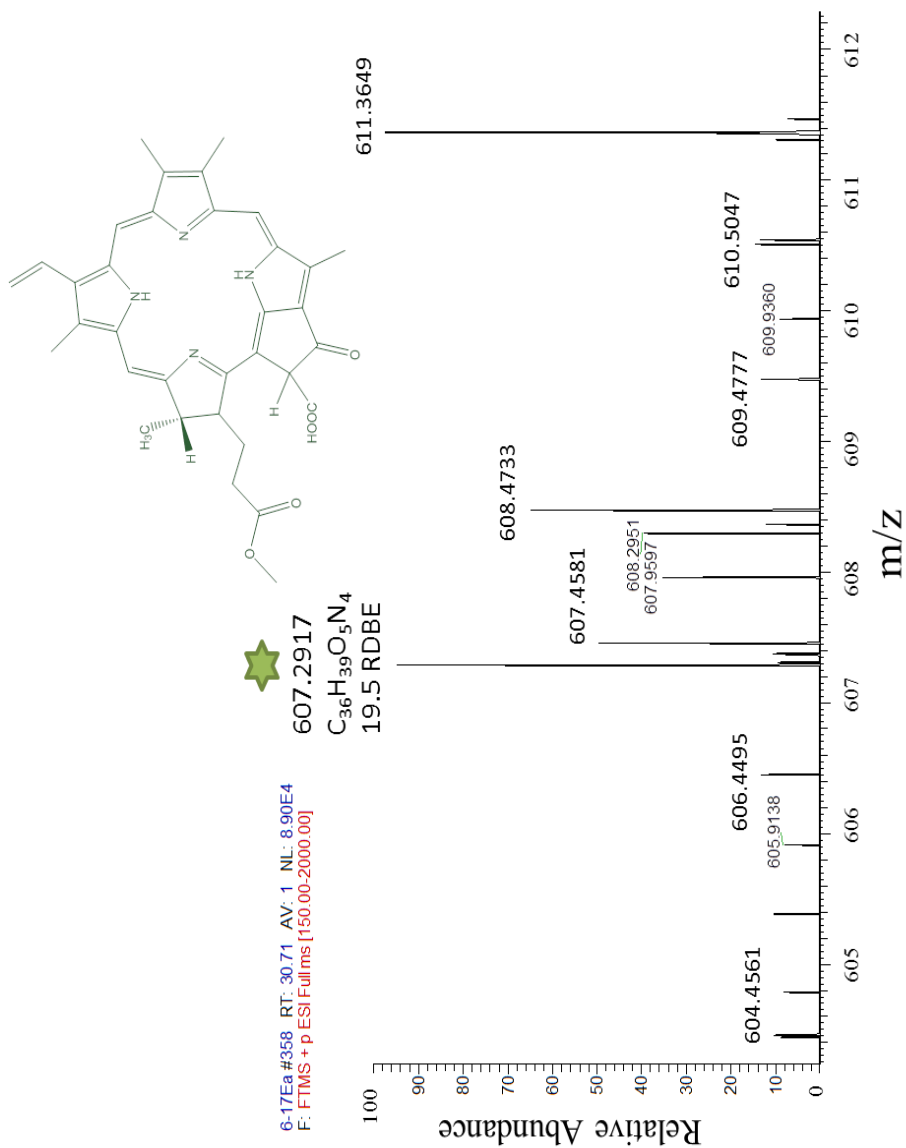


Figure 2.31 HRESI-MS chromatogram showing the relative abundance (y-axis) and the m/z (x-axis) of compound **4** (chemical formula and m/z indicated by the green asterisk). The corresponding molecular structure is embedded at the top right corner.

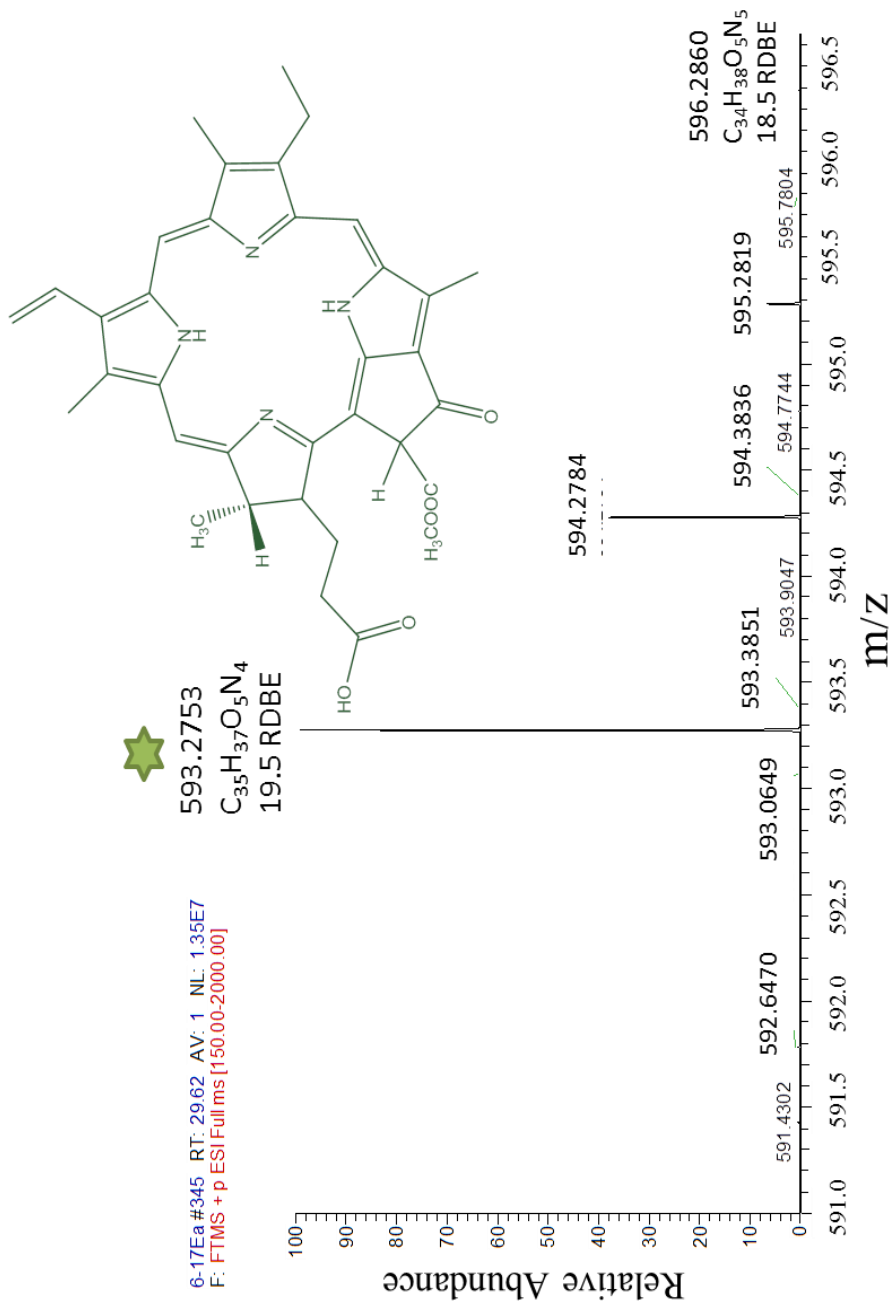


Figure 2.32 HRMSI-MS chromatogram showing the relative abundance (y-axis) and the m/z (x-axis) of compound **5** (chemical formula and m/z indicated by green asterisk). The corresponding molecular structure is embedded at the top right corner.

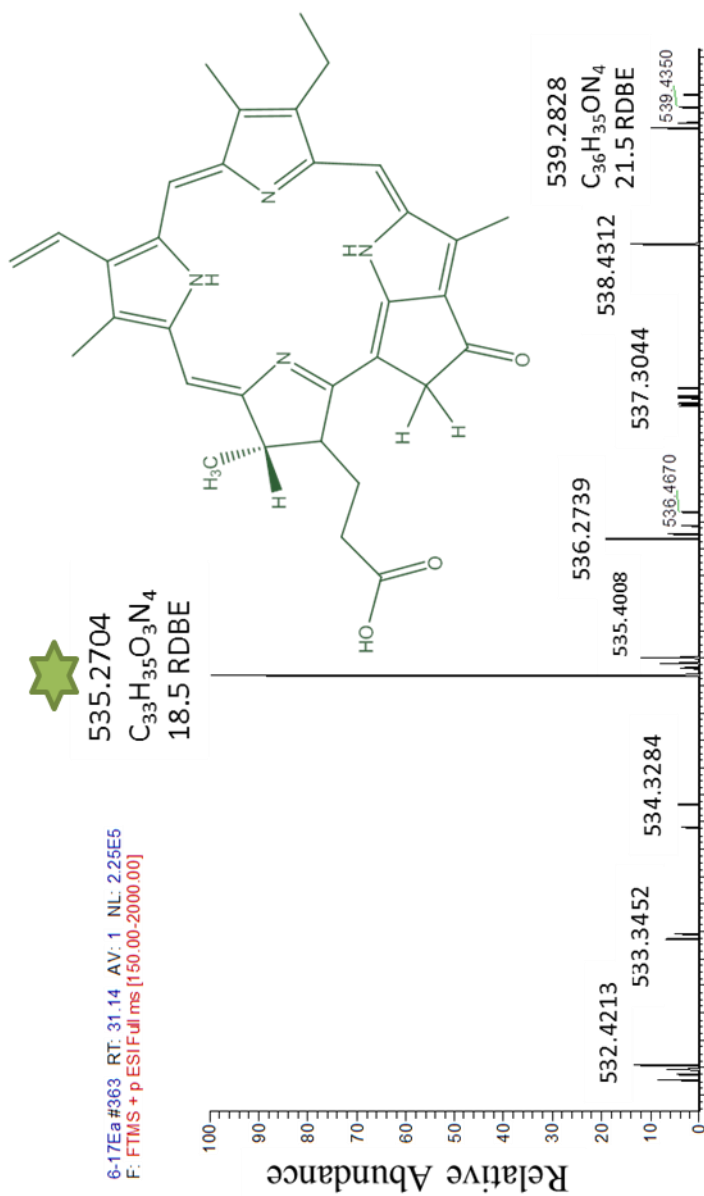


Figure 2.33 HRESI-MS chromatogram showing the relative abundance (y-axis) and the m/z (x-axis) of compound **6** (chemical formula and m/z indicated by green asterisk). The corresponding molecular structure is embedded at the top right corner.

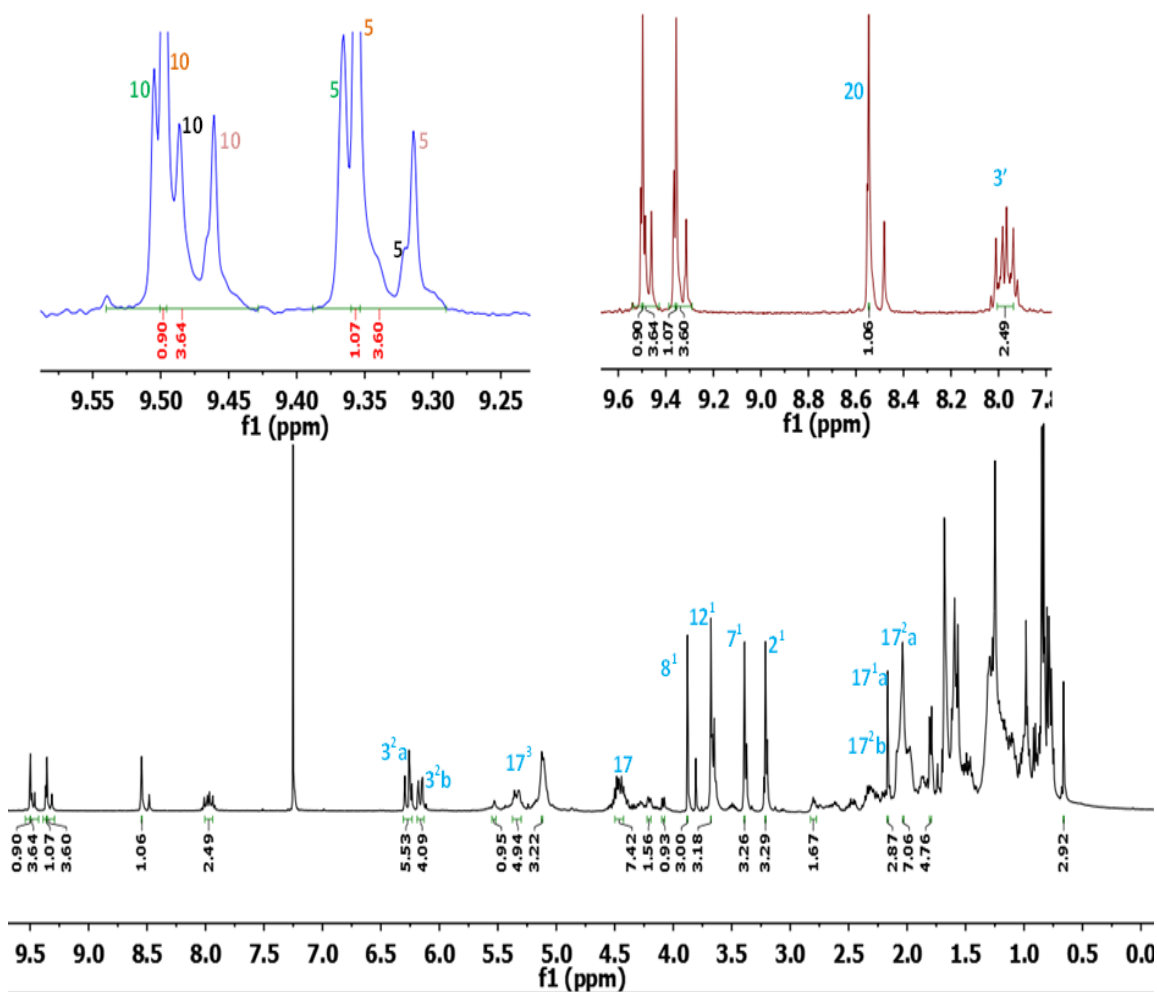


Figure 2.34 $^1\text{H-NMR}$ spectrum of pheophytin-a derivatives measured in CDCl_3 at 400MHz.

The different assignments are depicted in the figure. The expanded spectra highlights the distinguishing assignments; **green assignments** = compound **5**, **orange assignments** = compound **4**, **black assignments** = compound **3**, **pink assignments** = compound **6**, **blue assignments** = shared assignments among the compounds. The ratio of the compounds calculated from the integrals was computed for 17.8:46.5:14.9:18.6 respectively in percentages.

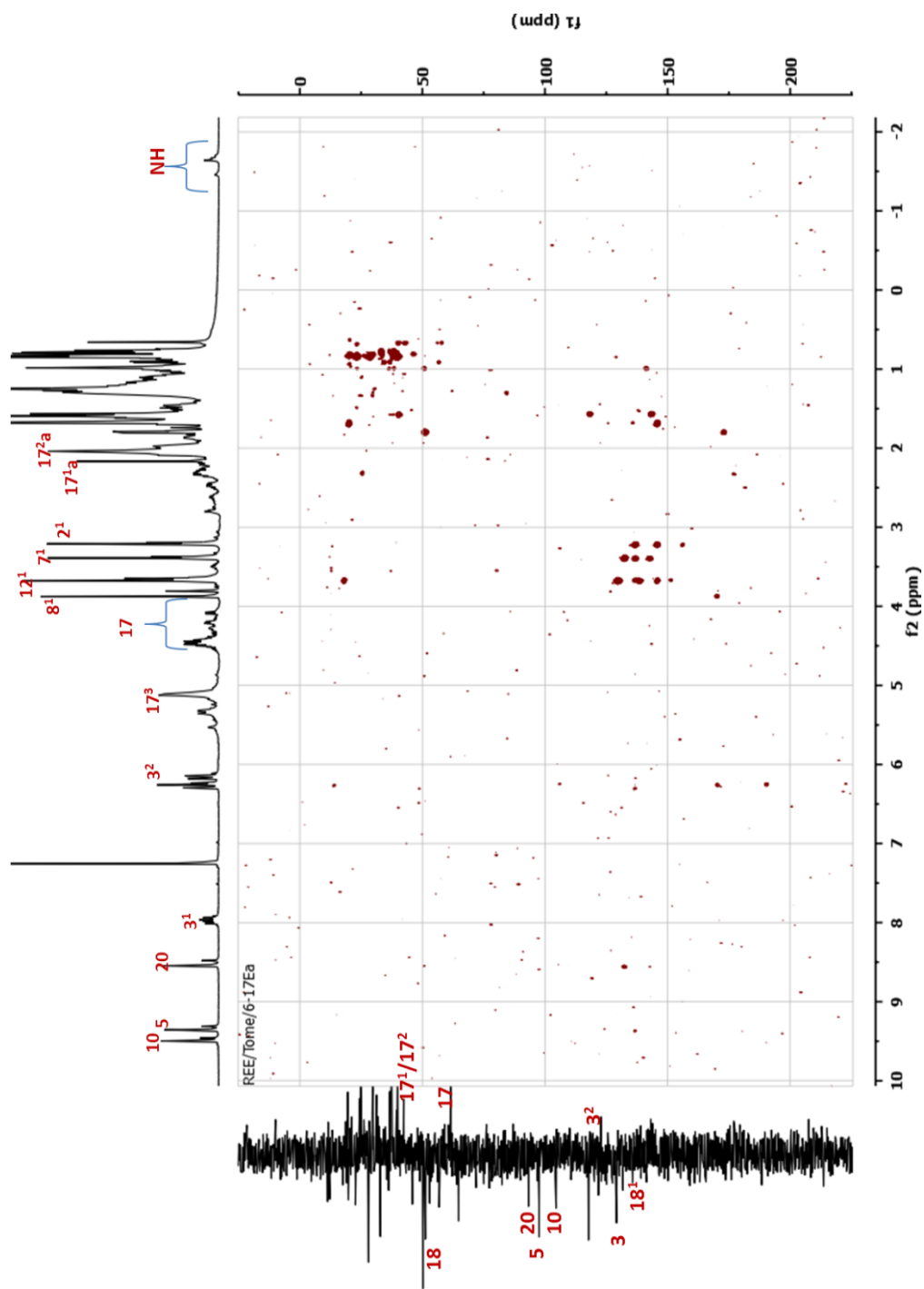


Figure 2.35 HMBC spectrum of pheophytin derivatives in CDCl_3 at 400 MHz. The carbon and proton assignments are outlined in Table 2.7 and 2.8

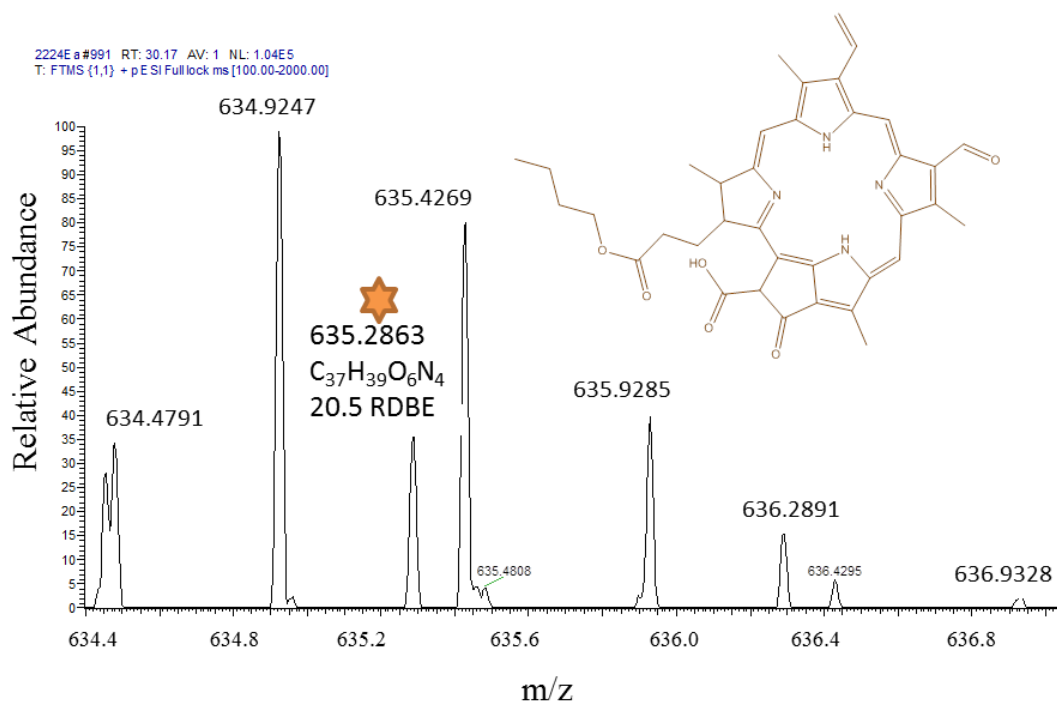


Figure 2.36 HRESI-MS chromatogram showing the relative abundance (y-axis) and the m/z (x-axis) of and molecular structure of compound **7** (chemical formula and m/z indicated by the brown-coloured asterisk).

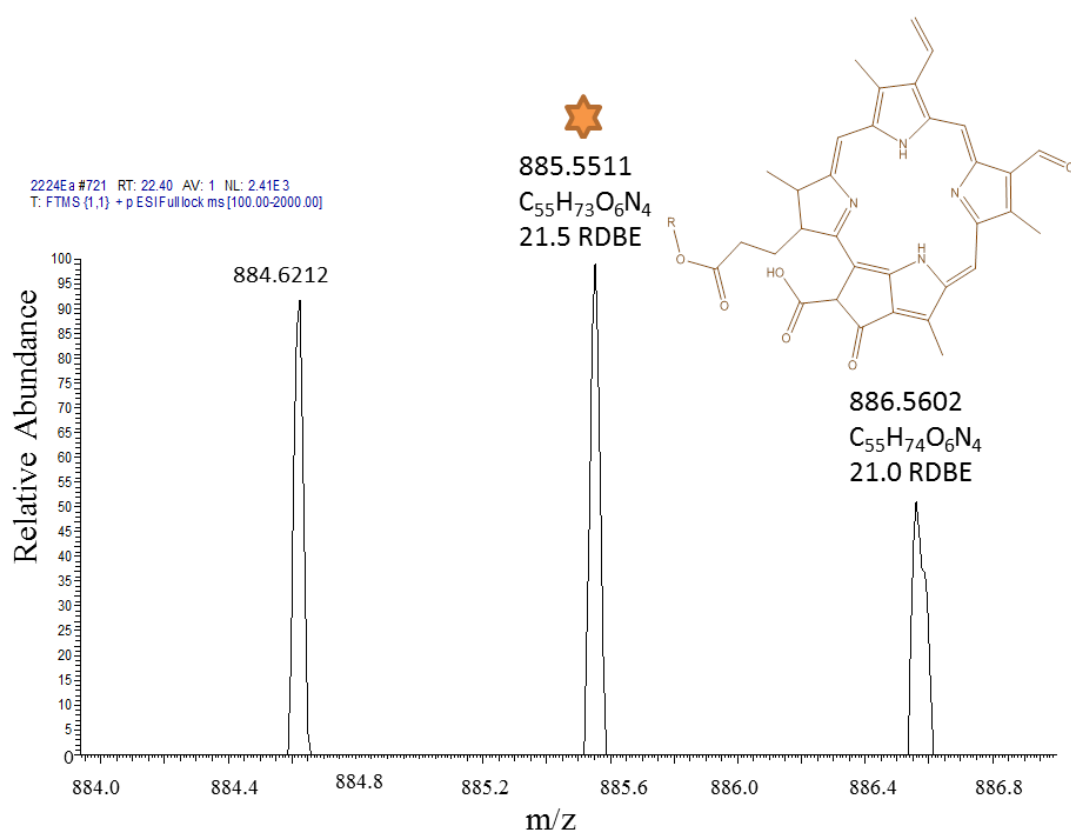


Figure 2.37 HRESI-MS chromatogram showing the relative abundance (y-axis), the m/z (x-axis) and the molecular structure of compound **8** (chemical formula and m/z indicated by the brown-coloured asterisk). R = C₂₁H₄₂.

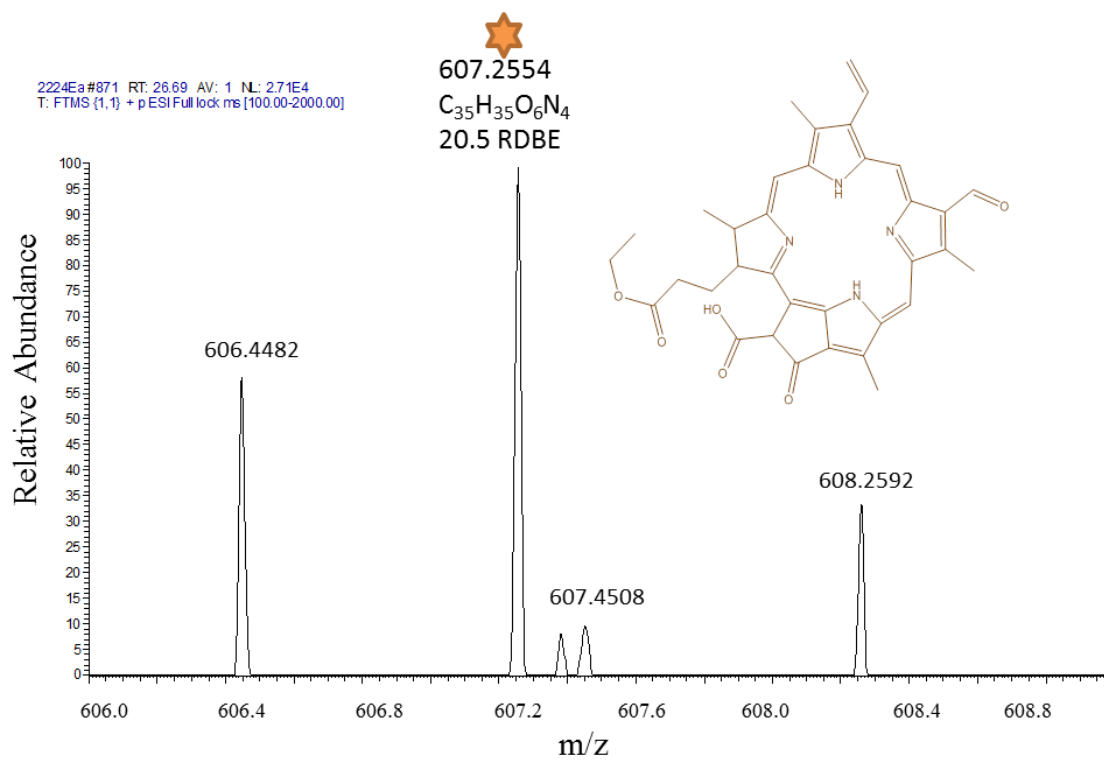


Figure 2.38 HRESI-MS chromatogram showing the relative abundance (y-axis), the m/z (x-axis) and molecular structure of compound **9** (chemical formula and m/z indicated by the brown-coloured asterisk).

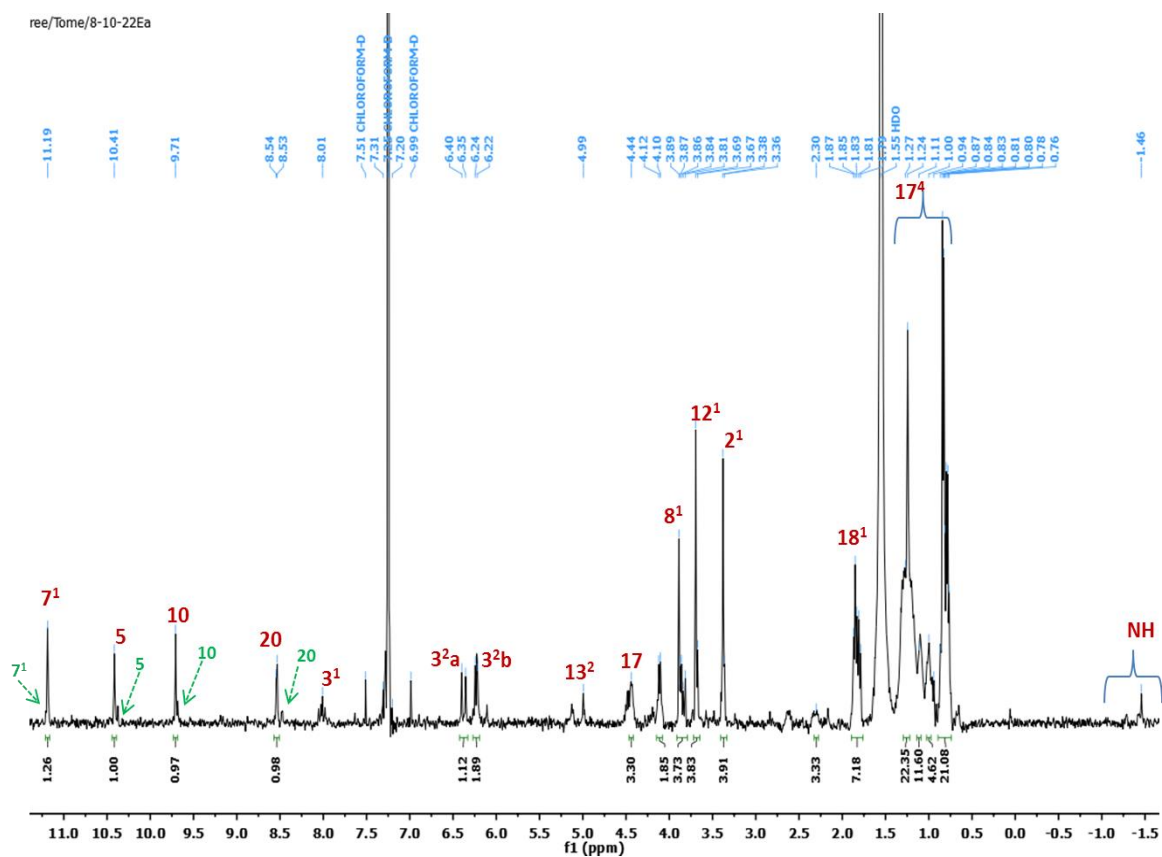


Figure 2.39 1D $^1\text{H-NMR}$ spectrum in CDCl_3 at 400 MHz of pheophorbide b derivatives (compound **7**) as the major compound and pheophorbide b, compound **8** (green arrows and font) as the minor compound in the spectrum. The ratio calculated from the integrals is 80:20 respectively in percentages.

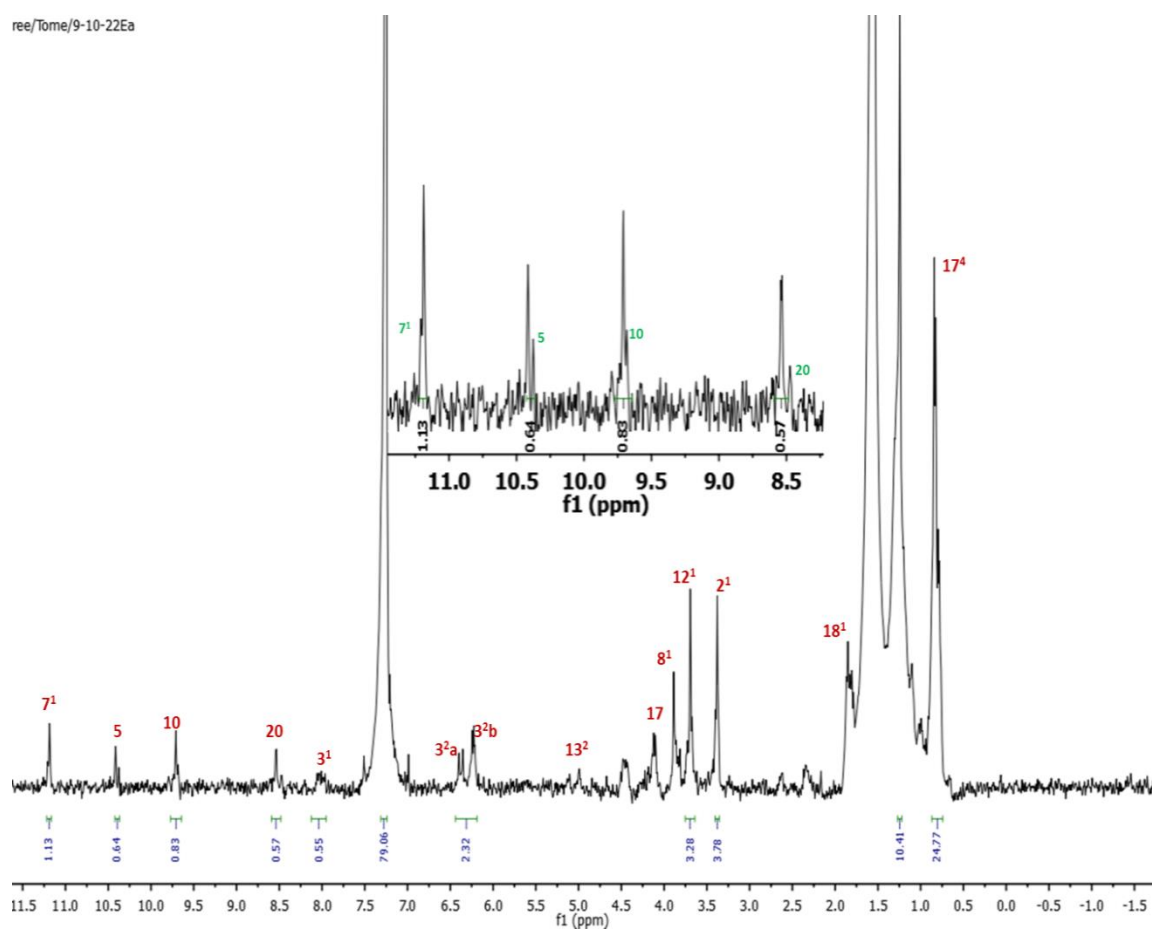


Figure 2.40 1D ¹H-NMR spectrum in CDCl₃ at 400 MHz of pheophorbide b, (compound **8**) and pheophytin b, compound **9**. The ratio calculated from the integrals is 76.6:23.4 respectively in percentages.

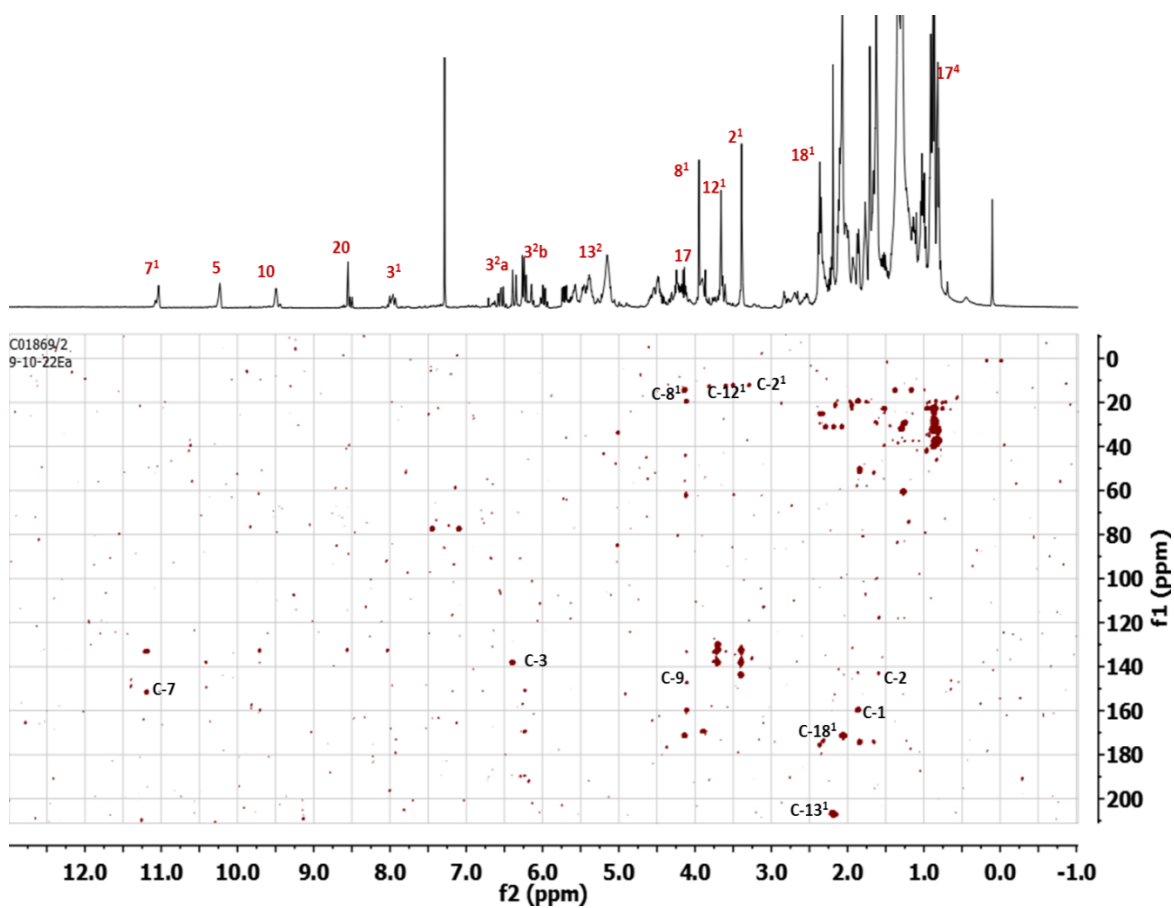


Figure 2.41 HMQC spectrum of **Fr.10-22Ea** (compounds **7**, **8** and **9**). The proton and carbon assignments are outlined in Tables 2.7 and 2.8 respectively. The compounds share common signals.

2.7.7.3 Flavonoid Derivatives

Fraction **28Ea** showed an orange fluorescence under UV light in the presence of Naturstoff reagents indicating the presence of flavonoids. Purification led to the isolation of four flavonoid compounds (**10-13**) all of which tested positive to Naturstoff test. However, low yield prevented further purification and individual bio-assessment of the compounds. Compound **10** was isolated as a green solid with an [M+H] peak at m/z 285.0757 in the HRESI-MS corresponding to the molecular formula $C_{16}H_{13}O_5$ (Fig. 2.42). The 1H -NMR and COSY spectrum of **10** showed a pair of ortho-coupled doublets ($J=8.11$ Hz) at δ 8.18 (2H) and 7.78 (2H) assigned to H-3',5' and H-6',2' and a sharp 1H singlet at δ 7.57 ascribed to H-3 (Fig. 2.43 and 2.45) indicated a 2' - oxygenated flavone (Muntha *et al.*, 2003). The methoxyl group at δ 3.95 was placed at C-7 as it showed a strong Nuclear Overhauser Enhancement (NOE) effect with irradiation of H-8 (δ 7.69, s) and vice versa in the 1D-NOE experiment (Fig. 2.44). H-6 was then assigned at δ 7.77, d and H-5 at 6.96, d. Compound **11** was also isolated as a green solid and the HRESI-MS showed a [M+H]⁺ (calculated for $C_{16}H_{19}O_3$, m/z 259.1330) (Fig. 2.46). The 1H -NMR spectrum showed a pair of AB doublets ($J = 16.2$ Hz) at δ 7.45 and 6.85 which has been described in the literatures and is consistent with *trans* olefinic-protons of a chalcone moiety (Muntha *et al.*, 2003). One methoxyl group at δ 3.95 was observed. The presence of eight aromatic protons at δ 6.30 (2H, d, $J = 8.10$ Hz), 6.96 (2H, d, $J = 8.10$ Hz), 7.70 (2H, d, $J = 8.10$ Hz) and 8.19 (2H, d, $J = 8.10$ Hz) (Fig. 2.47). Compound **12** appeared to be an isomer of compound **11** changing at the H-4 position (Fig. 2.47). Compound **13** was isolated as a green solid and the HRESI-MS showed a [M+H]⁺ peak (calculated for $C_{17}H_{19}O_5$, m/z 303.1226) (Fig. 2.48). The

$^1\text{H-NMR}$ spectrum showed a pair of AB doublets ($J = 15.83$ Hz) at δ 7.69 and 6.27, again consistent with *trans* olefinic-protons of a chalcone moiety (Muntha *et al.*, 2003). Two methoxyl groups δ 3.93 were observed along with 5 aromatic protons at δ 6.79 (1H, d, $J = 8.10$ Hz) assigned to H-2,6; 6.92 (1H, d, $J = 8.07$ Hz) assigned to H-3,5; 7.04 (1H, d, $J = 1.0$ Hz) assigned to H-6', 7.09 (1H, d, $J = 4.0$ Hz) assigned to H-3', 7.14 (1H, s) assigned to H-4' and 7.15 (1H, d, $J = 4.0$ Hz) assigned to H-4' and a glucopyranosyl moiety (δ 5.93, d, $J = 10.31$ Hz; 3.59-3.96, m; 4.15, m) (Fig. 2.49)

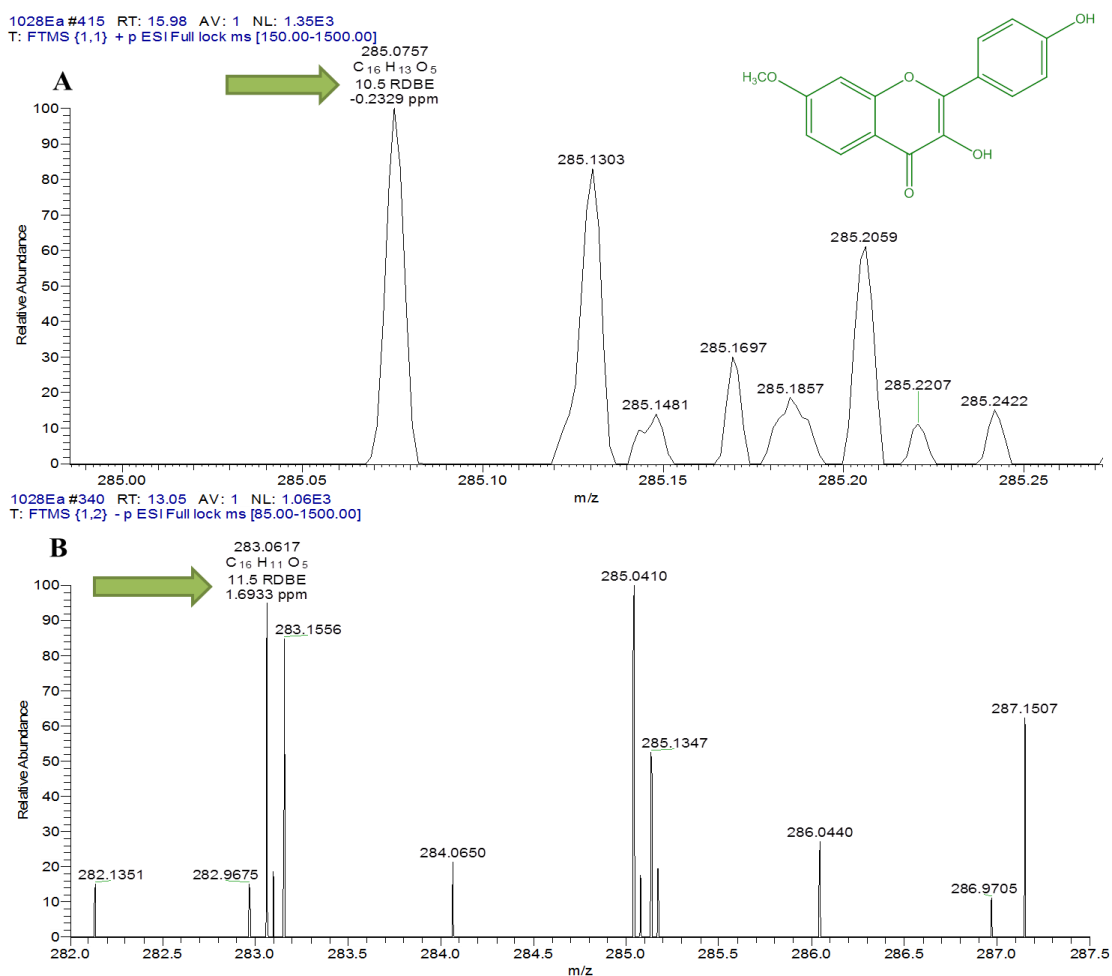


Figure 2.42 Positive (A) and negative (B) HRESI-MS chromatograms showing the relative abundance (y-axis) and the m/z (x-axis) of compound **10**. The green arrows point to the labelled peaks with corresponding molecular formulae, the deviation between theoretical and actual mass (in ppm) as well as the ring and double bond equivalents (RDBE).

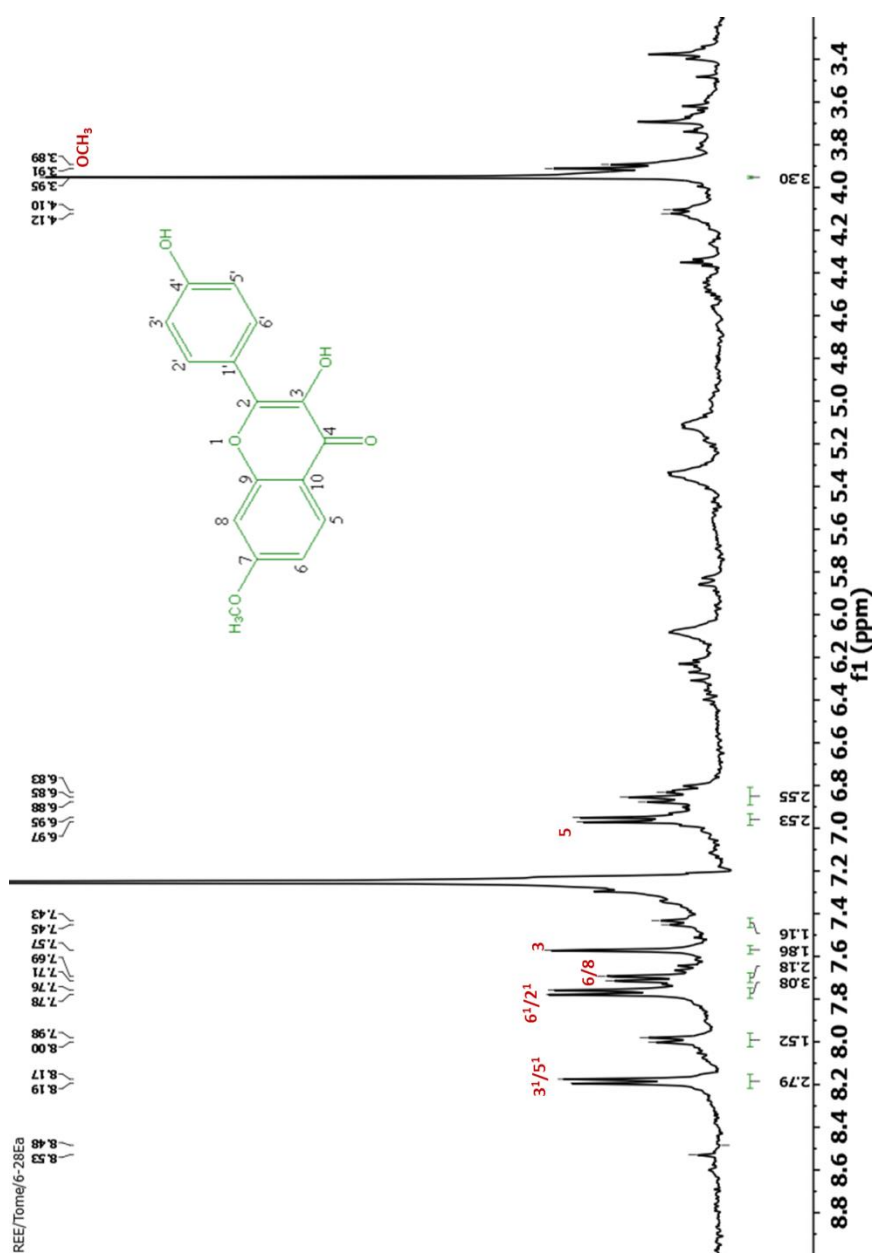


Figure 2.43 1D ¹H-NMR in CDCl₃ measured at 400 MHz showing the labelled peaks and molecular structure of compound **10**.

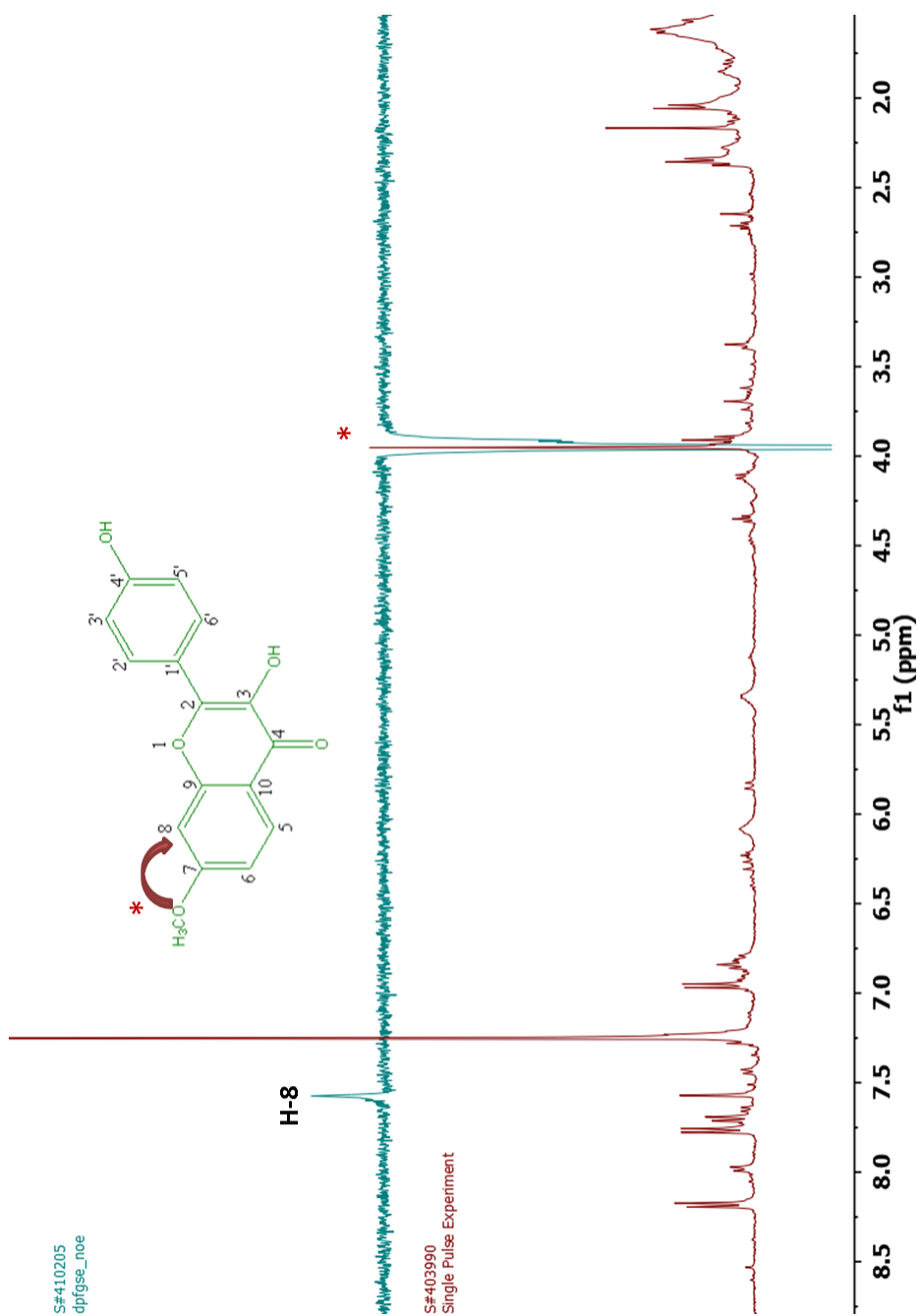


Figure 2.44 1D Nuclear Overhauser Enhancement Spectroscopy (NOESY) spectrum of compound **10** in CDCl₃ measured at 400 MHz. The arrow shows the correlation with H-8; * = irradiated point.

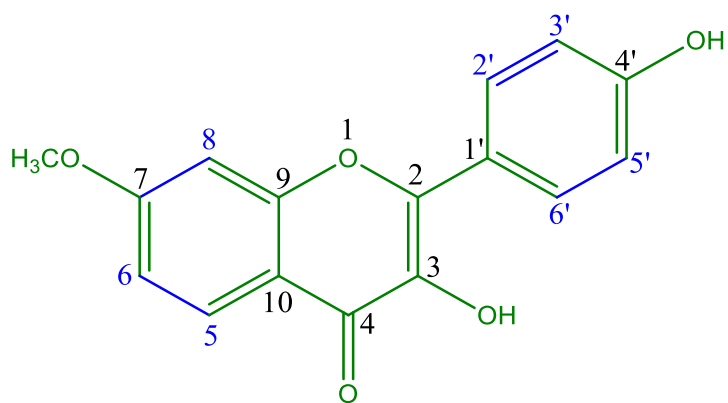
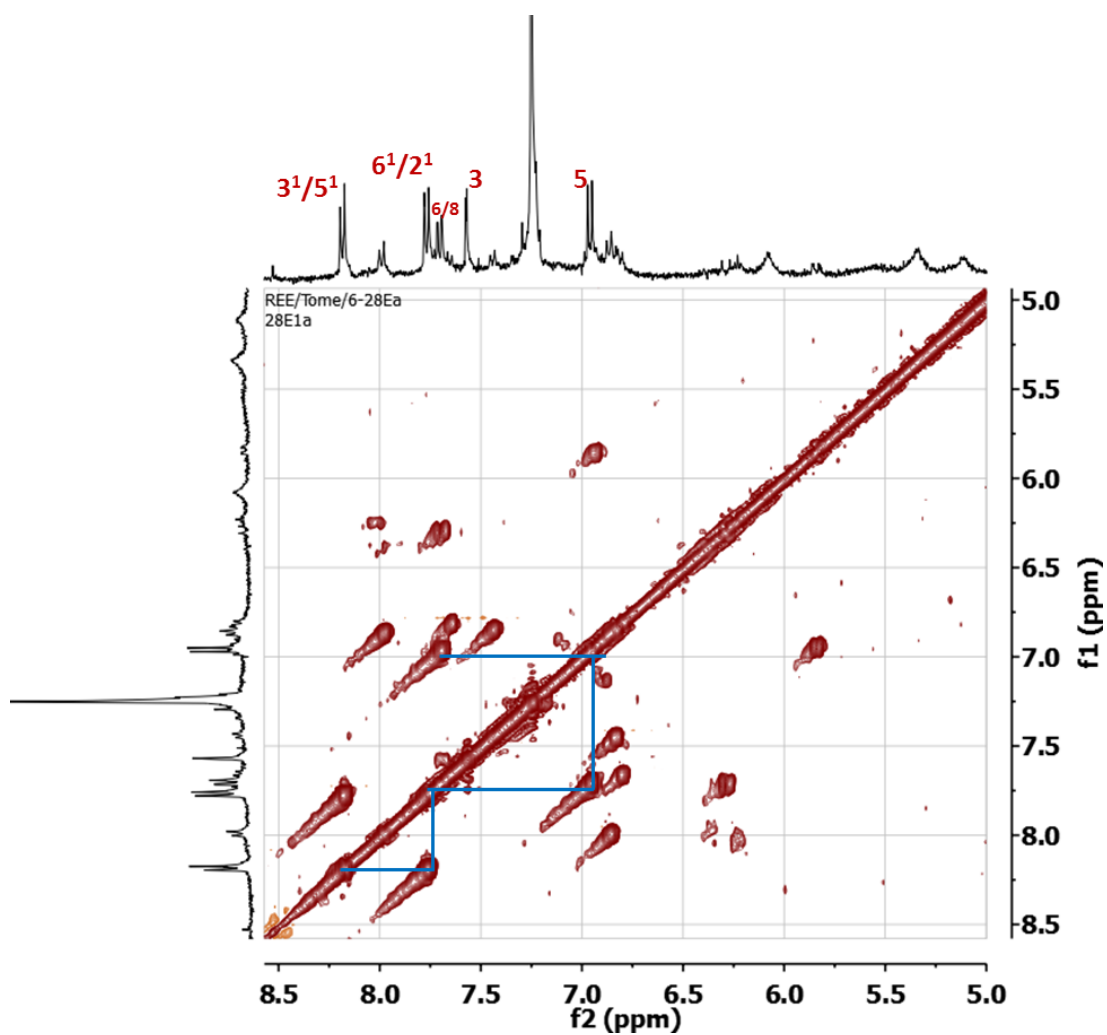
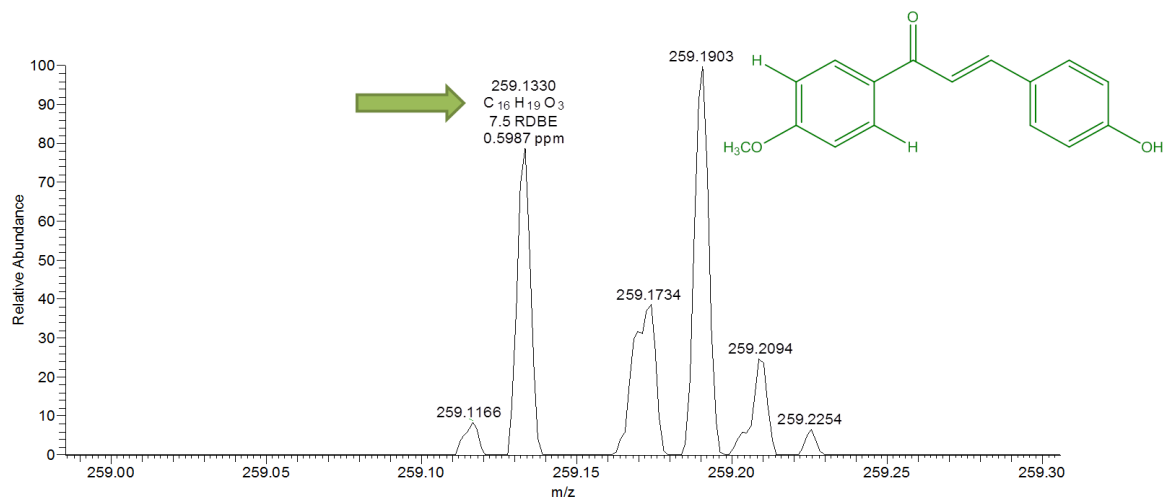


Figure 2.45 2D COSY spectrum of compound **10** in CDCl_3 measured at 400 MHz. The COSY correlations are highlighted in blue lines within the spectrum and the molecular structure.

928Ea #421 RT: 15.55 AV: 1 NL: 6.41E3
T: FTMS (1,1) +p ESI Full lock ms [150.00-1500.00]



928Ea #340 RT: 12.60 AV: 1 NL: 3.40E4
T: FTMS (1,2) -p ESI Full lock ms [85.00-1500.00]

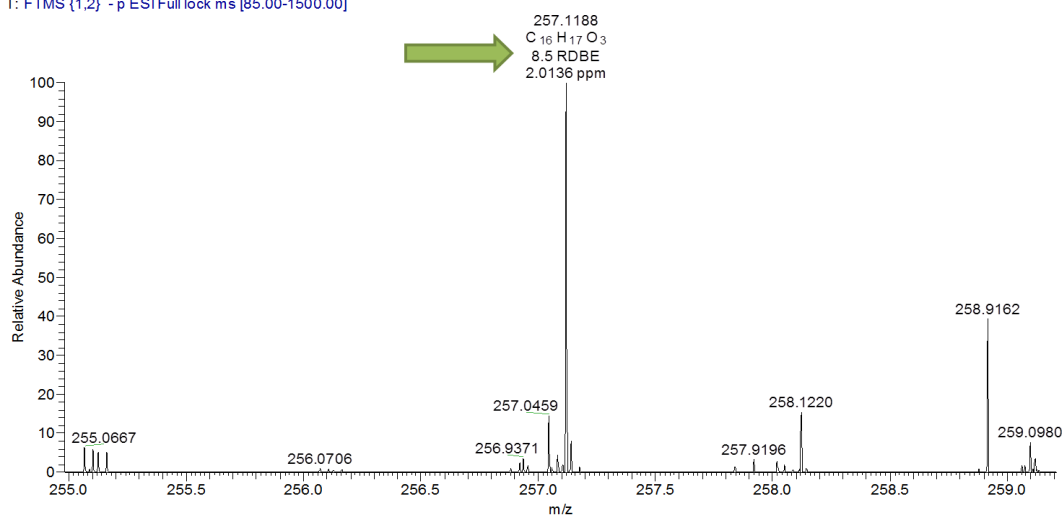
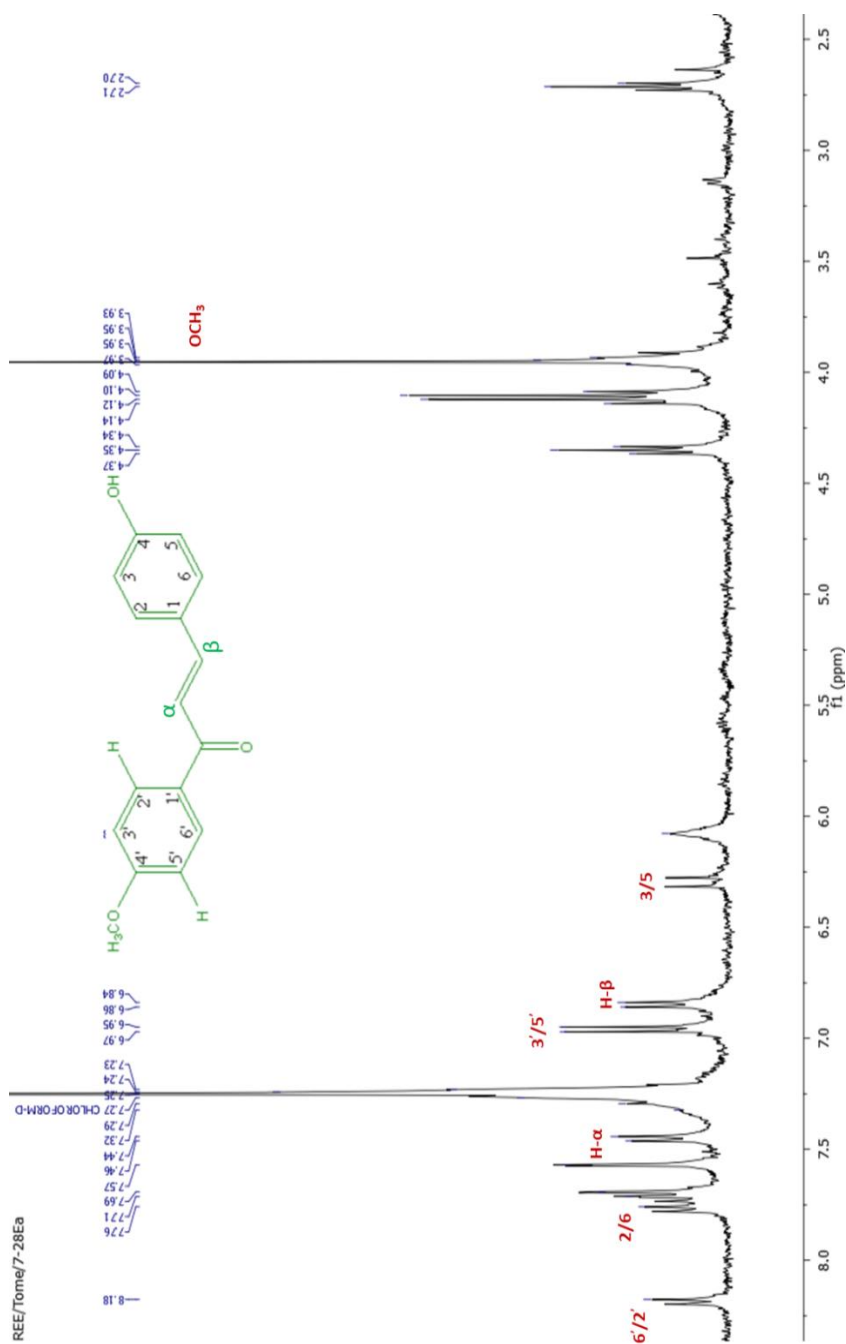


Figure 2.46 Positive (A) and negative (B) HRESI-MS chromatograms showing the relative abundance (y-axis) and the m/z (x-axis) of compound **11**. The green arrows point to the labelled peaks with corresponding molecular formulae, the deviation between theoretical and actual mass (in ppm) as well as the ring and double bond equivalents (RDBE).



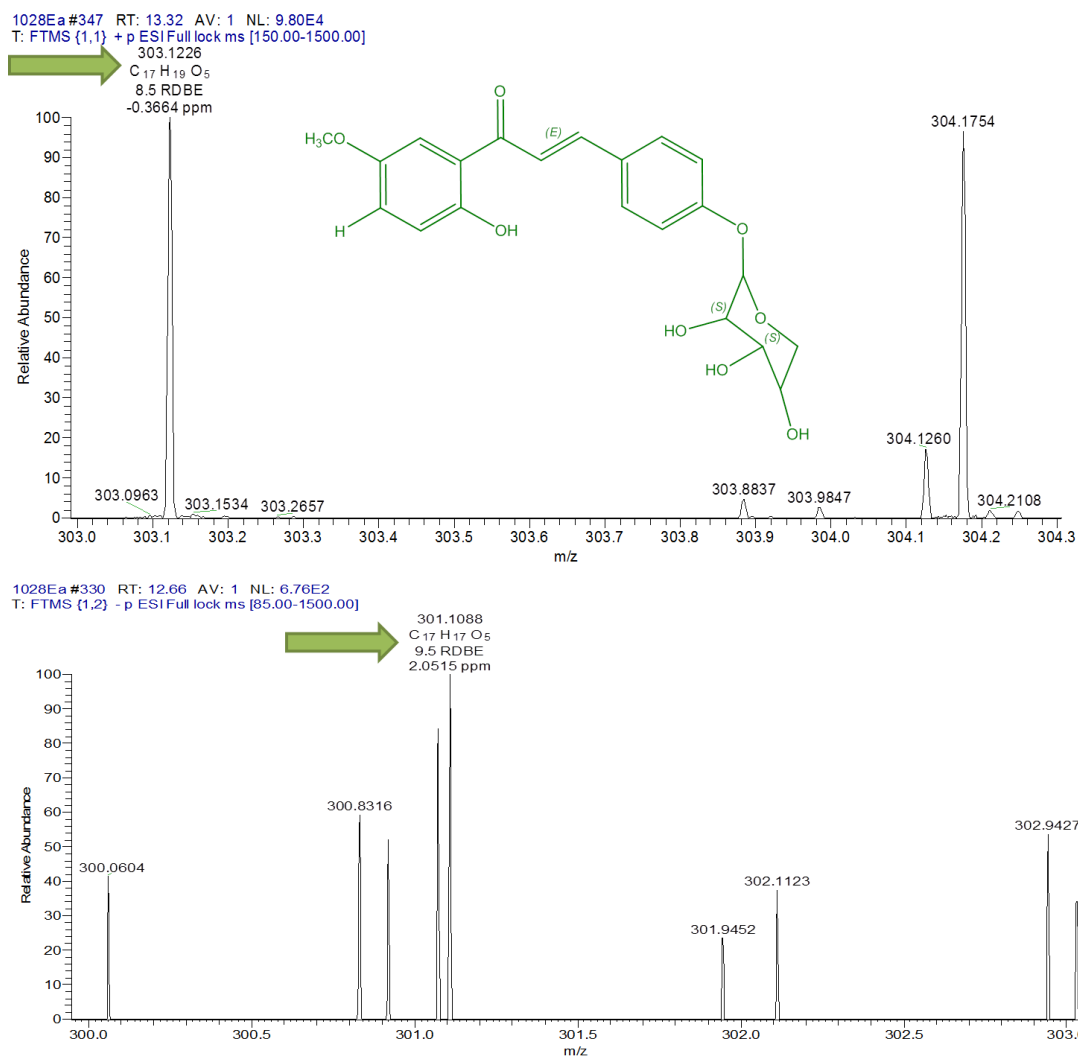


Figure 2.48 Positive (A) and negative (B) HRESI-MS chromatograms showing the relative abundance (y-axis) and the m/z (x-axis) of compound **13**. The green arrows point to the labelled peaks with corresponding molecular formulae, the deviation between theoretical and actual mass (in ppm) as well as the ring and double bond equivalents (RDBE).

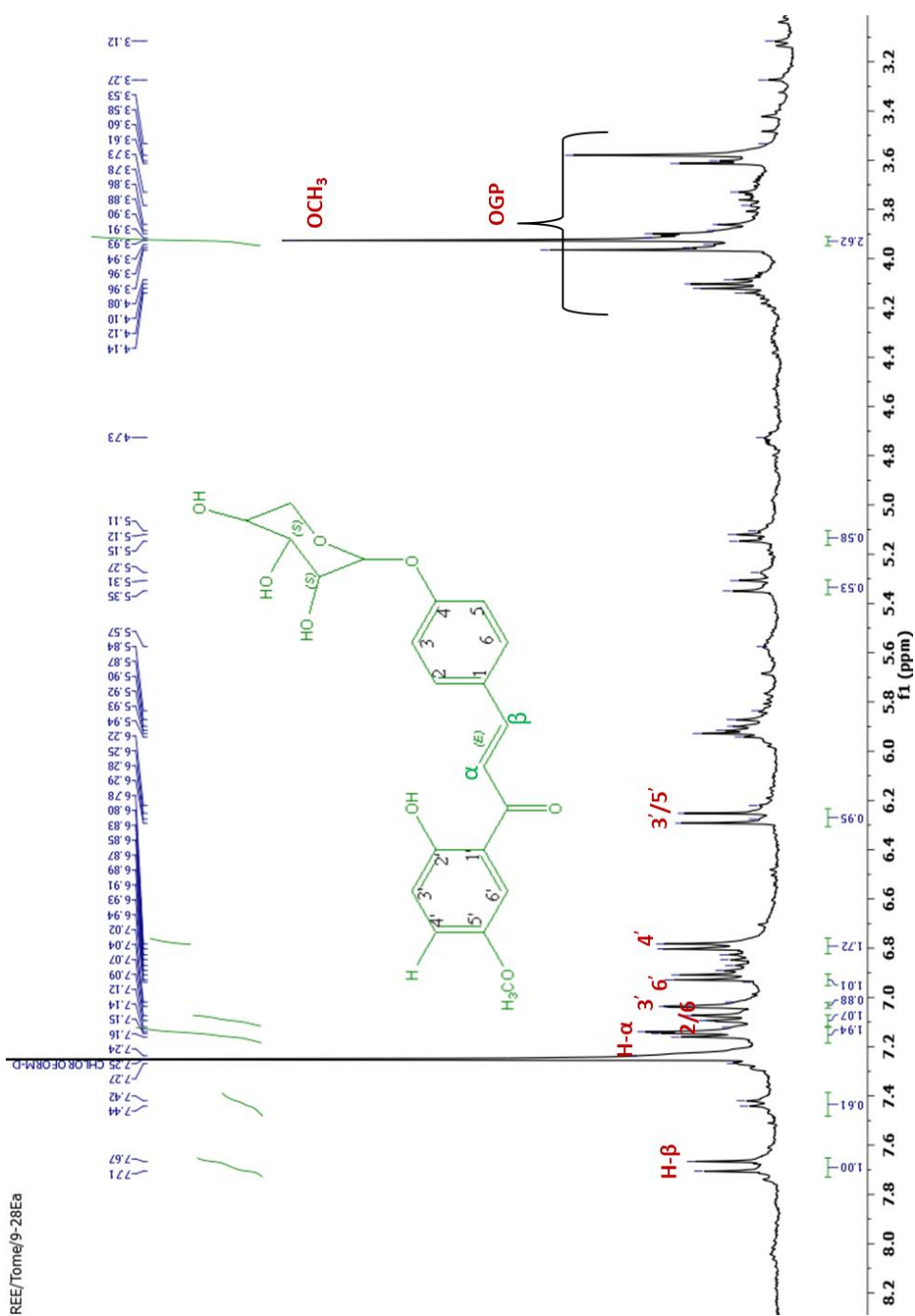
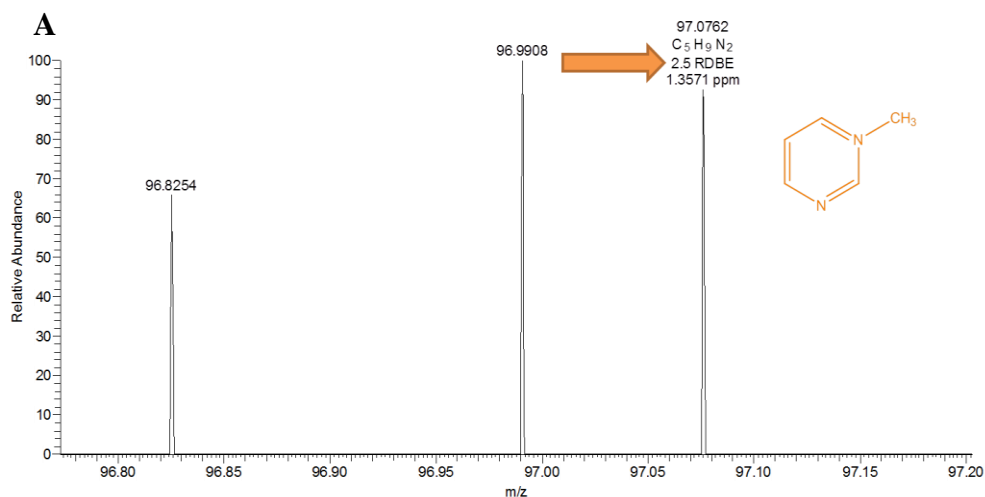


Figure 2.49 1D ¹H-NMR spectrum in CDCl₃ measured at 400MHz showing the labelled peaks and molecular structure of compound **13**.

2.7.7.4 N-Methyl Pyrimidine and Salt isolated from *F. exasperata*

N-Methyl pyrimidine (**14**) was also isolated from the active fractions of *F. exasperata*. Compound **14** was isolated with 70% purity. The fraction contained a mixture of compound **14** and fatty acid at a ratio of 70:30 in percentages. Compound **14** appeared as a brown solid with a characteristic odour. HRESI-MS showed a $[M-1]^-$ peak at m/z 95.0613 corresponding to a molecular formula of $C_5H_7N_2$ (Fig. 2.50). The 1H -NMR spectrum showed 4 aromatic protons δ 8.04 (1H, t, $J = 6.94$ Hz) assigned to H-5; δ 8.78 (1H, d, $J = 7.82$ Hz) assigned to H-4; δ 8.94 (1H, d, $J = 5.98$ Hz) assigned to H-6, and δ 9.22 (1H, s) assigned to H-2 (Fig. 2.51). The methyl group was observed at δ 4.38 (s, 3H), confirmed from the COSY which showed correlations with H-2 and H-4 (Fig. 2.52). Further assignments are presented in Table 2.9.

MC3 #355 RT: 4.55 AV: 1 NL: 1.16E3
T: FTMS (1,1) + p ESI Full lock ms [85.00-1200.00]



MC3 #134 RT: 1.66 AV: 1 NL: 2.41E3
T: FTMS (1,2) - p ESI Full lock ms [85.00-1200.00]

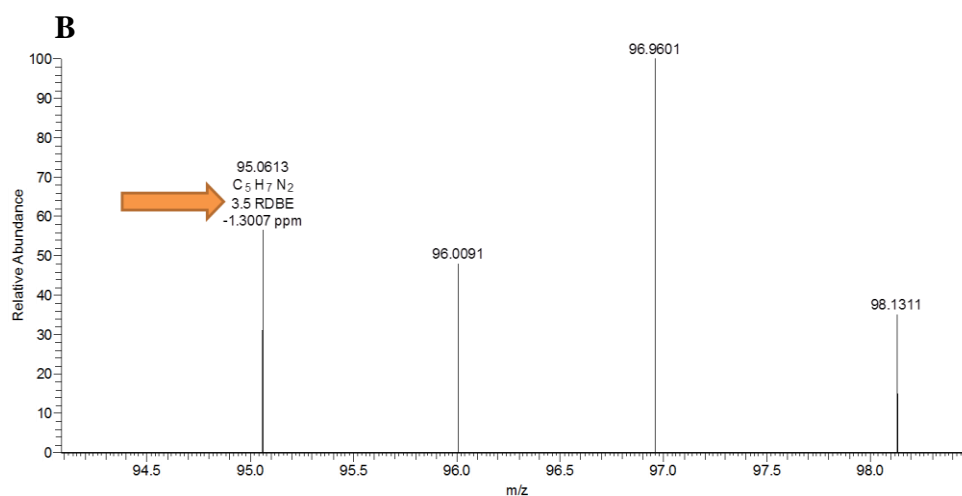


Figure 2.50 Positive (A) and negative (B) HRESI-MS chromatograms showing the relative abundance (y-axis) and the m/z (x-axis) of compound **14**. The orange arrows point to the labelled peaks with corresponding molecular formulae, the deviation between theoretical and actual mass (in ppm) as well as the ring and double bond equivalents (RDBE).

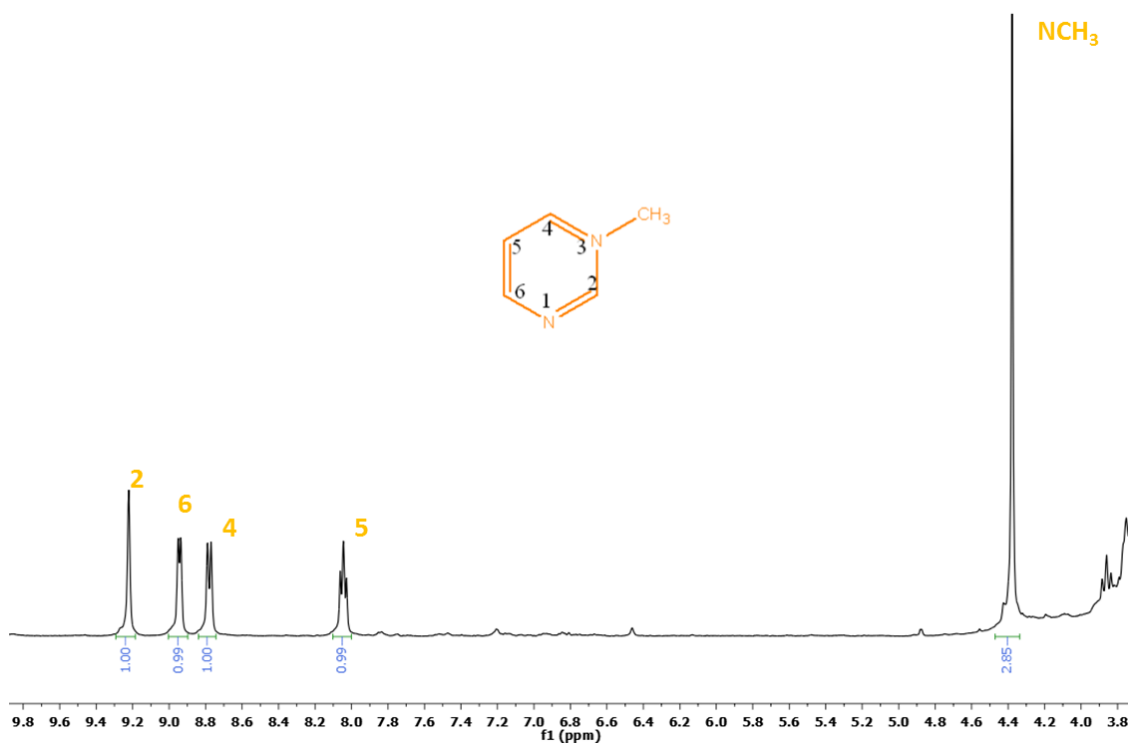


Figure 2.51 1D ¹H-NMR spectrum of compound **14** in CDCl₃ measured at 400 MHz.

The molecular structure is shown in orange within the spectrum.

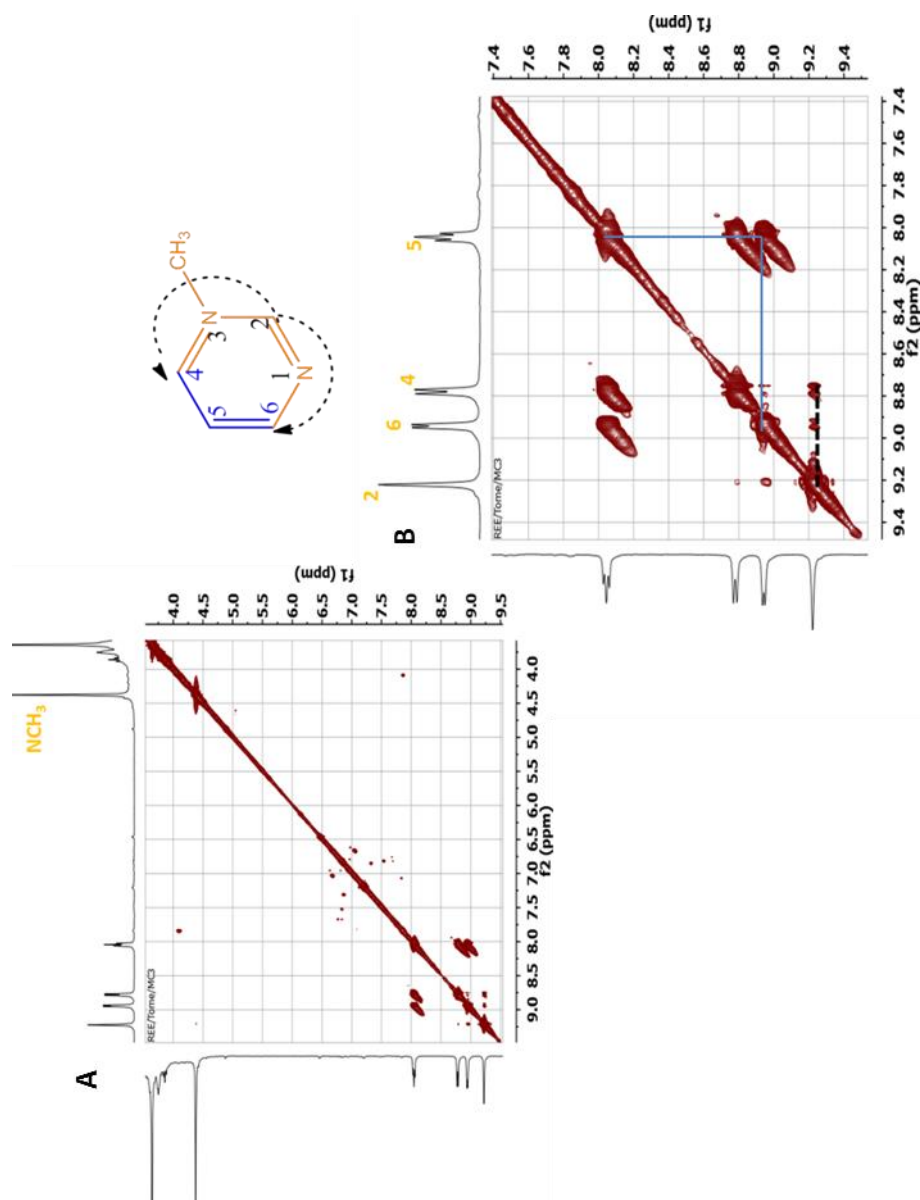


Figure 2.52 2D COSY spectra in CDCl₃ measured at 400 MHz showing the correlations in compound **14**. Panel A represents the COSY spectrum between 4.0 and 9.0 ppm while panel B represents an expanded spectrum showing chemical shifts between 7.4 and 9.4 ppm. The COSY correlations are highlighted with blue lines.

Table 2.9 ^1H -NMR, ^{13}C NMR, COSY and HMBC (400 MHz) of N-methyl pyrimidine (**14**) in CDCl_3

Position	^1H (ppm)	J (Hz)	COSY (H \rightarrow H)	HMBC (H \rightarrow C)	^{13}C
1	-	-	-	-	-
2	9.22 (s)	-	-	$3^1, 4, 6$	146.55
3	-	-	-	-	-
3¹	4.39 (s)	-	-	2,4,5,6	48.17
4	8.78 (d)	7.82	5,6	$3^1, 5, 6$	144.72
5	8.04 (t)	6.94	4,6	2,3 ¹ ,4,6	127.44
6	8.94 (d)	5.98	4,5	$3^1, 4, 5$	145.80

2.7.7.4.1 Compound 15

An inorganic salt was also extracted from the leaves of *F. exasperata* (Table 2.10). A ^1H -NMR spectrum of the compound showed an absence of compound peaks (Fig. 2.53).

{Compound 17}
{White crystalline solid}{ ^1H -NMR, DMSO- d_6 , AS400}

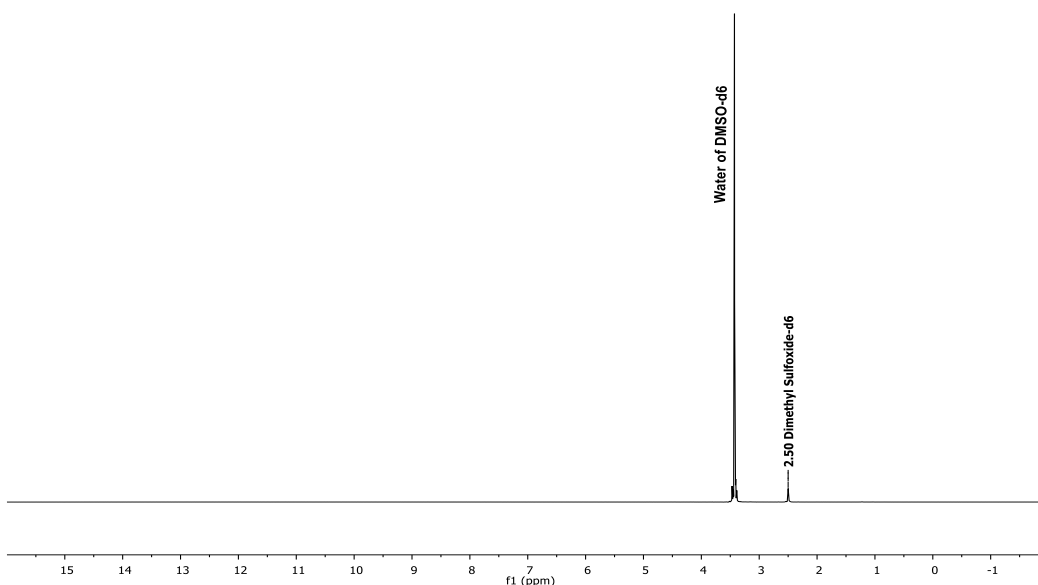


Figure 2.53 The ^1H -NMR spectrum of compound **15** in DMSO- d_6 from the leaves of *F. exasperata* measured on AS400-JEOL. No peaks corresponding to organic compounds were observed, the observed peaks in the figure are solvent peaks.

Table 2.10 Semi Quantitative Table showing ICP-MS analysis of Compound **15**Isolated from the leaves of *F. exasperata*

Element	Mass	Conc	Units	CPS	Time(sec)
Li	7	-61.703	ng/l	4,180.62	0.10
Be	9	26.973	ng/l	150.01	0.10
B	11	1.418	µg/l	6,011.17	0.10
C	12	1.160	mg/l	316,091.54	0.10
Na	23	61.317	mg/l	740,125,108.97	0.10
Mg	24	29.749	µg/l	147,433.74	0.10
Al	27	1.190	µg/l	12,334.47	0.10
Si	28	19.504	µg/l	15,897.20	0.10
P	31	25.597	µg/l	2,510.28	0.10
S	34	455.950	µg/l	9,302.64	0.10
Cl	35	147.242	mg/l	1,610,621.69	0.10
K	39	53.998	mg/l	128,230,248.09	0.10
Ca	42	53.058	µg/l	11,614.02	0.10
Sc	45	24.621	µg/l	1,191,352.72	0.10
Ti	47	574.878	ng/l	250.01	0.10
V	51	135.724	ng/l	10,563.40	0.10
Cr	52	242.426	ng/l	21,553.34	0.10
Mn	55	2.111	µg/l	31,257.54	0.10
Fe	56	2.455	µg/l	280,251.48	0.10
Co	59	-3733.001	ng/l	23,556.02	0.10
Ni	60	1.106	µg/l	20,071.63	0.10
Cu	63	900.135	ng/l	52,796.10	0.10
Zn	66	8.480	µg/l	38,501.55	0.10
Ga	69	-1990.918	ng/l	13,165.36	0.10
Ge	72	21.898	µg/l	620,032.37	0.10
As	75	95.952	ng/l	140.01	0.10
Se	78	1.843	µg/l	470.02	0.10
Br	79	450.681	µg/l	27,051.08	0.10
Rb	85	516.917	µg/l	554,615.46	0.10
Sr	88	7.434	µg/l	16,878.29	0.10
Y	89	-405112.086	ng/l	140.01	0.10

Highlighted rows indicate significantly detected elements; CPS = Count per seconds.

2.7.7.5 Summary of the Compounds Isolated from the Leaves of *F. exasperata*

(Figures 2.54 a-c)

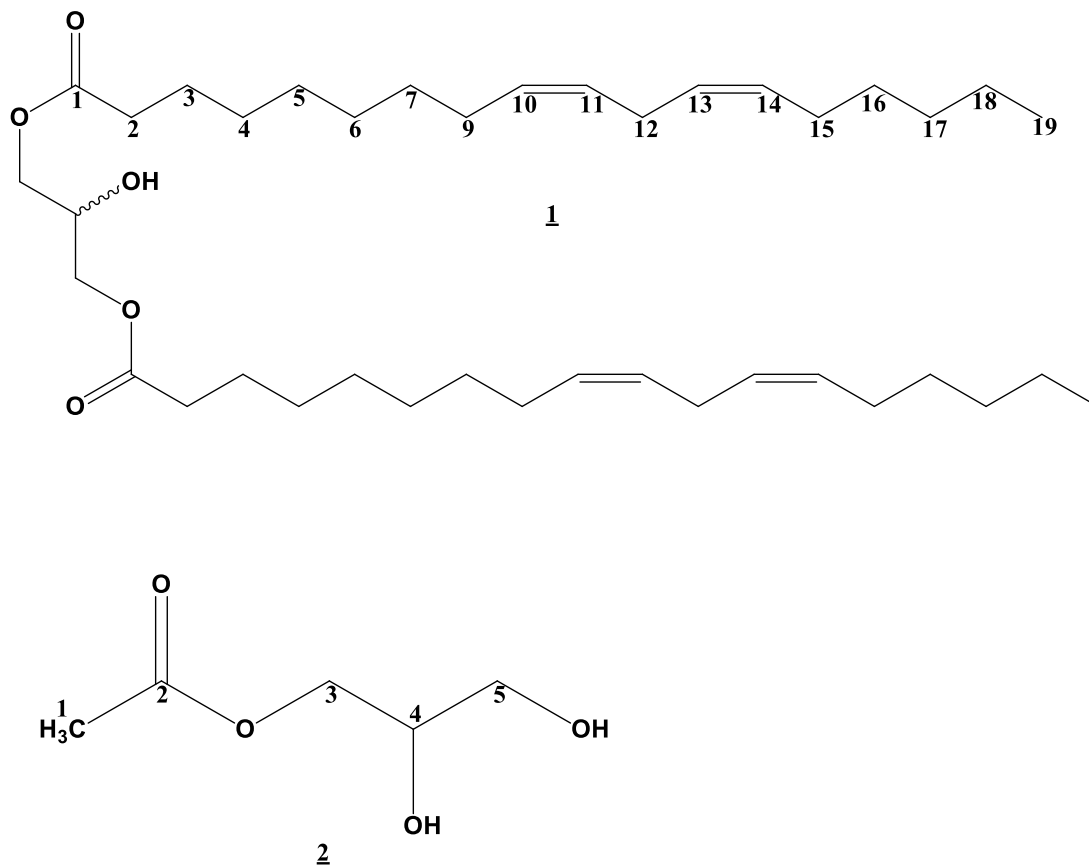
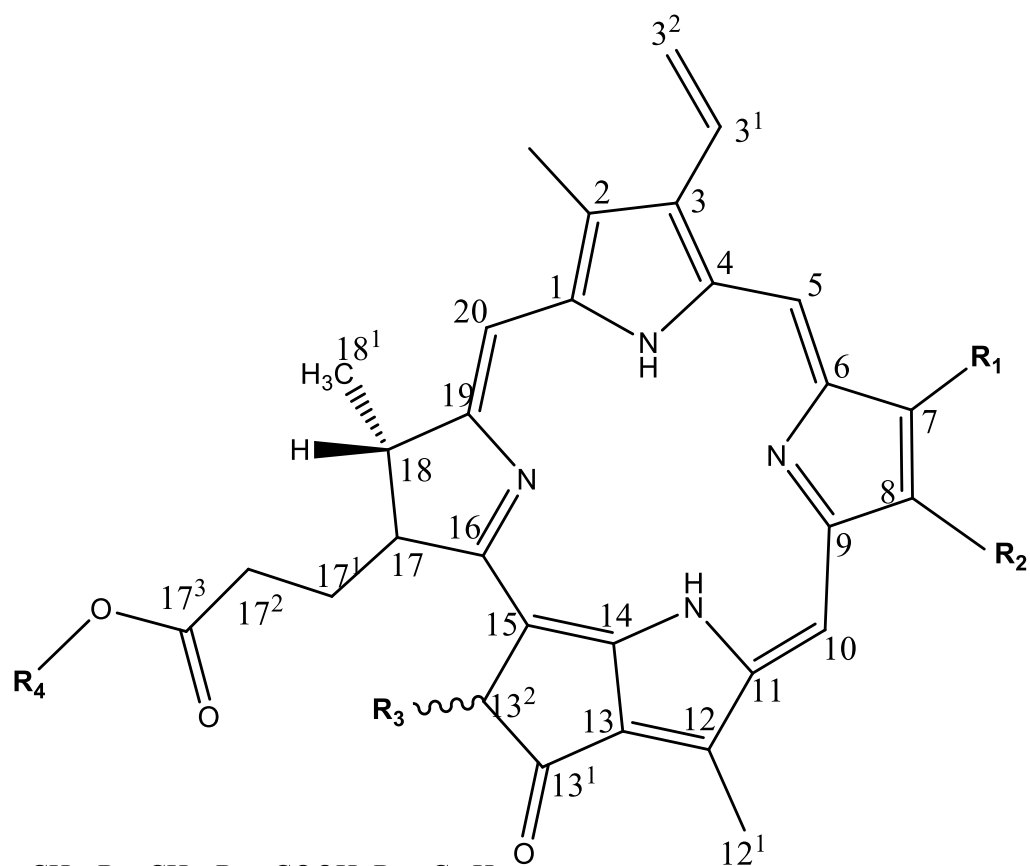


Figure 2.54a Compounds **1** and **2** isolated from the leaves of *F. exasperata*



- 3:** R₁=CH₃; R₂=CH₃; R₃=COOH; R₄=C₂₂H₄₂
4: R₁=CH₃; R₂=CH₃; R₃=COOH; R₄=CH₃
5: R₁=CH₃; R₂=C₂H₅; R₃=COOCH₃; R₄=H
6: R₁=CH₃; R₂=C₂H₅; R₃=H₂; R₄=H
7: R₁=CHO; R₂=CH₃; R₃=COOH; R₄=C₃H₇
8: R₁=CHO; R₂=CH₃; R₃=COOH; R₄=C₂₁H₄₂
9: R₁=CHO; R₂=CH₃; R₃=COOH; R₄=CH₃

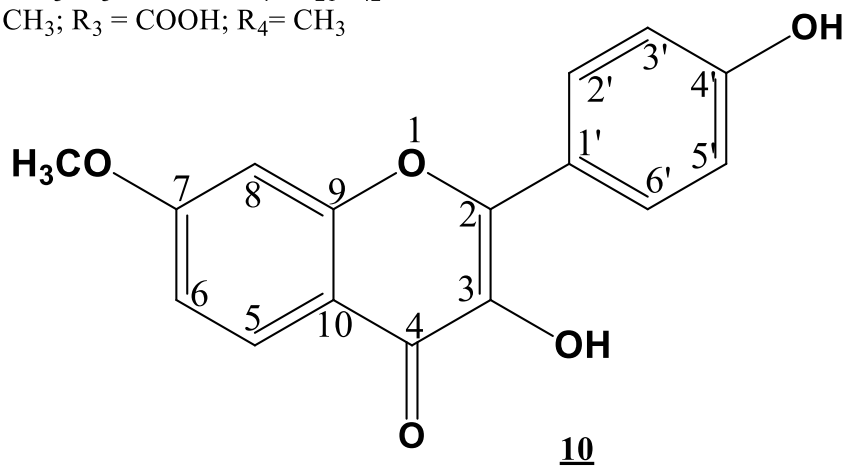
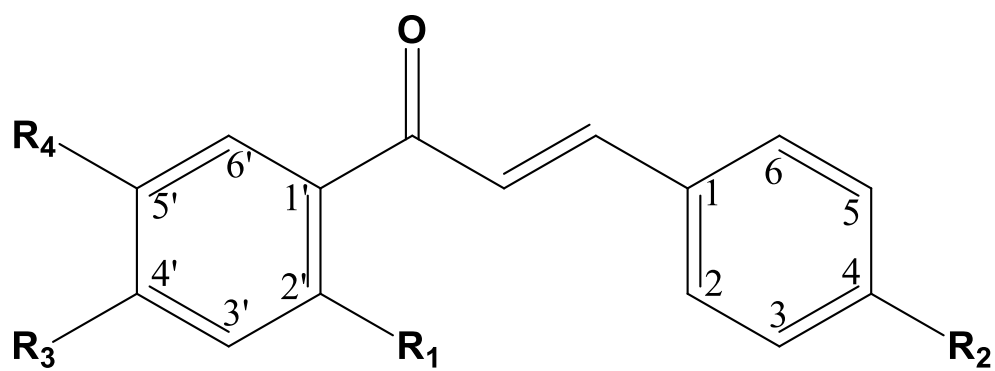


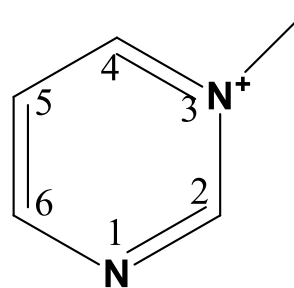
Figure 2.54b Compounds **3-10** isolated from the leaves of *F. exasperata*



11: $R_1=H$; $R_2=OH$; $R_3 = OCH_3$; $R_4 = H$

12: $R_1=OGP$; $R_2=OH$; $R_3 = H$; $R_4 = OCH_3$

13: $R_1=OH$; $R_2=OGP$; $R_3 = H$; $R_4 = OCH_3$



14

Figure 2.54c Compounds **11-14** isolated from the leaves of *F. exasperata*

2.7.8 Pharmacological Effects of Identified Compounds on Uterine Contractility

Representative tracings of the isolated compounds are shown in figures 2.55 – 2.64 below. The calculated effects of the different fractions on frequency, amplitude and area under the curve of uterine contraction are listed in Tables 2.11-2.13.

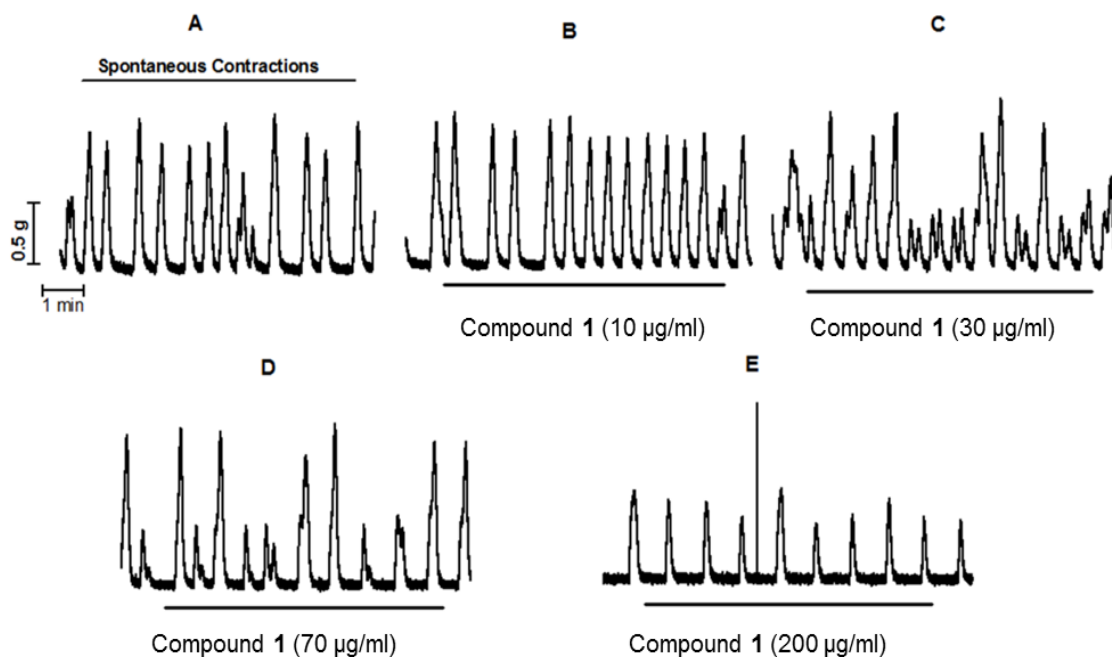


Figure 2.55 Representative tracings showing the effect of increasing concentrations of compound **1** (panel B - E) on spontaneous uterine contractions compared with the control recordings (represented in panel A). The tension and time scales shown in A above were the same for all figures A-E.

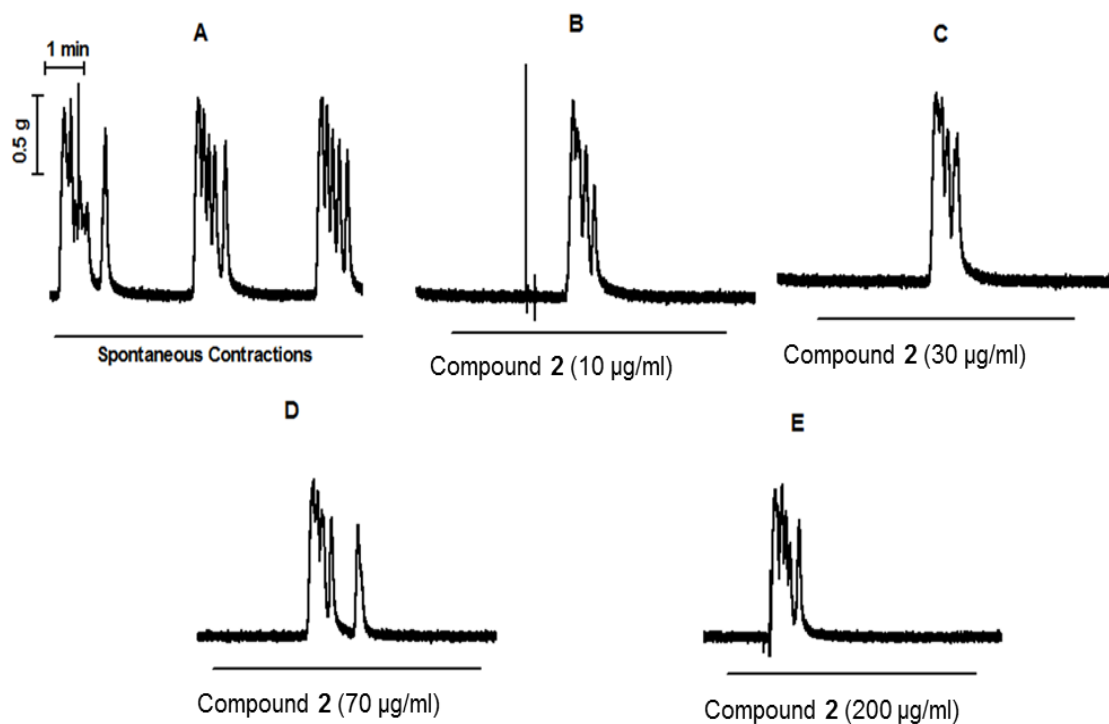


Figure 2.56 Representative recordings of increasing concentrations (10 – 200 µg/ml) of compound 2 on spontaneous uterine contractions compared with spontaneous contractions which were used as the control (A). The tension and time scales shown in A were the same for all figures A-E.

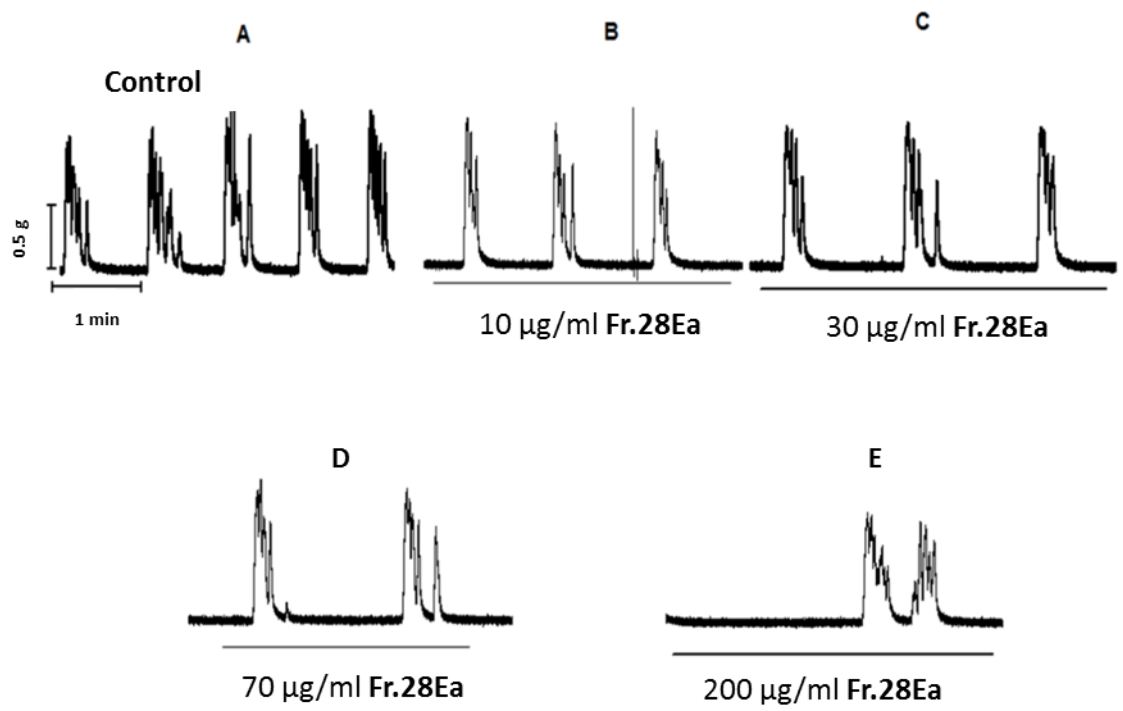


Figure 2.57 Original recordings showing increasing concentrations of **Fr. 28Ea** (panel B - E) on spontaneous uterine contractions compared with the control (panel A). The tension and time scales shown in A were the same for all figures A-E.

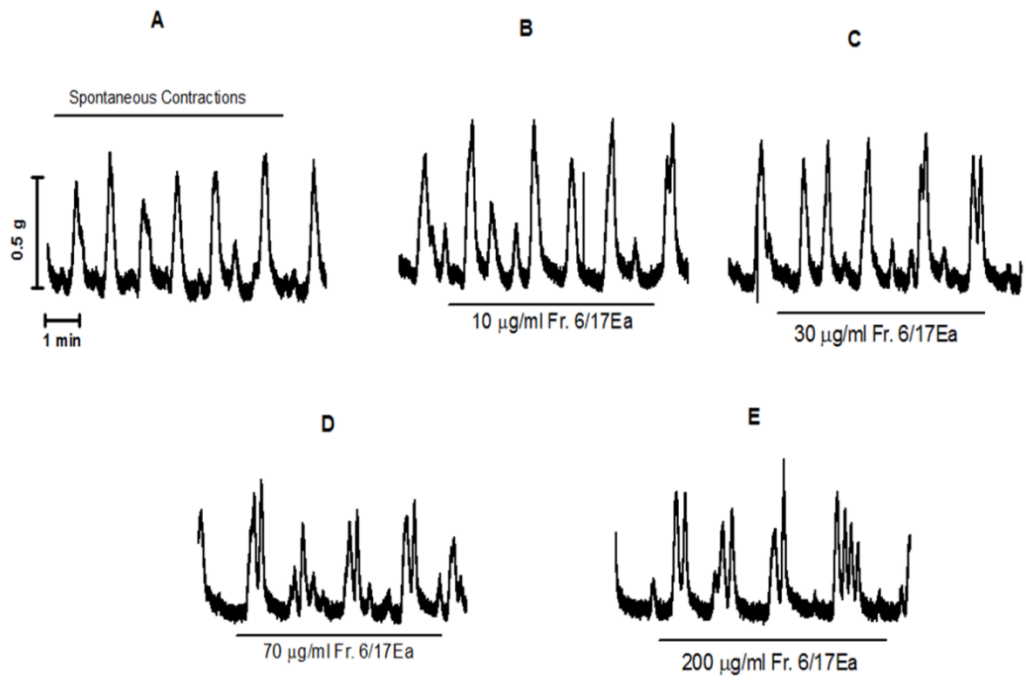


Figure 2.58 Representative tracings showing increasing concentrations of **Fr. 6/17Ea** (10 – 200 µg/ml) on spontaneous uterine contractions compared with the control (A). The tension and time scales shown in A were the same for all figures A-E.

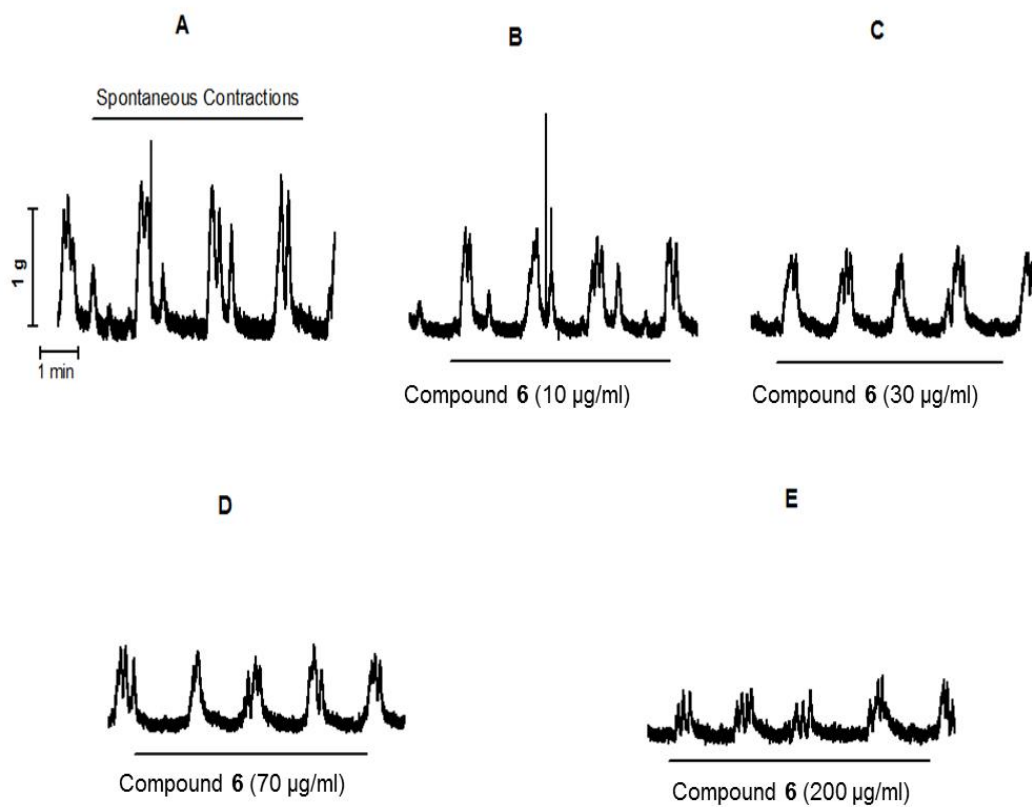


Figure 2.59 Original recordings of different concentrations of compound **6** on spontaneous uterine contractions compared with the control (A). The tension and time scales shown in A were the same for all figures A-E.

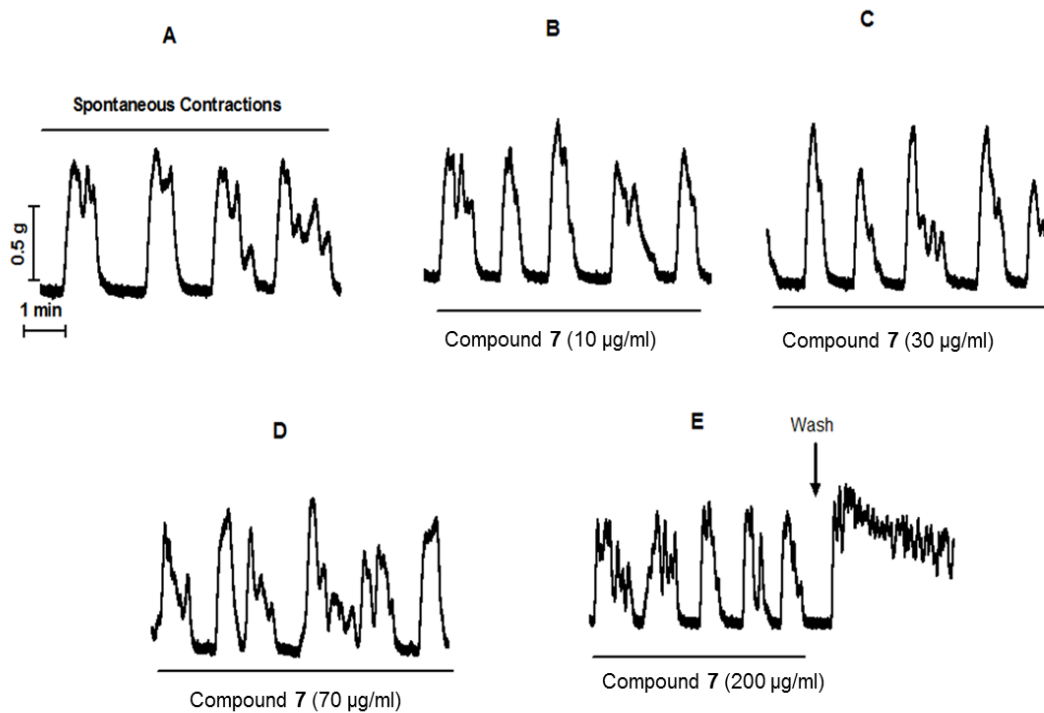


Figure 2.60 Representative recordings showing increasing concentrations of compound 7 (10 -200 $\mu\text{g/ml}$) on spontaneous uterine contractions compared with the control (A). The tension and time scales shown in A were the same for all figures A-E.

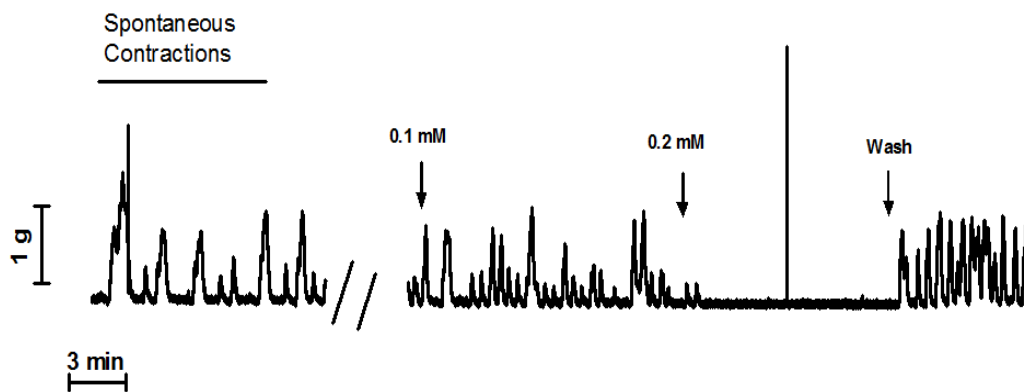


Figure 2.61 Representative recordings showing the effect of trilinolein on uterine smooth muscle. Contractions were restored upon washout.

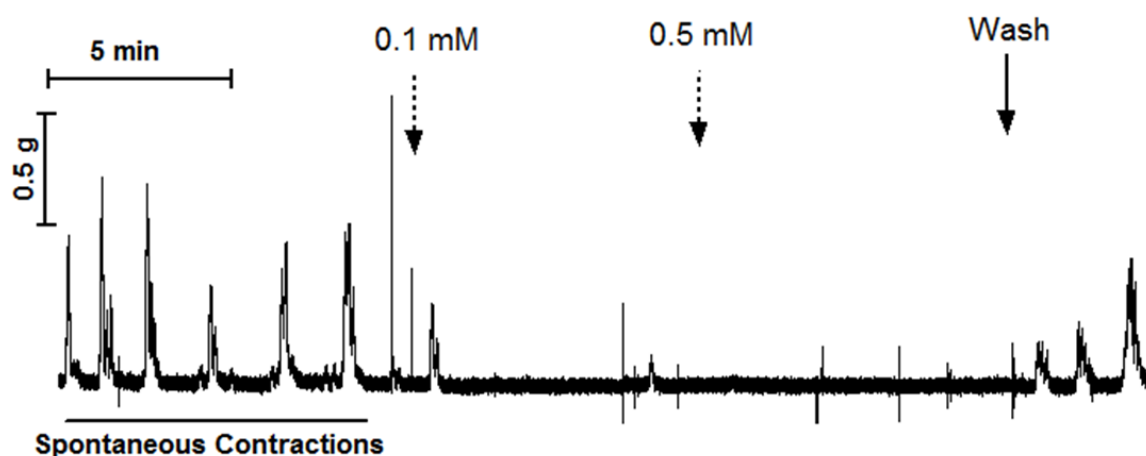


Figure 2.62 Representative recordings showing the effect of pyrimidine on uterine smooth muscle. Pyrimidine completely abolished uterine contractions at the concentrations used (0.1 - 0.5 mM). Contractions were however gradually restored upon washout.

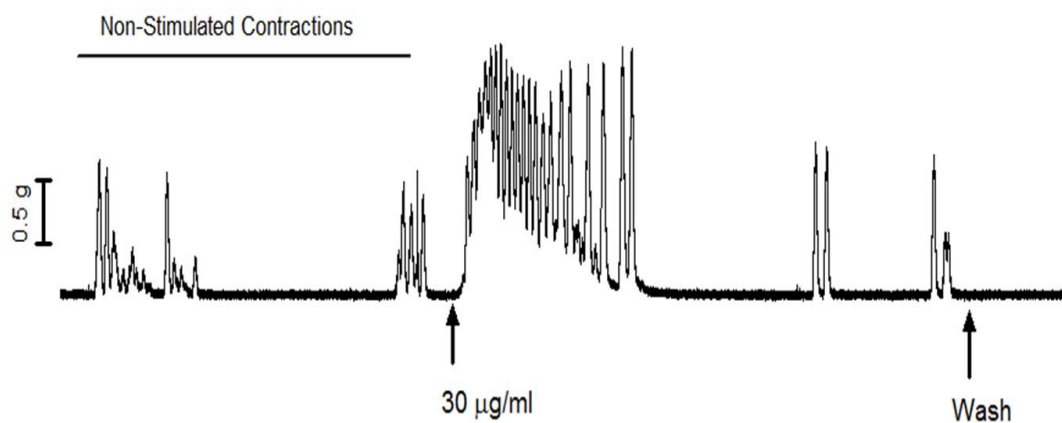


Figure 2.63 Representative tracing showing the effect of compound 14 on the non-stimulated uterus.

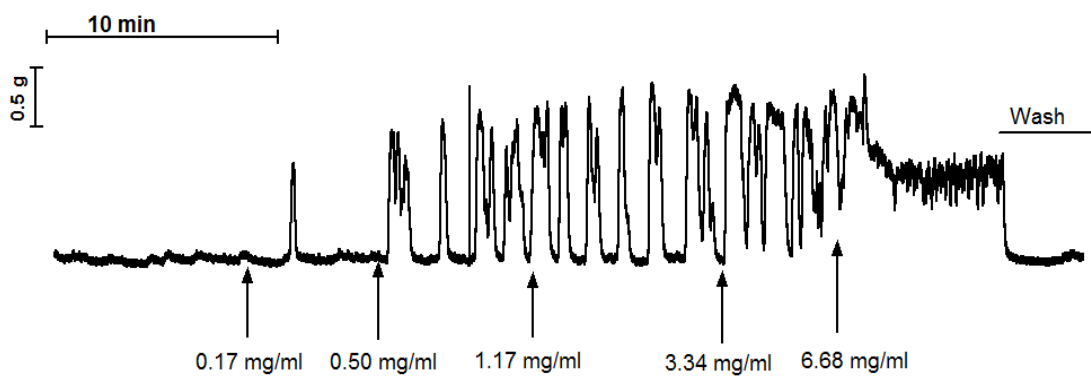


Figure 2.64 Representative tracing of the effects of compound **15** (KCl isolated from the leaves of *F. exasperata*) at different concentrations on the non-stimulated uterus.

Table 2.11 Effect of **E1a** Fractions on the Contraction Frequency (cycles/5 min) of the Uterus

Fractions	Control	50 µg/ml	150 µg/ml
11	9.3 ± 0.48	7.0 ± 1.15	12.3 ± 1.60
12	12.5 ± 1.44	15.8 ± 2.78 *	15.0 ± 0.41*
13	11.8 ± 1.18	11.5 ± 1.32	19.3 ± 0.48
14-16	15.0 ± 3.54	7.0 ± 6.12 *	2.3 ± 2.39**
17-19	8.8 ± 2.18	6.5 ± 2.53**	2.25 ± 3.15**
20	15.8 ± 3.25	14.5 ± 3.84	14.5 ± 3.22
21	10 ± 5.77	10 ± 1.44	12.75 ± 1.31
22-24	10.3 ± 2.17	7.5 ± 3.12	4.8 ± 4.27*
25	7.5 ± 3.23	10.3 ± 2.39	8.0 ± 4.08
26	9.0 ± 1.23	7.0 ± 4.56	7.0 ± 1.23
27	13.3 ± 4.48	9.3 ± 3.04*	6.0 ± 1.47**
28	12.5 ± 1.19	10.3 ± 2.75	5.3 ± 4.21**
29-30	12.8 ± 1.03	5.0 ± 1.08**	3.0 ± 2.89**
31-32	11.8 ± 2.75	8.8 ± 1.32	3.3 ± 5.15**
33	15.0 ± 2.89	8.5 ± 1.44**	5.3 ± 1.89**
34-36	39.3 ± 0.48	39.8 ± 0.48	45.5 ± 2.10
37-38	13.5 ± 1.44	8.5 ± 1.44*	5.7 ± 4.33**
39	14.5 ± 1.04	9.8 ± 0.63**	4.5 ± 2.10**
40-41	12.8 ± 1.60	10.3 ± 0.63	9.5 ± 0.65
42	10.0 ± 3.54	13.0 ± 1.23	10.8 ± 0.48
43-45	11.8 ± 1.18	7.3 ± 2.17*	5.3 ± 1.11**
46-48	8.8 ± 4.27	8.8 ± 4.30	6.3 ± 3.75
49-56	11.5 ± 3.6	10.4 ± 4.2	10.4 ± 2.6

Shaded rows indicate fractions of **E1** with significant effect on the contraction frequency of the uterus. *p<0.05; **p<0.01; n= 4-6 experiments

Table 2.12 Effect of **E1a** Fractions on the Contraction Amplitude (g) of the Uterus

Fractions	Control	50 µg/ml	150 µg/ml
11	4.92 ± 0.05	4.78 ± 0.11	4.25 ± 0.16
12	4.46 ± 0.56	5.36 ± 0.42	4.60 ± 0.35
13	4.94 ± 0.49	4.97 ± 0.22	4.69 ± 0.37
14-16	4.65 ± 0.41	4.39 ± 0.43	3.68 ± 0.27
17-19	4.76 ± 0.27	4.47 ± 0.11	4.34 ± 0.22
20	4.29 ± 0.22	4.42 ± 0.21	4.07 ± 0.08
21	5.2 ± 0.35	5.1 ± 0.18	4.4 ± 0.20
22-24	3.62 ± 0.10	3.20 ± 0.12	2.07 ± 0.19**
25	5.39 ± 0.09	5.16 ± 0.14	4.16 ± 0.05**
26	5.26 ± 0.02	4.69 ± 0.25	3.79 ± 0.27*
27	4.69 ± 0.12	4.50 ± 0.17	4.31 ± 0.05
28	4.26 ± 0.39	3.95 ± 0.12	3.82 ± 0.17
29-30	3.63 ± 0.27	3.00 ± 0.48	2.37 ± 0.12**
31-32	4.08 ± 0.08	3.46 ± 0.02 **	2.48 ± 0.19**
33	3.49 ± 0.02	3.08 ± 0.22*	2.48 ± 0.23**
34-36	4.33 ± 0.43	3.58 ± 0.42	2.87 ± 0.44?
37-38	3.49 ± 0.15	3.07 ± 0.33*	2.46 ± 0.19**
39	3.16 ± 0.42	3.01 ± 0.41	2.15 ± 0.29
40-41	3.37 ± 0.29	2.94 ± 0.34	2.22 ± 0.27*
42	2.97 ± 0.37	2.59 ± 0.25	2.91 ± 0.36
43-45	3.32 ± 0.21	2.77 ± 0.13	2.26 ± 0.15
46-48	3.34 ± 0.05	3.14 ± 0.02	2.84 ± 0.16**
49-56	3.19 ± 0.51	3.14 ± 0.29	2.44 ± 0.37

Shaded rows indicate fractions of **E1** with significant effect on the amplitude of uterine contraction. *p<0.05; **p<0.01; n= 4-6 experiments.

Table 2.13 Effect of **E1a** Fractions on the AUC (g. s) of the Uterus

Fractions	Control	50 µg/ml	150 µg/ml
11	318.89 ± 23.43	286.31 ± 28.41	236.05 ± 16.42
12	313.37 ± 12.19	261.49 ± 0.83*	242.25 ± 15.36**
13	304.48 ± 13.03	297.52 ± 24.50	239.54 ± 6.03*
14-16	187.72 ± 12.91	121.90 ± 10.07**	69.33 ± 4.79**
17-19	185.00 ± 8.66	129.43 ± 7.18**	71.79 ± 2.97**
20	189.05 ± 14.66	225.92 ± 6.04	202.42 ± 9.03
21	209.74 ± 3.09	254.89 ± 8.41	292.45 ± 9.61**
22-24	286.89 ± 9.09	258.45 ± 1.17*	174.32 ± 16.36**
25	254.81 ± 15.17	231.37 ± 7.36	197.46 ± 6.87 **
26	216.76 ± 5.47	189.88 ± 3.79**	149.21 ± 1.26**
27	220.01 ± 1.29	173.02 ± 5.95	134.92 ± 0.80**
28	211.36 ± 17.92	161.25 ± 16.08	125.82 ± 4.86**
29-30	321.02 ± 12.13	218.41 ± 14.94**	158.20 ± 12.61**
31-32	174.54 ± 10.34	128.36 ± 10.09*	62.66 ± 6.52 **
33	164.38 ± 15.92	114.42 ± 12.51*	64.62 ± 9.34**
34-36	445.16 ± 1.15	396.69 ± 17.87*	339.98 ± 10.83**
37-38	152.51 ± 15.95	102.12 ± 12.73*	65.39 ± 11.86**
39	360.17 ± 8.70	305.79 ± 17.72	258.71 ± 24.29**
40-41	318.91 ± 8.37	304.81 ± 2.78	220 ± 1.08**
42	302.52 ± 15.32	260.46 ± 16.31	316.70 ± 11.77
43-45	238.18 ± 4.58	184.26 ± 9.00**	143.46 ± 1.52**
46-48	291.23 ± 1.13	238.03 ± 3.34**	181.62 ± 1.19**
49-56	259.38 ± 6.90	205.74 ± 14.23**	187.00 ± 12.04**

*p<0.05; *p<0.01; n=4-6 experiments.

2.7.8.1 Effect on Spontaneous Uterine Contractility

Compounds **1**, **2**, **Fr. 28Ea**, **Fr. 6.17Ea** and **6** reduced the frequency and amplitude of spontaneous uterine contractions (Fig. 2.65 and 2.66). Each of these compounds exerted significant concentration-dependent inhibitory effects ($p < 0.01$) at all concentrations used. Commercially purchased trilinolein produced inhibitions at 0.1 mM (Fig. 2.67). However, **Fr. 28Ea** and **Fr. 6.17Ea** appeared to exhibit greater potency as these were mixtures containing more than three identified compounds. Compound **7** on the other hand appeared to produce varied effects of inhibition and stimulation, though the inhibitory component was considered statistically non-significant while significant stimulatory effects ($p < 0.01$) being very evident at 200 $\mu\text{g/ml}$ (Fig. 2.65C and 2.66C). Additionally, after each wash there was consistently observed an increase in tension (Fig. 2.60) which lasted for over 5 min. Trilinolein and pyrimidine which were commercially purchased were found to concentration-dependently inhibit uterine contractions at the concentrations used (Fig. 2.67).

Compound **14** stimulated significant increases ($p < 0.05$) in the frequency and amplitude of the isolated uterus at 30 $\mu\text{g/ml}$ (Fig. 2.63 and 2.69). Compound **15** similarly stimulated a concentration-dependent increase in the frequency and amplitude of the isolated uterus (Fig. 2.64 and 2.68).

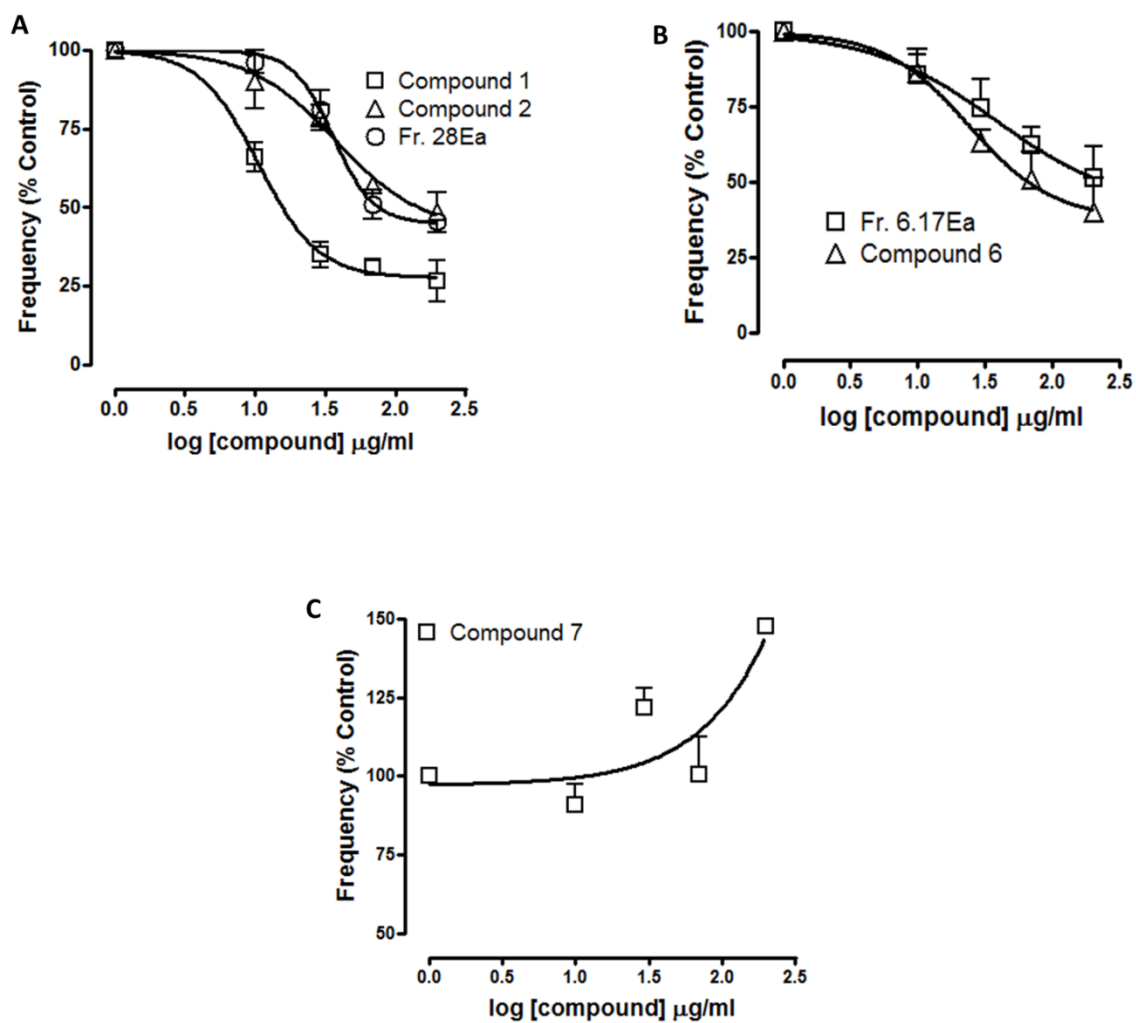


Figure 2.65 The effects of compounds from the leaves of *F. exasperata* on the frequency of spontaneous uterine contractions. Shown are concentration–response curves for compounds **1**, **2** and **Fr. 28Ea** (A) ($n = 5$ animals), **Fr. 6.17Ea**; Compound **6** (B) and compound **7** (C) ($n = 5$ animals). Data points for each set of experiments represent mean \pm S.E.M.

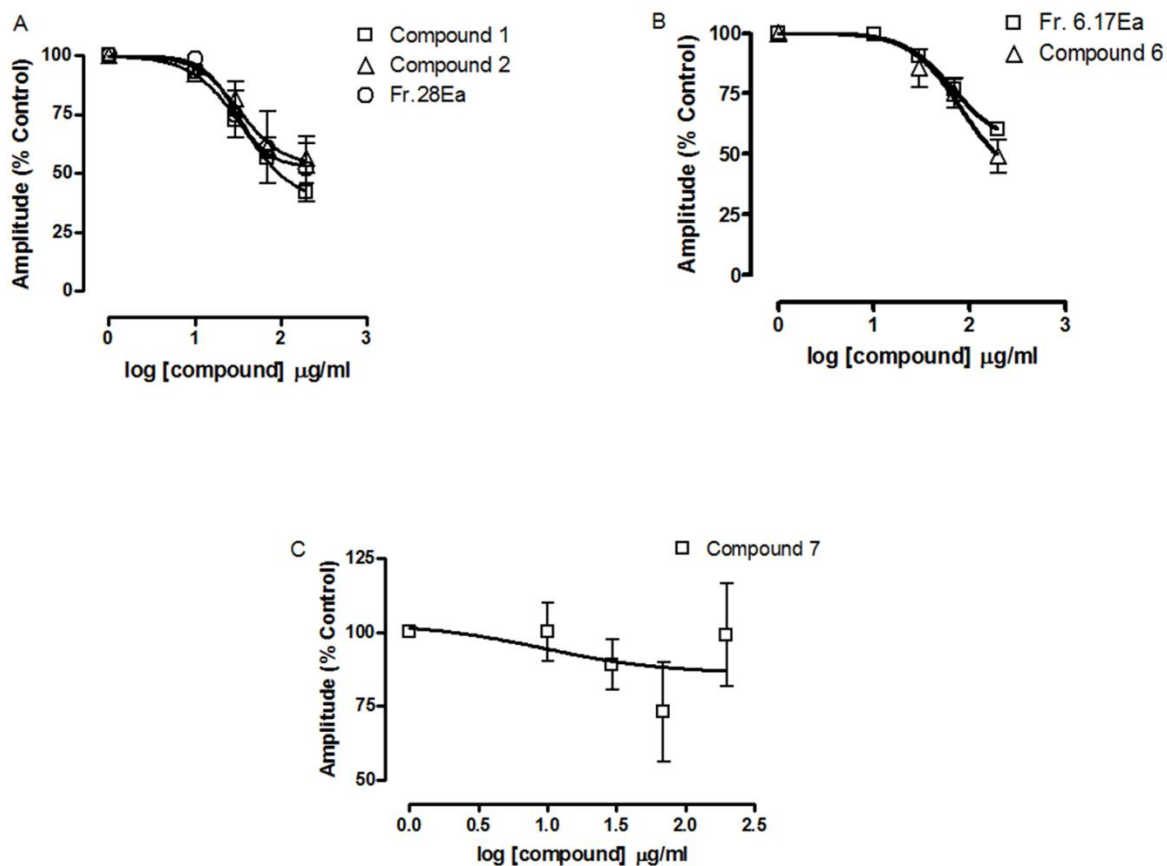


Figure 2.66 The effects of compounds from the leaves of *F. exasperata* on the amplitude of spontaneous uterine contractions. Shown are concentration–response curves for compounds **1**, **2** and **Fr. 28Ea** (A) ($n = 5$ animals), **Fr. 6.17Ea**; **6** (B) and compound **7** (C) ($n = 5$ animals). Data points for each set of experiments represent mean \pm S.E.M.

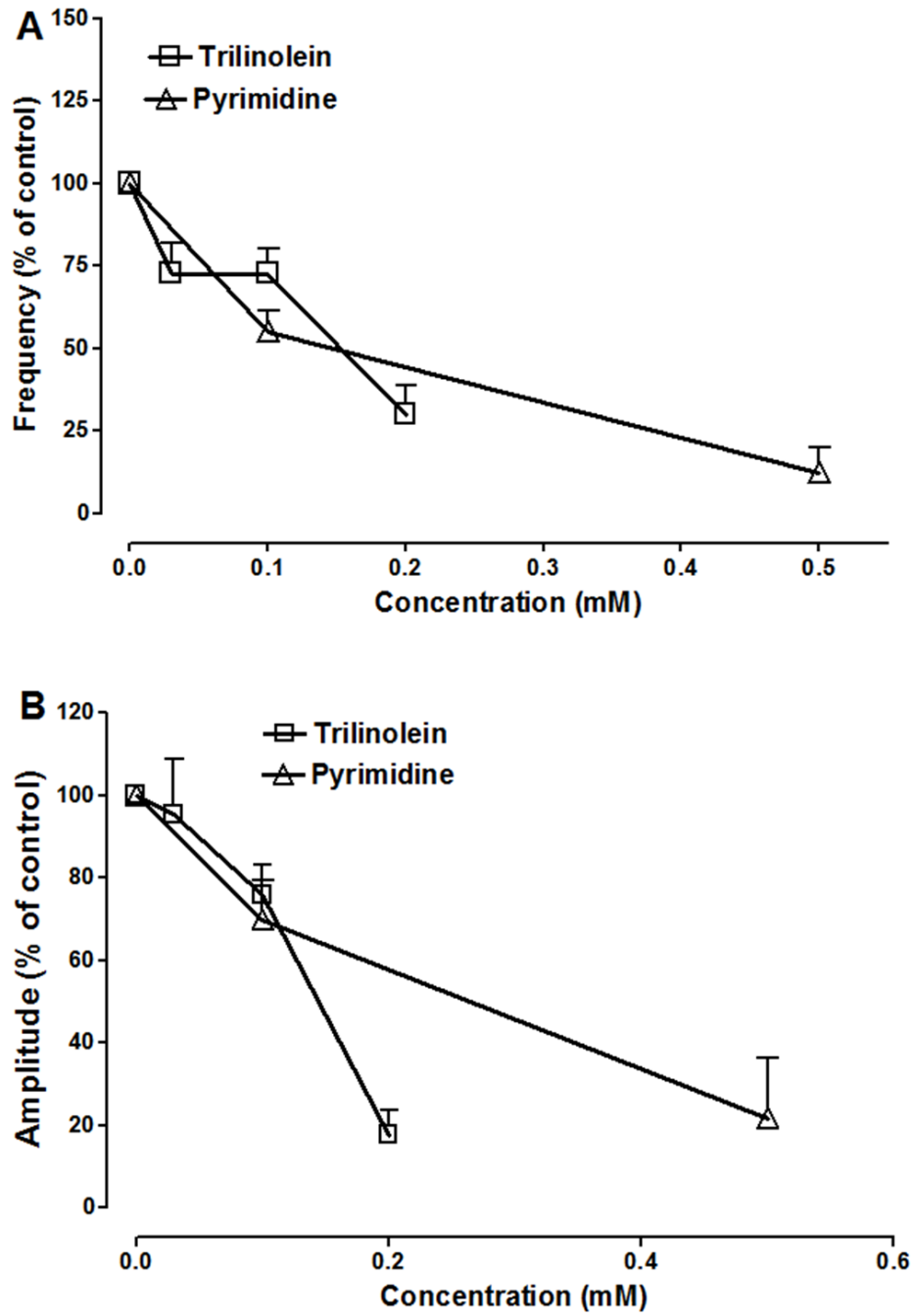


Figure 2.67 The effect of trilinolein and pyrimidine on the frequency and amplitude of spontaneous contractions, $n = 5$ animals. Data points for each set of experiments represent mean \pm SEM.

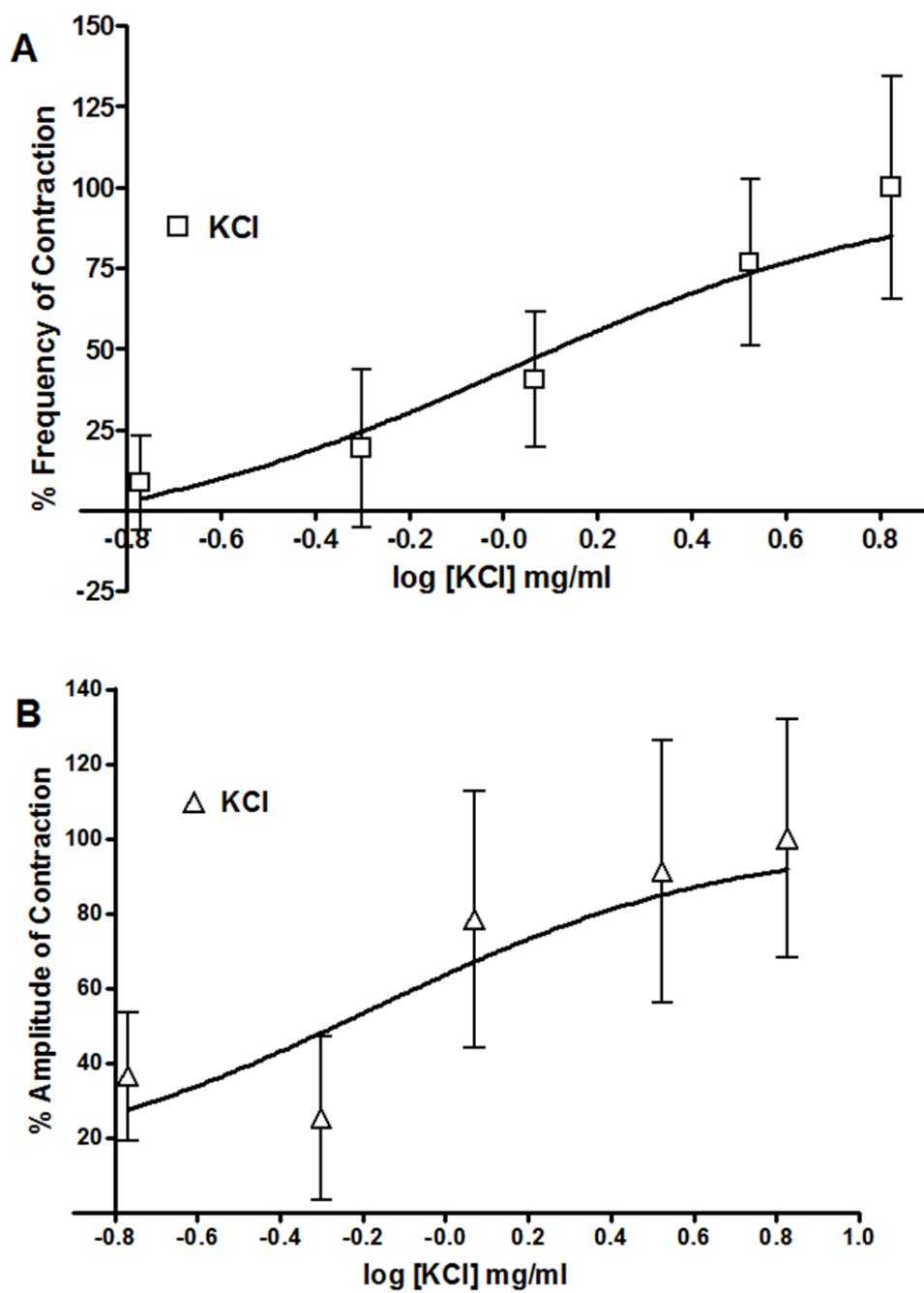


Figure 2.68 Concentration-response curves showing the effect of increasing concentrations of compound **15** (KCl isolated from the leaves of *F. exasperata*) on spontaneously contracting uterine tissue. The effect on frequency is shown in panel A and the effect on amplitude is shown in panel B. n= 5 animals.

Table 2.14 Contractility Parameters for Inhibitory Compounds on Spontaneous Contractions of the Isolated Non-Pregnant Mouse Uterus

Compounds	pEC ₅₀	E _{max} (cycles/5 min)	pEC ₅₀	E _{max} (g)
1	1.47 ± 0.08 ^a	24.64 ± 6.83 ^b	1.57±0.08 ^c	41.96 ± 4.0 ^d
2	1.49 ± 0.05 ^a	50.43 ± 11.03 ^b	1.46±0.02 ^c	56.51 ± 6.3 ^d
Fr.28Ea	1.45 ± 0.05 ^a	51.56 ± 11.43 ^{b*}	1.55 ± 0.11 ^c	51.91±13.99 ^d
Fr. 6.17Ea	1.37±0.11 ^a	63.33 ± 10.59 ^{b*}	1.64 ± 0.09 ^c	68.26 ± 2.52 ^d
6	1.5 ± 0.09 ^a	56.88 ± 5.70 [*]	1.54 ± 0.12 ^c	50.58 ± 9.71 ^d
7*	n.d.	n.d.	n.d.	n.d.

Maximum values are expressed as a percentage of the response to spontaneous contractions which was used as the control. E_{max} represents maximal effect and pEC_{50} represents the average half maximal effect. Data represents means ± SEM for $n = 5$ animals. Values with the same superscript are not significantly different from each other. $P \leq 0.05$ was considered significant in all cases.

The EC₅₀ for compound **7** could not be determined; n.d. = not detected

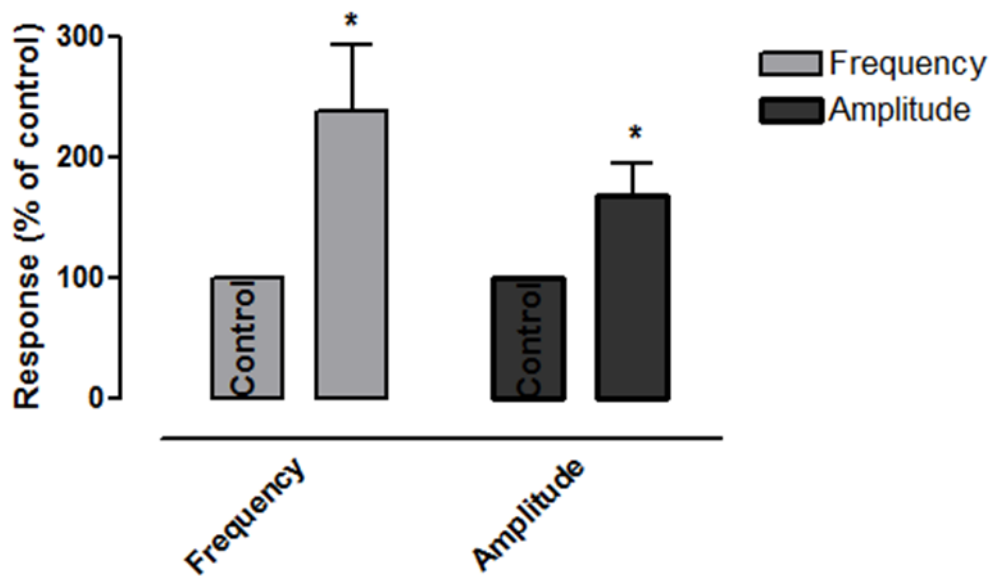


Figure 2.69 Bar graphs displaying the effect of compound **14** on uterine contractions. The percentage change in response is displayed in the left y-axis while the frequency and amplitude are displayed in the x-axis * $p < 0.05$; $n = 5$ animals.

2.7.8.2 Effect on Oxytocin-induced Uterine Contractions

Original representative recordings showing the effects of compounds **1**, **2**, **Fr. 28Ea**, **Fr. 6.17Ea**, **6** and **7** on OT-induced uterine contractions can be seen in figures 2.70, 2.71, 2.72, 2.73, 2.74, 2.75 respectively. An original representative tracing showing the effect of commercially purchased pyrimidine can also be seen in fig. 2.76. Compounds **1**, **2**, **Fr. 28Ea**, **Fr. 6.17Ea**, and **6** inhibited both the frequency and amplitude of OT-induced uterine contractions (Fig. 2.77 and 2.78). Compound **1**, compound **2** and **Fr. 28Ea** decreased the frequency of OT-induced contractions with variable effects on the amplitude (Fig. 2.77 and 2.78). Interestingly, however, compound **7** appeared to stimulate an increase in frequency but inhibit the amplitude of OT- induced contractions (Fig. 2.77 and 2.78).

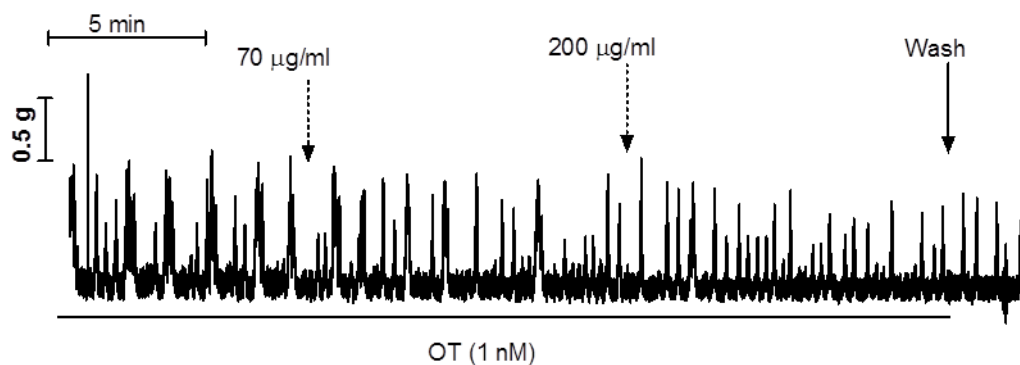


Figure 2.70 Original recording showing the effect of compound **1** on OT-induced uterine contractions. Compound **1** was added at concentrations of 70 and 200 µg/ml to OT-stimulated uterine contractions in order to assess the effect on agonist induced stimulation.

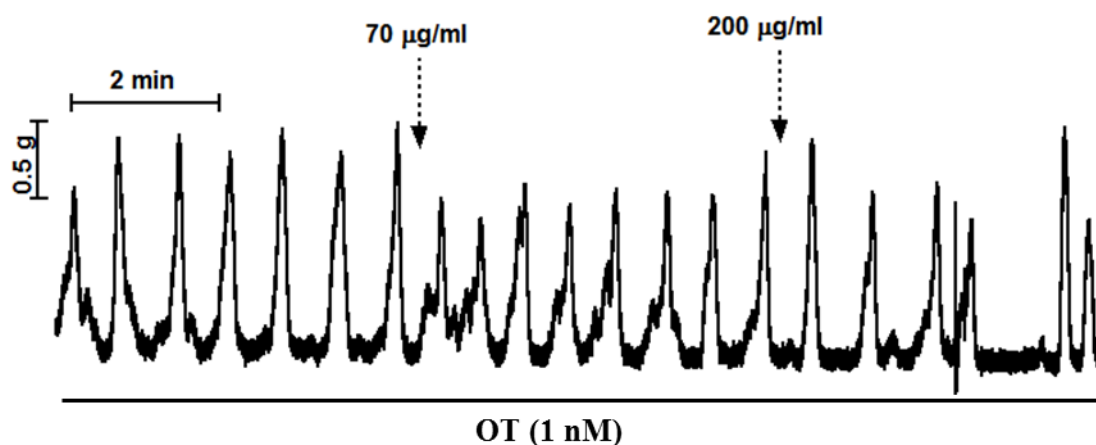


Figure 2.71 Original recording of compound **2** on OT-induced uterine contractions. At concentrations of 70 and 200 µg/ml, compound **2** was added into OT-stimulated uterine contractions to assess the effect on agonist stimulated contractions.

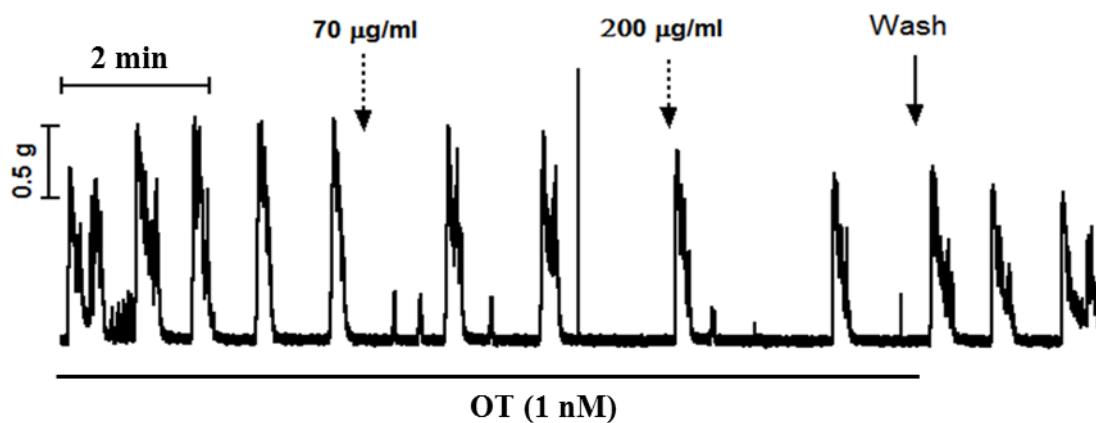


Figure 2.72 Original tracings of **Fr. 28Ea** on OT-induced uterine contractions. Fraction **28Ea** was added at concentrations of 70 and 200 $\mu\text{g/ml}$ to OT-stimulated uterine contractions in order to assess the effect on agonist induced stimulation.

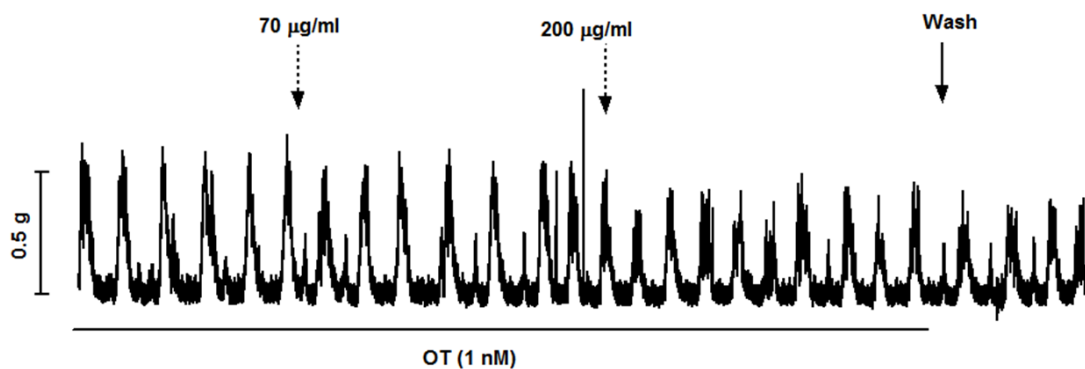


Figure 2.73 Original tracings of **Fr. 6.17Ea** on OT-induced uterine contractions. At concentrations of 70 and 200 $\mu\text{g/ml}$, **Fr.6.17Ea** was added into OT-stimulated uterine contractions to assess the effect on agonist stimulated contractions.

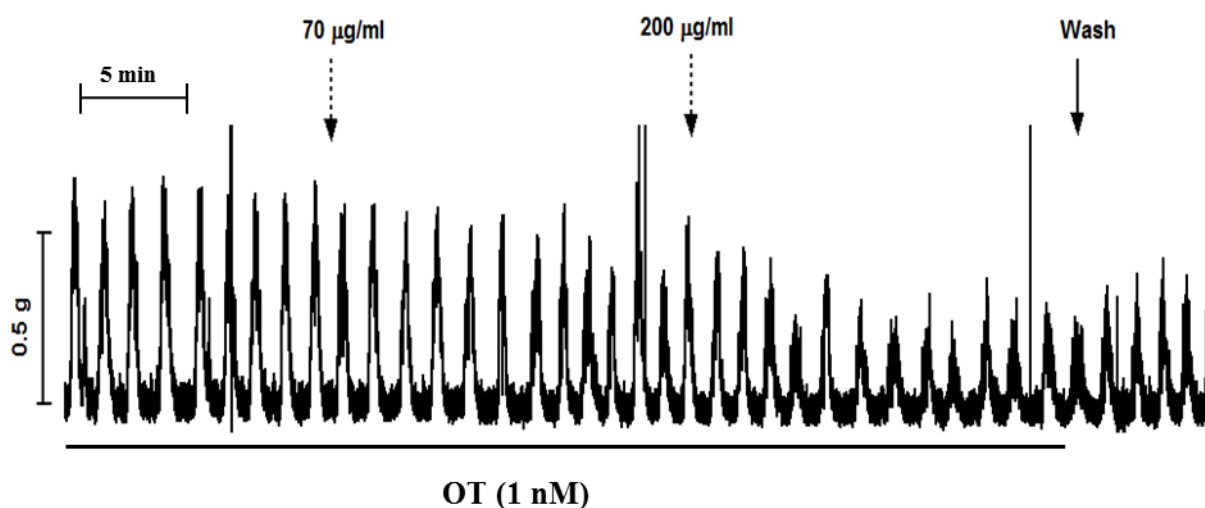


Figure 2.74 Representative tracing of compound **6** on OT-induced uterine contractions. Additions were made at concentrations of 70 and 200 µg/ml in the presence of OT and observed.

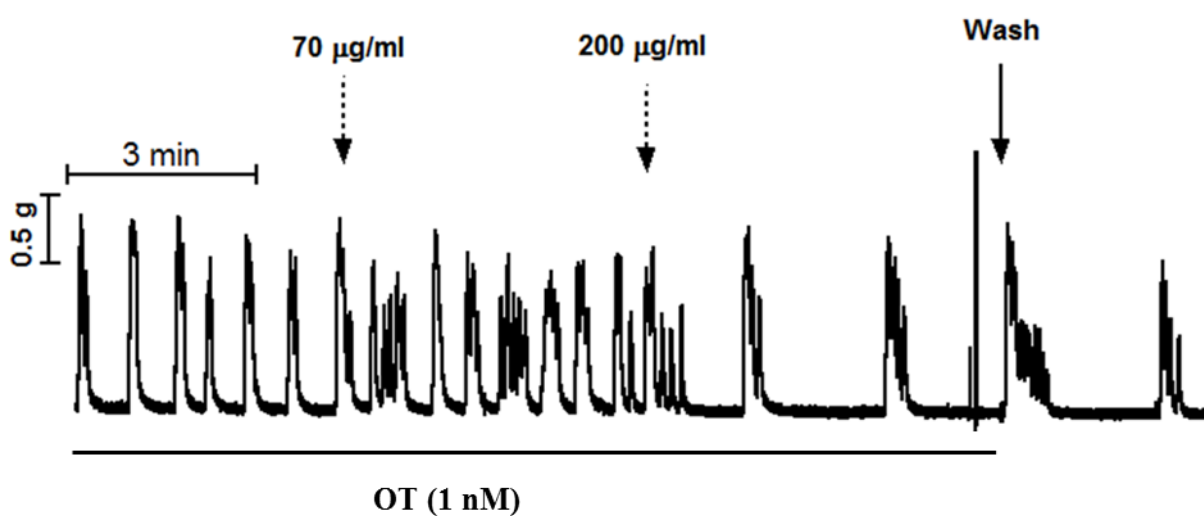


Figure 2.75 Representative tracing of compound **7** on OT-induced uterine contractions. The effect of compound **10** at concentrations of 70 and 200 µg/ml were observed in the presence of OT.

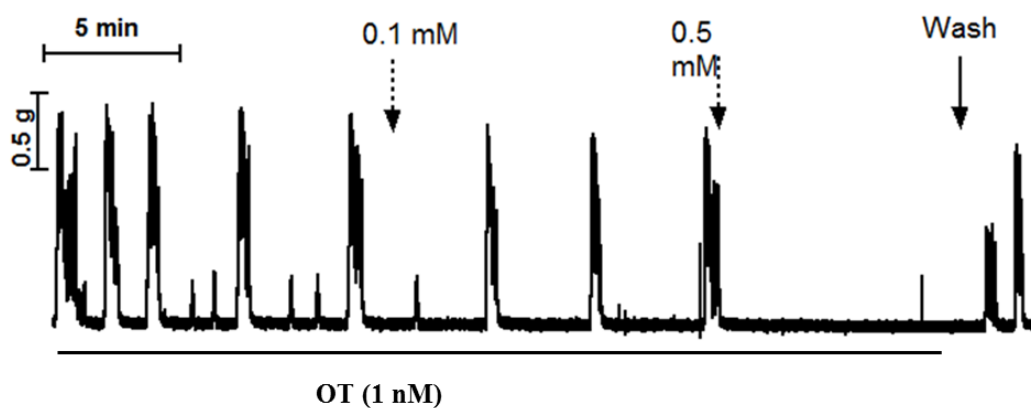


Figure 2.76 Original recording of the effect of pyrimidine on OT-induced contractions. At concentrations of 0.1 and 0.5 mM, pyrimidine was added into OT-stimulated uterine contractions to assess the effect on agonist stimulated contractions.

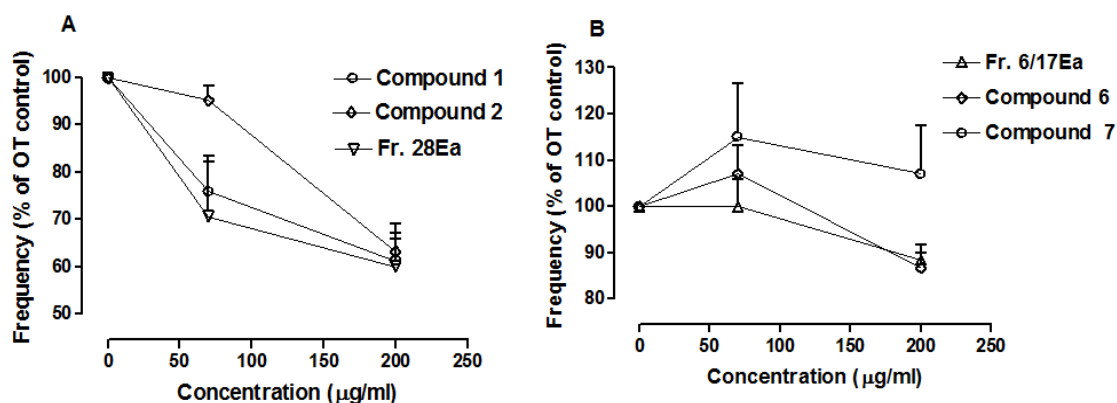


Figure 2.77 The effects of compounds from the leaves of *F. exasperata* on the frequency of OT-induced uterine contractions. Shown are concentration–response curves for **1**, **2** and **Fr. 28Ea** (A) (n = 5–6 animals), **Fr. 6/17Ea**; **6** and **7** (B) (n = 5–6 animals). Data points for each set of experiments represent mean ± S.E.M.

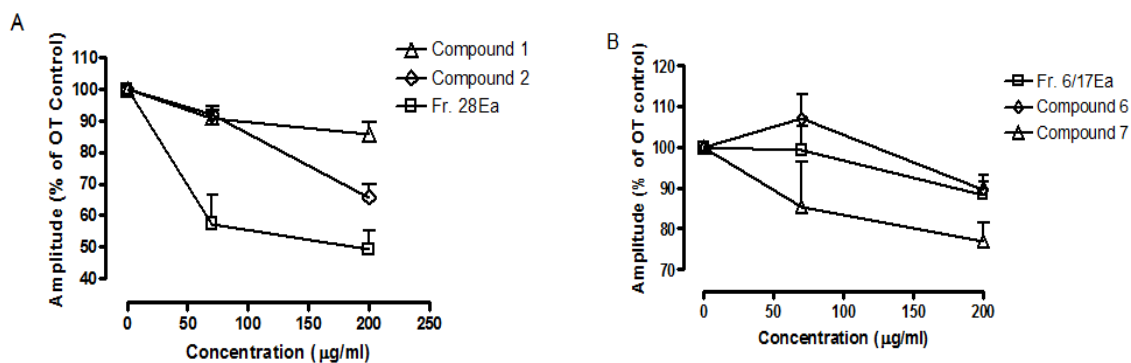


Figure 2.78 The effects of compounds from the leaves of *F. exasperata* on the amplitude of OT-induced uterine contractions. Shown are concentration–response curves for **1**, **2** and **Fr. 28Ea** (A) (n = 5–6 animals), **Fr. 6/17Ea**; **6** and **7** (B) (n = 5–6 animals). Data points for each set of experiments represent mean ± S.E.M.

2.7.8.3 Effect on KCl-induced Uterine Contractions

Compounds **1**, **2**, **Fr. 28Ea**, **Fr.6.17Ea** and **6** displayed no significant inhibition of 80 mM KCl-induced contractions including trilinolein.

Table 2.15 Summary Table for Active Compounds Isolated from the Leaves of *Ficus exasperata*

Compounds	Molecular Weight (g/mol)	Molecular Formula	Fraction	Uterine Activity
1	617.5139	C ₃₉ H ₆₉ O ₅	Fraction 14 E1	Inhibition
2	135.0650	C ₅ H ₁₁ O ₄	Fraction 37 E1	Inhibition
3	869.5582	C ₅₅ H ₇₃ N ₄ O ₅	Fraction 6-17 E1	Inhibition/Contraction
4	607.2917	C ₃₆ H ₃₉ N ₄ O ₅	Fraction 6-17 E1	Inhibition/Contraction
5	593.2754	C ₃₅ H ₃₇ N ₄ O ₅	Fraction 6-17 E1	Inhibition/Contraction
6	535.2704	C ₃₃ H ₃₅ N ₄ O ₃	Fraction 4-31 E1	Inhibition
7	635.2888	C ₃₇ H ₃₉ N ₄ O ₆	Fraction10-22 E1	Inhibition/Contraction
8	884.5430	C ₅₅ H ₇₃ N ₄ O ₆	Fraction10-22 E1	Inhibition/Contraction
9	607.2549	C ₃₅ H ₃₅ N ₄ O ₆	Fraction10-22 E1	Inhibition/Contraction
10	285.0757	C ₁₆ H ₁₃ O ₅	Fraction 28 E1	Inhibition
11	259.1330	C ₁₆ H ₁₃ O ₅	Fraction 28 E1	Inhibition
12	259.1330	C ₁₆ H ₁₃ O ₅	Fraction 28 E1	Inhibition
13	289.1432	C ₁₇ H ₁₉ O ₅	Fraction 28 E1	Inhibition
14	95.0604	C ₇ H ₅ N ₂	Fraction M1	Contraction
15	74.5513	KCl	Fraction M1	Contraction

2.8 Discussion

2.8.1 Plant Extraction

The extract yields obtained from the use of the two plant extraction procedures in this study, the maceration process and the Soxhlet Apparatus were examined. The results showed that the yields were comparable (Sections 2.6.2). That a non-polar solvent (such as hexane) was not employed during the maceration process may have resulted in more compounds in **E2** and the similarity between the ¹H-NMR of **H1** and **E2** as well as the subtle differences in the proton signals observed between **E1** and **E2** (Fig 2.11 a and b). This may also account for the slightly higher yield of **E2** compared with **E1**.

2.8.2 TLC Analysis of Extracts

Observation of the TLC plates under UV wavelength 365 nm showed some bands with distinguishable red fluorescing zones which were most probably due to chlorophyll (French and Huang, 1957; Emerson, 1957; Tomkins and Miller, 1994). These zones also appeared as green spots on the TLC plates (Fig. 2.2 and Fig. 2.3). Chlorophyll and its derivatives exist as either lipophilic or hydrophilic chlorophyll, thus depending on the solvent elution system applied, it could elute at differing distances along the TLC plate (Lavallee *et al.*, 1982; Ferruzzi and Blakeslee, 2007). Chlorophyll a, appears as dark green, while chlorophyll b may appear as pale yellow, yellow or orange (Thorne *et al.*, 1977). Pheophytin a and b are chlorophyll derivatives in which the chlorophyll lacks a magnesium ion and may also appear as green spots above the chlorophyll zones (Thorne *et al.*, 1977; Quach *et al.*, 2004). The yellowish colour observed at an R_f of 0.96 and 0.62 on the TLC plates that were not sprayed with reagents (Fig. 2.2 and 2.3) may represent the presence of fatty acids. Complex lipids such as glycosphingolipids and phospholipids usually remain at the origin and the simple lipids such as cholesterol esters, triglycerides, free fatty acids, cholesterol and diacylglycerol migrate along the plate when using mobile phases such as hexane and diethylether (Christie and Han, 2003) or in this instance ethyl acetate. Upon spraying with the anisaldehyde-sulphuric acid reagent a deep pink colour was observed. This deep pinkish colour was more intense at R_f 0.96 and 0.5 in **H1** and **E2** (Fig. 2.2 and Table 2.1) indicating the probable presence of a combination of simple lipids and some less complex lipids (Wagner *et al.*, 2009). The additional presence of carotenoids cannot be ruled out as they are usually in

combination with some lipids and are also observed as yellow bands on the TLC plates (Quach *et al.*, 2004).

The blue fluorescence observed under UV 365 nm which took up subtle violet colouration on plates sprayed with the anisaldehyde reagent respectively, at R_f 0.44 and 0.48 (Fig. 2.2, Fig. 2.3 and Table 2.1) may indicate the presence of alkaloids (Wagner *et al.*, 2009).

2.8.3 $^1\text{H-NMR}$ Analysis of Extracts of *F. exasperata*

The $^1\text{H-NMR}$ spectra of all extracts enabled a preliminary assessment of the range of peaks and likely classes of compounds expected. At the crude stage, each extract was a complex mixture of compounds, and definite conclusions could not be reached. However a few observations can be made. **E1** displayed some peaks up to 11.5 ppm signifying the probable presence of carboxylic acids. Also more peaks were observed in **E1** within the olefinic region and especially within the sugar and alcohol regions (4 - 5 ppm) compared to **E2**. The most intense of peaks in **M1** occurred within the aliphatic and olefinic region. There was observed a reduced density of peaks within the aliphatic region compared to **H1**, **E1** and **E2**. There was also observed broadening underneath the peaks at the olefinic regions (Fig. 2.11a) which are usually indicative of a number of factors one of which is the presence of salts or water. The peaks occurring in **W2** and **B2** showed similar distribution to each other in the chemical shifts from the aliphatic region to the aromatic region up to 9.2 ppm. The density of peaks in the aliphatic region was also much reduced compared to **H1**, **E1** and **E2**. **M1**, **W2**, and **B2** showed similarities in peaks (Fig. 2.11a and b)

however **M1** had the most number of peaks. **H1**, **E1** and **E2** also showed similarities in certain peaks (Fig. 2.11 a and b) but **E1** was distinctly different owing to the presence of peaks within 3.2 to 4.0 ppm which signifies the probable presence of alkyl groups attached to electronegative groups or the presence of alcohols or ethers.

2.8.4 LC-ESIMS Analysis of Extracts of *F. exasperata*

The total ion current chromatogram (TIC) and base peaks of the LC-HRFTMS data of the extracts were observed in the absence of a search for specific masses or peaks. The total ion chromatogram is a representation of the summed intensities of a range of masses across every point in the analysis where the masses are being detected (Anderegg, 1990). The base peak chromatogram on the other hand is quite similar to TIC but only the most intense peaks in the spectrum are displayed (Murray *et al.*, 2013). Base peak chromatograms therefore provide more information on the analytes than the TIC chromatogram. The information provided by the TIC is also quite limited compared to an extracted ion chromatogram (XIC) also called a reconstructed ion chromatogram (RIC) in which one or more specific m/z values are obtained or 'extracted' from the entire chromatographic analysis and are usually created using a data-analysis process. The XIC is useful for: detection of unknown analytes, detection of potential isomers, resolution of suspected co-eluting substances, or for the production of clean chromatograms with compounds of interest (Murray *et al.*, 2013). For the extracts, a base peak chromatogram was displayed as each extract was still at the crude stage. The peak at R_t 10.00 min which was common to all extracts (Fig. 2.12 and 2.13) was probably an artefact from the solvent. **M1** and **W2** exhibited fewer similar peaks which also occurred at the same retention times (Fig. 2.13). This

is suggestive of fewer compounds in the polar extracts compared to the others. Peaks exhibited by **B2** at Rt 6.9-8.3 min are suggestive of the presence of polar low molecular weight compounds (Fig. 2.13). A peak at Rt 27.70-27.72 min was common to **H1** and **E2** while a peak at Rt 41.3 min was common to **E1** and **E2** (Fig. 2.12). Peaks at 32.9-34.45 min were common to **M1** and **W2** while a peak at Rt 34.34 min was common to **M1**, **B2** and **W2** (Fig. 2.13).

2.8.5 Uterine Contractility Effect of Extracts

An assessment of the effect of the extracts on frequency and amplitude of uterine contractions was performed and the integral of the effects was also computed.

M1, **B2** and **H1** produced an increase in the frequency of uterine contractions, though the effect of **B2** can be considered transient. The reason for this is yet to be determined however possible hypotheses are interaction with voltage-dependent calcium channels, allowing an influx of extracellular calcium and enhancing contractions or due to inhibition of voltage-dependent potassium channels which Aaronson *et al.* (2006) proposed as a major contributing factors to basal myometrial contractility.

It was also observed that the extracts which increased the frequency of uterine contractions produced a concurrent decrease in the amplitude. A probable reason why a drug can affect the frequency of uterine contractions independent of the amplitude might be due to a lack of effect or an opposing effect on the endogenous pacemaker cells, which was noted by Mackler and colleagues, (1999) to reside in uterine tissues. The pacemaker cells in the uterus directly affect the gap junction

assembly and will either increase or decrease cellular communication, and consequently uterine contractions. The presence of endogenous oscillator within the uterus regulates the amplitude of contractions (Mackler *et al.*, 1999). This uterine oscillator differs from the neuroplexus pacemaker which coordinates smooth muscle activity in the gastrointestinal tract.

2.8.6 Fatty Acids Isolated from *F. exasperata*

The compound 1,3-dilinolein (compound **1**), as well as 3-O-glycerolmonoacetate (compound **2**) were isolated and identified from the leaves of *F. exasperata* and these were observed to exert significant inhibitory effects on the frequency and amplitude of uterine contractions. Fats as lipids have been described as biological compounds that include cholesterol, triacylglycerol and phospholipids, all of which play important biological roles (Mattos *et al.*, 2000). Phospholipids for instance make up the cellular membranes and act as precursors for several effector compounds e.g. the eicosanoids, while cholesterol, which is also a cell membrane component, acts as a precursor for steroidal hormones. The functions of these fatty acids are considered to be largely dependent on their structure. The esterification of fatty acids to the hydroxyl groups of glycerol results in the production of triacylglycerols (TGs), diacylglycerols and monoacylglycerols (Murphy *et al.*, 2007). The diacylglycerols can serve as intermediates both in the synthesis and metabolism of TGs but are also important signalling molecules (Murphy *et al.*, 2007). Essential fatty acids (EFAs) and metabolites of both the linoleic acid (LA, n-6) and linolenic acid (LnA, n-3) series contribute to the regulation of gestation and parturition (de Groot *et al.*, 2004). It has been reported that administration of very long chain n-3 fatty acids may

prolong the gestation periods in animals and humans through interference with the production of prostaglandins in reproductive tissues (de Groot *et al.*, 2004). This effect may also be related to the interference of arachidonic acid (ARA) metabolism *in vivo* which may ultimately regulate uterine contraction. Conjugated linoleic acids (CLA) have also been reported to inhibit prostaglandin synthesis *in-utero* (Harris *et al.*, 2001). Reduction of prostaglandin production and possibly extension of gestation period with the use of supplements of DHA or CLA is suggested to be beneficial in preterm birth (Harris *et al.*, 2001). The compound LA n-6, has been reported to inhibit ARA (Harris *et al.*, 2001) resulting in the accumulation of ARA subsequently activating stretch-dependent potassium channels (TREK) channels and further inhibition of uterine contractions (Tichenor *et al.*, 2005). Studies have also demonstrated LA n-6 direct inhibition of prostaglandins in the non-pregnant uterus *in vitro* (Cheng *et al.*, 2003; Cheng *et al.*, 2001). In general, fatty acids have been reported to directly activate calcium channels as well as modulate the effect of cell signalling pathways on the myometrium (Allen and Harris, 2001). All of these may explain in part the effect of 1,3-dilinolein as well as 3-O-glycerolmonoacetate on uterine contractility.

In consideration of possible structure-activity relationships, trilinolein was commercially purchased and tested and compared with the isolated 1,3-dilinolein (compound **1**) under the same conditions. It may appear that dilinolein is a more potent uterine inhibitory agent compared to trilinolein. Inhibition by dilinolein was observed to begin at 0.1 nM and a greater effect at 0.32 nM (calculated from the molecular weight) while trilinolein exhibited inhibition at 0.1 mM though producing an almost complete inhibition at 0.3 mM. Based on this observation it is suggested

that modification of the dilinolein structure may produce significantly potent tocolytic drugs, especially as it seems that the loss of an extra FA chain may increase activity. It is also proposed that modification of the monoacetate structure may increase activity probably by increasing the chain length and/or the hydroxyl groups.

2.8.7 Pheophorbides and Pheophytins

Chlorophylls are the natural pigments responsible for the green colour of vegetation (Hornero-Mendez *et al.*, 2005). During processing and storage, chlorophylls may undergo chemical and physical changes as a result of their structural properties and their ability to harvest energy. Therefore chlorophylls and their derivatives can be used as treatment (Hornero-Mendez *et al.*, 2005). During the extraction process, pheophytinization of the chlorophyll pigments occurs depending on the types of chlorophylls originally present. The pheophytins also appear to be a more stable form of chlorophyll. The pheophytins have been studied for their cytotoxic effects (Hajri *et al.*, 2002; Tan *et al.*, 2011; Wongsinkongman *et al.*, 2002) as a result of their ability to photosensitize. Pheophorbide-a derivatives such as pheophytin-a and pheophytin-a methyl esters, are frequently used as photosensitizers in photodynamic therapy (Dai *et al.*, 1992; Kessel and Smith, 1989). Pheophorbide-a, for instance is commonly utilized therapeutically for photodynamic therapy of certain diseases such as leukaemia, pigmented melanoma, colonic cancer, hepatoma and uterine carcinosarcoma by mechanisms of autopsies and autophagy (Bui-Xuan *et al.*, 2010). There have however been no reports, correlations or connections of pheophorbides with uterine contractility and this study would therefore be the first report of the effects of pheophorbide derivatives on uterine contractility.

New derivatives of both pheophorbide-a and -b were identified in this study. Pheophorbide-a is a metabolite of plant cells that is formed when chlorophyll a loses a magnesium ion and a phytol group through enzyme action (chlorophyllase) (Bui-Xuan *et al.*, 2010) and it is characterized by the absence of the aldehyde functional group on the ring structure. The mixture containing pheophorbide-a derivatives and pheophorbide a appeared to have an interesting effect on uterine contractility. It was observed that while the amplitude of contraction was moderately reduced there seemed to be an increase in frequency, which appeared in bursts of contractions rather than a rhythmic sequel. In the myometrial layer, the depolarizing phase responsible for the produced spikes is a result of inward currents carried by Ca^{2+} and Na^+ ions (Garfield and Maner, 2007), suggesting a possible involvement of the pheophorbide-a derivatives with calcium ions in uterine contractility. Pheophorbide b derivatives also displayed somewhat interesting activities on the uterus; the long chain pheophorbide b derivative was not tested in this study due to very low yield (2 mg). However, the short chain derivative appeared to exhibit dual activities (stimulation and inhibition) on spontaneously contracting tissues while inhibiting oxytocin-induced contraction. The contractile effect was not abolished after washing instead a sustained increase in both the frequency and amplitude of contractions after washing was observed. At this stage it is suggested that synthesis of the short chain pheophorbide-b derivative be performed and tested for further confirmation of its activity on the uterus, however the distinct contractile effect on spontaneous contraction makes it a potential agent for the management of dysfunctional labour.

2.8.8 Flavonoids

The term “flavonoid” is generally used to define an extensive range of natural products that consists of a C₆-C₃-C₆ carbon structure. Flavonoids can also be specifically described as having a phenylbenzopyran functionality. Several biological actions have been associated with the hydroxymethoxyflavones group of the flavonoids (e.g. chrysoeriol and diosmetin) (Park *et al.*, 2007). There are also the phytoestrogens, considered a very important and interesting group of flavonoids (e.g. isoflavones: genistein derivatives) and antioxidants (anthocyanins: flavonols and flavones (Prasain *et al.*, 2004). Studies have reported the isoflavones and chalcones to possess modest estrogenic activity possibly due to the structural similarities between the oestradiol nucleus and the flavonoids (Lain *et al.*, 1996; Liu *et al.*, 1994; Miksicek, 1995). Certain flavones have also been reported to inhibit the enzyme cytochrome P₄₅₀ (Zhai *et al.*, 1998). Overall these compounds may exert significant effect on the reproductive physiology. It was also reported that flavonoids present in the plant *B. pinnatum* may contribute to the inhibition of myometrial contractility (Wachter *et al.*, 2011). It has been suggested that flavonoids exert betamimetic activities on the myometrium (Revuelta *et al.*, 1999). In addition flavonoids may contribute to the increase in the phospholipid diacylglycerol and also play a role in the activation of the mammalian mitochondrial Ca²⁺ uniporter (Lee *et al.*, 2002). In contrast, naringenin and naringenin glycosides were reported to block hERG K⁺ channels (Zitron *et al.*, 2005) possibly via an indirect action on kinase activity. In this study the mixture containing five flavonoids was found to significantly inhibit uterine contractility. The mechanism at this stage is unknown as further pharmacological characterization could not be continued due to low yield. It is again

suggested that the flavonoids isolated from *F. exasperata* poses as potential tocolytic agents and further studies as well as synthetic modifications should be performed.

2.8.9 Pyrimidines

There is evidence to suggest that substituted pyrimidine derivatives promote myometrial relaxation. A relaxant effect on the uterus by a dihydropyrimidine derivative has been reported (Salwan *et al.*, 2011). Imatinib, a 2-phenylaminopyrimidine inhibits uterine contraction by alteration of pacemaker activities within the uterus (Allix *et al.*, 2008). It was therefore an interesting observation that N-methyl pyrimidine isolated from the leaves of *F. exasperata* contracted the uterus as opposed to the unsubstituted pyrimidine which was commercially purchased. The unsubstituted pyrimidine (commercially purchased) was found in this study to inhibit the frequency and amplitude of uterine contractions at concentrations of 0.1-0.5 mM, while the isolated N-methyl substituted pyrimidine stimulated both the frequency and amplitude of uterine contractions at concentrations of 30 µg/ml. Further evaluations were not possible due to low yield. Close observation of the structure-activity relationship suggests that methyl substitutions may promote stimulatory effects which may be potentiated by substitutions on the nitrogen rather than on the carbon moiety. Again, N-methyl pyrimidine poses as a potential agent for the management of dysfunctional labour and it is suggested that targeted modification of the pyrimidine structure might lead to the production of compounds with inhibitory activities on the one hand and with stimulatory effects on the other.

2.8.10 Compound 15

A white crystalline compound was also isolated from the leaves of *F. exasperata* which as described earlier was identified as potassium chloride salt with a weight of 4.45 g from **M1**. The absence of peaks in ¹H-NMR of the compound suggested the presence of an inorganic compound which significantly stimulated uterine contractions.

2.9 Conclusion

The isolation and improvement of natural products for medicinal use has been in existence and one of the earliest examples is the conversion of salicylic acid to aspirin (Rishton, 2008). To date this process of improving natural products is still on going and cuts across a wide range and source of natural products. In this study, uterine active chemical compounds have been isolated from the leaves of *F. exasperata*. With the increased search for efficacious, potent and safe drugs to curb preterm labour as well as for the management of dysfunctional labour, *F. exasperata* has offered new starting natural product materials which can be improved for further analysis targeting therapeutic efficacy in comparison with existing drugs for similar conditions. This study also supports previous findings which reported a dual effect of the crude aqueous extract of *F. exasperata* on uterine contractions.

CHAPTER THREE

DEVELOPMENT OF A METABOLOMIC MODEL FOR THE DETERMINATION OF MYOMETRIAL FUNCTION

3.0 Introduction

Animal models are frequently used in the study of diseases. Due to the low throughput observed with the use of conventional *invivo* animal models, coupled with the relatively large quantities of compounds required for testing in these systems, *invivo* assay-guided fractionation is currently considered by some as an ineffective approach for the discovery of drug-like natural products (Crawford *et al.*, 2011). By quantitative measurement of responses of several systems to different stimuli, metabolomics attempts to investigate the chemical changes and fluctuation within cells of organisms (Werth *et al.*, 2010). Metabolomics is therefore an important component in biomarker studies (Lu and Xu, 2008). Metabolites are functional units released within cells in response to signals. Measurement of these metabolites therefore can provide understanding into the basic mechanisms of several metabolic actions (Lin *et al.*, 2007). Sampling during metabolomic analysis measurement can include biofluids and/or tissues and in such instances the tissue samples can be used to investigate specific information related to the tissue or organ while the study of biofluids projects the metabolic changes that have occurred in an animal's organs (Heijne *et al.*, 2005). This process is commonly employed for the investigation of certain disease states (Pears *et al.*, 2005; Stentiford *et al.*, 2005) or toxicity sites (Garrod *et al.*, 2001).

The uterus has been described as 'the poor sister among isolated tissues in the pharmacologist's armamentarium' due to the extensive hormonal network, receptors, ion channels and signalling systems which makes the uterine tissue a significant biological challenge (Crankshaw, 2001). A better understanding of myometrial function, as a means of tackling conditions of reproductive abnormalities (e.g.

preterm birth) is required. Metabolomics is increasingly being employed in a wide variety of research fields. Its use is based on its effectiveness in the detection and identification of several spectral features that are used to identify metabolites released in response to cellular activity (Griffin, 2006; Varghese *et al.*, 2010; Wiklund *et al.*, 2008). Metabolomic methods which involve high resolution Fourier transform mass spectrometry (HRFTMS) and 1D/2D NMR have consistently proven effective for such analyses (Lokhov and Archakov, 2009). Detection of metabolites serves as fingerprints of the biological system, while taking into consideration both internal factors (e.g. genetic) and external factors (e.g. disease or drug treatment) (Wang *et al.*, 2008). Metabolomic techniques and technologies are increasingly being improved, and are an important part of systems biology and biomarker discovery. Mass spectrometry (MS) and NMR spectroscopy are the two core technologies used in metabolite analysis. Coupled with liquid chromatographic separation, the MS technique offers advantages in automation, resolution and sensitivity.

This study also attempts to identify biomarkers for the assessment of uterine function *in vitro*. An important question in many metabolomic studies is: has an altered metabolic state (e.g., disease, mutation, diet, and drugs) been observed to be different or similar to the reference state. One of the most common statistical approaches for the analysis of metabolomic data is principal component analysis (PCA) and partial least squares discriminant analysis (PLS-DA) (Werth *et al.*, 2010). PCA or PLS-DA transforms data obtained from high-throughput analysis or measurements into an informative visual presentation (scores plot). The score plot enhances understanding of the data as it groups biological samples into clusters of either similar or different groupings (Werth *et al.*, 2010). The PCA is used in the

determination of the uniformity of the imported data using the scatter plot (usually of the first two score vectors (t1-t2) and outliers, groupings, and trends are observed. Points that lie furthest from the rest of the group are referred to as strong outliers in the scatter plot. The SIMCA analytical software is commonly employed for the supervised classification method based on PCA. It enables the creation of a distinct PCA model for each known class of observations which are then used to classify the unknown. This is occurs by the calculation of these observations into each 95% confidence interval PCA class model. It has also been recommended that PCA is performed as the first process of statistical analysis in the analyses of multivariate data as it provides hidden information in the data. It has been suggested that additional information can be obtained through the use of more advanced multivariate methods (Trygg *et al.*, 2007). SIMCA uses projections to latent structures analysis in situations where it a measurable relationship between two data tables (X and Y) is required between a matrix, X . Where the X data is usually spectral or chromatographic data, and the matrix Y is usually quantitative values (e.g. concentrations of endogenous metabolites). In situations where the Y matrix contains qualitative values (e.g. gender and sample treatment), PLS can also be used. The generated PCA scores and loading plots and all residuals are employed to assist interpretation (Trygg *et al.*, 2007). There is also the orthogonal-PLS method (OPLS) which is a recent modification of the PLS method. OPLS creates a two part relationship between X and Y . In one part X is linearly related to Y and the other is orthogonal to Y . Creation of the two part relationship enhances better interpretation of the data and it's also easier to process the model on new samples. There is orthogonal partial least squares discriminant analysis (OPLS-DA) which creates a

model using two or more classes of data. This model helps to increase the separation between groups, assist in interpretations and very useful for the identification of potential biomarkers. OPLS-DA functions by combining the PLS-DA and SIMCA classification. O2PLS is a further modification of the OPLS method which can be used for two blocks of data by creating individual models for the joint and orthogonal variations in the **X** data.

3.1 Systematic Application/Interpretation of the Metabolomic Results

After analysis of the metabolomic data, the next step would be to appropriately interpret the results. In metabolomics, bias towards a particular class of compounds or samples should be avoided and interpretation should be objectively based on the relative alterations observed in the metabolite levels between experiments or treatments as discussed and reviewed by Teehan *et al.* (2006). Metabolomic analyses generally generate large quantities of data and unless major changes or differences are expected, or the data is too noisy, clearly defined clusters should be created (Griffin, 2006). Where the samples are not clearly defined further analysis is recommended. Furthermore where there are subgroups within the major clusters, these should be investigated and verified to ensure that it was not due to systematic errors probably during sample preparation or while data were acquired. Once a subgroup is found within a cluster, it is not statistically sound to treat B as one population and to compare it to A, by Student's t test for example. Several statistical methods can be employed to analyse metabolomic data e.g., multiple analysis of variance (MANOVA) or analysis of frequency distributions, but it should be noted that the statistical requirements for such tests must be met (Fiehn, 2001).

It is often also necessary to examine the relationship between the metabolomic data sets and known pathways. This can be performed using predictions models which have been created from a combination of mathematical or kinetic calculations (Chagoyen and Pazos, 2012). The KEGG pathway network is one of the publicly available pathway searches and can be used to visualize standard metabolic pathways in different organisms and situations (Okuda *et al.*, 2008). Other databases such as BRENDA and MetaCyc have also been suggested (Arita, 2004). Two basic approaches involving theoretical considerations can also be used when creating a relationship between pathways and metabolomic data: first, the use of metabolic control analysis which involves calculation of enzyme kinetics and stoichiometric consideration of enzymatic reactions (Fiehn, 2001).

3.2 Uterine Metabolomic Profiling

Comprehensive studies on uterine metabolite profiling appear to be sparse. The important roles played by metabolites in smooth muscle cells cannot be overemphasized. During uterine contraction a decrease in blood supply is said to occur, which can result in a decrease in the adenosine triphosphate (ATP) concentration and thus interfere with contraction (Wray, 1990). A fall in ATP in the rat uterus has been shown to occur when oxidative metabolism is inhibited and a decrease in ATP and phosphocreatine (PCr) as well as an increase in inorganic phosphate (Pi) have been shown to occur during contraction of the uterus (Ninomiya and Suzuki, 1983; Wray, 1990). An increase in the concentration of [Pi] can depress contraction in permeabilized myometrial preparations (Crichton *et al.*, 1993). An increase in K⁺ permeability makes the surface membrane more difficult to excite and

leads to relaxation (Heaton *et al.*, 1993). It is therefore important to understand the effect of metabolite changes (e.g. increased inorganic phosphate) on the production of force production by the uterus, in order to gain further insight into the mechanics of labour and uterine contraction in general.

3.3 Aim and Objectives of Study

In this study, the use of analytical and computational methods described above, for the characterization of myometrial metabolite alterations that have occurred in response to stimulatory and inhibitory drugs is reported. Typical functional pharmacological assays were performed on isolated uterine tissues involving the use of a standard uterine contraction stimulation agent (oxytocin) and uterine relaxation agent (ritodrine). In addition to tissue sampling, an innovative sampling approach which involves the utilization and assessment of bath fluids was also performed. This method was also aimed at correlating the metabolite released into the surrounding fluid with those detected within the myometrial tissues.

Oxytocin (OT) is one of the most potent uterotonic agents known and its effect on uterine contractility is of major pharmacological importance. It was therefore employed as the standard uterotonic drug in this study. It is known that oxytocin generates inositol 1,4,5-trisphosphate (IP₃) and diacylglycerol (DAG) (Schrey *et al.*, 1988) however the extensive clinical use of OT and OT receptor antagonists as well as some molecular and cellular mechanisms underlying oxytocin-induced modulation of uterine contractility are not completely understood (Ku *et al.*, 1995). Ritodrine (RIT), a β_2 -adrenoceptor mimetic, activates adenosine triphosphate

activated potassium (KATP) channels and large conductance potassium (BKCa) channels in the myometrium via cyclic adenosine monophosphate (cAMP)-dependent phosphorylation and/or directly via GTP (Andersson *et al.*, 1980; Khan *et al.*, 2001). RIT is occasionally used clinically for myometrial relaxation in preterm labour (Bulbring and Tomito, 1987; Jeyabalan and Caritis, 2002). A metabolomic study therefore will further aid the determination of the activity of RIT on the myometrium through identifying the metabolites related to the pathways mentioned above. In addition, the presence or absence of the predicted metabolites will provide evidence needed to validate the method and will be useful when determining the effect of unknown drugs. This method will additionally investigate the presence of alternate pathways if any that may be involved in the activity of these drugs on the myometrium. As a proof of principle, Shah and colleagues (2009) identified a number of proteins (desmoplakin isoform 1, stratifin and thrombospondin 1) as potential preterm birth protein biomarkers from cervical vaginal fluids (Shah *et al.*, 2009).

3.4 Materials and Methods

3.4.1 Animals

Female C57BL/6 strain laboratory mice weighing between 19-25 g, obtained from the Biological Procedures Unit of the University of Strathclyde, U.K. were used in this study. The animals were maintained in a controlled environment and in a conditioned room at 25°C, 60% relative humidity under a 12/12h cycle of light and dark with free access to food and water.

All experiments were carried out in accordance with the Animal Health and Welfare (Scotland) Act 2006 and the Public Health Service Policy on Humane Care and Use of Laboratory Animals 2002. Mice were euthanized under rising concentration of CO₂ and exsanguinated before excision of the uterine tissues.

3.4.2. Contractility Experiments

Mice in pro-oestrous and oestrous stages were used. Contractility experiments were performed on the dissected uteri which were cut into segments of approximately 0.5 - 0.8 cm in longitudinal length, cleaned of extra connective tissues to provide four preparations per mouse. The segments were then weighed and subsequently mounted in warmed (37°C) 3 ml organ baths containing normal Krebs-Henseleit physiological solution which was composed of; 118.4 NaCl, 25 NaHCO₃, 11.1 Glucose, 4.69 KCl, 2.41 MgSO₄, 1.18 KH₂PO₄, 2.5 CaCl₂ (mM) and continuously gassed with carbogen (95% O₂, 5% CO₂). Tissues were loaded with an initial tension of 1 g and equilibrated for 30 min before subsequent run of experiments. The differential force and frequency of spontaneous contractions in the longitudinal muscle layer were recorded through Grass (FTO3) isometric force transducers connected via Quad Bridge modules to a PowerLab 4/20 data acquisition system using Chart 3.3 software (AD Instruments, UK) which was used to store and analyze acquired data.

3.4.3 Concentration-Response Studies

OT (1 nM) was the uterine contractile agent used in this study while RIT (0.1 nM) was the uterine contraction inhibitory drug employed. In separate experiments, single concentrations of OT and RIT were added to the bath for 10 min following stable rhythmic spontaneous contractions. Without washing, the uterine tissues were

collected at the peak of each drug's effect and immediately flash frozen in liquid nitrogen. Flash freezing was achieved by rapidly lifting the tissues out of the organ bath and cutting the threads tethering the strips to the transducer and tissue holder. The tissues were then placed into cryovials, immediately capped and immersed into liquid nitrogen. The whole procedure lasted anywhere between 10-20 seconds. Fast and efficient flash freezing is important as cells/tissues will continue to respond to their perturbed environment until they are rendered physiologically incapable of doing so (Lin *et al.*, 2007). The bath fluids (3 ml) were similarly collected placed into pre-weighed vials and flash frozen. All samples were subsequently stored at -80°C prior to further experiments. A total of 4 animals each for individual experiments were employed. All graphs were prepared using Prism Software (version 4; GraphPad Software, CA).

3.5 Sampling

Choice of sampling, metabolite extraction and analytical techniques were chosen after careful consideration of the literature and also based on preliminary experiments. A minimum of 4 samples were collected to reduce the effect of biological variability and to obtain statistically validated data. The threads used in mounting the tissues were also collected for analysis.

3.5.1 Tissue Metabolite Extraction

Each flash frozen tissue was homogenized using an ULTRA-TURRAX T8 homogeniser (IKA®- WERKE GmbH & Co., Germany) in 400 µl cold methanol (MeOH). Combination of wet homogenization with direct extraction has been

reported as one of the best tissue disruption methods for metabolite extraction as it gives best metabolite reproducibility and increases the ease and speed of the extraction process (Griffin, 2006). The whole procedure was performed in the cold. The homogenate was vortexed for 60 s before being centrifuged using a Force 7 Fisher Scientific UK Limited (Leicestershire, UK) at 13,000 rpm, 5 min for MeOH extracts (polar extracts). The supernatant was collected using a micropipette syringe and dried in pre-weighed vials in preparation for further NMR and MS measurements. Using the same homogenized tissue the process was repeated with 400 μ l cold dichloromethane (DCM) but centrifuged at 13,000 rpm for 10 min to give the non-polar extracts. The time periods employed were predetermined from preliminary experiments.

3.5.2 Bath Fluid Metabolite Extraction

Each fluid sample was freeze dried in a Christ Alpha 2-4 (SciQuip, UK) freeze drier and weighed. The dried samples were then reconstituted with 500 μ l of cold MeOH and vortexed for 1 min. The solution of the mixture was pipetted out and centrifuged as previously described. The process was repeated with 600 μ l cold DCM on the residue obtained after MeOH extraction. The entire extraction procedure was performed under cold conditions.

3.6 HPLC-HRFTMS Data Acquisition

The MeOH extracts were reconstituted with 200 μ l of 100 % methanol while the DCM extracts were reconstituted in DCM : MeOH at a ratio of 30:70. The 30:70 ratio were predetermined from preliminary experiments as best suited for dissolving

the extracts. All solvents were of high pressure liquid chromatography (HPLC) grade. Samples were transferred into autosampler MS vials containing 200 μ l inserts for HPLC-MS analysis. HPLC-MS analysis was carried out using a Dionex UltiMate[®] 3000 HPLC system (Thermo Fisher Scientific Inc, Hemel Hempstead, UK) employing a C18 column (75.0 x 3.0mm) (HiChrom Limited, UK). The column was eluted with a linear gradient of 90% A (0.1% v/v formic acid in water) and 10% B (0.1% v/v formic acid in acetonitrile) mobile phases with a flow rate of 0.3 μ l/min over 0-35 min then 100% B for a further 5-min isocratic elution, and a return to starting conditions at 40 min for re-equilibration for the last 5 minutes, using up a total of 45 min for the run. MS identification and analysis were carried out using a ThermoScientific Exactive (Thermo Fisher Scientific Inc, Hemel Hempstead, UK) with a 10 μ l injection volume and the UV-MS hyphenated system using both positive and negative ion modes of detection with UV detection at 254 nm. Full scan data were collected from 50 to 1500 m/z (mass to charge ratio) with a scan time of 0.1 s. Capillary and cone voltages were set at 3.5 kV and 35 V, respectively; desolvation and source temperatures at 300°C and 120°C, respectively.

3.7 ¹H-NMR Data Acquisition

The dried MeOH extracts were weighed and reconstituted in 200 μ l DMSO vortexed for 30 seconds and placed in shigemi NMR tubes (5 mm) or capillary NMR inserts for 1D ¹H-NMR measurements while the DCM extracts were weighed and reconstituted in 200 μ l CDCl₃ and similarly placed in shigemi NMR tubes.

Presaturated ^1H -NMR experiments were carried out on a JEOL-LA400 FT-NMR spectrometer system (JEOL Ltd, UK) with an AS400 magnet and measured at 400 MHz for ^1H using a Pulse Field Gradient “Autotune” 40TH5AT/FG broadband high sensitivity probe to accept 5 mm tubes. One-dimensional ^1H -proton with presaturation of the residual water resonance NMR spectra were obtained using the following parameters; 32k data points, spectral width of 5998.4 Hz, an acquisition time of 2.73 s, a relaxation delay of 3.0 s., and pulse width of 5.47 requiring 3.85 min total acquisition time.

3.8 Data Processing and Analysis

3.8.1 HPLC-HRFTMS Profiles

The HPLC-HRFTMS metabolic profiles of polar and non-polar OT- and RIT-treated tissues and surrounding bath were analysed before and after drug treatment. The resulting data were then subjected to online metabolomic analysis (XCMS) for pre-processing. XCMS allows for the incorporation of novel nonlinear retention time alignment, matched filtration, peak detection, and peak matching (Patti *et al.*, 2012). After XCMS processing, 17154 and 9891 variables were acquired for polar (OTTP) and non-polar oxytocin treated tissues (OTTNP) respectively while 21340 and 16934 variables were acquired for polar (OTFP) and non-polar oxytocin treated fluids (OTFNP) respectively. For polar (RITTP) and non-polar (RITTNP) ritodrine-treated tissues, 14149 and 32051 variables were respectively acquired, while 23260 and 26770 variables were acquired for polar (RITFP) and non-polar ritodrine-treated

fluids (RITFNP) respectively. These numbers included isotopic and adduct ion peaks.

3.8.2 Preprocessing of HPLC-HRFTMS Data

The raw LC-MS data were first sliced into positive and negative ion modes before conversion to mzXML files prior to XCMS processing. With XCMS, peak identification in individual samples and peak alignment across samples is performed and this promotes comparison of the relative intensity of ions and the calculation of deviations in retention time. The peak-matching algorithm in XCMS contains an algorithm for peak-matching and this algorithm considers that LC-MS data are usually anisotropic in nature (Tautenhahn *et al.*, 2012). XCMS online was then employed to filter, detect and match peaks across samples to allow for retention time correction and relative ion intensity comparison. The data matrix was automatically normalized using the quantile normalization procedure. Statistical determination using the t-test was also performed at $p < 0.05$ for each pairwise comparison of control and drug-treated groups, with $p < 0.01$ considered highly significant. Identification of metabolites was performed within XCMS online using METLIN, which is a web-based database previously developed by the Scripps Research Institute in order to facilitate the identification of metabolites using accurate mass data. It includes an annotated list of structural information for known metabolites.

3.8.3 HPLC-HRFTMS Data Analysis

The XCMS peak areas were extracted and imported into the soft independent method of class analogy (SIMCA) –P (version 12.0, Umetrics AB, Umeå, Sweden) for PCA and OPLS-DA analysis. Statistical analyses based on a pairwise comparison of

control and treated groups were also acquired for the different drugs. Differentially expressed metabolites with p-values less than 5% and fold change greater than 150% were considered statistically significant and used for subsequent analyses. OPLS being a regression method was used to find the relationship between two data tables, **X** and **Y** in this case **X** is the LC-MS data and **Y** represents binary vectors (group descriptors (control or treated)). The OPLS model used was made up of two sets, the **Y** predictive set and the **Y** orthogonal set. The **Y** predictive provided information about inter-class variation and the **Y** orthogonal provided information about intra-class variation otherwise referred to as the uncorrelated variation. The predictive variation of **Y** in **X** is shown by the predictive components alone and a for a two group classification for instance, a single predictive component is required. The OPLS-DA method therefore enables an easy understanding and interpretation of the model without loss of the power of the model prediction. Prior to application of the OPLS-DA model, the data was first converted by scaling in order to eliminate noise. This was achieved by subjecting each variable to Pareto scaling ($1/\sqrt{SD}$ [SD= standard deviation]) prior to modeling (Eriksson *et al.*, 2006). In SIMCA-P software, a default sevenfold cross validation procedure was performed on the OPLS-DA model this action prevents model over fitting and creates diagnostic parameters R^2Y and Q^2Y which are used to determine and define the predictability and quality of the model. For visualization and interpretation the OPLS-DA score scatter plots, S plots and loading plots with confidence intervals were used The S-plot was employed in order to visualize the effect of the variables in each model, as it is able to bring together the covariance (contribution of magnitude) with correlation (contribution of effect and reliability) using scores of the model component. The statistical S plots

can therefore be applied in the identification of possible interesting compounds for both predictive and orthogonal variation. A plot of the loading vector $\text{Cov}(tp, X)$, represented as $p [1]$ with its corresponding jack-knifed confidence intervals was used to provide additional supporting information about metabolite variability in this study. The jack-knifed loading plot was additionally sorted by size in order to separate up- and down-regulated metabolites at each end of the plots.

3.8.4 Bioinformatic Analysis of HPLC-HRFTMS Data

Bioinformatic analysis was additionally performed using the Ingenuity Pathway Analysis (IPA) tool (Ingenuity Systems, Redwood City, CA) for the pathways search regulated by the identified metabolites. Some of the selected metabolites were further validated by MS/MS analysis. IPA-Metabolomics is a program within IPA that extracts rich pathway information from metabolomics data. Statistical significance was calculated using Fischer's exact test, $p < 0.05$ indicated a statistically significant no-random association. For a given data set, IPA automatically generates the pathways that are related to those metabolites.

3.8.5 NMR Pre-processing and Analysis

All NMR data sets were pre-processed using Mnova V 8.1. The imported spectra were manually phased, apodized at Gaussian = 1.0, and baseline corrected to Bernstein polynomial order fit (order 3). The spectra were binned between δ 0.5 – 9 ppm at bin value of δ 0.04 ppm width such that each bin can be integrated to yield vector containing intensity based descriptors of the original spectra. Bins representing the residual water and solvent peaks were removed. The total spectra area was then normalized to a total value of 100. This yielded a total of 163 and 165

contiguous data for the polar and non-polar datasets respectively. The resulting data yielded a 2D matrix ($n \times d$). The resulting data matrix was then exported into SIMCA-P software package (version 13.0, Umetrics AB, Umeå, Sweden). Mean centering was performed before principal component analysis (PCA) and OPLS-DA was applied to the datasets. PCA enabled examination of each data set for potential outliers as well as the degree of similarity between the metabolic fingerprints, in an unsupervised manner. In this pattern recognition technique, the algorithm calculates the highest amount of correlated variation along PC1, with subsequent PCs containing correspondingly smaller amounts of variance. For each model built, the loading vector for the PC was examined to identify which metabolites contributed to these clusters.

In the biplot, the scores and loadings were expressed via correlation scaling. Observations situated near variables expressed a high percentage of those variables and a lower percentage of variables relatively distant. The S-line which was also used in this study is similar to a statistical total correlation spectroscopy (STOCSY) (Cloarec *et al.*, 2005) and is useful for spectroscopy data. It projects both the covariance and the correlation structure between X-variables and the predictive scores $t[1]$. The original spectra is observed to be coloured according to the correlation loading ($p(\text{corr})$). The $p(\text{ctr})[1]$ loading colouring represents the absolute value of the correlation loading, and a high $p(\text{corr})$ points to a high reliability and a high $p(1)$ points to a high model influence. A colour scale which projects the chemical shifts that contributed to the separation between groups was placed beside the S line to increase interpretation.

3.8.6 ¹H-NMR Profiles

Pair-matched ¹H-NMR spectra of control versus treated mouse uterine tissues and respective bath fluids were presented in figures 3.20 - 3.27. The spectral resolution of the one dimensional (1D) spectra and 2D proton correlation spectroscopy combined with reported data from the literature (Celik *et al.*, 2004; Griffin *et al.*, 2003; Mazzei *et al.*, 2010; Ong *et al.*, 2009; Palama *et al.*, 2010; Reis *et al.*, 2003; Subramanian *et al.*, 2008; Vasskog *et al.*, 2012) enabled the identification and assignment of different metabolites (Table 3.4) at varying chemical shift ranges. Lipids and amino acids dominated each spectrum. In some cases, the 1D ¹H-NMR spectra of the uterine tissues and bath fluids contained similar metabolites in both the control and treated groups and classification was occasionally based on statistically significant differences between the relative amounts of the same metabolite. A flow chart showing the different steps involved in the assay is shown in figure 3.1.

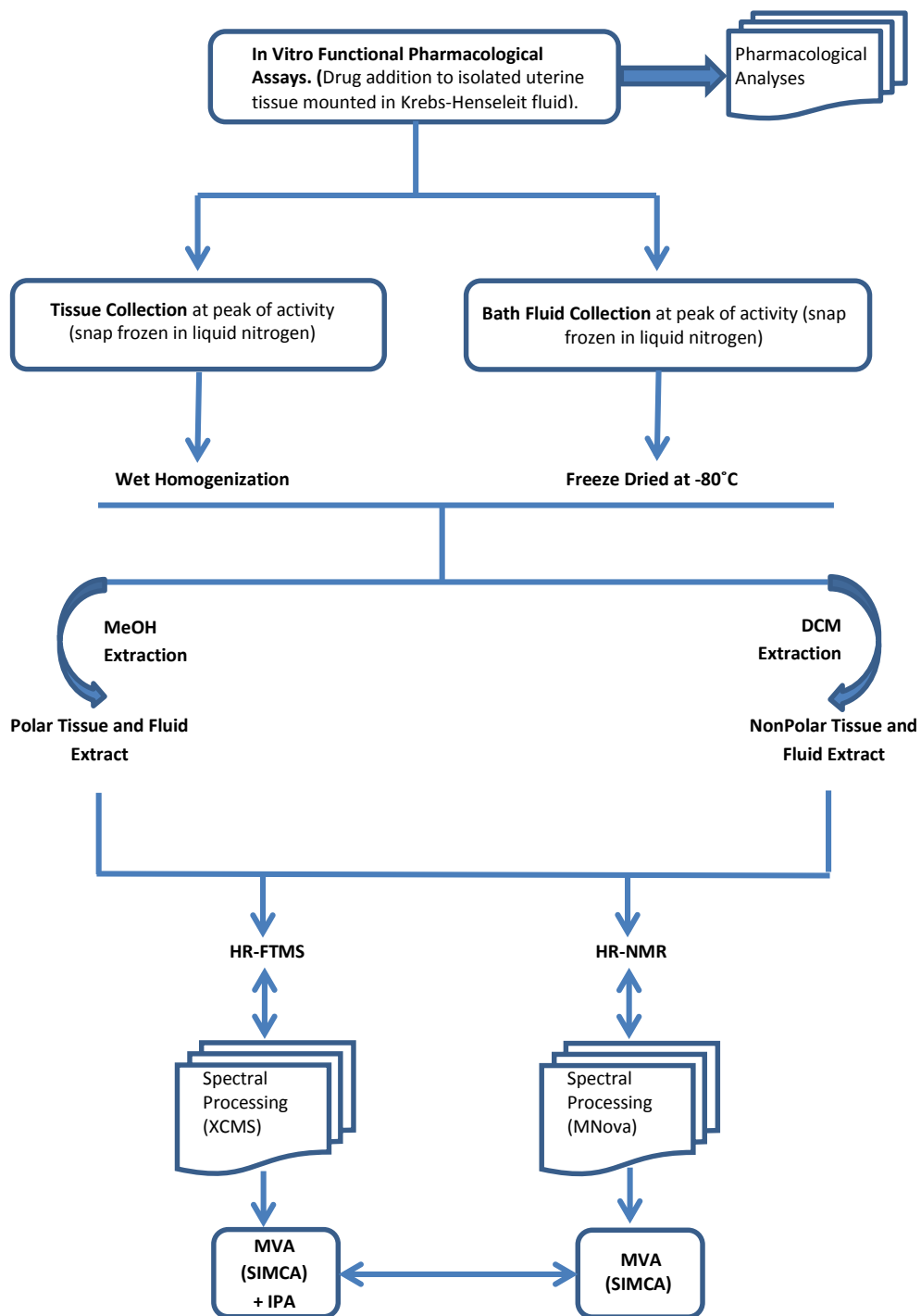


Figure 3.1 Flow chart showing the steps involved in the pharmaco-metabolomic analysis.

3.9 Results

3.9.1 Effect of Drugs on Spontaneous Uterine Contractions

Investigations on uterine contractility demonstrated that oxytocin (1 nM) produced phasic and tonic uterine contractions and increased the force and frequency of uterine contractions (Fig. 3.2). RIT (0.1 nM) however decreased contractility of spontaneously contracting tissues producing obvious decreases in the force and frequency of spontaneous uterine contractions (Fig. 3.3).

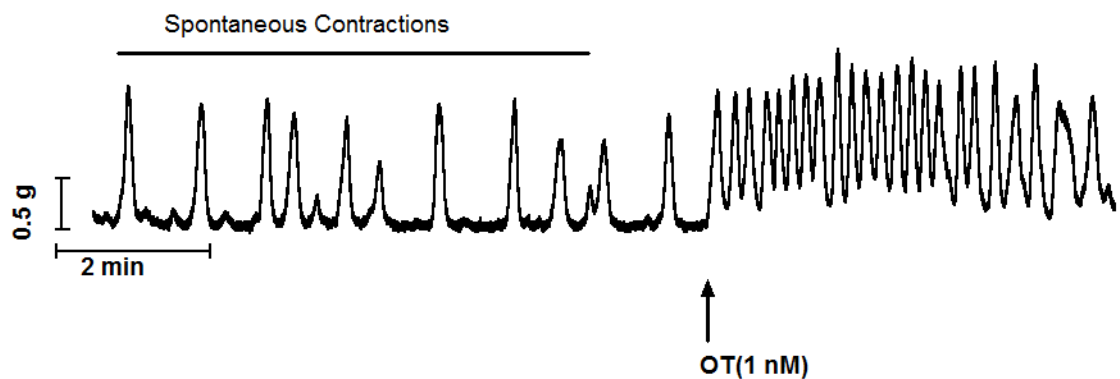


Figure 3.2 An example of a representative recording of the effect of oxytocin (OT (1 nM)) on spontaneously contracting mouse uterine tissues

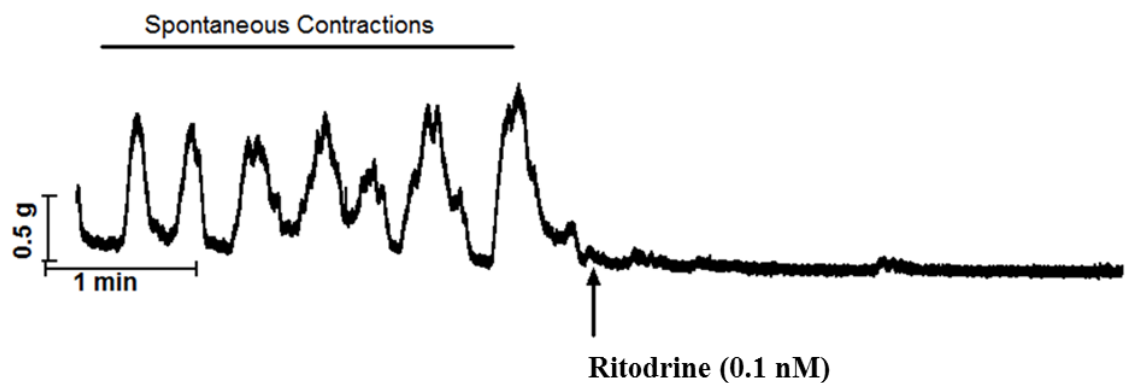


Figure 3.3 An example of a representative recording of the effect of ritodrine (RIT (0.1 nM)) on spontaneously contracting uterine tissues.

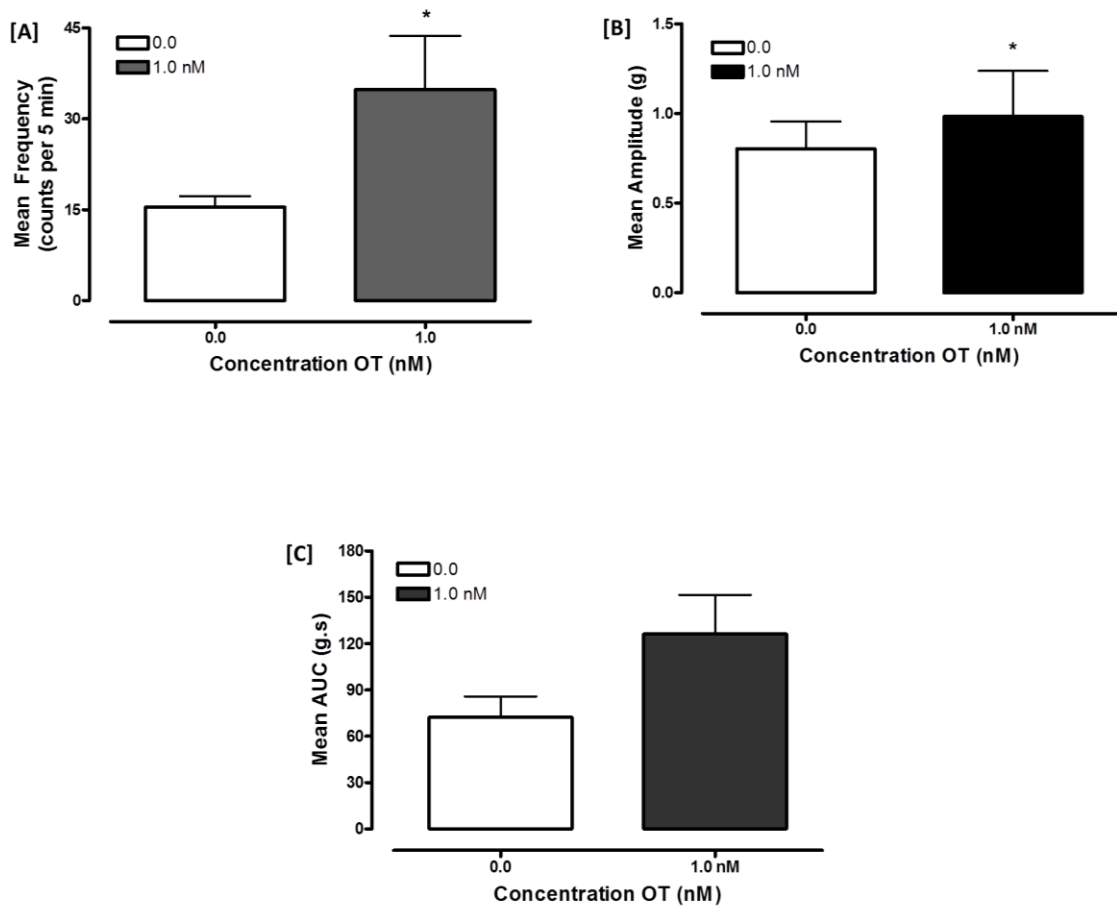


Figure 3.4 Mean responses (\pm S.E.M) of the isolated uterus to OT calculated within a 5 min time range. Frequency is represented in panel A; the amplitude of uterine contractions, in panel B and the area under the curve, in panel C. Spontaneous contractions which occurred in the absence of drug were considered as the control (0.0). Experiments were performed at 37°C. * = $p < 0.05$ compared with the control (analysed using the t-test). $n = 5$ animals.

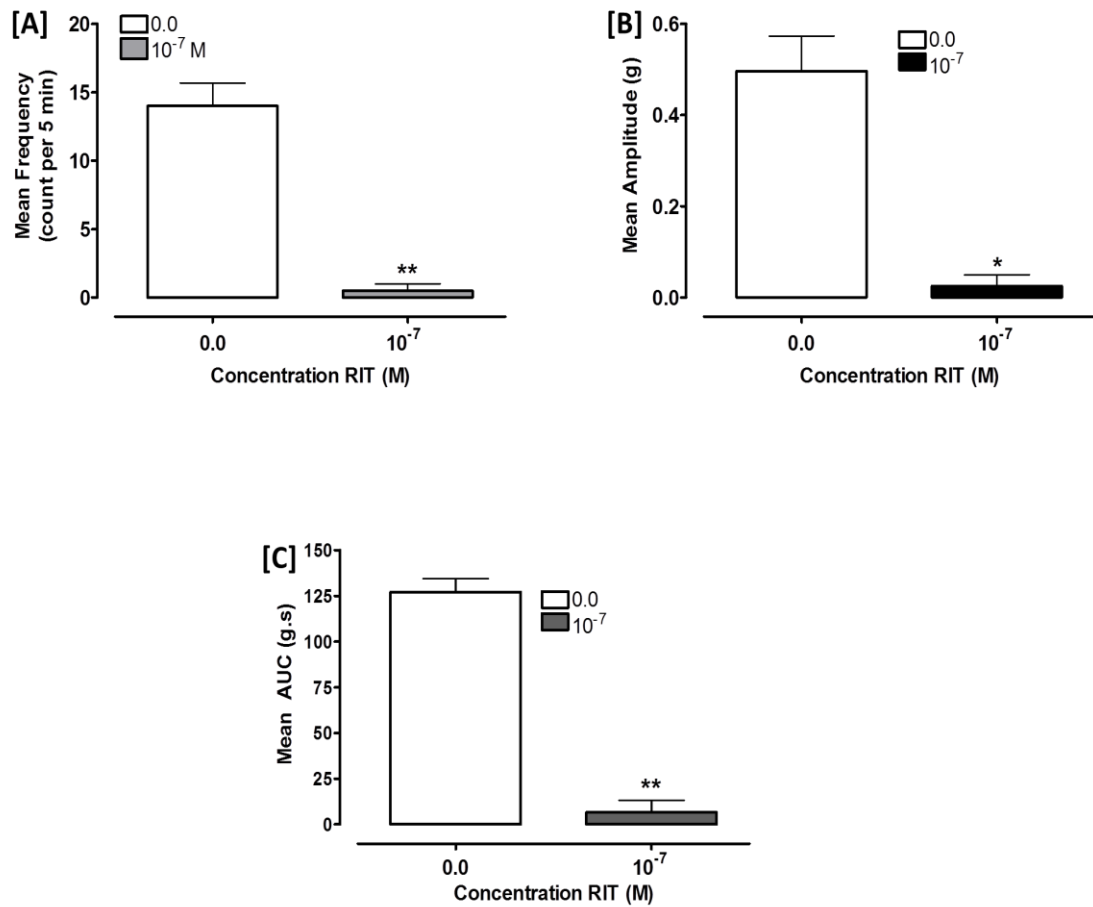


Figure 3.5 Mean responses (\pm S.E.M) of the isolated uterus to RIT calculated within a 5 min time range. Frequency is represented in panel A; the amplitude of uterine contractions, in panel B and the area under the curve, in panel C. Spontaneous contractions which occurred in the absence of drug were considered as the control (0.0). Experiments were performed at 37°C. * = $p < 0.05$; ** $p < 0.01$ compared with the control (calculated using the t-test). $n = 5$ animals.

3.9.2 Metabolomic Analyses of the Effect of Drugs on the Mouse Uterus

A summary of the parameters acquired for prediction and separation in the OPLS-DA models are shown in Table 3.1 and 3.2. The OPLS-DA parameters showed a scoring of greater than 0.5 in the MS models (Table 3.1), an indication of a high quality model for prediction and separation of the respective groups. The OPLS-DA parameters for $^1\text{H-NMR}$ data (Table 3.2) showed an R^2Y scoring of 1.0 in all models, a good indication of a satisfactory predictive model for the matched groups. The OPLS-DA score plot showed distinct separations between the control and treated in all experimental groups, OTTP and OTTNP, OTFP and OTFNP, RITTP and RITTNP, RITFP and RITFNP (Fig. 3.6 and 3.7). An S-plot, which is described as a variation of a scatter plot, was also utilized to explain the influence of the variables on the MS data. The S-plot combines covariance (x-axis: p_1) and correlation loading profiles (y-axis: $p(\text{corr})_1$), for the extraction of putative metabolites (Fig. 3.8 and 3.9). For this study, predictive and orthogonal S-plots were utilized. The farther along the x-axis the greater the contribution of the metabolites to the variance between the groups, while the farther along the y-axis the higher the reliability of the analytical result. From each plot, differentially significant metabolites were extracted using the jack knifed column plots with fitted confidence intervals. Peaks with confidence intervals that did not include 0, were selected and prioritized. These differentially regulated metabolites combined with those selected by the Ingenuity Pathway Analysis (IPA) bioinformatic software, have been highlighted (Table 3.3).

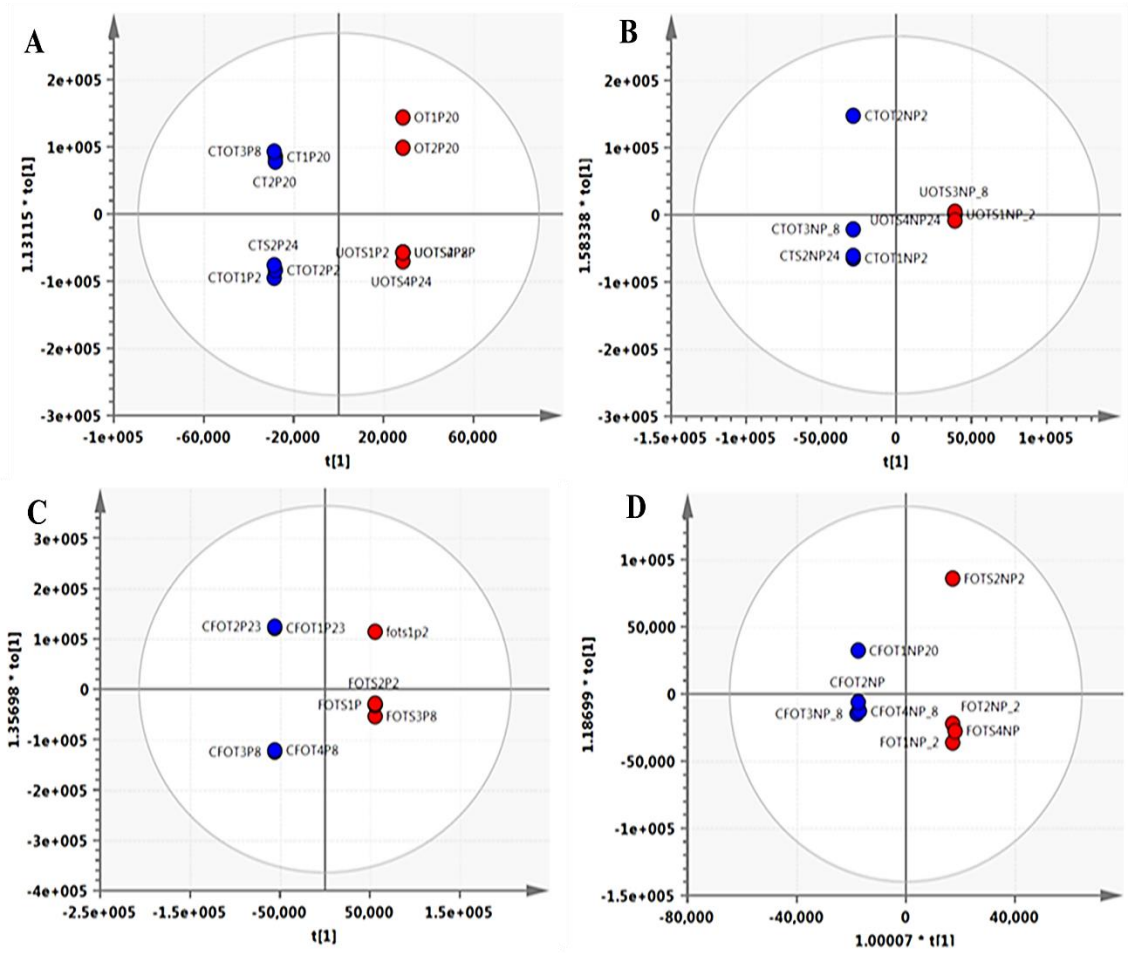


Figure 3.6 OPLS-DA scatter score plots of differentially synthesized metabolites observed on treatment of the isolated uterus with OT (A-D) as determined by HRFTMS. The red circles represent the treated groups while the blue circles represent the controls. n = 5 animals

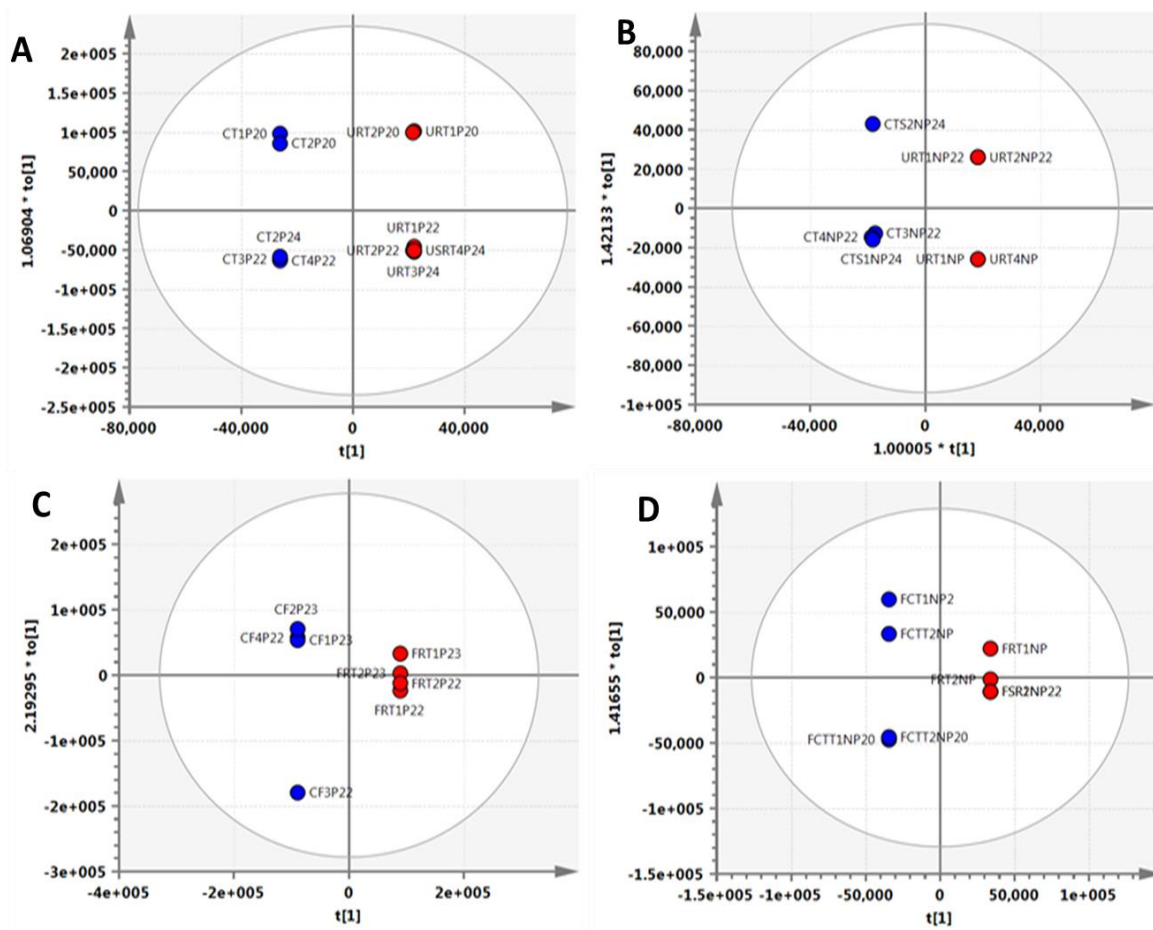


Figure 3.7 OPLS-DA scatter score plots of differentially synthesized metabolites observed on treatment of the isolated uterus with RIT (A-D) as determined by HRFTMS. The red circles represent the treated groups while the blue circles represent the controls. n = 5 animals

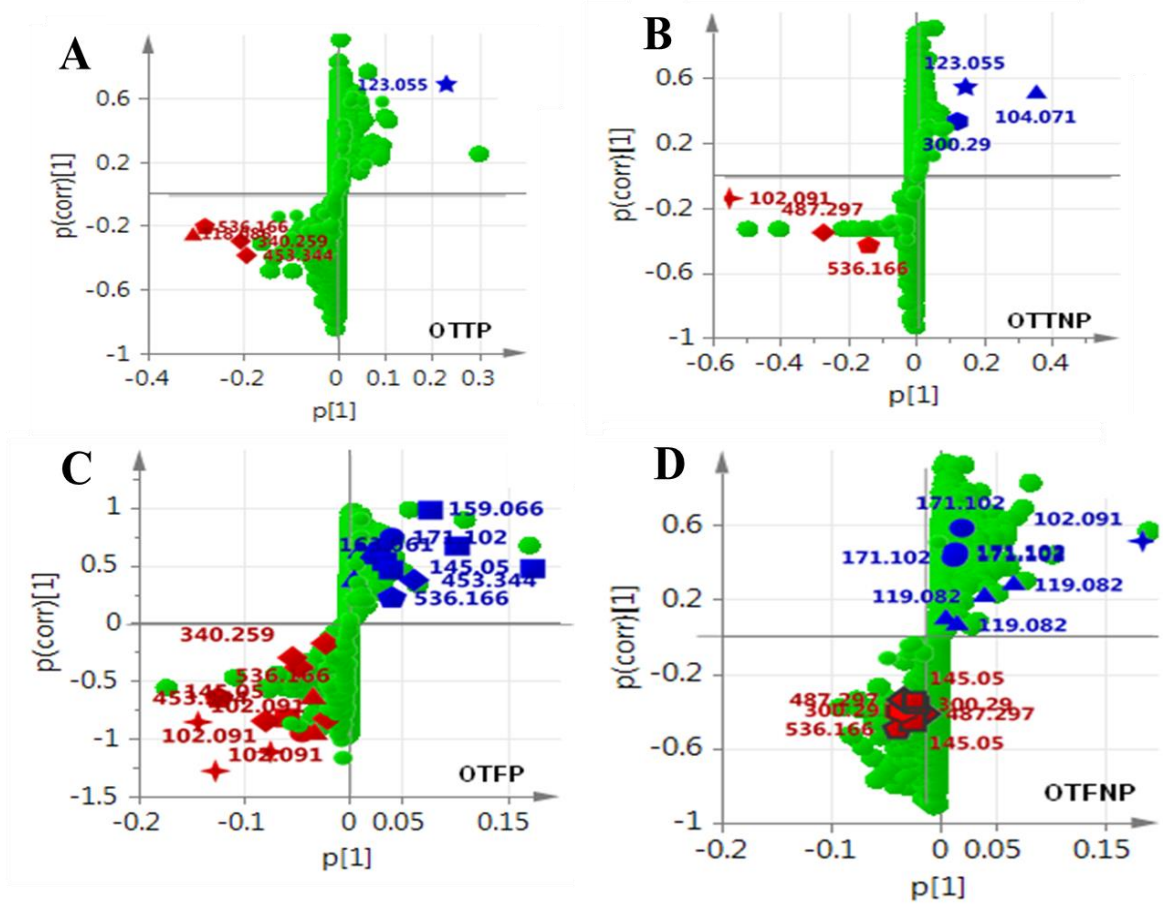


Figure 3.8 S-Plots of differentially synthesized metabolites with OT treatment of the isolated uterine tissues (A-B) and the bath fluids (C-D) as determined by HRFTMS. The green circles represent all metabolites detected for the particular group. Significantly regulated metabolites in the control groups are highlighted in blue shapes while those in the treated groups are highlighted in red shapes with corresponding m/z values. **OTTP** = OT-treated polar tissues; **OTTNP** = OT-treated non-polar tissues; **OTFP** = OT-treated polar bath fluids; **OTFNP** = OT-treated non-polar bath fluids.

● = Signal Transduction ($\text{PGF}_{1\alpha}$); ■ = Phosphatidyl-inositol signalling system; ▲ = Ligand-receptor interaction /LipidMetabolism(GABA);

◆ = cAMP biosynthesis; ● = Sphingolipid metabolism; ◆ = Cell Signalling (Arachidonic acid); ★ = Nicotine/Nicotinamide metabolism; † = Glycine, serine and threonine metabolism. The key metabolites that were perturbed are listed in Table 3.3. n = 5 animals

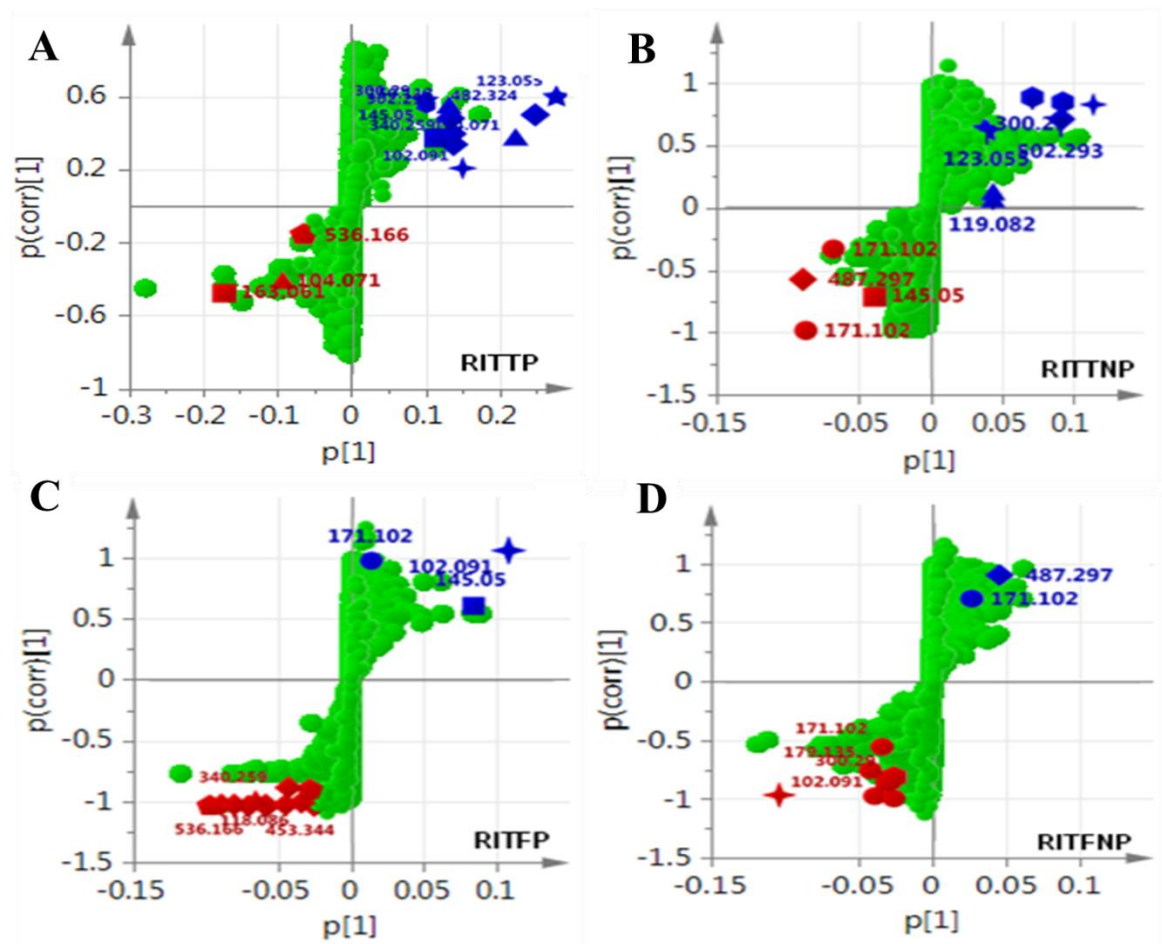


Figure 3.9 S-Plots of differentially synthesized metabolites with RIT treatment of the isolated uterine tissues (A-B) and the surrounding bath fluid (C-D) as determined by HRFTMS. The green circles represent all metabolites detected for the particular group. Significantly regulated metabolites in the control groups are highlighted in blue shapes while those in the treated groups are highlighted in red shapes with corresponding m/z values. **RITTP** = RIT-treated polar tissues; **RITTNP** = RIT-treated nonpolar tissues; **RITFP** = RIT-treated polar bath fluids; **RITFNP** = RIT-treated nonpolar bath fluids. ● = Signal Transduction (PGF1 α); ■ = Phosphatidyl-inositol signalling system; ▲ = Ligand-receptor Interaction/Lipid Metabolism(GABA); ◆ = cAMP biosynthesis; ● = Sphingolipid metabolism; ◆ = Cell Signalling (Arachidonic acid); ★ = Nicotine/Nicotinamide metabolism; † = Glycine, serine and threonine metabolism. The key metabolites that were perturbed are listed in Table 3.3. n = 5 animals

Table 3.1A Summary of OPLS-DA Parameters for the MS Data on Tissues

Group	Tissues				
	No ^a	OBS	R ² X(cum)	R ² Y(cum)	Q ² Y(cum)
OTTP	1P+8O	12	0.976	1.0	0.536
OTNP	1P+5O	7	1.000	1.0	1.000
RITP	1P+7O	11	0.956	1.0	0.144
RITNP	1P+3O	8	0.975	1.0	0.837

Table 3.1B Summary of OPLS-DA Parameters for the MS Data on Fluids

Group	Fluids				
	No ^a	OBS	R ² X(cum)	R ² Y(cum)	Q ² Y(cum)
OTTP	1P+4O	8	0.911	1.0	0.85
OTNP	1P+4O	8	0.904	1.0	0.615
RITP	1P+4O	8	0.939	1.0	0.762
RITNP	1P+4O	8	0.940	1.0	0.961

^a = Components required for a valid model and prediction; *P* = predictive component, *O* = orthogonal component; R²X_{cum}, represents the cumulative fraction of X-variation explained by all extracted components. R²Y_{cum} represents the cumulative SS of all the *y*-variables explained by the extracted components; Q²Y_{cum} = the cumulative Q² for all the *x*-variables and *y*-variables for the extracted components. The values of R²Y and Q²Y approaching 1.0 indicate a perfect model with a satisfactory predictive ability (cross-validation) and the value of Q²Y_{cum} ≥ 0.4 is considered a reliable model; OBS represents the number of observations.

**Table 3.2A Summary of Parameters for the OPLS-DA NMR Study Models on
Tissues**

Group	Tissues				
	No ^a	OBS	R ² X(cum)	R ² Y(cum)	Q ² Y(cum)
OTTP	1P+7O	11	0.987	1.0	0.367
OTNP	1P+1O	13	0.552	1.0	0.131
RITP	1P+9O	12	1.000	1.0	0.090
RITNP	1P+5O	8	0.996	1.0	0.949

**Table 3.2B Summary of Parameters for the OPLS-DA NMR Study Models on
Fluids**

Group	Fluids				
	No ^a	OBS	R ² X(cum)	R ² Y(cum)	Q ² Y(cum)
OTTP	1P+5O	12	1.0	1.0	0.380
OTNP	1P+10O	8	1.0	1.0	0.562
RITP	1P+6O	8	1.0	1.0	0.549
RITNP	1P+5O	8	1.0	1.0	0.977

^a = Components required for a valid model and prediction; *P* = predictive component, *O* = orthogonal component; R²X_{cum}, represents the cumulative fraction of X-variation explained by all extracted components. R²Y_{cum} represents the cumulative SS of all the y-variables explained by the extracted components; Q²Y_{cum} = the cumulative Q² for all the x-variables and y-variables for the extracted components. The values of R²Y and Q²Y approaching 1.0 indicate a perfect model with a satisfactory predictive ability (cross-validation) and the value of Q²Y_{cum} ≥ 0.4 is considered a reliable model; OBS represents the number of observations.

Table 3.3 Summary of Differentially Regulated Metabolites/Pathways Detected on Treatment of the Isolated Uterus with Oxytocin and Ritodrine

Abbreviations: DAG = diacyl glycerol; PC= phosphatidylcholine; PE= phosphoethanolamine; PS= phosphatidylserine; PG = glycerophosphate; TG=triacylglycerol; m/z = mass to charge; Rt = Retention time; FC = fold change; nd = not detected. A positive FC value indicates a relatively higher metabolite concentration in the treated groups, while a negative value is indicative of a relatively lower concentration in the treated groups.

Metabolic Pathway	Observed Metabolome	Adducts	m/z	Rt	Fold Change			
					Oxytocin		Ritodrine	
					Tissue	Fluid	Tissue	Fluid
Phosphatidylinositol Signalling	Myoinositol	[M+H-H ₂ O] ⁺	163.0607	1.75	nd	nd	-13.582	nd
			163.0608	1.75	nd	1.98	nd	nd
Nicotine/Nicotinamide metabolism	Niacinamide	[M+H] ⁺	123.0554	1.80	2.858	nd	nd	nd
			123.0554	1.82	nd	nd	4.691	nd
Glycine, Serine and Threonine metabolism	Betaine Aldehyde	[M+H] ⁺	102.0915	2.1	nd	nd	1.103	3.191
			102.0914	2.20	-1.332	3.506	nd	nd
Pyridine synthesis/ Valine, Leucine and Isoleucine biosynthesis	Norleucine	[M+H-H ₂ O] ⁺	340.2593	7.32	-2.337	-1.700	nd	nd
			340.2593	7.32	nd	nd	nd	-735.82
Cell Signalling	N-methyl arachidonyl amine	[M+Na] ⁺	340.2593	7.48	-2.337	-1.700	nd	nd
			340.2593	7.48	nd	nd	nd	-735.82
Cell Signalling	DAG (22:5) DAG isomer	[M+H-2H ₂ O] ⁺	679.5118	8.56	-5.989	-1.264	nd	nd
			679.5119	12.09	nd	nd	nd	-24582.825
Lipid metabolism	2-keto palmitic acid	[M+NH ₄] ⁺	288.2531	17.63	nd	-82.668	nd	nd
			288.2531	17.72	nd	nd	nd	-172.505
Sphingolipid metabolism	Sphingosine Sphingosine isomer	[M+H] ⁺	300.2897	19.03	2.213	1.678	nd	nd
			300.2897	21.31	nd	nd	2.525	nd
Glycerophospholipid metabolism	PC(18:2(2E, 4E)/0:0)	[M+H] ⁺	520.3403	19.40	nd	-252.938	nd	nd
			520.3403	19.51	nd	nd	nd	-451.904

Table 3.3 continued. Summary of Differentially Regulated Metabolites/Pathways Detected on Oxytocin and Ritodrine Treatment of the Isolated Uterus

Metabolic Pathway	Observed Metabolome	Adducts	m/z	Rt	Fold Change			
					Oxytocin		Ritodrine	
					Tissue	Fluid	Tissue	Fluid
Glycerophospholipid metabolism	PC(O-14:0/2:0)	[M+H] ⁺	496.3401	20.34	2.261	nd	nd	nd
			496.3400	20.34	nd	nd	2.108	nd
Glycerophospholipid metabolism	glycerophospho-N-oleoyl ethanolamine	[M+H] ⁺	480.3089	20.96	2.318	nd	nd	nd
			480.3087	21.00	nd	nd	2.422	nd
Glycerophospholipid metabolism	PC(O-16:1(11Z)/2:0)	[M+H] ⁺	522.3559	21.71	2.150	nd	nd	nd
			522.3558	21.72	nd	nd	nd	-55.707
Diacylglycerol biosynthesis	1-hexadecyl lysophosphatidic acid	[M+ACN+H] ⁺	438.2981	21.76	nd	nd	3.027	nd
			438.2981	21.78	2.867	-2.749	nd	nd
Glycerophospholipid metabolism	PE(18:0/0:0)	[M+H] ⁺	482.3243	24.84	nd	nd	2.175	nd
			482.3244	24.86	2.037	nd	nd	nd
Glycerophospholipid metabolism	PC(P-15:0/0:0)	[M+H] ⁺	466.3294	26.01	3.037	-1.427	nd	nd
			466.3294	26.10	nd	nd	2.880	nd
Diacylglycerol biosynthesis	1-Octadecyl Lysophosphatidic acid	[M+ACN+H] ⁺	466.3294	26.01	3.037	-1.427	nd	nd
			466.3294	26.10	nd	nd	2.880	nd
Steroid biosynthesis	dihydroxyvitamin D3	[M+H] ⁺	545.3850	26.22	nd	-4.637	nd	nd
			545.3851	26.67	nd	nd	nd	nd
Lipid Metabolism/Cell signalling	Oleamide	[M+H] ⁺	282.2791	29.31	2.691	2.085	nd	nd
			282.2791	29.54	nd	nd	5.242	nd
Catecholamines biosynthesis	N-Adenyl-L-phenylalanine	[M+ACN+H] ⁺	536.1659	34.52	nd	-3.606	nd	nd
			536.1659	35.04	nd	nd	nd	-15508.47

3.9.3 Bioinformatics

Bioinformatic information was obtained using the IPA system. Putative functions and pathways were extracted for oxytocin and ritodrine.

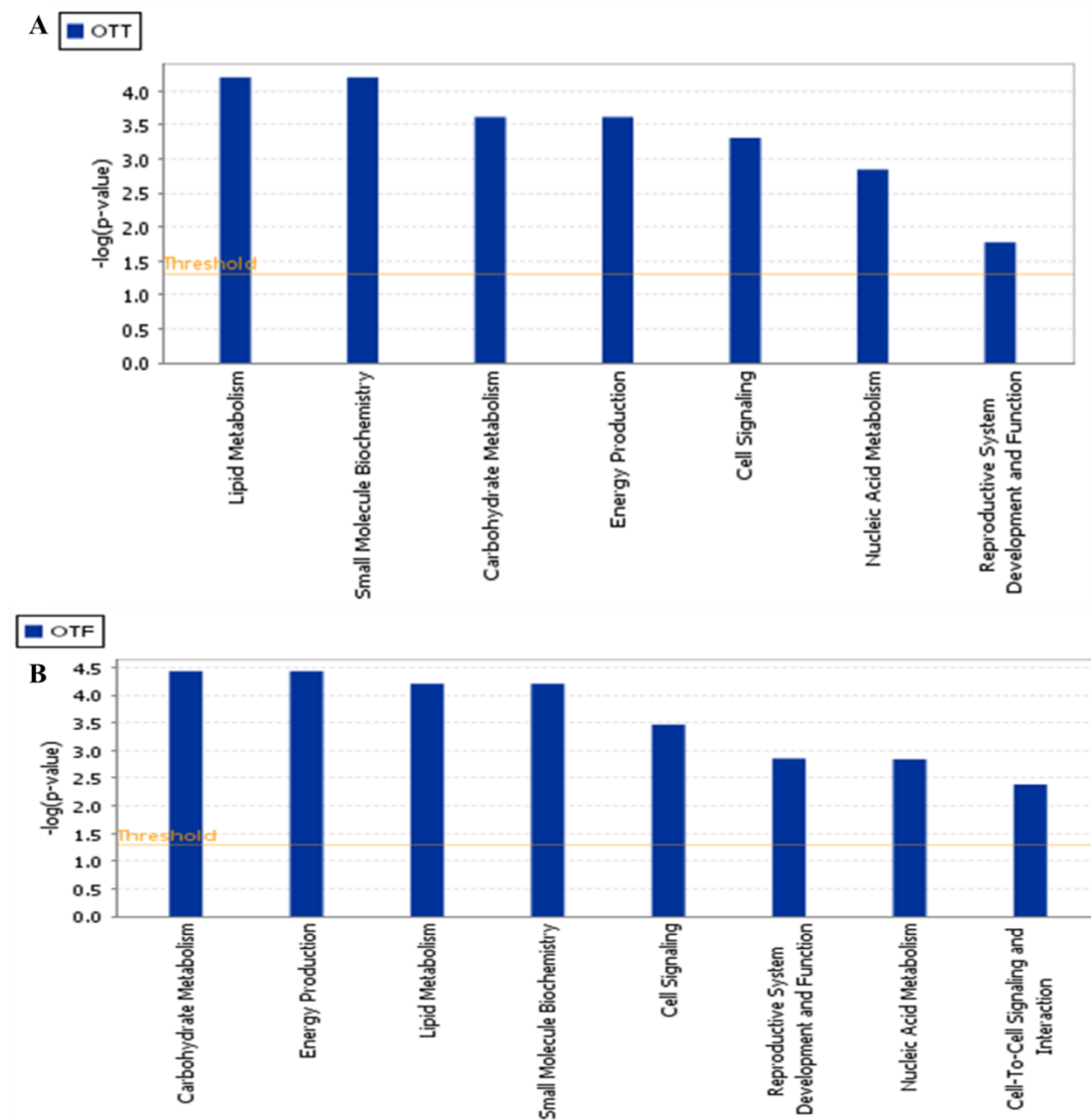


Figure 3.10 Top functions extracted by IPA software that have been perturbed on treatment of the isolated uterus with oxytocin. Functions associated with oxytocin- treated tissues and fluids are shown in A and B above along the x-axis while the $-\log(p\text{-value})$ is indicated on the left y-axis. Taller bars are more significant than shorter bars. The yellow line is indicative of the cut-off for significance $p < 0.05$ ($-\log = 1.3$). $n = 5$ animals

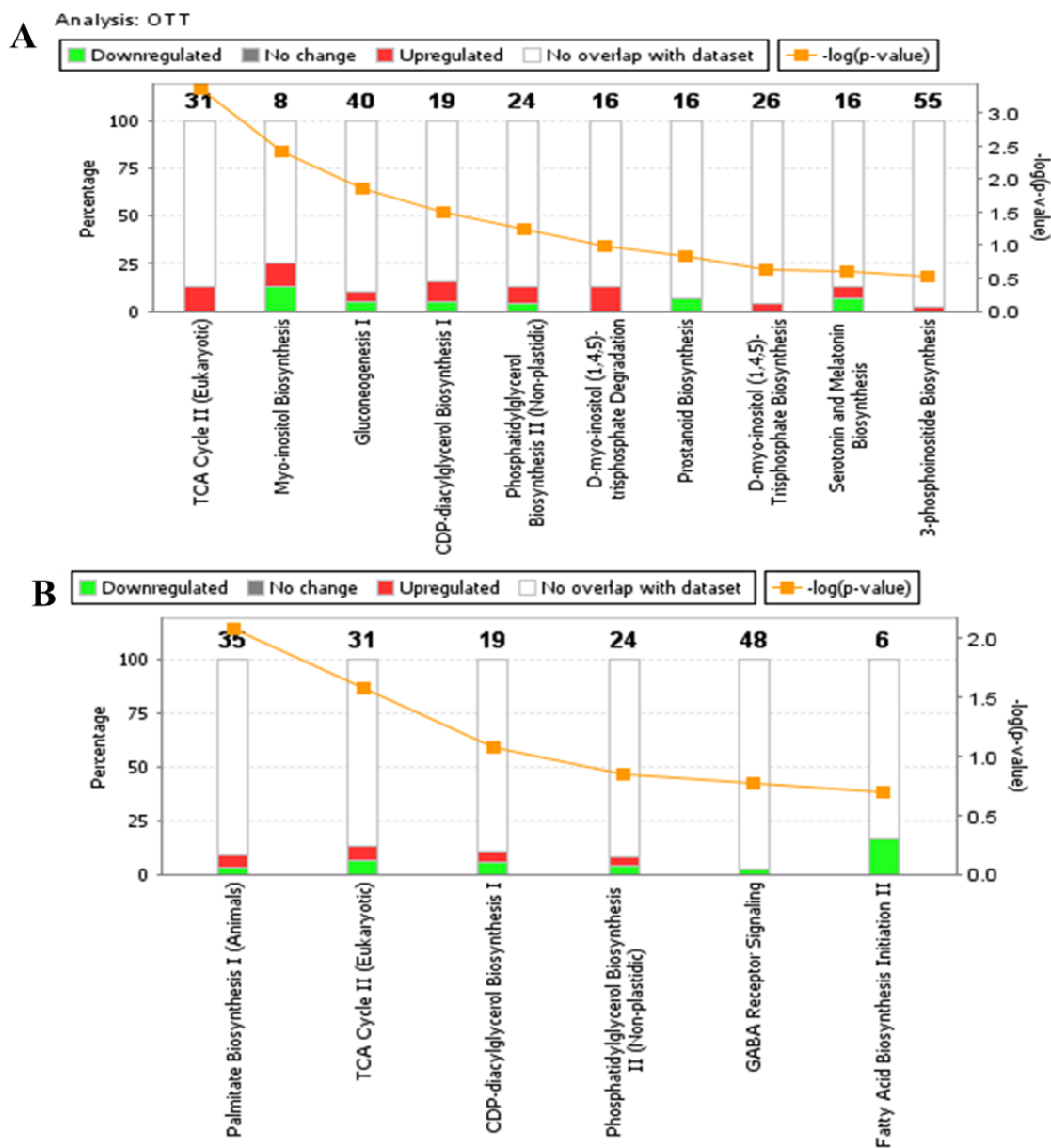


Figure 3.11 Top canonical pathways for OT extracted by IPA bioinformatics software. Pathways associated with OT-treated uterine tissues are shown in A while the bath fluids are shown in B. The pathways are displayed along the x-axis. The stacked bar charts represent the overlap of the analysis with the canonical pathways. The green bars represent downregulation and the red bars represent upregulation. The yellow line is indicative of the cut-off for significance $p < 0.05$. $n = 5$ animals

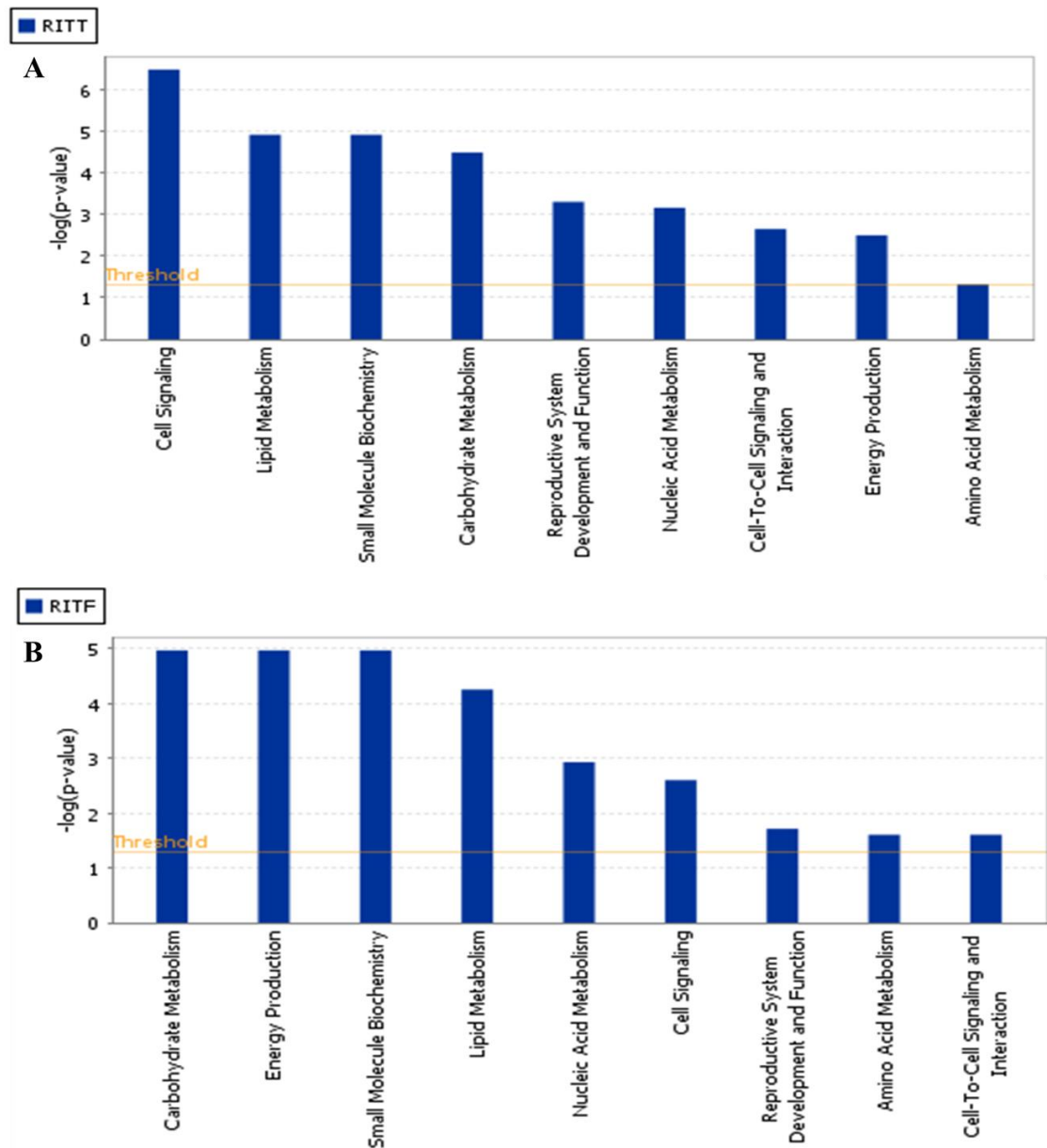


Figure 3.12 Top functions associated with the effect of RIT on uterine contraction. These functions were extracted using the IPA bioinformatics software. Functions associated with RIT - treated tissues and fluids are shown in A and B above along the x-axis while the $-\log(p\text{-value})$ is indicated on the left y-axis. Taller bars are more significant than shorter bars. The yellow line is indicative of the cut-off for significance $p < 0.05$ ($-\log = 1.3$). $n = 5$ animals

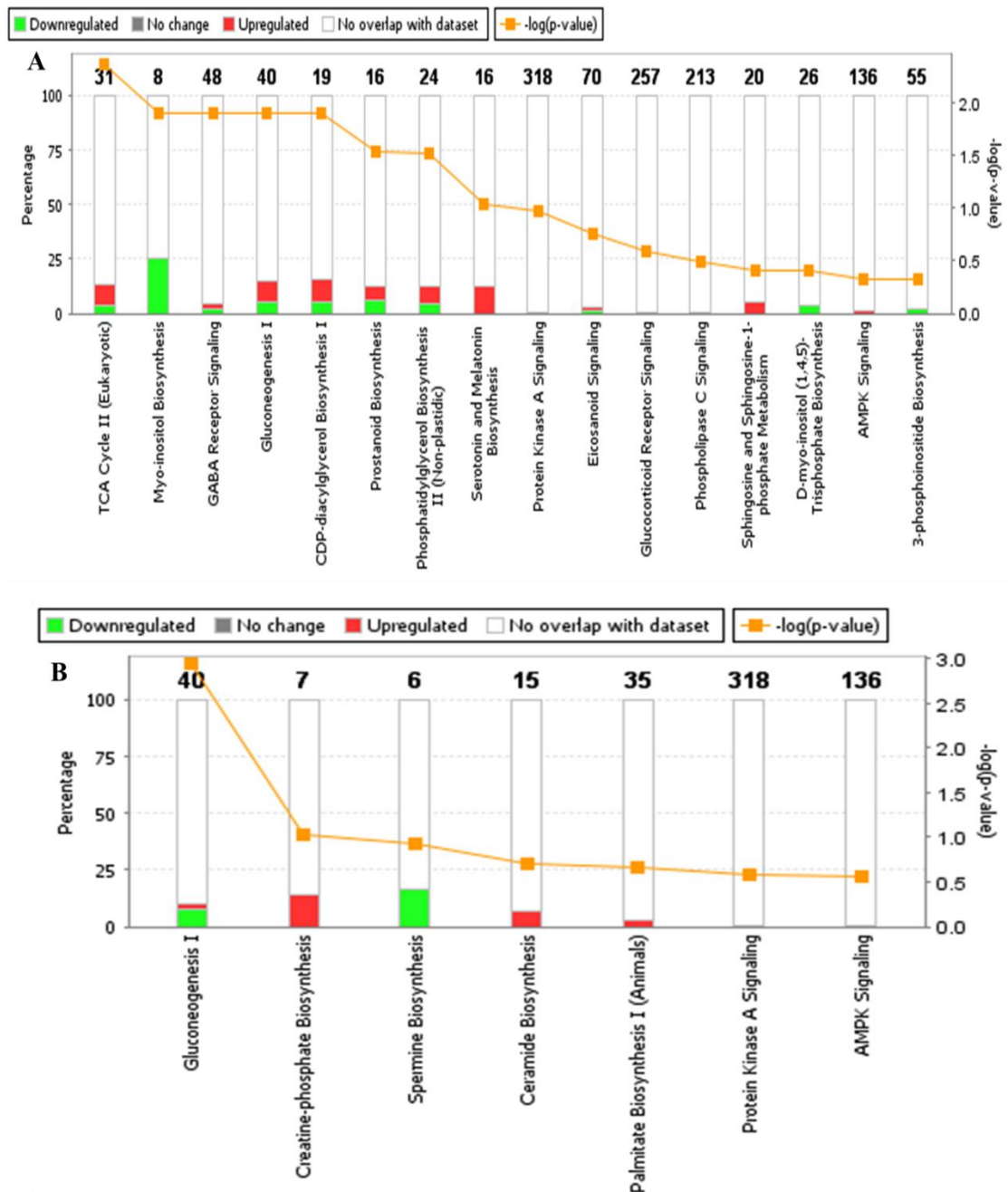


Figure 3.13 Top canonical pathways extracted by IPA bioinformatics software for the effect of RIT on uterine contraction are shown above. Pathways associated with RIT -treated uterine tissues are shown in A while the bath fluids are shown in B. The pathways are displayed along the x-axis. The stacked bar charts represent the overlap of the analysis with the canonical pathways. The green bars represent downregulation and the red bars represent upregulation. The yellow line is indicative of the cut-off for significance $p < 0.05$. $n = 5$ animals

Networks were also generated to show the interconnectivity between the derived pathways.

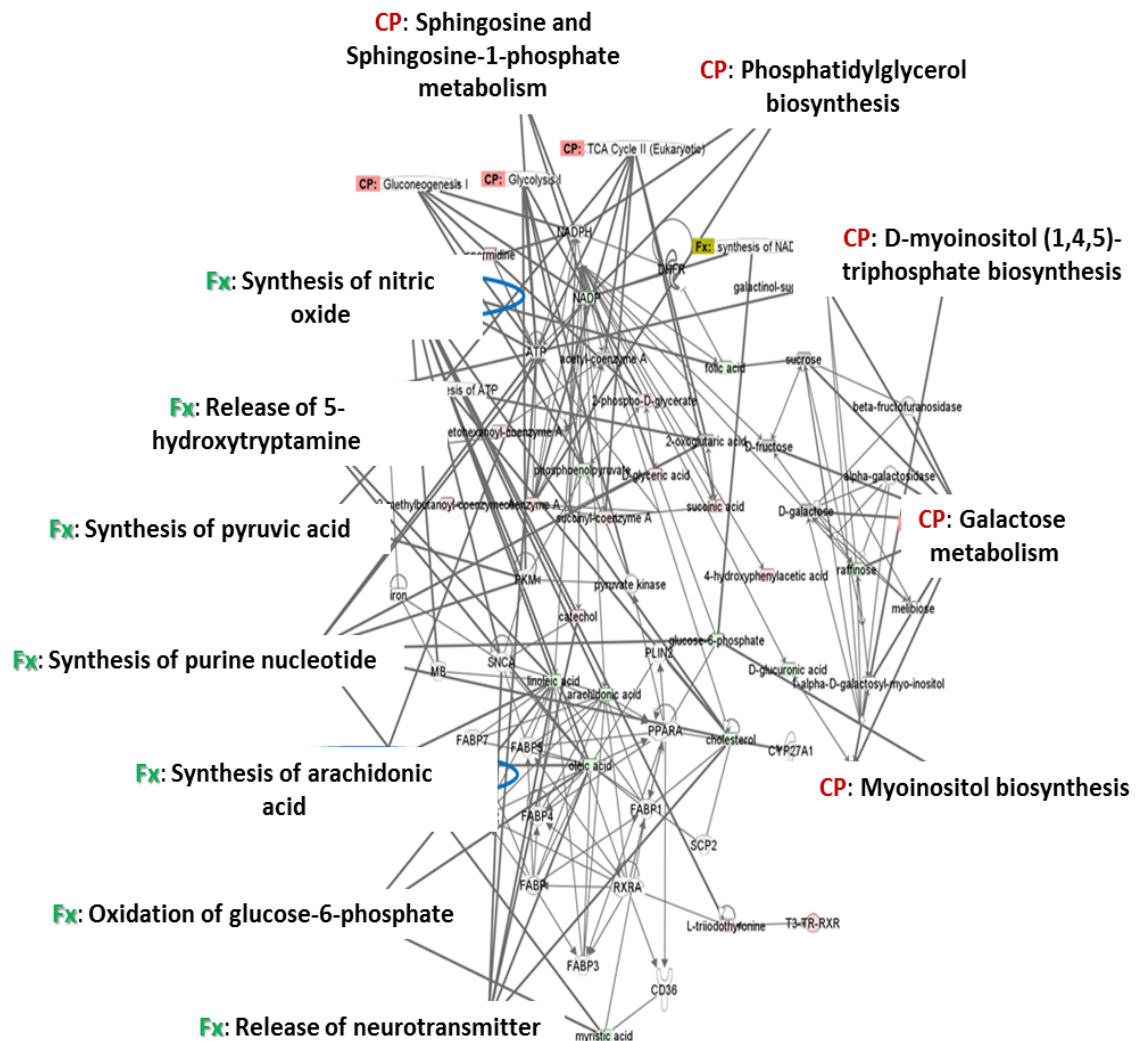


Figure 3.14 IPA network of top functions and signalling pathways detected on analysis of OT- treated uterine tissues. The network displays the interaction and interrelationship between the metabolites detected on OT treatment. The interconnectivities were then pulled together into specific biological functions and pathways. FX = function; CP= canonical pathways.

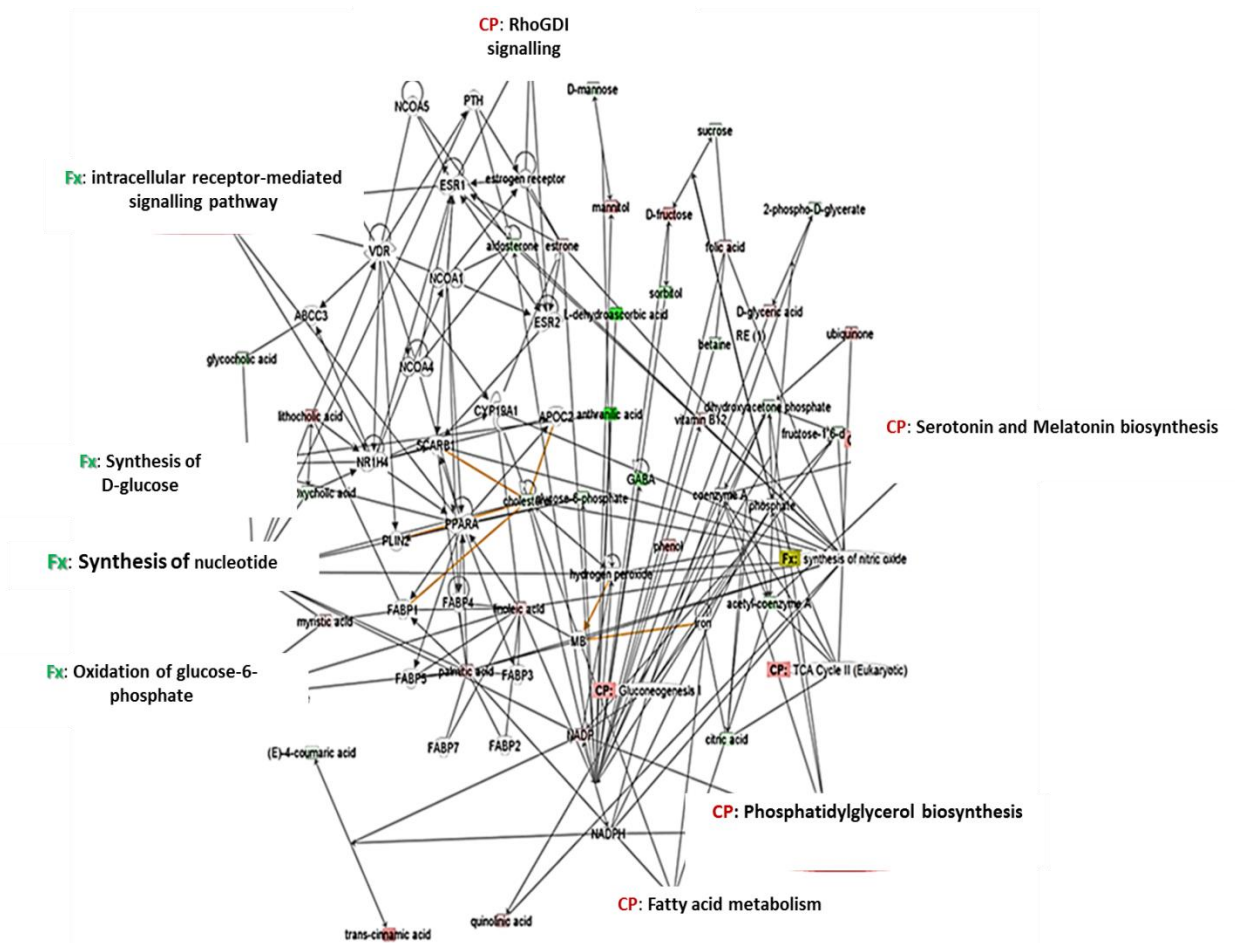


Figure 3.15 IPA network of top functions and signalling pathways detected on analysis of bath fluids in which OT - treated uterine tissues were immersed. The network displays the interaction and interrelationship between the metabolites released into the bath fluid on OT treatment. The interconnectivities were then pulled together into specific biological functions and pathways. FX = function; CP= canonical pathways.

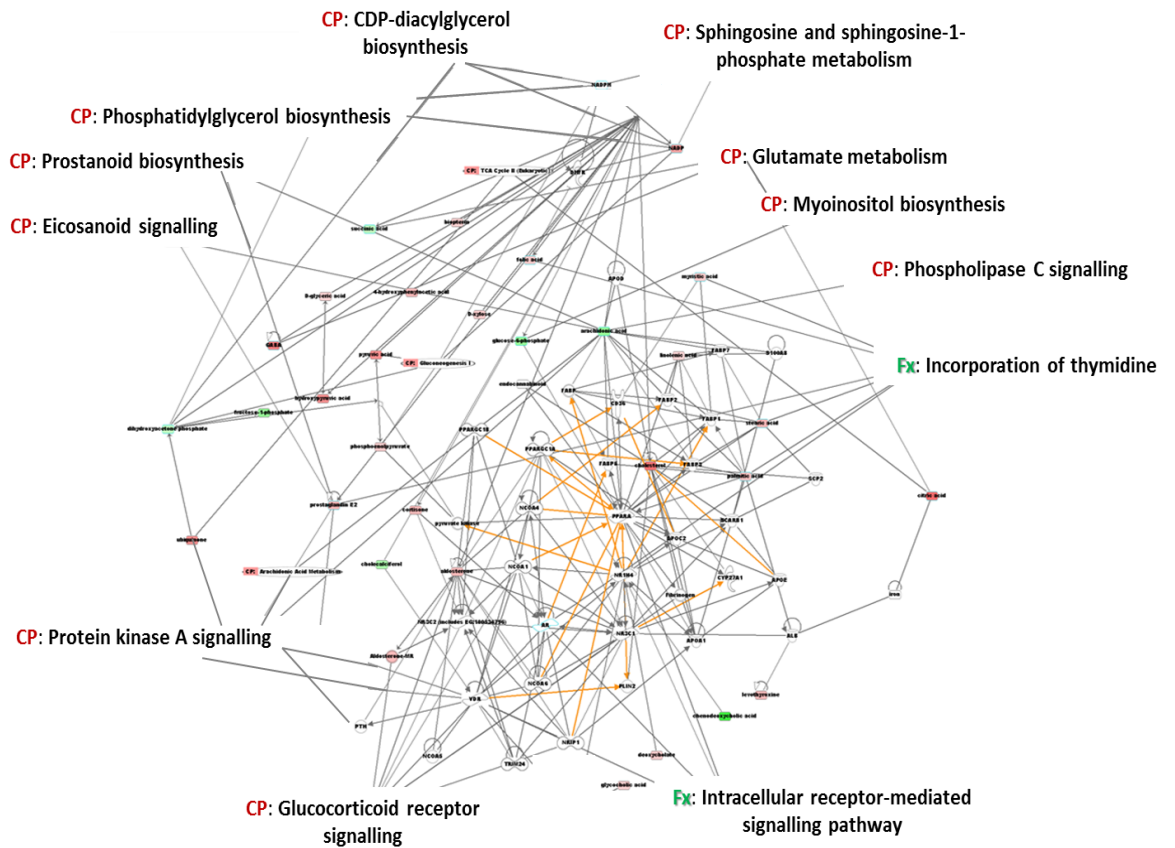


Figure 3.16 IPA network of top functions and signalling pathways detected on analysis of RIT- treated uterine tissues. The network displays the interaction and interrelationship between the metabolites detected on RIT treatment. The interconnectivities were then pulled together into specific biological functions and pathways. FX = function; CP= canonical pathways.

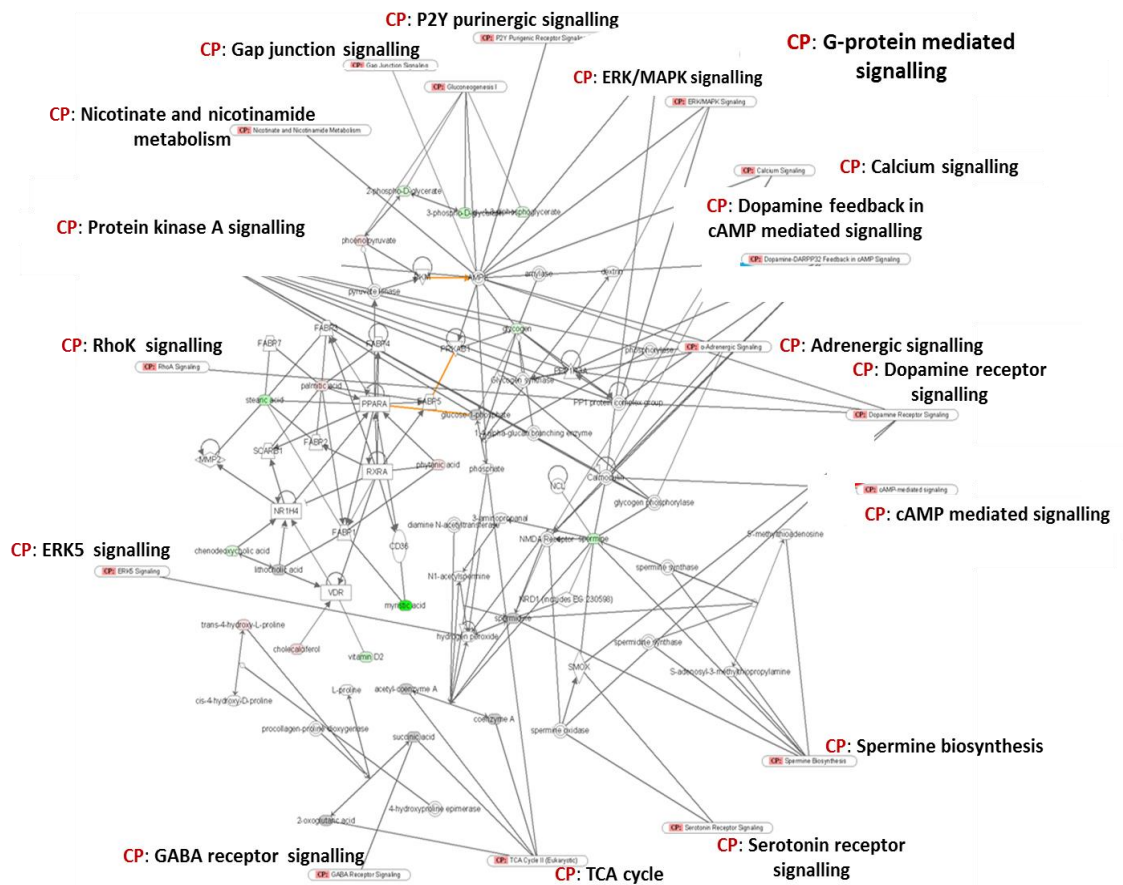


Figure 3.17 IPA network of top functions and signalling pathways detected on analysis of bath fluids in which RIT- treated uterine tissues were immersed. The network displays the interaction and interrelationship between the metabolites released into the bath fluid on RIT treatment. The interconnectivities were then pulled together into specific biological functions and pathways. FX = function; CP= canonical pathways.

3.9.4 Comparison of ¹H-NMR Metabolic Profiles of Uterine Tissues and Bath Fluids

Representative pair matched control versus treated ¹H-NMR spectra of mouse uterine tissues and respective bath fluids are presented for each data set. The spectral resolution of the one dimensional spectra combined with reported data from the literature enabled the identification and assignment of 57 different metabolites (Table 3.4). Biplots which simultaneously displays the relationship among scores and loadings (Fig. 3.18), and an S-line which is an analogue of a scatter S plot (Fig. 3.19), were utilized to explain the influence of the variables on the ¹H-NMR data derived from the OPLS-DA models.

Table 3.4: Chemical Shift Assignment of Uterine Metabolites		
Assigned Number	Metabolite	Chemical shift (ppm)
1	Lipid	0.65-0.7
2	DAG	0.7-1.0, 1.6-1.7, 2.0-2.1, 2.2-2.4, 2.75, 4.22, 5.0-5.33
3	Isoleucine + leucine	0.82
4	AEA	0.89, 1.25-1.40, 1.69-1.77, 2.05, 2.19-2.23, 2.62, 2.79-2.85, 3.40-3.44, 3.72, 5.30-5.43, 5.88-5.90
5	Valine	0.89, 0.97, 1.02-1.03, 2.25, 2.32, 3.59
6	Arachidonic acid	0.90, 2.15, 2.83, 5.36
7	Hydroxybutyrate	1.24
8	Lactate	1.30, 4.10-4.11
9	Threonine	1.32, 3.57, 4.24
10	Alanine	1.46, 1.51, 3.76-3.77
11	Lysine	1.55, 1.83, 3.03
12	Alanine	1.61
13	Leucine	1.77
14	Glutamate	1.88, 2.02-2.04, 2.12, 2.18-2.19, 2.33-2.35, 2.43, 3.74
15	GABA	1.89, 2.28-2.33, 3.00-3.01
16	Acetate	1.90, 1.93
17	N-Acetylaspartate	2.00, 2.48, 2.67, 4.38, 7.82
18	N-acetylaspartylglutamate	2.04, 2.51, 2.72, 4.60

Chemical Shift Assignment of Uterine Metabolites continued		
Assigned Number	Metabolite	Chemical shift (ppm)
19	Proline	2.06
20	Glycoprotein	2.08
21	Glutamine	2.1 – 2.32, 2.43-2.45, 3.75-3.76, 6.81, 7.52
22	Acetoacetate	2.22
23	Pyruvate	2.36
24	Succinate	2.39, 2.42
25	Glutamate	2.47
26	Aspartate	2.65-2.66, 2.80, 3.88-.89
27	Dimethylamine	2.72
28	Glucose	3.06, 4.27,4.91 3.23, 3.38-3.39, 3.42-3.47, 3.51, 3.62-3.88, 4.63, 5.21-5.30
29	Histamine	2.98, 3.03-3.04, 3.29-3.31
30	Creatine	3.02, 3.91, 6.64, 3.12
31	Tyrosine	3.03 -3.04, 3.19, 3.92, 6.88 – 6.89, 7.18, 7.50
32	Amino acids	3.10- 3.90
33	Phenylalanine	3.10-3.11, 3.27-3.28, 3.97-3.98, 7.20, 7.32-7.36, 7.42
34	Histidine	3.11, 3.18, 3.97-3.99, 7.05-7.10, 7.79, 7.90
35	Ethanolamine	3.14, 3.81
36	PE	3.17, 3.21, 3.97-3.98
37	Choline, Phosphocholine	3.18, 3.50, 4.05, 3.31
38	PC	3.20-3.21, 3.64, 4.28
39	Taurine	3.25, 3.42
40	Myoinositol	3.26, 3.51-3.52, 3.60-3.61, 4.04 - 4.05, 4.9-5.5
41	Tryptophan	3.28, 3.47, 7.19, 7.27, 7.30- 7.31, 7.53, 7.72
42	GPC	3.31
43	Betaine	3.35, 3.41
44	IP ₃	3.82, 4.11, 4.20, 4.43
45	Serine	3.84, 3.94, 3.97
46	Tyrosine	4.03, 6.0-7.5
47	TGs, Glyceryls	4.12-4.16
48	Adenosine nucleotide/ATP	4.20 - 4.29, 4.39, 4.61, 4.79, 6.12
49	Threonine	4.30 – 4.41
50	Glyceride/nucleotide sugars	4.41-4.52
51	PGF1 alpha	5.32, 5.76
52	AMP	5.39
53	Adenosine	5.92, 6.75, 5.22-8.23, 8.51-8.52,
54	Uridine	5.93, 7.93
55	Fumarate	6.55
56	Adenine	8.00 – 8.44
57	Unknown amine	>9.00

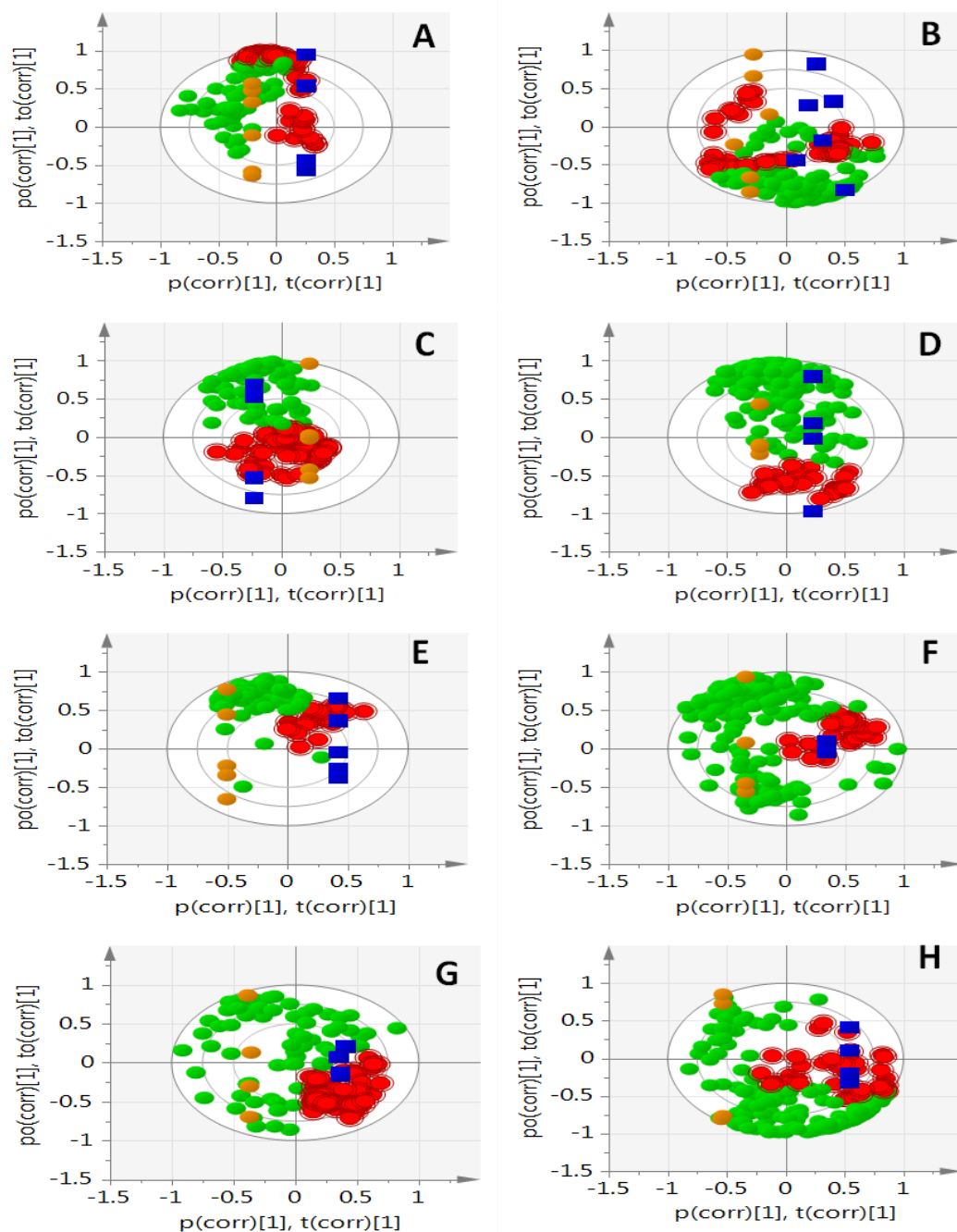


Figure 3.18 Biplots of oxytocin- and ritodrine-treated uterine tissues and surrounding bath fluids. The polar and non-polar extracts of oxytocin-treated uterine tissues are shown in A and B respectively and the surrounding bath fluid extracts are shown in C and D. Polar and non-polar extracts of ritodrine-treated uterine tissues are shown in E and F and the surrounding bath fluids in G and H. The biochemically significant metabolites are highlighted in red, the blue squares represent the treated groups while the brown circles represent the controls. n= 5 animals

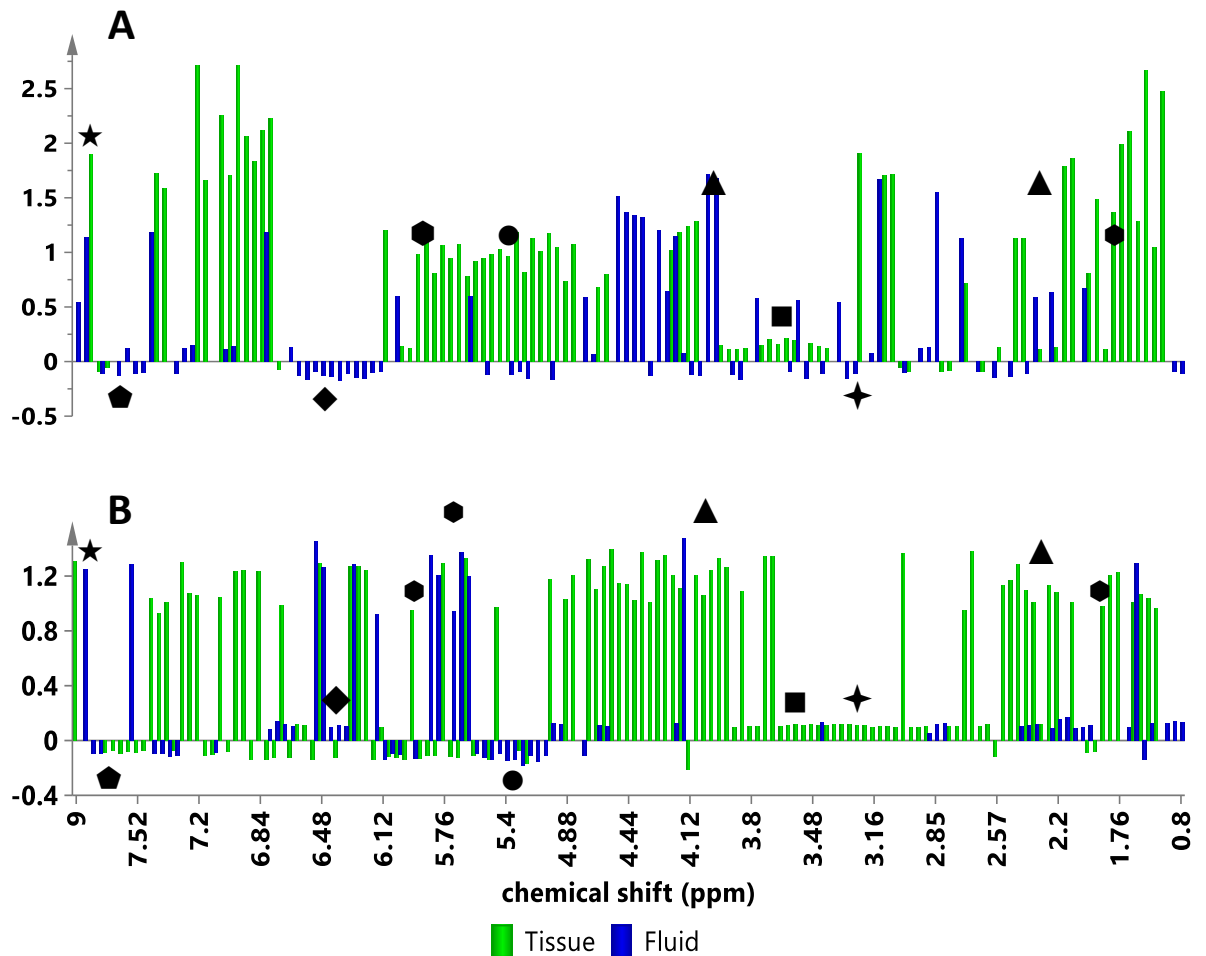


Figure 3.19 Differentially regulated metabolites with OT (A) and RIT (B) as determined by NMR. A positive p[1] value indicates a relatively higher metabolite concentration in the treated groups, while a negative value is indicative of a relatively lower concentration in the treated. ● = Signal Transduction (PGF_{1α}); ■ = Phosphatidyl-inositol signalling system (myoinositol); ▲ = Ligand-receptor Interaction/Lipid Metabolism (GABA/DAG); ◆ = cAMP biosynthesis (N-Adenylyl-L-phenylalanine); ● = Sphingolipid metabolism; ◆ = Cell Signalling (Arachidonic acid); ★ = Nicotine/Nicotinamide metabolism; † = Glycine, serine and threonine metabolism (betaine). n= 5 animals

3.9.5 Comparison of ^1H -NMR Metabolic Profiles of Oxytocin Treated Uterine Tissues and Bath Fluids with Controls

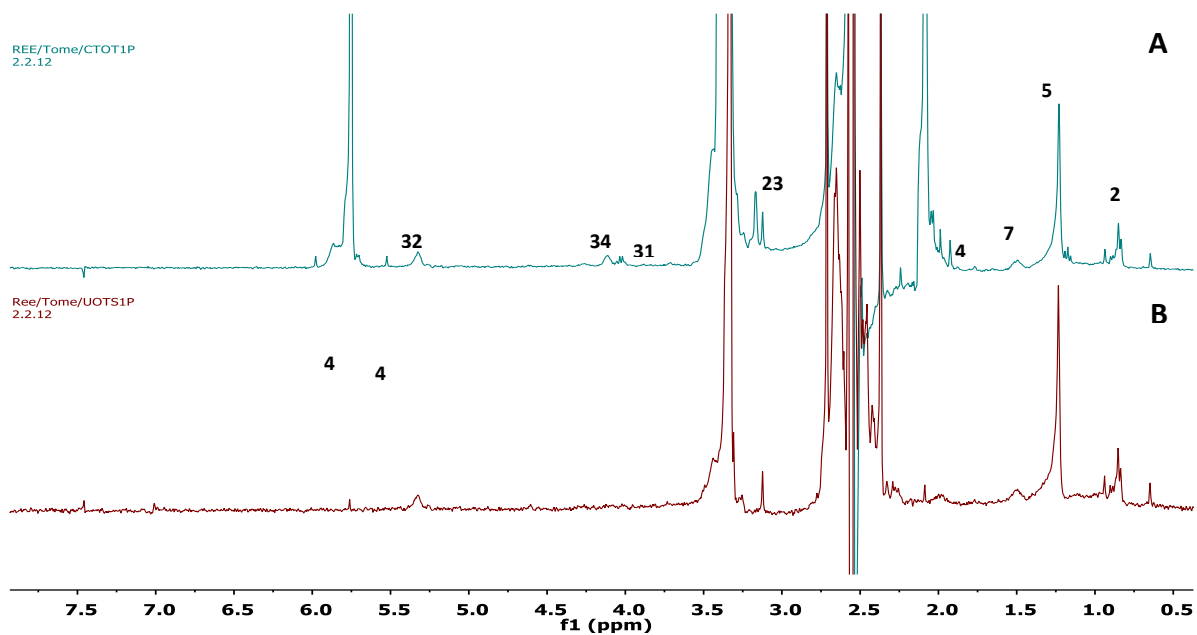


Figure 3.20 Pair matched 1D ^1H -NMR spectra showing polar extracts of control (**A**) versus oxytocin-treated (**B**) uterine tissues. The numbers indicate identified metabolites in Table 3.4.

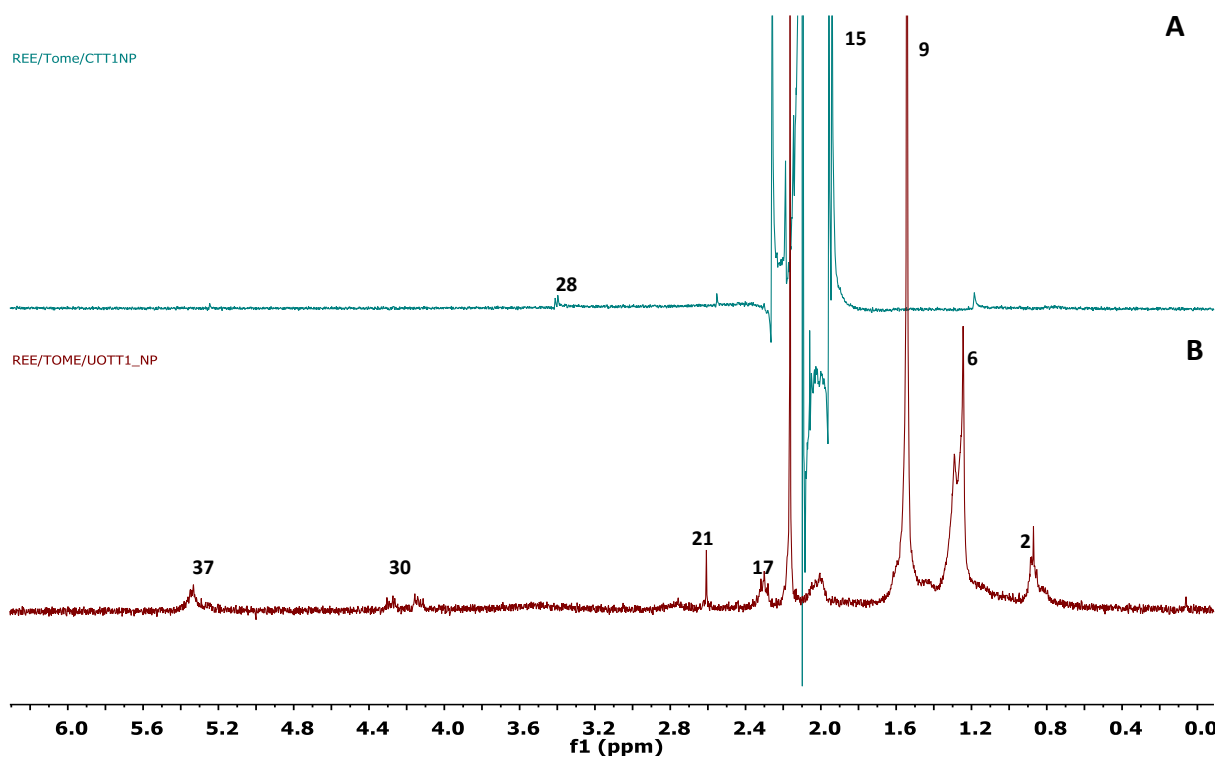


Figure 3.21 Pair matched 1D ¹H-NMR spectra showing nonpolar extracts of control (**A**) versus oxytocin-treated (**B**) uterine tissues. The numbers indicate identified metabolites in Table 3.4.

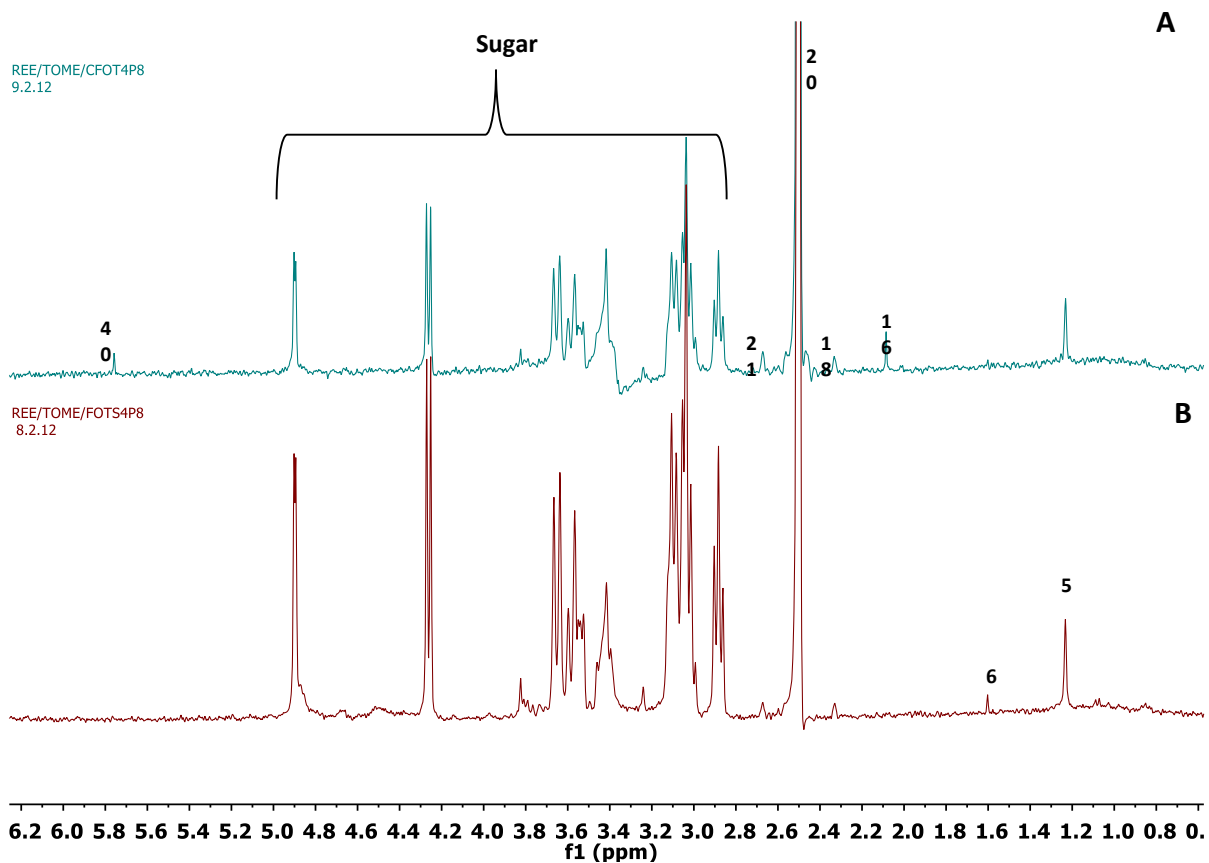


Figure 3.22 Representative pair matched 1D ^1H -NMR spectra showing polar extracts of control (A) versus oxytocin-treated (B) bath fluids. The numbers indicate identified metabolites in Table 3.4.

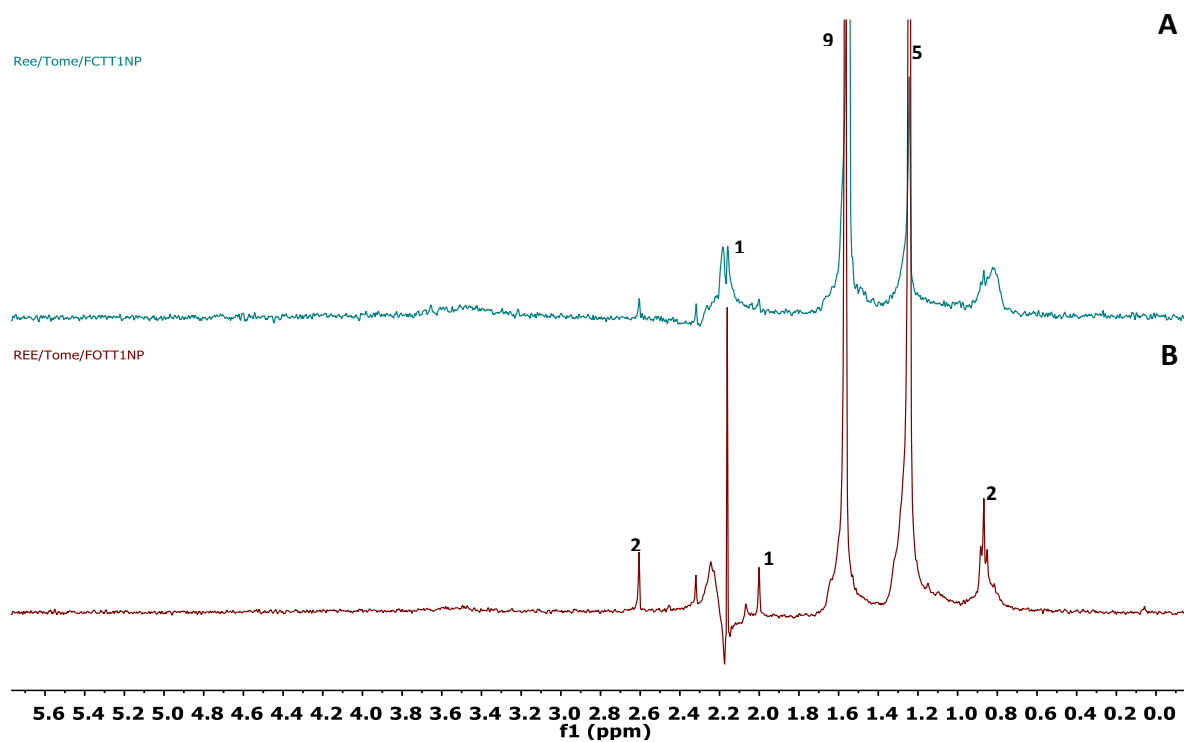


Figure 3.23 Representative pair matched 1D ¹H-NMR spectra showing nonpolar extracts of control (**A**) versus oxytocin-treated (**B**) bath fluids. The numbers indicate identified metabolites in Table 3.4.

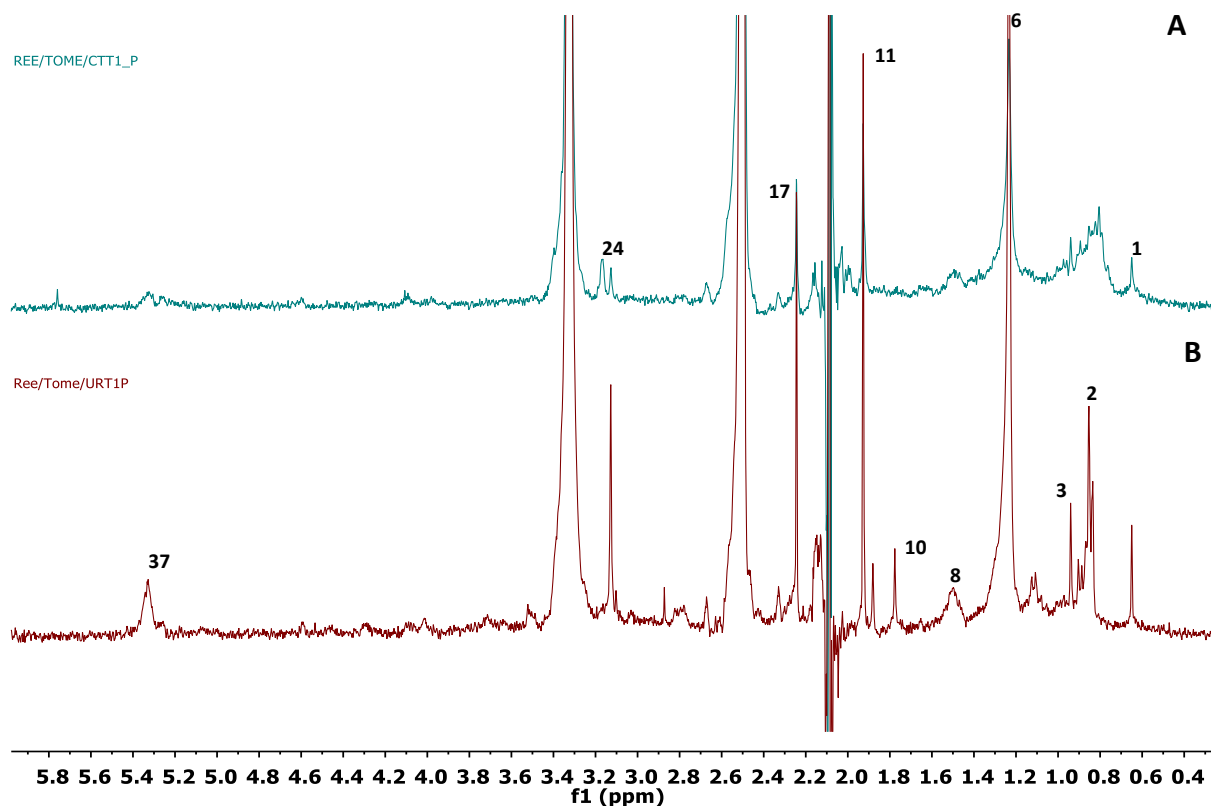


Figure 3.24 Representative pair matched 1D ^1H -NMR spectra showing polar extracts of control (**A**) versus ritodrine-treated (**B**) tissues. The numbers indicate identified metabolites in Table 3.4.

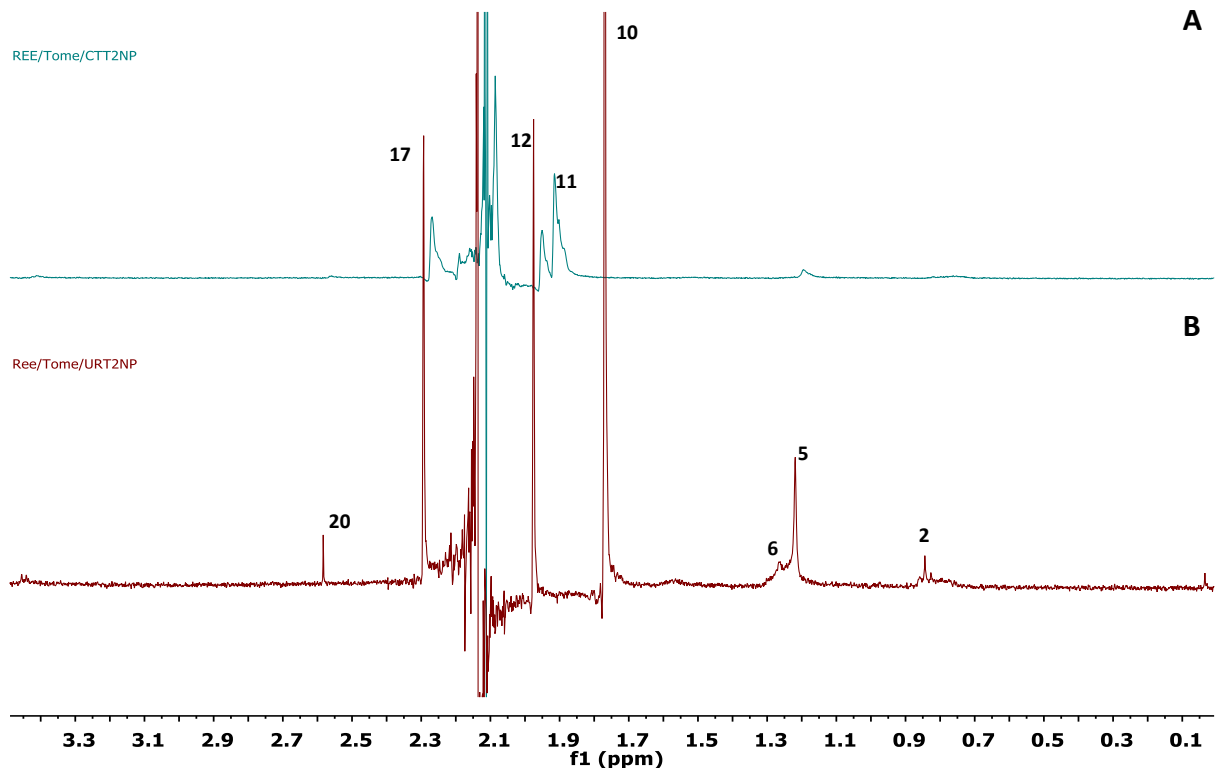


Figure 3.25 Representative pair matched 1D ¹H-NMR spectra showing nonpolar extracts of control (A) versus ritodrine-treated (B) tissue. The numbers indicate identified metabolites in Table 3.4.

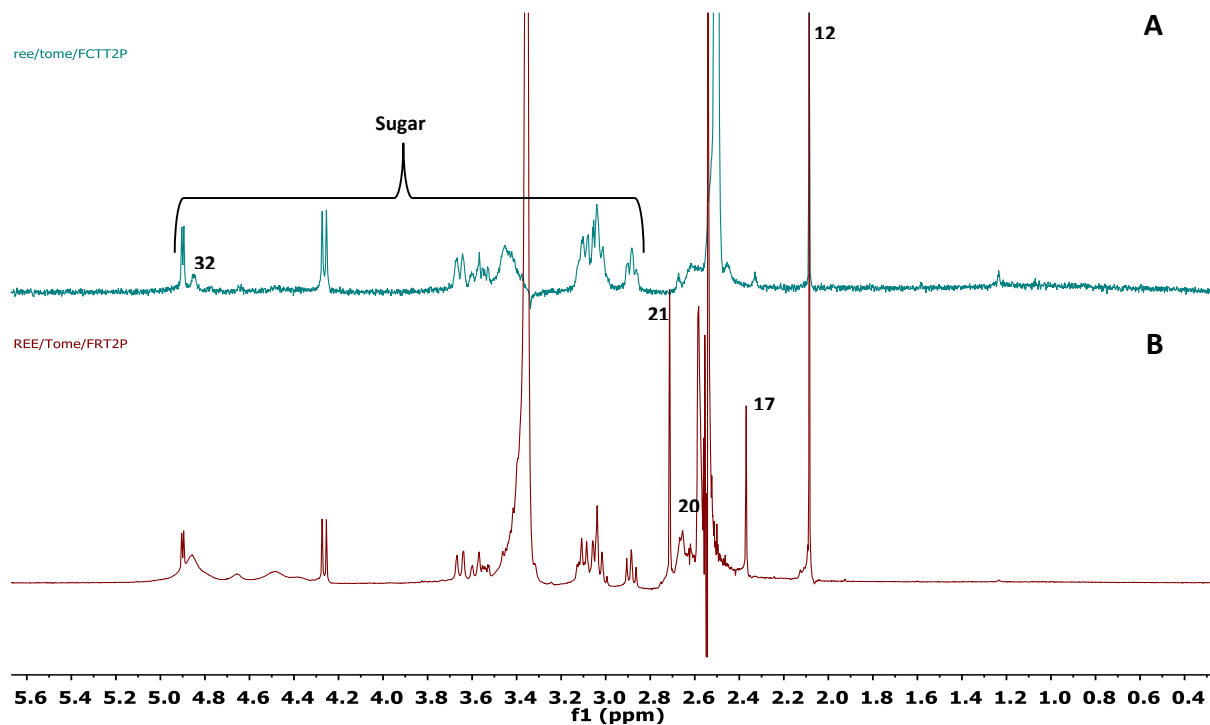


Figure 3.26 Representative pair matched 1D ^1H -NMR spectra showing polar extracts of control (**A**) versus ritodrine-treated (**B**) bath fluids. The numbers indicate identified metabolites as listed in Table 3.4.

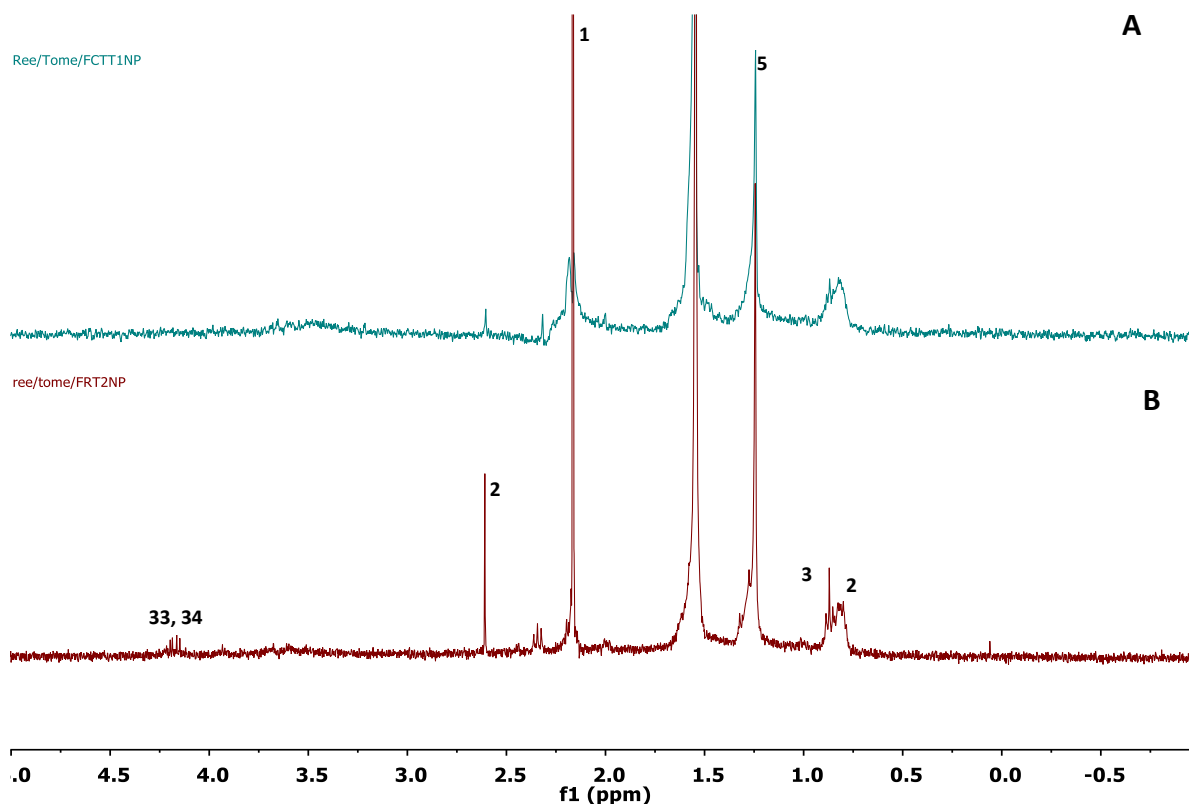


Figure 3.27 Representative pair matched 1D ^1H -NMR spectra showing nonpolar extracts of control (**A**) versus ritodrine-treated (**B**) bath fluids. The numbers indicate identified metabolites as listed in Table 3.4.

3.10 Discussion

It was observed that myoinositol, and diacylglycerol (DAG) were among the metabolites detected in the OT-treated myometrium (Tables 3.3, Fig. 3.8A-D). These findings correlate with previously documented activities reported on OT-induced uterine contraction (Gimpl and Fahrenholz, 2001; Ku *et al.*, 1995; Marc *et al.*, 1986; Nakamura *et al.*, 2000; Zingg and Laporte, 2003). Myoinositol is the cyclic alcohol derivative of glucose utilized in a number of signalling pathways one of which is the phosphatidylinositol signalling pathway (Downes and Macphee, 1990; Loewus and

Murthy, 2000) activated by OT in the uterus. In addition, other interesting findings were observed, some of which included the detection of nicotinic acid adenine dinucleotide phosphate (NADP), gamma amino butyric acid (GABA), metabolites involved in pyrimidine and purine biosynthesis and metabolites involved in nitric oxide synthesis (Table 3.3). Some of these metabolites had not been previously associated with the action of OT on the uterus. OT has been associated with the inhibition of K^+ -stimulated release of excitatory amino acids (glutamate, aspartate) in the supraoptic nerve via an indirect action on the terminals (Burbach *et al.*, 2006). Similarly, OT has been reported to inhibit GABA by suppressing presynaptic GABA neurons but these effects have never been reported to occur directly within the myometrium. In this study however as shown in Fig. 3.8, GABA was found to have been released into the bath fluids upon addition of OT to the isolated uterus. It is well established that an increase in calcium (Ca^{2+}) which could result from extracellular entry through membrane channels or intracellularly from the sarcoplasmic reticulum (SR) (Noble *et al.*, 2009) eventually leads to myometrial contraction. The role of NADP as an alternative second messenger and an effective regulator of calcium levels in the cytosol (besides the action of inositol triphosphate (IP_3) on SR during uterine contraction) is emerging (Aley *et al.*, 2010; Guse, 2009; Guse and Lee, 2008; Patel *et al.*, 2010). The two-pore channels have been associated with the NADP receptor in the endolysosomal system (Galione *et al.*, 2010) and activation of NADP-sensitive calcium channels produces significant changes in the calcium levels within the cytosol (Mandi and Bak, 2008). NADP component is coupled with the neurotransmitter glutamate (Pandey *et al.*, 2009) which was found significantly upregulated in this study (Appendix 4). A role for NADP in OT-induced uterine

contraction has been shown (Aley *et al.*, 2010) supporting results from this study in addition to cyclic ADP-ribose acting on ryanodine receptors (Barata *et al.*, 2004; Thompson *et al.*, 2004). Another interesting finding was the downregulation of arachidonic acid (AA) in some instances (Fig. 3.8) while a significant increase in prostaglandin concentration within the tissue was exhibited in response to OT treatment (Fig 3.8 A-D). AA has been associated with OT-induced prostaglandin release (Hertelendy *et al.*, 1995; Rauk and Chiao, 2000). Conversely but in correlation with our findings, a previous study strongly suggested that the effect of OT on the uterus is independent of prostaglandin release (Chan, 1980); but rather an outcome of two distinct actions, a uterotonic action on myometrial receptors and a prostaglandin-releasing action from endometrial receptors. Though AA is known to be the precursor of prostaglandins and as such associated with the connection between OT and PG on uterine action (Huszar and Roberts, 1982), AA can itself also serve as a second messenger (Piomelli, 1993). AA is liberated either directly or indirectly by different phospholipases (Dennis, 1983), some of which are Ca²⁺ dependent and others Ca²⁺ independent. The uterus develops spontaneous oscillatory contractions under appropriate conditions. In this study, OT was added to spontaneously contracting tissues and since AA modulates these spontaneous contractions by action on some ion channels (Bae *et al.*, 1999), this may be partly responsible for the observed decreased concentration of AA with the observed increase in PGE₁. However, there might be other sites of PGE synthesis besides AA metabolism. These observations were similarly supported by the results from the ¹H-NMR data (Fig. 3.19). Another interesting finding was the downregulation of N-arachidonyl amine (NAE) or anandamide (AEA) (Table 3.3) on OT treatment. There

has been no previous association of AEA with OT activity on the uterus. AEA activates cannabinoid receptors which have been recently found expressed in reproductive tissues (Battista *et al.*, 2008; Brighton *et al.*, 2009; Habayeb *et al.*, 2004; Marczylo *et al.*, 2010; Park *et al.*, 2003). Binding of AEA to its receptors has been associated with the reduction and increase of intracellular cAMP levels, regulation of ion channels and nitric oxide generation (Asala *et al.*, 2013). AEA has been reported to cause both stimulatory and inhibitory effects on uterine contractility (Brighton *et al.*, 2009; Dmitrieva and Berkley, 2002). The relationship between AEA and OT activities is yet to be investigated but bioinformatic analysis revealed an association of AEA and lipid metabolism during OT treatment. AEA was found to be increased in tissue analysis and decreased in the fluid analysis on OT treatment in this study. Sphingosine and kynurenic acid were also found associated with OT activity.

Metabolites generated from the action of RIT on spontaneous uterine contraction were listed in Table 3.3. In the presence of RIT, downregulation of PGF₁ with increased concentration of ARA in the bath fluid was exhibited (Fig. 3.9A-D). cAMP was not specifically identified in this study however, the bioinformatic analysis suggested the involvement of cAMP mediated signalling (Figure 3.17). Prostaglandins interact with specific receptors on plasma membranes to regulate myometrial activity (Asboth *et al.*, 1997; Chiossi *et al.*, 2012; Vane and Williams, 1973). A significant decrease in the concentration of myoinositol was also observed suggesting a reduction in the phosphatidylinositol signalling pathway in the presence of RIT, which supports recent studies linking cAMP signalling with phosphatidylinositol (Breuiller-Fouche *et al.*, 1991; Buxton, 2004). Increased

concentration of NADP, and a decreased concentration of AEA were also exhibited on RIT treatment (Table 3.3). These are new findings in connection with the uterine relaxant activity of RIT and possibly β_2 -adrenoceptor activation in the myometrium. It has however been suggested that S-nitrosylation and activation of NADP synthesis could subside membrane limited elevations in Ca^{2+} and constitute the cGMP-independent NO-mediated activation of K_{Ca} channels (Charpigny *et al.*, 2003) and may contribute to the seemingly dual role of NADP in the myometrium. In addition, GABA was found to be associated with RIT activity. Recent evidence has implicated a strong association of GABA receptors with lipid signalling and lipid rafts have been suggested to provide a platform for signal transduction (Becher *et al.*, 2004; Bowery *et al.*, 2002) and also play crucial roles in calcium signalling within the uterus (Noble *et al.*, 2006). As such, interference with the cholesterol or lipid content of the myometrial plasma membrane has been observed to cause a profound effect on both Ca^{2+} and force of contraction. The spontaneous contractions and Ca^{2+} transients associated with the myometrial longitudinal muscle, from rats and humans were greatly augmented upon cholesterol extraction and raft disruption (Bowery *et al.*, 2002). Lipid rafts can also rapidly recruit other signalling complexes into functional assemblies when an appropriate cell stimulus is applied (Brown and London, 1998; Simons and Toomre, 2000). There is strong evidence for the association of a significant fraction (30% - 40%) of the $\text{GABA}_{\text{B}}\text{R}$ with lipid raft domains (Becher *et al.*, 2001) and the presence of both the receptor and the G proteins in lipid rafts may indicate a possible functional role for the receptor raft association.

Lipids, amino acids, choline-containing compounds, creatine, inositols and lactate dominated the NMR spectra obtained in this study. In some cases, the 1D

¹H-NMR spectra of the uterine tissues and bath fluids mostly shared the same metabolites in both the control and treated groups. Glucose was significantly present in the fluids however increased levels were observed in some of the treated groups. On examination of the ¹H-NMR spectra of polar RIT- treated tissues (Fig. 3.24) and bath fluids (Fig. 3.26) lactate, leucine, acetate, GABA and glutamate were consistently present while the spectra of the nonpolar tissue (Fig. 3.25) and fluid (Fig. 3.27) extracts displayed the presence of HB, leucine, lactate, acetate, GABA and adenosine.

These findings on OT and RIT activity correlated with the OPLS-DA score plots and biplots on both the MS and NMR data which showed separations between OT-treated and RIT-treated tissues and control (Fig. 3.6, 3.7 and 3.18).

3.11 Conclusion

The detection of phosphatidylinositol and DAG pathways in connection with the activity of OT on the uterus as well as the detection of AMP, adenosine and components involved in the cAMP pathway in connection with the effect of RIT on the uterus validates the sensitivity of this method in the detection of metabolites associated with drug function. The discovery of the involvement of other metabolites such as sphingosine and AEA with the activity of OT and the association of GABA and AEA with the activity of RIT provides a knowledge-based hypothesis for further research. This new technique involving the utilization of pharmacology and metabolomics has therefore proven effective in the utilization of finger and footprints of myometrial tissue in the determination of the possible mechanism(s) of activity of

OT and RIT, as such, a useful tool in drug discovery for the rapid assessment of novel drug mechanisms of action.

CHAPTER FOUR

ELUCIDATION OF THE MECHANISM OF ACTION OF THE EXTRACTS OF *F. EXASPERATA* ON UTERINE CONTRACTION USING METABOLOMIC TECHNIQUES

4.1 INTRODUCTION

Development of novel drugs from natural products as well as determination of the mechanism of activity has become increasingly difficult in recent years due to the high cost and extended time period required (Yuliana *et al.*, 2011b). Also, as a natural product (NP) extract is made up of a complex mixture of compounds, the interactions of the different compounds could disguise the activity of compounds of interest or create false-positive results. Due to these difficulties the drug discovery process from plants were almost abandoned (Dickson and Gagnon, 2004; McChesney *et al.*, 2007). Some pharmaceutical companies (such as Pfizer) no longer screen NPs while others, such as Merck and Novartis, have placed emphasis on microbial NPs rather than plant NPs (Ortholand and Ganesan, 2004), which is also the trend today in most NP research centres. Between 1981 and 2002, 877 novel drugs were reported to have been developed and of these 6% were NP, 27% were NP derivatives and 16% were synthetically developed from an NP model (Newman *et al.*, 2003a). This therefore suggests that NPs still remain good sources of novel leads for drugs and has fuelled a renewed interest in drug discovery from NP. The ‘silver bullet’ approach to drug discovery is perceived to be the best approach where single compounds with a particular biological activity (single target–single compound paradigm) are tested at the molecular level (e.g. receptor binding inhibition or enzyme screening) (Verpoorte *et al.*, 2005). This approach has yielded some potent drugs such as the statins which are used in the reduction of cholesterol levels and the drug huperzine A which is used in the management of Alzheimer’s disease (Li *et al.*, 2004). However, it is not regarded as the best approach in NP screening programmes among some researchers due to the effects of synergism and pro-drugs in an extract

which could give misleading results (Verpoorte *et al.*, 2005). In order to improve on NP screening approach, a more holistic approach (a philosophy adopted by some traditional medicine practices such as Traditional Chinese Medicine (TCM) and Ayurveda, is being developed (Ulrich-Merzenich *et al.*, 2007; Verpoorte *et al.*, 2005; Wang *et al.*, 2005). In the holistic approach, whole herbal preparation (which is the crude complex mixture compounds) is taken to represent one active entity but may target multiple targets in organisms (Li *et al.*, 2004; Ulrich-Merzenich *et al.*, 2007). The system's response is observed using different physiological/pharmacological analytical tools which may include classic physiological observations (e.g. blood pressure, analgesic activity, sedative) and/or modern molecular observations (gene expression, proteome, metabolome). This is performed in order to ascertain the effect of the NP extract on the organism and has been termed 'systems biology approach' (Verpoorte *et al.*, 2005). Among these analytical tools are the 'omics' methods of which metabolomics, a relatively new member, is regarded as being the most helpful in understanding systems biology, as it extracts genotypic information (Sumner *et al.*, 2003). It is therefore considered a valuable tool and can be used to obtain information required in the holistic approach and particularly in the study of medicinal plants, creating new exciting opportunities for drug discovery from NP. Of the many challenges, deciphering the interaction between metabolites present in extracts has remained a significant challenge. Since extracts consist of mixtures of many compounds elaborate purification procedures are often required to isolate new pure compounds which can be extremely time consuming (Yuliana *et al.*, 2011a).

4.2 Metabolomics in Systems Biology

Metabolomics is aimed at the broad study and investigation of metabolites (the metabolome), within an organism, at a precise time and condition (Colquhoun, 2007; Hall, 2006; Mendes *et al.*, 2005; Ulrich-Merzenich *et al.*, 2007; Verpoorte *et al.*, 2007). A metabolome (which refers to a group of metabolites in a cell), as discussed in the preceding chapter is the outcome of several biochemical processes in cells and as such represents a fingerprint of biochemical network within individual cells. It is also a consequence of the exchange and communication that occurs within the organism's immediate environment and contributes in several signal transduction cascades. Therefore, the determination of all the metabolites, as well as the understanding the role played in cellular systems, is a major focus of current research. New methods have been designed and developed in this area which can be used in the determination of the metabolome, enabling a more accurate understanding of their functions (Saghatelian and Cravatt, 2005b) and for an increased understanding of the processes at the point of interaction between the proteome and the metabolome (Saghatelian and Cravatt, 2005a; Saghatelian and Cravatt, 2005b).

Limitations associated with the use of transcriptomics and proteomics profiles (such as the changes in the transcriptome or proteome) have been criticized because they seldom connect to biochemical phenotypes or sometimes the translated protein may not be an active enzyme (Nobeli and Thornton, 2006; Rochfort, 2005; Sumner *et al.*, 2003). Therefore, among the 'omics' technologies, metabolomics is often considered the most functional and reliable approach (Sumner *et al.*, 2003).

The techniques used in metabolomics for identification and quantification have been comprehensively reviewed (Bhalla *et al.*, 2005; Fiehn, 2002; Kell, 2004; Sumner *et al.*, 2003; Van der Greef and Smilde, 2005; Verpoorte *et al.*, 2008). Many reliable, robust and reproducible analytical methods with better selectivity and resolution have been developed which are able to quantitate multiple targets and provide an overview of compound classes (Fiehn, 2002). NMR provides high reproducibility though it's not as sensitive as MS (Colquhoun, 2007; Verpoorte *et al.*, 2007). NMR offers the advantage of rapid but simple sample preparation and measurement time, less automatization, advanced data analysis methods and the chance of structure determination of known or unknown compounds in a complex mixture using the innovative two-dimensional (2D) NMR methods (Colquhoun, 2007; Verpoorte *et al.*, 2007).

High dimensional data are usually obtained from metabolomics investigations and these call for multivariate data analysis (MVDA) methods which are often based on the classification of samples into different groups (e.g. treatment, genotype), both by supervised (e.g. discriminant function analysis, artificial neural networks) or unsupervised type data analysis method, e.g. principal component analysis (PCA), and hierarchical cluster analysis (HCA) (Nobeli and Thornton, 2006). MVDA can also be employed in the creation of a regression model between two data blocks often referred to as X and Y. In metabolomics-based NP studies, X may represent signals arising from different metabolites within plant extracts sampled at consistent time intervals, and Y the responses (e.g. product quality, bioactivity, and yield). The model created is then used to predict Y from X and can be applied to new

observations. The most common MVDA method for this modelling is the partial least square (PLS) method and its extended versions (Wold *et al.*, 2001).

Increased development in the holistic approach might help increase understanding of the mode of action of herbal or natural products and lead to the possible determination of their pharmacological activity. Additionally, measurement of the effect of a complex extract, either *in vitro* or *in vivo*, may assist in the identification of compounds correlated with activity. The holistic approach may also provide new or unanticipated mechanism(s) of action and targets (Verpoorte *et al.*, 2005).

4.3 Metabolomics in the Determination of Mode of Action of Herbal Medicines

Wang *et al.* (2005) studied the effect of three traditional Chinese medicines on insulin resistant transgenic mice by applying a ¹H-NMR and supervised MVDA method to measure metabolites in their urine (Wang *et al.*, 2005). The LC-MS measurement combined with MVDA was also applied to three TCM preparations to discover which was the most effective TCM with the lowest toxicity (Wang *et al.*, 2005).

The use of metabolomic profiling to study the mode of action of active natural products recently emerged in antimicrobial activity analysis. As an example, in one study, HPLC/DAD/ESI-MS application followed by PCA confirmed that dihydrocucurbitacin F-25-O-acetate was the main component having an antimicrobial activity in *Hemsleya pengxianensis*. The possible antibacterial mode of

action on *Staphylococcus aureus* CCTCC AB9105 was predicted by comparing the metabolite profile of *S. aureus* treated by the plant extract and commercial antibacterials with a known mode of action (Biao-Yi *et al.*, 2008).

The use of metabolomics to prove the efficacy of herbal medicines has also been reported. The anti-ageing effects of the total flavone content of the Chinese herb *Herba Epimedii* was investigated using ¹H NMR analysis as the analytical platform and PCA MVDA. Ten metabolites were identified as ageing markers in the rat urine profile (Wu *et al.*, 2008). Elsewhere, the study of *Epimedium brevicornum* Maxim, used for toning the kidney and bone strengthening was performed. The plasma metabolites of rats were analysed using UPLC-MS and PCA MVDA and an increase in the levels of three metabolites were found (Li *et al.*, 2007). The mechanism of action of the TCM preparation known as Xindi soft capsules used in the treatment of haematological disorders, was studied using UPLC-MS combined with quadrupole time of- flight tandem mass spectrometry (UPLC-QTOFMS) followed by PCA and PLS-DA analysis. Results of the study identified some potential biomarkers such as cholic acid, phenylalanine and kynurenic acid (Zhao *et al.*, 2008).

4.4 Aim of Current Study

Based on these reports it would therefore seem possible that metabolomics coupled with pharmacology could get us closer to mapping the pathways underlying the activity of NPs whether as a whole extract or purified compounds. This current study couples pharmacology with metabolomic methods described in the previous chapter

(chapter 3) in the determination of the mechanism of action of the extracts of the leaves of *F. exasperata* on uterine function.

4.5 Materials and Methods

Animals, contractility experiments, sampling, extraction, metabolomic measurements and analysis, pharmacological and statistical analysis are as previously described (Chapter 3).

4.6 Pharmacological Studies

Single concentrations of **E1** (800 µg/ml), **Fr. 14Ea** (200 µg/ml), compound **8** (Fr. 4-31Ea 200 µg/ml), **Fr. 6.17Ea** (200 µg/ml), **Fr. 28Ea** (200 µg/ml) were added to the bath for 10 min following stable rhythmic spontaneous contractions.

4.7 HR-FTLCMS Results

The OPLSDA scatter plots showed distinct separations between the control (blue circles) and treated (red circles) groups in all cases. Significantly regulated metabolites were also highlighted and mapped by the S plots in all analysis groups. A summary of all the metabolites and pathways detected are listed (Table 4.6).

4.7.1 HPLC-HRFTMS of E1

Multivariate analysis of HRFTMS experiments on **E1** using the OPLSDA plots showed clear separations between the control and treated groups (Fig. 4.1 and 4.3). Several metabolites were detected via HRFTMS analysis to have been perturbed on treatment of the uterine tissues with **E1** (Table 4.1). These metabolites ranged from amino acids (aa), to endocannabinoids, catecholamines, purine nucleosides, inositols, carbohydrates, and lipids. Some secondary plant metabolites were also identified such as pheophorbide a, and pyropheophorbide a (Table 4.1). An increase in cysteinyl-dopamine, adenosine, phosphatidylserine, phosphatidyl-ethanolamine, and tyrosine was detected on analysis of **E1**-treated uterine tissues (Table 4.1, Fig. 4.2 A, Fig. 4.4 A). Phenylalanine and aminobutyric acid were however decreased within the tissues (Table 4.1). These results were similarly detected in the bath fluids analysed but in addition myoinositol and phosphatidylinositol were detected to have been decreased (Table 4.1, Fig. 4.2 B, Fig. 4.4 B). Similar results were obtained with the polar and non-polar groups however it would appear that more metabolites were detected in the non-polar groups (Fig. 4.4 A and B). A summary of the major pathways detected are shown in figure 4.5.

Other fractions of **E1** were further subjected to metabolomic analysis.

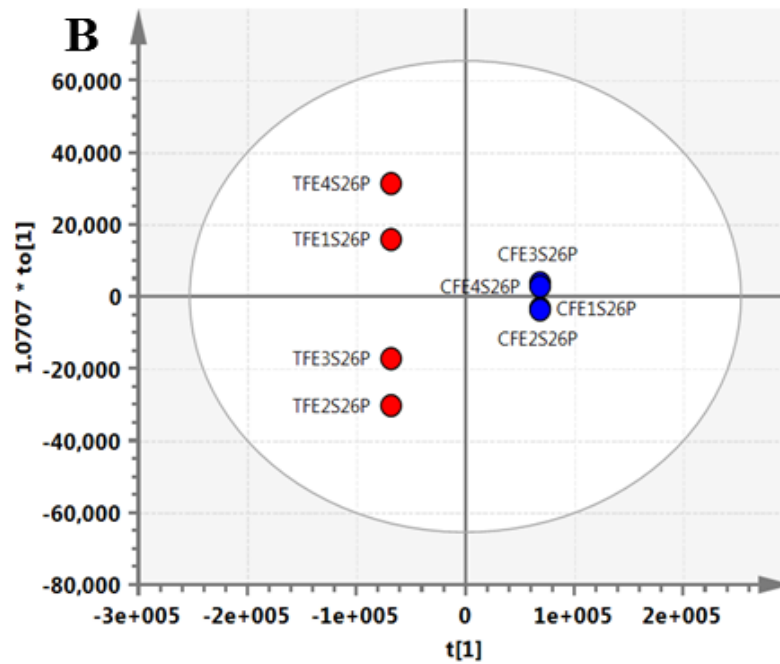
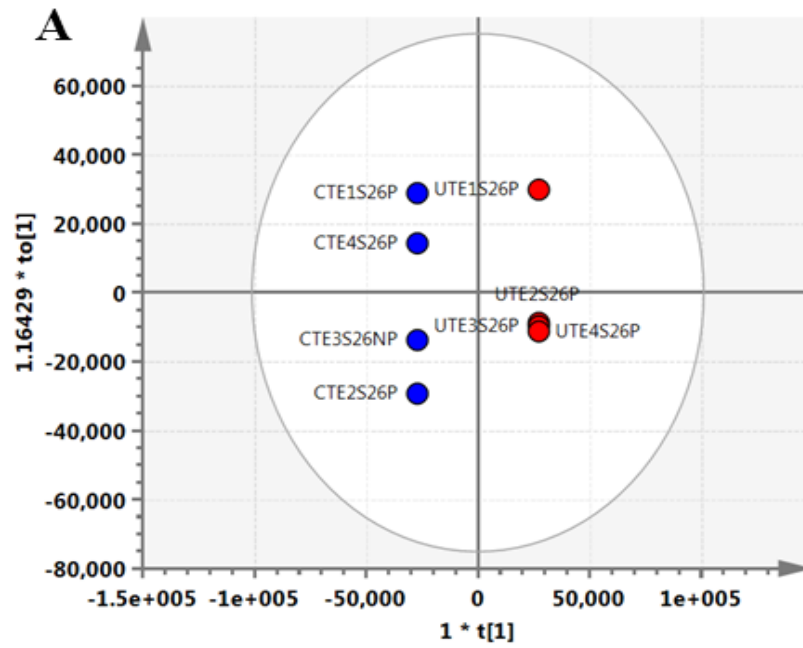


Figure 4.1 OPLSDA score plots (**A** and **B**) of polar **E1** treated groups. Blue circles represent control groups while red circles represent treated groups. Panel A shows the score plot for **E1**-treated uterine tissues while panel B shows the score plot generated for those associated with the bath fluids. n= 4 animals

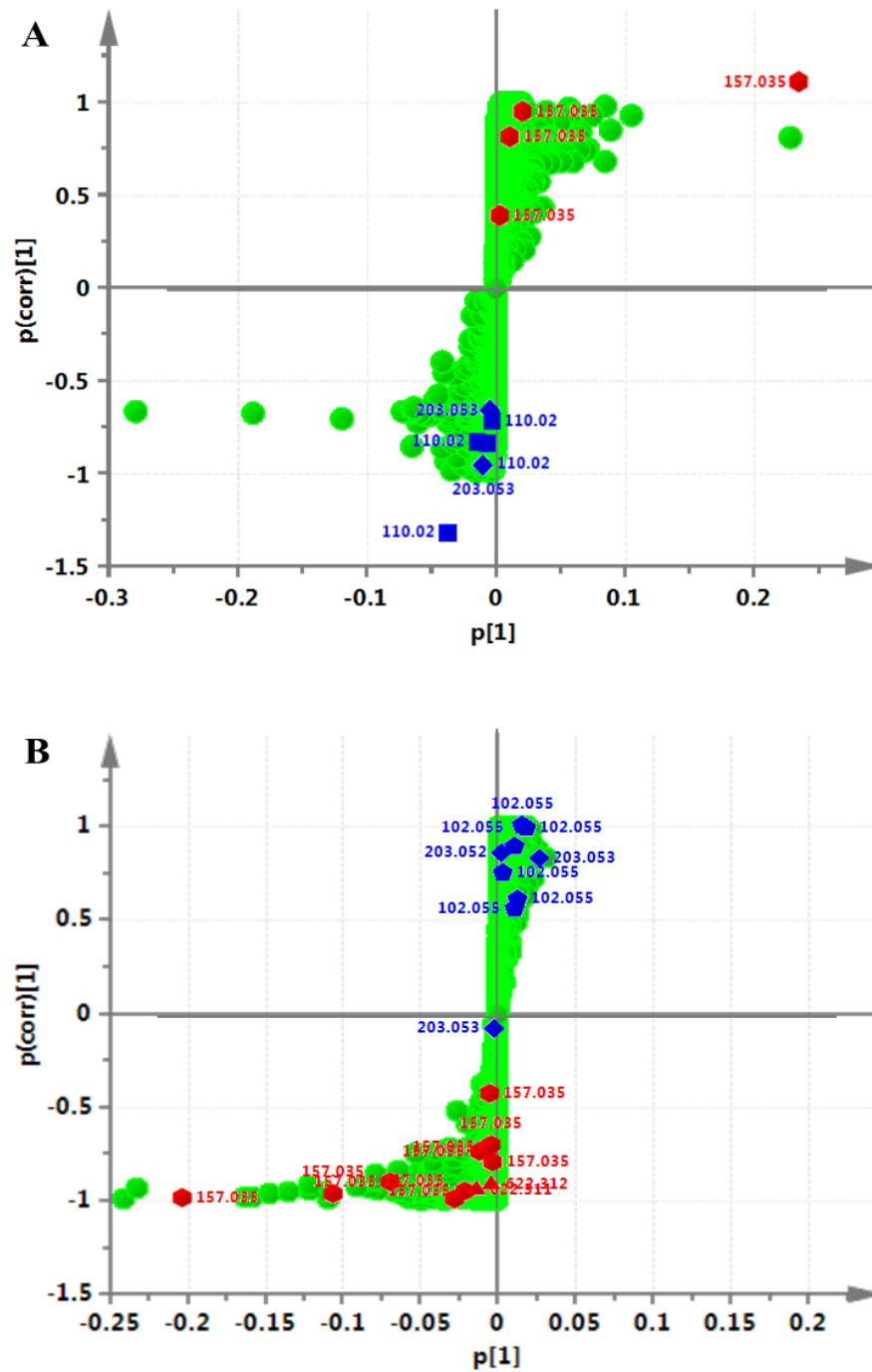


Figure 4.2 OPLSDA S plots of polar E1 treated groups. Panel A shows the S plot for E1-treated uterine tissues while panel B shows the S plot generated for those associated with the bath fluids. All metabolites detected are shown in green circles. Significantly regulated metabolites of the control groups are presented in blue shapes while those of the treated groups are presented in red shapes with their corresponding m/z values. ● = cAMP Metabolism; ▲= endocannabinoid metabolism; ▼= DAG/Lipid Metabolism; ■ = catecholamine synthesis; ◆ = MI Biosynthesis. Metabolites and corresponding m/z and pathways are listed in Table 4.1. n= 4 animals

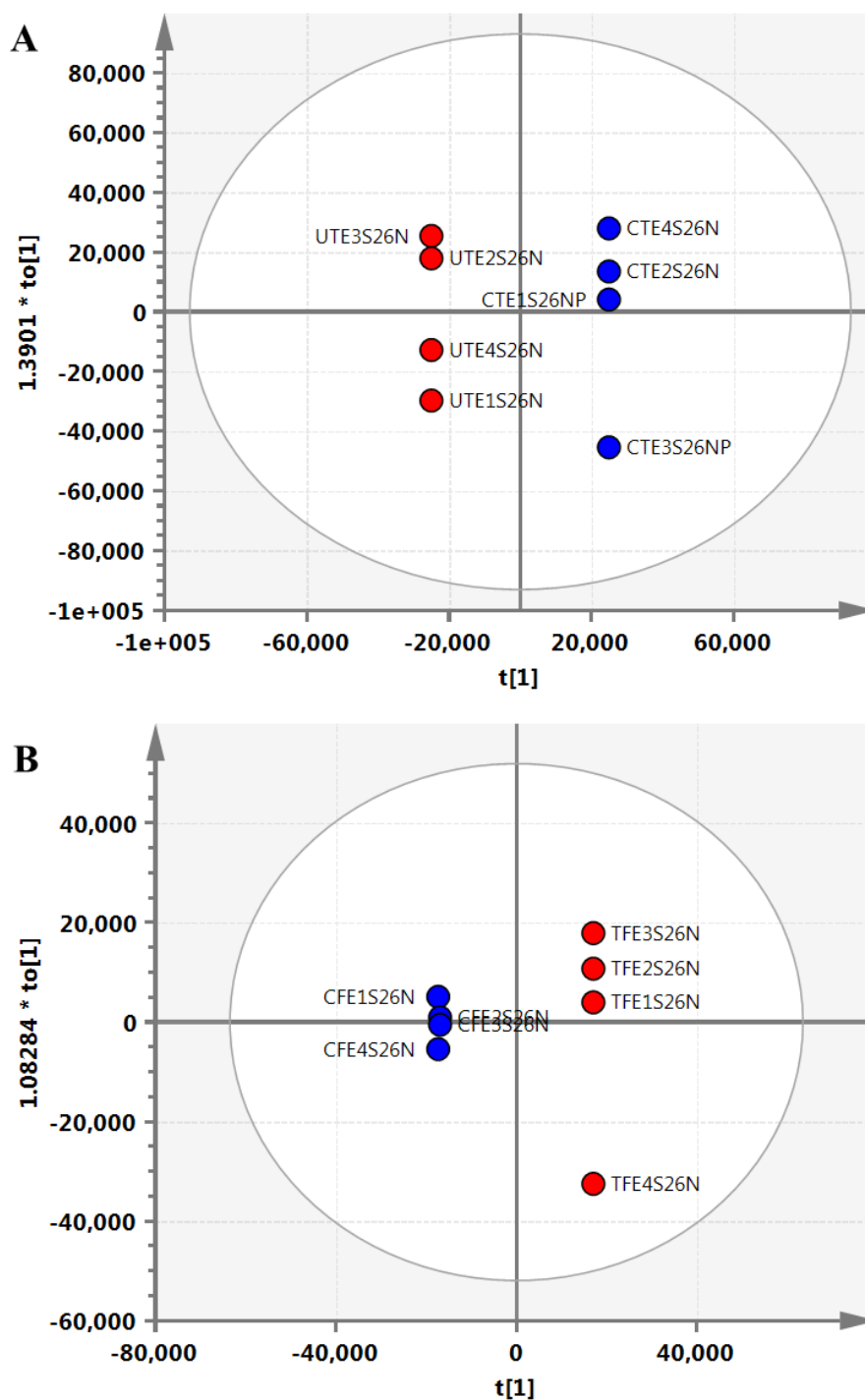


Figure 4.3 OPLSDA score plots (A and B) of non-polar E1 treated groups. Blue circles represent control groups while red circles represent treated groups. Panel A shows the score plot for E1-treated uterine tissues while panel B shows the score plot generated for those associated with the bath fluids.. n= 4 animals

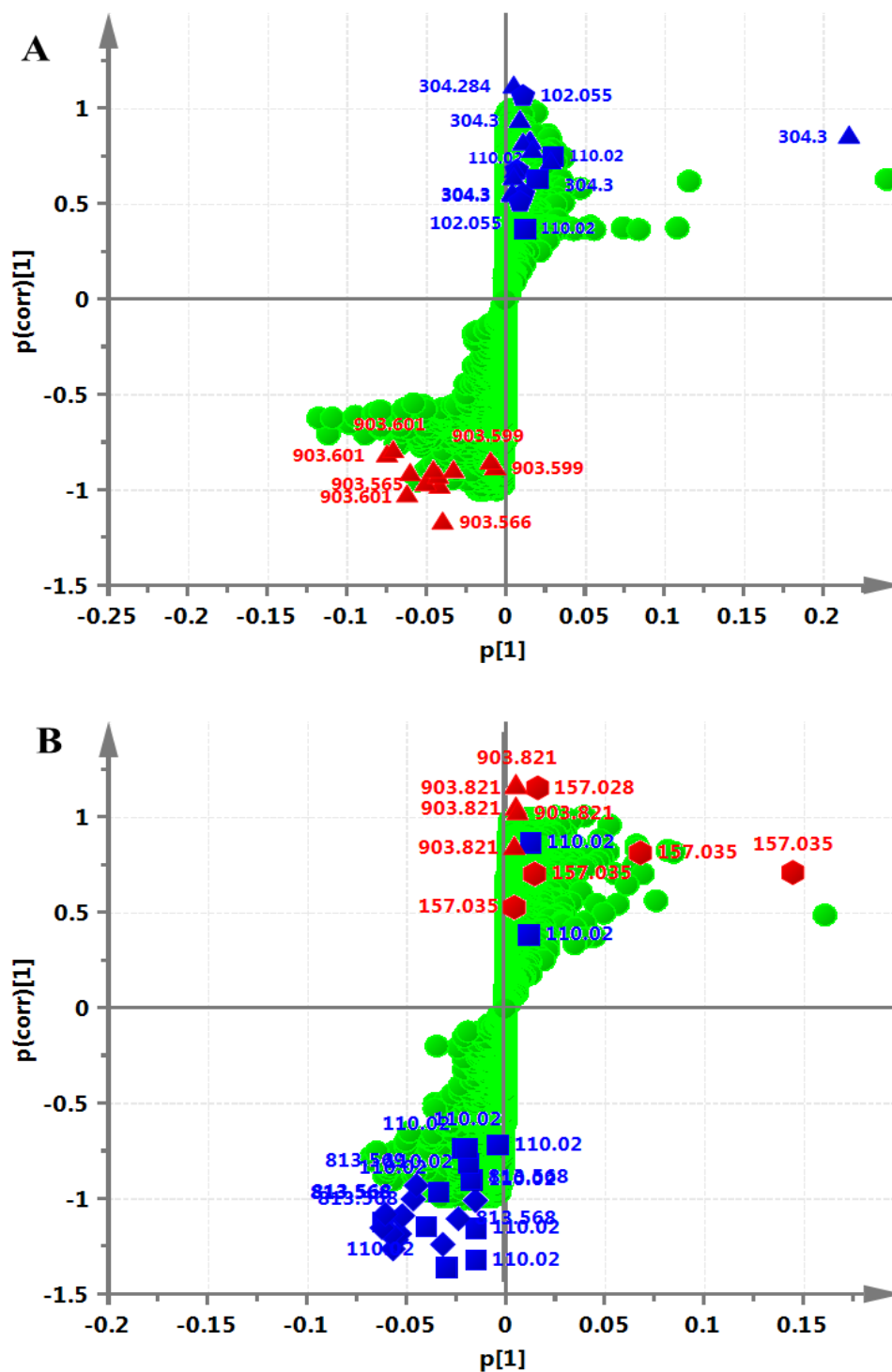


Figure 4.4 OPLSDA S plots of polar E1 treated groups. Panel A shows the S plot for E1-treated uterine tissues while panel B shows the S plot generated for those associated with the bath fluids. All metabolites detected are shown in green circles. Significantly regulated metabolites of the control groups are presented in blue shapes while those of the treated groups are presented in red shapes with their corresponding m/z values. ● = cAMP Metabolism; ▲ = endocannabinoid metabolism; ▼ = DAG/Lipid Metabolism; ■ = catecholamine synthesis; ◆ = MI Biosynthesis. Metabolites and corresponding m/z and pathways are listed in Table 4.1. n= 4 animals

Table 4.1 Pathways and Metabolites detected by HRFTMS on Treatment of the Uterus with E1

FC= Fold change; **GABA** = gamma aminobutyric acid; **CDPM**= cysteinyl dopamine; **cAMP**= cyclic adenosine monophosphate; **MI**= myoinositol; **DAG** = Diacylglycerol; **PS** = Phosphatidylserine; **PI**= Phosphatidylinositol; **PA** = Phosphatidic acid; **PE** = Phosphatidylethanolamine; **SM** = Sphingomyelin; **NA** = Nucleic Acid; **UDP-L-Ara4O** = Uridine 5'-diphospho -beta-L-threo-pentapyranos-4-ulose; **aa** =Amino acid; **Rt** = retention time; **m/z** = mass to charge ratio; **nd** = not detected

Pathway	Metabolome	Adduct	m/z	Rt	FC-Tissues	FC-Fluids
	unknown		182.9852	0.16	1.961	-1.764
	unknown		121.9744	1.21	nd	-2.3850
	unknown		142.0298	1.29	nd	160.666
aa metabolism	D-Proline	[M+H] ⁺	116.0707	1.32	-2.059	nd
NA metabolism	Betaine aldehyde	[M+CH ₃ OH+H] ⁺	134.1174	1.32	-3.639	nd
Dopamine synthesis	5-S-CDPM	[M+2Na] ²⁺	159.0308	1.36	7.794	432.165
	unknown		158.0385	1.37	288.700	nd
cAMP Metabolism	8-Azaadenosine	[M+2Na] ²⁺	157.0353	1.41	687.71	25042.330
aa metabolism	L-cysteine	[M+H] ⁺	162.0584	1.41	-2.796	nd
	unknown		128.5137	1.47	nd	58.253
	unknown		219.9724	1.51	nd	80.774
MI Biosynthesis	MI signalling	[M+Na] ⁺	203.0527	1.57	nd	-1.508
Cell/GABA signalling	Methylaminobutyrate	[M+H] ⁺	118.0863	1.60	-2.015	nd
Catecholamine Synthesis	Methylamino-alanine	[M+H] ⁺	119.0816	1.64	-102.2	nd
NA metabolism	UDP-L-Ara4O	[M+3H] ³⁺	179.0171	1.66	nd	2595.863

Table 4.1 Continued. Pathways and Metabolites detected by HRFTMS on Treatment of the Uterus with E1

Pathway	Metabolome	Adduct	m/z	Rt	FC-Tissues	FC-Fluids
	unknown		210.1159	1.77	8.393	nd
Gluconeogenesis	2-Deoxy-D-Ribose	[M+H] ⁺	135.0652	1.78	nd	24.415
aa Metabolism	L-Methionine	[M+H] ⁺	150.0585	1.78	2.453	nd
	unknown		159.0278	1.78	47.89	nd
Catecholamine Synthesis	DL-Tyrosine	[M+H] ⁺	182.0813	1.78	-2.415	nd
	unknown		138.0568	1.8	nd	26.674
TCA Cycle	4-Fluoro-L-threonine	[M+H] ⁺	138.0567	1.81	18.32	nd
Secondary metabolite	9,12-hexadecadienoic acid	[M+H+Na] ²⁺	138.1025	1.82	29.078	nd
Leucine Metabolism	L-Leucine	[M+H] ⁺	132.1019	1.83	-3.593	nd
	unknown		133.1051	1.83	-0.072	nd
Catecholamine Synthesis	Tyramine	[M+H-H ₂ O] ⁺	120.0808	2.29	-3.417	nd
Catecholamine Synthesis	D-Phenylalanine	[M+H] ⁺	166.0863	2.29	-3.259	nd
	unknown		167.0895	2.29	-3.305	nd
	unknown		156.9907	3.00	nd	825.775
Leucine Metabolism	L-isoleucyl--decanoyl-sn-Glycerol	[M+H] ⁺	229.1546	3.32	4.393	nd
TCA Cycle	Succinylacetone	[M+H] ⁺	159.0653	3.42	nd	30.613
Energy Production	7-methylguanosine phosphate	[M+H+Na] ²⁺	201.0392	3.60	nd	-23.722
Catecholamine Synthesis	Glycyl-Phenylalanine	[M+H-H ₂ O] ⁺	205.0971	3.62	-2.056	nd
Lipid Metabolism	Dodecatetraenoic acid	[M+H] ⁺	225.1484	5.71	nd	27.603

Table 4.1 continued. Pathways and Metabolites detected by HRFTMS on Treatment of the Uterus with E1

Pathway	Metabolome	Adduct	m/z	Rt	FC-Tissues	FC-Fluids
	unknown		309.1267	7.28	-5.973	nd
Cell/GABA signalling	2-Phenylbutyric acid	[M+CH ₃ OH+H] ⁺	197.1171	7.5	nd	2740.432
Endocannabinoid Signalling	Oleoyl ethanolamide (OEA)	[M+CH ₃ OH+H] ⁺	304.2999	19.65	nd	-8.596
	unknown		305.3031	19.65	nd	-8.791
Lipid Metabolism/Cell Signalling	SM(d18:1/16:0)	[M+H] ⁺	703.5757	23.81	991.92	nd
Lipid Metabolism/Cell Signalling	Cholesteryl ester	[M+CH ₃ OH+H] ⁺	703.6046	25.16	366.35	nd
Lipid Metabolism/Cell Signalling	Cholesteryl ester	[M+CH ₃ OH+H] ⁺	703.6032	25.51	302.12	nd
	unknown		625.2665	28.00	nd	1198.768
Lipid Metabolism/Cell Signalling	Cholesteryl ester	[M+CH ₃ OH+H] ⁺	703.6041	28.37	237.76	nd
Lipid Metabolism/Cell Signalling	SM(d18:2/24:0)	[M+H] ⁺	813.6849	29.11	nd	-3.684
Secondary Metabolite	Pheophorbide b	[M+CH ₃ OH+H] ⁺	639.2819	29.12	nd	2528.316
	unknown		640.2847	29.12	nd	2645.829
Secondary Metabolite	Pheophorbide a		593.2766	29.43	nd	869.783
Secondary Metabolite	Pheophorbide b	[M+CH ₃ OH+H] ⁺	639.2828	30.55	nd	1025.141
Secondary Metabolite	Pyropheophorbide a	[M+H] ⁺	535.2709	30.67	nd	737.261
	unknown		639.3186	30.67	nd	496.263
Secondary Metabolite	Pyropheophorbide a	[M+H] ⁺	535.2709	30.89	nd	97.818
Secondary Metabolite	Evasterioside C	[M+H-H ₂ O] ⁺	653.2995	31.59	nd	859.989
Secondary Metabolite	Evasterioside B	[M+H-H ₂ O] ⁺	667.3137	32.35	nd	18417.31
	unknown		919.5499	32.58	29.809	nd
MI Biosynthesis/signalling	PI(18:4/22:4)	[M+CH ₃ OH+H] ⁺	939.5609	32.65	1383.9	nd
MI Biosynthesis/signalling	PI(P-18:0/18:1)	[M+H-H ₂ O] ⁺	813.5684	32.67	nd	-107.481
	unknown		621.3078	33.01	nd	1937.269

Table 4.1 continued. Pathways and Metabolites detected by HRFTMS on Treatment of the Uterus with E1

Pathway	Metabolome	Adduct	m/z	Rt	FC-Tissues	FC-Fluids
Endo-Cannabinoid Signalling	PS(22:2/0:0)	[M+CH ₃ OH+H] ⁺	622.311	33.01	nd	903.833
	unknown		918.5824	33.12	1907.1	nd
Endo-cannabinoid Signaling	PE(22:4/22:6)	[M+CH ₃ OH+H] ⁺	903.5636	34.21	129.36	nd
	unknown		918.5828	34.74	66.987	nd
MI Biosynthesis/signalling	PI(20:4/22:6)[U]	[M+CH ₃ OH+H] ⁺	917.5797	35.58	26.046	nd
Endo-cannabinoid Signaling	PE(22:4/22:6)	[M+CH ₃ OH+H] ⁺	903.5645	36.22	165.16	nd
Endo-cannabinoid Signaling	PE(22:4/22:6)	[M+CH ₃ OH+H] ⁺	903.5646	36.67	162.94	nd
	unknown		969.5147	37.66	-882.2	nd
Cell signalling	5-Phenylvaleric acid	[M+H] ⁺	179.1065	39.65	-36.16	nd
Cell/GABA signalling	Aminohydroxybutyric acid	[M+H-H ₂ O] ⁺	102.0551	41.56	nd	-74.968

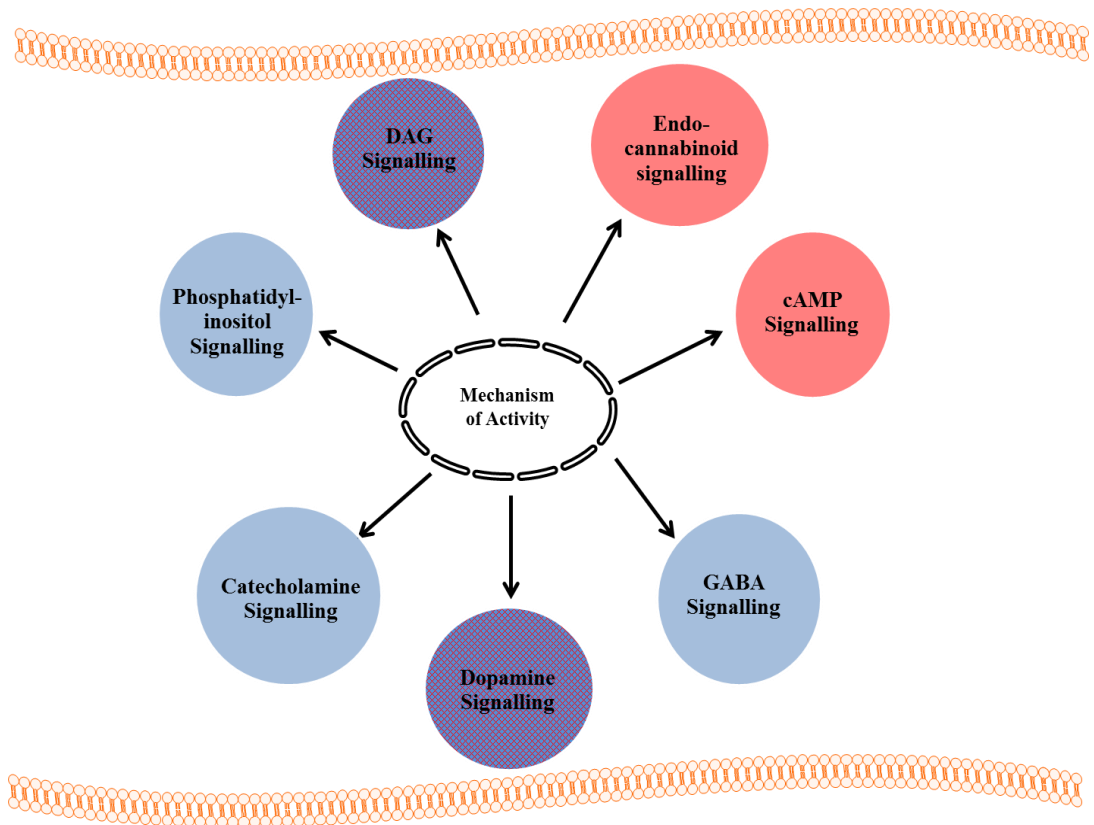


Figure 4.5 Predicted significantly regulated pathways of **E1** on uterine contraction. The red circles represent upregulated pathways and the blue circles represent downregulated pathways. The gradient blue and red circles represent possibly up- and downregulated pathways. **cAMP** = cyclic adenosine monophosphate; **DAG** = diacylglycerol; **GABA** = gamma aminobutyric acid.

4.7.2 HR-FTLCMS of F14

OPLSDA multivariate analysis of HR-FTLCMS experiments on **F14** showed distinct separations between the control and treated groups of both the polar (Fig. 4.6 A and B) and non-polar groups (Fig. 4.8 A and B). Several metabolites were detected via HR-FTLCMS analysis to have been perturbed on treatment of the uterine tissues with **F14** (Table 4.2). The spectra were dominated by amino acids and lipids. Some secondary plant metabolites were also identified such as pheophytin a, and triglycerides (Table 4.2). From the S plots generated, cAMP, DAG and dopamine signalling were upregulated while MI and endocannabinoid signalling were downregulated in the **F14** treated tissues (Fig. 4.7 and Fig. 4.9) These findings were similarly observed in the bath fluids but DAG was observed to be dominant (Fig. 4.7 B and 4.9 B). Additionally, an increase in cysteinyl dopamine, adenosine, nicotinic acid, phosphatidic acid, diacylglycerol, histidinol, glycerol phosphate and phosphatidyl serine were detected on analysis of **F14**-treated uterine tissues (Table 4.2). Betaine aldehyde, choline and phosphatidylcholine were however decreased within the tissues (Table 4.2). These results were similarly detected in the bath fluids (Table 4.2). Similar results were obtained with the polar and non-polar groups however it would appear that more metabolites were detected in the non-polar groups (Fig. 4.9 A and B). The IPA bioinformatic analysis showed lipid metabolism, cell signalling, nucleic and amino acid metabolism as high-level functional categories involved in **F14**-treatment of uterine tissues (Fig. 4.10 a and b). Canonical pathways generated by IPA bioinformatics showed myo-inositol, GABA, IP₃ and serotonin to have been upregulated and detected in the tissues (Fig. 4.10a) and CDP-DAG and

catecholamine synthesis to have been additionally upregulated in the bath fluids (Fig. 4.10b).

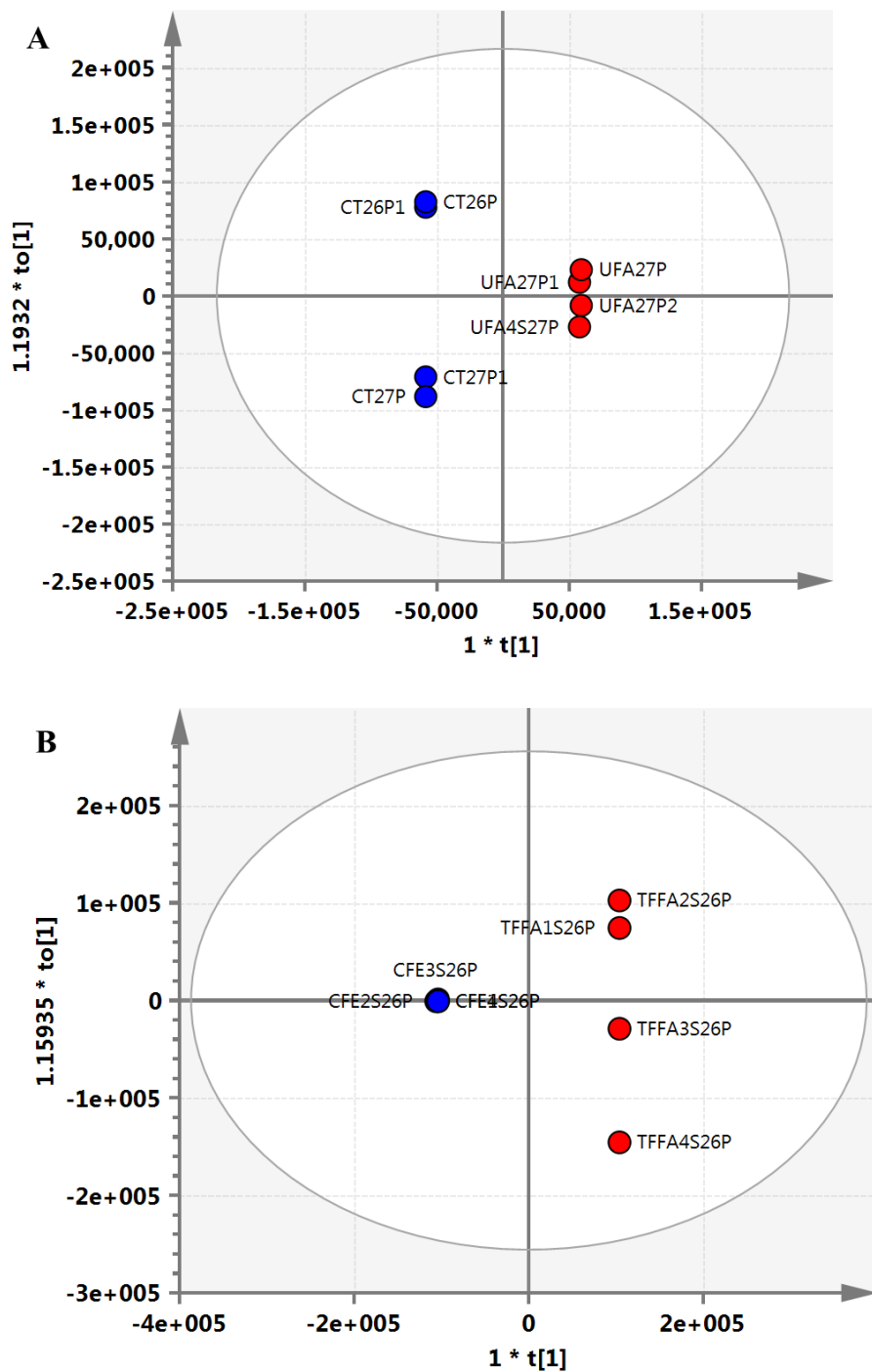


Figure 4.6 OPLSDA score plots (A and B) of polar **F14** treated groups. Blue circles represent control groups while red circles represent treated groups. Panel A shows the score plot for **F14**-treated uterine tissues while panel B shows the score plot generated for those associated with the bath fluids. n = 4 animals

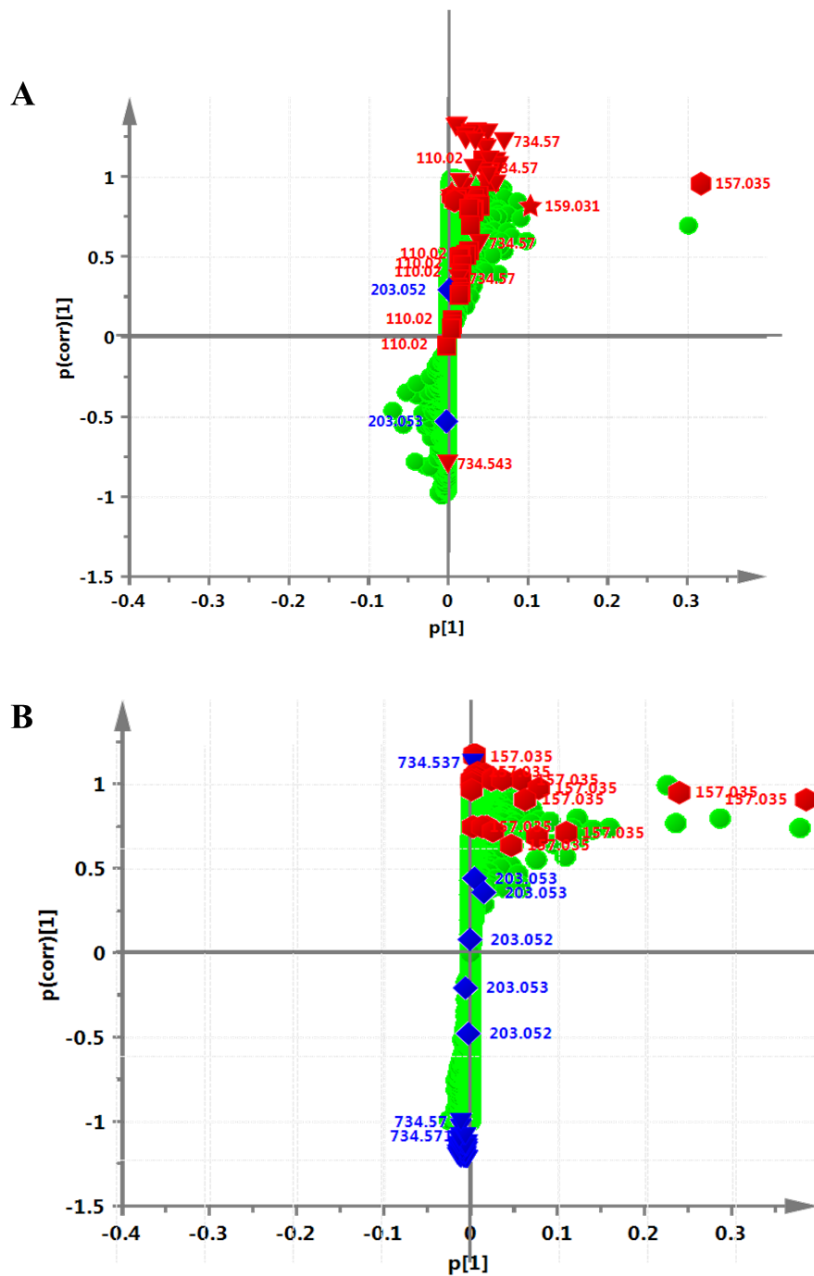


Figure 4.7 OPLSDA S plots of polar **F14** treated groups. Panel A shows the S plot for **F14**-treated uterine tissues while panel B shows the S plot generated for those associated with the bath fluids. All metabolites detected are shown in green circles. Significantly regulated metabolites of the control groups are presented in blue shapes while those of the treated groups are presented in red shapes with their corresponding m/z values. \bullet = cAMP signalling; \blacktriangle = endocannabinoid signalling; \blacktriangledown = DAG signalling; \blacksquare = catecholamine synthesis; \blacklozenge = MI biosynthesis/signalling; \blackstar = dopamine metabolism. n = 4 animals

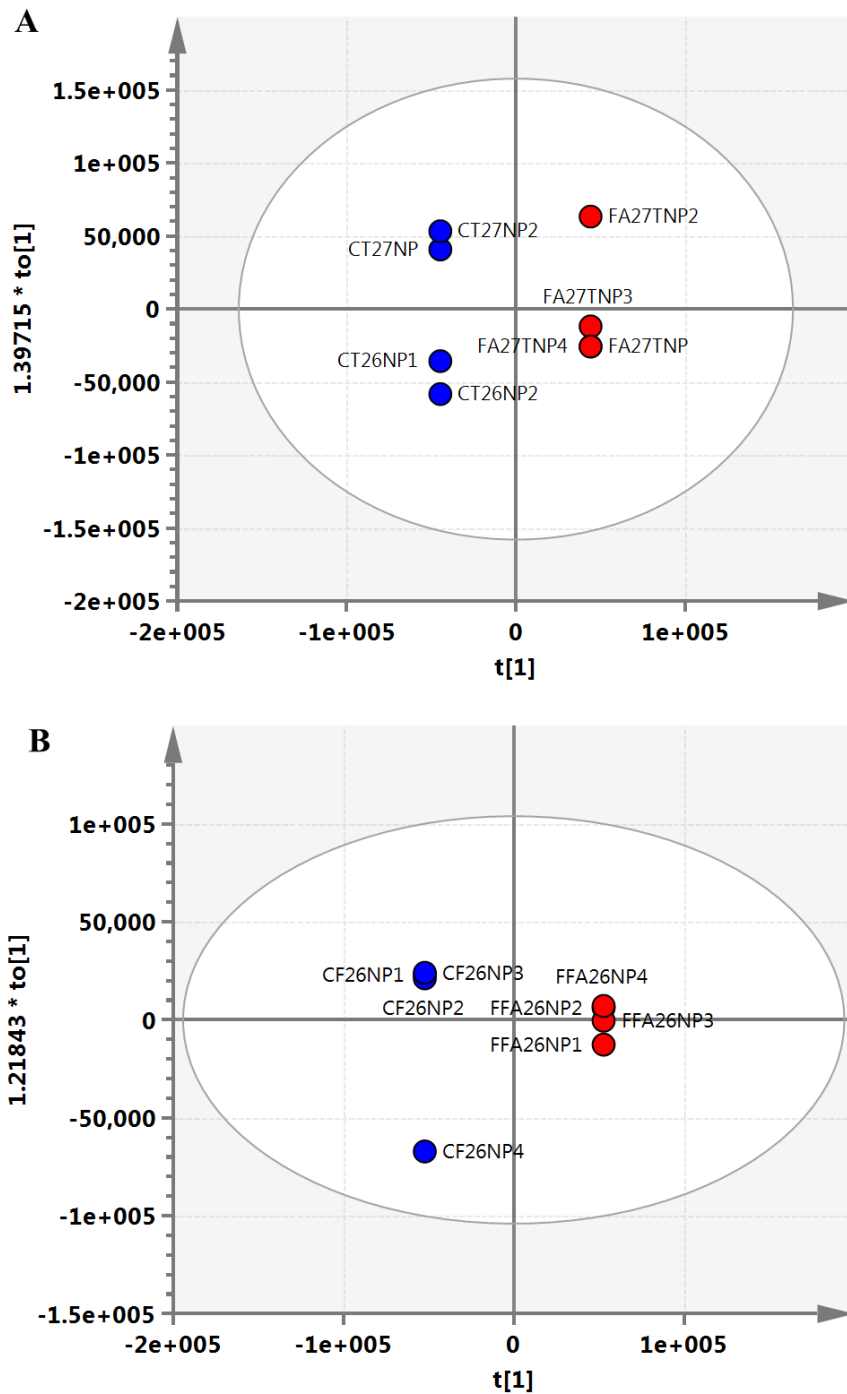


Figure 4.8 OPLSDA score plots (**A** and **B**) of non-polar **F14** treated groups. Blue circles represent control groups while red circles represent treated groups. Panel A shows the score plot for **F14**-treated uterine tissues while panel B shows the score plot generated for bath fluids in which the treated tissues were immersed. n = 4 animals

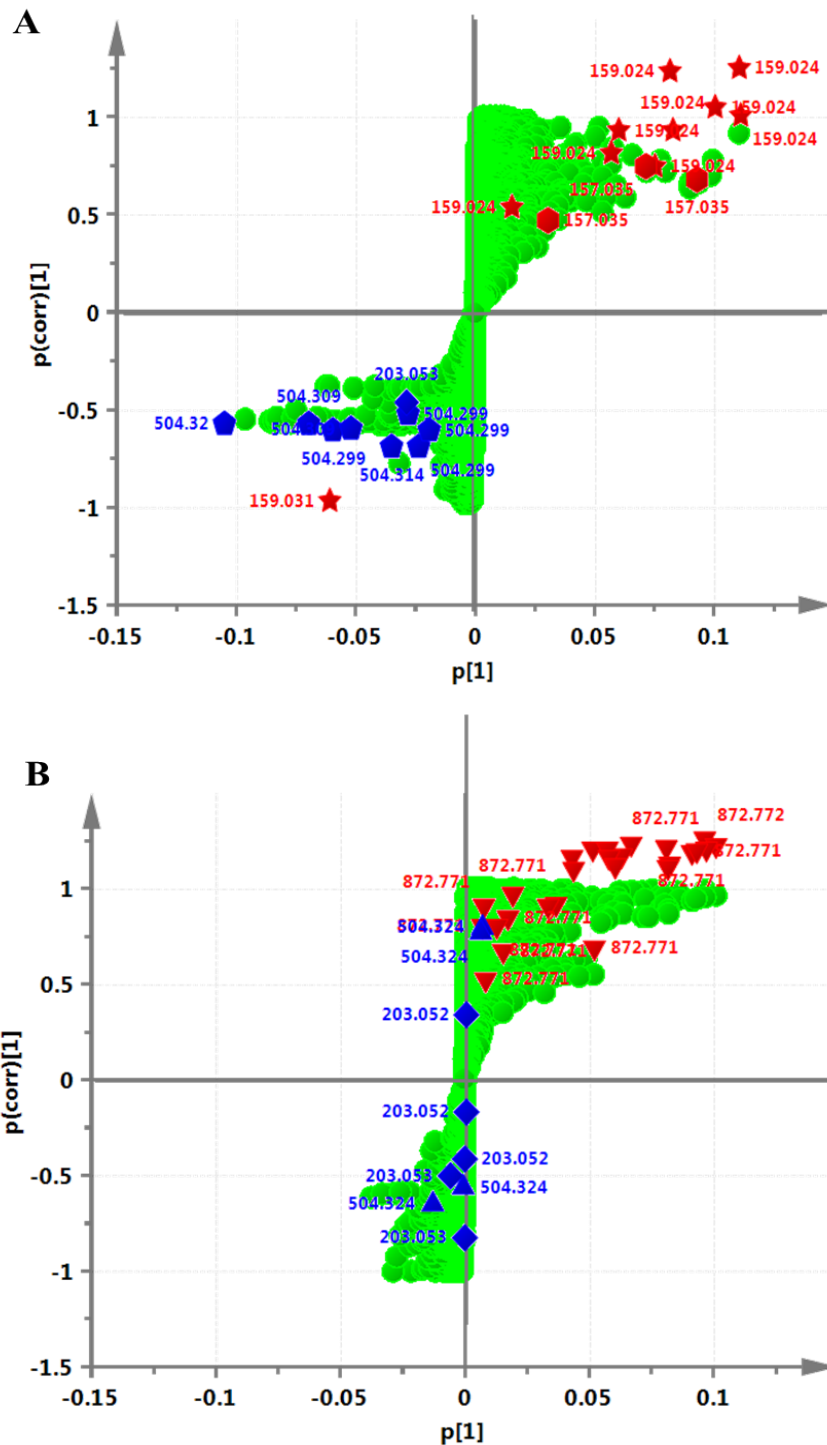


Figure 4.9 OPLSDA S plots of non-polar **F14** treated groups. Panel A = S plot for **F14**-treated uterine tissues while panel B shows S plot generated for those associated with the bath fluids. All metabolites detected are represented by the green circles. Metabolites that were significantly regulated in the control groups are presented in blue shapes while those of the treated groups are presented in red shapes with corresponding m/z values. \blacklozenge = cAMP signalling; \blacktriangle = endocannabinoid signalling; \blacktriangledown = DAG signalling; \blacksquare = catecholamine synthesis; \blacklozenge = aa metabolism; \blacklozenge = MI biosynthesis/signalling; \star = dopamine metabolism. n = 4 animals

Table 4.2 Pathways and Metabolites detected by HRFTMS on Effect of F14 on Uterine Contractility

FC= fold change; **GABA** = gamma aminobutyric acid; **CDPM**= cysteinyl dopamine; **cAMP**= cyclic adenosine monophosphate; **MI**= myoinositol; **DAG** = diacylglycerol; **PS** = phosphatidylserine; **PI**= phosphatidylinositol; **PA** = phosphatidic acid; **PE** = phosphatidylethanolamine; **SM** = sphingomyelin; **NA** = nucleic acid; **UDP-L-Ara4O** = uridine 5'-diphospho -beta-L-threo-pentapyranos-4-ulose; **TG**= triacylglycerol; **PC**= phosphatidylcholine; **aa** =Amino acid; **Rt** =Retention time; **m/z** = mass to charge ratio; **nd** = not detected

Pathway	Metabolome	Adduct	m/z	Rt	FC-Tissues	FC-Fluids
NA Metabolism	Betaine aldehyde	$[M+CH_3OH+H]^+$	134.1174	1.33	-2.9544	nd
	unknown		116.9771	1.33	nd	374.4446
Choline Metabolism	Choline	$[M+H]^+$	104.1071	1.37	1.9532	nd
Amino sugar and nucleotide sugar metabolism	UDP-L-Ara4O	$[M+3H]^{3+}$	179.0171	1.45	nd	54743.18
Serotonin biosynthesis	5-S-CDPM	$[M+2Na]^{2+}$	159.0307	1.46	133.6072	nd
cAMP Metabolism	8-Azaadenosine	$[M+2Na]^{2+}$	157.0353	1.48	5438.0291	1434.018
Gluconeogenesis and Glycolysis	3-Dehydro-L-gulonate	$[M+H-2H_2O]^+$	159.0305	1.69	nd	1637.055
GABA Signalling	2,3-dihydroxy-3-methylbutyric acid	$[M+Na]^+$	157.0473	1.77	nd	104186.8
	Dimethyl sulfoxide	$[M+ACN+Na]^+$	142.0298	1.77	nd	172.0802
	unknown		137.0018	1.77	-6.3764	
	unknown		141.9587	1.77	nd	681.5441

Table 4.2 continued. Pathways and Metabolites detected by HRFTMS on Effect of F14 on Uterine Contractility

Pathway	Metabolome	Adduct	m/z	Rt	FC-Tissues	FC-Fluids
Gluconeogenesis and Glycolysis	Methyl nicotinate	[M+H-H ₂ O] ⁺	120.0445	1.86	162.6332	nd
	unknown		158.9861	2.29	nd	2889.017
	unknown		159.0252	2.66	nd	1030.808
	unknown		158.9614	2.77	nd	735.8927
	unknown		156.9907	4.21	nd	1353.117
Catecholamine Biosynthesis	L-Tyrosine	[M+2H+Na] ³⁺	110.0201	4.55	nd	2.1354
	unknown		102.0339	8.97	nd	3.4336
	unknown		304.2999	19.62	nd	-314.307
Endocannabinoid Signalling	PC(O-14:0/2:0)	[M+H] ⁺	496.3401	21.41	-2.6099	nd
	unknown		332.3312	22.29	nd	-3133
MI Biosynthesis/Signalling	PA(17:1/22:2)	[M+ACN+H] ⁺	782.5700	28.83	3.8447	nd
DAG signalling	DAG(20:5/22:3/0:0)	[M+ACN+H] ⁺	734.5702	28.85	24.5178	nd
DAG signalling	DAG(20:5/22:3)	[M+ACN+H] ⁺	734.5701	29.69	5.4107	nd
DAG signalling	DAG(22:3/22:6/0:0)	[M+ACN+H] ⁺	760.5865	29.69	2.9383	nd
DAG synthesis	SM(d18:1/16:0)	[M+H] ⁺	703.5755	30.08	7.6167	nd

Table 4.2 continued. Pathways and Metabolites detected by HRFTMS on Effect of F14 on Uterine Contractility

Pathway	Metabolome	Adduct	m/z	Rt	FC-Tissues	FC-Fluids
DAG signalling	DAG(22:3/22:6/0:0)	[M+ACN+H] ⁺	760.5855	30.12	5.2189	-8.2758
Endocannabinoid signalling	PC(16:0/20:4)	[M+H] ⁺	782.5699	30.12	3.6909	nd
Pentose phosphate and Purine metabolism	L-Histidinol	[M+H-H ₂ O] ⁺	124.0869	30.34	3.7838	73.1934
DAG synthesis	TG(17:1/17:2/18:0)	[M+ACN+H] ⁺	898.7865	30.54	-51.2965	nd
DAG synthesis	TG(18:2/20:2/20:2)	[M+H-2H ₂ O] ⁺	899.7902	31.13	-35.4867	nd
Secondary Metabolite	Pheophytin a	[M+H] ⁺	871.5743	32.27	2366.645	nd
	unknown		900.7936	32.38	-52.3959	nd
DAG synthesis	TG(16:0/17:1)	[M+ACN+H] ⁺	872.7707	34.19	2.3563	16.5108
DAG synthesis	TG(18:2/20:2/20:2)	[M+H-2H ₂ O] ⁺	899.7898	34.28	nd	11.6516
DAG synthesis	TG(18:2/18:3/20:0)	[M+H-2H ₂ O] ⁺	873.7744	34.29	nd	8.9541
DAG synthesis	TG(17:1/17:2/18:0)	[M+ACN+H] ⁺	898.7865	34.29	nd	11.1758
DAG synthesis	TG(17:2/17:2/18:0)	[M+ACN+H] ⁺	896.7696	34.46	9.3149	nd
	unknown		914.7810	34.51	7.157	nd
	unknown		663.4551	34.62	nd	-45.7102

Table 4.2 continued. Pathways and Metabolites detected by HRFTMS on Effect of F14 on Uterine Contractility

Pathway	Metabolome	Adduct	m/z	Rt	FC-Tissues	FC-Fluids
MI Biosynthesis	PA(O-16:0/20:5)	[M+H] ⁺	681.4843	34.62	nd	-44.9568
	unknown		680.4811	34.62	nd	-66.4065
			685.4361	34.62	nd	-1265.54
MI Biosynthesis	PG(O-18:0/22:6)	[M+ACN+Na] ⁺	872.5779	35.97	16106.02	nd
	unknown		900.7931	36.10	-43.1712	nd
MI Biosynthesis	PA(O-16:0/20:5)	[M+H] ⁺	681.4836	36.56	553.4892	nd
Endocannabinoid Signalling	PS(O-18:0/18:3)	[M+H-2H ₂ O] ⁺	736.5261	36.58	1201.437	nd
			735.5226	36.63	838.1367	nd
	unknown		940.7818	36.69	nd	2067.523
	unknown		663.4542	36.70	409.0791	nd
Endocannabinoid Signalling	PS(P-16:0/12:0)	[M+H] ⁺	664.4574	36.70	769.8695	nd
Endocannabinoid Signalling	PS(22:1/22:6)	[M+H-H ₂ O] ⁺	872.5774	36.70	7348.963	nd
	unknown		1534.0203	36.70	2.9681	nd
	unknown		1344.9327	36.79	19320.42	nd
DAG synthesis	TG(17:2/17:2/18:1)	[M+ACN+H] ⁺	894.7551	37.11	10.2863	nd
Inositol Phosphate synthesis	PI(O-16:0/20:1)	[M+Na] ⁺	873.5806	37.14	1625.086	nd

Table 4.2 continued. Pathways and Metabolites detected by HRFTMS on Effect of F14 on Uterine Contractility

Pathway	Metabolome	Adduct	m/z	Rt	FC-Tissues	FC-Fluids
DAG synthesis	TG(18:2/18:3/20:0)	[M+H-2H ₂ O] ⁺	873.7746	37.15	nd	21.5008
	unknown		680.4809	37.30	63.2369	nd
	unknown		940.7813	37.41	nd	2067.523
	unknown		874.7779	37.51	nd	8.5346
	unknown		192.9764	37.77	nd	-39.6321
DAG synthesis	TG(17:1/17:2/18:0)	[M+ACN+H] ⁺	898.7869	37.79	nd	4073.58
			179.0608	37.93	nd	-148.5
DAG synthesis	TG(16:0/17:1)	[M+ACN+H] ⁺	872.7725	38.09	nd	61371.03
	unknown		182.9853	38.20	5.0843	nd
Secondary Metabolite	Pheophytin a	[M+H] ⁺	871.5757	38.32	nd	10662.89
	unknown		900.7936	39.04	nd	2.8927
	unknown		208.0392	39.28	nd	14.4786
	unknown		122.5471	44.58	2.8541	3.8539

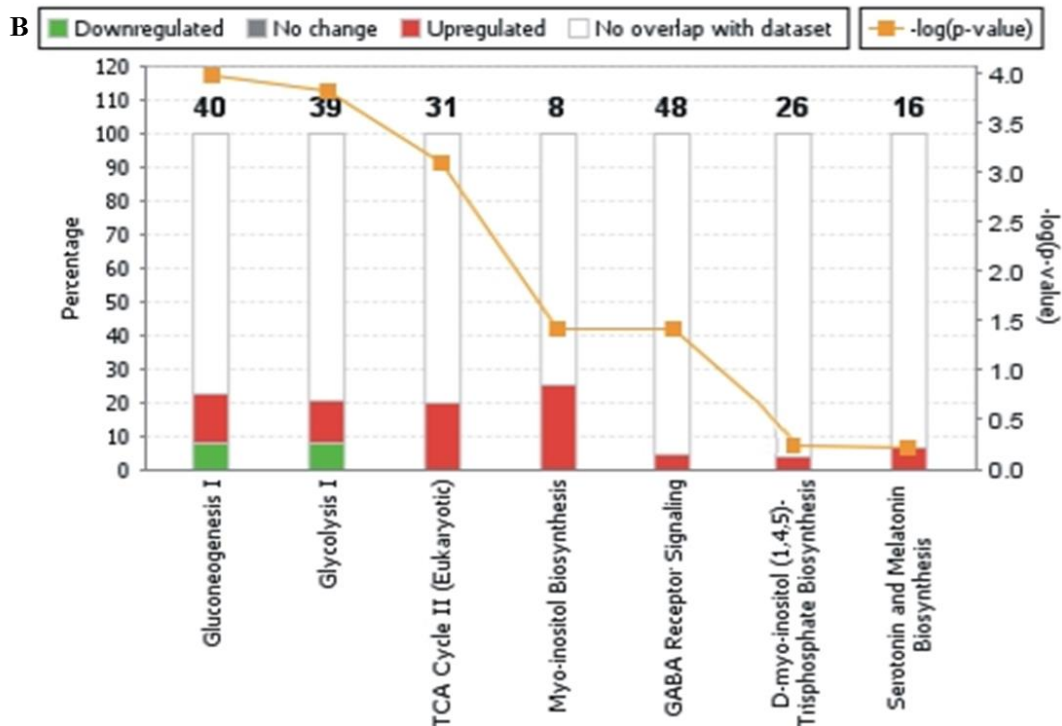
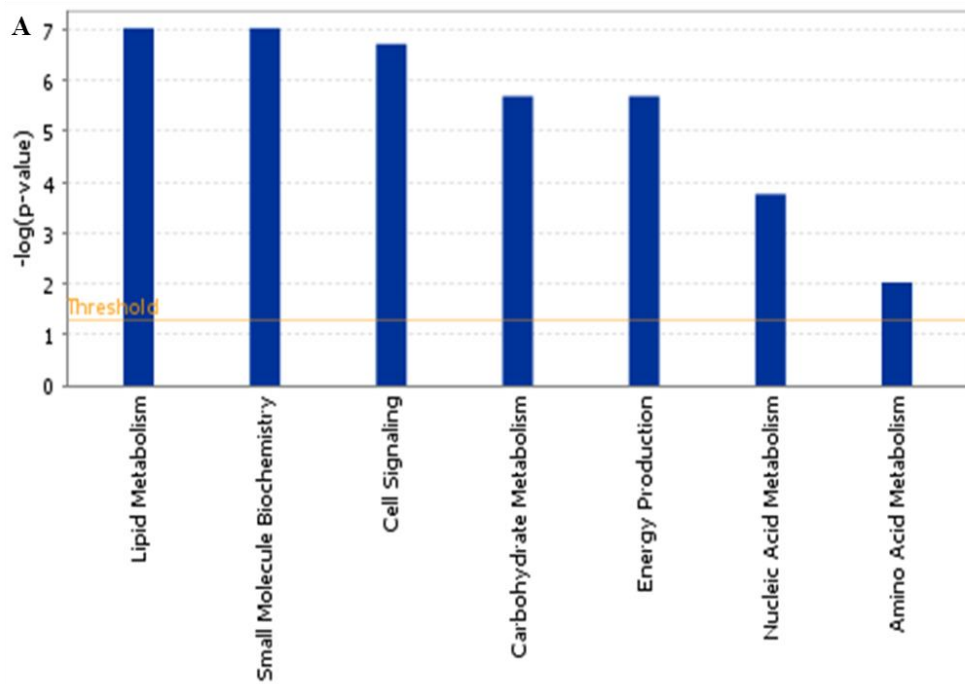


Figure 4.10a Bar charts displaying top functions (A) and canonical pathways (B) extracted by IPA software for **F14** treated uterine tissues. The high level functional categories associated with **F14**- treated tissues are displayed along the x-axis in A above while high level canonical pathways are shown in B. The y-axis displays the $-\log$ significance. Taller bars in A are more significant than the shorter bars and functions are listed from most significant to least. The orange horizontal line in A and B denotes the cut-off for significance (p-value of 0.05).

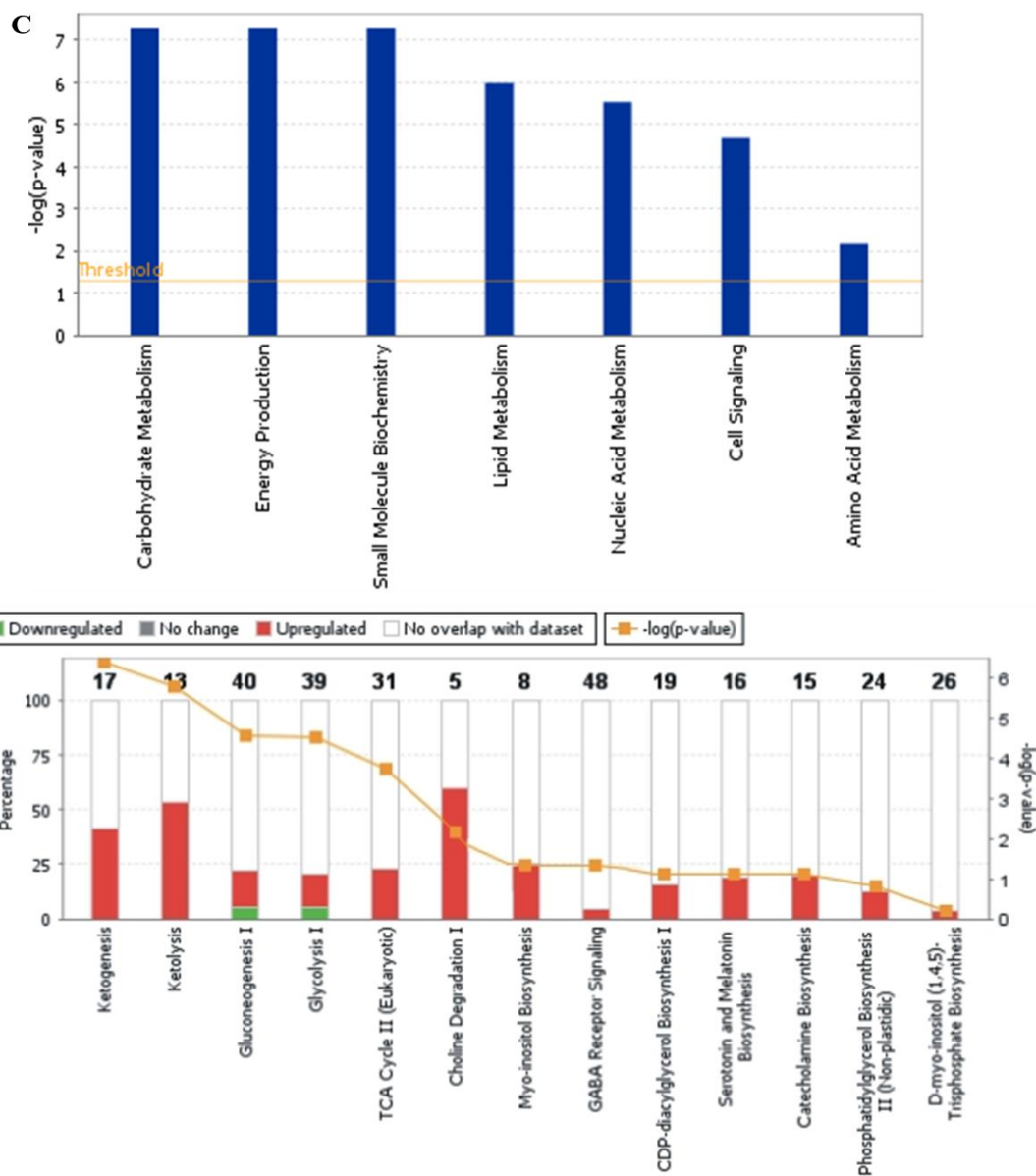


Figure 4.10b IPA-generated bar charts displaying top functions (C) and canonical pathways (D) for bath fluids in which the **F14** treated uterine tissues were immersed. Significantly associated functional categories of **F14**- treated fluids are displayed along the x-axis in C above while significant canonical pathways are shown in the x-axis of D above. The y-axis in C displays the $-\log$ significance while the left y-axis in D displays the percentage change. Taller bars in C are more significant than the shorter bars. Functions in C have been listed from most significant to least significant; the orange horizontal line in C and D denotes the cut-off for significance (p-value of 0.05).

4.7.3 HPLC-HRFTMS of F4-31

HR-FTLCMS experiments were analysed using the multivariate analysis and the bioinformatics software IPA. Multivariate OPLSDA plots showed distinct separations between the control (blue circles) and treated (red circles) groups (Fig. 4.11 and Fig. 4.13). Multivariate S-plots were also generated which represented every metabolite detected within the groups compared and also showed significantly regulated metabolites in the control (highlighted in blue) and treated groups (highlighted in red) (Fig. 4.12 and 4.14). The different pathways associated with the significantly regulated metabolites are presented in different shapes (Fig. 4.12 and Fig. 4.14). cAMP, catecholamine and endocannabinoid signalling were upregulated (Fig. 4.12 and Fig. 4.14) while MI signalling was downregulated (Fig. 4.12 and 4.14). Other detected metabolites are listed in Table 4.3. These metabolites ranged from amino acids to inositols, and phospholipids (Table 4.3). An increase in threonine and adenosine were observed in the tissues and fluids (Table 4.3) while a decrease in GABA, glutamate, tyrosine, methionine, threonine and phenylalanine were detected in the tissues (Table 4.3). Additional metabolites were detected in the fluids and these included an increase in nicotinic acid, UDP-L-Ara4O, cysteinyl dopamine, and ceramide while MI, sphingosine, phosphatidylinositol and phosphatidic acid were observed in the bath fluids to have been decreased (Table 4.3). Some secondary plant metabolites were also identified in the process, these included hexadecadienoic acid, furaneol-4-glucoside, pheophorbide a, pheophorbide b, pyropheophorbide-a and vinaginsenoside (Table 4.3). The IPA bioinformatics software showed lipid metabolism, small molecule chemistry, nucleic acid metabolism and cell signalling as top functions associated with F4-31 (Fig. 4.15a and

Fig. 4.15b). Canonical pathways generated by IPA displayed an upregulation of nicotinic acid, eicosanoids, CDP-DAG, 5-HT, GABA and MI pathways (Fig. 4.15a and b).

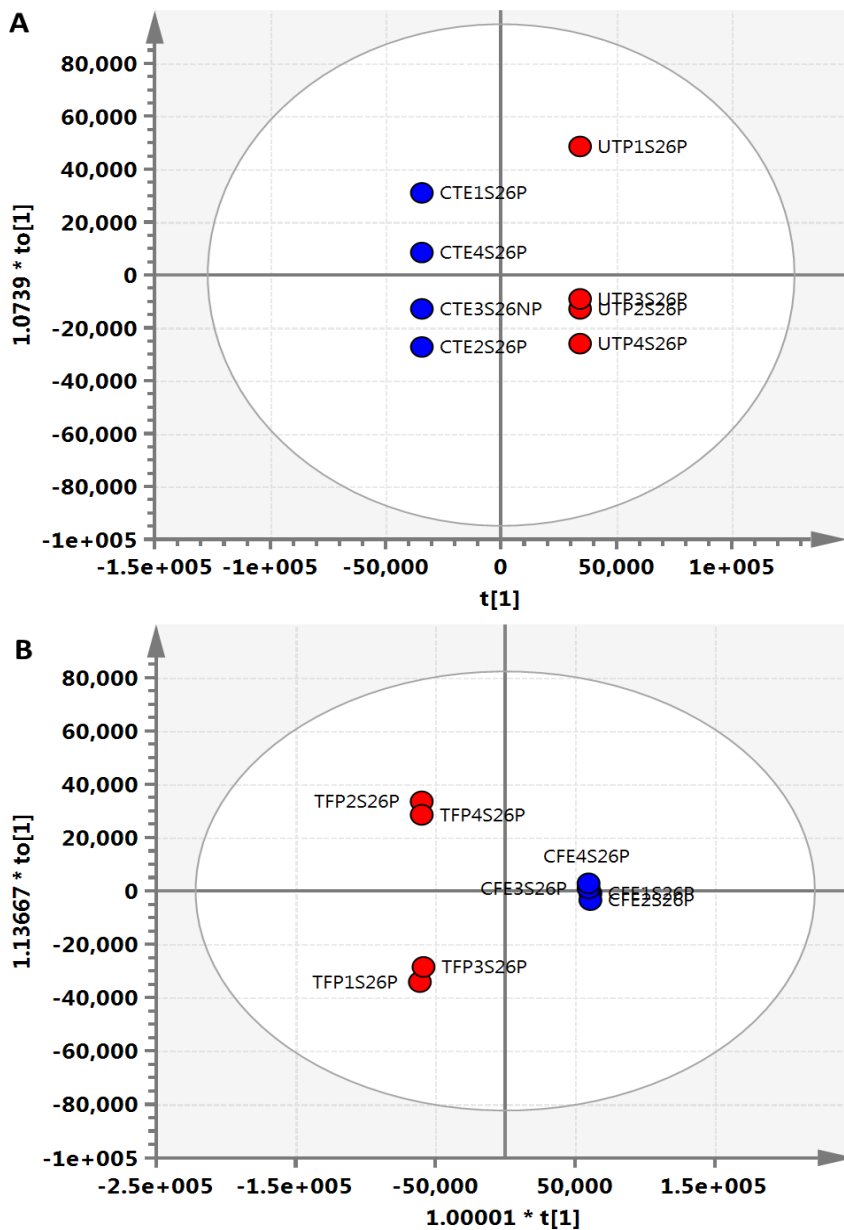


Figure 4.11 OPLSDA score plots (A and B) of polar **F4-31** treated groups. Blue circles represent control groups while red circles represent treated groups. Panel A shows the score plot for **F4-31** treated uterine tissues while panel B shows the score plot generated for those associated with the bath fluids. n = 4 animals

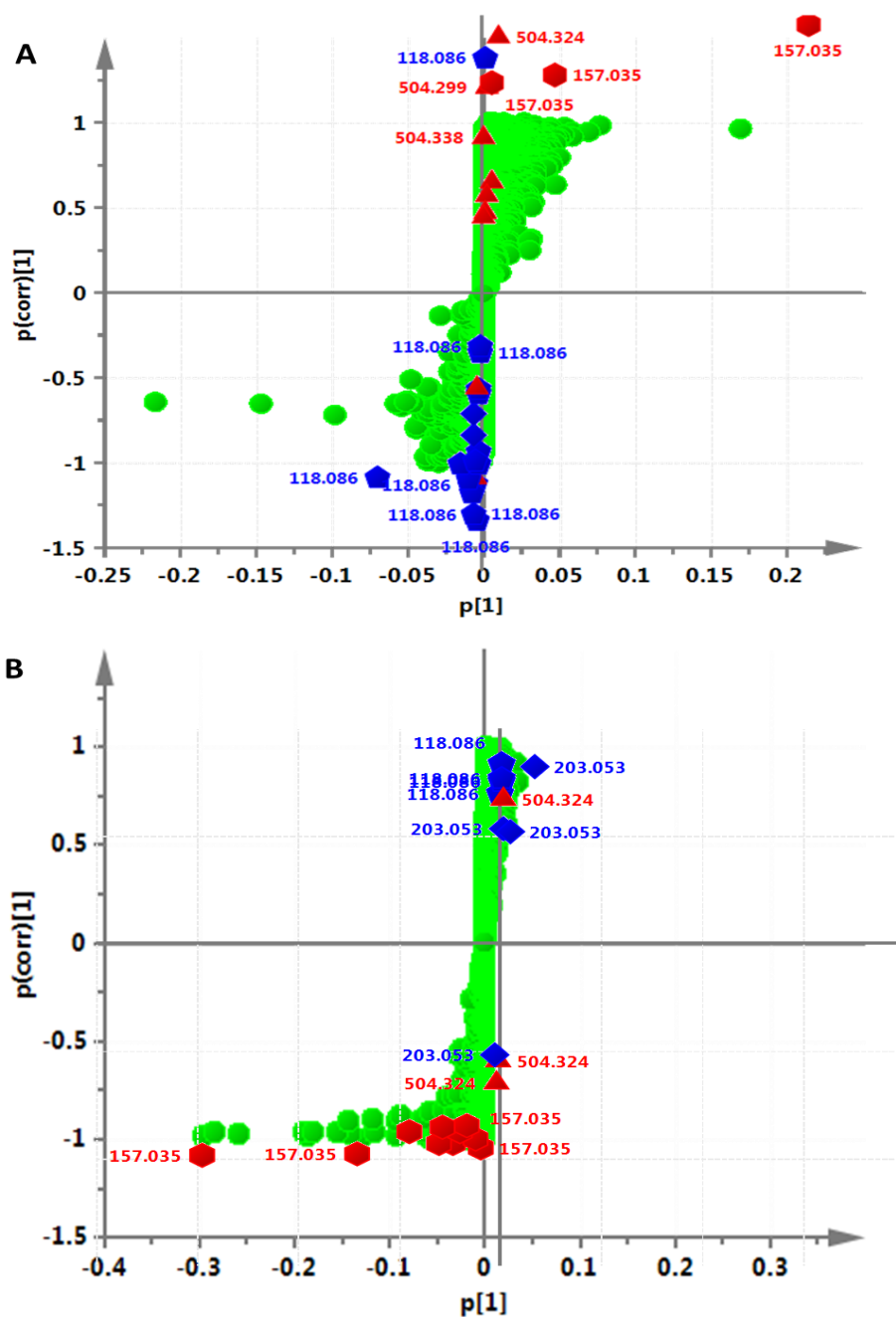


Figure 4.12 OPLSDA S plots of polar **F4-31** treated groups. Panel A shows the S plot for **F4-31**-treated uterine tissues while panel B shows the S plot generated for those associated with the bath fluids. All metabolites detected are shown in green circles. Significantly regulated metabolites of the control groups are presented in blue shapes while those of the treated groups are presented in red shapes with corresponding m/z values. \bullet = cAMP signalling; \blacktriangle = endocannabinoid signalling; \blacktriangledown = DAG signalling; \blacksquare = catecholamine synthesis; \blacklozenge = MI biosynthesis/signalling; \star = dopamine metabolism. n = 4 animals

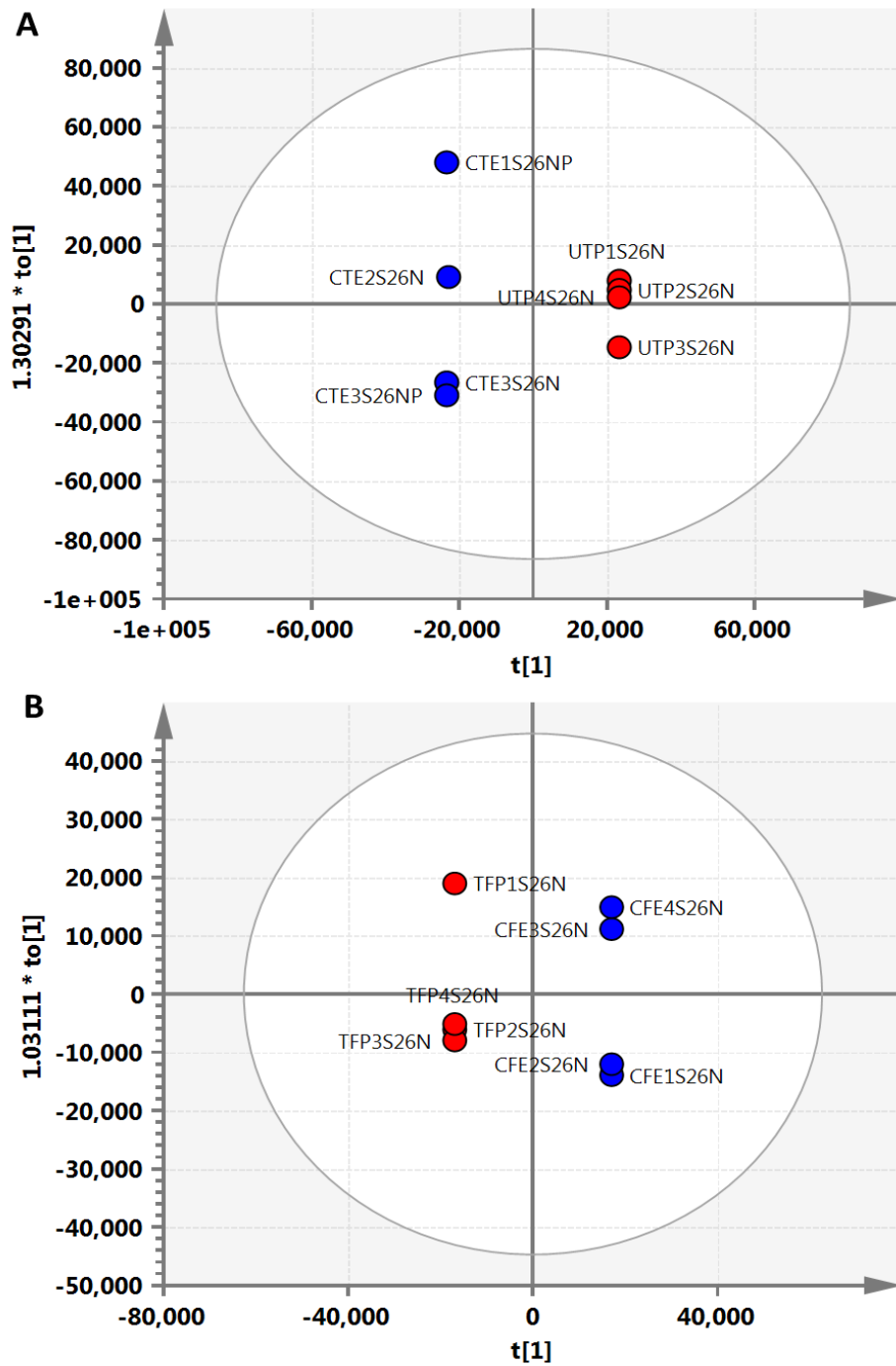


Figure 4.13 OPLSDA score plots (A and B) of non-polar **F4-31** treated groups. Blue circles represent control groups while red circles represent treated groups. Panel A shows the score plot for **F4-31** treated uterine tissues while panel B shows the score plot generated for bath fluids in which the treated tissues were immersed. n = 4 animals

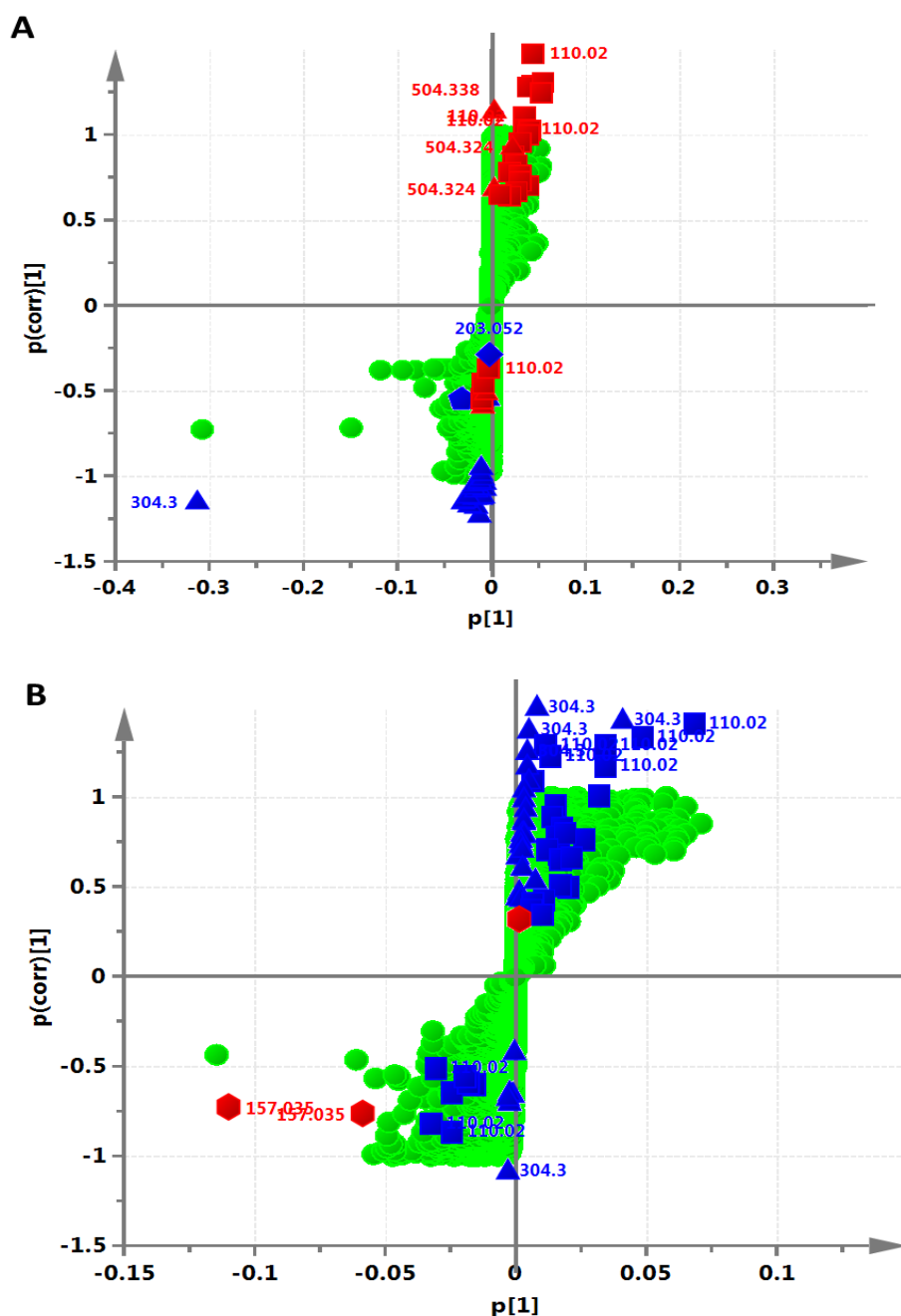


Figure 4.14 OPLSDA S plots of non-polar **F4-31** treated groups. Panel A shows the S plot for **F4-31**-treated uterine tissues while panel B shows the S plot generated for those associated with the bath fluids. All metabolites detected are shown in green circles. Significantly regulated metabolites of the control groups are presented in blue shapes while those of the treated groups are presented in red shapes with corresponding m/z values. ● = cAMP signalling; ▲ = endocannabinoid signalling; ▼ = DAG signalling; ■ = catecholamine synthesis; ◆ = MI biosynthesis/signalling; ★ = dopamine metabolism. n = 4 animals

Table 4.3 Pathways and Metabolites detected by HPLC-HRFTMS on Effect of F4-31 on Uterine Contractility

FC= fold change; GABA = gamma aminobutyric acid; CDPM= cysteinyl dopamine; cAMP= cyclic adenosine monophosphate; MI= myoinositol; DAG = diacylglycerol; PS = phosphatidylserine; PI= phosphatidylinositol; PA = phosphatidic acid; PE = phosphatidylethanolamine; SM = sphingomyelin; NA = nucleic acid; UDP-L-Ara4O = Uridine 5'-diphospho -beta-L-threo-pentapyranos-4-ulose; CER= ceramide; PC = phosphatidylcholine; Rt = retention time; m/z = mass to charge ratio; nd = not detected

Pathway	Metabolome	Adduct	m/z	Rt	FC-Tissues	FC-Fluids
Secondary Metabolite	Kaempferol 3,7-di-O-sulphate	[M+2H] ²⁺	223.9883	0.24	nd	2.4210221
	unknown		200.9725	0.99	-12.3654	nd
Gluconeogenesis	Glycolaldehyde	[M+H] ⁺	102.0549	1.04	nd	2.938571
Gluconeogenesis	Lactaldehyde	[M+ACN+H] ⁺	116.0707	1.32	-2.3778	nd
Lipid Metabolism/ Cell Signalling	Caproic acid	[M+NH ₄] ⁺	134.1174	1.32	-2.4534	nd
	Methyl nicotinate	[M+H] ⁺	138.0551	1.32	nd	27.117456
Sphingosine Metabolism	unknown		181.0126	1.33	nd	1018.1743
	GABA	[M+H] ⁺	118.0863	1.37	-1.9603	nd
GABA Receptor Signalling	GABA	[M+H] ⁺	118.0863	1.37	-1.9603	nd
aa and nucleotide sugar metabolism	UDP-L-Ara4O	[M+3H] ³⁺	179.0169	1.37	nd	37416.1
GABA Receptor Signalling	Glutamate	[M+H] ⁺	148.0606	1.37	-1.6216	nd
	unknown		121.9744	1.38	nd	-3.8105

Table 4.3 Continued. Pathways and Metabolites detected by HRFTMS on Effect of F4-31 on Uterine Contractility

Pathway	Metabolome	Adduct	m/z	Rt	FC-Tissues	FC-Fluids
	unknown		102.9988	1.39	nd	253.39797
aa metabolism	L-cysteine	[M+H] ⁺	162.0584	1.41	-2.9115	nd
cAMP synthesis	8-Azaadenosine	[M+2Na] ²⁺	157.0353	1.42	498.8266	1393.8791
	unknown		128.5137	1.48	nd	52.435029
	unknown		219.9725	1.49	nd	62.637065
Catecholamine Synthesis	L-Tyrosine	[M+2H+Na] ³⁺	110.0201	1.56	nd	-1.9912
MI Biosynthesis/Signalling	MI	[M+Na] ⁺	203.0526	1.68	nd	-1.498
Amino and nucleotide sugar metabolism	UDP-L-Ara4O	[M+3H] ³⁺	179.0171	1.72	nd	-4010.3903
	unknown		158.0384	1.77	nd	1317.5852
Catecholamine Synthesis/ Cell Signalling	CDPM	[M+2Na] ²⁺	159.0308	1.78	nd	315.95094
Phospholipid Synthesis	Methionine	[M+H] ⁺	150.0585	1.79	-2.3909	nd
Catecholamine Synthesis	L-Tyrosine	[M+H] ⁺	182.0813	1.79	-2.3937	nd
TCA Cycle	4-Fluoro-L-threonine	[M+H] ⁺	138.0567	1.81	14.975425	nd
Secondary Metabolite	9,12-hexadecadienoic acid	[M+H+Na] ²⁺	138.1025	1.82	23.444361	nd

Table 4.3 Continued. Pathways and Metabolites detected by HRFTMS on Effect of F4-31 on Uterine Contractility

Pathway	Metabolome	Adduct	m/z	Rt	FC-Tissues	FC-Fluids
Protein Synthesis/Cell Signalling	L-Leucine	[M+H] ⁺	132.1019	1.83	-3.5026	nd
	unknown		133.1051	1.84	-4.0141	nd
Protein Synthesis/Cell Signalling	Glycyl-Isoleucine	[M+H] ⁺	189.1234	1.84	-7.8112	nd
Secondary Metabolite	Furaneol 4-glucoside	[M+H+Na] ²⁺	157.0483	1.95	nd	20702.771
	unknown		158.0029	2.05	nd	305.1943
Catecholamine Metabolism	Tyramine	[M+H-H ₂ O] ⁺	120.0808	2.29	-3.4054	nd
Catecholamine Synthesis	D-Phenylalanine	[M+H] ⁺	166.0864	2.29	-3.2755	nd
aa metabolism	4-Guanidinobutanamide	[M+Na] ⁺	167.0895	2.30	-3.3457	nd
Glutamate Metabolism	L-isoleucyl-L-proline	[M+H] ⁺	229.1546	3.31	-5.5293	nd
	unknown		156.9907	3.35	nd	499.9947
Catecholamine Synthesis	L-Tyrosine	[M+2H+Na] ³⁺	110.0201	3.66	1.4794	nd
	unknown		197.1172	6.34	nd	-11.7734
	unknown		309.1267	7.26	-10.4258	nd

Table 4.3 Continued. Pathways and Metabolites detected by HRFTMS on Effect of F4-31 on Uterine Contractility

Pathway	Metabolome	Adduct	m/z	Rt	FC-Tissues	FC-Fluids
GABA Receptor Signalling	3-Phenylbutyric acid	[M+CH ₃ OH+H] ⁺	197.1172	7.56	nd	1283.3689
Endocannabinoid Metabolism	Oleoyl ethanolamide	[M+H-2H ₂ O] ⁺	304.2999	19.71	-24.8789	-1.2906
	unknown		305.3031	19.71	-26.3138	nd
	unknown		306.3061	19.71	-28.7571	nd
	unknown		332.3312	22.54	1.6238737	-1.5618
	unknown		597.2714	26.27	nd	6970.0291
Secondary metabolite	Pheophorbide a	[M+CH ₃ OH+H] ⁺	625.3027	27.36	nd	464.1722
	unknown		625.2664	28.09	nd	1010.5702
MI Biosynthesis/Signalling	PC(16:0/18:1)	[M+H] ⁺	760.5859	29.12	nd	2.837
MI Biosynthesis/Signalling	PC(16:0/20:1)	[M+H] ⁺	788.6172	29.12	nd	-7.4079
Sphingosine Metabolism	SM(d18:1/24:1)	[M+H] ⁺	813.6849	29.12	nd	-9.2151
	unknown		814.6884	29.12	nd	-9.4795
	unknown		640.2849	29.18	nd	3050.0209
Secondary Metabolite	Pheophorbide a	[M+H] ⁺	593.2765	29.36	nd	1271.3816
	unknown		1069.5331	30.81	nd	6.7649
	unknown		1070.5363	30.81	nd	6.6622

Table 4.3 Continued. Pathways and Metabolites detected by HRFTMS on Effect of F4-31 on Uterine Contractility

Pathway	Metabolome	Adduct	m/z	Rt	FC-Tissues	FC-Fluids
Secondary Metabolites	Pyropheophorbide a	[M+H] ⁺	535.2707	30.81	69.6248	2868.9572
	unknown		536.2736	30.81	nd	3416.0911
	unknown		537.2767	30.81	nd	3154.8818
Secondary Metabolites	Pyropheophorbide a	[M+H] ⁺	535.2709	30.92	nd	133.3165
Sphingosine Metabolism	Cer d18:1/22:0)	[M+3H] ³⁺	705.7237	31.73	nd	51.6002
MI Biosynthesis/Signalling	PA(22:0/22:2)	[M+H] ⁺	813.6388	32.58	nd	-69.4274
	unknown		814.6423	32.59	nd	-61.7095
Sphingosine Metabolism	Cer(d18:1/20:0)	[M+2H+Na] ³⁺	727.7058	32.59	nd	57.4416
Lipid Metabolism/ Cell Signalling	TG(16:0/16:0/16:0)	[M+ACN+H] ⁺	848.7709	33.41	nd	2.5155
MI Biosynthesis/Signalling	PI(O-16:0/20:2)	[M+H-2H ₂ O] ⁺	813.5683	34.29	nd	-120.9246
MI Biosynthesis/Signalling	Glycerophosphocholine	[M+H] ⁺	814.5718	35.93	nd	-152.0414
MI Biosynthesis/Signalling	PA(22:0/22:2)	[M+H] ⁺	813.6391	36.06	nd	-109.6111
	unknown		706.7274	36.64	nd	40.1577
Secondary Metabolite	Vinaginsenoside R3	[M+H] ⁺	931.5591	37.66	-88.9506	nd
Secondary Metabolite	Vinaginsenoside R4	[M+K] ⁺	969.5147	37.66	-1685.5944	nd

Table 4.3 Continued. Pathways and Metabolites detected by HRFTMS on Effect of F4-31 on Uterine Contractility

Pathway	Metabolome	Adduct	m/z	Rt	FC-Tissues	FC-Fluids
Secondary Metabolite	Vinaginsenoside R4	[M+K] ⁺	969.5147	37.66	-1685.5944	nd
	unknown		190.9795	37.88	3.0024	nd
	unknown		241.9845	37.98	-14.0817	nd
	unknown		241.9849	38.84	-75.5218	nd
Tyrosinase Inhibitor	Nonanedioic acid	[M+H-H ₂ O] ⁺	171.1021	40.16	nd	-4.0766
	unknown		200.9724	43.77	nd	8.0858
	unknown		182.9852	44.09	nd	1.3304

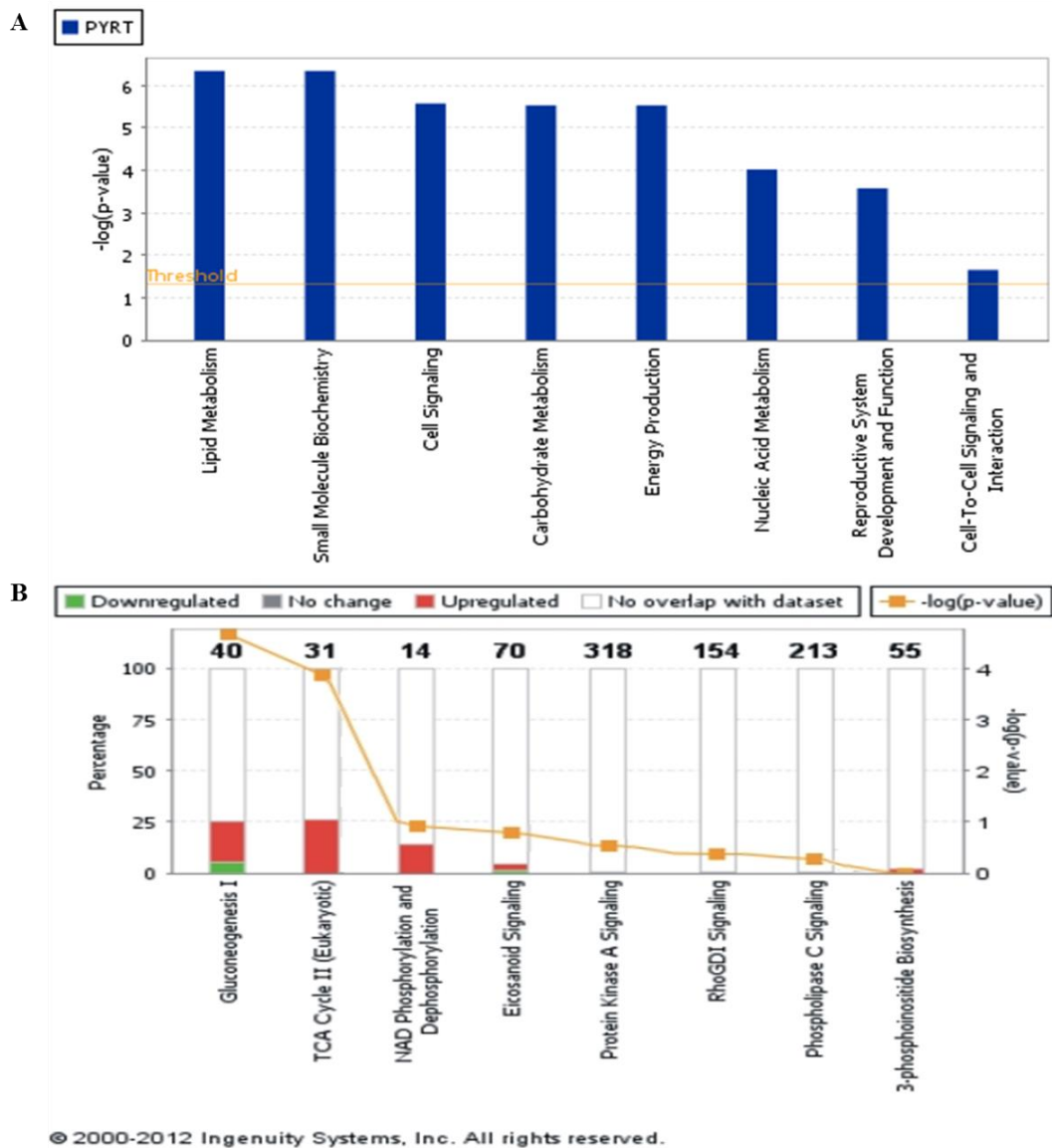


Figure 4.15a Bar charts displaying top functions (A) and canonical pathways (B) extracted by IPA software for **F4-31** treated uterine tissues. The high level functional categories associated with **F4-31**- treated tissues are displayed along the x-axis in A above while high level canonical pathways are shown in B above. The y-axis displays the $-\log$ significance. Taller bars in A are more significant than the shorter bars. Functions are listed from most significant to least and the orange horizontal line in A and B denotes the cutoff for significance (p-value of 0.05).

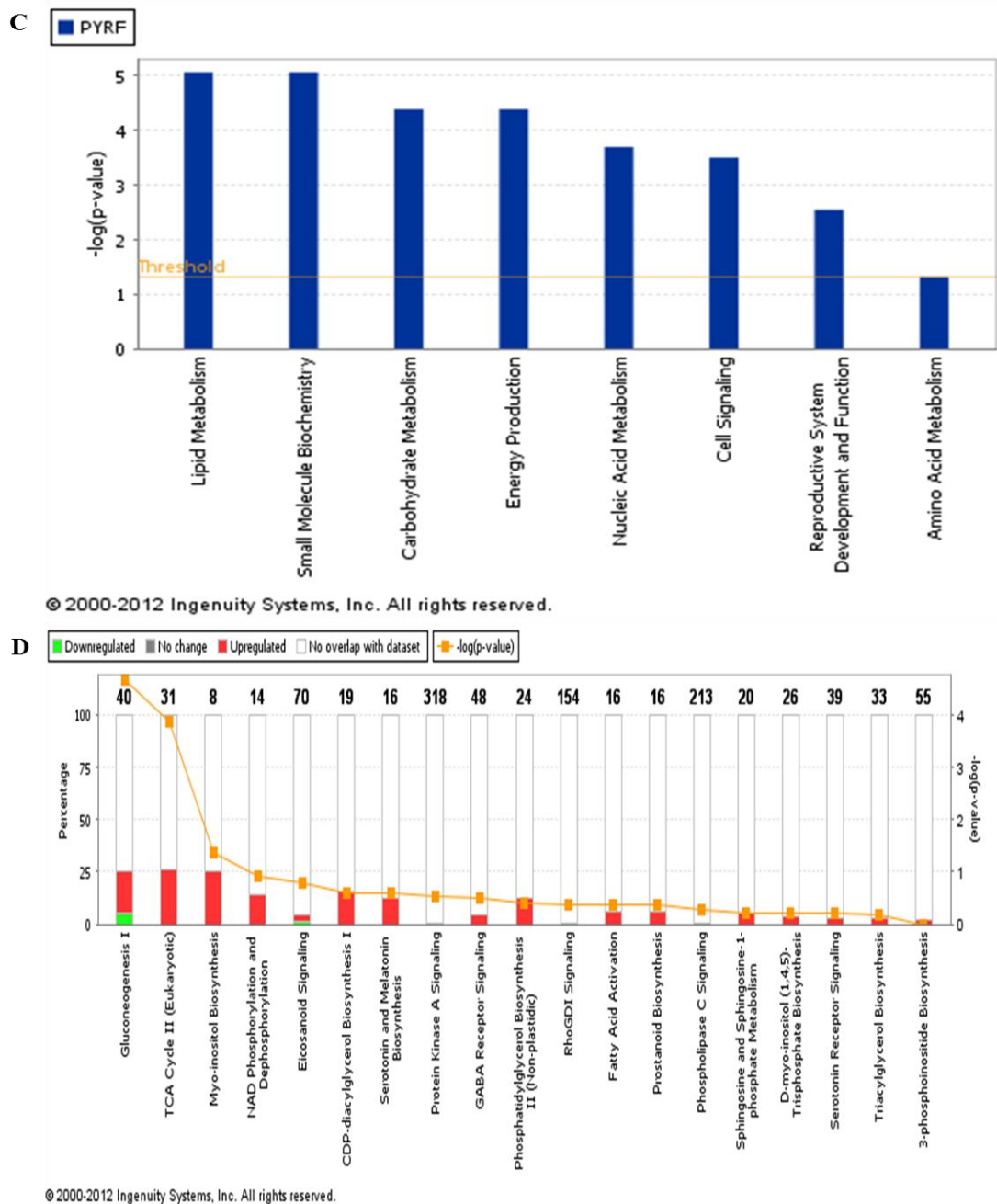


Figure 4.15b IPA-generated bar charts displaying top functions (C) and canonical pathways (D) for bath fluids in which the **F14** treated uterine tissues were immersed. Significantly associated functional categories of **F14**- treated fluids are displayed along the x axis in C above while significant canonical pathways are shown in the x-axis of D above. The y-axis in C displays the $-\log$ significance while the left y-axis in D displays the percentage change. Taller bars in C are more significant than the shorter bars. Functions in C have been listed from most significant to least significant; the orange horizontal line in C and D denotes the cutoff for significance (p-value of 0.05).

4.7.4. HPLC-HRFTMS of F6.17

HRFTMS experiments were analysed using the multivariate analysis and the bioinformatics software IPA. Multivariate OPLSDA plots showed distinct separations between the control (blue circles) and treated (red circles) groups (Fig. 4.16 and Fig. 4.18). Multivariate S-plots were also generated which represented every metabolite detected within the groups compared. Significantly regulated metabolites and pathways were also displayed as blue shapes in the control and red shapes in the treated (Fig. 4.17 and Fig. 4.19). cAMP, endocannabinoid and catecholamine signalling were upregulated while MI, and endocannabinoids signalling were downregulated control group was downregulated (Fig. 4.17 and Fig. 4.19). Other detected metabolites are listed in Table 4.4. These metabolites ranged from amino acids to lipids (Table 4.4). An increase in adenosine, cysteinyl dopamine, phosphatidyl ethanolamine, glycerolphosphate, phosphatidyl serine, triglyceride were observed in the tissues and fluids while a decrease in MI, noradrenaline, tyrosine, and phosphatidylinositol were observed (Table 4.4). Some secondary plant metabolites were also identified in the process, these included herbetene, pheophorbide a, and pyropheophorbide a (Table 4.4). The IPA bioinformatic software showed cell signalling, lipid metabolism, small molecule biochemistry, nucleic and amino acid metabolism as high level functions associated with **F6.17** while myoinositol signalling CDP-DAG and serotonin pathways were observed to be associated with the effect of **F6.17** on uterine contractility (Fig. 4.20 a and b).

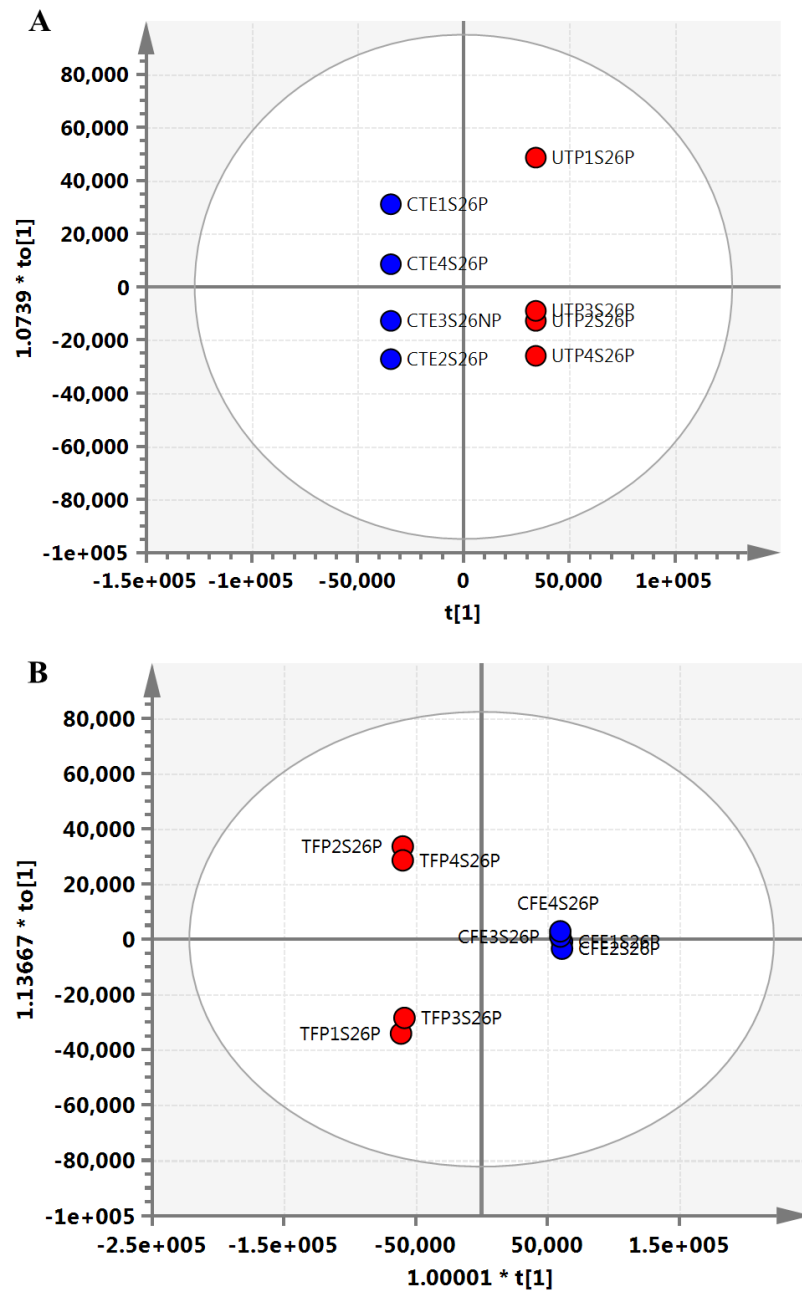


Figure 4.16 OPLSDA score plots (A and B) of polar **F6.17** treated groups. Blue circles represent control groups while red circles represent treated groups. Panel A shows the score plot for **F6.17** treated uterine tissues while panel B shows the score plot generated for those associated with the bath fluids. n = 4 animals

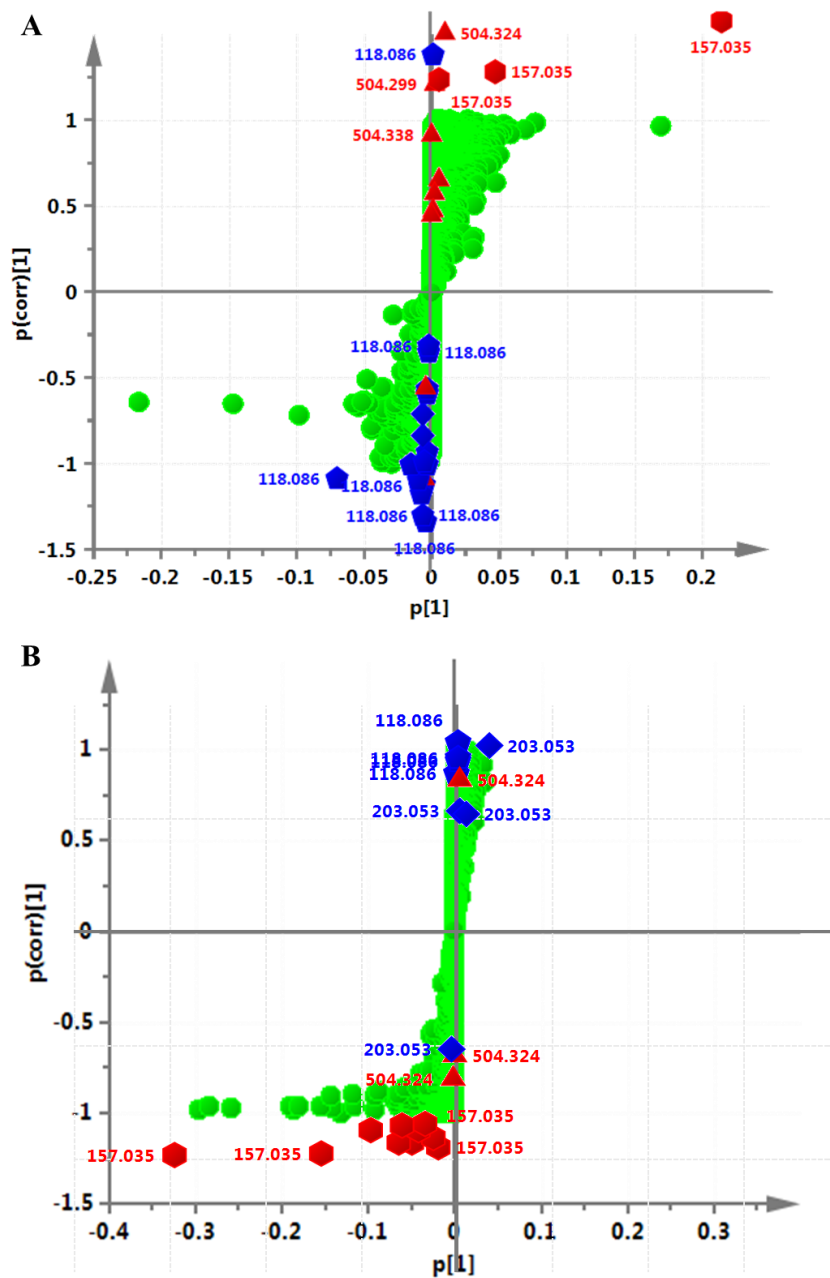


Figure 4.17 OPLSDA S plots of polar **F6.17** treated groups. Panel A shows the S plot for **F6.17**-treated uterine tissues while panel B shows the S plot generated for those associated with the bath fluids. The green circles represent all metabolites detected in the analysis. Significantly regulated metabolites of the control groups are presented in blue shapes while those of the treated groups are presented in red shapes with their corresponding m/z values. \blacklozenge = cAMP signalling; \blacktriangle = endocannabinoid signalling; \blacklozenge = aa signalling; \blacktriangledown = DAG signalling; \blacksquare = catecholamine synthesis; \blacklozenge = MI biosynthesis/signalling. n = 4 animals

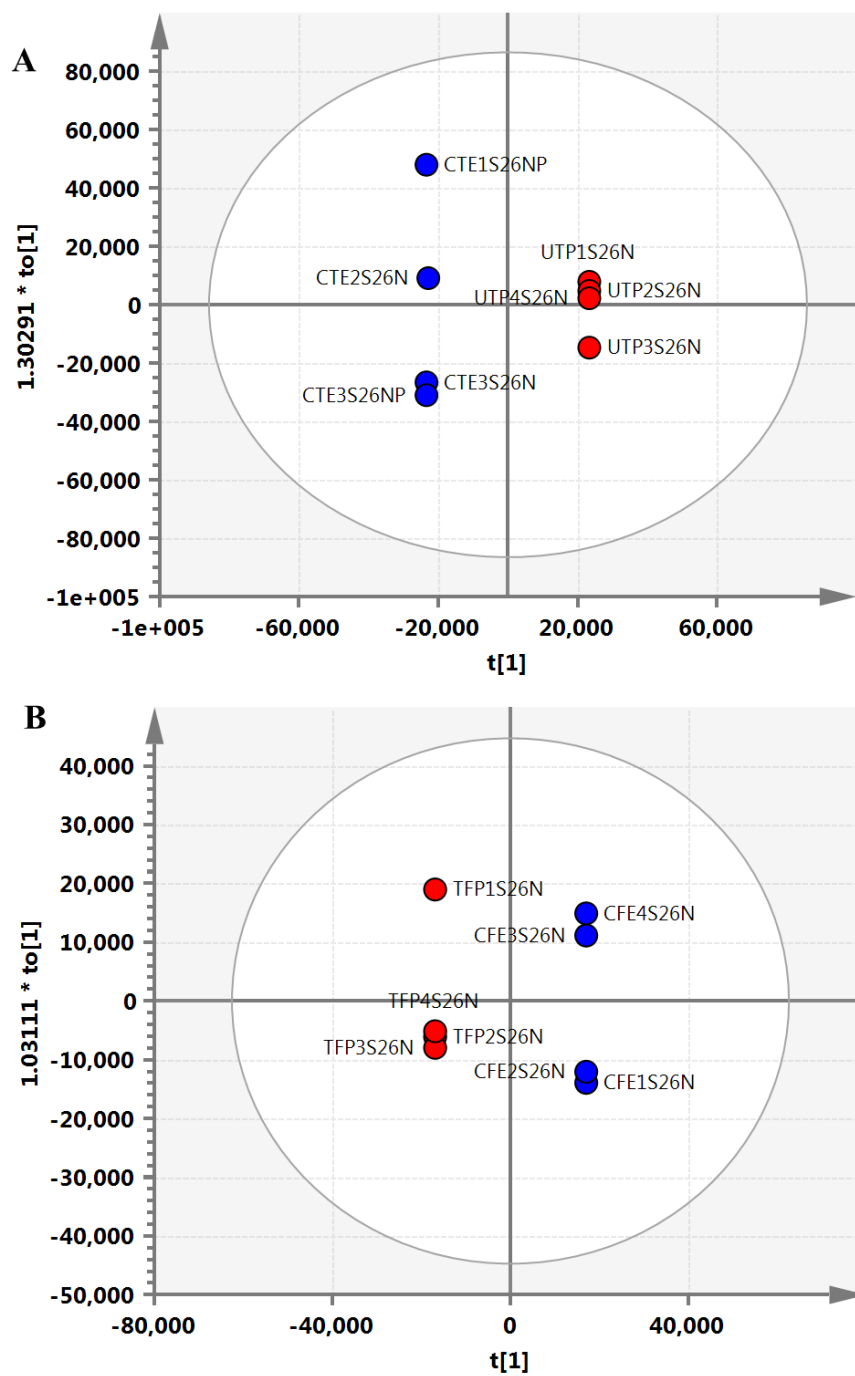


Figure 4.18 OPLSDA score plots (A and B) of non-polar **F6.17** treated groups. Blue circles represent control groups while red circles represent treated groups. Panel A shows the score plot for **F6.17** treated uterine tissues while panel B shows the score plot generated for those associated with the bath fluids. n = 4 animals

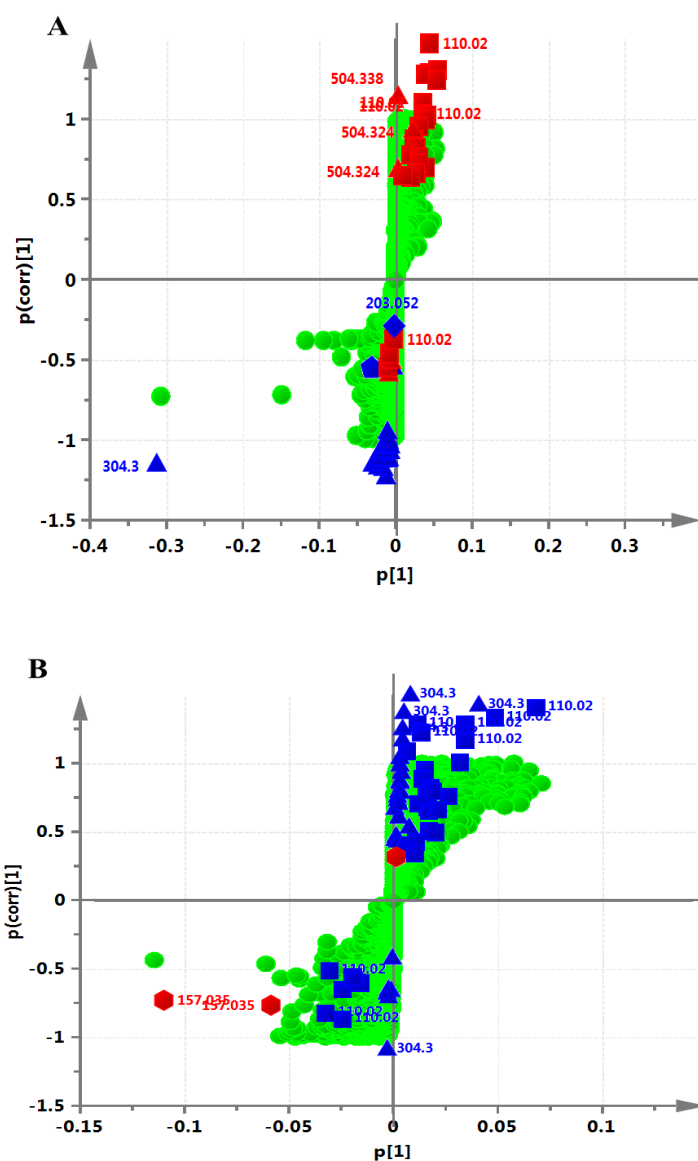


Figure 4.19 OPLSDA S plots of non-polar **F6.17** treated groups. Panel A shows the S plot for **F6.17**-treated uterine tissues while panel B shows the S plot generated for those associated with the bath fluids. All metabolites detected are shown in green circles. Significantly regulated metabolites of the control groups are presented in blue shapes while those of the treated groups are presented in red shapes with corresponding m/z values. ● = cAMP signalling; ▲ = endocannabinoid signalling; ▼ = DAG signalling; ■ = catecholamine synthesis; ◆ = MI biosynthesis/signalling. n = 4 animals

Table 4.4 Pathways and Metabolites detected by HRFTMS on Effect of F6.17 on Uterine Contractility

FC= fold change; **aa** = amino acid; **GABA** = gamma aminobutyric acid; **CDPM**= cysteinyl dopamine; **cAMP**= cyclic adenosine monophosphate; **MI**= myoinositol; **DAG** = diacylglycerol; **PS** = phosphatidylserine; **PI**= phosphatidylinositol; **PA** = phosphatidic acid; **PE** = phosphatidylethanolamine; **SM** = sphingomyelin; **NA** = nucleic acid; **UDP-L-Ara4O** = uridine 5'-diphospho -beta-L-threo-pentapyranos-4-ulose; **PG**= glycerophosphate; **TG**= triacylglycerol; **Rt**= Retention time; **m/z** = mass to charge ratio; **nd** = not detected

Pathway	Metabolome	Adduct	m/z	Rt	FC-Tissues	FC-Fluids
	unknown		122.5472	0.09	30.4936	nd
	unknown		122.5472	1.09	nd	-1.7316
aa Metabolism	Taurine	[M+Na] ⁺	148.0041	1.32	-4.9836	nd
	unknown		120.0767	1.34	-36.7203	nd
Energy production	Lactaldehyde	[M+ACN+H] ⁺	116.0707	1.35	-5.9186	nd
	unknown		116.9771	1.37	nd	465.0968
	L-Prolinamide	[M+H] ⁺	115.087	1.38	nd	3.5970
	Aminobenzoate	[M+H] ⁺	138.055	1.38	99.8340	nd
aa Metabolism/ Serotonin Signalling	Cysteine	[M+NH ₄] ⁺	139.0536	1.39	nd	130.6774
	unknown		158.0384	1.40	nd	138.7658
aa Metabolism	Betaine aldehyde	[M+CH ₃ OH+H] ⁺	134.1174	1.41	-5.4066	nd
	unknown		139.0214	1.50	199.4688	nd

Table 4.4 Continued. Pathways and Metabolites detected by HRFTMS on Effect of F6.17 on Uterine Contractility

Pathway	Metabolome	Adduct	m/z	Rt	FC-Tissues	FC-Fluids
TCA Cycle/ GABA Signalling	Succinate	[M+H+Na] ²⁺	120.5276	1.57	100.2912	nd
cAMP metabolism	8-Azaadenosine	[M+2Na] ²⁺	157.0352	1.60	11433.3826	9785.7196
Dopamine synthesis	5-S-CDPM	[M+2Na] ²⁺	159.0306	1.60	805.3107	nd
	unknown		158.0381	1.65	355.7425	8426.7705
MI Biosynthesis/signalling	MI	[M+Na] ⁺	203.0527	1.69	nd	-1.3952
NA Metabolism	UDP-L-Ara4O	[M+3H] ³⁺	179.0170	1.72	nd	14787.6064
DAG Metabolism/Glycerolipid Metabolism	Acylglycerone phosphate	[M+H-H ₂ O] ⁺	180.9898	1.76	nd	1462.5095
NA Metabolism	Dihydropteridine	[M+Na] ⁺	157.0483	1.76	nd	14878.8020
	unknown		141.9587	1.77	nd	1039.7553
aa Metabolism/ Serotonin Signalling	Cysteine	[M+NH ₄] ⁺	139.0536	1.77	34.3804	nd
Dopamine Metabolism	5-S-CDPM	[M+2Na] ²⁺	159.0304	1.78	nd	3601.7490
	unknown		137.0018	1.83	-14.1527	nd
Dopamine Metabolism	5-S-CDPM	[M+2Na] ²⁺	159.0309	1.85	nd	19.4752
Leucine Metabolism	L-Leucine	[M+H] ⁺	132.1019	1.88	-2.5470	nd

Table 4.4 Continued. Pathways and Metabolites detected by HRFTMS on Effect of F6.17 on Uterine Contractility

Pathway	Metabolome	Adduct	m/z	Rt	FC-Tissues	FC-Fluids
	unknown		158.0029	1.89	nd	2288.3669
	unknown		156.9909	1.93	3939.8379	nd
	unknown		158.9613	1.96	182.4889	805.9703
	unknown		158.9618	2.25	nd	1383.2920
NA Metabolism/NADP Metabolism	2-Chloro-3-oxoadipate	[M+H-2H ₂ O] ⁺	158.9861	2.29	nd	2261.6683
Lipid Metabolism/ Cell Signalling	Succinic acid	[M+K] ⁺	156.9905	2.32	690.0647	nd
Adrenergic signalling	Methylnoradrenaline	[M+H-H ₂ O] ⁺	166.0864	2.46	-3.1303	nd
	8-Azaadenosine	[M+2Na] ²⁺	157.0353	2.48	nd	29.1782
	unknown		156.9907	2.68	nd	10534.9220
aa Metabolism	Betaine aldehyde	[M+H] ⁺	102.0914	3.37	nd	-7.9259
Secondary Metabolite	1,13-Dihydroxy-herbertene	[M+H] ⁺	235.1691	5.01	nd	254.0582
	unknown		122.5472	5.77	2.6587	nd
	unknown		102.0339	6.90	nd	-1.6618

Table 4.4 Continued. Pathways and Metabolites detected by HRFTMS on Effect of F6.17 on Uterine Contractility

Pathway	Metabolome	Adduct	m/z	Rt	FC-Tissues	FC-Fluids
Catecholamine Synthesis	L-Tyrosine	[M+2H+Na] ³⁺	110.0201	9.85	nd	-1.7568
	unknown		122.5472	11.38	nd	-1.3957
	unknown		305.303	19.62	77480.8832	nd
Endocannabinoid Signalling	PC(O-14:0/2:0)	[M+H] ⁺	496.3401	21.36	-2.8513	nd
Endocannabinoid Signalling	N- arachidonoyl amine	[M+NH ₄] ⁺	504.3241	23.38	nd	7.3176
Lipid Metabolism/ Endocannabinoid synthesis	PE(21:0/0:0)	[M+H] ⁺	524.3715	26.46	1.9740	nd
Lipid Metabolism/ Cell Signalling	PC(16:0/18:1(9Z))	[M+H] ⁺	760.5856	29.23	nd	83.2337
	Pheophorbide a	[M+H] ⁺	593.2765	29.70	nd	21905.4735
	PG(20:5/0:0)	[M+ACN+Na] ⁺	594.2794	29.70	nd	46467.7011
Secondary metabolite	Beberine	[M+H] ⁺	595.2824	29.70	nd	4.8995
Secondary metabolite	Pheophorbide a	[M+H] ⁺	593.2765	30.29	2.9054	nd
Glycerophospholipid metabolism	PG(20:5/0:0)	[M+ACN+Na] ⁺	594.2796	30.29	2.9022	nd
Secondary metabolite	Pheophorbide a	[M+H] ⁺	593.2766	30.40	nd	2.7199
	unknown		608.2954	30.49	nd	232.5424

Table 4.4 Continued. Pathways and Metabolites detected by HRFTMS on Effect of F6.17 on Uterine Contractility

Pathway	Metabolome	Adduct	m/z	Rt	FC-Tissues	FC-Fluids
Secondary metabolite	Pyropheophorbide a	[M+H] ⁺	535.2708	31.16	nd	3361.4904
Secondary metabolite	Resiniferatoxin	[M+CH ₃ OH+H] ⁺	661.3029	31.38	nd	5.0646
Endocannabinoid Signalling	PC(20:4/22:6)	[M+CH ₃ OH+H] ⁺	886.5932	31.50	nd	-4.2569
Lipid Metabolism/ Cell Signalling	TG(17:1/17:2/18:0)	[M+ACN+H] ⁺	898.7866	31.80	1038.9446	7.7292
MI signalling	PI(17:1/22:2)	[M+H-H ₂ O] ⁺	885.5895	31.92	nd	-5.4249
	unknown		675.3183	32.06	nd	4.9225
	unknown		607.2925	32.26	nd	3650.4381
	unknown		608.2955	32.26	nd	5756.5133
	unknown		607.2921	32.28	9117.3047	nd
MI Biosynthesis/Signalling	PI(17:1/22:2)	[M+H-H ₂ O] ⁺	885.5897	32.42	nd	-6.7596
	unknown		880.7611	32.46	nd	-145.6427
Lipid Metabolism/ Cell Signalling	TG(17:2/17:2/17:2)	[M+ACN+H] ⁺	878.7276	32.50	nd	15.8852
Lipid Metabolism/ Cell Signalling	TG(17:2/17:2/20:3)	[M+H] ⁺	877.7265	32.52	nd	9.5732
GABA Signalling	Linalyl isobutyrate	[M+H+Na] ²⁺	124.0869	32.79	3.8062	62.9969
	unknown		621.3078	32.87	96001.1760	nd

Table 4.4 Continued. Pathways and Metabolites detected by HRFTMS on Effect of F6.17 on Uterine Contractility

Pathway	Metabolome	Adduct	m/z	Rt	FC-Tissues	FC-Fluids
	unknown		874.7778	33.12	nd	6.0879
Lipid Metabolism/ Cell Signalling	PS(22:2/0:0)	[M+2Na-H] ⁺	622.3110	33.18	nd	3361.4851
	unknown		621.3077	33.28	nd	1553.4127
Lipid Metabolism	TG(18:2/18:3/20:0)	[M+H-2H ₂ O] ⁺	873.7746	33.49	nd	7.2787
	unknown		682.4880	34.03	nd	140.8014
	unknown		680.4809	34.06	236.5634	26.9456
Secondary metabolite	Pheophorbide a	[M+H-H ₂ O] ⁺	549.2866	34.10	nd	628.2744
Lipid Metabolism/ Cell Signalling	PA(O-16:0/20:5)	[M+H] ⁺	681.4845	34.14	nd	257.5960
	unknown		735.5234	34.14	nd	195.3836
Lipid Metabolism	TG(17:1/17:2/18:0)	[M+ACN+H] ⁺	898.7865	34.28	759.7382	3.3984
	unknown		663.4545	34.30	73.4568	100.5055
Lipid Metabolism/ Cell Signalling	Lipid A - disaccharide-1-P	[M+NH ₄] ⁺	1342.9266	34.34	15718.3668	nd
Lipid Metabolism/ Cell Signalling	Lipid A - disaccharide-1-P	[M+NH ₄] ⁺	1343.9297	34.34	6290.3069	nd
	PS(P-16:0/12:0)	[M+H] ⁺	664.4581	34.41	nd	31.1625
	unknown		680.4803	34.54	17.5514	nd

Table 4.4 Continued. Pathways and Metabolites detected by HRFTMS on Effect of F6.17 on Uterine Contractility

Pathway	Metabolome	Adduct	m/z	Rt	FC-Tissues	FC-Fluids
	unknown		900.7939	34.60	nd	3.4810
	unknown		888.7661	34.82	6.6627	nd
	unknown		900.7931	34.96	nd	5.1916
Lipid Metabolism/ Cell Signalling	TG(16:0/17:1(9Z)/17:1(9Z))	[M+ACN+H] ⁺	872.7714	35.46	124.3982	nd
	unknown		906.7762	35.54	nd	-31.4020
Lipid Metabolism/ Cell Signalling	TG(17:2/17:2/18:0)	[M+ACN+H] ⁺	896.7709	35.60	nd	11644.6557
Lipid Metabolism/ Cell Signalling	TG(18:3/20:2/20:2)	[M+H-2H ₂ O] ⁺	897.7743	35.60	nd	584.8636
Lipid Metabolism/ Cell Signalling	TG(18:2/18:3/20:0)	[M+H-2H ₂ O] ⁺	873.7743	35.83	nd	9.7240
Lipid Metabolism/ Cell Signalling	TG(16:0/17:1(9Z)/17:1(9Z))	[M+ACN+H] ⁺	872.7708	35.89	nd	7.0803
	unknown		932.7922	35.89	nd	-20.3652
	unknown		907.7796	36.36	nd	-32.9128
Lipid Metabolism	TG(16:0/17:1(9Z)/17:1(9Z))	[M+ACN+H] ⁺	872.7717	36.63	86.9237	nd
Lipid Metabolism	TG(18:2/20:2/20:2)	[M+H-H ₂ O] ⁺	899.7901	36.71	2442.5931	nd

Table 4.4 Continued. Pathways and Metabolites detected by HRFTMS on Effect of F6.17 on Uterine Contractility

Pathway	Metabolome	Adduct	m/z	Rt	FC-Tissues	FC-Fluids
	unknown		1733.4662	36.78	nd	22.7211
Lipid Metabolism/ Cell Signalling	TG(17:1/17:2/18:0)	[M+ACN+H] ⁺	899.7899	36.81	nd	2.2150
	unknown		900.7938	37.21	51.2180	nd
	unknown		997.7766	37.27	813.1830	nd
	unknown		900.7934	37.60	42.1432	nd
	unknown		296.9708	37.64	nd	1.7011
Catecholamine Synthesis	L-Tyrosine	[M+2H+Na] ³⁺	110.0201	37.73	nd	-2.2789
	unknown		208.0394	37.87	7.2853	nd
	unknown		167.0129	37.88	5.9285	nd
	unknown		141.1136	37.90	25.0014	1.7879
	unknown		122.5472	37.93	12.8460	nd
Lipid Metabolism/ Cell Signalling	4Z,7-octadienoic acid	[M+H] ⁺	141.0912	37.98	nd	3.9567
Tyrosine Metabolism	Succinylacetone	[M+H-H ₂ O] ⁺	141.0546	38.15	nd	328.6351
	unknown	[M+H-2H ₂ O] ⁺	182.9853	38.26	7.4940	nd
Catecholamine Synthesis	L-Tyrosine	[M+2H+Na] ³⁺	110.0201	38.49	4.0729	nd
aa Metabolism	Betaine aldehyde	[M+H] ⁺	102.0913	44.08	nd	-12.0518

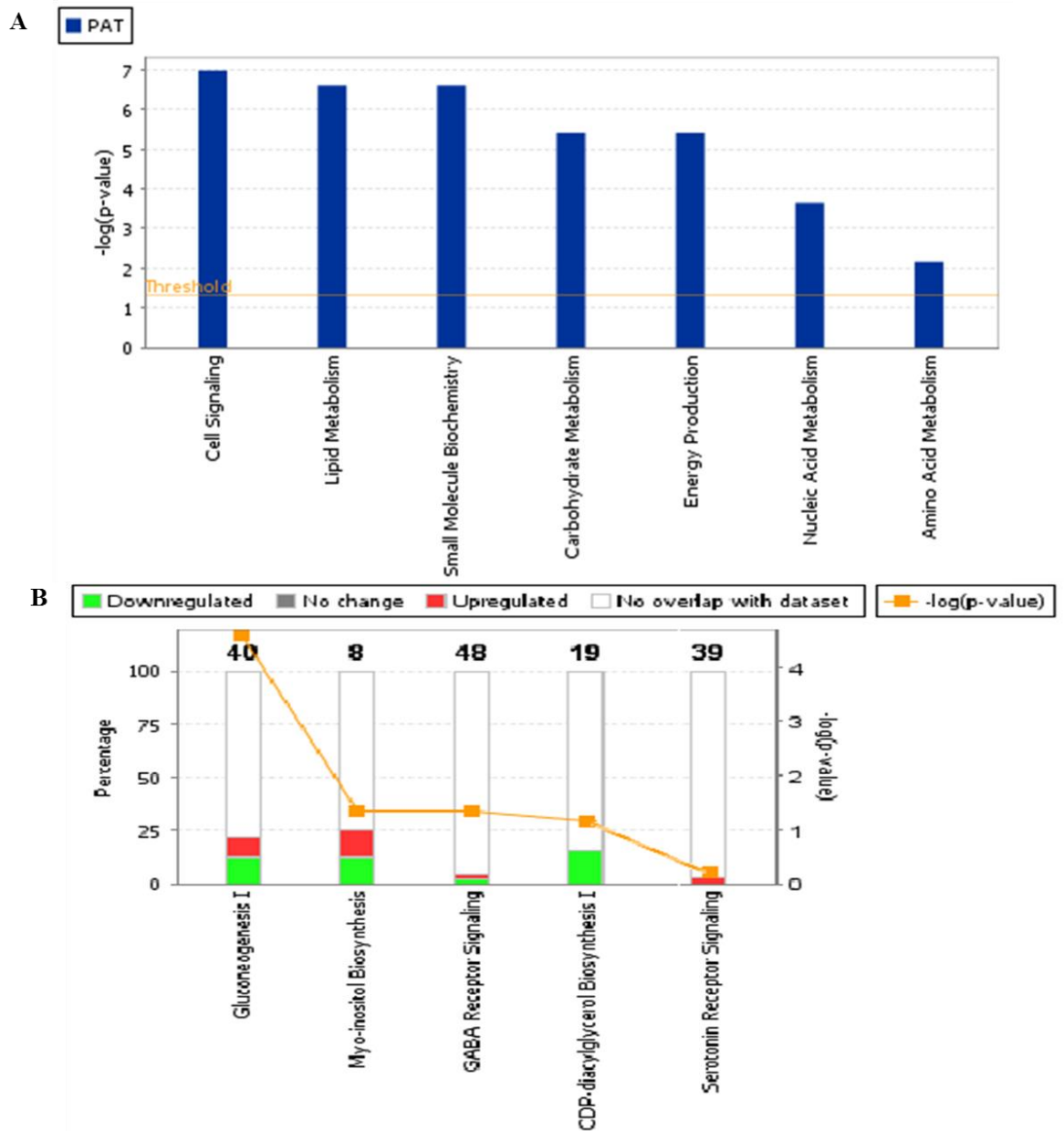


Figure 4.20a Bar charts displaying top functions (A) and canonical pathways (B) extracted by IPA software for **F6.17** treated uterine tissues. The high level functional categories associated with **F6.17**- treated tissues are displayed along the x-axis in A while high level canonical pathways are shown in B. The y-axis displays the $-\log$ significance. Taller bars in A are more significant than the shorter bars and are listed from most significant to least. The orange horizontal line in A and B denotes the cut-off for significance (p -value of 0.05).

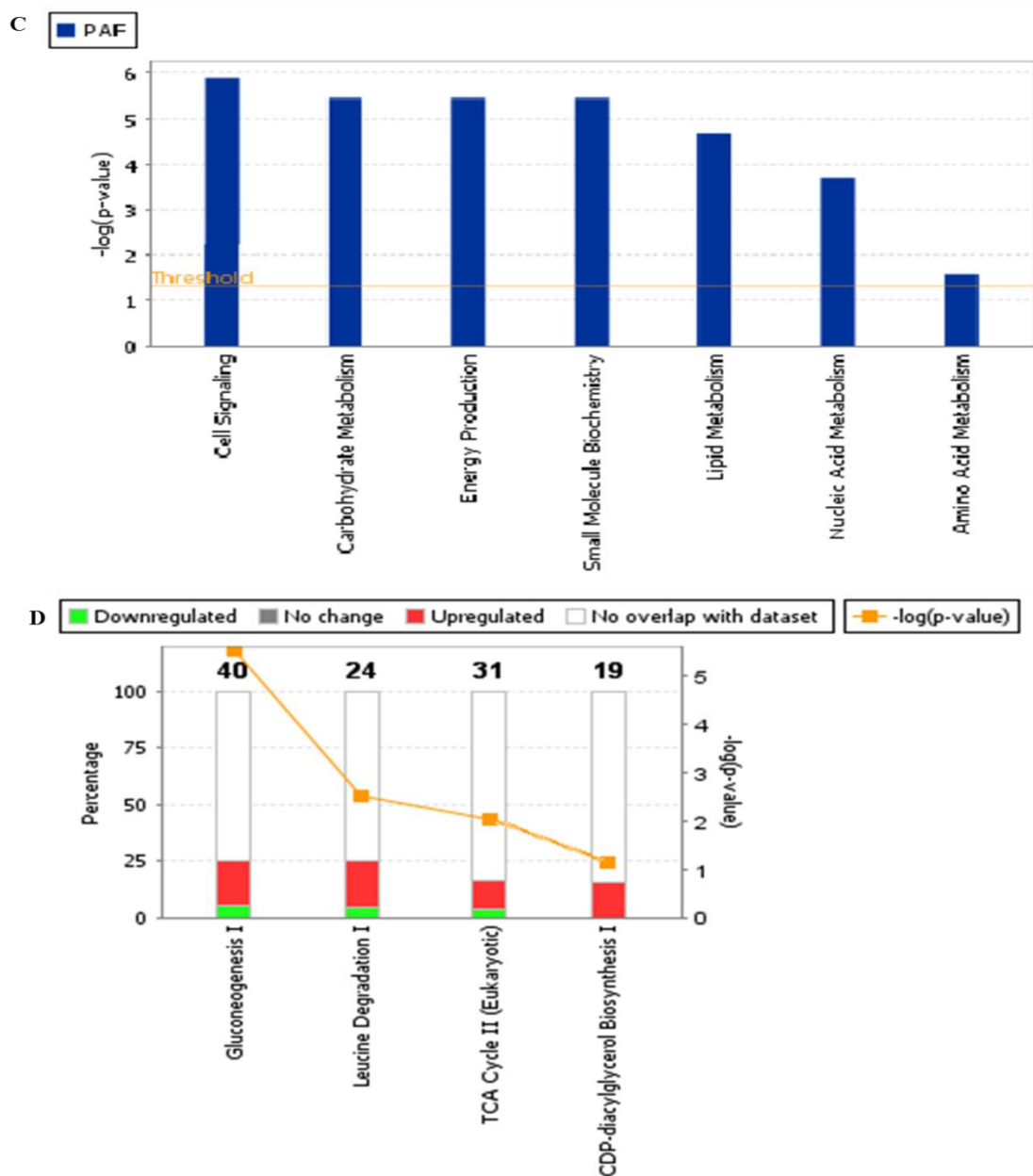


Figure 4.20b IPA-generated bar charts displaying top functions (C) and canonical pathways (D) for bath fluids in which the **F6.17** treated uterine tissues were immersed. Significantly associated functional categories of **F6.17**- treated fluids are displayed along the x-axis in C above while significant canonical pathways are shown in the x-axis of D above. The y-axis in C displays the $-\log$ significance while the left y-axis in D displays the percentage change. Taller bars in C are more significant than the shorter bars and are listed from most to least significant; the orange horizontal line in C and D denotes the cut-off for significance (p-value of 0.05).

4.7.5 HPLC-HRFTMS of F28

OPLSDA multivariate analysis of HR-FTLCMS experiments on **F28** showed distinct separations between the control and treated groups of both the polar (Fig. 4.21) and non-polar groups (Fig. 4.23). From the S plots generated, cAMP, and catecholamine signalling were upregulated while MI and DAG signalling were downregulated in the **F28** treated tissues (Fig. 4.22 A and Fig. 4.24 A). These findings were similarly observed in the bath fluids (Fig. 4.22 B and 4.24 B). Several metabolites were detected via HRFTMS analysis to have been perturbed on treatment of the uterine tissues with **F28** (Table 4.5). Some secondary plant metabolites were also identified such as coumestrol 3-o-glucoside, Furaneol-4-glucoside, 3-(Acetylthio-)2-methylfuran (Table 4.5). Additionally, an increase in nicotinamide, adenosine, adenine, and cysteinyl dopamine, were detected on analysis of **F28**-treatment while MI and phosphatidyl ethanolamine were decreased (Table 4.5). The IPA bioinformatic analysis showed lipid metabolism, cell signalling, nucleic and amino acid metabolism and small molecule biochemistry as high-level functional categories associated with **F28**-treatment of uterine tissues (Fig. 4.25 a and b). Canonical pathways generated by IPA bioinformatics showed myo-inositol, GABA, IP₃, MI and serotonin to have been upregulated (Fig.4.25 a and b).

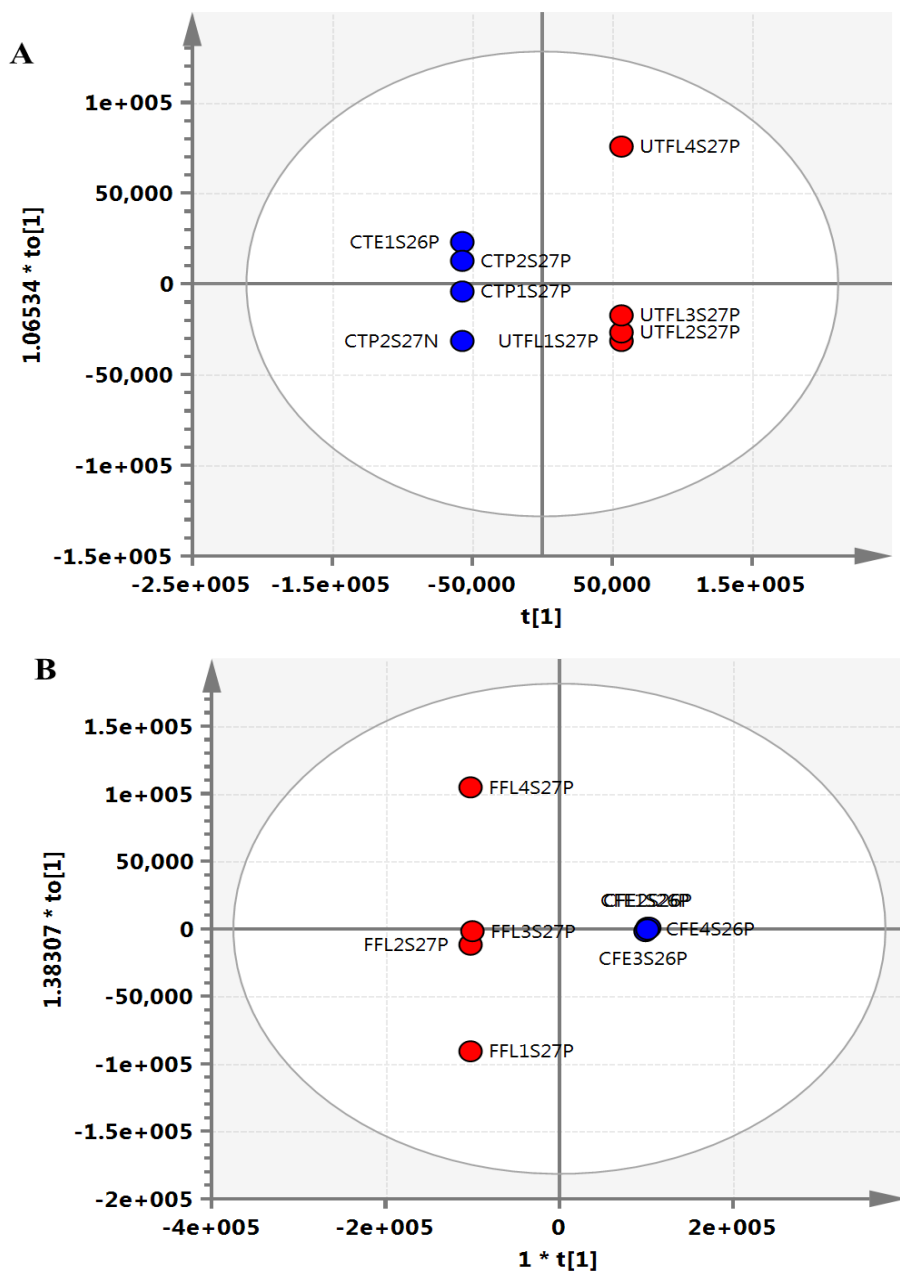


Figure 4.21 OPLSDA score plots (A and B) of polar **F28** treated groups. Blue circles represent control groups while red circles represent treated groups. Panel A shows the score plot for **F28** treated uterine tissues while panel B shows the score plot generated for those associated with the bath fluids. n = 4 animals

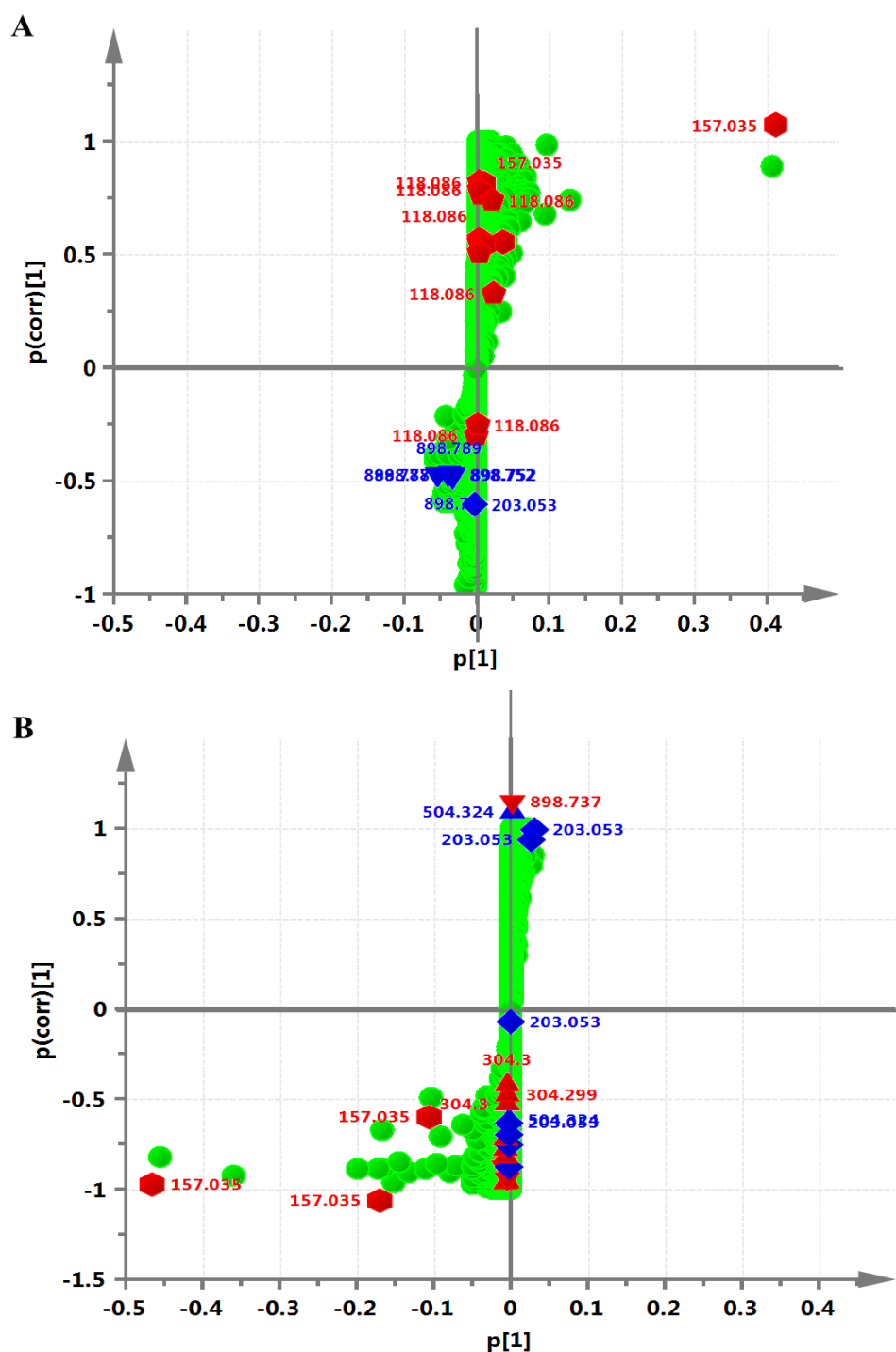


Figure 4.22 OPLSDA S plots of polar **F28** treated groups. Panel A shows the S plot for **F28**-treated uterine tissues while panel B shows the S plot generated for those associated with the bath fluids. All metabolites detected are shown in green circles. Significantly regulated metabolites of the control groups are presented in blue shapes while those of the treated groups are presented in red shapes with corresponding m/z values. \blacklozenge = cAMP signalling; \blacktriangle = endocannabinoid signalling; \blacktriangledown = DAG signalling; \blacksquare = catecholamine synthesis; \blacklozenge = MI biosynthesis/signalling. n = 4 animals

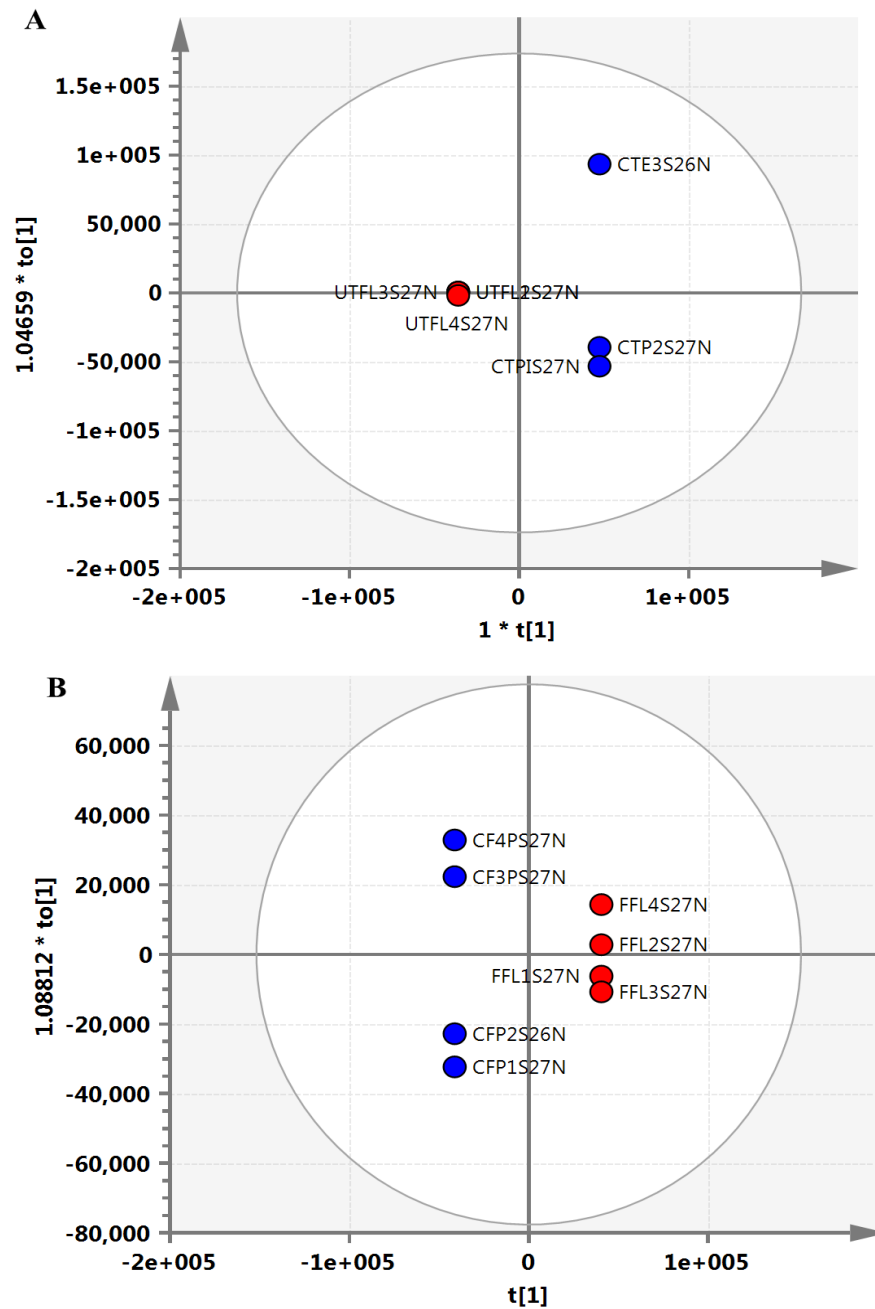


Figure 4.23 OPLSDA score plots (A and B) of non-polar **F28** treated groups. Blue circles represent control groups while red circles represent treated groups. Panel A shows the score plot for **F28** treated uterine tissues while panel B shows the score plot generated for those associated with the bath fluids. n = 4 animals

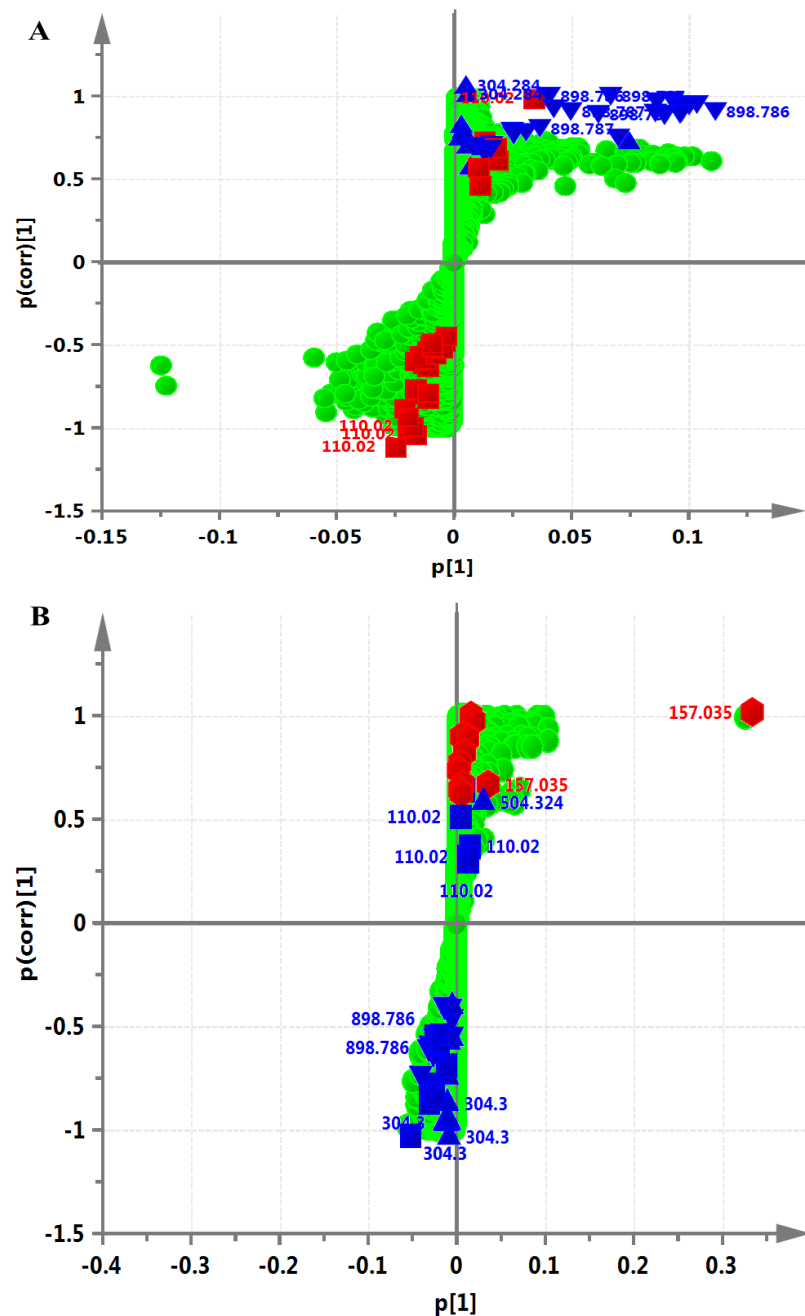


Figure 4.24 OPLSDA S plots of non-polar **F28** treated groups. Panel A shows the S plot for **F28**-treated uterine tissues while panel B shows the S plot generated for those associated with the bath fluids. All metabolites detected are shown in green circles. Significantly regulated metabolites of the control groups are presented in blue shapes while those of the treated groups are presented in red shapes with corresponding m/z values. \blacklozenge = cAMP signalling; \blacktriangle = endocannabinoid signalling; \blacktriangledown = DAG signalling; \blacksquare = catecholamine synthesis; \blacklozenge = MI biosynthesis/signalling. n = 4 animals

Table 4.5 Pathways and Metabolites detected by HRFTMS on Effect of F28 on Uterine Contractility

FC= fold change; **GABA** = gamma aminobutyric acid; **CDPM**= cysteinyl dopamine; **cAMP**= cyclic adenosine monophosphate; **MI**= myoinositol; **DAG** = diacylglycerol; **PS** = phosphatidylserine; **PI**= phosphatidylinositol; **PA** = phosphatidic acid; **PE** = phosphatidylethanolamine; **SM** = sphingomyelin; **NA** = nucleic acid; **UDP-L-Ara4O** = uridine 5'-diphospho -beta-L-threo-pentapyranos-4-ulose; **PG**= glycerophosphate; **CER** = ceramide; **TG** = triacylglycerol; **Rt** =Retention time; **m/z** = mass to charge ratio; aa = amino acid; **nd** = not detected

Pathway	Metabolome	Adduct	m/z	Rt	FC-Tissues	FC-Fluids
MI						
Biosynthesis/Signalling	MI	[M+Na] ⁺	203.0526	1.21	nd	-2.0978
Dopamine Metabolism	5-S-CDPM	[M+2Na] ²⁺	159.0307	1.35	131.9353	nd
cAMP Metabolism	8-Azaadenosine	[M+2Na] ²⁺	157.0353	1.40	nd	21394.7338
Catecholamine Metabolism	5-S-CDPM	[M+2Na] ²⁺	159.0308	1.41	nd	255.3661
aa metabolism	L-Cysteine	[M+NH ₄] ⁺	139.0536	1.41	nd	135.7910
	unknown		138.0568	1.42	nd	128.7474
DAG Metabolism/Cell Signalling	Nicotinamide N-oxide	[M+H] ⁺	139.0503	1.44	37.8491	nd
cAMP Metabolism	2,8-Dihydroxyadenine	[M+H] ⁺	168.0518	1.45	209.7970	nd
Lipid Metabolism	Creatinine	[M+H] ⁺	114.0663	1.47	27.4254	nd
aa Metabolism	L-Proline	[M+H] ⁺	116.0707	1.48	3.0362	nd
Secondary metabolite	3-(Acetylthio)-2-methylfuran	[M+H-H ₂ O] ⁺	139.0214	1.51	nd	279.1276

Table 4.5 Pathways and Metabolites detected by HRFTMS on Effect of F28 on Uterine Contractility

Pathway	Metabolome	Adduct	m/z	Rt	FC-Tissues	FC-Fluids
DAG Metabolism/Cell Signalling	UDP-L-Ara4O	[M+3H] ³⁺	179.0171	1.56	nd	19685.8142
	unknown		122.5472	1.64	nd	-6.2191
MI Biosynthesis/Signalling	MI	[M+Na] ⁺	203.0530	1.65	nd	-2.9784
	unknown		181.0120	1.69	nd	2199.4096
cAMP Metabolism	8-Azaadenosine	[M+2Na] ²⁺	157.0350	1.70	15703.2665	11304.1783
Secondary Metabolites	Furaneol 4-glucoside		157.0483	1.76	nd	132125.6893
DAG Metabolism/Cell Signalling	Nicotinamide N-oxide	[M+H] ⁺	139.0503	1.77	40.2363	nd
	unknown		141.9587	1.78	nd	507.8939
Dopamine Metabolism	5-S-CDPM	[M+2Na] ²⁺	159.0304	1.88	689.3141	3844.5666
	unknown		158.0029	1.89	nd	1993.9714
	unknown		158.9641	1.91	nd	1564.0228
	unknown		122.5472	1.97	3.1059	3.7939
	unknown		156.9910	2.23	nd	16882.2743
	unknown		158.9618	2.25	nd	1850.0061
	2-Chloro-3-oxoadipate	[M+H-2H ₂ O] ⁺	158.9861	2.29	nd	2894.1997

Table 4.5 Pathways and Metabolites detected by HRFTMS on Effect of F28 on Uterine Contractility

Pathway	Metabolome	Adduct	m/z	Rt	FC-Tissues	FC-Fluids
Secondary Metabolite	Coumestrol 3-O-glucoside	[M+2Na+H] ³⁺	159.0252	2.49	nd	1431.6192
aa metabolism	4-Fluoro-L-threonine	[M+H-H ₂ O] ⁺	120.0461	2.51	nd	637.6850
	unknown		156.9910	2.68	nd	6520.9585
	unknown		156.9907	3.14	nd	1544.8049
	unknown		122.5472	3.53	2.7385	nd
Leucine Metabolism	Leucine	[M+H-H ₂ O] ⁺	114.0914	3.67	37.7390	nd
	unknown		156.9907	3.76	nd	1468.9710
	unknown		156.9907	4.51	nd	825.6455
	unknown		156.9910	5.28	nd	1670.9034
	unknown		122.5472	7.35	4.4897	nd
DAG Metabolism/Cell Signalling	TG(16:0/17:1/17:1)	[M+ACN+H] ⁺	872.7713	29.58	nd	5.3276
DAG Metabolism/Cell Signalling	TG(16:0/17:1/17:1)	[M+ACN+H] ⁺	872.7713	32.73	-8.6456	5.0730
	unknown		900.7929	33.32	-6.3575	nd

Table 4.5 Pathways and Metabolites detected by HRFTMS on Effect of F28 on Uterine Contractility

Pathway	Metabolome	Adduct	m/z	Rt	FC-Tissues	FC-Fluids
DAG Metabolism/Cell Signalling	TG(18:2/18:3/20:0)	[M+H-2H ₂ O] ⁺	873.7740	34.11	nd	-39.9441
DAG Metabolism/Cell Signalling	TG(16:0/17:1/17:1)	[M+ACN+H] ⁺	872.7709	34.22	-6.9353	6.0068
	unknown		914.7799	34.57	14.8475	nd
	unknown		680.4811	35.47	nd	4.2257
	unknown		1343.9300	35.54	229.2043	56.7479
DAG Metabolism/Cell Signalling	TG(16:0/17:1/17:1)	[M+ACN+H] ⁺	872.7708	35.58	-7.8883	5.2553
	unknown		680.4805	35.64	95.1138	22.5529
	unknown		663.4542	35.66	82.4886	22.9148
	unknown		735.5229	35.70	nd	8.2292
MI Biosynthesis	PS(P-16:0/12:0)	[M+H] ⁺	664.4576	35.95	nd	29.5071
Lipid Metabolism/Cell Signalling	Lipid A - disaccharide	[M+NH ₄] ⁺	1342.9270	35.95	nd	58.6173
	unknown		900.7930	35.99	-5.7075	nd
MI Biosynthesis	PA(O-16:0/20:5)	[M+H] ⁺	681.4841	36.04	nd	21.9442
DAG Metabolism/Cell Signalling	TG(16:0/17:1/17:1)	[M+ACN+H] ⁺	872.7715	36.34	-5.2972	nd

Table 4.5 Pathways and Metabolites detected by HRFTMS on Effect of F28 on Uterine Contractility

Pathway	Metabolome	Adduct	m/z	Rt	FC-Tissues	FC-Fluids
	unknown	nd	900.7933	36.90	-4.0451	nd
DAG Metabolism/Cell Signalling	TG(16:0/17:1/17:1)	[M+ACN+H] ⁺	872.7714	37.06	-4.6421	nd
Endocannabinoid Metabolism	PE(22:4/22:6)	[M+ACN+Na] ⁺	903.5636	37.34	-312.8630	nd
Lipid Metabolism/Cell Signalling	Cer(d18:1/20:0)	[M+3H] ³⁺	913.7694	37.60	44.6479	nd
GABA Signalling	2,4-diaminobutyric acid	[M+H] ⁺	119.0816	38.84	nd	-163.3174
GABA Signalling	2,4-diaminobutyric acid	[M+H] ⁺	119.0816	39.83	nd	-224.6762

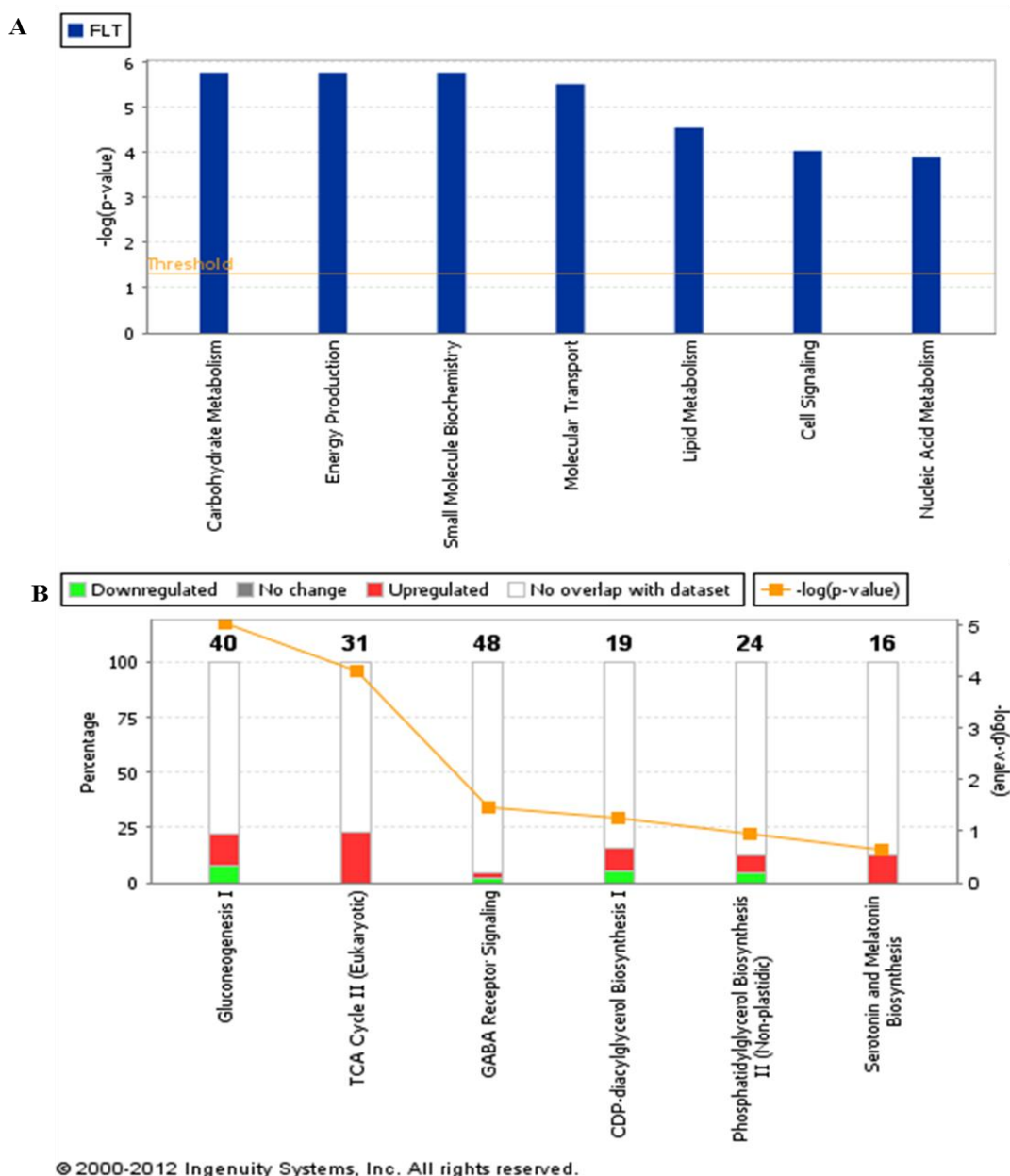


Figure 4.25a Bar charts displaying top functions (A) and canonical pathways (B) extracted by IPA software for **F28** treated uterine tissues. The high level functional categories associated with **F28**- treated tissues are displayed along the x in A above while high level canonical pathways are shown in B above. The y-axis displays the $-\log$ significance. Taller bars in A are more significant than the shorter bars. Functions in A are listed from most significant to least. The orange horizontal line in A and B denotes the cut-off for significance (p -value of 0.05).

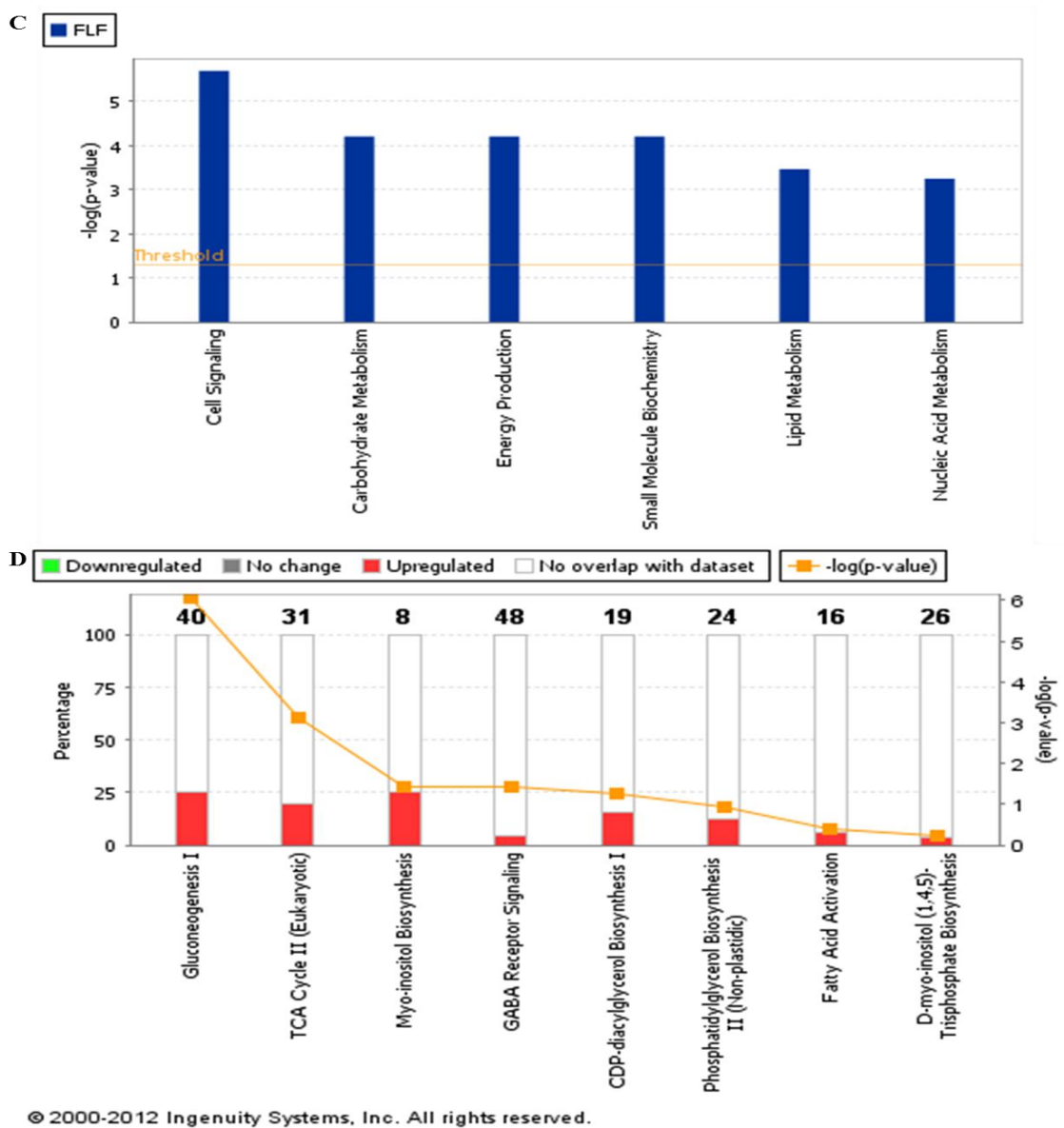


Figure 4.25b IPA-generated bar charts displaying top functions (C) and canonical pathways (D) for bath fluids in which the **F28** treated uterine tissues were immersed. Significantly associated functional categories of **F28**- treated fluids are displayed along the x-axis in C above while significant canonical pathways are shown in the x-axis of D above. The y-axis in C displays the $-\log$ significance while the left y-axis in D displays the percentage change. Taller bars in C are more significant than the shorter bars. Functions in C have been listed from most significant to least significant; the orange horizontal line in C and D denotes the cut-off for significance (p-value of 0.05).

Table 4.6 Summary of Pathways and Metabolites detected by HR-FTLCMS on Effect of Fractions of *F. exasperata* on Uterine Contractility

FC= Fold change; GABA = gamma aminobutyric acid; CDPM= cysteinyl dopamine; cAMP= cyclic adenosine monophosphate; MI= myoinositol; DAG = Diacylglycerol; PS = Phosphatidylserine; PI= Phosphatidylinositol; PA = Phosphatidic acid; PE = Phosphatidylethanolamine; TG = Triacylglycerol; m/z = mass to charge ratio; Rt = Retention time; nd = not detected

Pathway	Metabolome	Adduct	m/z	Rt	FC-E1		FC-F14		FC-F4_31		FC-F6_17		FC-F28	
					Tissues	Fluids	Tissues	Fluid	Tissues	Fluids	Tissues	Fluids	Tissues	Fluids
GABA Receptor Signalling	GABA	[M+H] ⁺	118.0863	1.36	nd	nd	nd	nd	1.365	-1.9603	nd	nd	nd	nd
Dopamine Synthesis	5-S-CDPM	[M+2Na] ²⁺	159.0308	1.36	7.794	432.165	nd	nd	nd	nd	nd	nd	nd	nd
			159.0308	1.46	nd	nd	133.6072	nd	nd	nd	nd	nd	nd	nd
GABA Receptor Signalling	Glutamate	[M+H] ⁺	148.0606	1.37	nd	nd	nd	nd	-1.6216	nd	nd	nd	nd	nd
cAMP Metabolism	8-Azaadenosine	[M+2Na] ²⁺	157.0353	1.41	687.711	25042.326	nd	nd	nd	nd	11433.3826	9785.7196	nd	21394.7338
			157.0353	1.48	nd	nd	5438.029	1434.018	498.8266	1393.879	nd	nd	nd	nd
MI Biosynthesis	MI	[M+Na] ⁺	203.0527	1.57	nd	-1.508	nd	nd	nd	-1.498	nd	-1.3952	nd	nd
			203.0530	1.65	nd	nd	nd	nd	nd	nd	nd	nd	nd	-2.9784
GABA signalling	4-Methylaminobutyrate	[M+H] ⁺	118.0863	1.60	-2.015	nd	nd	nd	nd	nd	nd	nd	nd	nd
Catecholamine Synthesis	D-Phenylalanine	[M+H] ⁺	166.0863	2.29	-3.259	nd	nd	nd	nd	nd	nd	nd	nd	nd
Catecholamine Synthesis	L-Tyrosine	[M+2H+Na] ³⁺	110.0201	3.66	nd	nd	nd	nd	1.47941	nd	nd	nd	nd	nd
			110.0201	4.55	1.960	-2.027	2.1354	nd	nd	nd	-1.7568	nd	nd	nd
Endocannabinoid Metabolism	Oleoylethanolamide	[M+H-2H ₂ O] ⁺	304.2999	19.71	nd	nd	nd	nd	-24.8789	-1.2906	nd	nd	nd	nd
DAG Metabolism/Endocannabinoid Signalling	N- arachidonoyl amine	[M+NH ₄] ⁺	504.3241	23.38	nd	nd	nd	nd	nd	nd	nd	7.3176	nd	nd
Lipid metabolism	PA(17:1/22:2)	[M+ACN+H] ⁺	782.5700	28.83	nd	nd	3.8447	nd	nd	nd	nd	nd	nd	nd
DAG signalling	DAG(20:5/22:3/0:0)	[M+ACN+H] ⁺	734.5702	28.85	nd	nd	24.5178	nd	nd	nd	nd	nd	nd	nd
Sphingosine Metabolism	PS(21:0/22:4)	[M+H] ⁺	904.6039	32.06	1973.397	nd	nd	nd	nd	nd	nd	nd	nd	nd
MI Biosynthesis	PI(17:1/22:2)	[M+H-H ₂ O] ⁺	885.5897	32.42	nd	nd	nd	nd	nd	nd	nd	-6.7596	nd	nd
MI Biosynthesis	PI(P-18:0/18:1)	[M+H] ⁺	813.5684	32.67	nd	-107.481	nd	nd	nd	nd	nd	nd	nd	nd
MI Biosynthesis	PI(O-16:0/20:2)	[M+H-2H ₂ O] ⁺	813.5683	34.29	nd	nd	nd	nd	nd	-120.925	nd	nd	nd	nd
Endocannabinoid Metabolism	PE(22:4/22:6)	[M+ACN+Na] ⁺	903.5636	34.21	129.360	nd	nd	nd	nd	nd	nd	nd	nd	nd
			903.5636	37.34	nd	nd	nd	nd	nd	nd	nd	nd	nd	-312.8630

4.8 ¹H-NMR Results

Table 4.7 Summarised table showing significant metabolites and pathways detected by ¹H-NMR analysis to be involved in the action of *Ficus* fractions on uterine contraction.

GABA =gamma aminobutyric acid; **NA** = nucleic acid; **aa** = amino acid; **TCA** = tricarboxylic acid cycle; **cAMP** = cyclic adenosine monophosphate; **MI** = myoinositol; **PC** = phosphatidylcholine; **PS**= phosphatidylserine; **PGF1**= prostaglandinF1; **PHE** = phenylalanine; **PE**= phosphatidylethanolamine; **AA** = arachidonic acid; **AEA** = anandamide; **U** = unknown; **DAG** = diacylglycerol; **ATP** = adenosinetriphosphate; **NA** = nucleic acid; **ERK** = extracellular signal regulated kinase; **RhoA** = Ras homolog gene family, member A, **mTOR** = mammalian target of rapamycin; **NAA** = N-acetylaspartate; **nd** = not detected

Pathway	Metabolome	Shift (ppm)	E1		F14		F4-31		F6.17		F28	
			p[1]Tissues	p[1]Fluids	p[1]Tissues	p[1]Fluids	p[1]Tissues	p[1]Fluids	p[1]Tissues	p[1]Fluids	p[1]Tissues	p[1]Fluids
DAG Signalling	DAG	0.72	nd	nd	-0.0815	-0.0815	nd	-0.1308	nd	nd	nd	-0.116
DAG Signalling	DAG	0.76	nd	nd	nd	-0.1022	nd	-0.1731	nd	nd	nd	-0.1526
DAG Signalling	DAG	0.80	nd	-0.1371	-0.1658	-0.1375	nd	-0.2088	nd	nd	-0.1327	-0.2046
Endocannabinoid	AEA	0.88	nd	nd	nd	-0.1579	0.078	nd	nd	0.0258	-0.0511	nd
Prostanoid Signalling	AA	0.92	nd	nd	-0.0343	-0.122	nd	nd	nd	nd	-0.0382	nd
Prostanoid Signalling	AA	0.96	nd	nd	-0.0367	-0.0809	nd	nd	-0.0368	-0.0482	-0.0387	nd
Prostanoid Signalling	AA	1.00	nd	nd	-0.031	-0.1172	nd	nd	-0.0378	-0.0658	-0.0332	nd
Prostanoid Signalling	AA	1.04	nd	nd	-0.0329	-0.1316	-0.0907	nd	-0.0361	-0.0658	-0.0332	nd
Prostanoid Signalling	AA	1.08	nd	nd	-0.0417	-0.1295	-0.0862	-0.0183	-0.0367	nd	-0.038	-0.125
Endocannabinoid Signalling	AEA	1.24	nd	nd	nd	nd	nd	-0.0469	nd	0.0421	-0.0743	-0.2319
Endocannabinoid Signalling	AEA	1.28	nd	nd	0.3912	-0.2555	nd	nd	nd	0.0343	0.3334	nd

Table 4.7 Continued. Summarised table showing significant metabolites and pathways detected by ¹H-NMR analysis to be involved in the action of *Ficus* fractions on uterine contraction.

GABA =gamma aminobutyric acid; **NA** = nucleic acid; **aa AA** = amino acid; **TCA** = tricarboxylic acid cycle; **cAMP** = cyclic adenosine monophosphate; **MI** = myoinositol; **PC** = phosphatidylcholine; **PS**= phosphatidylserine; **PGF1**= prostaglandinF1; **PHE** = phenylalanine; **PE**= phosphatidylethanolamine; **AEA** = anandamide; **U** = unknown; **DAG** = diacylglycerol; **ATP** = adenosinetriphosphate; **NA** = nucleic acid; **ERK** = extracellular signal regulated kinase; **RhoA** = Ras homolog gene family, member A, **mTOR** = mammalian target of rapamycin; **NAA** = N-acetylaspartate; **nd** = not detected

Pathway	Metabolome	Shift (ppm)	E1		F14		F4-31		F6.17		F28	
			p[1]Tissues	p[1]Fluids	p[1]Tissues	p[1]Fluids	p[1]Tissues	p[1]Fluids	p[1]Tissues	p[1]Fluids	p[1]Tissues	p[1]Fluids
Endocannabinoid Signalling	AEA	1.36	nd	nd	0.1159	-0.1326	nd	nd	nd	nd	-0.0278	nd
DAG Signalling	DAG	1.60	nd	0.0244	nd	nd	nd	nd	nd	-0.3338	nd	nd
DAG Signalling	DAG	1.64	nd		nd	nd	nd	nd	nd	-0.1475	nd	nd
DAG Signalling	DAG	1.68	nd	0.0254	nd	nd	nd	nd	nd	nd	nd	0.2822
Endocannabinoid Signalling	AEA	1.72	nd	nd	nd	nd	nd	nd	nd	0.0786	nd	0.2316
Endocannabinoid Signalling	AEA	1.76	nd	nd	nd	nd	nd	nd	nd	0.1103	nd	nd
Endocannabinoid Signalling	AEA	1.80	0.015	nd	nd	nd	nd	nd	0.0535	0.0971	nd	nd
GABA Signalling	Glutamate	1.88	nd	0.0236	nd	nd	nd	nd	nd	0.0819	nd	nd
ERK½ signalling	NAA	2.00	nd	0.0375	nd	nd	-0.1297	nd	nd	0.1327	0.1137	nd
Glutamate Signalling	NAG	2.04	nd	nd	nd	nd	-0.1373	nd	nd	0.0839	0.1575	nd
GABA/Glutamate metabolism	Glutamine	2.12	nd	nd	nd	nd	nd	nd	0.0959	0.1067	0.0875	nd

Table 4.7 Continued. Summarised table showing significant metabolites and pathways detected by ¹H-NMR analysis to be involved in the action of *Ficus* fractions on uterine contraction.

GABA =gamma aminobutyric acid; **NA** = nucleic acid; **aa** = amino acid; **TCA** = tricarboxylic acid cycle; **cAMP** = cyclic adenosine monophosphate; **MI** = myoinositol; **PC** = phosphatidylcholine; **PS**= phosphatidylserine; **PGF1**= prostaglandinF1; **PHE** = phenylalanine; **PE**= phosphatidylethanolamine; **AEA** = anandamide; **U** = unknown; **DAG** = diacylglycerol; **ATP** = adenosinetriphosphate; **NA** = nucleic acid; **ERK** = extracellular signal regulated kinase; **RhoA** = Ras homolog gene family, member A, **mTOR** = mammalian target of rapamycin; **NAA** = N-acetylaspartate; **nd** = not detected

Pathway	Metabolome	Shift (ppm)	E1		F14		F4-31		F6.17		F28	
			p[1]Tissues	p[1]Fluids	p[1]Tissues	p[1]Fluids	p[1]Tissues	p[1]Fluids	p[1]Tissues	p[1]Fluids	p[1]Tissues	p[1]Fluids
Glutamate Signalling	Glutamate	2.44	nd	nd	nd	nd	nd	nd	nd	nd	nd	nd
ERK½ signalling	NAA	2.48	nd	nd	nd	nd	nd	nd	0.0312	nd	0.029	nd
ERK½ signalling	Aspartate	2.64	nd	nd	0.1222	0.0403	0.2028	nd	nd	0.1027	nd	0.3735
ERK½ signalling	Aspartate	2.68	0.0259	nd	0.0803	nd	0.1535	nd	0.0792	nd	nd	0.1428
GABA Signalling	N-acetylaspartylglutamate	2.72	0.0397	0.1096	0.0821	nd	nd	0.0552	nd	nd	nd	0.1011
ERK½ signalling	Aspartate	2.80	0.0404	nd	nd	nd	nd	nd	nd	-0.0553	0.062	nd
Endocannabinoid Signalling	AEA	2.84	0.0309	nd	nd	nd	nd	nd	nd	-0.0874	0.0549	nd
GABA Signalling	GABA	3.00	nd	nd	nd	nd	nd	0.0699	nd	-0.1127	nd	nd
Catecholamine Synthesis	Tyrosine	3.04	nd	-0.2807	nd	-0.2773	nd	-0.3466	nd	-0.2621	nd	-0.2871
Endocannabinoid Signalling	AEA	3.40	nd	-0.1024	0.2413	nd	nd	-0.1451	nd	-0.1539	nd	-0.1446
Endocannabinoid Signalling	AEA	3.44	nd	-0.1316	nd	0.3187	nd	-0.1849	0.3265	nd	nd	-0.129

Table 4.7 Continued. Summarised table showing significant metabolites and pathways detected by ¹H-NMR analysis to be involved in the action of *Ficus* fractions on uterine contraction.

GABA =gamma aminobutyric acid; **NA** = nucleic acid; **aa** = amino acid; **TCA** = tricarboxylic acid cycle; **cAMP** = cyclic adenosine monophosphate; **MI** = myoinositol; **PC** = phosphatidylcholine; **PS**= phosphatidylserine; **PGF1**= prostaglandinF1; **PHE** = phenylalanine; **PE**= phosphatidylethanolamine; **AEA** = anandamide; **U** = unknown; **DAG** = diacylglycerol; **ATP** = adenosinetriphosphate; **NA** = nucleic acid; **ERK** = extracellular signal regulated kinase; **RhoA** = Ras homolog gene family, member A, **mTOR** = mammalian target of rapamycin; **NAA** = N-acetylaspartate; **nd** = not detected

Pathway	Metabolome	Shift (ppm)	E1		F14		F4-31		F6.17		F28	
			p[1]Tissues	p[1]Fluids	p[1]Tissues	p[1]Fluids	p[1]Tissues	p[1]Fluids	p[1]Tissues	p[1]Fluids	p[1]Tissues	p[1]Fluids
Catecholamine Synthesis	PHE	3.96	nd	nd	-0.03	-0.0341	nd	nd	-0.0546	-0.0616	-0.0426	nd
Endocannabinoid Signalling	PC	4.04	nd	nd	-0.0436	nd	nd	nd	nd	nd	nd	nd
RhoA/Rho-kinase/mTOR Signalling	Threonine	4.24	nd	-0.0915	-0.1796	-0.107	nd	-0.1075	-0.1922	-0.115	nd	-0.0833
NA Metabolism	ATP	4.28	nd	-0.21	-0.2413	-0.2047	-0.3187	-0.2665	-0.2531	-0.1326	-0.2162	-0.1936
RhoA/Rho-kinase/mTOR Signalling	Threonine	4.32	0.4685	nd	-0.2134	nd	-0.246	-0.0358	-0.2249	nd	0.0789	nd
RhoA/Rho-kinase/mTOR Signalling	Threonine	4.36	0.293	nd	-0.2043	nd	nd	nd	-0.2186	-0.067	0.057	0.202
RhoA/Rho-kinase/mTOR Signalling	Threonine	4.40	nd	nd	-0.2042	nd	nd	0.0764	-0.218	-0.0636	0.0364	nd

Table 4.7 Continued. A summarised table showing significant metabolites and pathways detected by ¹H-NMR analysis to be involved in the action of *Ficus* fractions on uterine contraction.

GABA =gamma aminobutyric acid; **NA** = nucleic acid; **aa** = amino acid; **TCA** = tricarboxylic acid cycle; **cAMP** = cyclic adenosine monophosphate; **MI** = myoinositol; **PC** = phosphatidylcholine; **PS**= phosphatidylserine; **PGF1**= prostaglandin F₁; **PHE** = phenylalanine; **PE**= phosphatidylethanolamine; **AEA** = anandamide; **U** = unknown; **DAG** = diacylglycerol; **ATP** = adenosinetriphosphate; **NA** = nucleic acid; **ERK** = extracellular signal regulated kinase; **RhoA** = Ras homolog gene family, member A, **mTOR** = mammalian target of rapamycin; **NAA** = N-acetylaspartate; **nd** = not detected

Pathway	Metabolome	Shift (ppm)	E1		F14		F4-31		F6.17		F28	
			p[1]Tissues	p[1]Fluids	p[1]Tissues	p[1]Fluids	p[1]Tissues	p[1]Fluids	p[1]Tissues	p[1]Fluids	p[1]Tissues	p[1]Fluids
DAG Signalling	DAG	5.08	0.0575	nd	-0.0223	nd	nd	-0.0189	nd	-0.038	nd	nd
DAG Signalling	DAG	5.12	0.0597	nd	nd	nd	nd	nd	nd	-0.038	nd	nd
DAG Signalling	DAG	5.16	0.0492	nd	-0.0088	nd	nd	nd	nd	-0.0369	nd	nd
cAMP synthesis/NA Metabolism	Adenosine	5.20	0.0414	nd	nd	nd	nd	nd	nd	-0.0334	0.0302	nd
cAMP synthesis/NA Metabolism	Adenosine	5.24	0.0387	nd	-0.0075	nd	nd	nd	nd	-0.029	nd	nd
MI Signalling	MI	5.28	nd	nd	-0.0127	nd	nd	nd	-0.0158	-0.0227	nd	nd
Endocannabinoid Signalling	AEA	5.32	nd	nd	nd	nd	nd	nd	nd	-0.0157	nd	nd
Endocannabinoid Signalling	AEA	5.36	nd	nd	nd	nd	nd	-0.02	nd	nd	0.1111	nd
cAMP Signalling	AMP	5.40	0.0553	nd	nd	nd	0.054	nd	nd	nd	0.1165	nd
Endocannabinoid Signalling	AEA	5.44	0.0377	nd	nd	nd	0.0361	nd	nd	nd	0.0871	nd
cAMP Signalling	Adenosine	5.48	0.0277	nd	nd	nd	0.0233	nd	nd	nd	0.0568	nd

Table 4.7 Continued. Summarised table showing significant metabolites and pathways detected by ¹H-NMR analysis to be involved in the action of *Ficus* fractions on uterine contraction.

GABA =gamma aminobutyric acid; **NA** = nucleic acid; **aa** = amino acid; **TCA** = tricarboxylic acid cycle; **cAMP** = cyclic adenosine monophosphate; **MI** = myoinositol; **PC** = phosphatidylcholine; **PS**= phosphatidylserine; **PGF1**= prostaglandinF1; **PHE** = phenylalanine; **PE**= phosphatidylethanolamine; **AEA** = anandamide; **U** = unknown; **DAG** = diacylglycerol; **ATP** = adenosinetriphosphate; **NA** = nucleic acid; **ERK** = extracellular signal regulated kinase; **RhoA** = Ras homolog gene family, member A, **mTOR** = mammalian target of rapamycin; **NAA** = N-acetylaspartate; **nd** = not detected

Pathway	Metabolome	Shift (ppm)	E1		F14		F4-31		F6.17		F28	
			p[1]Tissues	p[1]Fluids	p[1]Tissues	p[1]Fluids	p[1]Tissues	p[1]Fluids	p[1]Tissues	p[1]Fluids	p[1]Tissues	p[1]Fluids
Endocannabinoid Signalling	AEA	5.88	nd	nd	-0.0083	nd	nd	-0.0378	nd	nd	nd	nd
cAMP Signalling	Adenosine	5.92	nd	nd	nd	nd	0.0393	nd	nd	nd	nd	nd
Catecholamine Synthesis	Tyrosine	6.00	nd	nd	nd	nd	0.0201	nd	0.0309	nd	nd	nd
Catecholamine Synthesis	Tyrosine	6.16	nd	nd	-0.0081	nd	nd	nd	nd	nd	nd	nd
Catecholamine Synthesis	Tyrosine	7.00	nd	nd	-0.0074	nd	nd	nd	nd	nd	nd	nd
Catecholamine synthesis	PHE	7.24	-0.0229	nd	-0.0101	nd	nd	nd	nd	0.107	nd	nd
Catecholamine Synthesis	PHE	7.32	nd	nd	nd	nd	nd	nd	nd	0.0983	nd	nd
Serotonin Signalling	Tryptophan	7.72	-0.0177	nd	nd	nd	nd	nd	nd	nd	nd	nd
GABA Signalling	GABA	2.28	nd	nd	0.0417	nd	nd	nd	nd	-0.058	0.0536	nd

Table 4.7 Continued. Summarised table showing significant metabolites and pathways detected by ¹H-NMR analysis to be involved in the action of *Ficus* fractions on uterine contraction.

Pathway	Metabolome	Shift (ppm)	E1		F14		F4-31		F6.17		F28	
			p[1]Tissues	p[1]Fluids	p[1]Tissues	p[1]Fluids	p[1]Tissues	p[1]Fluids	p[1]Tissues	p[1]Fluids	p[1]Tissues	p[1]Fluids
Glutamine Signalling	Glutamine	2.44	nd	0.0468	nd	nd	nd	0.0429	0.0508	nd	0.037	nd
MI Signalling	MI	4.96	nd	nd	-0.0371	nd	nd	nd	-0.0384	nd	nd	nd
MI Signalling	DAG	5.00	0.06	nd	-0.0312	nd	nd	nd	-0.0316	nd	nd	nd
NA Metabolism	ATP	4.60	-0.1466	nd	-0.1584	nd	-0.1844	0.0301	-0.1668	nd	-0.1413	nd
NA Metabolism	ATP	4.64	-0.1711	nd	-0.1515	0.0292	-0.2034	nd	-0.1609	nd	-0.1361	nd
MI Signalling	MI	4.92	-0.1802	0.0197	-0.0479	nd	nd	nd	-0.0492	nd	-0.0429	-0.2113
MI Signalling	MI	3.60	nd	nd	0.064	nd	nd	-0.2344	nd	-0.2436	-0.0345	nd
Endocannabinoid Signalling	Serine	3.84	nd	nd	nd	nd	nd	nd	nd	-0.0631	nd	nd
DAG Signalling	DAG	5.04	0.0524	nd	-0.0258	nd	nd	-0.0509	nd	-0.0412	nd	nd
cAMP synthesis/NA Metabolism	Adenosine	5.56	0.0236	nd	-0.0053	nd	0.0181	nd	nd	nd	nd	nd
Prostanoid Signalling	PGF ₁	5.76	nd	-0.0644	-0.0785	nd	nd	-0.0826	0.0691	nd	nd	nd
Prostanoid Signalling	PGF ₁	5.80	nd	nd	-0.0335	nd	nd	nd	nd	nd	nd	nd
Glutamate Signalling	Glutamate	2.16	nd	nd	nd	nd	0.0313	nd	nd	-0.032	nd	nd
cAMP synthesis/NA Metabolism	Adenosine	5.52	0.0271	nd	nd	nd	nd	nd	nd	nd	nd	nd
Catecholamine Synthesis	Tyrosine	3.92	nd	nd	-0.022	nd	nd	nd	-0.0328	-0.0665	nd	nd
DAG Signalling	DAG	2.20	0.0272	nd	nd	nd	0.0403	nd	nd	-0.038	nd	nd

4.8.1 ¹H-NMR Multivariate Analysis of the fractions of *F. exasperata*

The ¹H-NMR data obtained for the fractions tested on uterine contractility were subjected to multivariate analysis. Clear separations between the control and treated groups were observed in the OPLSDA score plots of all fractions tested (Fig. 4.26, 4.28, 4.30, 4.32, 4.34, 4.36, 4.38, 4.40, 4.42, and 4.44). Several metabolites were detected and the significant metabolites are listed in Table 4.7.

From the analysis of **E1**-treated groups, cAMP, DAG and endocannabinoid signalling were detected in the treated groups while MI and nucleic acid signalling were detected in the control groups (Fig. 4.27 and 4.29). Anandamide (AEA), DAG, and adenosine were significantly upregulated in the uterine tissues, this was similarly detected in the bath fluids but in addition glutamate, N-acetylaspartate and MI were also upregulated (Table 4.7). Some metabolites were also detected to have been downregulated in the tissues, these included phenylalanine, tryptophan, adenosinetriphosphate (ATP) and MI, while metabolites found to have been downregulated in the bath fluids in which the uterine tissues were immersed included tyrosine, ATP, and threonine.

For **F14** groups, endocannabinoid signalling was detected in both control and treated groups (Fig. 4.31 and 4.33). In addition, GABA signalling was detected in the treated groups while MI and catecholamine signalling in the control (Fig. 4.31 and 4.33). Other specific metabolites detected by NMR in the **F14** treated groups included AEA, aspartate, and GABA which were upregulated in the tissues; aspartate was similarly detected to have been upregulated in the bath fluids. In addition, DAG, AA, phenylalanine, phosphatidylcholine, threonine, tyrosine and prostaglandin F₁ were detected to have been downregulated in the tissues these were similarly

observed in the bath fluids but in addition, adenosine and MI were also downregulated (Table 4.7).

For **F4-31** groups, endocannabinoids signalling was also found in both control and treated groups (Fig. 4.35 and Fig. 4.37). GABA signalling was detected in the control while catecholamine and cAMP signalling were detected in the treated groups (Fig. 4.35 and Fig. 4.37). Other metabolites detected included adenosine, glutamate, DAG, adenosine monophosphate, AEA, and aspartate which were upregulated in the tissues while glutamine, ATP and GABA were detected as upregulated in the bath fluids. ATP and AA were observed to have been downregulated in the tissues and in the bath fluids and in addition MI, DAG, prostaglandin F₁, AEA, threonine, were downregulated in the bath fluids (Table 4.7).

For **F6.17** groups, RhoA, nucleic acid, cAMP and nucleic acid signalling were detected in the control tissues (Fig. 4.39 and 4.41) while MI, RhoA and cAMP were detected in the control fluids (Fig. 4.39 and 4.41). Endocannabinoid and DAG signalling were detected in the treated tissues and bath fluids (Fig. 4.39 and Fig. 4.41). Glutamine and tyrosine were detected to have been upregulated in the uterine tissues while AEA, glutamate, aspartate, glutamine and phenylalanine were upregulated in the bath fluids (Table 4.7). AA, AEA, MI, DAG, ATP were detected to have been downregulated in the uterine tissues, these were similarly observed in the bath fluids but in addition GABA, tyrosine, phenylalanine and threonine were downregulated (Table 4.7).

For **F28** groups, nucleic acid, GABA, endocannabinoids and DAG signalling were detected in the control tissues while cAMP and also DAG signalling were

detected in the control group of bath fluids (Fig. 4.43 and Fig. 4.45). For the **F28** treated tissues cAMP, endocannabinoids and GABA signalling were detected while both GABA and endocannabinoids signalling were detected in the treated bath fluids (Fig. 4.43 and Fig. 4.45). Aspartate, glutamate, glutamine, adenosine, AEA and GABA were upregulated in the **F28**-treated uterine tissues while DAG, AEA and threonine were upregulated in the bath fluids (Table 4.7). DAG, AEA, AA, phenylalanine, ATP and MI were detected to have been downregulated in the tissues and these similarly occurred in the bath fluids in which the **F28** treated uterine tissues were immersed (Table 4.7).

Some intriguing observations were detected where one metabolite was upregulated in the tissues but downregulated in the bath fluids or vice versa. For **E1** some of those metabolites included DAG, which was upregulated in the tissues at 5.08, 5.12 and 5.16 ppm and in the bath fluids at 1.60 ppm but also downregulated in the bath fluids at 0.80 ppm (Table 4.7), other metabolites were AEA which was downregulated in the bath fluids at 3.40 and 3.44 pm but upregulated in the tissues at 1.80 ppm and 2.84 ppm; MI which was upregulated in the fluids but downregulated in the tissues at 4.92 ppm (Table 4.7). For **F14**, AEA was downregulated in the bath fluids but upregulated in the tissues at 1.80 ppm (Table 4.7). For **F4-31**, these included ATP which was downregulated in the tissues but upregulated in the tissues at 4.60 ppm and AEA which was upregulated in uterine tissues at 0.88 ppm and but downregulated in the bath fluids at 1.24 ppm (Table 4.7). It should be noted however, that at 4.28 ppm ATP was downregulated in both the tissues and bath fluids (Table 4.7). For **F6.17**, these included tyrosine which was upregulated in the tissues at 6.00 ppm and downregulated in the bath fluids at 3.04 ppm (Table 4.7). For **F28**,

AEA was found to have been upregulated in tissues at 1.28 ppm and 1.72 ppm in the tissues and bath fluids respectively but downregulated in the tissues at 0.88 and 1.36 ppm in the tissues and at 1.24 and at 1.24 ppm in the bath fluids (Table 4.7).

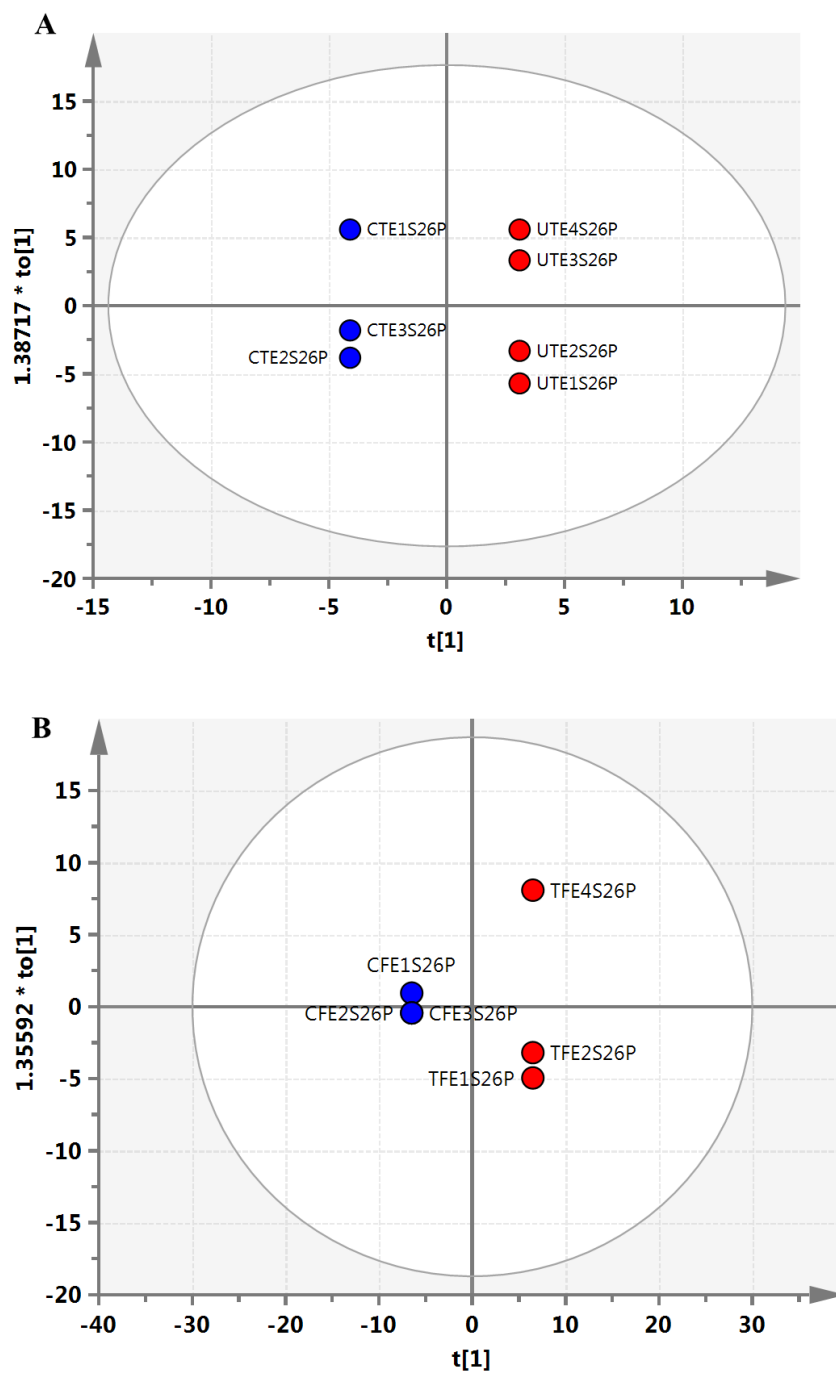


Figure 4.26 OPLSDA scatter plots showing ¹H-NMR analysis of polar **E1** treated uterine tissues (A) and those associated with the bath fluids. (B). The blue circles represent the control groups while the red circles represent the treated groups. n = 4 animals.

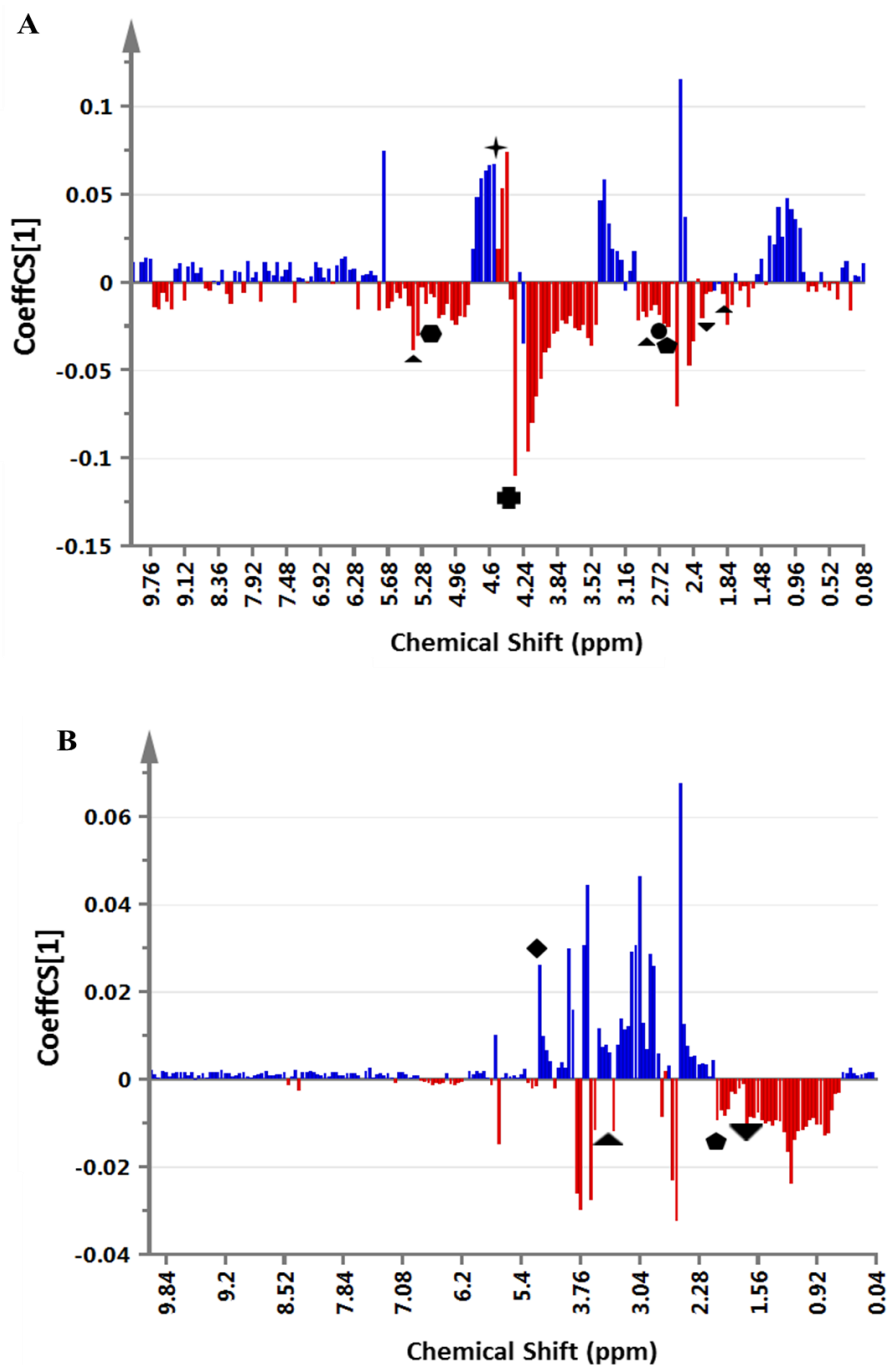


Figure 4.27 Correlation coefficient plots showing the distribution of metabolites in the NMR spectra of the polar **E1**-treated groups. Plot of NMR data for tissues are in A while plots for those associated with the bath fluids are in B. The blue columns represent the control groups and the red columns represent the treated groups. Significant metabolites have been highlighted and represented according to the corresponding pathways. ● = cAMP signalling; ▲ = endocannabinoid signalling; ▼ = DAG signalling/lipid metabolism; ◆ = aa metabolism/signalling; † = NA metabolism; ◆ = MI biosynthesis/signalling. These pathways were found to be strongly correlated with the action of **E1**. n= 4 animals.

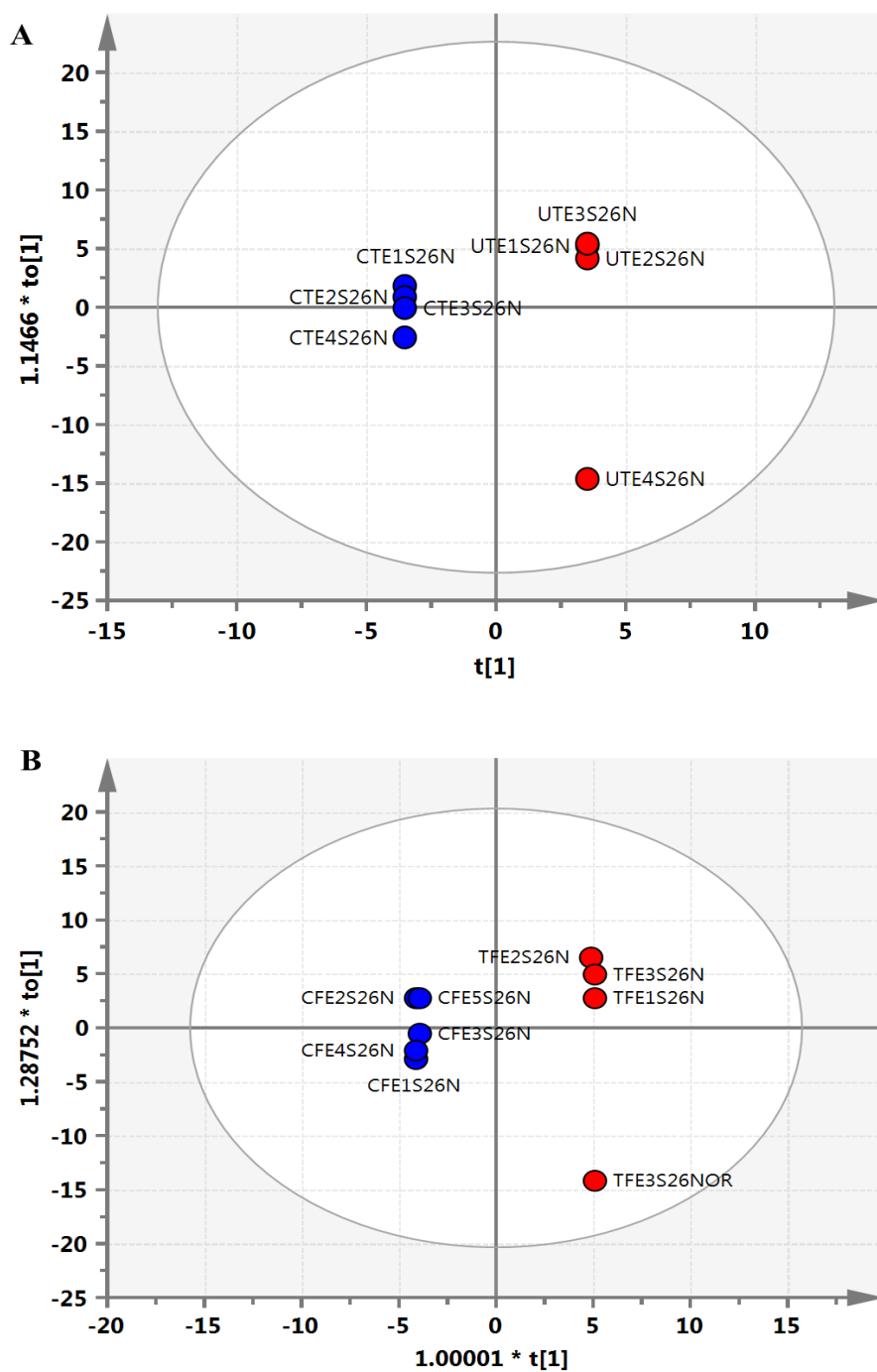


Figure 4.28 OPLSDA scatter plots showing $^1\text{H-NMR}$ analysis of non-polar **E1** treated uterine tissues (A) and those associated with the bath fluids (B). The blue circles represent the control groups while the red circles represent the treated groups. Successful separation was achieved between both groups. $n = 4$ animals.

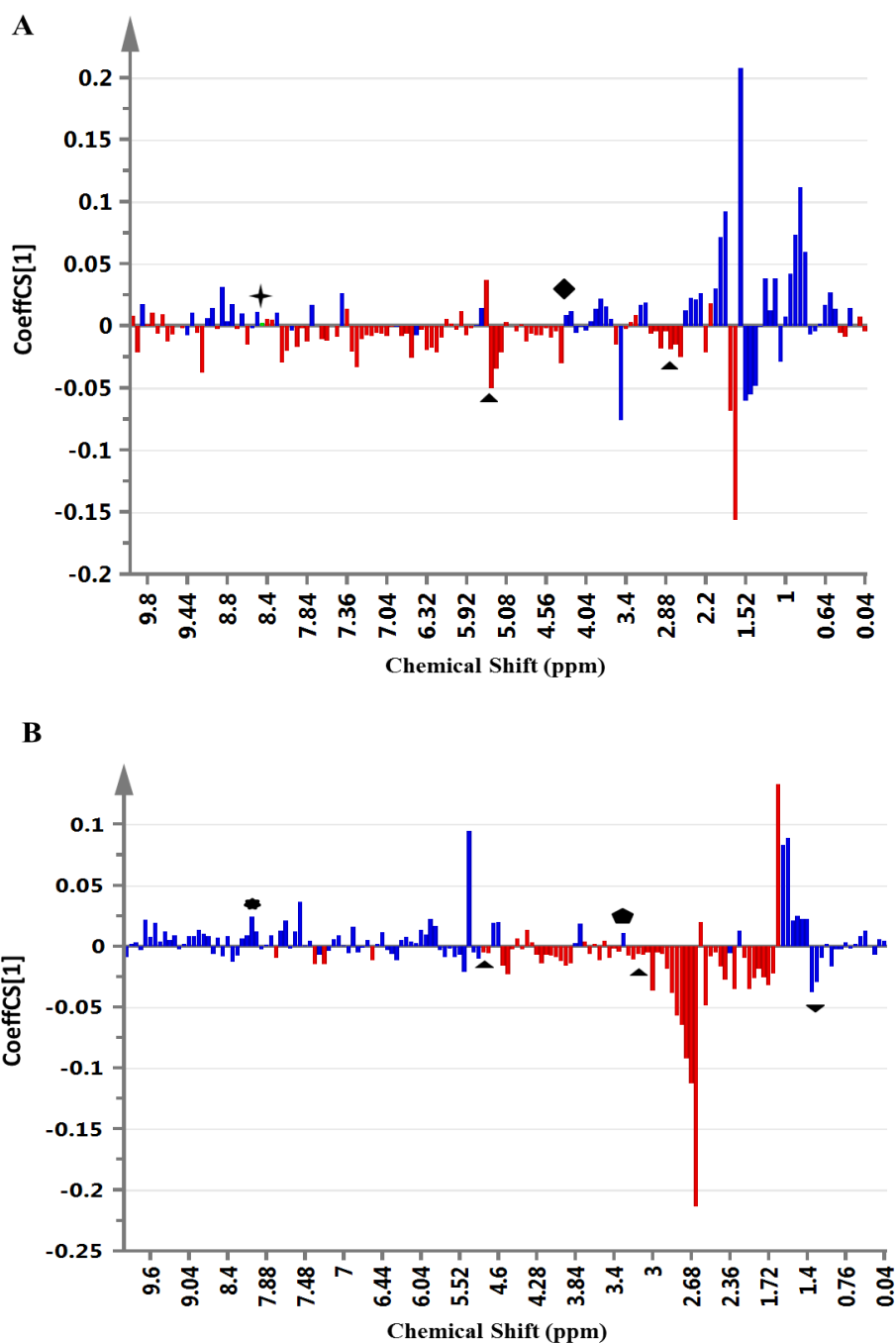


Figure 4.29 Correlation coefficient plots showing the distribution of metabolites in the NMR spectra of the non-polar **E1**-treated groups. Plot of NMR data for tissues are in A while plots for those associated with the bath fluids are in B. The blue columns represent the control groups and the red columns represent the treated groups. Significant metabolites have been highlighted and represented according to the corresponding pathways. \blacklozenge = cAMP Metabolism; \blacktriangleup = endocannabinoid metabolism; \blacktriangledown = DAG signalling/lipid metabolism; \blackstar = NA metabolism; \bullet = GABA signalling; \blacklozenge = MI biosynthesis/signalling; \bullet = serotonin signalling. These pathways were found to be strongly correlated with the action of **E1**. n= 4 animals.

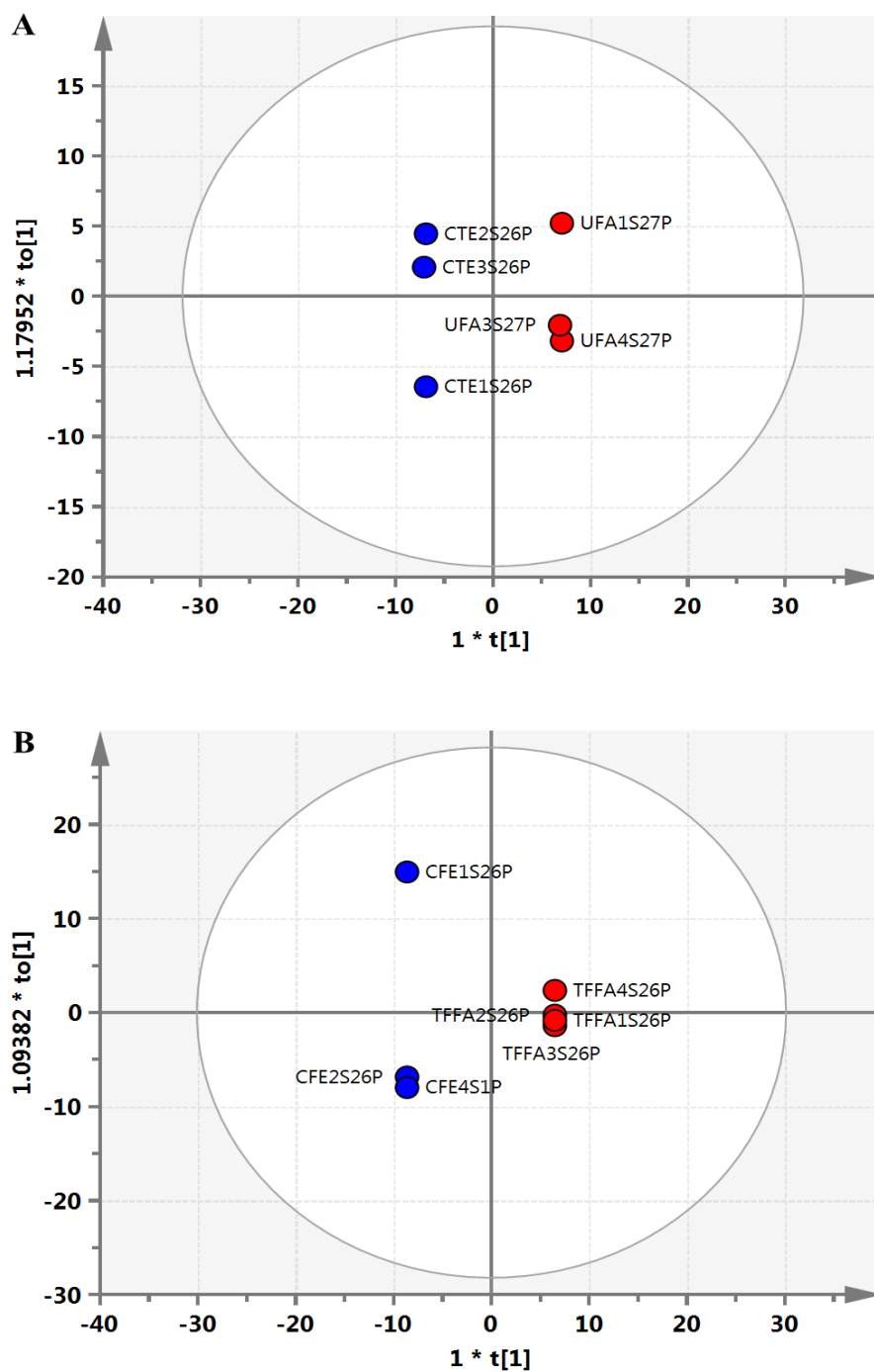


Figure 4.30 OPLSDA score plots showing $^1\text{H-NMR}$ analysis of polar **F14** treated uterine tissues (A) and those associated with the bath fluids (B). The blue circles represent the control groups while the red circles represent the treated groups. Successful separation was achieved between both groups. $n = 4$ animals.

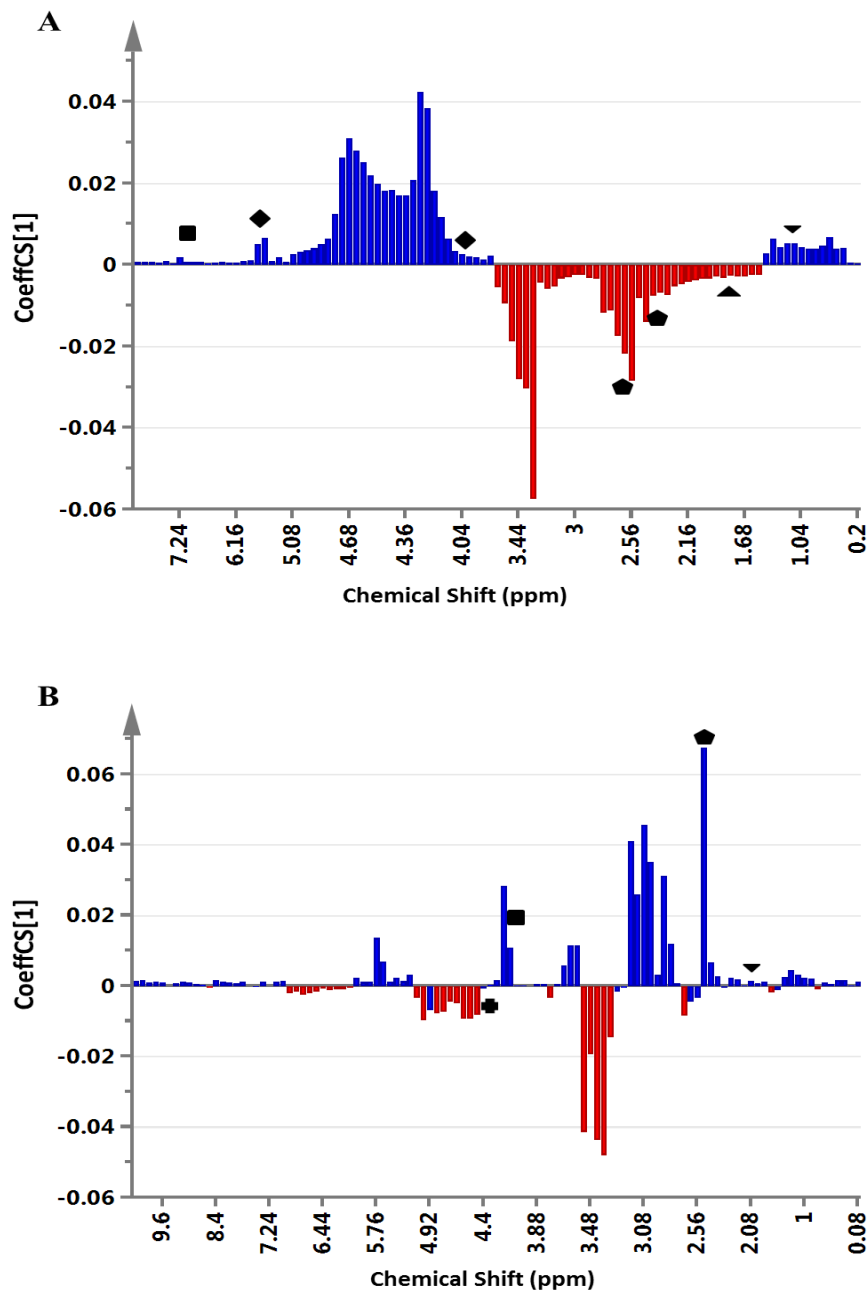


Figure 4.31 Correlation coefficient plots showing the distribution of metabolites in the NMR spectra of the polar **F14**-treated groups. Plot of NMR data for tissues are in A while plots for those associated with the bath fluids are in B. The blue columns represent the control groups and the red columns represent the treated groups. Significant metabolites have been highlighted and represented according to the corresponding pathways. \blacklozenge = cAMP signalling; \blacktriangle = endocannabinoid signalling; \blacktriangledown = DAG signalling/lipid metabolism; \blackcross = NA metabolism; \blacklozenge = MI biosynthesis/signalling; \blacksquare = RhoA signalling; \blacksquare = catecholamine signalling; \blacklozenge = GABA signalling. These pathways were found to be strongly correlated with the action of **F14**. n= 4 animals.

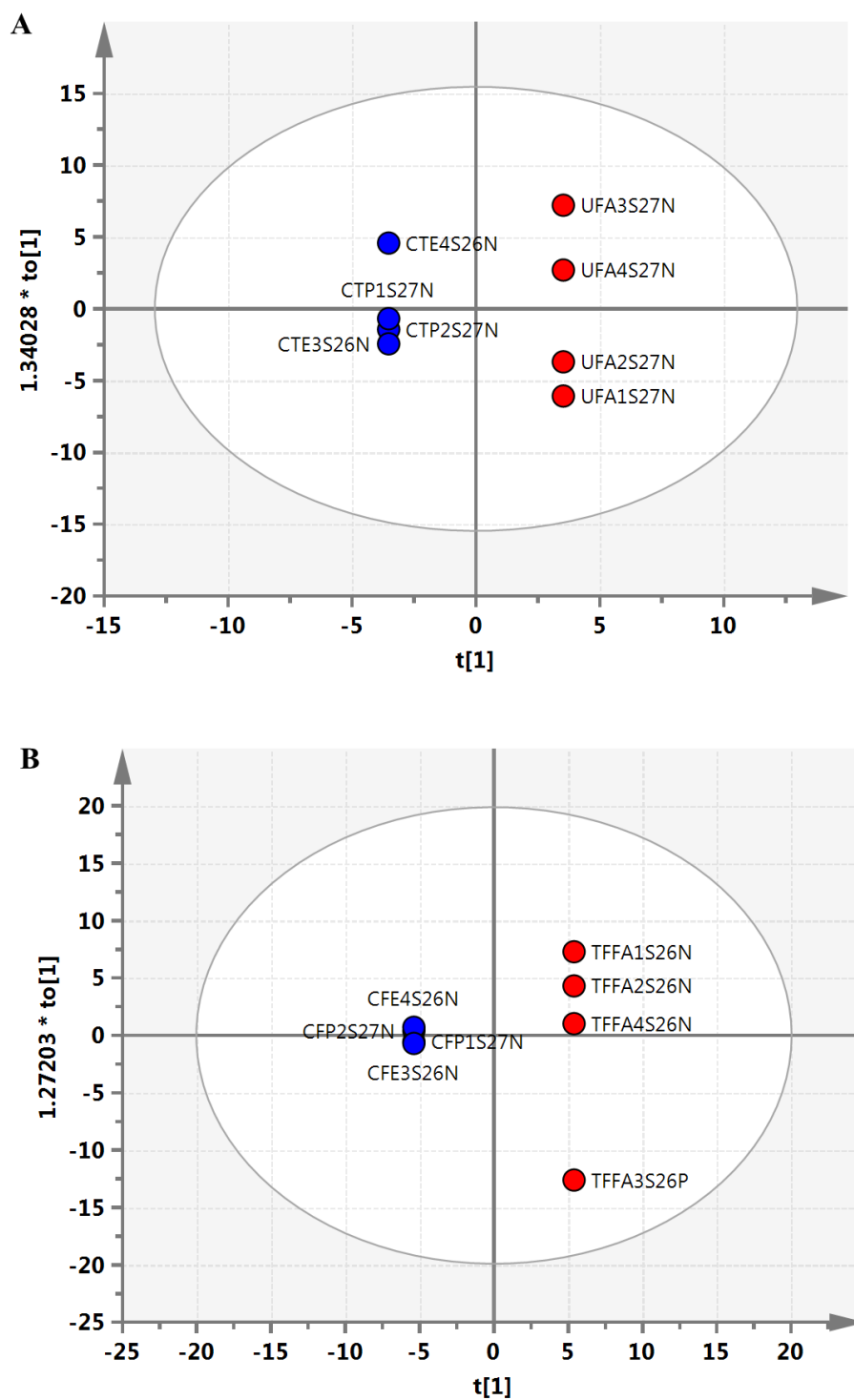


Figure 4.32 OPLSDA score plots showing $^1\text{H-NMR}$ analysis of non-polar **F14** treated uterine tissues (A) and those associated with the bath fluids (B). The blue circles represent the control groups while the red circles represent the treated groups. Successful separation was achieved between both groups. $n = 4$ animals.

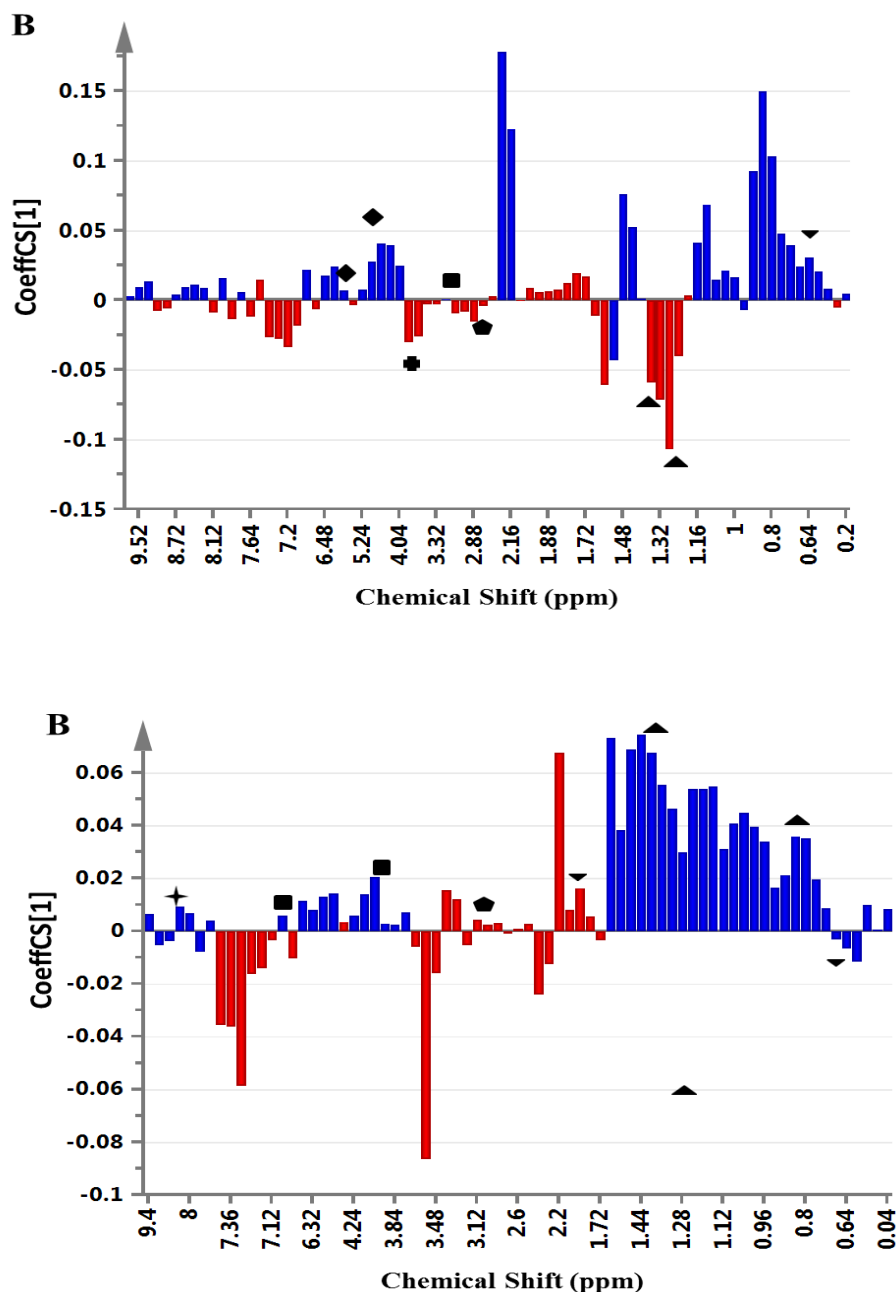


Figure 4.33 Correlation coefficient plots showing the distribution of metabolites in the NMR spectra of the non-polar **F14**-treated groups. Plot of NMR data for tissues are in A while plots for those associated with the bath fluids are in B. The blue columns represent the control groups and the red columns represent the treated groups. Significant metabolites have been highlighted and represented according to the corresponding pathways. ◆ = cAMP signalling; ▲ = endocannabinoid signalling; ▼ = DAG signalling/lipid metabolism; + = NA metabolism; ◆ = MI biosynthesis/signalling; ■ = RhoA signalling; ■ = catecholamine signalling; ◆ = GABA signalling. These pathways were found to be strongly correlated with the action of **F14**. n= 4 animals.

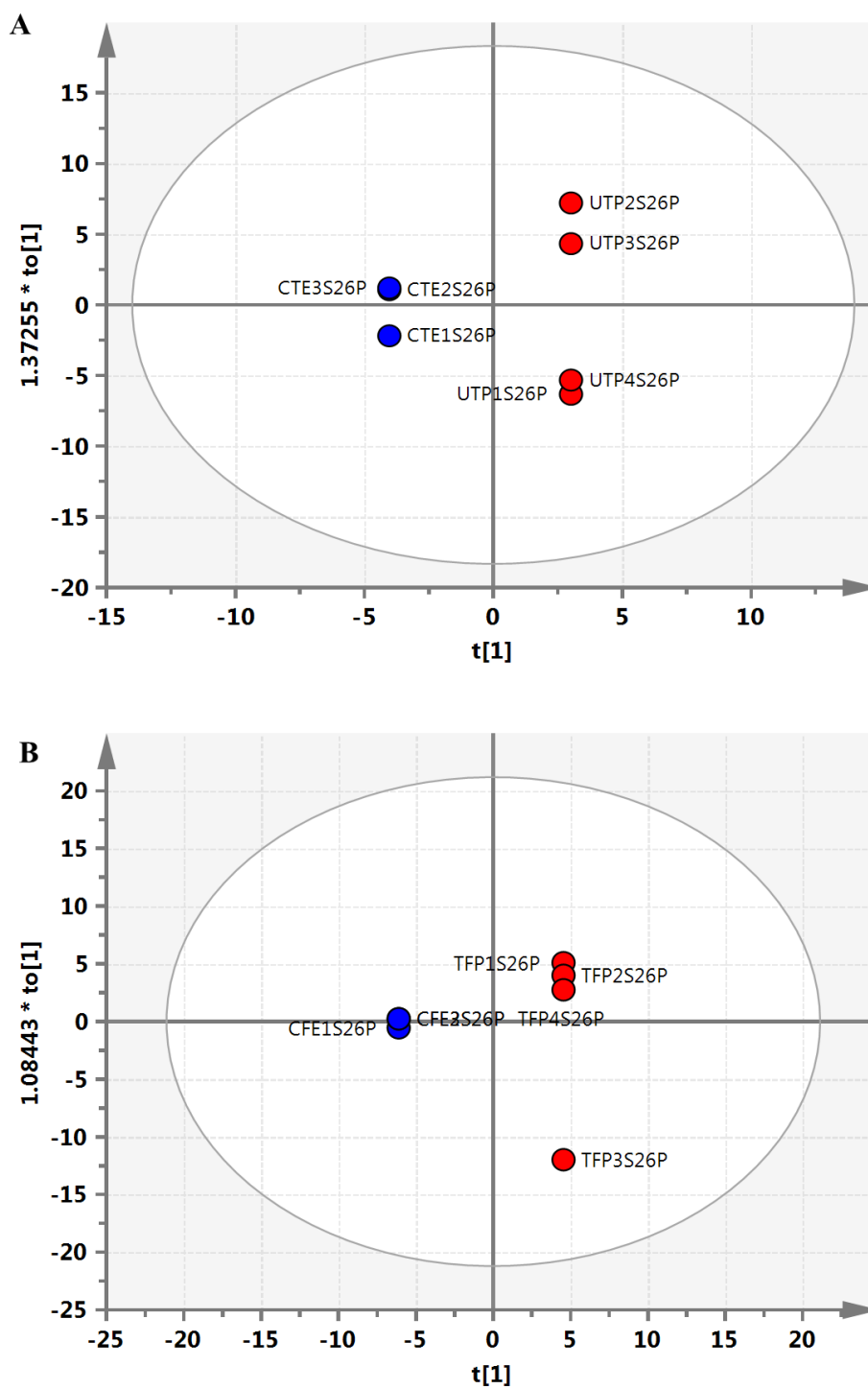


Figure 4.34 OPLSDA score plots showing $^1\text{H-NMR}$ analysis of polar **F4-31** treated uterine tissues (A) and those associated with the bath fluids (B). The blue circles represent the control groups while the red circles represent the treated groups. Successful separation was achieved between both groups. $n = 4$ animals.

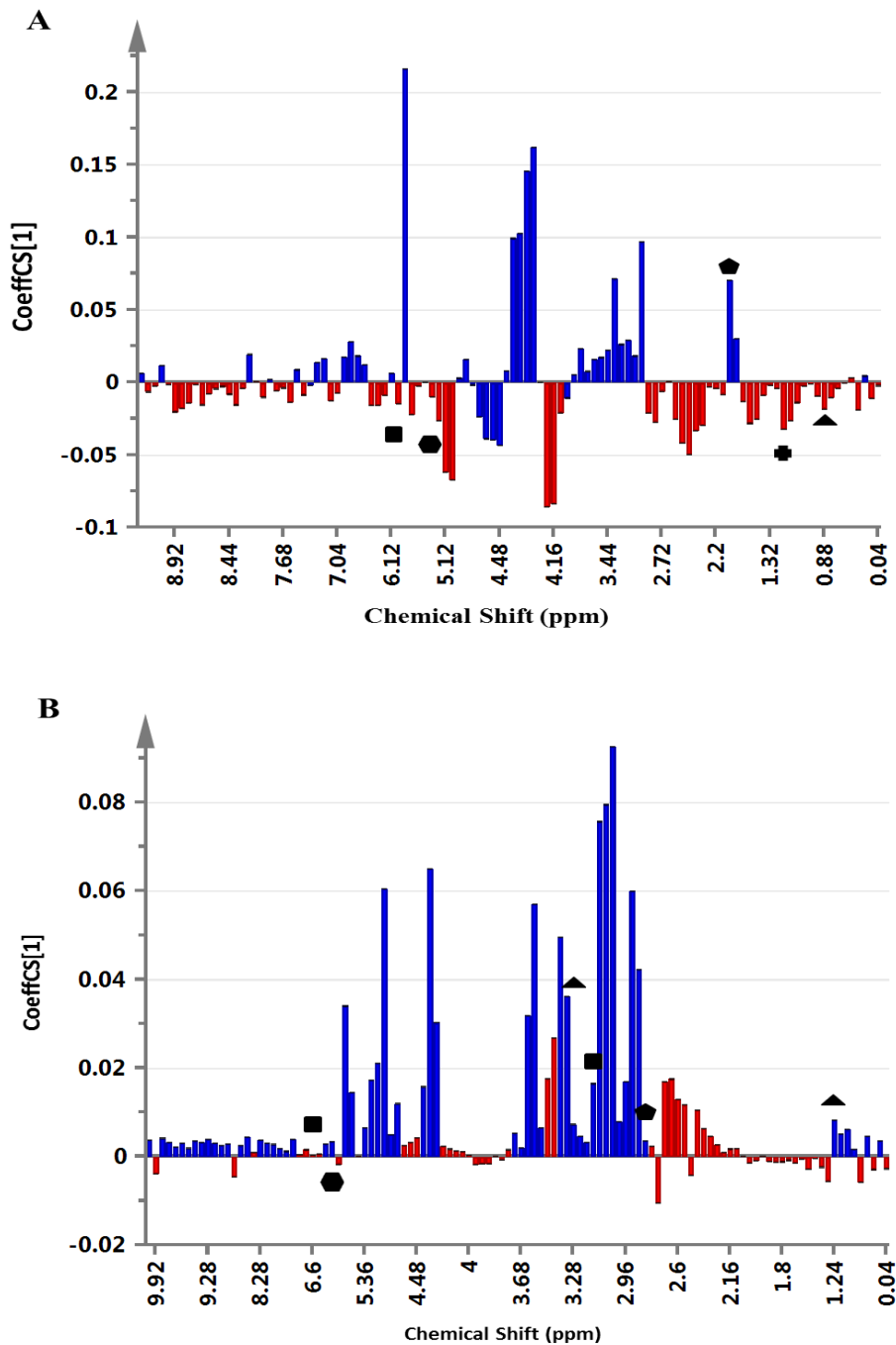


Figure 4.35 Correlation coefficient plots showing the distribution of metabolites in the NMR spectra of the polar **F4-31**-treated groups. Plot of NMR data for tissues are in A while plots for those associated with the bath fluids are in B. The blue columns represent the control groups and the red columns represent the treated groups. Significant metabolites have been highlighted and represented according to the corresponding pathways. ● = cAMP signalling; ▲ = endocannabinoid signalling; ▼ = DAG signalling/lipid metabolism; ✦ = NA metabolism; ◆ = MI biosynthesis/signalling; ■ = RhoA signalling; ■ = catecholamine signalling; ⬠ = GABA signalling. These pathways were found to be strongly correlated with the action of **F4-31**. n = 4 animals.

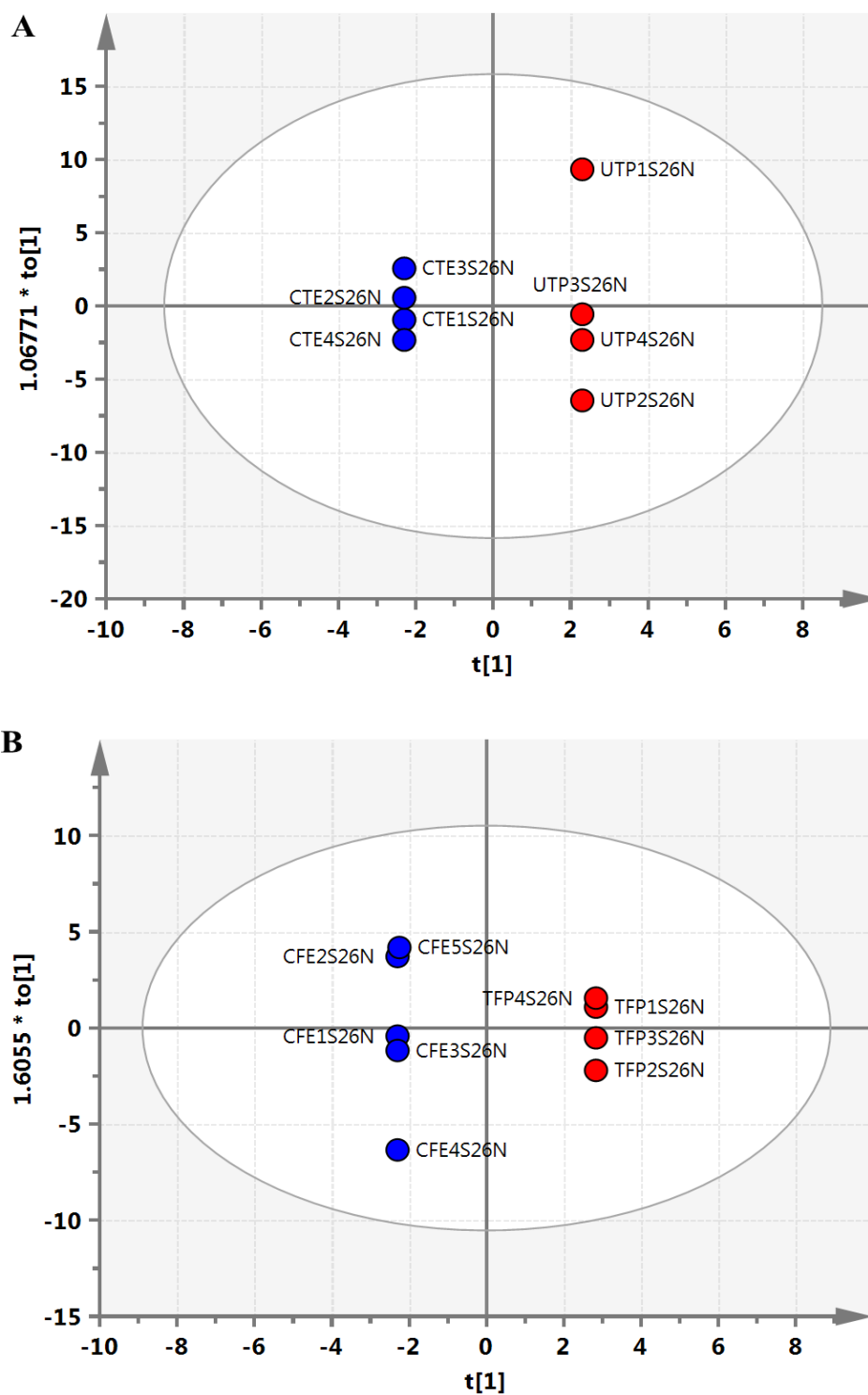


Figure 4.36 OPLSDA score plots showing $^1\text{H-NMR}$ analysis of non-polar **F4-31** treated uterine tissues (A) and those associated with the bath fluids (B). The blue circles represent the control groups while the red circles represent the treated groups. Successful separation was achieved between both groups. $n = 4$ animals.

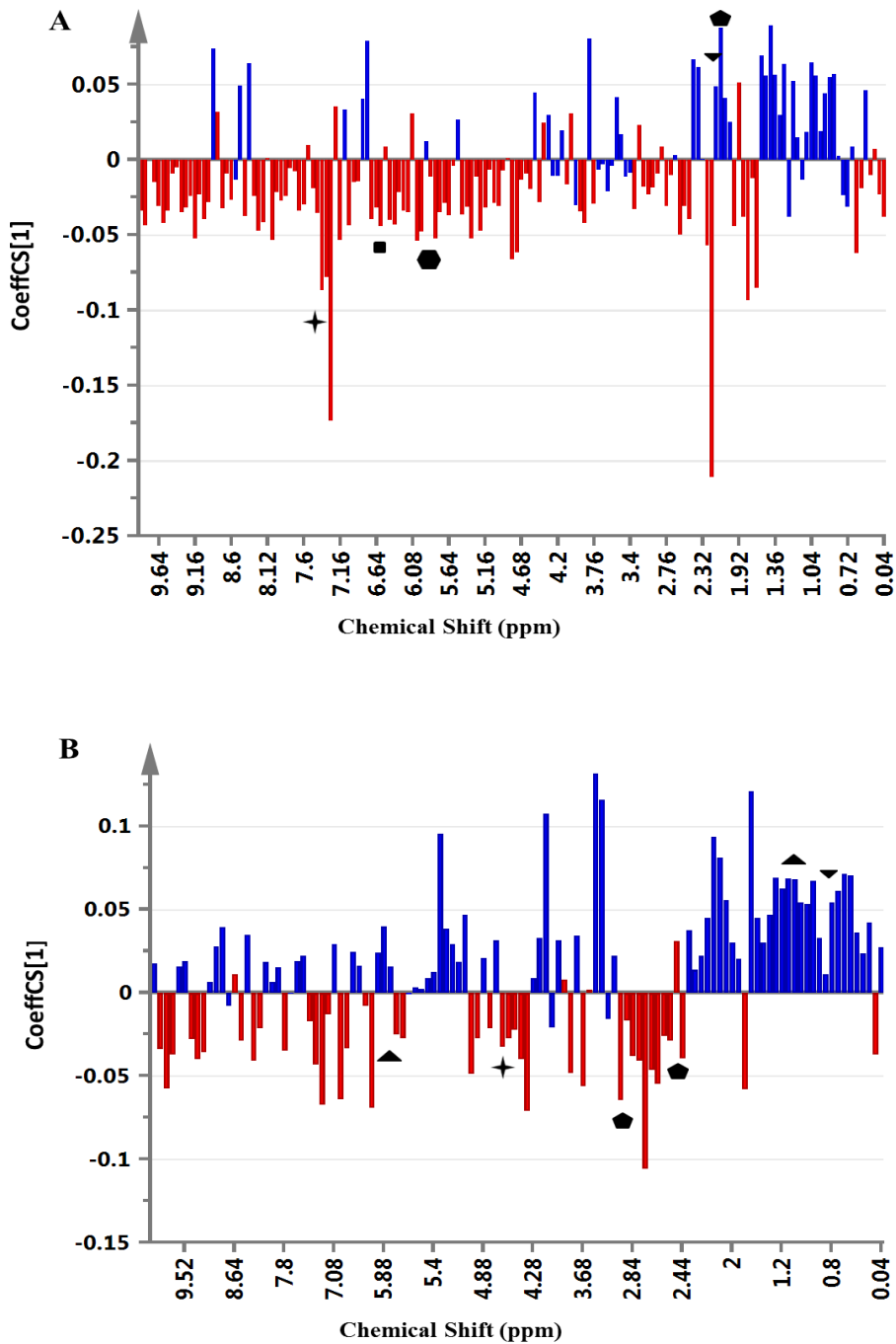


Figure 4.37 Correlation coefficient plots showing the distribution of metabolites in the NMR spectra of the non-polar **F4-31**-treated groups. The plot of NMR data for tissues are in A while the plot for those associated with the bath fluids are in B. The blue columns represent the control groups and the red columns represent the treated groups. Significant metabolites have been highlighted and represented according to the corresponding pathways. \blacklozenge = cAMP signalling; \blacktriangleup = endocannabinoid signalling; \blacktriangledown = DAG signalling/lipid metabolism; \blackplus = NA metabolism; \blacklozenge = MI biosynthesis/signalling; \blacksquare = catecholamine signalling; \blacklozenge = GABA signalling. These pathways were found to be strongly correlated with the action of **F4-31**. n= 4 animals.

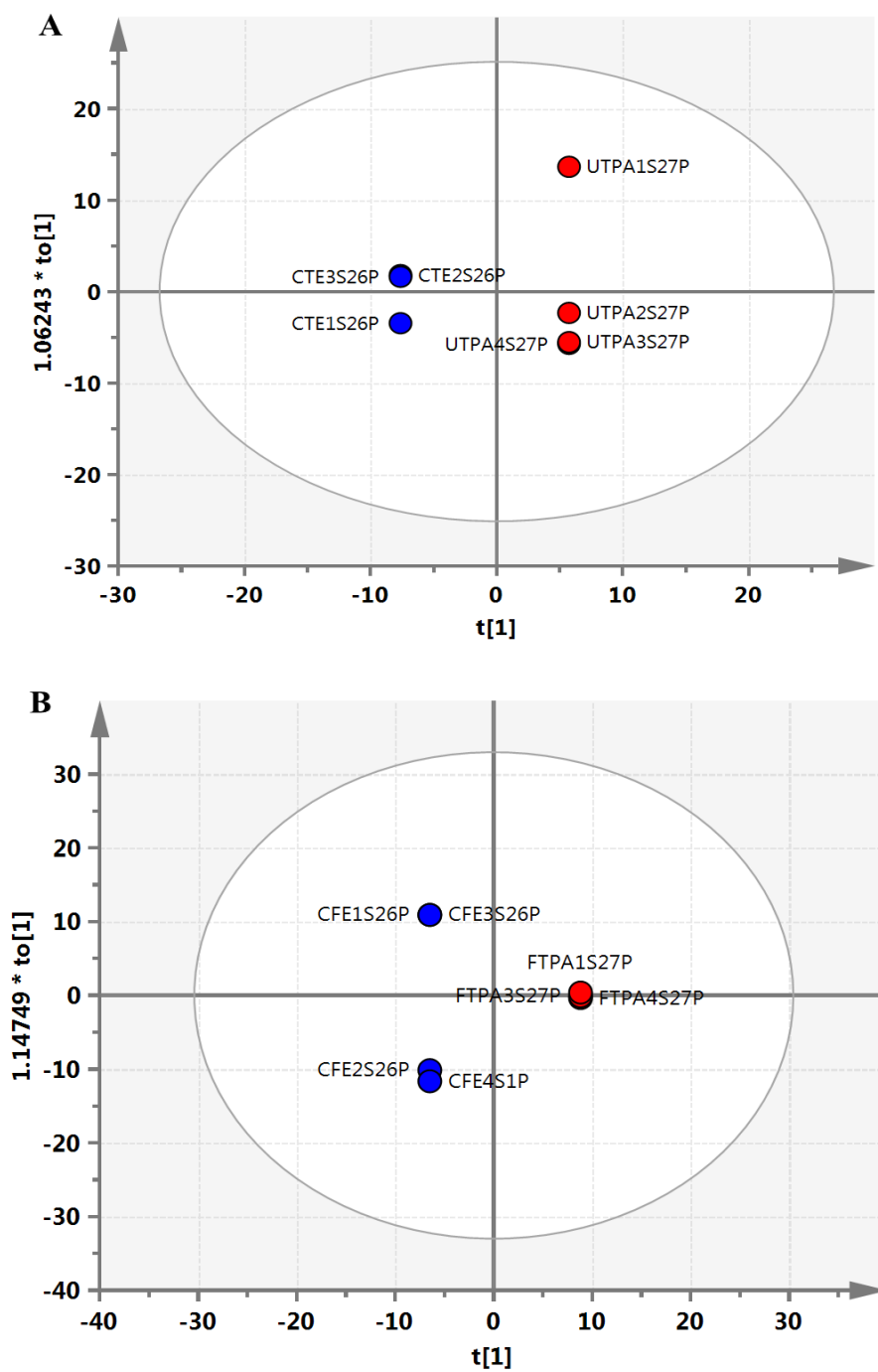


Figure 4.38 OPLSDA score plots showing $^1\text{H-NMR}$ analysis of polar **F6.17** treated uterine tissues (A) and bath fluids (B). The blue circles represent the control groups while the red circles represent the treated groups. Successful separation was achieved between both groups. $n = 4$ animals.

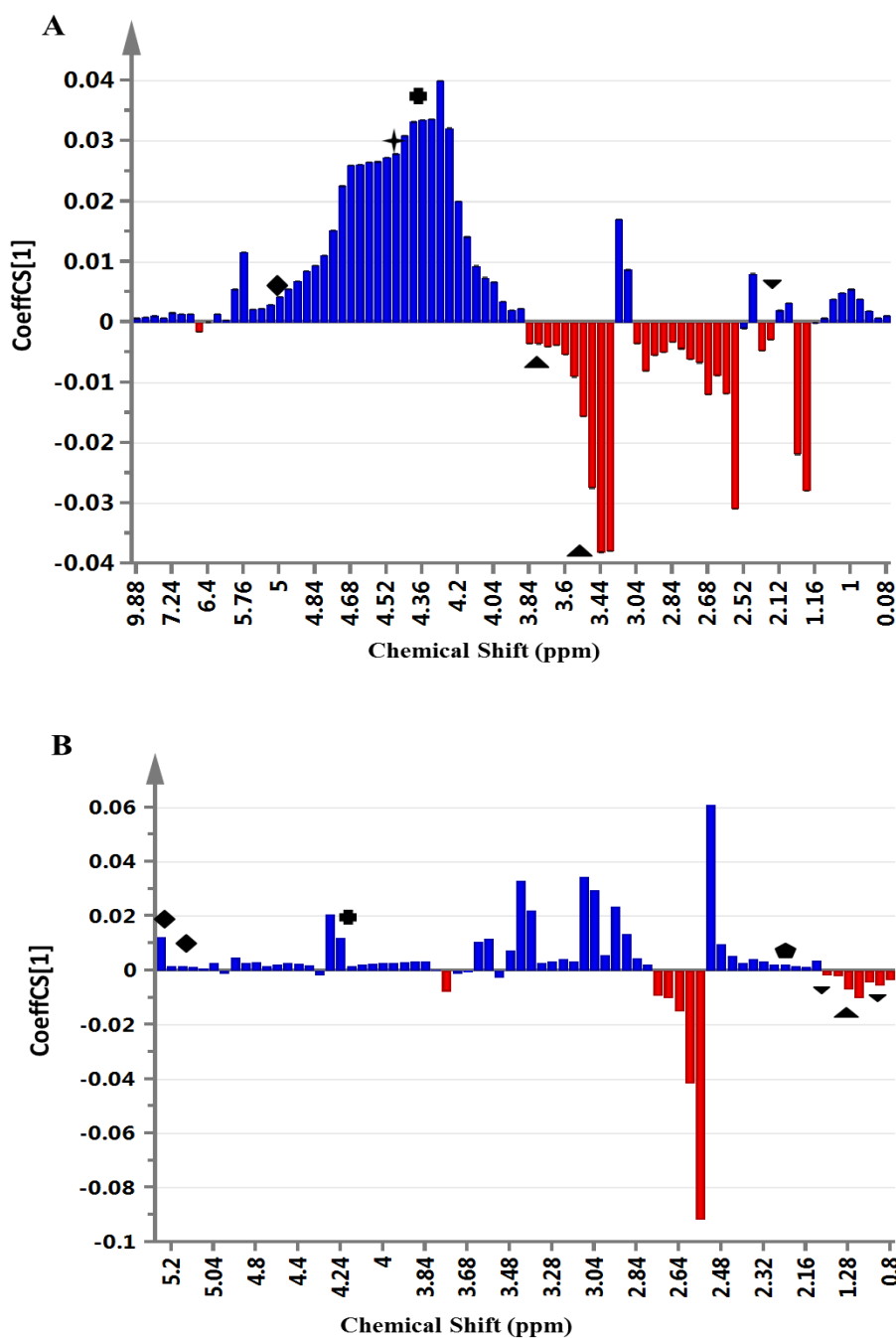


Figure 4.39 Correlation coefficient plots showing the distribution of metabolites in the NMR spectra of the polar **F6.17**-treated groups. The plot of NMR data for tissues are in A while the plot for those associated with the bath fluids are in B. The blue columns represent the control groups and the red columns represent the treated groups. Significant metabolites have been highlighted and represented according to the corresponding pathways. ◆ = cAMP signalling; ▲ = endocannabinoid signalling; ▼ = DAG signalling/lipid metabolism; † = NA metabolism; ◆ = MI biosynthesis/signalling; ▲ = RhoA signalling; ● = catecholamine signalling; ● = GABA signalling. These pathways were found to be strongly correlated with the action of **F6.17** on uterine contractility. n= 4 animals.

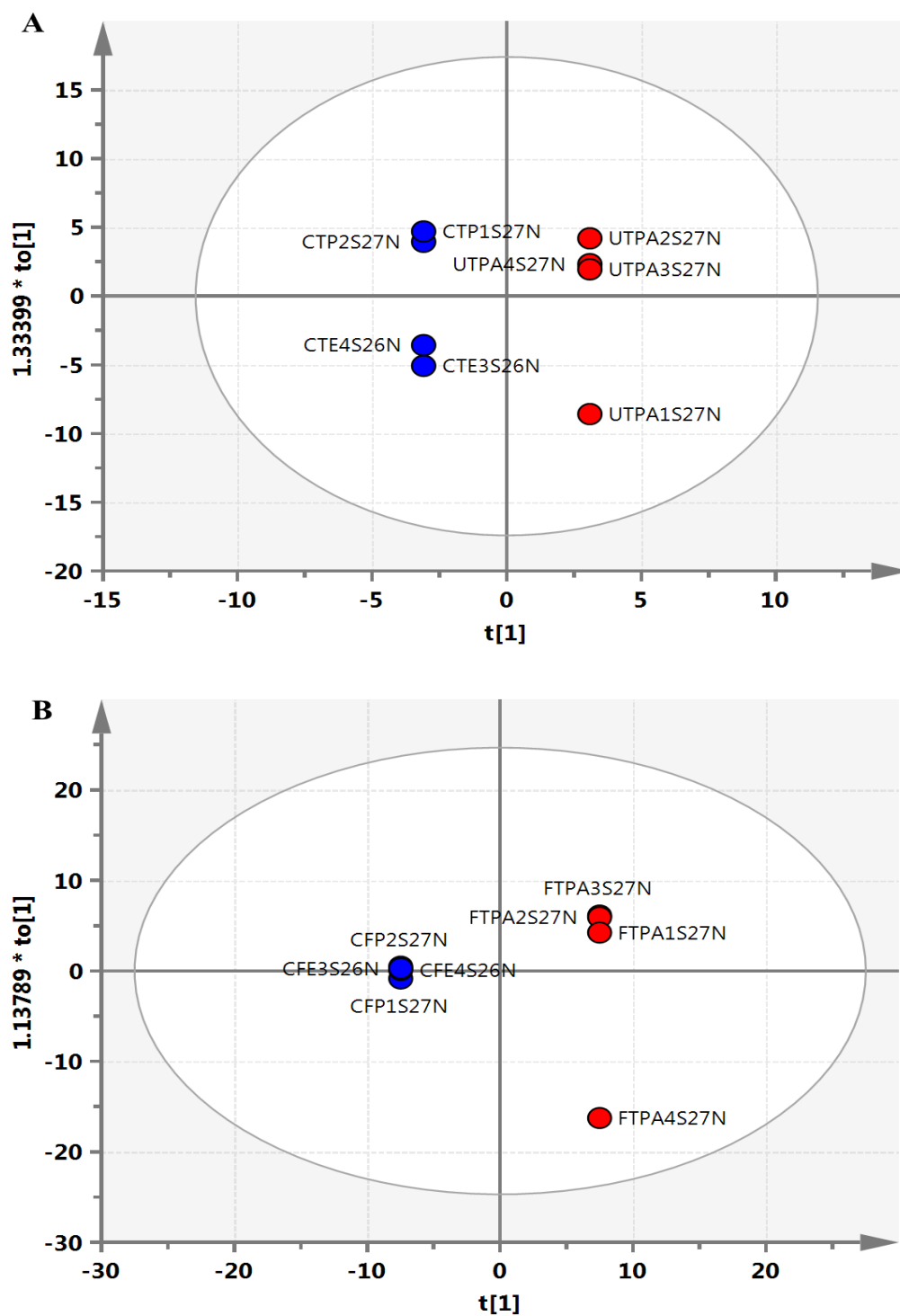


Figure 4.40 OPLSDA score plots showing $^1\text{H-NMR}$ analysis of non-polar **F6.17** treated uterine tissues (A) and those associated with the bath fluids (B). The blue circles represent the control groups while the red circles represent the treated groups. Successful separation was achieved between both groups. $n = 4$ animals.

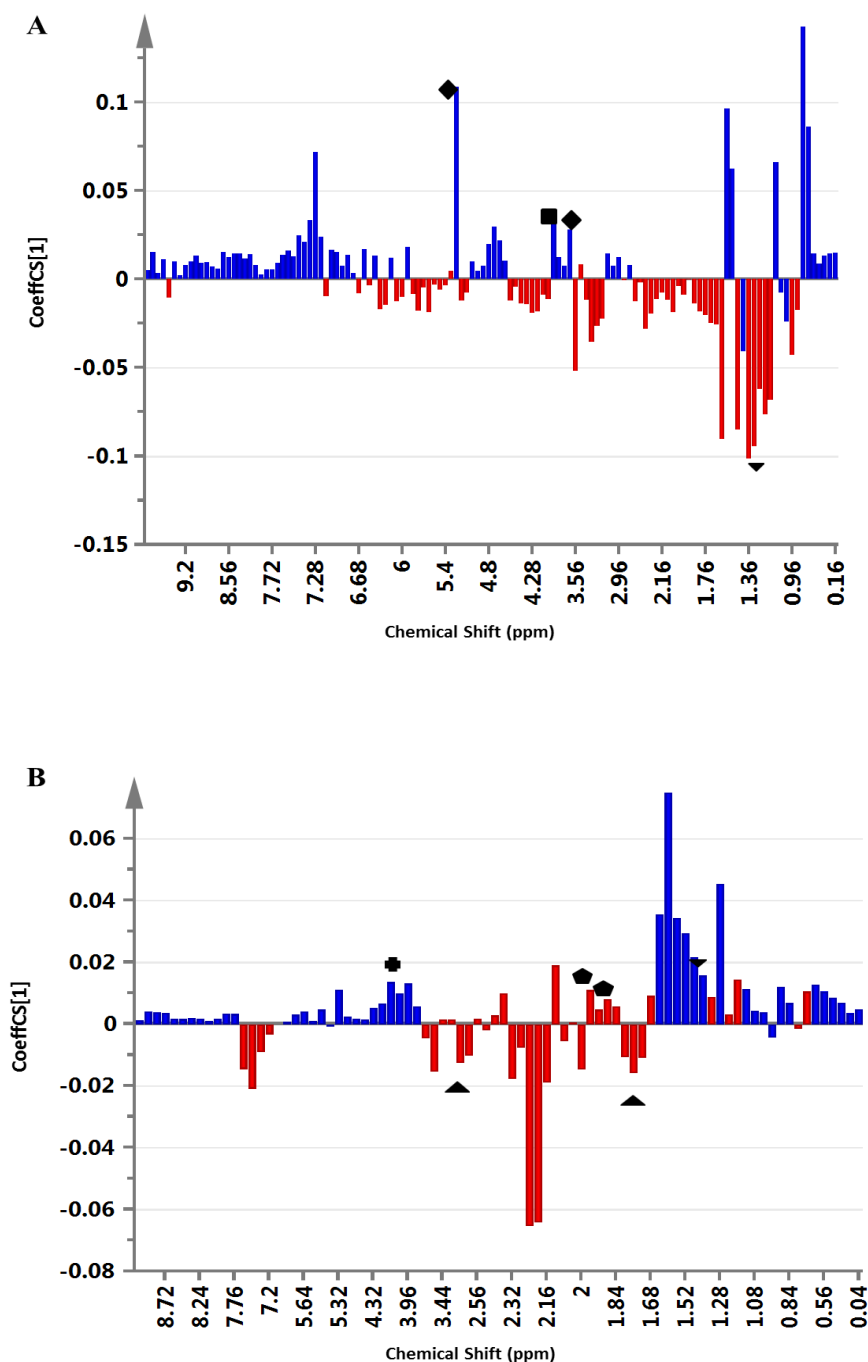


Figure 4.41 Correlation coefficient plots showing the distribution of metabolites in the NMR spectra of the non-polar **F6.17** treated groups. The plot of NMR data for tissues are in **A** while the plot for those associated with the bath fluids are in **B**. The blue columns represent the control groups and the red columns represent the treated groups. Significant metabolites have been highlighted and represented according to the corresponding pathways. ● = cAMP signalling; ▲ = endocannabinoid signalling; ▼ = DAG signalling/lipid metabolism; † = NA metabolism; ◆ = MI biosynthesis/signalling; ■ = RhoA signalling; ■ = catecholamine signalling; ◆ = GABA signalling. These pathways were found to be strongly correlated with the action of **F6.17** on uterine contractility. n= 4 animals.

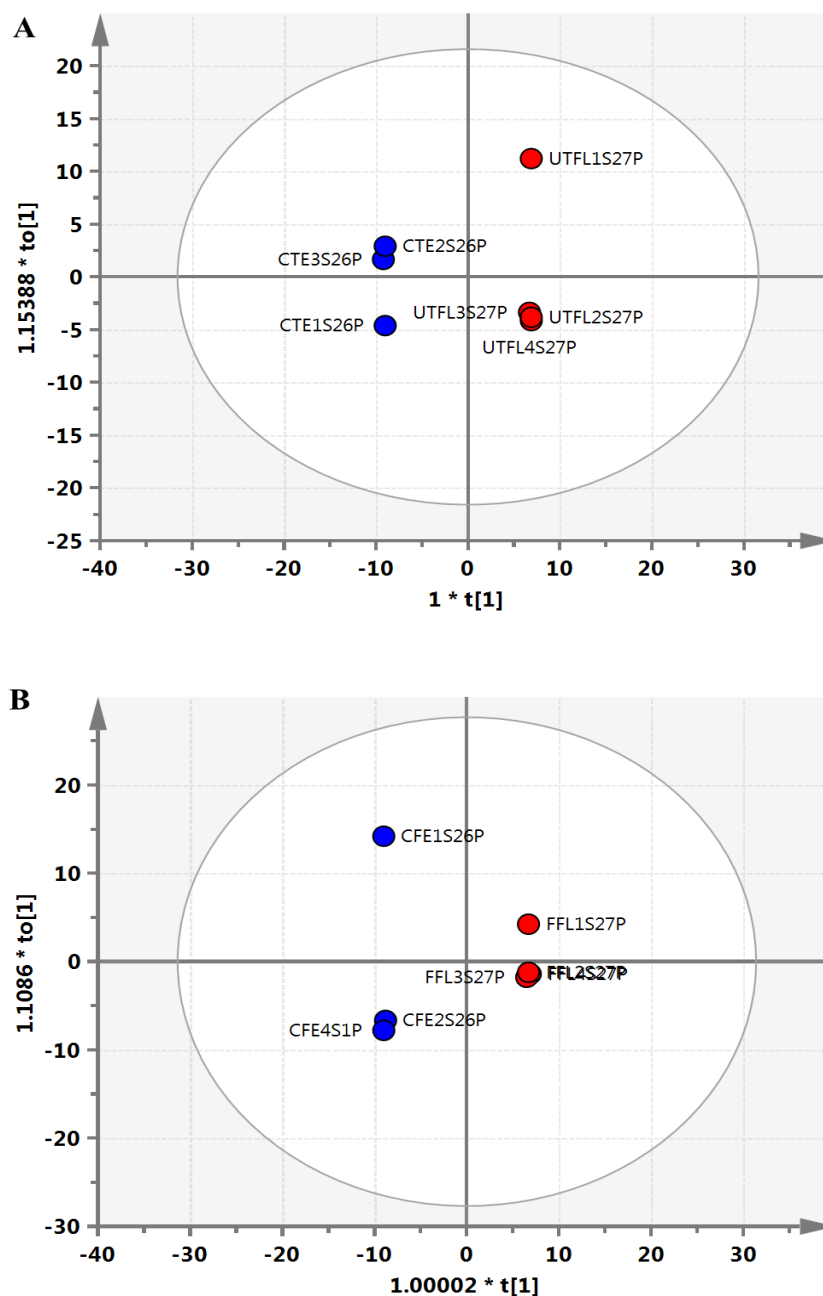


Figure 4.42 OPLSDA score plots showing ¹H-NMR analysis of polar **F28** treated uterine tissues (A) and bath fluids in which the uterine tissues were immersed (B). The blue circles represent the control groups while the red circles represent the treated groups. Successful separation was achieved between both groups. n = 4 animals.

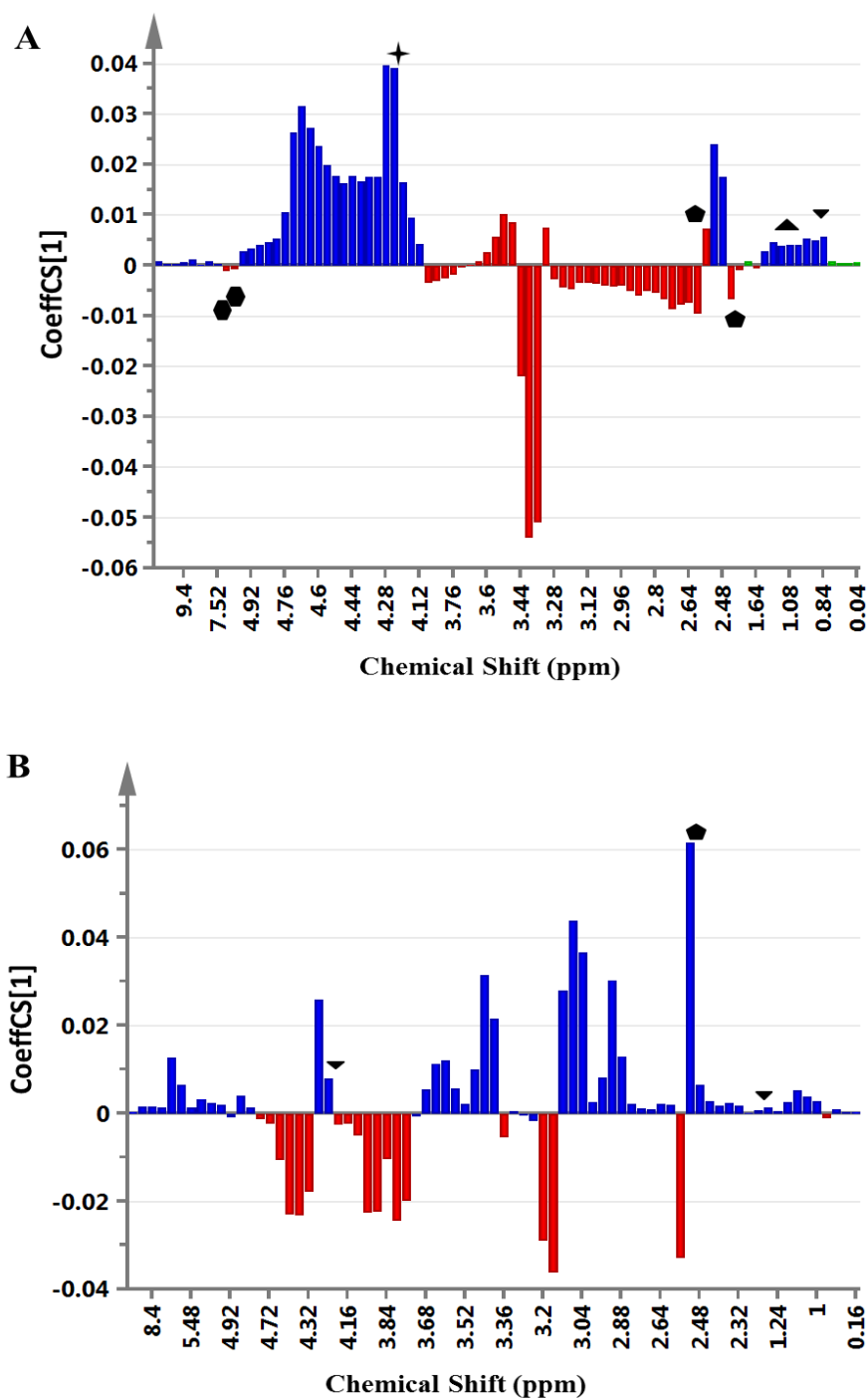


Figure 4.43 Correlation coefficient plots showing the distribution of metabolites in the NMR spectra of the polar **F28**-treated groups. The plot of NMR data for tissues are in A while the plot for those associated with the bath fluids are in B. The blue columns represent the control groups and the red columns represent the treated groups. Significant metabolites have been highlighted and represented according to the corresponding pathways. \blacklozenge = cAMP signalling; \blacktriangleup = endocannabinoid signalling; \blacktriangledown = DAG signalling/lipid metabolism; \blackstar = NA metabolism; \blacklozenge = MI biosynthesis/signalling; \blacksquare = RhoA signalling; \blacksquare = catecholamine signalling; \bullet = GABA signalling. n = 4 animals.

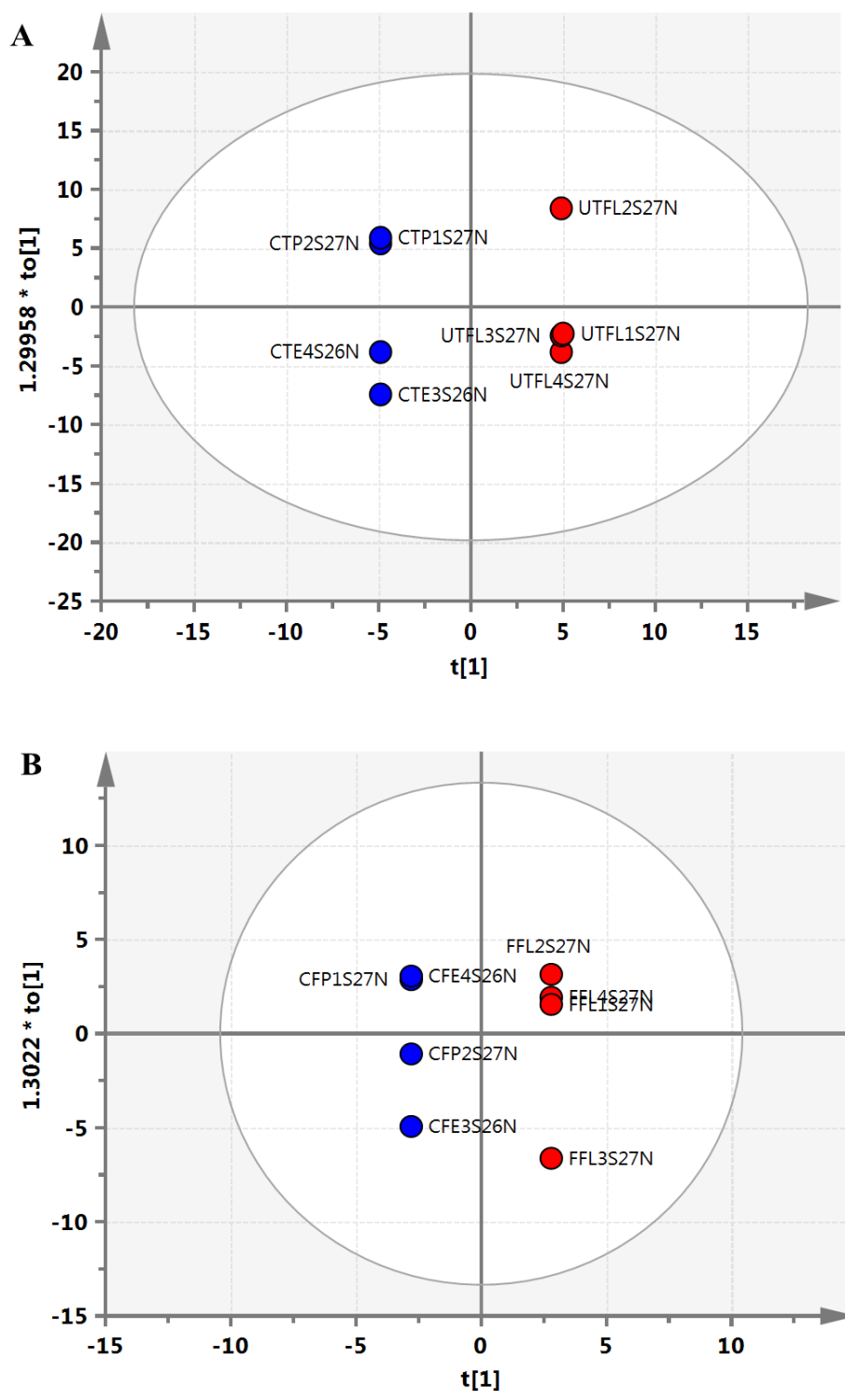


Figure 4.44 OPLSDA score plots showing ¹H-NMR analysis of non-polar **F28** treated uterine tissues (A) and those associated with the bath fluids (B). The blue circles represent the control groups while the red circles represent the treated groups. Successful separation was achieved between both groups. n = 4 animals.

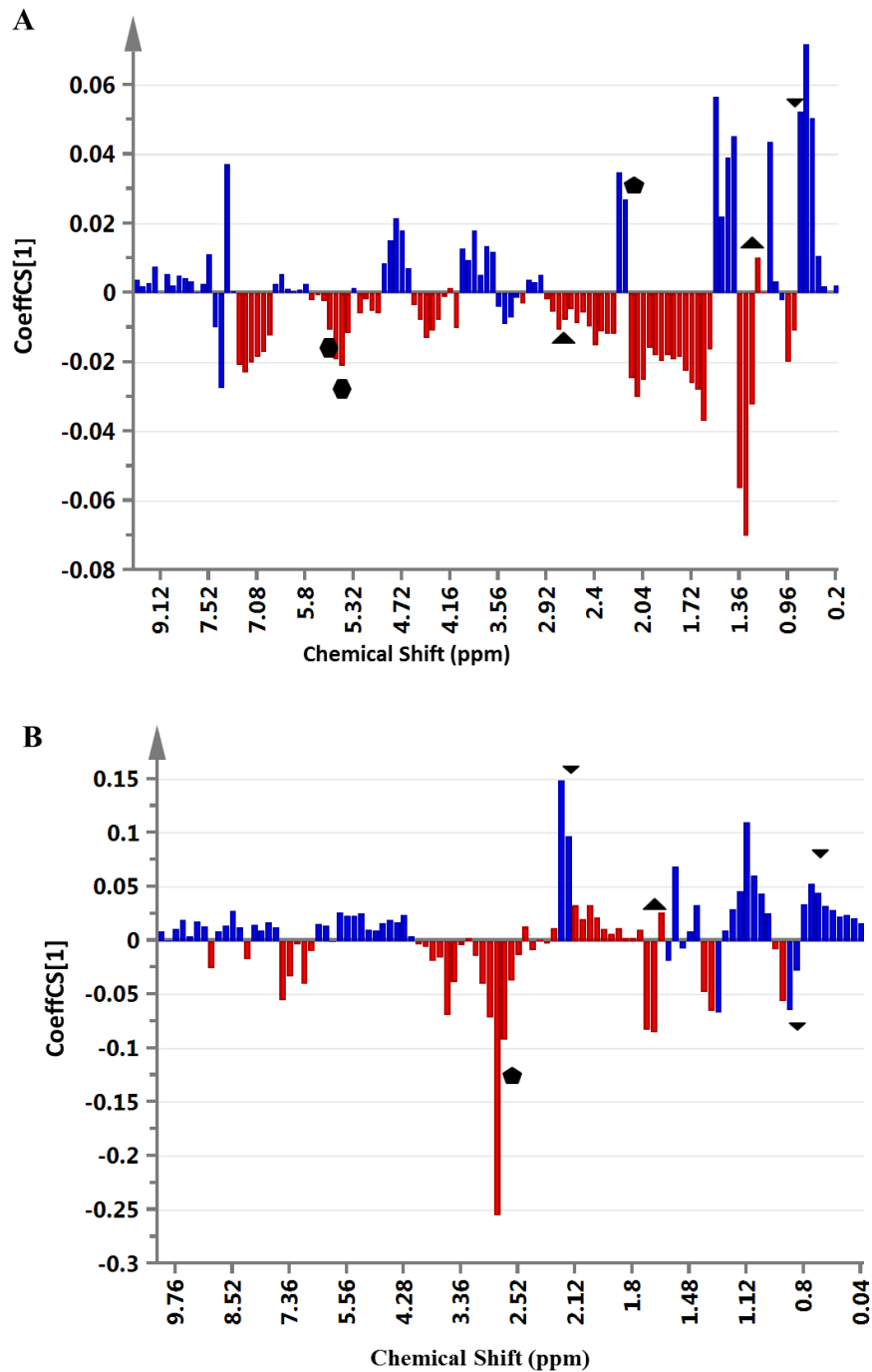


Figure 4.45 Correlation coefficient plots showing the distribution of metabolites in the NMR spectra of the non-polar **F28**-treated groups. The plot of NMR data for tissues are in A while the plot for those associated with the bath fluids are in B. The blue columns represent the control groups and the red columns represent the treated groups. Significant metabolites have been highlighted and represented according to the corresponding pathways. \blacklozenge = cAMP signalling; \blacktriangle = endocannabinoid signalling; \blacktriangledown = DAG signalling/lipid metabolism; \blackplus = NA metabolism; \blacklozenge = MI biosynthesis/signalling; \blacksquare = RhoA signalling; \blacksquare = catecholamine signalling; \blacklozenge = GABA signalling. These pathways were found to be strongly correlated with the action of **F28**. n= 4 animals.

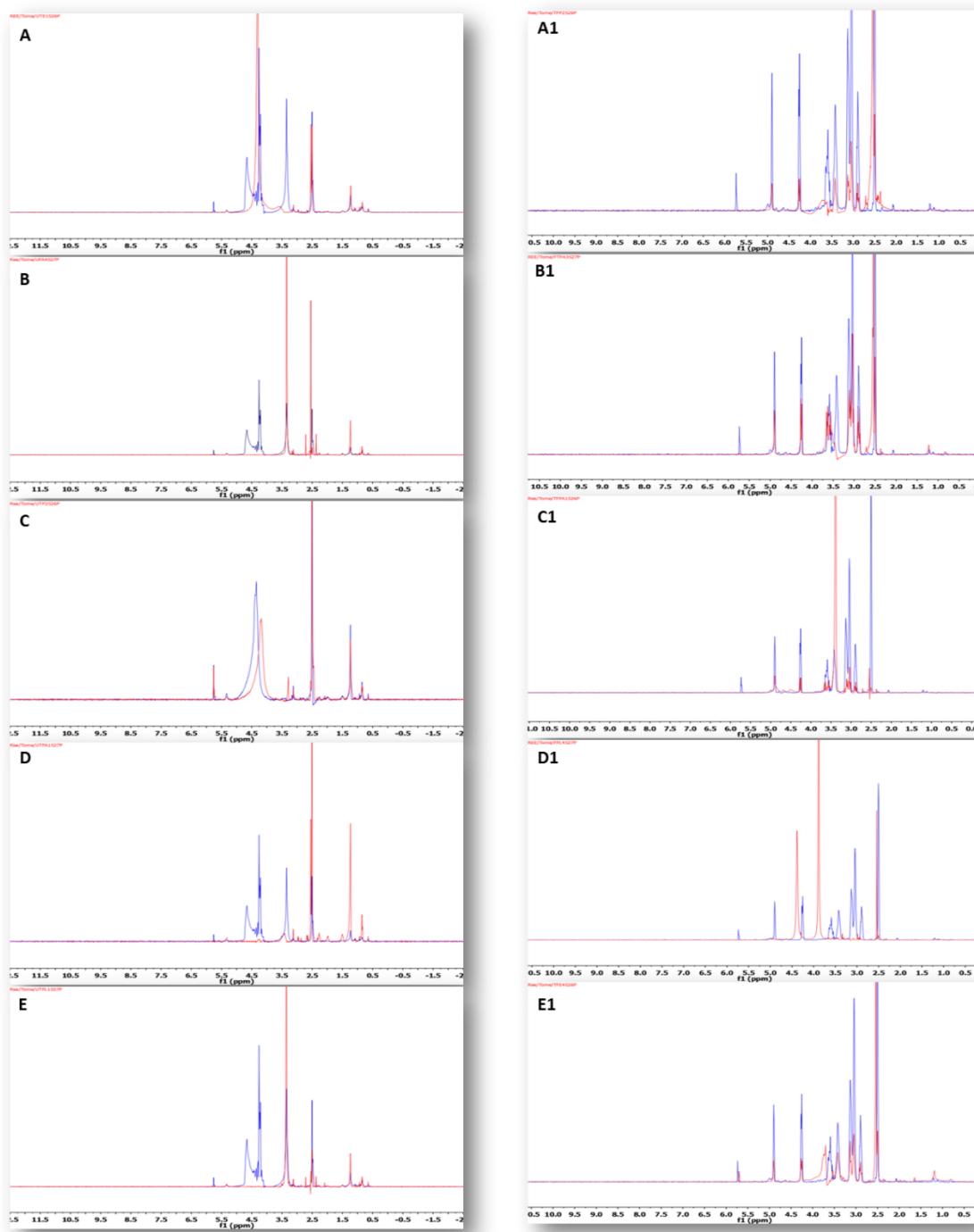


Figure 4.46 Typical ^1H -NMR spectra showing polar extracts of uterine tissues (A-E) and bath fluids in which the uterine tissues were immersed (A1-E1) that have been treated with fractions of *F. exasperata* **E1**; **F14**; **F4-31**; **F6.17**; **F28** (across from top to bottom). The superimposed spectra show the control (blue peaks) and treated (red peaks) groups

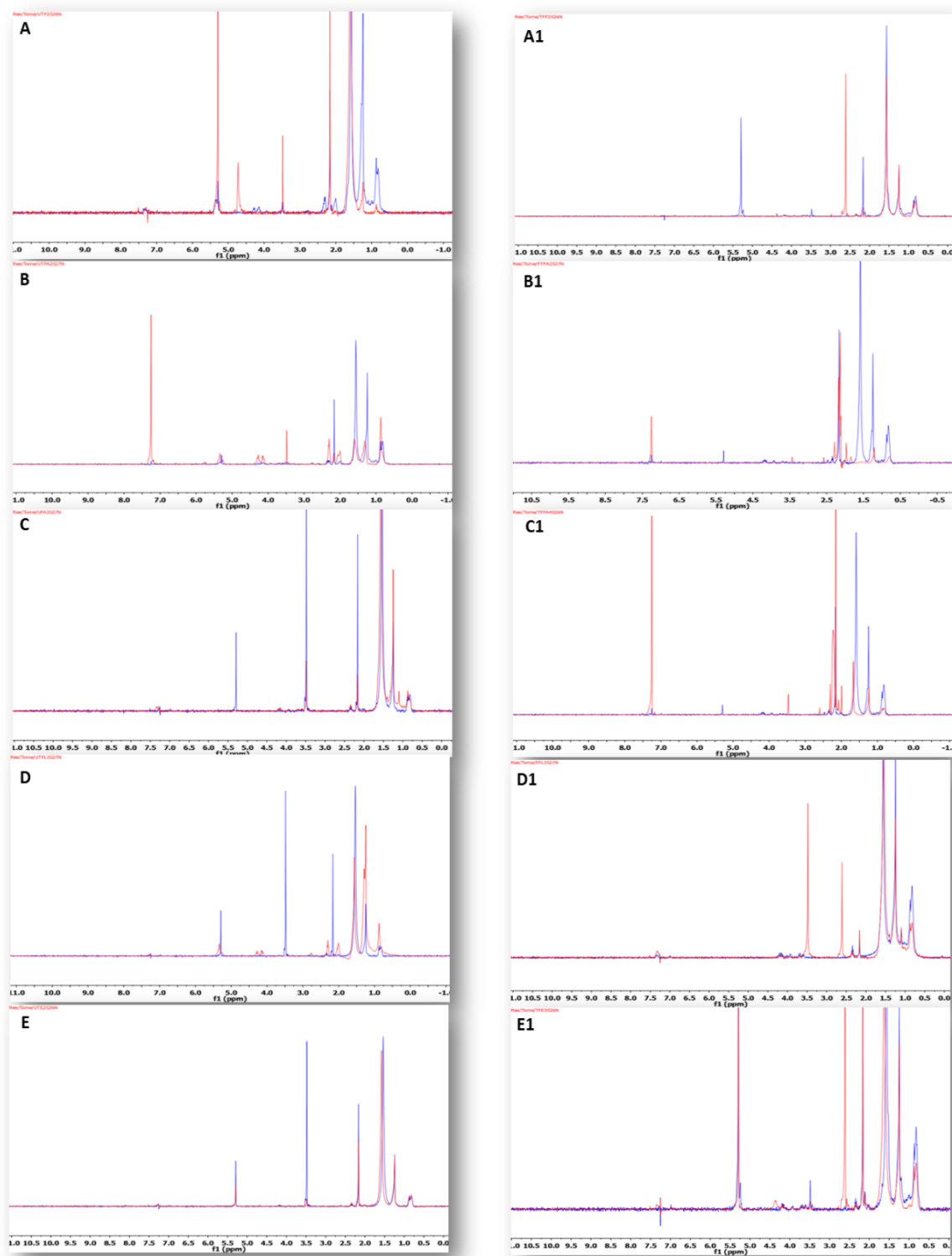


Figure 4.47 Typical ^1H -NMR spectra showing non-polar extracts of uterine tissues (A-E) and bath fluids in which the uterine tissues were immersed (A1-E1) that have been treated with fractions of *F. exasperata* E1; F14; F4-31; F6.17; F28 (across from top to bottom). The superimposed spectra show the control (blue peaks) and treated (red peaks) groups.

Table 4.8a Summary of the Proposed Mechanism(s) of Action of crude extract E1 of *Ficus exasperata* leaves

Determined from Metabolomic Analysis

GABA = gamma aminobutyric acid; **cAMP** = cyclic adenosine monophosphate; **MI** = myoinositol; **DAG** = diacylglycerol; **ERK** = extracellular signal regulated kinase; **RhoA** = Ras homolog gene family member A; **nd** = not detected; [↑] = increase; [↓] = decrease

Extract/ Fraction	Uterine Smooth Muscle Activity	MS Metabolomic Pathways		NMR Metabolomic Pathways	
		Uterine Tissues	Bath Fluids	Uterine Tissues	Bath Fluids
E1 (crude extract)	Inhibition	cAMP signalling [↑]	cAMP signalling [↑]	cAMP signalling [↑]	nd
		nd	MI signalling [↑]	MI signalling [↑]	nd
		GABA signalling [↑]	nd	nd	nd
		Catecholamine Synthesis [↓]	nd	Catecholamine Synthesis [↓]	Catecholamine Synthesis [↓]
		Endocannabinoid Signalling [↑]	Endocannabinoid Signalling [↑]	Endocannabinoid Signalling [↑]	Endocannabinoid Signalling [↓]
		Dopamine Signalling [↑]	Dopamine Signalling [↑]	nd	nd
		nd	nd	DAG Signalling [↑]	DAG Signalling [↑]
		nd	nd	nd	Glutamate Signalling [↑]
		nd	nd	RhoA Signalling [↓]	RhoA Signalling [↑]

Table 4.8b Summary of the Proposed Mechanism(s) of Action of F14 of *Ficus exasperata* leaves

Determined from Metabolomic Analysis

GABA = gamma aminobutyric acid; **cAMP** = cyclic adenosine monophosphate; **MI** = myoinositol; **DAG** = diacylglycerol; **ERK** = extracellular signal regulated kinase; **RhoA** = Ras homolog gene family member A; **nd** = not detected; [↑] = increase; [↓] = decrease

Extract/ Fraction	Active Compound (s)	Uterine Smooth Muscle Activity	MS Metabolomic Pathways		NMR Metabolomic Pathways	
			Uterine Tissues	Bath Fluids	Uterine Tissues	Bath Fluids
F14	Dilinolein and fatty acid series	Inhibition/Contraction	cAMP signalling [↑]	cAMP signalling [↑]	nd	nd
			nd	GABA signalling [↑]	GABA signalling [↑]	GABA signalling [↑]
			nd	Catecholamine synthesis [↑]	Catecholamine synthesis [↓]	nd
			nd	nd	Prostanoid signalling [↓]	Prostanoid signalling [↓]
			nd	DAG Signalling [↓]	DAG Signalling [↓]	DAG Signalling [↓]
			Endocannabinoid signalling [↓]	Endocannabinoid signalling [↑]	Endocannabinoid signalling [↓]	Endocannabinoid signalling [↑]
			MI signalling [↑]	nd	MI signalling [↓]	MI signalling [↑]
			nd	nd	ERK1/2 signalling [↑]	ERK1/2 signalling [↑]

Table 4.8c Summary of the Proposed Mechanism(s) of Action of F4-31 of *Ficus exasperata* leaves

Determined from Metabolomic Analysis

GABA = gamma aminobutyric acid; **cAMP** = cyclic adenosine monophosphate; **MI** = myoinositol; **DAG** = diacylglycerol; **ERK** = extracellular signal regulated kinase; **RhoA** = Ras homolog gene family member A; **nd** = not detected; [↑] = increase; [↓] = decrease

Extract/ Fraction	Active Compound (s)	Uterine Smooth Muscle Activity	MS Metabolomic Pathways		NMR Metabolomic Pathways	
			Uterine Tissues	Bath Fluids	Uterine Tissues	Bath Fluids
F4-31	Pyropheophorbide a	Inhibition	nd	Sphingosine signalling [↑]	nd	nd
			GABA signalling [↓]	nd	nd	GABA signalling [↑]
			cAMP signalling [↑]	cAMP signalling [↑]	nd	nd
			Catecholamine Synthesis [↓]	Catecholamine Synthesis [↓]	nd	Catecholamine Synthesis [↓]
			Glutamate Metabolism [↓]	nd	nd	nd
			Endocannabinoid Signalling [↓]	Endocannabinoid Signalling [↓]	Endocannabinoid Signalling [↓]	Endocannabinoid Signalling [↓]
			nd	MI signalling [↓]	nd	MI signalling [↓]
			nd	nd	nd	DAG Signalling [↓]
			nd	nd	Glutamate Signalling [↑]	Glutamate Signalling [↑]
			nd	nd	ERK1/2 Signalling [↓]	nd
nd	nd	RhoA Signalling [↓]	RhoA Signalling [↓]			

Table 4.8d. Summary of the Proposed Mechanism(s) of Action of F6.17 of *Ficus exasperata* leaves

Determined from Metabolomic Analysis

GABA = gamma aminobutyric acid; **cAMP** = cyclic adenosine monophosphate; **MI** = myoinositol; **DAG** = diacylglycerol; **ERK** = extracellular signal regulated kinase; **RhoA** = Ras homolog gene family member A; **nd** = not detected; [↑] = increase; [↓] = decrease

Extract/ Fraction	Active Compound (s)	Uterine Smooth Muscle Activity	MS Metabolomic Pathways		NMR Metabolomic Pathways	
			Uterine Tissues	Bath Fluids	Uterine Tissues	Bath Fluids
F6-17	Pheophytin a series	Inhibition/Contraction	cAMP signalling [↑]	cAMP signalling [↑]	nd	cAMP signalling [↑]
			Dopamine signalling [↑]	nd	nd	nd
				MI signalling [↓]	MI signalling [↓]	nd
			Catecholamine Synthesis [↓]	Catecholamine Synthesis [↓]	Catecholamine Synthesis [↓]	Catecholamine Synthesis [↓]
			nd	Endocannabinoid Signalling [↑]	Endocannabinoid Signalling [↑]	Endocannabinoid Signalling ^{↑↓}
			nd	nd	RhoA Signalling ^{↑↓}	RhoA Signalling [↓]
			Prostanoid Signalling [↓]	Prostanoid Signalling [↓]	Prostanoid Signalling [↓]	Prostanoid Signalling [↓]
			nd	nd	nd	nd
			nd	nd	DAG Signalling [↓]	DAG Signalling [↓]
			nd	nd	nd	GABA signalling [↓]
			nd	nd	ERK1/2 Signalling [↑]	ERK1/2 Signalling [↑]
			nd	nd	Glutamate Signalling [↑]	Glutamate Signalling [↑]

Table 4.8e Summary of the Proposed Mechanism(s) of Action of F28 of *Ficus exasperata* leaves

Determined from Metabolomic Analysis

GABA = gamma aminobutyric acid; **cAMP** = cyclic adenosine monophosphate; **MI** = myoinositol; **DAG** = diacylglycerol; **ERK** = extracellular signal regulated kinase; **RhoA** = Ras homolog gene family member A; **nd** = not detected; [↑] = increase; [↓] = decrease

Extract/ Fraction	Active Compound (s)	Uterine Smooth Muscle Activity	MS Metabolomic Pathways		NMR Metabolomic Pathways	
			Uterine Tissues	Bath Fluids	Uterine Tissues	Bath Fluids
F28	Flavonoid series	Inhibition	nd	MI signalling [↓]	MI signalling [↓]	nd
			Dopamine signalling [↑]	Dopamine signalling [↑]	nd	nd
			cAMP signalling [↑]	cAMP signalling [↑]	cAMP signalling [↑]	nd
			nd	nd	nd	DAG Signalling [↓]
			nd	nd	Endocannabinoid Signalling ^{↓↑}	nd
			nd	nd	RhoA Signalling [↓]	nd
			nd	nd	ERK1/2 Signalling [↑]	ERK1/2 Signalling [↑]
			nd	nd	GABA signalling [↑]	nd

4.9 DISCUSSION

During our pharmacological screening, the leaf extract which showed greater inhibition of uterine contractility was **E1**. It was therefore selected for metabolomic analysis. Observation of metabolic changes using MS and NMR revealed the possibility of the interaction of several pathways responsible for the observed activity.

The observed discrepancies in some instances of the same metabolite are not surprising as this might result from the presence of different interacting phytochemical constituents present in **E1**. The MS analysis also enabled the detection of several phytochemical compounds which had been previously identified and isolated, these include the pheophytin-a and -b series, fatty acids and flavonoids (Table 4.1). A comprehensive list of significant metabolites detected by the NMR analysis is shown in appendix 3.

4.9.1 Metabolomic Analysis of Extract and Fractions

An increase in cAMP pathway was detected by both MS and NMR to have played a role in the effects of **E1**, **F14**, **F4-31**, **F6.17** and **F28** on uterine contraction. Increase in myometrial cAMP concentration often results in inhibition of uterine contraction. The complete mechanism by which this is achieved appears to be somewhat still unknown (Nohara *et al.*, 1996). Several mechanisms of cAMP –induced relaxation has been proposed. Increase cAMP has been reported to activate $\text{Na}^+/\text{Ca}^{2+}$ pump and promote intracellular storage of Ca^{2+} (Scheid *et al.*, 1979). Recent studies have also suggested that cAMP blocks signal transmission from Ras to Raf-1 by interaction

with protein kinase A this prevents mitogen activated protein kinase (MAPK) activation (Hordijk *et al.*, 1994; Sevetson *et al.*, 1993). An inhibition of PI turnover has also been suggested (Sanborn, 1995).

Myoinositol (MI) signalling was also detected to play a role in the effect of all fractions and extracts tested but it was increased in some and decreased in others. For instance MI signalling was detected to have been increased upon **E1** and **F14** treatment of uterine tissues while it was observed to have been decreased upon **F4-31**, **F6.17** and **F28** treatment. MI is an isomer of cyclohexane hexol in eukaryotic cells and a precursor of the inositol phospholipids. In addition to the popular function of diacylglycerol (DAG) production as well as IP₃ which both act as second messengers resulting in an increase in Ca²⁺ in the cytosol (Berridge and Irvine, 1984; Berridge and Irvine, 1989; Downes, 1989), there are several other inositol phospholipid pathways some of which include the complex metabolism of IP₃ (Majerus *et al.*, 1988), the metabolism of inositol polyphosphates (Cosgrove and Irving, 1980), the novel inositol phospholipid pathway initiated by phosphatidylinositol 3-kinase which might be regulated by tyrosine kinases (Whitman *et al.*, 1988), and the synthesis of phosphatidylinositols (PtdIns) glycans (Low, 1989). The metabolism of inositol phosphate has been described as being extremely complex (Berridge and Irvine, 1989). Summarily, the metabolism of inositol results in the generation of several inositol phosphates the commonly known include IP₃, inositol 1,3,4,5 phosphate (IP₄), inositol-5-phosphate, inositol 3, 4, 5, 6, tetrakisphosphate and inositol-6-phosphate which have different biologic functions (Downes and Macphee, 1990). IP₄ has also been implicated in Ca²⁺ signalling (Irvine and Moor, 1987; Irvine *et al.*, 1988). Some studies have shown that IP₄ may exert

both facilitatory and inhibitory feedback on calcium signalling as it inhibits IP₃ receptors at certain concentrations (Hermosura *et al.*, 2000). IP₄ has been reported to also inhibit IP₃ metabolism through IP₃ 5-phosphatase thus facilitating the activation of store operated Ca²⁺ current (*I*_{CRAC}). IP₄ receptors are located on the nuclear membranes, activation of which results in calcium uptake and inhibition of IP₃. It has also been proposed that IP₄ calcium uptake might be mediated through the stimulation of calcium pumps (Koppler *et al.*, 1993). From the foregoing, it would seem that MI generates several functional metabolites besides IP₃ which may play a role in smooth muscle relaxation through inhibition of IP₃ or calcium uptake. The exact MI metabolite responsible for the uterine inhibitory effect observed with **E1** and **F14** is unknown at the moment and further studies would be required to elucidate the specific MI pathway or the relationship between MI and the observed **E1** effect however it is proposed that in **F4-31**, **F6.17** and **F28** a decrease in IP₃ contributed to the pharmacological effect seen.

An increase in GABA signalling was observed across **E1** and fractions except for **F6.17** where a decrease was observed. GABA and receptor binding sites of GABA have been shown to occur in the uterus of the rat and rabbit (Erdo, 1984). GABA has been shown to activate GABA_B to elicit excitatory responses in the rabbit uterus (Riesz and Erdo, 1985) while activation of GABA_A receptors in the uterus promotes inhibition of uterine contractility and has been proposed to play a role in the modulation of uterine contractility (Erdo, 1984; Erdo *et al.*, 1989; Riesz and Erdo, 1985). It has also been suggested that the density of the GABA receptor type present in an organ may determine the response observed (and it seems that the prevailing hormonal environment (such as occurs during pregnancy or during the

oestrous cycle) may determine the type and density of receptors present in the uterus (Erdo *et al.*, 1989; Follesa *et al.*, 1998; Westerling *et al.*, 1991).

Catecholamines (adrenaline and noradrenaline) have been reported to contribute in the regulation of myometrial contraction via interaction with the β - and α -adrenergic receptors present in the uterus (Marshall, 1981). The myometrial inhibitory effect observed upon activation of the β -adrenergic receptors occur through the upregulation of adenylyl cyclase (Wray, 1993) while myometrial stimulation is observed upon activation of α -adrenergic receptors through upregulation of the $G\alpha_{q/11}$ protein and phospholipase C stimulation (Breuiller-Fouche *et al.*, 1991; Limon-Boulez *et al.*, 1997). However in this study, catecholamine synthesis was found to have been decreased upon treatment of the uterus with the extract and fractions. It may therefore be that catecholamines do not play any significant role in the effects of *F. exasperata* on uterine contraction however their role in the regulation of spontaneous uterine contraction had to be decreased or inhibited in order for the effect of the fractions of Ficus to be observed.

The endogenous cannabinoids were also found to be perturbed upon treatment of the uterus by *Ficus* fractions. Endocannabinoids were increased on **E1** and **F6.17** treatment while a decrease was observed in the tissues and an increase observed in the bath fluids upon treatment with **F14**, a decrease was observed upon treatment of uterine tissues with **F4-31** and a simultaneous increase and decrease were observed in the uterine tissues of **F28**. These endocannabinoids belong to a class of fatty amides. N-Acylethanolamines (NAEs) are ethanolamides of long chain fatty acids and exist in various organisms including animals and plants (Hansen *et al.*, 2000; Schmid *et al.*, 1990). Of these, anandamide (AEA) or *N*-

arachidonylethanolamide has attracted special interest because of its marked biological activities ('ananda' means inner bliss and tranquility in Sanskrit). NAEs are currently considered to be a class of endogenous lipid mediators (Di Marzo and De Petrocellis, 2012; Maccarrone *et al.*, 2010). Upon its identification in 1992 from porcine brain (Devane *et al.*, 1992), AEA has so far been the most extensively characterized NAE, which functions as an endogenous ligand of cannabinoid receptors and transient receptor potential vanilloid 1 channels and actually exerts a variety of central and peripheral activities through these receptors (Pacher *et al.*, 2006). Like the pharmacologically active compounds in marijuana or cannabis (from *Cannabis sativa*), its effects is exerted through binding to and activating specific cannabinoid receptors (CBR) and along with 2-arachidonoyl-glycerol AEA they have been termed endogenous cannabinoids or 'endocannabinoid' (Brown *et al.*, 2013). Both cannabinoid receptors CB₁ and CB₂ are membrane-bound G-protein coupled receptors (Vogel *et al.*, 1993). CB₁ is mainly found in the central nervous system (Herkenham *et al.*, 1991) and in organs such as the heart, uterus, testis and small intestine, while the CB₂ receptor is found primarily in the spleen and other cells associated with immunochemical functions, as well as some peripheral cells (Munro *et al.*, 1993). More recently some CB and non-CB ligands have been reported to also bind G-protein 55 (GPR55) (Lauckner *et al.*, 2008; Pertwee, 2007; Ryberg *et al.*, 2007). This suggests that the latter protein might act as a novel "type-3 (CB₃)" cannabinoid receptor (Moriconi *et al.*, 2010). Endocannabinoids have been demonstrated in the uterus with one of the highest levels detected in the mouse uterus (Schmid *et al.*, 1997). A role has also been implicated in the regulation of the female reproductive cycle. Cannabinoid receptors have also been reported in the uterus

(Paria *et al.*, 1995). There have been a couple of investigations into the effects of endocannabinoids on uterine contractions and there also appear to be contradictory reports on the effect of endocannabinoids on uterine contractility. Dennedy *et al.* (2004) reported a relaxant effect of AEA on uterine contractility and demonstrated that this relaxant effect may be linked to a reduction in uterine prostaglandin synthesis (Dennedy *et al.*, 2004). In contrast, an increase in the force of spontaneous uterine contraction was reported for the endocannabinoids (Dmitrieva and Berkley, 2002), which was purportedly due partly to a cannabinoid-induced production of PGE₂ and PGF_{2α} resulting in a decrease in the intracellular concentration of cAMP (Asala *et al.*, 2013). Similarly, some seemingly contradictory reports on the mechanisms of action of endocannabinoids exist. Some researchers report on a direct regulation of uterine contraction via binding with CB₁ and CB₂ receptors that preferentially couple to inhibitory Gai/o proteins to inhibit adenylate cyclase activity, and consequently reduce intracellular cAMP levels (Howlett and Mukhopadhyay, 2000), while yet some researchers report on an observed increase in cAMP levels following CB₁ activation (Busch *et al.*, 2004), suggesting a possible coupling to Gα_s of the G protein receptors. Other signalling events, including increased activity of MAPK, inhibition of voltage-gated Ca²⁺ channels, activation of K⁺ channels, and nitric oxide (NO) generation, have also been suggested to follow CB receptor subtypes activation under different conditions (Asala *et al.*, 2013). It may seem therefore that binding of endocannabinoids to their receptors can result in activation/regulation of a number of signal transduction pathways which are dependent on the agonist involved and the factors in place upon binding. For instance binding to their receptor can result in activation of pathways outlined in Table 4.9.

Briefly, binding can result in inhibition of Ca^{2+} channels; inhibition of adenylyl cyclase and corresponding decrease of cAMP-dependent protein kinase which leads to decreased phosphorylation of the K^+ channels and regulation of ionic currents; activation of focal adhesion kinase and activation of MAPK cascades (Pertwee, 2005), which includes extracellular signal-regulated kinases (ERK) p38 MAPK cascades (Derkinderen *et al.*, 2001; Gertsch *et al.*, 2004), as well as the stimulation of other intracellular pathways such as the phosphatidylinositol 3-kinase (PI_3K)/Akt (also known as Protein Kinase B (PKB)) pathway through CB_2 (Molina-Holgado *et al.*, 2002). It is a serine/threonine-specific protein kinase that plays a key role in multiple cellular processes such as glucose metabolism, apoptosis, cell proliferation, transcription and cell migration (Staal *et al.*, 1977). Different subtypes of Akt exist but Akt_1 is involved in the $\text{PI}_3\text{K}/\text{AKT}/\text{mTOR}$ pathway and other signalling pathways (Chen *et al.*, 2005). Activation of GPR55, (“ CB_3 ” cannabinoid receptor), has been linked to: an increase in intracellular Ca^{2+} increase (Lauckner *et al.*, 2008); activation of the small GTPase proteins RhoA, Rac, and Cdc42 (Henstridge *et al.*, 2009; Ryberg *et al.*, 2007); and ERK phosphorylation (Oka *et al.*, 2009; Oka *et al.*, 2007). It has also been observed that muscarinic and glutamate receptors have allosteric sites for AEA binding (Lanzafame *et al.*, 2004). It can therefore be seen that endocannabinoids exert a highly complex network of interactions (Lopez-Moreno *et al.*, 2008) which may probably be extended to its role in modulating uterine contractions.

Dopamine was also detected to contribute to the effects of *Ficus* fractions on uterine contractions. It was observed to have been increased on **E1**, **F6.17** and **F28** treatment. Dopamine has been reported to inhibit uterine contractions in the

non-pregnant uterus via action on adrenergic receptors (Estan *et al.*, 1988; Czerski *et al.*, 2005). However at early and term pregnancy, dopamine has been reported to stimulate myometrial contractility (Lal and Sharma, 1983; Sizov, 1992; Urban *et al.*, 1982). Dopamine can oftentimes exert different and opposing effects on organs or tissues and this observation has been associated with the species involved as well as the receptors present since dopamine is known to act on both dopaminergic and adrenergic receptors (Czerski *et al.*, 2005). Endogenous dopamine has been previously detected in the uterus (Arkininstall and Jones, 1985). Interestingly in this study, while catecholamine synthesis was detected to be decreased, dopamine signalling was detected as being increased. It was also observed that in each case where dopamine was increased endocannabinoids signalling was also increased simultaneously. It is therefore possible that the increased dopamine detected in this study is a product of the AEA pathway. N-arachidonyldopamine (NADA) has been detected as an endogenous component of certain mammalian tissues (Sagar *et al.*, 2004). NADA binds to the CB₁ receptor and transient receptor potential vanilloid type 1 (TRPV1) channels and regulates calcium mobilization (Bisogno *et al.*, 2000; Huang *et al.*, 2002). Biosynthesis is believed to occur mainly by conjugation of dopamine with arachidonic acid, catalysed by a fatty acid amide hydrolase (not via the CoA ester), although there are suggestions that some might be derived from arachidonoyltyrosine (Hu *et al.*, 2009; Hu *et al.*, 2004). Studies have shown the inhibition of T-type Ca²⁺ channels by NADA (Ross *et al.*, 2009) and sarcoendoplasmic reticulum calcium transport ATPase (SERCA) uncoupling (Mahmmoud and Gaster, 2012). Unfortunately, it would appear that not many studies have been done on the relationship between NADA and uterine contractility.

RhoA signalling was also detected in this study. An increase in rhoA signalling was detected in uterine tissues treated by **E1** but a decrease was observed in the bath fluids. A decrease was detected on treatment with **F4-31** and **F6.17**. The role of the small G protein rhoA (a member of the Rho subfamily of the Ras superfamily of monomeric GTPases) in the regulation of myometrial contractility has recently received considerable attention. It has been suggested to be involved in agonist-induced Ca^{2+} -sensitization by acting downstream on receptor occupancy (Otto *et al.*, 1996) as it has been shown to increase myosin light chain (MLC) phosphorylation at a constant Ca^{2+} concentration (Noda *et al.*, 1995). Inactivation of rhoA therefore would inhibit Ca^{2+} -sensitization. An effector molecule rho-associated kinase (ROK) appears to play a role in the Ca^{2+} -sensitising effects of rhoA activation (Uehata *et al.*, 1997). ROK inhibits the activity of myosin phosphatase (Amano *et al.*, 1996; Kimura *et al.*, 1996) through the inhibition of myosin binding subunits (Tahara *et al.*, 2002). Activation of certain receptors in the myometrium results in the translocation of rhoA from the cytoplasm to the cell membranes as was reported to occur with muscarinic receptors (Taggart *et al.*, 1999). RhoA and ROK have been shown to be involved in oxytocin-induced myometrial contractility (Tahara *et al.*, 2002). Caveolins have also been shown to regulate the activities of rhoA and probably ROK (Taggart *et al.*, 1999). Thus a reduction in rhoA would result in the inhibition of myometrial contractility.

Extracellular signal-related kinases (ERK) signalling was detected in this study to have been increased on **F14**, **F6.17** and **F28** treatment of uterine smooth muscle but a decrease was observed with **F4-31**. The involvement of the ERK pathway has been proposed to play a role in the regulation of agonist-induced smooth

muscle contraction, activation of which has been shown to stimulate contraction (Adam *et al.*, 1995; Childs *et al.*, 1992; Dessy *et al.*, 1998; Watts, 1996; Xiao and Zhang, 2002). ERK also seems to be involved in spontaneous uterine contractility (Li *et al.*, 2003). However, it has been proposed that the ERK pathway may not affect Ca^{2+} channels directly (Xiao and Zhang, 2002). ERK pathway has been shown to be involved in OT-induced uterine contraction (Nohara *et al.*, 1996) as well as prostaglandin $F_{2\alpha}$ – induced uterine contraction (Ohmichi *et al.*, 1997) and has been proposed to exert its effect by phosphorylation of caldesmon (CAD) (Adam *et al.*, 1995).

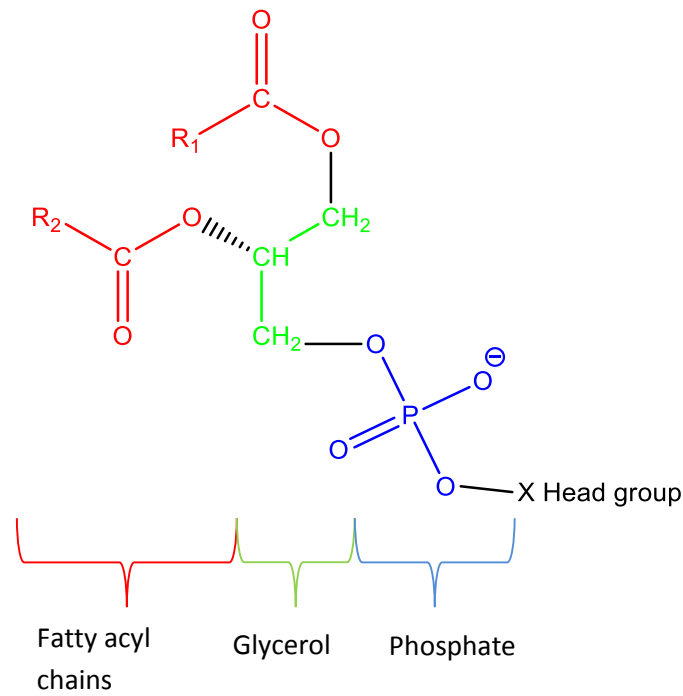
The idea of cross talk between signalling pathways is currently being investigated by several scientists particularly G-proteins and their second messenger pathways. For instance stimulation of the CB_1 cannabinoid receptor has been shown to lead to an increase in dopamine turnover (Romero *et al.*, 1995; Szabo *et al.*, 1999) while the stimulation of D_2 receptors leads to an increase in the endocannabinoid AEA (Giuffrida *et al.*, 1999). Activation of either CB_1 or D_2 receptors results in the inhibition of adenylyl cyclase, however simultaneous stimulation of both receptors appears to lead to the accumulation and increase in cAMP, and ERK receptor activation (Kearn *et al.*, 2005) suggesting the presence of associated signalling pathways regulated when both receptors are activated by agonists (Glass and Felder, 1997; Kearn *et al.*, 2005). Increase in cAMP has also been reported to induce an increase in cGMP-dependent protein kinase which further potentiates relaxation of smooth muscles (Kotlikoff and Kamm, 1996) and inhibit the rhoA signalling pathway (Sah *et al.*, 2000; Somlyo and Somlyo, 2000).

A summary of the fractions tested and corresponding pharmacological effect and metabolomic analysis are listed in table 4.8.

4.9.2 The Phospholipids and their involvement in this Study

There was considerable involvement of the phospholipids, phosphatidylserine (PS), phosphatidylcholine (PC), phosphatidylethanolamine (PE) and phosphatidylinositol (PI) in this study. This is not entirely surprising as they are known to play roles in the regulation of the signal transduction pathways. Phospholipids serve as a reservoir/precursor for signalling molecules, such as AA, phosphatidate, DAG and IP₃ (Vance and Vance, 2009). The synthesis of phospholipids is based on the phosphatidic acid (PA) backbone while DAG is used in the subsequent biosynthetic pathways for PC and PE and is also the precursor to the main storage form of energy, triacylglycerol (Vance, 2008). Structures are shown in fig. 4.48.

PS and PE, also called aminophospholipids, are metabolically related and are present in cell membranes with PC being the most abundant (20% of the total phospholipids) and followed closely by PE (which accounts for approximately 15% of total phospholipids) (Vance, 2008). The majority of phospholipids are synthesized in the endoplasmic reticulum (ER) while the mitochondria provide a minor contribution (Vance, 2008).



When X = H (phosphatidic acid); **==** $-\text{CH}_2-\text{CH}_2-\text{N}(\text{CH}_3)_3$ (PC); **==** $-\text{CH}_2-\text{CH}_2-\text{NH}_3$ (PE); **=** $-\text{CH}_2-\text{CH}(\text{OH})-\text{CH}_2\text{OH}$ (phosphatidylglycerol).

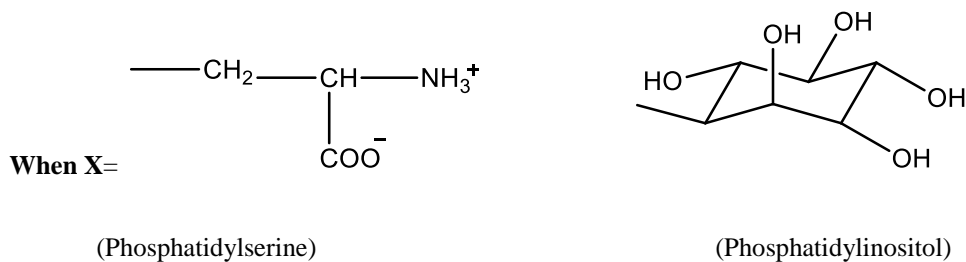


Figure 4.48 Structure of Phospholipids showing the different functional groups.

4.9.2.1 Physiological Role of Phosphatidylserine

Several important physiological processes initiate a redistribution of PS from the inner, to the outer, surface of the plasma membrane of mammalian cells. Several intracellular processes also make use of PS (Johnson *et al.*, 2000; Munnix *et al.*, 2003; van Genderen *et al.*, 2008). One primary function of PS is as the precursor of

PE through decarboxylation via the mitochondrial enzyme PS decarboxylase. The anionic nature of PS is responsible for most of its intracellular functions (Vance and Tasseva, 2013). This is confirmed because some key signalling proteins, such as the tyrosine kinase Src, and the Ras and Rho family of GTPases which contain positively-charged motifs, bind to PS resulting in membrane targeting and activation of these proteins (Lemmon, 2008). PS also modifies the catalytic activity of several key signalling proteins that contain C2 domains (Lemmon, 2008). Thus, although PS represents a quantitatively minor phospholipid in mammalian cells, the presence of PS is required for many fundamental cellular processes.

4.9.2.2 Phosphatidylethnaolamine (PE) and Anandamide (AEA)

PE is a precursor for the synthesis of AEA (anandamide) or N-arachidonylamine (NAE), the ligand for cannabinoid receptors (Jin *et al.*, 2007). In mammalian cells this protein dominates regulation of cholesterol homeostasis, and the protein processing is regulated by the level of cholesterol, not PE, in the ER (Brown *et al.*, 2000). In addition to its structural role in membranes, PE serves multiple important cellular functions that were until recently unrecognized. An association of PE with uterine contraction was observed by Phoenix and Wray in 1994 (Phoenix and Wray, 1994). This association suggests a PE-specific phospholipase C signalling pathway in the uterus as it is possible that phosphoethnaolamine is being released from membrane PE as a source of DAG, as such might also suggest a role for the involvement of PE and calcium signalling with the effect of *Ficus* fractions on uterine contraction.

4.9.2.3 Physiological Role of Phosphatidylcholine (PC)

Phosphatidylcholine (PC) once called lecithin is the major phospholipid component of mammalian cell membranes, accounting for over 50% of cell membrane phospholipids and more than 30% of total cellular lipid content. PCs are actually a diverse group of related species (Ekroos *et al.*, 2003; van Meer *et al.*, 2008). In addition to its function as a membrane constituent, PC may have a role in signalling via the generation of DAG, especially in the nucleus. The plasmalogen form of PC may also have a signalling function, as thrombin treatment of endothelial cells activates a selective hydrolysis (phospholipase A₂) of molecular species containing AA in the *sn*-2 position, releasing this fatty acid for eicosanoid production (Bills *et al.*, 1977; Lapetina *et al.*, 1981; McKean *et al.*, 1981). Other studies also support the involvement of PC with AA synthesis and release (Chien *et al.*, 1984; Grillone *et al.*, 1988; Price *et al.*, 1989). PC is the biosynthetic precursor of sphingomyelin (Voelker and Kennedy, 1982) and as such must have some influence on the many metabolic pathways that constitute the sphingomyelin cycle. It is also a precursor for phosphatidic acid (Lassegue *et al.*, 1993), lysoPC and platelet-activating factor (Stremmler *et al.*, 1989), and of PS (Juneja *et al.*, 1989) each with important signalling functions. PC synthesis is also observed when 3-deaza-adenosine, an inhibitor of the transmethylation pathway, is administered to rats (Pritchard *et al.*, 1982). Cyclic AMP also stimulates phospholipid methyltransferase. A study showed that stimulation of β -adrenergic receptors activated phospholipid methyltransferase facilitating the coupling of β -receptor-adenylate cyclase (Hirata *et al.*, 1979). Thus cAMP promotes inhibition of the synthesis of PC (Marin-Cao *et al.*, 1983) and both cAMP and PC were found to be some of the dominant metabolites

mediating the action of *Ficus* fractions on the uterus. Interestingly, a crosstalk between PC appears to occur with different pathways this includes synthesis of PE and consequently AEA, as well as the indirect inhibition of cAMP.

4.9.2.4 Physiological Role of Phosphatidylinositol (PI)

Phosphatidylinositol (PI) is an acidic (anionic) phospholipid that in essence consists of a phosphatidic acid backbone, linked via the phosphate group to inositol (Barlow *et al.*, 2010). In most organisms, the stereochemical form of the latter is *myo*-D-inositol (Parthasarathy and Eisenberg, 1986). PI is present in all tissues and cell types. There is usually less of it than of PC, PE and PS (Barlow *et al.*, 2010). PI is formed biosynthetically from the precursor cytidine diphosphate diacylglycerol (CDP-DAG) by reaction with inositol, and catalysed by the enzyme CDP-DAG inositol phosphatidyltransferase (PI synthase) (Lykidis *et al.*, 1997). The enzyme is also located mainly in the ER, and PI is then delivered to other membranes either by vesicular transport or via the use of specific transfer proteins (Christie and Han, 2010). In animal tissues, PI is the primary source of the AA required for biosynthesis of eicosanoids and also the main source of DAG that serve as a signalling molecule (Berridge and Irvine, 1984). 2-Arachidonoyl-glycerol, an endogenous cannabinoid receptor ligand, may also be a product of PI catabolism (Boss and Im, 2012).

Generally, phosphoinositides have a central and general function in the fields of cell signalling and regulation. They are able to achieve signalling effects directly by binding to cytosolic proteins or specific cytosolic domains of membrane proteins via their polar head groups, thereby triggering downstream signalling cascades. In this way, they can regulate the function of innumerable proteins integral to

membranes, for example by relocating a protein from one area of the cell to another, usually from the cytosol to the inner leaflet of the plasma membrane, or they can attract cytoskeletal and signalling components to the membrane. Amongst the proteins that bind to phosphoinositides in this way are phospholipases, protein kinases, regulators of membrane trafficking, and cytoskeletal, scaffold and ion channel proteins (Vicinanza *et al.*, 2008). It is therefore not surprising that PI has functional and probably regulatory roles in the action of *Ficus* fractions on the uterus and is also linked to the MI signalling observed.

Table 4.9 Signal Transduction Pathways in the Uterus Activated by Endocannabinoids on Binding to Different Receptors

RECEPTOR	SIGNAL TRANSDUCTION	PHYSIOLOGICAL EFFECT
CB ₁ and CB ₂	<ul style="list-style-type: none"> •Decrease in adenylyate cyclase; •Increase focal adhesion kinase (FAK) and mitogen-activated protein kinase (MAPK); •Increase extracellular signal regulated kinases (ERK), p38 through CB₁,and PI3K/Akt through CB₂; •Increase K⁺ channels; •Decrease Ca²⁺ channels 	<p>Uterine contraction;</p> <p>Uterine contraction;</p> <p>Uterine contraction;</p> <p>Uterine relaxation;</p> <p>Uterine relaxation</p>

Table 4.9 continued. Signal Transduction Pathways in the Uterus Activated by Endocannabinoids on Binding to Different Receptors

RECEPTOR	SIGNAL TRANSDUCTION	PHYSIOLOGICAL EFFECT
GPR55 (G protein coupled receptor 55)	<ul style="list-style-type: none"> •Increase Intracellular [Ca²⁺]; •Increase RhoA, Rac, and Cdc42; •Increase ERK phosphorylation 	Uterine contraction; Uterine contraction; Uterine contraction
TRPV1 (transient receptor potential vanilloid 1)	<ul style="list-style-type: none"> •Increase Intracellular [Ca²⁺]; •Increase Caspases; •Increase Cytochrome c release; •Increase Mitochondrial uncoupling; •Increase Pro-apoptotic kinases 	Uterine contraction; Uterine relaxation; Uterine relaxation; Uterine relaxation; Not entirely applicable
PPARs (peroxisome proliferator-activated receptors)	<ul style="list-style-type: none"> •Increase ROS; •Increase Tyrosine kinases; •Increase Adiponectin and lipoprotein lipase 	Uterine contraction

Modified (Battista *et al.*, 2012).

4.9.3 CONCLUSION

From the pharmaco-metabolomic analysis, several signalling pathways have been detected to be involved in the effect of the leaves of *Ficus* on uterine contractility. These pathways include cAMP, phosphoinositide, GABA, RhoA, ERK, and endocannabinoids. Certainly further verification studies are required. However, it would also make for interesting future research to investigate the possibility of

crosstalk in the mechanism of activity of *Ficus*, as it may well be that activation of just one or two receptors may have led to interaction with other pathways due to the intraconnectivity. The significance of phospholipids and endocannabinoids both of which play regulatory roles in the uterus is worth further investigation as not many studies have been performed on this. Especially since it has become increasingly evident that a dysregulation of endocannabinoids is connected to pathological conditions, therefore modulation of the activities of endocannabinoids is expected to have a massive potential for research and intervention in multiple areas of human health (Battista *et al.*, 2012). Some alternative strategies to treat pain syndromes and spontaneous abortion are already being investigated based on the enhancement of the endocannabinoids tone, through the inhibition of endocannabinoids - hydrolyzing enzymes (Jhaveri *et al.*, 2007). An in-depth understanding of signal transduction pathways discovered from this study could therefore provide a significant aid in the design of compounds such as those isolated from *F. exasperata* and might prove useful in the treatment and prevention of preterm labour/birth.

CHAPTER FIVE

SUMMARY, FUTURE RESEARCH AND CONCLUDING REMARKS

This study was designed to investigate the effect of the leaf extracts of *F. exasperata* on uterine contractility and it was based primarily on the need to search for and develop new uterine active compounds to treat and manage existing uterine disorders which represent a significant health burden such as preterm birth and complications of labour. The plant, *F. exasperata*, was chosen based on its common use by traditional healers in Africa and particularly Nigeria for the treatment of uterine disorders. The goal of this study was to identify the phytochemical constituents of the active extracts and fractions and also to pharmacologically analyse these constituents using the isolated mouse uterus. The study also aimed to map out possible mechanisms of activity of the active constituents. In the process, several uterine active constituents belonging to different phytochemical classes were isolated and identified, and possible mechanisms of activity were also provided with the aid of a metabolomic technique developed in the course of study. In general, the study sought to answer these questions:

1. Are there uterine active compounds in the leaves of *F. exasperata*?
2. Are these compounds novel?
3. What are the possible mechanisms of activity of these compounds?

5.1 Isolation and Identification of Uterine Active Phytochemical Constituents of *F. exasperata*

In the course of this study, fourteen phytochemical compounds belonging to 4 general phytochemical classes were isolated and identified as having effects on uterine contractility. These compounds were isolated from the ethylacetate and the methanol leaf extracts of *F. exasperata*. The phytochemical classes identified included: (1) Fatty acids from which two active compounds were identified; (2) Pheophorbides and Pheophytins from which seven active compounds were identified; (3) Flavonoids from which four active compounds were identified and, (4) Pyrimidines from which one active compound was identified. In addition, KCl was found in high yields in the methanol extract. Eight of these compounds were found to be new compounds as they have never been previously discovered, therefore supporting the hypothesis that the leaves of *F. exasperata* contain new uterine active compounds. These compounds were found to exhibit varied effects of inhibition and stimulation of contractility on the uterus. Since none of the compounds were of 100% purity it is suggested that the minute presence of the salt may have contributed in some way to the contractile activities observed in some of these compounds. It is therefore suggested that further studies be performed to synthesize these compounds. It is also suggested that further pharmacological assays be performed on the synthesized compounds (which lack the presence of salts) to compare the effects between the synthesized compounds and those observed with the compounds in their natural state.

5.2 Development of a Metabolomic Model for the Investigation of Drug Action

A new model which was evaluated and found to be very useful in the determination of mechanisms of action of natural products was also developed in the course of this study. The development of this model was necessitated by the need to evaluate pharmacological activities of natural products after several fractionation processes. Oftentimes after the second or third fractionation/purification process, the quantities of the samples are drastically reduced and may not allow for further pharmacological or physiological evaluations. This may therefore force a re-extraction and/or re-fractionation which are very expensive and largely time-consuming. This model was designed such that functional pharmacological assays are performed using a pre-determined set of animals or tissues and the drug-treated tissues are subjected to ¹H-NMR and mass spectrometric analysis. Briefly, while the drug is still in contact with the tissues, the tissues are flash-frozen in liquid nitrogen; the physiological fluids are also collected and flash-frozen. The samples are then stored in -80°C until further studies. The samples are then extracted and subjected to metabolomic assays which provide fingerprints of metabolites that were perturbed within the tissues under the influence of the drugs. Application of this model therefore completely erases the processes of re-extraction and re-evaluation while significantly reducing the number of animals that would have been employed in the re-evaluation phase. At the same time, this model speeds up the process of developing hypotheses for mechanisms of activity of the compound being tested. This it does by the creation of knowledge-based hypotheses through the combination of multivariate analyses and bioinformatics applied to the resulting metabolomic data. Validation of this model

was achieved by applying this model to the evaluation of oxytocin and ritodrine which are both uterine active drugs with known mechanisms of action. The model also provided added information by assessment of the metabolites released into the surrounding physiological fluid into which the uterine tissue was immersed for assessment. This new technique that involves coupling of functional pharmacological assays with metabolomics therefore provides a new model in the pharmacological evaluation of the function of drugs.

5.3 Application of Pharmacology coupled with Metabolomics in the Evaluation of the Mechanism of Action of the Fractions

In this study also, metabolomics was systematically applied in the evaluation of the mechanism of action of the fractions obtained in this study. From this study, the following mechanisms of action are being proposed for the fractions of *F. exasperata* on uterine contractility:

- 1). The fraction **F14** which contained compound **1**, acts primarily by affecting the regulation of cAMP, endocannabinoids, GABA and MI. The possibility of a connection with the catecholamines, DAG, ERK1/2 and prostanoids is also postulated.
- 2). The fraction **F4-31** which contained compound **6**, acts primarily by affecting cAMP, sphingosine, glutamate and GABA. Possible connection with catecholamines, endocannabinoids, ERK1/2, RhoA, DAG and MI is also postulated.

3). The fraction **F6.17**, which contained compounds **3**, **4**, and **5**, acts primarily by affecting cAMP, Dopamine, ERK1/2 and glutamate. Possible connection with other catecholamines, prostanoids, MI, RhoA and GABA is also suggested.

4). The fraction, **F28**, which contained compounds, **10**, **11**, **12** and **13**, acts primarily via interaction with dopamine, cAMP, ERK1/2, and GABA. Possible connection with MI, endocannabinoids and DAG is also suggested.

The other compounds could not be evaluated as they were almost completely exhausted during the pharmacological analysis. This model has however generated a framework of possible mechanisms of activity on which further supporting and confirmatory assays can be done. The possibility of receptor crosstalk can also be examined.

5.4 Future Research

From the outcome of this study, it is recommended that each identified active compound be synthesized in sufficient quantities to allow for further evaluation. The synthesized compounds should then be subjected to cytotoxicity assays and pharmacokinetic assays in order to generate profiles on toxicity, absorption, distribution, metabolism and excretion parameters. In-depth cellular assays on mechanism of activity based on the data generated from the pharmaco-metabolomic assay should also be performed. Assessment of the potency of these compounds in comparison with other known tocolytic agents is also suggested. The possibility of encapsulating these compounds in novel nanocarriers should be examined in future research as well as the possible development of target proteins that deliver the

encapsulated drugs directly to the myometrium. These latter ideas offer an innovative direction to the future of this research.

Optimisation of the metabolomic model such that it can be effectively positioned as a technique that largely replaces or minimizes the use of *in vitro* models requiring isolated tissues is suggested. This can involve application of the model in uterine cell assays.

5.5 Conclusion

Conclusively, this study has provided lead chemical series from the tropical plant *F. exasperata* in the discovery of drugs that can be developed further for the management of preterm labour and uterine disorders. Finally, the pharmacometabolomic model positions itself as a lead technique that can be employed in drug discovery research laboratories and pharmaceutical industries alike as a fast and efficient method for investigating the mechanisms of drug action and function.

6.0 REFERENCES

- Aaronson, P. I., Sarwar, U., Gin, S., Rockenbauch, U., Connolly, M., Tillet, A., Watson, S., Liu, B. & Tribe, R. M. (2006). A role for voltage-gated, but not Ca²⁺-activated, K⁺ channels in regulating spontaneous contractile activity in myometrium from virgin and pregnant rats. *British Journal of Pharmacology*, 147: 815-824.
- Abo, K. A., Fred-Jaiyesimi, A. A. & Jaiyesimi, A. E. (2008). Ethnobotanical studies of medicinal plants used in the management of diabetes mellitus in South Western Nigeria. *Journal of Ethnopharmacology*, 115: 67-71.
- Abotsi, W. M., Woode, E., Ainooson, G. K., Amo-Barimah, A. K. & Boakye-Gyasi, E. (2010). Antiarthritic and antioxidant effects of the leaf extract of *Ficus exasperata* P. Beauv. (Moraceae). *Pharmacognosy Research*, 2: 89-97.
- Achrekar, S., Kaklij, G. S., Pote, M. S. & Kelkar, S. M. (1991). Hypoglycemic activity of *Eugenia jambolana* and *Ficus bengalensis*: mechanism of action. *In Vivo*, 5 : 143-147.
- Adam, L. P., Franklin, M. T., Raff, G. J. & Hathaway, D. R. (1995). Activation of mitogen-activated protein kinases in porcine carotid arteries. *Circulation Research*, 76: 183-190.
- Adewole, S. O., Adenowo, T. K., Naicker, T., & Ojewole, J. A. (2011). Hypoglycaemic and hypotensive effects of *Ficus exasperata* Vahl.(Moraceae) leaf aqueous extracts in rats. *African Journal of Traditional, Complementary and Alternative Medicines*, 8(3) : 275-283.

Adjanohoun, E., Adjakidje, V., Ahyi, M. R. A., Akpagana, K., Chibon, P., El-Hadji, A., Eyme, J., Garba, M., Gassita, J. N., Gbeassor, M., Goudote, E., Guinko, S., Hodouto, K. K., Houngnon, P., Keita, A., Keoula, W. P., Kluga-Ocloo, I., Lo, K. M. & Siamevi, K. K. (1986). Contribution aux études ethnobotaniques et floristiques au Togo. Paris. p. 671

Agrawal, S. & Agarwal, S. S. (1990). Preliminary observations on leukaemia specific agglutinins from seeds. *Indian Journal of Medical Research*, 92: 38-42.

Aguilar, H. N. & Mitchell, B. F. (2010). Physiological pathways and molecular mechanisms regulating uterine contractility. *Human Reproduction Update*, 16: 725-744.

Ahmad, S., Rao, H., Akhtar, M., Ahmad, I., & Munawar, M. (2011). Phytochemical composition and pharmacological prospectus of *Ficus bengalensis* Linn.(Moraceae) A review. *Journal of Medicinal Plants Research*,5(28) :6393-6400.

Ahmed, F. & Urooj, A. (2010). Hepatoprotective effects of *Ficus racemosa* stem bark against carbon tetrachloride-induced hepatic damage in albino rats. *Pharmaceutical Biology*, 48: 210-216.

Akah, P. A., Gamaniel, K. S., Wambebe, C. N., Shittu, A., Kapu, S. D., & Kunle, O. O. (1997). Studies on the gastrointestinal properties of *Ficus exasperata*. *Fitoterapia*, 68(1) : 17-20.

Akah, P. A., Orisakwe, O. E., Gamaniel, K. S. & Shittu, A. (1998). Evaluation of Nigerian traditional medicines: II. Effects of some Nigerian folk remedies on peptic ulcer. *Journal of Ethnopharmacology*, 62: 123-127.

- Aley, P. K., Noh, H. J., Gao, X., Tica, A. A., Brailoiu, E. & Churchill, G. C. (2010). A functional role for nicotinic acid adenine dinucleotide phosphate in oxytocin-mediated contraction of uterine smooth muscle from rat. *Journal of Pharmacology and Experimental Therapeutics*, 333: 726-735.
- Allen, K. G. & Harris, M. A. (2001). The role of n-3 fatty acids in gestation and parturition. *Experimental Biology and Medicine*, 226: 498-506.
- Allix, S., Reyes-Gomez, E., Aubin-Houzelstein, G., Noel, D., Tiret, L., Panthier, J. J. & Bernex, F. (2008). Uterine contractions depend on KIT-positive interstitial cells in the mouse: genetic and pharmacological evidence. *Biology of Reproduction*, 79: 510-517.
- Amano, M., Ito, M., Kimura, K., Fukata, Y., Chihara, K., Nakano, T., Matsuura, Y. & Kaibuchi, K. (1996). Phosphorylation and activation of myosin by Rho-associated kinase (Rho-kinase). *Journal of Biological Chemistry*, 271: 20246-20249.
- Anderegg, R. J. (1990). Mass spectrometry: an introduction. *Methods of Biochemical Analysis*, 34: 1-89.
- Andersson, R. G., Berg, G., Johansson, S. R. & Ryden, G. (1980). Effects of non-selective and selective beta-adrenergic agonists on spontaneous contractions and cyclic AMP levels in myometrial strips from pregnant women. *Gynecologic and Obstetric Investigation*, 11: 268-293.
- Anotayanonth, S., Subhedar, N. V., Garner, P., Neilson, J. P. & Harigopal, S. (2004). Betamimetics for inhibiting preterm labour. *Cochrane Database of Systematic Reviews*: CD004352.

Anowi, C. F., Emezio, U. U. A. U., & Utoh-Nedosa, A. U. (2012). Anti-diarrhoeal, antispasmodic and phytochemical properties of ethanol extract of the leaves of *Ficus exasperata*. *Asian Journal of Research in Pharmaceutical Sciences*, 2(1) : 26-32.

Anwer, K., Oberti, C., Perez, G. J., Perez-Reyes, N., McDougal, J. K., Monga, M., Sanborn, B. M., Stefani, E. & Toro, L. (1993). Calcium-activated K⁺ channels as modulators of human myometrial contractile activity. *American Journal of Physiology*, 265: 976-985.

Arita, M. (2004). Brief Functional Genomic. *Proteomic*, 77:2201-2209.

Arkininstall, S. J. & Jones, C. T. (1985). Regional changes in catecholamine content of the pregnant uterus. *Journal of Reproduction and Fertility*, 73: 547-557.

Asala, A. K., Diab, A. A., Atia, K. I. & Fatthy, M. A. (2013). Cannabinoid Induced Changes in rat Uterine Contractility. *Zagazig University Medical Journal*, 19: 154-168.

Asboth, G., Phaneuf, S. & Lopez Bernal, A. L. (1997). Prostaglandin E receptors in myometrial cells. *Acta Physiologica Hungarica*, 85: 39-50.

Aubin, Y., Freedberg, D.I., & Keire, D.A. (2014). One- and Two- Dimensional NMR Techniques for Biopharmaceuticals, In Biophysical Characterization of Proteins in Developing Biopharmaceuticals. In Biophysical Characterization of Proteins in Developing Biopharmaceuticals. Damian J. HoudeSteven A. (eds.) Berkowitz, Elsevier, Amsterdam. Pages 341-383.

Augusti, K. T. (1975). Hypoglycaemic action of bengalenoside, a glucoside isolated from *Ficus bengalensis* Linn, in normal and alloxan diabetic rabbits. *Indian Journal of Physiology and Pharmacology*, 19: 218-220.

Ayinde, B. A., Omogbai, E. K. & Amaechina, F. C. (2007). Pharmacognosy and hypotensive evaluation of *Ficus exasperata* Vahl (Moraceae) leaf. *Acta Poloniae Pharmaceutica*, 64: 543-546.

Babiychuk, E. B., Monastyrskaya, K., Burkhard, F. C., Wray, S. & Draeger, A. (2002). Modulating signaling events in smooth muscle: cleavage of annexin 2 abolishes its binding to lipid rafts. *FASEB Journal*, 16: 1177-1184.

Bae, J., Peters-Golden, M. & Loch-Carusio, R. (1999). Stimulation of pregnant rat uterine contraction by the polychlorinated biphenyl (PCB) mixture aroclor 1242 may be mediated by arachidonic acid release through activation of phospholipase A2 enzymes. *Journal of Pharmacology and Experimental Therapeutics*, 289: 1112-1120.

Bafor, E. E. & Igbinuwen, O. (2009). Acute toxicity studies of the leaf extract of *Ficus exasperata* on haematological parameters, body weight and body temperature. *Journal of Ethnopharmacology*, 123: 302-307.

Bafor, E. E., Nwiko, M., Omogbai, E. K. I., Ozolua, R. I., & Nworgu, Z. A. M. (2009a). Evaluation of the Proposed Inhibitory Effect of the Aqueous Stem-Bark Extract of *Ficus exasperata* on Uterine Preparations in vitro. *International Journal of Pharmacology*, 5(1) : 94-97.

- Bafor, E. E., Omogbai, E. K. & Ozolua, R. I. (2010a). In vitro determination of the uterine stimulatory effect of the aqueous leaf extract of *Ficus exasperata*. *Journal of Ethnopharmacology*, 127: 502-507.
- Bafor, E. E., Omogbai, E. K. & Ozolua, R. I. (2011). Oxytocin inhibiting effect of the aqueous leaf extract of *Ficus exasperata* (Moraceae) on the isolated rat uterus. *Acta Poloniae Pharmaceutica*, 68: 541-547.
- Bafor, E. E., Omogbai, E. K. I. & Ozolua, R. I. (2009b). Evaluation of the uterotonic activity of the aqueous leaf extract of *Ficus exasperata* Vahl. (Moraceae). *Research Journal of Medicinal Plants*, 3: 34-40.
- Bafor, E. E., Uwumarongie, H. O. & Idiake, J. O. (2010b). Antipyretic effects of the aqueous, ethylacetate and hexane extracts of *Ficus exasperata* (Moraceae) in mice. *Thermal Biology*, 35: 275-279.
- Bakker, J., & Baum, M. J. (2000). Neuroendocrine regulation of GnRH release in induced ovulators. *Frontiers in neuroendocrinology*, 21(3) : 220-262.
- Barata, H., Thompson, M., Zielinska, W., Han, Y. S., Mantilla, C. B., Prakash, Y. S., Feitoza, S., Sieck, G. & Chini, E. N. (2004). The role of cyclic-ADP-ribose-signaling pathway in oxytocin-induced Ca²⁺ transients in human myometrium cells. *Endocrinology*, 145: 881-889.
- Barlow, C.A., Laishram, R. S. & Anderson, R. A. (2010). Nuclear phosphoinositides: a signaling enigma wrapped in a compartmental conundrum. *Trends in Cell Biology*, 20: 25-35.

- Barton, E. R., Morris, L., Kawana, M., Bish, L. T. & Toursel, T. (2005). Systemic administration of L-arginine benefits mdx skeletal muscle function. *Muscle and Nerve*, 32: 751-760.
- Battista, N., Di Tommaso, M., Bari, M. & Maccarrone, M. (2012). The endocannabinoid system: an overview. *Frontiers in Behavioural Neuroscience*, 6: 9.
- Battista, N., Pasquariello, N., Di Tommaso, M. & Maccarrone, M. (2008). Interplay between endocannabinoids, steroids and cytokines in the control of human reproduction. *Journal of Neuroendocrinology*, 20 Suppl 1: 82-89.
- Becher, A., Green, A., Ige, A. O., Wise, A., White, J. H. & Mcilhinney, R. A. (2004). Ectopically expressed gamma-aminobutyric acid receptor B is functionally down-regulated in isolated lipid raft-enriched membranes. *Biochemical and Biophysical Research Communications*, 321: 981-987.
- Becher, A., White, J. H. & Mcilhinney, R. A. (2001). The gamma-aminobutyric acid receptor B, but not the metabotropic glutamate receptor type-1, associates with lipid rafts in the rat cerebellum. *Journal of Neurochemistry*, 79: 787-795.
- Beck, S., Wojdyla, D., Say, L., Betran, A. P., Merialdi, M., Requejo, J. H., Rubens, C., Menon, R. & Van Look, P. F. (2010). The worldwide incidence of preterm birth: a systematic review of maternal mortality and morbidity. *Bulletin of the World Health Organization*, 88: 31-38.
- Berridge, M. J. & Irvine, R. F. (1984). Inositol trisphosphate, a novel second messenger in cellular signal transduction. *Nature*, 312: 315-321.

Berridge, M. J. & Irvine, R. F. (1989). Inositol phosphates and cell signalling. *Nature*, 341: 197-205.

Berridge, M. J. (2008). Smooth muscle cell calcium activation mechanisms. *Journal of Physiology*, 586: 5047-50461.

Bhalla, R., Narasimhan, K. & Swarup, S. (2005). Metabolomics and its role in understanding cellular responses in plants. *Plant Cell Reports*, 24: 562-571.

Biao-Yi, Z., Yu, Y. & Zeng-Liang, Y. (2008). Investigation of antimicrobial model of *Hemsleya pengxianensis* W.J. Chang and its main active component by metabolomics technique. *Journal of Ethnopharmacology*, 116: 89-95.

Bills, T. K., Smith, J. B. & Silver, M. J. (1977). Selective release of arachidonic acid from the phospholipids of human platelets in response to thrombin. *Journal of Clinical Investigation*, 60: 1-6.

Bisogno, T., Melck, D., Bobrov, M., Gretskaya, N. M., Bezuglov, V. V., De Petrocellis, L. & Di Marzo, V. (2000). N-acyl-dopamines: novel synthetic CB(1) cannabinoid-receptor ligands and inhibitors of anandamide inactivation with cannabimimetic activity in vitro and in vivo. *Biochemical Journal*, 351 (3): 817-824.

Blanch, G., Lavender, T., Walkinshaw, S. & Alfirevic, Z. (1998). Dysfunctional labour: a randomised trial. *British Journal of Obstetrics and Gynaecology*, 105: 117-120.

Blaustein, M. P., Golovina, V. A., Song, H., Choate, J., Lencesova, L., Robinson, S. W. & Wier, W. G. (2002). Organization of Ca²⁺ stores in vascular smooth muscle:

functional implications. *Novartis Foundation Symposium*, 246: 125-137; discussion 137-141, 221-227.

Boss, W. F. & Im, Y. J. (2012). Phosphoinositide signaling. *Annual Review of Plant Biology*, 63: 409-429.

Bowery, N. G., Bettler, B., Froestl, W., Gallagher, J. P., Marshall, F., Raiteri, M., Bonner, T. I. & Enna, S. J. (2002). International Union of Pharmacology. XXXIII. Mammalian gamma-aminobutyric acid(B) receptors: structure and function. *Pharmacological Reviews*, 54: 247-264.

Brainard, A. M., Miller, A. J., Martens, J. R. & England, S. K. (2005). Maxi-K channels localize to caveolae in human myometrium: a role for an actin-channel-caveolin complex in the regulation of myometrial smooth muscle K⁺ current. *American Journal of Physiology, Cell Physiology*, 289: C49-C57.

Breuiller-Fouche, M., Doualla-Bell Kotto Maka, F., Geny, B. & Ferre, F. (1991). Alpha-1 adrenergic receptor: binding and phosphoinositide breakdown in human myometrium. *Journal of Pharmacology and Experimental Therapeutics*, 258: 82-87.

Brighton, P. J., McDonald, J., Taylor, A. H., Challiss, R. A., Lambert, D. G., Konje, J. C. & Willets, J. M. (2009). Characterization of anandamide-stimulated cannabinoid receptor signaling in human ULTR myometrial smooth muscle cells. *Molecular Endocrinology*, 23: 1415-1427.

Bronson F.H., Dagg, C. P., Snell, G. D. (1966). *Reproduction*. New York: Dover Publications, Inc.;

- Brown, D. A. & London, E. (1998). Functions of lipid rafts in biological membranes. *Annual Review Cell and Developmental Biology*, 14: 111-136.
- Brown, I., Cascio, M. G., Rotondo, D., Pertwee, R. G., Heys, S. D. & Wahle, K. W. (2013). Cannabinoids and omega-3/6 endocannabinoids as cell death and anticancer modulators. *Progress in Lipid Research*, 52: 80-109.
- Brown, M. S., Ye, J., Rawson, R. B. & Goldstein, J. L. (2000). Regulated intramembrane proteolysis: a control mechanism conserved from bacteria to humans. *Cell*, 100: 391-398.
- Bui-Xuan, N. H., Tang, P. M., Wong, C. K. & Fung, K. P. (2010). Photo-activated pheophorbide-a, an active component of *Scutellaria barbata*, enhances apoptosis via the suppression of ERK-mediated autophagy in the estrogen receptor-negative human breast adenocarcinoma cells MDA-MB-231. *Journal of Ethnopharmacology*, 131: 95-103.
- Bulbring E and Tomito T. (1987). Catecholamine action on smooth muscle. *Pharmacology Reviews*, 39: 49–96.
- Bulletti, C., De Ziegler, D., De Moustier, B., Polli, V., Bolelli, G., Franceschetti, F. & Flamigni, C. (2001). Uterine contractility: vaginal administration of the beta-adrenergic agonist, terbutaline. Evidence of direct vagina-to-uterus transport. *Annals of the New York Academy of Sciences*, 943: 163-171.
- Burbach, J. P. H., Young, L. J. & Russell, A. J. (2006). Oxytocin: Synthesis, Secretion and Reproductive Functions. In: NEIL, J. D. (ed.) *Knobil and Neil's Physiology of Reproduction*. 3rd ed. U. S. A: Elsevier Academy Press. p. 3095.

Burdyga, T. & Wray, S. (2005). Action potential refractory period in ureter smooth muscle is set by Ca²⁺ sparks and BK channels. *Nature*, 436: 559-562.

Burdyga, T., Wray, S. & Noble, K. (2007). In situ calcium signaling: no calcium sparks detected in rat myometrium. *Annals of the New York Academy of Sciences*, 1101: 85-96.

Busch, L., Sterin-Borda, L. & Borda, E. (2004). Expression and biological effects of CB1 cannabinoid receptor in rat parotid gland. *Biochemical Pharmacology*, 68: 1767-1774.

Buxton, I. L. (2004). Regulation of uterine function: a biochemical conundrum in the regulation of smooth muscle relaxation. *Molecular Pharmacology*, 65: 1051-1059.

Cabral, R., Gutierrez, M., Fernandez, A. I., Cantabrana, B. & Hidalgo, A. (1994). Progesterone and pregnanolone derivatives relaxing effect on smooth muscle. *General Pharmacology*, 25: 173-178.

Cai, H., Liu, X., Chen, Z., Liao, S. & Zou, Y. (2013). Isolation, purification and identification of nine chemical compounds from *Flammulina velutipes* fruiting bodies. *Food Chemistry*, 141: 2873-2879.

Caligioni, C. 2009. Assessing Reproductive Status/Stages in Mice. *Current Protocol in Neuroscience*. APPENDIX: Appendix-4I. doi:10.1002/0471142301.nsa04is48

Cannell, R. J. P. (1998). How to Approach the Isolation of a Natural Product. In: CANNELL, R. J. P. (ed.) *Natural Products Isolation*. New Jersey, U. S. A.: Humana press. p 1-52.

- Carew, B. A. R., Mosi, A. K., Mba, A. U. & Egbunike, G. N. (1980). The potential of browse plants in the nutrition of small ruminants in the humid forest and derived savanna zones of Nigeria. *Browse in Africa*, 20: 307-311.
- Casey, M. L., Korte, K. & Macdonald, P. C. (1988). Epidermal growth factor stimulation of prostaglandin E₂ biosynthesis in amnion cells. Induction of prostaglandin H₂ synthase. *Journal of Biological Chemistry*, 263: 7846-7854.
- Cavanagh, J., Fairbrother, W. J., Plamer, A.G., Rance, M., & Skelton, N.J. (2007). Protein NMR spectroscopy, principles and practice. San Diego: Elsevier Academic Press.
- Celik, O., Sarac, K., Hascalik, S., Alkan, A., Mizrak, B. & Yologlu, S. (2004). Magnetic resonance spectroscopy features of uterine leiomyomas. *Gynecologic and Obstetric Investigation*, 58: 194-201.
- Chagoyen, M., Pazos, F., (2012). Tools for the functional interpretation of metabolomic experiments. *Briefings in Bioinformatics* doi:10.1093/bib/bbs055
- Challis, J. R. G. & Lye, S. J. (1994). Parturition. In: KNOBIL, E. & NEILL, J. D. (eds.) *The Physiology of Reproduction*. New York, U. S. A: Raven Press. p 985-1031.
- Chan, W. Y. (1980). The separate uterotonic and prostaglandin-releasing actions of oxytocin. Evidence and comparison with angiotensin and methacholine in the isolated rat uterus. *Journal of Pharmacology and Experimental Therapeutics*, 213: 575-579.

Charpigny, G., Leroy, M. J., Breuiller-Fouche, M., Tanfin, Z., Mhaouty-Kodja, S., Robin, P., Leiber, D., Cohen-Tannoudji, J., Cabrol, D., Barberis, C. & Germain, G. (2003). A functional genomic study to identify differential gene expression in the preterm and term human myometrium. *Biology of Reproduction*, 68: 2289-2296.

Chen, C. S., Weng, S. C., Tseng, P. H., Lin, H. P. & Chen, C. S. (2005). Histone acetylation-independent effect of histone deacetylase inhibitors on Akt through the reshuffling of protein phosphatase 1 complexes. *Journal of Biological Chemistry*, 280: 38879-38887.

Cheng, H., Lederer, W. J. & Cannell, M. B. (1993). Calcium sparks: elementary events underlying excitation-contraction coupling in heart muscle. *Science*, 262: 740-744.

Cheng, Z., Elmes, M., Abayasekara, D. R. & Wathes, D. C. (2003). Effects of conjugated linoleic acid on prostaglandins produced by cells isolated from maternal intercotyledonary endometrium, fetal allantochorion and amnion in late pregnant ewes. *Biochimica et Biophysica Acta*, 1633: 170-178.

Cheng, Z., Robinson, R. S., Pushpakumara, P. G., Mansbridge, R. J. & Wathes, D. C. (2001). Effect of dietary polyunsaturated fatty acids on uterine prostaglandin synthesis in the cow. *Journal of Endocrinology*, 171: 463-473.

Chien, K. R., Han, A., Sen, A., Buja, L. M. & Willerson, J. T. (1984). Accumulation of unesterified arachidonic acid in ischemic canine myocardium. Relationship to a phosphatidylcholine deacylation-reacylation cycle and the depletion of membrane phospholipids. *Circulation Research*, 54: 313-322.

Childs, T. J., Watson, M. H., Sanghera, J. S., Campbell, D. L., Pelech, S. L. & Mak, A. S. (1992). Phosphorylation of smooth muscle caldesmon by mitogen-activated protein (MAP) kinase and expression of MAP kinase in differentiated smooth muscle cells. . *Journal of Biological Chemistry*, 267: 22853–22859.

Chiossi, G., Costantine, M. M., Bytautiene, E., Kechichian, T., Hankins, G. D., Sbrana, E., Saade, G. R. & Longo, M. (2012). The effects of prostaglandin E1 and prostaglandin E2 on in vitro myometrial contractility and uterine structure. *American Journal of Perinatology*, 29: 615-622.

Christie, W. W. & Han, X. (2003). *Lipid Analysis: Isolation separation, identification and structural analysis of lipid*, London, UK, Oily Press

Christie, W. W. & Han, X. (2010). *Lipid Analysis - Isolation, Separation, Identification and Lipidomic Analysis*, Bridgwater, UK, Cambridge, UK, Oily Press, Woodhead Publishing, Ltd. p 446.

Ciray, H. N., Guner, H., Hakansson, H., Tekelioglu, M., Roomans, G. M. & Ulmsten, U. (1995). Morphometric analysis of gap junctions in nonpregnant and term pregnant human myometrium. *Acta Obstetricia et Gynecologica Scandinavica*, 74: 497-504.

Circosta, C., De Pasquale, R., Samperi, S., Pino, A. & Occhiuto, F. (2007). Biological and analytical characterization of two extracts from *Valeriana officinalis*. *Journal of Ethnopharmacology*, 112: 361-367.

Cirriolo, R., Enrico, G. T., Matthias, K. S., Anna, Q., Alexander, S., Marc, M., Jerome, D., Anthony, N., Francesco, B., Claudio, G., Lucia, G., Paolo, M., Russell, J.

T., Claude, C., Florence, L., Karine, P., Claude, B. & Andre, C. (2003). Pharmacology of (2S-4Z)-N-[(2S)-2-Hydroxy-2-Phenylethyl]-4-(Methoxyimino)-1-[(2'-methyl[1,1'-biphenyl]-4-yl)carbonyl]-2-pyrrolidinocarboxamide, a New Potent and Selective Nonpeptide Antagonist of Oxytocin Receptor. *Journal of Pharmacology and Experimental Therapeutics*, 306: 253-261.

Clardy, J. & Walsh, C. (2004). Lessons from natural molecules. *Nature*, 432: 829-837.

Claridge, T. (1999). High-resolution NMR techniques in organic chemistry. Oxford: Pergamon Press.

Cloarec, O., Dumas, M. E., Craig, A., Barton, R. H., Trygg, J., Hudson, J., Blancher, C., Gauguier, D., Lindon, J. C., Holmes, E. & Nicholson, J. (2005). Statistical total correlation spectroscopy: an exploratory approach for latent biomarker identification from metabolic ¹H NMR data sets. *Analytical Chemistry*, 77: 1282-1289.

Coelli, A. P., Nascimento, L. R., Mill, J. G. & Molina Mdel, C. (2011). [Preterm birth as a risk factor for high blood pressure in children: a systematic review]. *Cadernos de Saude Publica*, 27: 207-218.

Colquhoun, I. J. (2007). Use of NMR for metabolic profiling in plant systems. *Journal of Pesticide Science*, 32: 200-212.

Conde, E., Cadahia, E. & Garcia-Vallejo, M. C. (1992). Optimization of TLC for research on the flavonoids in wood and bark of species of the genus *Eucalyptus* L'Heritier. *Chromatographia*, 33: 418-426.

- Conde-Agudelo, A., Romero, R. & Kusanovic, J. P. (2011). Nifedipine in the management of preterm labor: a systematic review and metaanalysis. *American Journal of Obstetrics and Gynecology*, 204: 134 e131-120.
- Cordell, A. G. & Colvard, M. D. (2005). Some thoughts on the future of ethnopharmacology. *Journal of Ethnopharmacology*, 60: 52-60.
- Cosgrove, D. J. & Irving, G. C. J. (1980). Inositol phosphates: their chemistry, biochemistry and physiology, Amsterdam, Elsevier. p 191.
- Cragg, G. M. & Newman, D. J. (2013). Natural products: a continuing source of novel drug leads. *Biochimica et Biophysica Acta*, 1830: 3670-3695.
- Crankshaw, D. J. & Morrison, J. J. (2011). Methodology and pharmacological analysis of effects of uterotonic compounds in human myometrium in vitro. *American Journal of Obstetrics and Gynecology*, 205: 155 e151-e156.
- Crankshaw, D. J. (2001). Pharmacological techniques for the in vitro study of the uterus. *Journal of Pharmacological and Toxicological Methods*, 45: 123-140.
- Crawford, A. D., Liekens, S., Kamuhabwa, A. R., Maes, J., Munck, S., Busson, R., Rozenski, J., Esguerra, C. V. & De Witte, P. A. (2011). Zebrafish bioassay-guided natural product discovery: isolation of angiogenesis inhibitors from East African medicinal plants. *PLoS One*, 6: e14694.
- Crichton, C. A., Taggart, M. J., Wray, S. & Smith, G. L. (1993). Effects of pH and inorganic phosphate on force production in alpha-toxin-permeabilized isolated rat uterine smooth muscle. *Journal of Physiology*, 465: 629-645.

- Crowther, C. A., Hiller, J. E., Doyle, L. W., Haslam, R. R. & Australasian Collaborative Trial of Magnesium Sulphate Collaborative, G. (2003). Effect of magnesium sulfate given for neuroprotection before preterm birth: a randomized controlled trial. *Journal of the American Medical Association*, 290: 2669-2676.
- Czerski, A., Zawadzki, W., Zawadski, M. & Czerska, Z. (2005). Influence of dopamine on rat uterine motility in vitro. *Acta Veterinaria Brno*, 74: 9-15.
- Dabertrand, F., Morel, J. L., Sorrentino, V., Mironneau, J., Mironneau, C. & Macrez, N. (2006). Modulation of calcium signalling by dominant negative splice variant of ryanodine receptor subtype 3 in native smooth muscle cells. *Cell Calcium*, 40: 11-21.
- Dai, R., Shoemaker, R., Farrens, D., Han, M. J., Kim, C. S. & Song, P. S. (1992). Characterization of silkworm chlorophyll metabolites as an active photosensitizer for photodynamic therapy. *Journal of Natural Products Sciences*, 55: 1241-1251.
- Datwyler, S. L., & Weiblen, G. D. (2004). On the origin of the fig: phylogenetic relationships of Moraceae from ndhF sequences. *American Journal of Botany*, 91(5) : 767-777.
- Dawood, M. Y. (1988). Nonsteroidal anti-inflammatory drugs and changing attitudes toward dysmenorrhea. *American Journal of Medicine*, 84: 23-29.
- Dawood, M. Y. (1993). Nonsteroidal antiinflammatory drugs and reproduction. *American Journal of Obstetrics and Gynecology*, 169: 1255-1265.
- Dawson, M. J. & Wray, S. (1985). The effects of pregnancy and parturition on phosphorus metabolites in rat uterus studied by ³¹P nuclear magnetic resonance. *Journal of Physiology*, 368: 19-31.

- De Groot, R. H., Hornstra, G., Van Houwelingen, A. C. & Roumen, F. (2004). Effect of alpha-linolenic acid supplementation during pregnancy on maternal and neonatal polyunsaturated fatty acid status and pregnancy outcome. *American Journal of Clinical Nutrition*, 79: 251-260.
- De Ziegler, D., Bulletti, C., Fanchin, R., Epiney, M. & Brioschi, P. A. (2001). Contractility of the nonpregnant uterus: the follicular phase. *Annals of the New York Academy of Sciences*, 943: 172-184.
- Dennedy, M. C., Friel, A. M., Houlihan, D. D., Broderick, V. M., Smith, T. & Morrison, J. J. (2004). Cannabinoids and the human uterus during pregnancy. *American Journal of Obstetrics and Gynecology*, 190: 2-9; discussion 3A.
- Dennis, E. A. (1983). 9 Phospholipases. *The Enzymes*, 16: 307-353.
- Deraniyagala, S. A., Wijesundera, R. L. C. & Weerasena, O. V. D. S. J. (1998). Antifungal activity of *Ficus racemosa* leaf extract and isolation of the active compound. *Journal of the National Science Foundation of Sri Lanka*, 26: 19-26.
- Derkinderen, P., Ledent, C., Parmentier, M. & Girault, J. A. (2001). Cannabinoids activate p38 mitogen-activated protein kinases through CB1 receptors in hippocampus. *Journal of Neurochemistry*, 77: 957-960.
- Dessy, C., Kim, I., Sougnez, C. L., Laporte, R. & Morgan, K. G. (1998). A role for MAP kinase in differentiated smooth muscle contraction evoked by alpha-adrenoceptor stimulation. *American Journal of Physiology*, 275: C1081-C1086.
- Devane, W. A., Hanus, L., Breuer, A., Pertwee, R. G., Stevenson, L. A., Griffin, G., Gibson, D., Mandelbaum, A., Etinger, A. & Mechoulam, R. (1992). Isolation and

structure of a brain constituent that binds to the cannabinoid receptor. *Science*, 258: 1946-1949.

Di Marzo, V. & De Petrocellis, L. (2012). Why do cannabinoid receptors have more than one endogenous ligand? *Philosophical Transactions of the Royal Society of London. Series B, Biological Sciences*, 367: 3216-3228.

Dickson, M. & Gagnon, J. P. (2004). Key factors in the rising cost of new drug discovery and development. *Nature Reviews, Drug Discovery*, 3: 417-429.

Dmitrieva, N. & Berkley, K. J. (2002). Contrasting effects of WIN 55212-2 on motility of the rat bladder and uterus. *Journal of Neuroscience*, 22: 7147-7153.

Dongfack, M. D., Lallemand, M. C., Kuete, V., Mbazona, C. D., Wansi, J. D., Trinh-van-Dufat, H., ... & Wandji, J. (2011). A new sphingolipid and furanocoumarins with antimicrobial activity from *Ficus exasperata*. *Chemical & Pharmaceutical Bulletin*, 60(8), 1072-1075.

Downes, C. P. & Macphee, C. H. (1990). myo-inositol metabolites as cellular signals. *European Journal of Biochemistry*, 193: 1-18.

Downes, C. P. (1989). Twenty-fifth Colworth medal lecture. The cellular functions of myo-inositol. *Biochemical Society Transactions*, 17: 259-268.

Draeger, A., Wray, S. & Babiychuk, E. B. (2005). Domain architecture of the smooth-muscle plasma membrane: regulation by annexins. *The Biochemical Journal*, 387: 309-314.

- Dussourd DE, Eisner T. 1987. Vein-cutting behavior: insect counterploy to the latex defense of plants. *Science* 237: 898– 901.
- Earley, L. & Wray, S. (1993). Effects of hypoxia on force produced by agonists and depolarization and arising spontaneously in the rat uterus. *Journal of Reproduction and Fertility*, 99: 539-544.
- Ekroos, K., Ejsing, C. S., Bahr, U., Karas, M., Simons, K. & Shevchenko, A. (2003). Charting molecular composition of phosphatidylcholines by fatty acid scanning and ion trap MS3 fragmentation. *Journal of Lipid Research*, 44: 2181-2192.
- Emerson, R., (1957). Dependence of yield of photosynthesis in longwave red on wavelength and intensity of supplementary light, *Science*, 125:746.
- Erdo, S. L. (1984). Identification of GABA receptor binding sites in rat and rabbit uterus. *Biochemical and Biophysical Research Communication*, 125: 18-24.
- Erdo, S. L., Villanyi, P. & Laszlo, A. (1989). Gestational changes of GABA levels and GABA binding in the human uterus. *Life Sciences*, 44: 2009-2014.
- Eriksson, L., Johansson, E., Kettaneh-Wold, N., Trygg, J., Wikstrom, C. & Wold, S. (2006). Centering and Scaling. Multi- and Megavariate Data Analysis Part I: Basic Principles and Applications. Second ed. Sweden: Umetrics AB. p 208.
- Estan, L., Martinez-Mir, I., Rubio, E. & Morales-Olivas, F. J. (1988). Relaxant effect of dopamine on the isolated rat uterus. *Naunyn-Schmiedeberg's Archives of Pharmacology*, 338: 484-488.

- Evans, J.N.S. (1995). *Biomolecular NMR spectroscopy*. Oxford: Oxford University Press.
- Fenn, J. B., Mann, M., Meng, C. K., Wong, S. F. & Whitehouse, C. M. (1989). Electrospray ionization for mass spectrometry of large biomolecules. *Science*, 246: 64-71.
- Ferruzzi, M. G. & Blakeslee, J. (2007). Digestion, absorption, and cancer preventative activity of dietary chlorophyll derivatives. *Nutrition Research*, 27: 1-12.
- Fiehn, O. (2001). Combining genomics, metabolome analysis, and biochemical modelling to understand metabolic networks. *Comparative and Functional Genomics*, 2: 155-168.
- Fiehn, O. (2002). Metabolomics--the link between genotypes and phenotypes. *Plant Molecular Biology*, 48: 155-171.
- Follesa, P., Floris, S., Tuligi, G., Mostallino, M. C., Concas, A. & Biggio, G. (1998). Molecular and functional adaptation of the GABA(A) receptor complex during pregnancy and after delivery in the rat brain. *European Journal of Neuroscience*, 10: 2905-2912.
- Fox, S. I. (2002). Reproduction. In: Fox, S. I. (ed.) *Human Physiology*. 7th ed. U. S. A.: McGraw Hill. p 677-678.
- Freeman, ME. The neuroendocrine control of the ovarian cycle in the rat. In: Knobil, E.; Neill, JD., editors. *Physiology of Reproduction*. Raven; New York: 1994. p. 613-658.

- French, C. S., & Huang, H. S. (1957). The shape of the red absorption band of chlorophyll in live cells, *Carnegie Institution Washington Yearbook* No. 56: 266.
- Galione, A., Morgan, A. J., Arredouani, A., Davis, L. C., Rietdorf, K., Ruas, M. & Parrington, J. (2010). NAADP as an intracellular messenger regulating lysosomal calcium-release channels. *Biochemical Society Transactions*, 38: 1424-1431.
- Garcia, S., Heinzen, H., Martinez, R. & Moyna, P. (1993). Identification of flavonoids by TLC scanning analysis. *Chromatographia*, 35: 430-434.
- Garfield, R. E. & Maner, W. L. (2007). Physiology and electrical activity of uterine contractions. *Seminars in Cell and Developmental Biology*, 18: 289-295.
- Garfield, R. E. & Yallampali, C. (1994). Structure and Function of the Uterus. In: Chard, T. & Grudzinkas, G. (eds.) *The Uterus*. United Kingdom: Cambridge University Press. p 54.
- Garrod, S., Humpher, E., Connor, S. C., Connelly, J. C., Spraul, M., Nicholson, J. K. & Holmes, E. (2001). High-resolution (1)H NMR and magic angle spinning NMR spectroscopic investigation of the biochemical effects of 2-bromoethanamine in intact renal and hepatic tissue. *Magnetic Resonance in Medicine*, 45: 781-790.
- Gertsch, J., Schoop, R., Kuenzle, U. & Suter, A. (2004). Echinacea alkylamides modulate TNF-alpha gene expression via cannabinoid receptor CB2 and multiple signal transduction pathways. *FEBS Letters*, 577: 563-569.
- Gibbons, S. & Gray, A. I. (1998). Isolation by planar chromatography. *Natural products isolation*. New Jersey, U. S. A.: Humana Press. p 209-245.

- Gibbs, R. S., Romero, R., Hillier, S. L., Eschenbach, D. A. & Sweet, R. L. (1992). A review of premature birth and subclinical infection. *American Journal of Obstetrics and Gynecology*, 166: 1515-1528.
- Gilani, H. A. & Rahman, A. (2005). Trends in Ethnopharmacology. *Journal of Ethnopharmacology*, 100: 43-49.
- Gill, L. S. (1992). Ethnomedicinal uses of plants in Nigeria, Benin City, Nigeria, University of Benin Press. p 350.
- Gimpl, G. & Fahrenholz, F. (2001). The oxytocin receptor system: structure, function, and regulation. *Physiological Reviews*, 81: 629-683.
- Giuffrida, A., Parsons, L. H., Kerr, T. M., Rodriguez De Fonseca, F., Navarro, M. & Piomelli, D. (1999). Dopamine activation of endogenous cannabinoid signaling in dorsal striatum. *Nature Neuroscience*, 2: 358-363.
- Glass, M. & Felder, C. C. (1997). Concurrent stimulation of cannabinoid CB1 and dopamine D2 receptors augments cAMP accumulation in striatal neurons: evidence for a Gs linkage to the CB1 receptor. *Journal of Neuroscience*, 17: 5327-5333.
- Goldenberg, R. L. (2002). The management of preterm labor. *Obstetrics and Gynecology*, 100: 1020-1037.
- Goldenberg, R. L., Culhane, J. F., Iams, J. D. & Romero, R. (2008). Epidemiology and causes of preterm birth. *Lancet*, 371: 75-84.
- Gravina, F. S., Parkington, H. C., Kerr, K. P., De Oliveira, R. B., Jobling, P., Coleman, H. A., Sandow, S. L., Davies, M. M., Imtiaz, M. S. & Van Helden, D. F.

- (2010). Role of mitochondria in contraction and pacemaking in the mouse uterus. *British Journal of Pharmacology*, 161: 1375-1390.
- Griffin, J. L. (2006). The Cinderella story of metabolic profiling: does metabolomics get to go to the functional genomics ball? *Philosophical Transactions of the Royal Society of London. Series B, Biological Sciences*, 361: 147-161.
- Griffin, J. L., Pole, J. C., Nicholson, J. K. & Carmichael, P. L. (2003). Cellular environment of metabolites and a metabonomic study of tamoxifen in endometrial cells using gradient high resolution magic angle spinning ^1H NMR spectroscopy. *Biochimica et Biophysica Acta*, 1619: 151-158.
- Grillone, L. R., Clark, M. A., Godfrey, R. W., Stassen, F. & Crooke, S. T. (1988). Vasopressin induces V1 receptors to activate phosphatidylinositol- and phosphatidylcholine-specific phospholipase C and stimulates the release of arachidonic acid by at least two pathways in the smooth muscle cell line, A-10. *Journal of Biological Chemistry*, 263: 2658-2663.
- Grison-Pige, L., Hossaert-Mckey, M., Greeff, J. M. & Bessiere, J. M. (2002). Fig volatile compounds--a first comparative study. *Phytochemistry*, 61: 61-71.
- Gruber, C. W. & O'brien, M. (2011). Uterotonic plants and their bioactive constituents. *Planta Medica*, 77: 207-220.
- Gurib-Fakim A. (2006). Medicinal plants: traditions of yesterday and drugs of tomorrow. *Molecular Aspects of Medicine*, 27(1) : 193.
- Guse, A. H. & Lee, H. C. (2008). NAADP: a universal Ca^{2+} trigger. *Science Signaling*, 1: re10.

Guse, A. H. (2009). Second messenger signaling: multiple receptors for NAADP. *Current Biology*, 19: R521-R523.

Habayeb, O. M., Taylor, A. H., Evans, M. D., Cooke, M. S., Taylor, D. J., Bell, S. C. & Konje, J. C. (2004). Plasma levels of the endocannabinoid anandamide in women - a potential role in pregnancy maintenance and labor? *Journal of Clinical Endocrinology and Metabolism*, 89: 5482-5487.

Haeberle J R , Hathaway, D R & Ve-Paoli-Roach, A. A. (1985). Dephosphorylation of myosin by the catalytic subunit of a type-2 phosphatase produces relaxation of chemically skinned uterine smooth muscle. *Journal of Biological Chemistry*, 260 : 9965-9968.

Hajri, A., Wack, S., Meyer, C., Smith, M. K., Leberquier, C., Keding, M. & Aprahamian, M. (2002). In vitro and in vivo efficacy of photofrin and pheophorbide a, a bacteriochlorin, in photodynamic therapy of colonic cancer cells. *Photochemistry and Photobiology*, 75: 140-148.

Hall, R. D. (2006). Plant metabolomics: from holistic hope, to hype, to hot topic. *New Phytologist*, 169: 453-468.

Hansen, H. S., Moesgaard, B., Hansen, H. H. & Petersen, G. (2000). N-Acylethanolamines and precursor phospholipids - relation to cell injury. *Chemistry and Physics of Lipids*, 108: 135-150.

Harris, M. A., Hansen, R. A., Vidsudhiphan, P., Koslo, J. L., Thomas, J. B., Watkins, B. A. & Allen, K. G. (2001). Effects of conjugated linoleic acids and docosahexaenoic acid on rat liver and reproductive tissue fatty acids, prostaglandins

and matrix metalloproteinase production. *Prostaglandins, Leukotrienes, and Essential Fatty Acids*, 65: 23-29.

Heaton, R. C., Wray, S. & Eisner, D. A. (1993). Effects of metabolic inhibition and changes of intracellular pH on potassium permeability and contraction of rat uterus. *Journal of Physiology*, 465: 43-56.

Heijne, W. H., Kienhuis, A. S., Van Ommen, B., Stierum, R. H. & Groten, J. P. (2005). Systems toxicology: applications of toxicogenomics, transcriptomics, proteomics and metabolomics in toxicology. *Expert Review of Proteomics*, 2: 767-780.

Henstridge, C. M., Balenga, N. A., Ford, L. A., Ross, R. A., Waldhoer, M. & Irving, A. J. (2009). The GPR55 ligand L-alpha-lysophosphatidylinositol promotes RhoA-dependent Ca²⁺ signaling and NFAT activation. *FASEB Journal*, 23: 183-193.

Herkenham, M., Lynn, A. B., Johnson, M. R., Melvin, L. S., De Costa, B. R. & Rice, K. C. (1991). Characterization and localization of cannabinoid receptors in rat brain: a quantitative in vitro autoradiographic study. *Journal of Neuroscience*, 11: 563-583.

Hermosura, M. C., Takeuchi, H., Fleig, A., Riley, A. M., Potter, B. V., Hirata, M. & Penner, R. (2000). InsP4 facilitates store-operated calcium influx by inhibition of InsP3 5-phosphatase. *Nature*, 408: 735-740.

Hertelendy, F., Molnar, M. & Rigo, J., Jr. (1995). Proposed signaling role of arachidonic acid in human myometrium. *Molecular and Cellular Endocrinology*, 110: 113-118.

Hirata, F., Strittmatter, W. J. & Axelrod, J. (1979). beta-Adrenergic receptor agonists increase phospholipid methylation, membrane fluidity, and beta-adrenergic receptor-adenylate cyclase coupling. *Proceedings of the National Academy of Sciences of the United States of America*, 76: 368-372.

Hoja, H., Marquet, P., Verneuil, B., Lotfi, H., Penicaut, B., & Lachatre, G. (1997). Applications of liquid chromatography –mass spectrometry in analytical toxicology: a review. *Journal of Analytical Toxicology*, 21: 116-126.

Hordijk, P. L., Verlaan, I., Van Corven, E. J. & Moolenaar, W. H. (1994). Protein tyrosine phosphorylation induced by lysophosphatidic acid in Rat-1 fibroblasts. Evidence that phosphorylation of map kinase is mediated by the Gi-p21ras pathway. *Journal of Biological Chemistry*, 269: 645-651.

Hornero-Mendez, D., Gandul-Rojas, B. & Minguez-Mosquera, M. I. (2005). Routine and sensitive SPE-HPLC method for quantitative determination of pheophytin a and pyropheophytin a in olive oils. *Food Research International*, 38: 1067-1072.

Houghton, P. J. & Raman, A. (1998). *Laboratory Handbook for the Fractionation of Natural Extracts*, London, UK, Chapman and Hall. 19.

Howlett, A. C. & Mukhopadhyay, S. (2000). Cellular signal transduction by anandamide and 2-arachidonoylglycerol. *Chemistry and Physics of Lipids*, 108: 53-70.

Hu, S. S., Bradshaw, H. B., Benton, V. M., Chen, J. S., Huang, S. M., Minassi, A., Bisogno, T., Masuda, K., Tan, B., Roskoski, R., Jr., Cravatt, B. F., Di Marzo, V. & Walker, J. M. (2009). The biosynthesis of N-arachidonoyl dopamine (NADA), a

putative endocannabinoid and endovanilloid, via conjugation of arachidonic acid with dopamine. *Prostaglandins, Leukotrienes, and Essential Fatty Acids*, 81: 291-301.

Hu, S., Chen, J., Minassi, A., Roskoski, R., Di Marzo, V. & Walker, M. J. (2004). Studies of the biosynthesis of N-arachidonoyl-dopamine (NADA). 14th Annual Symposium on the Cannabinoids (International Cannabinoid Research Society), Burlington, Vermont. . p 10.

Huang, S. M., Bisogno, T., Trevisani, M., Al-Hayani, A., De Petrocellis, L., Fezza, F., Tognetto, M., Petros, T. J., Krey, J. F., Chu, C. J., Miller, J. D., Davies, S. N., Geppetti, P., Walker, J. M. & Di Marzo, V. (2002). An endogenous capsaicin-like substance with high potency at recombinant and native vanilloid VR1 receptors. *Proceedings of the National Academy of Sciences of the United States of America*, 99: 8400-8405.

Huszar, G. & Roberts, J. M. (1982). Biochemistry and pharmacology of the myometrium and labor: regulation at the cellular and molecular levels. *American Journal of Obstetrics and Gynecology*, 142: 225-237.

Ijeh, I. I. & Agbo, C. A. (2006). Body organ weight changes following the administration of aqueous extracts of *Ficus exasperata* Vahl. *Journal of Animal Veterinary Advances*, 5: 277-279.

Ijeh, I. I. & Ukwani, A. I. (2007). Acute effect of administration of ethanol extracts of *Ficus exasperata* vahl on kidney function in albino rats. *Journal of Plants and Medicinal Research*, 1: 27-29.

- Irene, I. I., & Iheanacho, U. A. (2007). Acute effect of administration of ethanol extracts of *Ficus exasperata* vahl on kidney function in albino rats. *Journal of Medicinal Plants Research*, 1: 27-9.
- Irvine, R. F. & Moor, R. M. (1987). Inositol(1,3,4,5)tetrakisphosphate-induced activation of sea urchin eggs requires the presence of inositol trisphosphate. *Biochemical and Biophysical Research Communications*, 146: 284-290.
- Irvine, R. F., Moor, R. M., Pollock, W. K., Smith, P. M. & Wreggett, K. A. (1988). Inositol phosphates: proliferation, metabolism and function. *Philosophical Transactions of the Royal Society of London. Series B, Biological Sciences*, 320: 281-298.
- Izumi, H., Garfield, R. E., Morishita, F. & Shirakawa, K. (1994). Some mechanical properties of skinned fibres of pregnant human myometrium. *European Journal of Obstetrics, Gynecology, and Reproductive Biology*, 56: 55-62.
- Jeyabalan A and Caritis SN. Pharmacologic inhibition of preterm labor. *Clinical Obstetrics and Gynecology* 45: 99–113, 2002.
- Jhaveri, M. D., Richardson, D. & Chapman, V. (2007). Endocannabinoid metabolism and uptake: novel targets for neuropathic and inflammatory pain. *British Journal of Pharmacology*, 152: 624-632.
- Jin, X. H., Okamoto, Y., Morishita, J., Tsuboi, K., Tonai, T. & Ueda, N. (2007). Discovery and characterization of a Ca²⁺-independent phosphatidylethanolamine N-acyltransferase generating the anandamide precursor and its congeners. *Journal of Biological Chemistry*, 282: 3614-3623.

Jochle W. Current research in coitus-induced ovulation: A review. *Journal of Reproduction and Fertility Suppl* 1975, 22: 165–207.

Johnson, J. E., Giorgione, J. & Newton, A. C. (2000). The C1 and C2 domains of protein kinase C are independent membrane targeting modules, with specificity for phosphatidylserine conferred by the C1 domain. *Biochemistry*, 39: 11360-11369.

Jones, A. E. (2004). Managing the pain of primary and secondary dysmenorrhoea. *Nursing Times*, 100: 40-43.

Jork, I. H. H., Funk W., Fischer W., Wimmer H., , Weinheim, VHC. (1990). Thin-Layer Chromatography Reagents and Detection Methods, Vol. 1a: Physical and Chemical Detection Methods: Fundamentals, Reagents. Germany.

Joseph, B. & Raj, J. S. (2010). Phytopharmacological properties of *Ficus racemosa* Linn – An overview. *International Journal of Pharmaceutical Sciences Review and Research*, 3: 134-138.

Joshi, H., Joshi, A. B., Sati, H., Gururaja, M. P., Shetty, P. R., Subrahmanyam, E. V. S. & Satyanaryana, D. (2009). Fatty Acids from *Memecylon umbellatum* (Burm.). *Asian Journal of Research in Chemistry*, 2: 178-180.

Juneja, L. R., Kazuoka, T., Goto, N., Yamane, T. & Shimizu, S. (1989). Conversion of phosphatidylcholine to phosphatidylserine by various phospholipases D in the presence of L-or D-serine. *Biochimica et Biophysica Acta (BBA)-Lipids and Lipid Metabolism*, 1003: 277-283.

- Kaingu, C. K., Kanui, T., & Oduma, J. A. (2012). Preliminary investigation of contractile activity of *Ricinus communis*. *Journal of Ethnopharmacology*, 142(2), : 496-502
- Kearn, C. S., Blake-Palmer, K., Daniel, E., Mackie, K. & Glass, M. (2005). Concurrent stimulation of cannabinoid CB1 and dopamine D2 receptors enhances heterodimer formation: a mechanism for receptor cross-talk? *Molecular Pharmacology*, 67: 1697-1704.
- Kell, D. B. (2004). Metabolomics and systems biology: making sense of the soup. *Current Opinion in Microbiology*, 7: 296-307.
- Kendrick, A. J., Zhang, J., Tattersall, M., Bricker, L., Quenby, S. & Wray, S. (2004). Calcium signalling, caveolae and human myometrial contractility. *Proceedings of the Physiological Society*, 560P: C50.
- Kerharo, J. & Bouquet, A. (1950). *Plantes médicinales et toxiques de la Côte-d'Ivoire*. November 15, 2012 ed. Belgium: BeBIF Provider.
- Kessel, D. & Smith, K. (1989). Photosensitization with derivatives of chlorophyll. *Photochemistry and Photobiology*, 49: 157-160.
- Khan, R. N., Matharoo-Ball, B., Arulkumar, S. & Ashford, M. L. (2001). Potassium channels in the human myometrium. *Experimental Physiology*, 86: 255-264.
- Kimura, K., Ito, M., Amano, M., Chihara, K., Fukata, Y., Nakafuku, M., Yamamori, B., Feng, J., Nakano, T., Okawa, K., Iwamatsu, A. & Kaibuchi, K. (1996).

Regulation of myosin phosphatase by Rho and Rho-associated kinase (Rho-kinase). *Science*, 273: 245-248.

King, J., Flenady, V., Cole, S. & Thornton, S. (2005). Cyclo-oxygenase (COX) inhibitors for treating preterm labour. *Cochrane Database of Systematic Reviews*: CD001992.

Klein, U., Gimpl, G. & Fahrenholz, F. (1995). Alteration of the myometrial plasma membrane cholesterol content with beta-cyclodextrin modulates the binding affinity of the oxytocin receptor. *Biochemistry*, 34: 13784-13793.

Koppler, P., Matter, N. & Malviya, A. N. (1993). Evidence for stereospecific inositol 1,3,4,5-[3H]tetrakisphosphate binding sites on rat liver nuclei. Delineating inositol 1,3,4,5-tetrakisphosphate interaction in nuclear calcium signaling process. *Journal of Biological Chemistry*, 268: 26248-26252.

Kosterin, S. A., Babich, L. G. & Shlykov, S. G. (1994). [Mg²⁺, ATP-dependent accumulation of Ca²⁺ in smooth muscle cells stimulated by oxalate and suppressed by thapsigargin]. *Doklady Akademii Nauk/ [Rossiiskaia akademii nauk]*, 335: 511-514.

Kotlikoff, M. I. & Kamm, K. E. (1996). Molecular mechanisms of beta-adrenergic relaxation of airway smooth muscle. *Annual Reviews of Physiology*, 58: 115-141.

Ku, C. Y., Qian, A., Wen, Y., Anwer, K. & Sanborn, B. M. (1995). Oxytocin stimulates myometrial guanosine triphosphatase and phospholipase-C activities via coupling to G alpha q/11. *Endocrinology*, 136: 1509-1515.

- Kumar, R. V. & Augusti, K. T. (1989). Antidiabetic effect of a leucocyanidin derivative isolated from the bark of *Ficus bengalensis* Linn. *Indian Journal of Biochemistry and Biophysics*, 26: 400-404.
- Kupittayanant, S., Burdyga, T. & Wray, S. (2001). The effects of inhibiting Rho-associated kinase with Y-27632 on force and intracellular calcium in human myometrium. *Pflugers Archiv: European Journal of Physiology*, 443: 112-114.
- Kupittayanant, S., Luckas, M. J. & Wray, S. (2002). Effect of inhibiting the sarcoplasmic reticulum on spontaneous and oxytocin-induced contractions of human myometrium. *International Journal of Obstetrics and Gynaecology*, 109: 289-296.
- Lain, R., Ahmadi, M., Smith, H. J., Nicholls, P. J. & Whomsley, R. (1996). Some Flavones and Isoflavones as Inhibitors of Human Placental 17 β -Hydroxysteroid Dehydrogenase In-vitro. *Pharmacy and Pharmacology Communications*, 2: 21-23.
- Lal, R. & Sharma, P. L. (1983). Preliminary study on the mechanism of dopamine action on rabbit myometrium. *Indian Journal of Medical Research*, 77: 265-270.
- Lansky, E. P., Paavilainen, H. M., Pawlus, A. D. & Newman, R. A. (2008). *Ficus* spp. (fig): ethnobotany and potential as anticancer and anti-inflammatory agents. *Journal of Ethnopharmacology*, 119: 195-213.
- Lanzafame, A. A., Guida, E. & Christopoulos, A. (2004). Effects of anandamide on the binding and signaling properties of M1 muscarinic acetylcholine receptors. *Biochemical Pharmacology*, 68: 2207-2219.
- Lapetina, E. G., Billah, M. M. & Cuatrecasas, P. (1981). The initial action of thrombin on platelets. Conversion of phosphatidylinositol to phosphatidic acid

preceding the production of arachidonic acid. *Journal of Biological Chemistry*, 256: 5037-5040.

Larcombe-Mcdouall, J. B., Harrison, N. & Wray, S. (1998). The in vivo relationship between blood flow, contractions, pH and metabolites in the rat uterus. *Pflugers Archiv: European Journal of Physiology*, 435: 810-817.

Larcombe-Mcdouall, J., Buttell, N., Harrison, N. & Wray, S. (1999). In vivo pH and metabolite changes during a single contraction in rat uterine smooth muscle. *Journal of Physiology*, 518 (3): 783-790.

Lassegue, B., Alexander, R. W., Clark, M., Akers, M. & Griendling, K. K. (1993). Phosphatidylcholine is a major source of phosphatidic acid and diacylglycerol in angiotensin II-stimulated vascular smooth-muscle cells. *Biochemical Journal*, 292 (2): 509-517.

Lauckner, J. E., Jensen, J. B., Chen, H. Y., Lu, H. C., Hille, B. & Mackie, K. (2008). GPR55 is a cannabinoid receptor that increases intracellular calcium and inhibits M current. *Proceedings of the National Academy of Sciences of the United States of America* 105: 2699-2704.

Lauderdale JW. (2009). ASAS Centennial Paper: Contributions in the Journal of Animal Science to the development of protocols for breeding management of cattle through synchronization of estrus and ovulation. *Journal of Animal Science*, 87:801–12.

- Lavallee, D. K., Huggins, E. & Lee, S. (1982). Kinetics and mechanism of the hydrolysis of chlorophyll a in ternary solvent microemulsion media. *Inorganic Chemistry*, 21: 1552-1553.
- Lawn, J. E., Cousens, S., Zupan, J. & Lancet Neonatal Survival Steering, T. (2005). 4 million neonatal deaths: when? Where? Why? *Lancet*, 365: 891-900.
- Lawn, J. E., Kerber, K., Enweronu-Laryea, C. & Cousens, S. (2010). 3.6 million neonatal deaths--what is progressing and what is not? *Seminars in Perinatology*, 34: 371-386.
- Lee, E. H., Meissner, G. & Kim, D. H. (2002). Effects of quercetin on single Ca(2+) release channel behavior of skeletal muscle. *Biophysical Journal*, 82: 1266-1277.
- Lemmon, M. A. (2008). Membrane recognition by phospholipid-binding domains. *Nature Reviews. Molecular Cell Biology*, 9: 99-111.
- Li, F., Lu, X., Liu, H., Liu, M. & Xiong, Z. (2007). A pharmaco-metabonomic study on the therapeutic basis and metabolic effects of Epimedium brevicornum Maxim. on hydrocortisone-induced rat using UPLC-MS. *Biomedical Chromatography*, 21: 397-405.
- Li, R. W., Leach, D. N., Myers, S. P., Lin, G. D., Leach, G. J. & Waterman, P. G. (2004). A new anti-inflammatory glucoside from *Ficus racemosa* L. *Planta Medica*, 70: 421-426.
- Li, Y., Je, H. D., Malek, S. & Morgan, K. G. (2003). ERK1/2-mediated phosphorylation of myometrial caldesmon during pregnancy and labor. *American*

Journal of Physiology. Regulatory, Integrative and Comparative Physiology, 284: R192-R199.

Limon-Boulez, I., Mhaouty-Kodja, S., Coudouel, N., Benoit De Coignac, A., Legrand, C. & Maltier, J. P. (1997). The alpha1B-adrenergic receptor subtype activates the phospholipase C signaling pathway in rat myometrium at parturition. *Biology of Reproduction*, 57: 1175-1182.

Lin, C. Y., Wu, H., Tjeerdema, R. S. & Viant, M. R. (2007). Evaluation of metabolite extraction strategies from tissue samples using NMR metabolomics. *Metabolomics*, 3: 55-67.

Liu, H., Wormke, M., Safe, S. H. & Bjeldanes, L. F. (1994). Indolo[3,2-b]carbazole: a dietary-derived factor that exhibits both antiestrogenic and estrogenic activity. *Journal of the National Cancer Institute*, 86: 1758-1765.

Loch-Caruso, R. K., Criswell, K. A., Grindatti, C. M. & Brant, K. A. (2003). Sustained inhibition of rat myometrial gap junctions and contractions by lindane. *Reproductive Biology and Endocrinology*, 1: 62.

Loch-Caruso, R., Pahl, M. S. & Juberg, D. R. (1992). Rat myometrial smooth muscle cells show high levels of gap junctional communication under a variety of culture conditions. *In Vitro Cellular and Developmental Biology*, 28A: 97-101.

Loewus, F. A. & Murthy, P. P. N. (2000). Myo-inositol metabolism in plants. *Plant Science*, 150: 1-19.

Lokhov, P. G. & Archakov, A. I. (2009). Mass spectrometry methods in metabolomics. *Biochemistry (Moscow) Supplement Series B: Biomedical Chemistry*, 3: 1-9.

Lopez-Moreno, J. A., Gonzalez-Cuevas, G., Moreno, G. & Navarro, M. (2008). The pharmacology of the endocannabinoid system: functional and structural interactions with other neurotransmitter systems and their repercussions in behavioral addiction. *Addiction Biology*, 13: 160-187.

Lourenço, E. L. B., Muller, J. C., Boareto, A. C., Gomes, C., Lourenço, A. C., Minatovicz, B., Crestani, S., Gasparotto Jr, A., Martino-Andrade, A. J. & Dalsenter, P. R. (2012). Screening for in vivo (anti) estrogenic and (anti) androgenic activities of *Tropaeolum majus* L. and its effect on uterine contractility. *Journal of Ethnopharmacology*, 141(1) : 418-423.

Low, M. G. (1989). Glycosyl-phosphatidylinositol: a versatile anchor for cell surface proteins. *FASEB Journal*, 3: 1600-1608.

Lu, X. & Xu, G. (2008). LC-MS metabonomics methodology in biomarker discovery. *Biomarker methods in drug discovery and development*. New Jersey, U. S. A: Humana press. p 291-315.

Lykidis, A., Jackson, P. D., Rock, C. O. & Jackowski, S. (1997). The role of CDP-diacylglycerol synthetase and phosphatidylinositol synthase activity levels in the regulation of cellular phosphatidylinositol content. *Journal of Biological Chemistry*, 272: 33402-33409.

Lynch, G. S., Hinkle, R. T., Chamberlain, J. S., Brooks, S. V. & Faulkner, J. A. (2001). Force and power output of fast and slow skeletal muscles from mdx mice 6-28 months old. *Journal of Physiology*, 535: 591-600.

Maccarrone, M., Gasperi, V., Catani, M. V., Diep, T. A., Dainese, E., Hansen, H. S. & Avigliano, L. (2010). The endocannabinoid system and its relevance for nutrition. *Annual Review of Nutrition*, 30: 423-440.

Macfoy, C. A., & Cline, E. I. (1990). In vitro antibacterial activities of three plants used in traditional medicine in Sierra Leone. *Journal of Ethnopharmacology*, 28(3), 323-327.

Mackler, A. M., Ducsay, C. A., Veldhuis, J. D. & Yellon, S. M. (1999). Maturation of spontaneous and agonist-induced uterine contractions in the peripartum mouse uterus. *Biology of Reproduction*, 61: 873-878.

Macmillan, K. L., and C. R. Burke. (1996). Effects of oestrous cycle control on reproductive efficiency. *Animal Reproduction Science* 42:307– 320.

Macmillan, K. L., Taufan, V. K., Day, A. M., & McDougall, S. (1995). Some effects of using progesterone and oestradiol benzoate to stimulate oestrus and ovulation in dairy cows with anovulatory anoestrus. *Proceedings of the New Zealand Society of Animal Production* 55:242–244.

Mahmmoud, Y. A. & Gaster, M. (2012). Uncoupling of sarcoplasmic reticulum Ca²⁺(+)-ATPase by N-arachidonoyl dopamine. Members of the endocannabinoid family as thermogenic drugs. *British Journal of Pharmacology*, 166: 2060-2069.

Majerus, P. W., Connolly, T. M., Bansal, V. S., Inhorn, R. C., Ross, T. S. & Lips, D. L. (1988). Inositol phosphates: synthesis and degradation. *Journal of Biological Chemistry*, 263: 3051-3054.

Malairajan, P., Geetha, G., Narasimhan, S. & Jessi Kala Veni, K. (2006). Analgesic activity of some Indian medicinal plants. *Journal of Ethnopharmacology*, 106: 425-428.

Mandal, S. C. & Kumar, A. C. K. (2002). Studies on anti-diarrhoeal activity of *Ficus hispida*. Leaf extract in rats. *Fitoterapia*, 73: 663-667.

Mandal, S. C., Maity, T. K., Das, J., Saba, B. P. & Pal, M. (2000). Anti-inflammatory evaluation of *Ficus racemosa* Linn. leaf extract. *Journal of Ethnopharmacology*, 72: 87-92.

Mandal, S. C., Mukherjee, P. K., Saha, K. & Saha, B. P. (1997). Antidiarrheal evaluation of *Ficus racemosa* Linn. leaf extract. *Journal of Natural Products Sciences*, 3: 100-103.

Mandi, M. & Bak, J. (2008). Nicotinic acid adenine dinucleotide phosphate (NAADP) and Ca²⁺ mobilization. *Journal of Receptor and Signal Transduction Research*, 28: 163-184.

Marc, S., Leiber, D. & Harbon, S. (1986). Carbachol and oxytocin stimulate the generation of inositol phosphates in the guinea pig myometrium. *FEBS Letters*, 201: 9-14.

Marczylo, T. H., Lam, P. M., Amoako, A. A. & Konje, J. C. (2010). Anandamide levels in human female reproductive tissues: solid-phase extraction and measurement

by ultraperformance liquid chromatography tandem mass spectrometry. *Analytical Biochemistry*, 400: 155-162.

Marin-Cao, D., Alvarez Chiva, V. & Mato, J. M. (1983). Beta-adrenergic control of phosphatidylcholine synthesis by transmethylation in hepatocytes from juvenile, adult and adrenalectomized rats. *Biochemical Journal*, 216: 675-680.

Marjoribanks, J., Proctor, M. L. & Farquhar, C. (2003). Nonsteroidal anti-inflammatory drugs for primary dysmenorrhoea (Cochrane Review). *The Cochrane Library*, 4.

Marshall, J. M. (1981). Effects of ovarian steroids and pregnancy on adrenergic nerves of uterus and oviduct. *American Journal of Physiology*, 240: C165-C174.

Marquet, P. (2002). Progress of liquid chromatography – mass spectrometry in clinical and forensic toxicology. *Therapeutic Drug Monitoring*, 24: 255-276.

Martinez-Gaudio, M., Yoshiba, T. & Bengtsson, L. P. (1973). Propagated and non propagated myometrial contraction in normal menstrual cycle. *American Journal of Obstetrics and Gynecology*, 115: 107-111.

Matschke, K., Babiychuk, E. B., Monastyrskaya, K. & Draeger, A. (2006). Phenotypic conversion leads to structural and functional changes of smooth muscle sarcolemma. *Experimental Cell Research*, 312: 3495-3503.

Matthew, A., Shmygol, A. & Wray, S. (2004). Ca²⁺ entry, efflux and release in smooth muscle. *Biological Research*, 37: 617-624.

Mattos, R., Staples, C. R. & Thatcher, W. W. (2000). Effects of dietary fatty acids on reproduction in ruminants. *Reviews of Reproduction*, 5: 38-45.

Maurer, H. H. (1999). Systematic toxicological analysis procedures for acidic drugs and/or doping control. *Journal of Chromatographic B Biomedical Sciences and Applications*, 733: 3-25.

Mazzei, P., Piccolo, A., Nugnes, L., Mascolo, M., De Rosa, G. & Staibano, S. (2010). Metabolic profile of intact tissue from uterine leiomyomas using high-resolution magic-angle-spinning (1)H NMR spectroscopy. *NMR in Biomedicine*, 23: 1137-1145.

Mcchesney, J. D., Venkataraman, S. K. & Henri, J. T. (2007). Plant natural products: back to the future or into extinction? *Phytochemistry*, 68: 2015-2022.

Mccormick, M. C., Litt, J. S., Smith, V. C. & Zupancic, J. A. (2011). Prematurity: an overview and public health implications. *Annual Review of Public Health*, 32: 367-379.

Mckean, M. L., Smith, J. B. & Silver, M. J. (1981). Formation of lysophosphatidylcholine by human platelets in response to thrombin. Support for the phospholipase A2 pathway for the liberation of arachidonic acid. *Journal of Biological Chemistry*, 256: 1522-1524.

Mckillen, K., Thornton, S. & Taylor, C. W. (1999). Oxytocin increases the [Ca²⁺]_i sensitivity of human myometrium during the falling phase of phasic contractions. *The American Journal of Physiology*, 276: E345-351.

Mendes, P., Camacho, D. & De La Fuente, A. (2005). Modelling and simulation for metabolomics data analysis. *Biochemical Society Transactions*, 33: 1427-1429.

Miksicek, R. J. (1993). Commonly occurring plant flavonoids have estrogenic activity. *Molecular Pharmacology*, 44: 37-43.

Miksicek, R. J. (1995). Estrogenic flavonoids: structural requirements for biological activity. *Proceedings of the Society for Experimental Biology and Medicine*, 208: 44-50.

Miriel, V. A., Mauban, J. R., Blaustein, M. P. & Wier, W. G. (1999). Local and cellular Ca²⁺ transients in smooth muscle of pressurized rat resistance arteries during myogenic and agonist stimulation. *The Journal of Physiology*, 518 (Pt 3): 815-824.

Molina-Holgado, F., Molina-Holgado, E., Guaza, C. & Rothwell, N. J. (2002). Role of CB1 and CB2 receptors in the inhibitory effects of cannabinoids on lipopolysaccharide-induced nitric oxide release in astrocyte cultures. *Journal of Neuroscience Research*, 67: 829-836.

Moore, F. & Lopez Bernal, A. (2003). Chronic exposure to TXA₂ increases expression of ROCK1 in human myometrial cells. *Prostaglandins and Other Lipid Mediators*, 71: 23-32.

Moriconi, A., Cerbara, I., Maccarrone, M. & Topai, A. (2010). GPR55: Current knowledge and future perspectives of a purported "Type-3" cannabinoid receptor. *Current Medicinal Chemistry*, 17: 1411-1429.

Munnix, I. C., Harmsma, M., Giddings, J. C., Collins, P. W., Feijge, M. A., Comfurius, P., Heemskerk, J. W. & Bevers, E. M. (2003). Store-mediated calcium

entry in the regulation of phosphatidylserine exposure in blood cells from Scott patients. *Thrombosis and Haemostasis*, 89: 687-695.

Munro, S., Thomas, K. L. & Abu-Shaar, M. (1993). Molecular characterization of a peripheral receptor for cannabinoids. *Nature*, 365: 61-65.

Murphy, R. C., James, P. F., Mcanoy, A. M., Krank, J., Duchoslav, E. & Barkley, R. M. (2007). Detection of the abundance of diacylglycerol and triacylglycerol molecular species in cells using neutral loss mass spectrometry. *Analytical Biochemistry*, 366: 59-70.

Murray, K. K., Boyd, R. K., Eberlin, M. N., Langley, G. J., Li, L. & Naito, Y. (2013). Definitions of terms relating to mass spectrometry (IUPAC Recommendations 2013). *Pure and Applied Chemistry*, 85: 1512-1609.

Mussalli, G. M., Blanchard, R., Brunnert, S. R. & Hirsch, E. (1999). Inflammatory cytokines in a murine model of infection-induced preterm labor: cause or effect? *Journal of the Society for Gynecologic Investigation*, 6: 188-195.

Nakamura, H., Itakura, A., Okamura, M., Ito, M., Iwase, A., Nakanishi, Y., Okada, M., Nagasaka, T. & Mizutani, S. (2000). Oxytocin stimulates the translocation of oxytocinase of human vascular endothelial cells via activation of oxytocin receptors. *Endocrinology*, 141: 4481-4485.

Nelson, M. T., Cheng, H., Rubart, M., Santana, L. F., Boney, A. D., Knot, H. J. & Lederer, W. J. (1995). Relaxation of arterial smooth muscle by calcium sparks. *Science*, 270: 633-637.

Newman, D. J., Cragg, G. M. & Snader, K. M. (2003a). Natural products as sources of new drugs over the period 1981-2002. *Journal of Natural Products Sciences*, 66: 1022-10237.

Newman, D. J., Cragg, G. M. & Snader, K. M. (2003b). Natural products as sources of new drugs over the period 1981-2002. *Journal of Natural Products*, 66: 1022-1037.

Niangadouma, R., 2010. *Ficus exasperata* Vahl. In: Brink, M. & Achigan-Dako, E.G. (Editors). *Prota 16: Fibres/Plantes à fibres*. [CD-Rom]. PROTA, Wageningen, Netherlands.

Nimenibo-Uadia, R. (2003). *Ficus exasperata*: effects on diabetes mellitus in an experimental rat model. *Global Journal of Pure and Applied Science*, 9: 529-532.

Ninomiya, J. G., Suzuki, H. (1983). Electrical Responses of smooth muscle cells of the mouse uterus to adenosine triphosphate. *Journal of Physiology*, 342, 499-515.

Nobeli, I. & Thornton, J. M. (2006). A bioinformatician's view of the metabolome. *Bioessays*, 28: 534-545.

Noble, K. & Wray, S. (2002). The role of the sarcoplasmic reticulum in neonatal uterine smooth muscle: enhanced role compared to adult rat. *The Journal of Physiology*, 545: 557-566.

Noble, K., Matthew, A., Burdyga, T. & Wray, S. (2009). A review of recent insights into the role of the sarcoplasmic reticulum and Ca entry in uterine smooth muscle. *European Journal of Obstetrics, Gynecology, and Reproductive Biology*, 144 Suppl 1: S11-S19.

Noble, K., Zhang, J. & Wray, S. (2006). Lipid rafts, the sarcoplasmic reticulum and uterine calcium signalling: an integrated approach. *Journal of Physiology*, 570: 29-35.

Noda, M., Yasuda-Fukazawa, C., Moriishi, K., Kato, T., Okuda, T., Kurokawa, K. & Takuwa, Y. (1995). Involvement of rho in GTP gamma S-induced enhancement of phosphorylation of 20 kDa myosin light chain in vascular smooth muscle cells: inhibition of phosphatase activity. *FEBS Letters*, 367: 246-250.

Noe, M., Kunz, G., Herbertz, M., Mall, G. & Leyendecker, G. (1999). The cyclic pattern of the immunocytochemical expression of oestrogen and progesterone receptors in human myometrial and endometrial layers: characterization of the endometrial-subendometrial unit. *Human Reproduction*, 14: 190-197.

Nohara, A., Ohmichi, M., Koike, K., Masumoto, N., Kobayashi, M., Akahane, M., Ikegami, H., Hirota, K., Miyake, A. & Murata, Y. (1996). The role of mitogen-activated protein kinase in oxytocin-induced contraction of uterine smooth muscle in pregnant rat. *Biochemical and Biophysical Research Communications*, 229: 938-944.

Odunbaku, O. A., Ilusanya, O. A. & Akasoro, K. S. (2008). Antibacterial activity of ethanolic leaf extract of *Ficus exasperata* on *Escherichia coli* and *Staphylococcus albus*. *Scientific Research and Essays*, 3: 562-564.

Ogunleye, D. S., Adeyemi, A. A., & Sanni, A. M. (2005). Hypoglycaemic activities of the stem bark of *Cola acuminata* Vahl and leaf of *Ficus exasperata* (P. Beauv) Schott and Endl. *Nigerian Quarterly Journal of Hospital Medicine*, 13(1) : 58-60.

Ohmichi, M., Koike, K., Kimura, A., Masuhara, K., Ikegami, H., Ikebuchi, Y., Kanzaki, T., Touhara, K., Sakaue, M., Kobayashi, Y., Akabane, M., Miyake, A. & Murata, Y. (1997). Role of mitogen-activated protein kinase pathway in prostaglandin F₂α-induced rat puerperal uterine contraction. *Endocrinology*, 138: 3103-3111.

Oka, S., Nakajima, K., Yamashita, A., Kishimoto, S. & Sugiura, T. (2007). Identification of GPR55 as a lysophosphatidylinositol receptor. *Biochemical and Biophysical Research Communications*, 362: 928-934.

Oka, S., Toshida, T., Maruyama, K., Nakajima, K., Yamashita, A. & Sugiura, T. (2009). 2-Arachidonoyl-sn-glycero-3-phosphoinositol: a possible natural ligand for GPR55. *Journal of Biochemistry*, 145: 13-20.

Okafor, J. I., Eze, E. A., & Njoku, O. U. (2001). Antifungal Activities of the Leaves of *Baphia nitida*, *Cassia alata*, *Ficus exasperata* and *Gossypium arboreum*. *Nigerian Journal of Natural Products and Medicine*, 5(1) : 59-60.

Okazaki, M., Matsuyama, T., Kohno, T., Shindo, H., Koji, T., Morimoto, Y. & Ishimaru, T. (2005). Induction of epithelial cell apoptosis in the uterus by a mouse uterine ischemia-reperfusion model: possible involvement of tumor necrosis factor-α. *Biology of Reproduction*, 72: 1282-1288.

Okuda, S., Yamada, T., Hamajima, M., Itoh, M., Katayama, T., Bork, P., Goto, S., Kanehisa, M. (2008). KEGG Atlas mapping for global analysis of metabolic pathways. *Nucleic acids Research*, 36: W423-426.

- Oladosu, I. A., Zubair, M. F., Ali, M. S., & Olawore, N. O. (2009). Anticandidal activity of volatile compounds from the root bark of *Ficus exasperata* Vahl-Holl (Moraceae). *Journal of Essential Oil Bearing Plants*, 12(5) : 562-568.
- Ong, E. S., Chor, C. F., Zou, L. & Ong, C. N. (2009). A multi-analytical approach for metabolomic profiling of zebrafish (*Danio rerio*) livers. *Molecular Biosystems*, 5: 288-298.
- Ortholand, J. Y. & Ganesan, A. (2004). Natural products and combinatorial chemistry: back to the future. *Current Opinion in Chemical Biology*, 8: 271-280.
- Otto, B., Steusloff, A., Just, I., Aktories, K. & Pfitzer, G. (1996). Role of Rho proteins in carbachol-induced contractions in intact and permeabilized guinea-pig intestinal smooth muscle. *Journal of Physiology*, 496 (Pt 2): 317-329.
- Pacher, P., Batkai, S. & Kunos, G. (2006). The endocannabinoid system as an emerging target of pharmacotherapy. *Pharmacological Reviews*, 58: 389-462.
- Palama, T. L., Fock, I., Choi, Y. H., Verpoorte, R. & Kodja, H. (2010). Biological variation of *Vanilla planifolia* leaf metabolome. *Phytochemistry*, 71: 567-573.
- Pandey, V., Chuang, C. C., Lewis, A. M., Aley, P. K., Brailoiu, E., Dun, N. J., Churchill, G. C. & Patel, S. (2009). Recruitment of NAADP-sensitive acidic Ca²⁺ stores by glutamate. *Biochemical Journal*, 422: 503-512.
- Paria, B. C., Das, S. K. & Dey, S. K. (1995). The preimplantation mouse embryo is a target for cannabinoid ligand-receptor signaling. *Proceedings of the National Academy of Sciences of the United States of America*, 92: 9460-9464.

- Park, B., Gibbons, H. M., Mitchell, M. D. & Glass, M. (2003). Identification of the CB1 cannabinoid receptor and fatty acid amide hydrolase (FAAH) in the human placenta. *Placenta*, 24: 990-995.
- Park, Y., Moon, B. H., Yang, H., Lee, Y., Lee, E. & Lim, Y. (2007). Complete assignments of NMR data of 13 hydroxymethoxyflavones. *Magnetic Resonance in Chemistry: MRC*, 45: 1072-1075.
- Parkening, T.A., Collins, T.J., Smith, E.R. (1982). Plasma and pituitary concentrations of LH, FSH, and prolactin in aging C57BL/6 mice at various times of the estrous cycle. *Neurobiology of Aging*, 3:31–35.
- Parratt, J., Taggart, M. & Wray, S. (1994). Abolition of contractions in the myometrium by acidification in vitro. *Lancet*, 344: 717-718.
- Parthasarathy, R. & Eisenberg, F., Jr. (1986). The inositol phospholipids: a stereochemical view of biological activity. *Biochemical Journal*, 235: 313-322.
- Patel, S., Marchant, J. S. & Brailoiu, E. (2010). Two-pore channels: Regulation by NAADP and customized roles in triggering calcium signals. *Cell Calcium*, 47: 480-490.
- Patti, G. J., Tautenhahn, R. & Siuzdak, G. (2012). Meta-analysis of untargeted metabolomic data from multiple profiling experiments. *Nature Protocols*, 7: 508-516.
- Pawson, T. & Scott, J. D. (1997). Signaling through scaffold, anchoring, and adaptor proteins. *Science*, 278: 2075-2080.

- Pears, M. R., Cooper, J. D., Mitchison, H. M., Mortishire-Smith, R. J., Pearce, D. A. & Griffin, J. L. (2005). High resolution ^1H NMR-based metabolomics indicates a neurotransmitter cycling deficit in cerebral tissue from a mouse model of Batten disease. *Journal of Biological Chemistry*, 280: 42508-42514.
- Pertwee, R. G. (2005). Pharmacological actions of cannabinoids. *Handbook of Experimental Pharmacology*, p 1-51.
- Peters, F. T. (2011). Recent advances of liquid chromatography – (tandem) mass spectrometry in clinical and forensic toxicology. *Clinical Biochemistry*, 44: 54-65.
- Pertwee, R. G. (2007). GPR55: a new member of the cannabinoid receptor clan? *British Journal of Pharmacology*, 152: 984-986.
- Pfaff, D. W., & Sakuma, Y. (1979). Facilitation of the lordosis reflex of female rats from the ventromedial nucleus of the hypothalamus. *The Journal of Physiology*, 288(1) : 189-202.
- Phoenix, J. & Wray, S. (1994). Changes in human and rat uterine phosphoethanolamine and taurine with pregnancy and parturition. *Experimental Physiology*, 79: 601-604.
- Pierce, S. J., Kupittayanant, S., Shmygol, T. & Wray, S. (2003). The effects of pH change on Ca^{++} signaling and force in pregnant human myometrium. *American Journal of Obstetrics and Gynecology*, 188: 1031-1038.
- Piomelli, D. (1993). Arachidonic acid in cell signaling. *Current Opinion in Cell Biology*, 5: 274-280.

Pitt, C., Greco, G., Powell-Jackson, T. & Mills, A. (2010). Countdown to 2015: assessment of official development assistance to maternal, newborn, and child health, 2003-08. *Lancet*, 376: 1485-1496.

Poyser, N. L. (1984). Prostaglandin production by the early pregnant guinea-pig uterus in relation to implantation and luteal maintenance, and the effect of oestradiol. *Journal of Reproduction and Fertility*, 72: 117-127.

Ppaff, D. W., Diakow, C., Zigmond, R. E. & Kow, L.-M. (1974). Neural and hormonal determinants of female mating behavior in rats . In *The Neurosciences: Third Study Program*, ed SchmirT, F. O. & Worden, F. G., pp. 621-646. Cambridge, Mass. and London, England: M.I.T. Press.

Prange, A. & Schaumloffel, D. (2002). Hyphenated techniques for the characterization and quantification of metallothionein isoforms. *Analytical and Bioanalytical Chemistry*, 373: 441-453.

Prasain, J. K., Wang, C. C. & Barnes, S. (2004). Mass spectrometric methods for the determination of flavonoids in biological samples. *Free Radical Biology and Medicine*, 37: 1324-1350.

Price, B. D., Morris, J. D., Marshall, C. J. & Hall, A. (1989). Stimulation of phosphatidylcholine hydrolysis, diacylglycerol release, and arachidonic acid production by oncogenic ras is a consequence of protein kinase C activation. *Journal of Biological Chemistry*, 264: 16638-16643.

- Pritchard, K. A., Jr., Karpen, C. W., Merola, A. J. & Panganamala, R. V. (1982). Influence of dietary vitamin E on platelet thromboxane A₂ and vascular prostacyclin I₂ in rabbit. *Prostaglandins, Leukotrienes, and Medicine*, 9: 373-378.
- Quach, H. T., Steeper, R. L. & Griffin, W. G. (2004). An improved method for the extraction and thin-layer chromatography of chlorophyll a and b from spinach. *Journal of Chemical Education*, 81: 385.
- Quenby, S., Pierce, S. J., Brigham, S. & Wray, S. (2004). Dysfunctional labor and myometrial lactic acidosis. *Obstetrics and Gynecology*, 103: 718-723.
- Rajaratnam, J. K., Marcus, J. R., Flaxman, A. D., Wang, H., Levin-Rector, A., Dwyer, L., Costa, M., Lopez, A. D. & Murray, C. J. (2010). Neonatal, postneonatal, childhood, and under-5 mortality for 187 countries, 1970-2010: a systematic analysis of progress towards Millennium Development Goal 4. *Lancet*, 375: 1988-2008.
- Ramsey, E. M. (1994). *Anatomy of the Human Uterus*, United Kingdom, Cambridge Press. p 18.
- Rang, H. P., Dale, M. M., Ritter, J. M. & Flower, P. K. (2007). *Pharmacology*, London, UK, Churchill Livingstone Elsevier. p 456-457.
- Rao, B. R., Murugesan, T., Sinha, S., Saba, B. P., Pal, M. & Mandal, S. C. (2002). Glucose lowering efficacies of *Ficus racemosa* bark extract in normal and alloxan diabetic rats. *Phytotherapy Research*, 16: 590-592.
- Ratnasooriya, W. D., Jayakody, J. R. & Nadarajah, T. (2003). Antidiuretic activity of aqueous bark extract of Sri Lankan *Ficus racemosa* in rats. *Acta Biologica Hungarica*, 54: 357-363.

- Rauk, P. N. & Chiao, J. P. (2000). Oxytocin signaling in human myometrium is impaired by prolonged exposure to interleukin-1. *Biology of Reproduction*, 63: 846-850.
- Ray, S., Ahmed, H., Basu, S. & Chatterjee, B. P. (1993). Purification, characterisation, and carbohydrate specificity of the lectin of *Ficus cunia*. *Carbohydrate Research*, 242: 247-263.
- Reis, M. G., Faria, A. D., Amaral, M. C. E. & Marsaiolia, A. J. (2003). Oncidinol—a novel diacylglycerol from *Ornithophora radicans* Barb. Rodr. (Orchidaceae) floral oil. *Tetrahedron letters*, 44: 8519-8523.
- Revuelta, M. P., Hidalgo, A. & Cantabrana, B. (1999). Involvement of cAMP and beta-adrenoceptors in the relaxing effect elicited by flavonoids on rat uterine smooth muscle. *Journal of Autonomic Pharmacology*, 19: 353-358.
- Riesz, M. & Erdo, S. L. (1985). GABAB receptors in the rabbit uterus may mediate contractile responses. *European Journal of Pharmacology*, 119: 199-204.
- Rishton, G. M. (2008). Natural products as a robust source of new drugs and drug leads: past successes and present day issues. *American Journal of Cardiology*, 101: 43D-49D.
- Ritter, M., Sui, Z., Philipson, K. D., Li, F., Spitzer, K. W., Ishida, H. & Barry, W. H. (2003). Ca²⁺ sparks induced by Na/Ca exchange. *Cell Calcium*, 34: 11-17.
- Rizzo, G., Capponi, A., Pietropolli, A., Bufalino, L. M., Arduini, D. & Romanini, C. (1994). Fetal cardiac and extracardiac flows preceding intrauterine death. *Ultrasound in Obstetrics and Gynecology*, 4: 139-142.

Roberts, J. M., Riemer, R. K., Bottari, S. P., Wu, Y. Y., & Goldfien, A. (1989). Hormonal regulation myometrial adrenergic responses: the receptor and beyond. *Journal of developmental physiology*, 11(3) :125-134.

Rochfort, S. (2005). Metabolomics reviewed: a new "omics" platform technology for systems biology and implications for natural products research. *Journal of Natural Products*, 68: 1813-18120.

Romero, J., Garcia, L., Cebeira, M., Zadrozny, D., Fernandez-Ruiz, J. J. & Ramos, J. A. (1995). The endogenous cannabinoid receptor ligand, anandamide, inhibits the motor behavior: role of nigrostriatal dopaminergic neurons. *Life Sciences*, 56: 2033-20340.

Romero, R., Espinoza, J., Chaiworapongsa, T. & Kalache, K. (2002). Infection and prematurity and the role of preventive strategies. *Seminars in Neonatology*, 7: 259-274.

Ross, H. R., Gilmore, A. J. & Connor, M. (2009). Inhibition of human recombinant T-type calcium channels by the endocannabinoid N-arachidonoyl dopamine. *British Journal of Pharmacology*, 156: 740-750.

Rubnov, S., Kashman, Y., Rabinowitz, R., Schlesinger, M. & Mechoulam, R. (2001). Suppressors of cancer cell proliferation from fig (*Ficus carica*) resin: isolation and structure elucidation. *Journal of Natural Product*, 64: 993-996.

Ryberg, E., Larsson, N., Sjogren, S., Hjorth, S., Hermansson, N. O., Leonova, J., Elebring, T., Nilsson, K., Drmota, T. & Greasley, P. J. (2007). The orphan receptor

GPR55 is a novel cannabinoid receptor. *British Journal of Pharmacology*, 152: 1092-1101.

Sagar, D. R., Smith, P. A., Millns, P. J., Smart, D., Kendall, D. A. & Chapman, V. (2004). TRPV1 and CB(1) receptor-mediated effects of the endovanilloid/endocannabinoid N-arachidonoyl-dopamine on primary afferent fibre and spinal cord neuronal responses in the rat. *European Journal of Neuroscience*, 20: 175-184.

Saghatelian, A. & Cravatt, B. F. (2005a). Discovery metabolite profiling--forging functional connections between the proteome and metabolome. *Life Sciences*, 77: 1759-1766.

Saghatelian, A. & Cravatt, B. F. (2005b). Global strategies to integrate the proteome and metabolome. *Current Opinion in Chemical Biology*, 9: 62-68.

Sah, V. P., Seasholtz, T. M., Sagi, S. A. & Brown, J. H. (2000). The role of Rho in G protein-coupled receptor signal transduction. *Annual Reviews of Pharmacology and Toxicology*, 40: 459-489.

Saigal, S. & Doyle, L. W. (2008). An overview of mortality and sequelae of preterm birth from infancy to adulthood. *Lancet*, 371: 261-269.

Sakamoto, K., Hori, M., Izumi, M., Oka, T., Kohama, K., Ozaki, H. & Karaki, H. (2003). Inhibition of high K⁺-induced contraction by the ROCKs inhibitor Y-27632 in vascular smooth muscle: possible involvement of ROCKs in a signal transduction pathway. *Journal of Pharmacological Sciences*, 92: 56-69.

- Sales, K. J. & Jabbour, H. N. (2003). Cyclooxygenase enzymes and prostaglandins in pathology of the endometrium. *Reproduction*, 126: 559-567.
- Salwan, S., Walia, R., Baja, V. K., Kaur, B. & Salwan, P. (2011). Salwan, S., Walia, R., Bajaj, V. K., Kaur, B., & Salwan, P. (2011). Smooth muscle relaxant activity of a synthetic dihydropyrimidine derivative 5-acyl-6-methyl-4 (2, 3methylenedioxy) phenyl-2-s-benzyl-1, 4-dihydro Pyrimidine (bk-vii) on isolated rat uterus and rabbit aortic strip. *Journal of Research in Medical Education & Ethics*, 1: 113-118.
- Sanborn, B. M. (1995). Ion channels and the control of myometrial electrical activity. *Seminars in Perinatology*, 19: 31-40.
- Sanborn, B. M. (2001). Hormones and calcium: mechanisms controlling uterine smooth muscle contractile activity. *The Litchfield Lecture. Experimental Physiology*, 86: 223-237.
- Sanborn, B. M., Ku, C. Y., Shlykov, S. & Babich, L. (2005). Molecular signaling through G-protein-coupled receptors and the control of intracellular calcium in myometrium. *Journal of the Society for Gynecologic Investigation*, 12: 479-487.
- Sandabe, U. K., Onyeyili, P. A., & Chibuzo, G. A. (2006). Phytochemical screening and effect of aqueous extract of *Ficus sycomorus* L.(Moraceae) stem bark on muscular activity in laboratory animals. *Journal of Ethnopharmacology*, 104(1) : 283-285.
- Sarkar, D.K., Chiappa, S.A., Fink, G., Sherwood, N.M.(1976). Gonadotropin-releasing hormone surge in prooestrous rats. *Nature.*; 264:461–463.

Scheid, C. R., Honeyman, T. W. & Fay, F. S. (1979). Mechanism of beta-adrenergic relaxation of smooth muscle. *Nature*, 277: 32-36.

Schild, H. O. (1983). The Uterus. In: SCHILD, H. O. (ed.) Applied Pharmacology. UK: Churchill Livingstone. p 217-219.

Schmid, H. H., Schmid, P. C. & Natarajan, V. (1990). N-acylated glycerophospholipids and their derivatives. *Progress in Lipid Research*, 29: 1-43.

Schmid, P. C., Paria, B. C., Krebsbach, R. J., Schmid, H. H. & Dey, S. K. (1997). Changes in anandamide levels in mouse uterus are associated with uterine receptivity for embryo implantation. *Proceedings of the National Academy of Sciences of the United States of America*, 94: 4188-4192.

Schrey, M. P., Cornford, P. A., Read, A. M. & Steer, P. J. (1988). A role for phosphoinositide hydrolysis in human uterine smooth muscle during parturition. *American Journal of Obstetrics and Gynecology*, 159: 964-970.

Seeger, C. (2012). Usage and Limitations of liquid chromatography-tandem mass spectrometry (LC-MS/MS) in clinical routine laboratories. *Wien Med Wochenschr*, 162: 499- 504.

Sevetson, B. R., Kong, X. & Lawrence, J. C., Jr. (1993). Increasing cAMP attenuates activation of mitogen-activated protein kinase. *Proceedures of the National Academy of Sciences of the United States of America*, 90: 10305-10309.

Shah, S. J., Yu, K. H., Sangar, V., Parry, S. I. & Blair, I. A. (2009). Identification and quantification of preterm birth biomarkers in human cervicovaginal fluid by liquid

chromatography/tandem mass spectrometry. *Journal of Proteome Research*, 8: 2407-2417.

Sheu, Y. W., Chiang, L. C., Chen, I. S., Chen, Y. C. & Tsai, I. L. (2005). Cytotoxic flavonoids and new chromenes from *Ficus formosana* f. *formosana*. *Planta Medica*, 71: 1165-1167.

Shih, H. C., Hsu, C. S. & Yang, L. L. (2009). In vitro study of the tocolytic effect of oroxilin A from *Scutellaria baicalensis* root. *Journal of Biomedical Science*, 16: 27.

Shmigol, A. V., Eisner, D. A. & Wray, S. (1999). The role of the sarcoplasmic reticulum as a Ca²⁺ sink in rat uterine smooth muscle cells. *The Journal of Physiology*, 520(1) : 153-163.

Shmigol, A., Eisner, D. A. & Wray, S. (1998). Carboxyeosin decreases the rate of decay of the [Ca²⁺]_i transient in uterine smooth muscle cells isolated from pregnant rats. *Pflugers Archiv: European Journal of Physiology*, 437: 158-160.

Shmygol, A. & Wray, S. (2004). Functional architecture of the SR calcium store in uterine smooth muscle. *Cell Calcium*, 35: 501-508.

Shmygol, A., Noble, K. & Wray, S. (2007). Depletion of membrane cholesterol eliminates the Ca²⁺-activated component of outward potassium current and decreases membrane capacitance in rat uterine myocytes. *Journal of Physiology*, 581: 445-456.

Shukla, R., Gupta, S., Gambhir, J. K., Prabhu, K. M. & Murthy, P. S. (2004). Antioxidant effect of aqueous extract of the bark of *Ficus bengalensis* in hypercholesterolaemic rabbits. *Journal of Ethnopharmacology*, 92: 47-51.

Sigger, J. N., Harding, R. & Jenkin, G. (1984). Relationship between electrical activity of the uterus and surgically isolated myometrium in the pregnant and nonpregnant ewe. *Journal of Reproduction and Fertility*, 70: 103-114.

Simmons, L. E., Rubens, C. E., Darmstadt, G. L. & Gravett, M. G. (2010). Preventing preterm birth and neonatal mortality: exploring the epidemiology, causes, and interventions. *Seminars in Perinatology*, 34: 408-415.

Simon, P. N., Chaboud, A., Darbour, N., Di Pietro, A., Dumontet, C., Lurel, F., Raynaud, J. & Barron, D. (2001). Modulation of cancer cell multidrug resistance by an extract of *Ficus citrifolia*. *Anticancer Research*, 21: 1023-1027.

Simons, K. & Toomre, D. (2000). Lipid rafts and signal transduction. *Nature Reviews, Molecular Cell Biology*, 1: 31-39.

Singh, R. K., Mehta, S., Jaiswal, D., Rai, P. K. & Watal, G. (2009). Antidiabetic effect of *Ficus bengalensis* aerial roots in experimental animals. *Journal of Ethnopharmacology*, 123: 110-114.

Sizov, P. I. (1992). [Action of GABA-positive preparations on uterus-stimulating effects of activating neuromediators, prostaglandin F2 alpha and oxytocin]. *Biulleten' Eksperimental'noi Biologii i Meditsiny*, 113: 387-389.

Smith, G. N., Guo, Y., Wen, S. W., Walker, M. C. & Canadian Preterm Labor Nitroglycerin Trial, G. (2010). Secondary analysis of the use of transdermal nitroglycerin for preterm labor. *American Journal of Obstetrics and Gynecology*, 203: 565 e561-e566.

Smith, R. C., McClure, M. C., Smith, M. A., Abel, P. W. & Bradley, M. E. (2007). The role of voltage-gated potassium channels in the regulation of mouse uterine contractility. *Reproductive Biology and Endocrinology*, 5: 41.

Smith, R. D., Babiychuk, E. B., Noble, K., Draeger, A. & Wray, S. (2005). Increased cholesterol decreases uterine activity: functional effects of cholesterol alteration in pregnant rat myometrium. *American Journal of Physiology, Cell Physiology*, 288: C982-C988.

Solberg, P. (2004). Examination of vaginal smears in the rat [Online]. Oslo, U. S. A.: Laboratory Animal Unit, National Institute of Public Health. Available: <http://oslovet.norecopa.no/teaching/rat/oestrus/> [Accessed 28th August 2011].

Soloff, M. S. & Sweet, P. (1982). Oxytocin inhibition of (Ca²⁺ + Mg²⁺)-ATPase activity in rat myometrial plasma membranes. *The Journal of Biological Chemistry*, 257: 10687-10693.

Somlyo, A. P. & Somlyo, A. V. (2000). Signal transduction by G-proteins, rho-kinase and protein phosphatase to smooth muscle and non-muscle myosin II. *Journal of Physiology*, 522 Pt 2: 177-185.

Staal, S. P., Hartley, J. W. & Rowe, W. P. (1977). Isolation of transforming murine leukemia viruses from mice with a high incidence of spontaneous lymphoma. *Proceedings of the National Academy of Sciences of the United States of America*, 74: 3065-3067.

Stahl E. (1975). Techniques of thin layer chromatography. In Chromatography- A laboratory handbook of chromatographic and electrophoretic methods. Springer-Verlag. p.164

Stahl, E. (1988). Thin layer chromatography, 2nd edition, Springer-Verlag Berlin, Reprint.

Stahl, E. (1956). [Thin-layer chromatography; methods, influencing factors and an example of its use]. *Die Pharmazie*, 11: 633-637.

Stentiford, G. D., Viant, M. R., Ward, D. G., Johnson, P. J., Martin, A., Wenbin, W., Cooper, H. J., Lyons, B. P. & Feist, S. W. (2005). Liver tumors in wild flatfish: a histopathological, proteomic, and metabolomic study. *OMICS: a journal of integrative biology*, 9: 281-299.

Stobiecki, M. & Kachliki, P. (2006). Isolation and Identification of Flavonoids. The Science of Flavonoids. New York, U. S. A: Springer. p 47-69.

Stremmler, K. E., Stafforini, D. M., Prescott, S. M., Zimmerman, G. A. & McIntyre, T. M. (1989). An oxidized derivative of phosphatidylcholine is a substrate for the platelet-activating factor acetylhydrolase from human plasma. *Journal of Biological Chemistry*, 264: 5331-5334.

Stull, J.T., Hsu, L.C., Tansey, M.G., Kamm, K.E. (1990). Myosin light chain kinase phosphorylation in tracheal smooth muscle. *Journal of Biological Chemistry*, 265: 16683-16690.

Subramanian, A., Shankar Joshi, B., Roy, A. D., Roy, R., Gupta, V. & Dang, R. S. (2008). NMR spectroscopic identification of cholesterol esters, plasmalogen and

phenolic glycolipids as fingerprint markers of human intracranial tuberculomas. *NMR in Biomedicine*, 21: 272-288.

Sumner, L. W., Mendes, P. & Dixon, R. A. (2003). Plant metabolomics: large-scale phytochemistry in the functional genomics era. *Phytochemistry*, 62: 817-836.

Szabo, B., Muller, T. & Koch, H. (1999). Effects of cannabinoids on dopamine release in the corpus striatum and the nucleus accumbens in vitro. *Journal of Neurochemistry*, 73: 1084-1089.

Taggart, M. J. & Wray, S. (1993). Occurrence of intracellular pH transients during spontaneous contractions in rat uterine smooth muscle. *Journal of Physiology*, 472: 23-31.

Taggart, M. J. & Wray, S. (1998). Contribution of sarcoplasmic reticular calcium to smooth muscle contractile activation: gestational dependence in isolated rat uterus. *The Journal of Physiology*, 511 (Pt 1): 133-144.

Taggart, M. J. (2001). Smooth muscle excitation-contraction coupling: a role for caveolae and caveolins? *News in Physiological Sciences*, 16: 61-65.

Taggart, M. J., Lee, Y. H. & Morgan, K. G. (1999). Cellular redistribution of PKC α , rhoA, and ROK α following smooth muscle agonist stimulation. *Experimental Cell Research*, 251: 92-101.

Tahara, M., Morishige, K., Sawada, K., Ikebuchi, Y., Kawagishi, R., Tasaka, K. & Murata, Y. (2002). RhoA/Rho-kinase cascade is involved in oxytocin-induced rat uterine contraction. *Endocrinology*, 143: 920-929.

- Taiwo, B. J., & Aderogba, M. A. (2007). Antioxidant lignans from the leaves of *Ficus exasperata*. *Nigerian Journal of Natural Products and Medicine*, 10(1) : 111-113.
- Tan, P. J., Ong, C. Y., Danial, A., Yusof, H. M., Neoh, B. K. & Lee, H. B. (2011). Cyclic Tetrapyrrolic Photosensitisers from the leaves of *Phaeanthus ophthalmicus*. *Chemistry Central Journal*, 5: 32.
- Tautenhahn, R., Patti, G. J., Rinehart, D. & Siuzdak, G. (2012). XCMS Online: a web-based platform to process untargeted metabolomic data. *Analytical Chemistry*, 84: 5035-5039.
- Teehan, O., Gamble, S., Holmes, E., Waxman, J., Nicholson, J. K., Bevan, C., Keun, H. C. (2006). Impact of Analytical Bias in Metabonomic Studies of Human Blood Serum and Plasma. *Analytical Chemistry*, 78:4307-4318.
- Thomas, J., Callwood, A. & Paranjothy, S. (2000). National Sentinel Caesarean Section Audit: update. *Practical Midwife*, 3: 20.
- Thompson, M., Barata Da Silva, H., Zielinska, W., White, T. A., Bailey, J. P., Lund, F. E., Sieck, G. C. & Chini, E. N. (2004). Role of CD38 in myometrial Ca²⁺ transients: modulation by progesterone. *American Journal of Physiology, Endocrinology and Metabolism*, 287: E1142-E1148.
- Thorne, S. W., Newcomb, E. H., & Osmond, C. B., (1977). Identification of chlorophyll b in extracts of prokaryotic algae by fluorescence spectroscopy. *Proceedings of the National Academy of Science USA*, 74 (2) : 575-578.

- Tichenor, J. N., Hansen, E. T. & Buxton, I. L. (2005). Expression of stretch-activated potassium channels in human myometrium. *Proceedings of the Western Pharmacology Society*, 48: 44-48.
- Tolstikov, V.V., Fiehn, O. & Tanaka, N. (2007). Application of Liquid Chromatography-Mass Spectrometry Analysis in Metabolomics: Reversed-Phase Monolithic Capillary Chromatography Coupled to Electrospray Ionization-Mass Spectrometry. In: Weckworth, W. (ed.) *Metabolomics: Methods and Protocols*. Totowa, New Jersey: Humana press Inc.
- Tomkins, S. P. & Miller, M. B. (1994). A rapid extraction and fast separation of leaf pigments using thin layer chromatography. *School Science Review*, 75: 69-72.
- Trygg, J., Holmes, E. & Lundstedt, T. (2007). Chemometrics in metabonomics. *Journal of Proteome Research*, 6: 469-479.
- Turi, A., Kiss, A. L. & Mullner, N. (2001). Estrogen downregulates the number of caveolae and the level of caveolin in uterine smooth muscle. *Cell Biology International*, 25: 785-794.
- Tweheyo, M. & Lye, K. A. (2007). Phenology of figs in Budongo forests Uganda and its importance for the chimpanzee diet. *African Journal of Ecology*, 41: 306-316.
- Uehata, M., Ishizaki, T., Satoh, H., Ono, T., Kawahara, T., Morishita, T., Tamakawa, H., Yamagami, K., Inui, J., Maekawa, M. & Narumiya, S. (1997). Calcium sensitization of smooth muscle mediated by a Rho-associated protein kinase in hypertension. *Nature*, 389: 990-994.

- Ulrich-Merzenich, G., Zeitler, H., Jobst, D., Panek, D., Vetter, H. & Wagner, H. (2007). Application of the "-Omic-" technologies in phytomedicine. *Phytomedicine*, 14: 70-82.
- Urban, J., Radwan, J., Laudanski, T. & Akerlund, M. (1982). Dopamine influence on human uterine activity at term pregnancy. *British Journal of Obstetrics and Gynaecology*, 89: 451-455.
- Usman, H., Abdulrahman, F. I., & Usman, A. (2009). Qualitative phytochemical screening and in vitro antimicrobial effects of methanol stem bark extract of *Ficus thonningii* (Moraceae). *African Journal of Traditional, Complementary and Alternative Medicines*, 6(3).
- Van Der Greef, J. & Smilde, A. K. (2005). Symbiosis of chemometrics and metabolomics: past, present, and future. *Journal of Chemometrics* 19: 376-386.
- Van Genderen, H. O., Kenis, H., Hofstra, L., Narula, J. & Reutelingsperger, C. P. (2008). Extracellular annexin A5: functions of phosphatidylserine-binding and two-dimensional crystallization. *Biochimica et Biophysica Acta*, 1783: 953-963.
- Van Meer, G., Voelker, D. R. & Feigenson, G. W. (2008). Membrane lipids: where they are and how they behave. *Nature Reviews. Molecular Cell Biology*, 9: 112-124.
- Vance, D. E. & Vance, J. E. (2009). Physiological consequences of disruption of mammalian phospholipid biosynthetic genes. *Journal of Lipid Research*, 50 Suppl: S132-S137.

Vance, J. E. & Tasseva, G. (2013). Formation and function of phosphatidylserine and phosphatidylethanolamine in mammalian cells. *Biochimica et Biophysica Acta*, 1831: 543-554.

Vance, J. E. (2008). Phosphatidylserine and phosphatidylethanolamine in mammalian cells: two metabolically related aminophospholipids. *Journal of Lipid Research*, 49: 1377-1387.

Vane, J. R. & Williams, K. I. (1973). The contribution of prostaglandin production to contractions of the isolated uterus of the rat. *British Journal of Pharmacology*, 48: 629-639.

Varghese, R. S., Cheema, A., Cheema, P., Bourbeau, M., Tuli, L., Zhou, B., Jung, M., Dritschilo, A. & Ransom, H. W. (2010). Analysis of LC-MS data for characterizing the metabolic changes in response to radiation. *Journal of Proteome Research*, 9: 2786-2793.

Vasskog, T., Andersen, J. H., Hansen, E. & Svenson, J. (2012). Characterization and cytotoxicity studies of the rare 21:4 n-7 acid and other polyunsaturated fatty acids from the marine opisthobranch *Scaphander lignarius*, isolated using bioassay guided fractionation. *Marine Drugs*, 10: 2676-2690.

Veerapur, V. P., Prabhakar, K. R., Parihar, V. K., Kandadi, M. R., Ramakrishana, S., Mishra, B., Satish Rao, B. S., Srinivasan, K. K., Priyadarsini, K. I. & Unnikrishnan, M. K. (2009). *Ficus racemosa* Stem Bark Extract: A Potent Antioxidant and a Probable Natural Radioprotector. Evidence-Based Complementary and Alternative Medicine : *eCAM*, 6: 317-324.

- Velardo, J. T. (1959). Steroid hormones and uterine growth. *Annals of the New York Academy of Science*, 75: 441-462.
- Verpoorte, R., Choi, Y. H. & Kim, H. K. (2005). Ethnopharmacology and systems biology: a perfect holistic match. *Journal of Ethnopharmacology*, 100: 53-56.
- Verpoorte, R., Choi, Y. H. & Kim, H. K. (2007). NMR-based metabolomics at work in phytochemistry. *Phytochemistry Reviews*, 6: 3-14.
- Verpoorte, R., Choi, Y. H., Mustafa, N. R. & Kim, H. K. (2008). Metabolomics: back to basics. *Phytochemistry Reviews*, 7: 525-537.
- Versace, F., Sporkert, F., Mangin, P., & Staub, C. (2012). Rapid sample pre-treatment prior to GC-MS and GC-MS/MS urinary toxicological screening. *Talanta*, 101: 299-306.
- Viant, M. R. (2007). Revealing the Metabolome of Animal Tissues using ¹H Nuclear magnetic Resonance Spectroscopy. In: Weckworth, W, (ed.) *Metabolomics: Methods and Protocols*. Totowa, New Jersey: Humana press Inc.
- Vicinanza, M., D'angelo, G., Di Campli, A. & De Matteis, M. A. (2008). Function and dysfunction of the PI system in membrane trafficking. *EMBO Journal*, 27: 2457-2470.
- Voelker, D. R. & Kennedy, E. P. (1982). Cellular and enzymic synthesis of sphingomyelin. *Biochemistry*, 21: 2753-2759.

Vogel, Z., Barg, J., Levy, R., Saya, D., Heldman, E. & Mechoulam, R. (1993). Anandamide, a brain endogenous compound, interacts specifically with cannabinoid receptors and inhibits adenylate cyclase. *Journal of Neurochemistry*, 61: 352-355.

Wachter, R., Brenneisen, R., Hamburger, M., Mennet, M., Schnelle, M., Worel, A. M., Simoes-Wust, A. P. & Von Mandach, U. (2011). Leaf press juice from *Bryophyllum pinnatum* (Lamarck) Oken induces myometrial relaxation. *Phytomedicine*, 19: 74-82.

Wagner, H., Bladt, S. & Rickl, V. (2009). *Plant Drug Analysis: A Thin Layer Chromatography Atlas*, Germany, Springer. 151.

Walmer, D.K., Wrona, M.A., Hughes, C.L., Nelson, K.G. (1992). Lactoferrin expression in the mouse reproductive tract during the natural estrous cycle: correlation with circulating estradiol and progesterone. *Endocrinology*, 131:1458–1466.

Wang, H. T., Shi, Q. L. & Yin, W. P. (2001). Isolation and identification of lipid from *Setaria italic*. *Chinese Traditional and Herbal Drugs*, 32: 291-293.

Wang, J. N., Zhou, Y., Zhu, T. Y., Wang, X. & Guo, Y. L. (2008). Prediction of acute cellular renal allograft rejection by urinary metabolomics using MALDI-FTMS. *Journal of Proteome Research*, 7: 3597-3601.

Wang, L., Wang, X., Wang, W., Chen, C., Ronnennberg, A. G., Guang, W., Huang, A., Fang, Z., Zang, T., Wang, L. & Xu, X. (2004). Stress and dysmenorrhea: a population based prospective study. *Occupational and Environmental Medicine* 61: 1021-1026.

Wang, M., Lamers, R. J., Korthout, H. A., Van Nesselrooij, J. H., Witkamp, R. F., Van Der Heijden, R., Voshol, P. J., Havekes, L. M., Verpoorte, R. & Van Der Greef, J. (2005). Metabolomics in the context of systems biology: bridging traditional Chinese medicine and molecular pharmacology. *Phytotherapy Research*, 19: 173-182.

Wang, Z. B. & Ma, H. I. (2005). Study on anticancer components on fig residues with super (sic) critical fluid CO₂ extracting technique. *Zhongguo Zhong Yao Za Zhi*, 30: 1443-1447.

Watcho, P., Ngadjui, E., Alango Nkeng-Efouet, P., Benoit Nguelefack, T. & Kamanyi, A. (2011). Evaluation of In Vitro Uterotonic Activities of Fruit Extracts of *Ficus asperifolia* in Rats. *Evidence-Based Complementary and Alternative Medicine*, 2011: 783413.

Watcho, P., Ngadjui, E., Alango, N. E., Benoit, N. T. & Kamanyi, A. (2009). Reproductive effects of *Ficus asperifolia* (Moraceae) in female rats. *African Health Sciences*, 9: 49-53.

Watts, S. W. (1996). Serotonin activates the mitogen-activated protein kinase pathway in vascular smooth muscle: use of the mitogen-activated protein kinase inhibitor PD098059. *Journal of Pharmacology and Experimental Therapeutics*, 279: 1541-1550.

Werth, M. T., Halouska, S., Shortridge, M. D., Zhang, B. & Powers, R. (2010). Analysis of metabolomic PCA data using tree diagrams. *Analytical Biochemistry*, 399: 58-63.

- Westerling, P., Lindgren, S. & Meyerson, B. (1991). Functional changes in GABAA receptor stimulation during the oestrous cycle of the rat. *British Journal of Pharmacology*, 103: 1580-1584.
- Whitman, M., Downes, C. P., Keeler, M., Keller, T. & Cantley, L. (1988). Type I phosphatidylinositol kinase makes a novel inositol phospholipid, phosphatidylinositol-3-phosphate. *Nature*, 332: 644-646.
- Wiklund, S., Johansson, E., Sjoström, L., Mellerowicz, E. J., Edlund, U., Shockcor, J. P., Gottfries, J., Moritz, T. & Trygg, J. (2008). Visualization of GC/TOF-MS-based metabolomics data for identification of biochemically interesting compounds using OPLS class models. *Analytical Chemistry*, 80: 115-122.
- Wilson, L., Jr., Parsons, M. T., Ouano, L. & Flouret, G. (1990). A new tocolytic agent: development of an oxytocin antagonist for inhibiting uterine contractions. *American Journal of Obstetrics and Gynecology*, 163: 195-202.
- Wiltbank, M. C., & Pursley, J. R. (2014). The cow as an induced ovulator: Timed AI after synchronization of ovulation. *Theriogenology*, 81(1) : 170-185.
- Wold, S., Sjoström, M. & Eriksson, L. (2001). PLS-regression: a basic tool of chemometrics. *Chemometrics and Intelligent Laboratory Systems*, 58: 109-130.
- Wongsinkongman, P., Brossi, A., Wang, H. K., Bastow, K. F. & Lee, K. H. (2002). Antitumor agents. Part 209: Pheophorbide-a derivatives as photo-Independent cytotoxic agents. *Bioorganic and Medicinal Chemistry*, 10: 583-591.

Woode, E., Poku, R. A., & Abotsi, W. K. (2011). Anticonvulsant effects of a leaf extract of *Ficus exasperata* Vahl (Moraceae) in mice. *International Journal of Pharmacology*, 7: 405-9.

Woode, E., Poku, R. A., Ainosoon, G. K., Abotsi, W. M. K., Mensah, T. L. & Amoh-Barimah, A. K. (2009). An Evaluation of the Anti-inflammatory and Antinociceptive Effects of *Ficusexasperata*Vahl Leaf Extract. *Journal of Pharmacology and Toxicology*, 4: 138-151.

Woodland, D. W. (1997). Contemporary plant systematics, Berrien Springs, Michigan, Andrews University Press.

Wray, S. & Noble, K. (2008). Sex hormones and excitation-contraction coupling in the uterus: the effects of oestrous and hormones. *Journal of Neuroendocrinology*, 20: 451-461.

Wray, S. & Shmygol, A. (2007). Role of the calcium store in uterine contractility. *Seminars in Cell and Developmental Biology*, 18: 315-320.

Wray, S. (1988). Regulation of intracellular pH in rat uterine smooth muscle, studied by ³¹P NMR spectroscopy. *Biochimica et Biophysica Acta*, 972: 299-301.

Wray, S. (1990). The effects of metabolic inhibition on uterine metabolism and intracellular pH in the rat. *Journal of Physiology*, 423: 411-423.

Wray, S. (1993). Uterine contraction and physiological mechanisms of modulation. *American Journal of Physiology*, 264: C1-C18.

Wray, S. (2007). Insights into the uterus. *Experimental Physiology*, 92: 621-631.

Wray, S., Jones, K., Kupittayanant, S., Li, Y., Matthew, A., Monir-Bishty, E., Noble, K., Pierce, S. J., Quenby, S. & Shmygol, A. V. (2003). Calcium signaling and uterine contractility. *Journal of the Society for Gynecologic Investigation*, 10: 252-264.

Wray, S., Kupittayanant, S., Shmygol, A., Smith, R. D. & Burdyga, T. (2001). The physiological basis of uterine contractility: a short review. *Experimental Physiology*, 86: 239-246.

Wu, H., Southam, A. D., Hines, A. & Viant, M. R. (2008). High-throughput tissue extraction protocol for NMR- and MS-based metabolomics. *Analytical Biochemistry*, 372: 204-212.

Wynn, R. (1977). Biology of the Uterus. In: WYNN, R. (ed.) Histology and ultrastructure of the human endometrium. New York, U. S. A: Plenum Press. p 341-376.

Xiao, D. & Zhang, L. (2002). ERK/ MAP kinases regulate smooth muscle contraction in ovine uterine artery: effect of pregnancy. *American Journal of Physiology. Heart and Circulatory Physiology*, 282: H292-H300.

Young, R. C., Smith, L. H. & McLaren, M. D. (1993). T-type and L-type calcium currents in freshly dispersed human uterine smooth muscle cells. *American Journal of Obstetrics and Gynecology*, 169: 785-792.

Yuan, C., Chen, D., Wang, S. (2014). Drug confirmation by mass spectrometry: Identification criteria and complicating factors. *Clinica Chimica Acta*, 438: 119-125.

Yuliana, N. D., Khatib, A., Choi, Y. H. & Verpoorte, R. (2011a). Metabolomics for bioactivity assessment of natural products. *Phytotherapy Research*, 25: 157-169.

Yuliana, N. D., Khatib, A., Verpoorte, R. & Choi, Y. H. (2011b). Comprehensive extraction method integrated with NMR metabolomics: a new bioactivity screening method for plants, adenosine A1 receptor binding compounds in *Orthosiphon stamineus* Benth. *Analytical Chemistry*, 83: 6902-6906.

Zhai, S., Dai, R., Friedman, F. K. & Vestal, R. E. (1998). Comparative inhibition of human cytochromes P450 1A1 and 1A2 by flavonoids. *Drug Metabolism and Disposition*, 26: 989-992.

Zhang, X., Shen, P., Coleman, M., Zou, W., Loggie, B. W., Smith, L. M. & Wang, Z. (2005). Caveolin-1 down-regulation activates estrogen receptor alpha expression and leads to 17beta-estradiol-stimulated mammary tumorigenesis. *Anticancer Research*, 25: 369-375.

Zhao, X., Zhang, Y., Meng, X., Yin, P., Deng, C., Chen, J., Wang, Z. & Xu, G. (2008). Effect of a traditional Chinese medicine preparation Xindi soft capsule on rat model of acute blood stasis: a urinary metabonomics study based on liquid chromatography-mass spectrometry. *Journal of Chromatography B Analytical Technologies in the Biomedical and Life Sciences*, 873: 151-158.

Zhou, X., Brotman, R. M., Gajer, P., Abdo, Z., Schuette, U., Ma, S., Ravel, J. & Forney, L. J. (2010). Recent advances in understanding the microbiology of the female reproductive tract and the causes of premature birth. *Infectious Diseases in Obstetrics and Gynecology*, 2010: 737425.

Zingg, H. H. & Laporte, S. A. (2003). The oxytocin receptor. *Trends in Endocrinology and Metabolism*, 14: 222-227.

Zitron, E., Scholz, E., Owen, R. W., Luck, S., Kiesecker, C., Thomas, D., Kathofer, S., Niroomand, F., Kiehn, J., Kreye, V. A., Katus, H. A., Schoels, W. & Karle, C. A. (2005). QTc prolongation by grapefruit juice and its potential pharmacological basis: HERG channel blockade by flavonoids. *Circulation*, 111: 835-838.

APPENDIX

APPENDIX 1

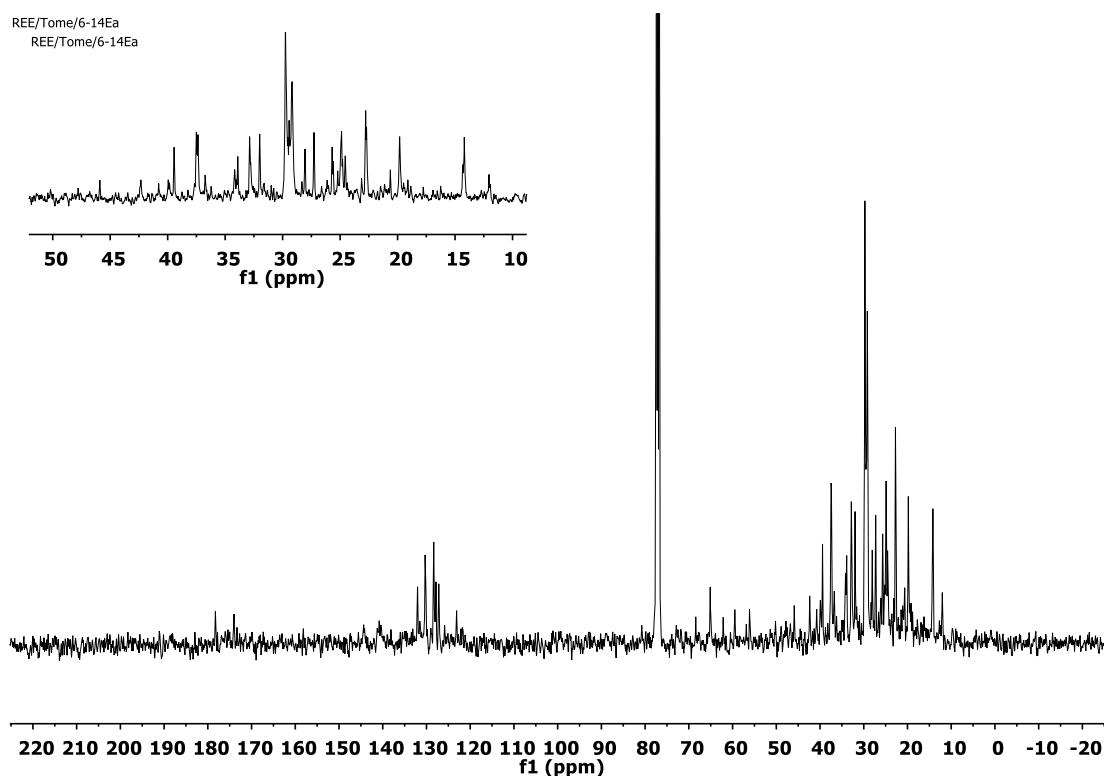


Figure A1.1 ^{13}C NMR of Compound **4** in CDCl_3 with an expansion of the crowded region between 10 and 50 ppm.

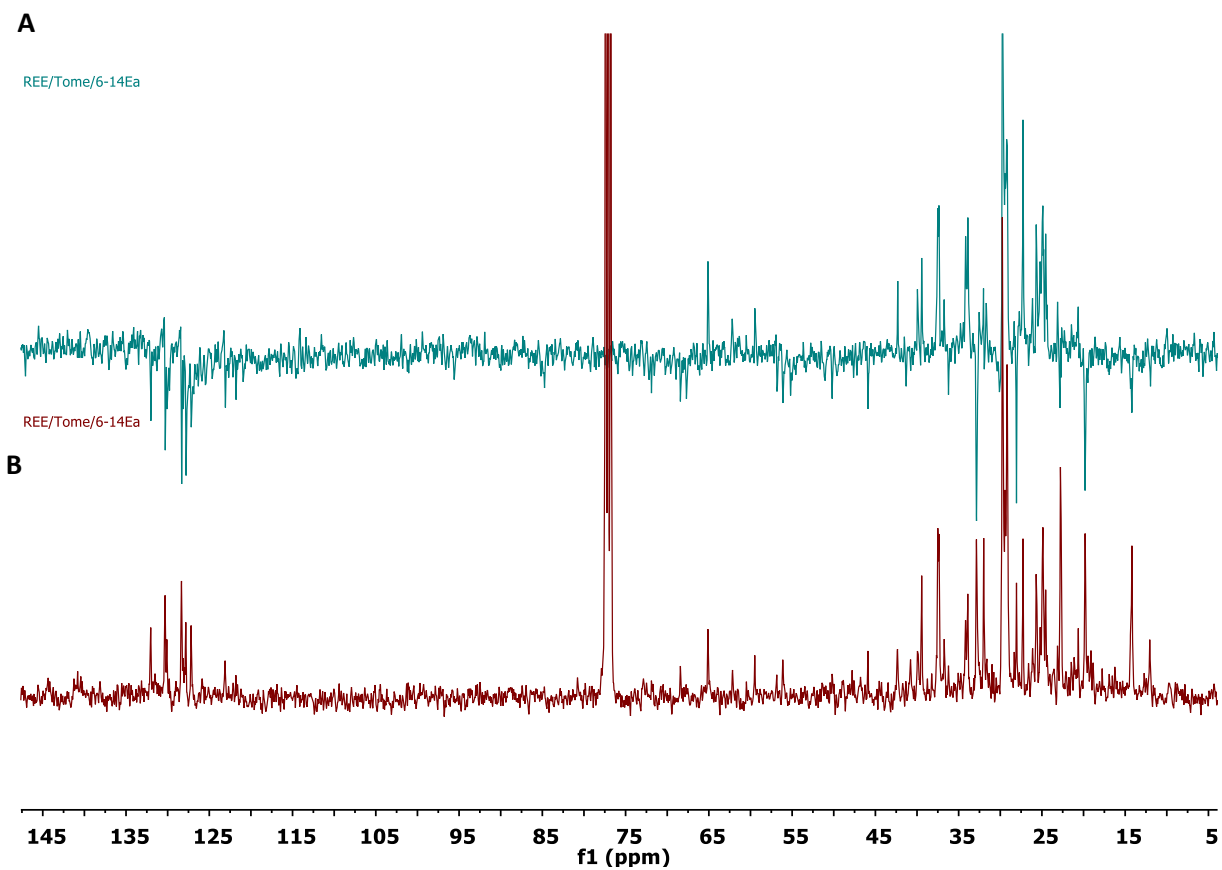


Figure A1.2 Figure showing DEPT (A) and ^{13}C (B) NMR of Compound **4** in CDCl_3 .

APPENDIX 2

Pharmacological Screening of the Methanol Fractions

The uterine activity of the active methanol fractions are shown below:

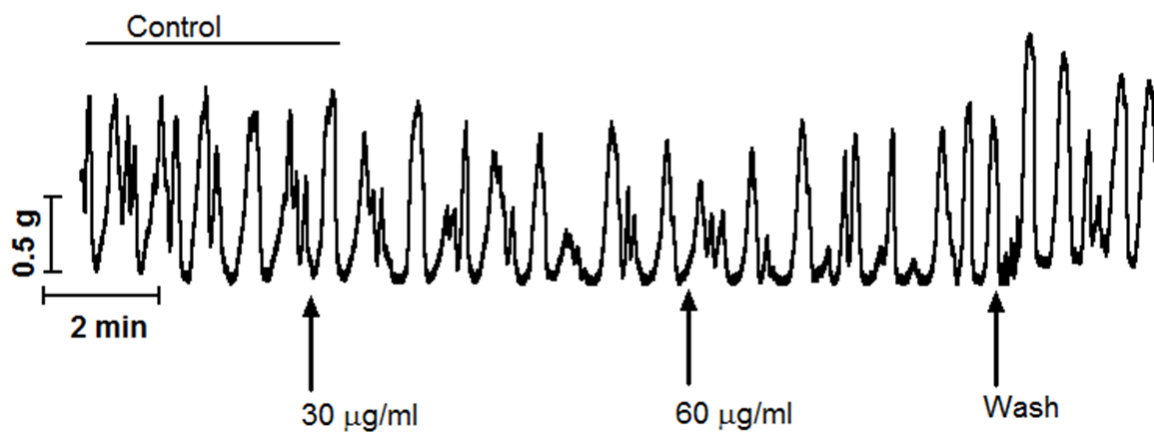


Figure A2.1 Representative recording of the effect of **1M1a** on lidocaine-induced (control) uterine contraction.

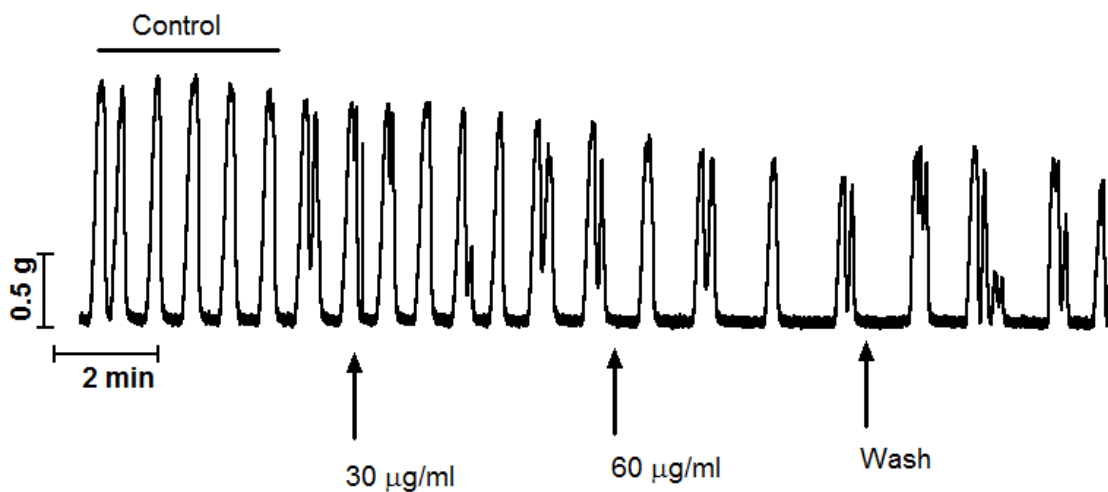


Figure A2.2 Representative recording of the effect of **2M1a** on lidocaine-induced (control) uterine contraction.

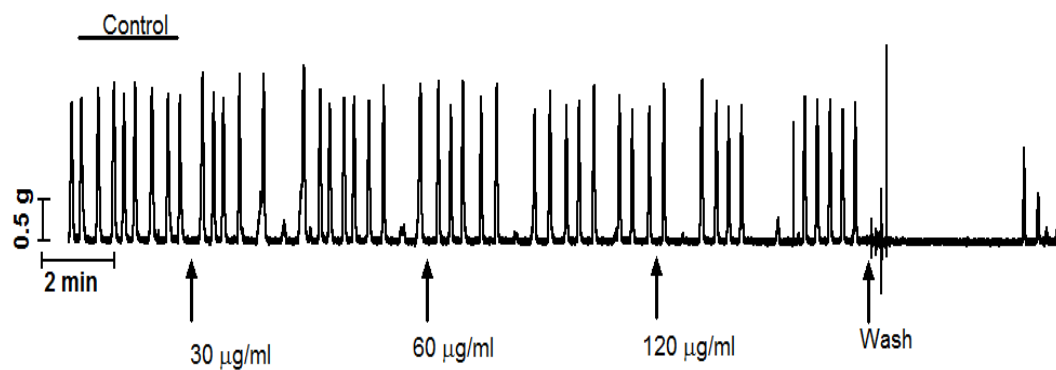


Figure A2.3 Original recording of the effect of **3M1a** on lidocaine-induced (control) uterine contractions.

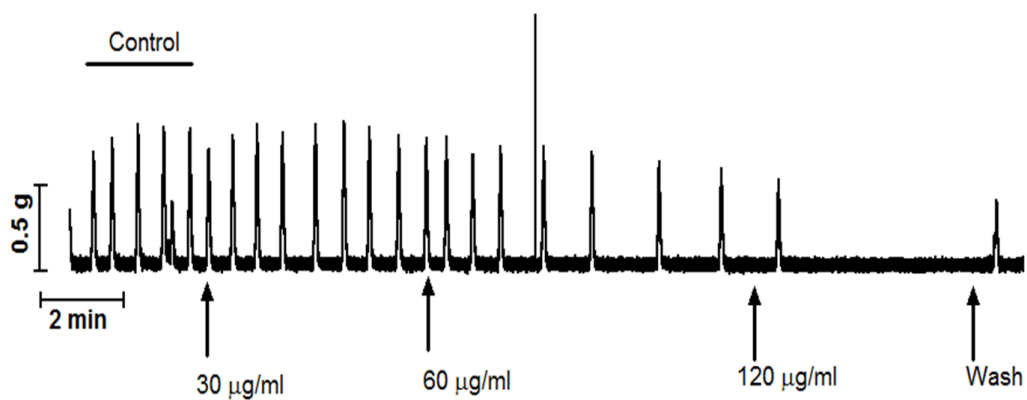


Figure A2.4 Effect of **5M1a** on lidocaine-induced (control) uterine contractions.

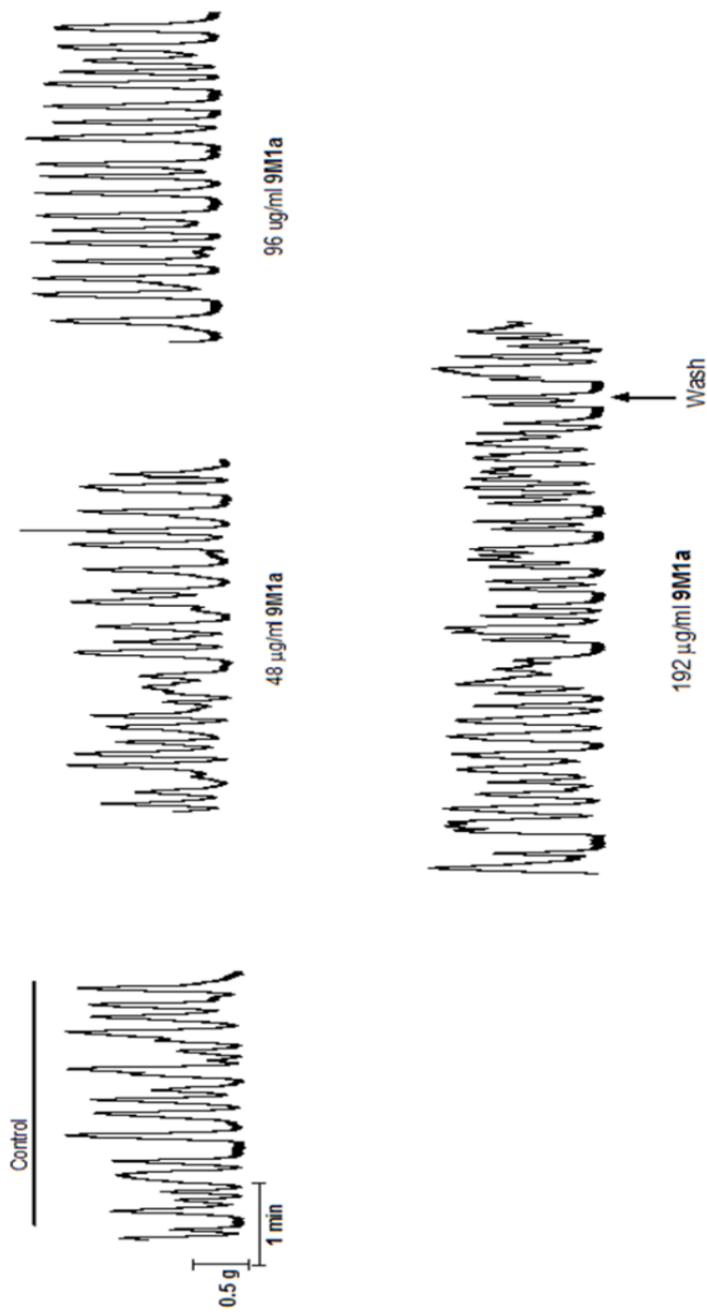


Figure A2.5 Effect of **9M1a** on lidocaine-induced (control) uterine contractions.

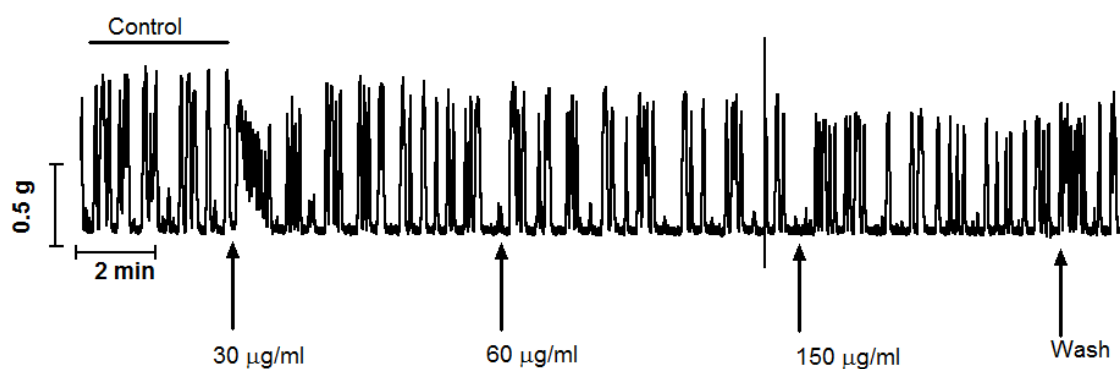


Figure A2.6 Effect of **11M1a** on lidocaine-induced (control) uterine contractions

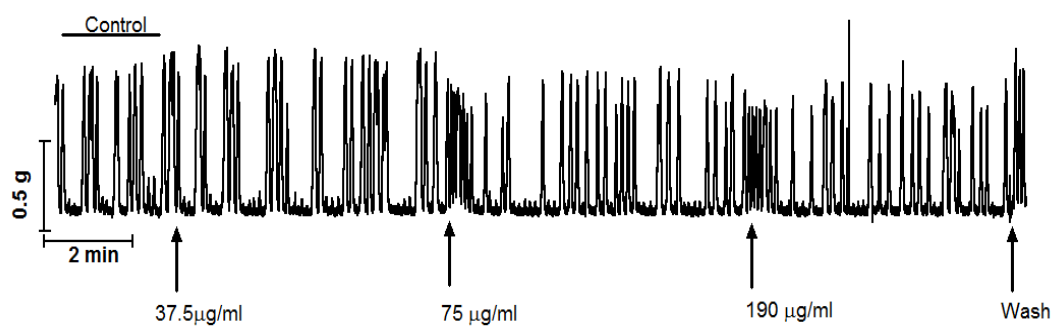


Figure A2.7 Effect of **15M1a** on lidocaine-induced (control) uterine contractions.

APPENDIX 3

Table A3.1 Significant metabolites and pathways extracted for the action of E1 on the uterus

GABA = gamma aminobutyric acid; **NA** = nucleic acid; **aa** = amino acid; **TCA** = tricarboxylic acid cycle; **cAMP** = cyclic adenosine monophosphate; **MI** = myoinositol; **PC** = phosphatidylcholine; **PS** = phosphatidylserine; **PGF1** = prostaglandinF1; **PHE** = phenylalanine; **PE** = phosphatidylethanolamine; **AEA** = anandamide; **U** = unknown; **DAG** = diacylglycerol; **ATP** = adenosinetriphosphate; **AA** = arachidonic acid; **NA** = nucleic acid; **ERK** = extracellular signal regulated kinase; **RhoA** = Ras homolog gene family, member A, **mTOR** = mammalian target of rapamycin; **NAA** = N-acetylaspartate; **nd** = not detected

Pathway	Metabolome	Shift (ppm)	p[1]Tissues	p[1]Fluids
	U	0.12	0.0200	nd
	U	0.28	0.0181	nd
	U	0.40	0.0316	nd
Lipid Metabolism	Lipids	0.68	-0.0299	nd
DAG Signalling	DAG	0.80	nd	-0.1371
	U	0.84	-0.2195	nd
DAG Signalling	DAG	0.84	nd	-0.1591
	U	1.40	nd	-0.0841
aa Metabolism	Alanine	1.44	nd	-0.1223
aa Metabolism	Alanine	1.48	nd	-0.1617
aa Metabolism	Alanine	1.52	nd	-0.2412
aa Metabolism	Lysine	1.56	-0.5716	-0.4574
DAG Signalling	DAG	1.60	nd	0.0244
DAG Signalling	DAG	1.68	nd	0.0254
Endocannabinoid Signalling	AEA	1.80	0.0150	nd
GABA Signalling	Glutamate	1.88	nd	0.0236
	U	1.92	nd	0.0269
	U	1.96	nd	0.0314
ERK1/2 signalling	NAA	2.00	nd	0.0375
	Glycoprotein	2.08	nd	-0.0378
DAG Signalling	DAG	2.20	0.0272	nd
TCA cycle	pyruvate	2.36	nd	-0.0513
DAG Signalling	DAG	2.40	0.0440	nd
Glutamine Signalling	Glutamine	2.44	nd	0.0468
	U	2.52		-0.3954
	U	2.56	nd	0.5167
	U	2.60	nd	0.1076
ERK1/2 Signalling	Aspartate	2.68	0.0259	nd
GABA Signalling	N-acetylaspartyl glutamate	2.72	0.0397	0.1096

Table A3.1 continued. Significant metabolites and pathways extracted for the action of E1 on the uterus by ¹H-NMR

Pathway	Metabolome	Shift (ppm)	p[1]Tissues	p[1]Fluids
ERK1/2 Signalling	Aspartate	2.80	0.0404	nd
Endocannabinoid Signalling	AEA	2.84	0.0309	nd
	U	2.88	nd	-0.1514
	U	2.92	nd	-0.1967
	U	2.96	nd	-0.0502
Histamine Metabolism	Histamine	3.04	nd	-0.2807
	U	3.08	nd	-0.2489
aa Metabolism	AA	3.12	-0.0438	-0.2040
aa Metabolism	AA	3.16	-0.0533	-0.1624
Endocannabinoid Signalling	AEA	3.40	nd	-0.1024
Endocannabinoid Signalling	AEA	3.44	nd	-0.1316
	U	3.48	nd	-0.0920
RhoA/Rho-kinase/mTOR Signalling	Threonine	4.24	nd	-0.0915
NA Metabolism	ATP	4.28	nd	-0.2100
RhoA/Rho-kinase/mTOR Signalling	Threonine	4.32	0.4685	nd
RhoA/Rho-kinase/mTOR Signalling	Threonine	4.36	0.2930	nd
NA Metabolism	ATP	4.60	-0.1466	nd
NA Metabolism	ATP	4.64	-0.1711	nd
	U	4.84	nd	0.0256
MI Signalling	MI	4.92	-0.1802	0.0197
DAG Signalling	DAG	5.00	0.0600	nd
DAG Signalling	DAG	5.04	0.0524	nd
DAG Signalling	DAG	5.08	0.0575	nd
DAG Signalling	DAG	5.12	0.0597	nd
DAG Signalling	DAG	5.16	0.0492	nd
cAMP synthesis/NA Metabolism	Adenosine	5.20	0.0414	nd
cAMP synthesis/NA Metabolism	Adenosine	5.24	0.0387	nd

Table A3.1 continued. Significant metabolites and pathways extracted for the action of **E1** on the uterus by ¹H-NMR

Pathway	Metabolome	Shift (ppm)	p[1]Tissues	p[1]Fluids
cAMP synthesis/NA Metabolism	Adenosine	5.24	0.0387	nd
cAMP synthesis/NA Metabolism	Adenosine	5.28	nd	nd
Endocannabinoid Signalling	AEA	5.40	0.0553	nd
Endocannabinoid Signalling	AEA	5.44	0.0377	nd
	U	5.48	0.0277	nd
cAMP synthesis/NA Metabolism	Adenosine	5.52	0.0271	nd
cAMP synthesis/NA Metabolism	Adenosine	5.56	0.0236	nd
	U	5.60	0.0231	nd
Prostanoid Signalling	PGF1	5.76	nd	-0.0644
	U	7.12	-0.0133	nd
Catecholamine synthesis	PHE	7.24	-0.0229	nd
Serotonin Signalling	Tryptophan	7.72	-0.0177	nd
	N-Acetylaspartate	7.84	0.0124	nd
	U	7.88	-0.0103	nd
Purine metabolism	Adenine	8.28	-0.0184	nd
	U	9.04	-0.0148	nd
	U	9.16	0.0227	nd
	U	9.48	nd	-0.0198
	Amines	9.84	-0.0146	nd
	Amines	9.88	-0.0128	nd

Table A3.2 Identified Metabolomes and Pathways of **F14**-Treated Tissues and Fluids

GABA =gamma aminobutyric acid; **NA** = nucleic acid; **aa** = amino acid; **TCA** = tricarboxylic acid cycle; **cAMP** = cyclic adenosine monophosphate; **MI** = myoinositol; **PC** = phosphatidylcholine; **PS**= phosphatidylserine; **PGF1**= prostaglandinF1; **PHE** = phenylalanine; **PE**= phosphatidylethanolamine; **AEA** = anandamide; **U** = unknown; **DAG** = diacylglycerol; **ATP** = adenosinetriphosphate; **AA** = arachidonic acid; **NA** = nucleic acid; **ERK** = extracellular signal regulated kinase; **RhoA** = Ras homolog gene family, member A, **mTOR** = mammalian target of rapamycin; **NAA** = N-acetylaspartate; **nd** = not detected

Pathways	Metabolome	Chemical Shift (ppm)	p[1]TP	p[1]FP
	U	0.04	nd	-0.0182
	U	0.20	-0.0076	nd
	U	0.32	-0.0069	nd
	U	0.44	-0.0070	nd
	U	0.60	nd	-0.0525
Lipid metabolism	Lipid	0.64	-0.0193	-0.0597
Lipid metabolism	Lipid	0.68	-0.0235	-0.0723
DAG Signalling	DAG	0.72	-0.0815	-0.0815
DAG Signalling	DAG	0.76	nd	-0.1022
DAG Signalling	DAG	0.80	-0.1658	-0.1375
DAG Signalling	DAG	0.84	-0.0473	-0.1857
Endocannabinoid Signalling	AEA	0.88	nd	-0.1579
Prostanoid Signalling	AA	0.92	-0.0343	-0.1220
Prostanoid Signalling	AA	0.96	-0.0367	-0.0809
Prostanoid Signalling	AA	1.00	-0.0310	-0.1172
Prostanoid Signalling	AA	1.04	-0.0329	-0.1316
Prostanoid Signalling	AA	1.08	-0.0417	-0.1295
	U	1.12	-0.0414	-0.0262
	U	1.16	-0.0342	-0.1419
	U	1.20	-0.0386	-0.0280
Endocannabinoid Signalling	AEA	1.28	0.3912	-0.2555
RhoA/Rho-kinase/mTOR Signalling	Threonine	1.32	0.2693	-0.1718
Endocannabinoid Signalling	AEA	1.36	0.1159	-0.1326
Endocannabinoid Signalling	AEA	1.40	-0.1569	-0.1235
Endocannabinoid Signalling	AEA	1.44	-0.2257	-0.1500
	U	1.48	-0.1956	-0.1850
aa metabolism	Lysine	1.56	nd	-0.3906
DAG Signalling	DAG	2.08	nd	-0.0471

Table A3.2 continued. Significant metabolites and pathways extracted for the action of F14 on the uterus by ¹H-NMR

Pathway	Metabolome	Shift (ppm)	p[1]Tissues	p[1]Fluids
GABA Signalling	GABA	2.28	0.0417	nd
GABA Signalling	Succinate	2.40	0.0987	nd
Glutamate/GABA Signalling	NAG	2.52	nd	-0.4175
	U	2.56	0.2066	nd
	U	2.60	0.1516	nd
ERK1/2 Signalling	Aspartate	2.64	0.1222	0.0403
ERK1/2 Signalling	NAA	2.68	0.0803	nd
Glutamate/GABA Signalling	NAG	2.72	0.0821	nd
	U	2.88	0.0193	-0.1664
	U	2.92	0.0204	-0.1984
Catecholamine Synthesis	Tyrosine	3.04	nd	-0.2773
	U	3.08	nd	-0.2093
	Creatine	3.12	nd	-0.1689
Endocannabinoid Signalling	PE	3.16	nd	-0.2114
	PC	3.32	0.0212	nd
NA Metabolism	Betaine	3.36	0.4871	nd
NA Metabolism	Betaine	3.40	0.2413	nd
	U	3.44	nd	0.3187
	U	3.48	0.1410	nd
Gluconeogenesis	Glucose	3.52	0.1204	nd
Gluconeogenesis	Glucose	3.56	0.0790	nd
	U	3.60	0.0640	nd
	U	3.72	nd	-0.0380
	U	3.80	-0.0109	nd
Catecholamine Synthesis	Tyrosine	3.92	-0.0220	nd
Catecholamine Synthesis	PHE	3.96	-0.0300	-0.0341
	U	4.00	-0.0343	nd
Endocannabinoid Signalling	PC	4.04	-0.0436	nd
	U	4.08	-0.0506	nd
Lipid Metabolism/ Energy production	TG	4.12	-0.0664	nd

Table A3.2 continued. Significant metabolites and pathways extracted for the action of F14 on the uterus by ¹H-NMR

Pathway	Metabolome	Shift (ppm)	p[1]Tissues	p[1]Fluids
Lipid Metabolism/ Energy production	TG	4.16	-0.0925	-0.0303
Energy production	ATP	4.20	-0.1229	-0.0482
Energy production	ATP	4.24	-0.1796	-0.1070
Energy production	ATP	4.28	-0.2413	-0.2047
RhoA/Rho-kinase/mTOR Signalling	Threonine	4.32	-0.2134	nd
RhoA/Rho-kinase/mTOR Signalling	Threonine	4.36	-0.2043	nd
RhoA/Rho-kinase/mTOR Signalling	Threonine	4.40	-0.2042	nd
NA Metabolism	Nucleotide sugars	4.44	-0.1892	nd
NA Metabolism	Nucleotide sugars	4.52	-0.1681	nd
	U	4.56	-0.1628	nd
	U	4.60	-0.1584	nd
	U	4.64	-0.1515	0.0292
	U	4.68	-0.1454	nd
	U	4.72	-0.1275	nd
	U	4.76	-0.0950	0.0441
MI Signalling	MI	4.92	-0.0479	nd
MI Signalling	MI	4.96	-0.0371	nd
MI Signalling	MI	5.00	-0.0312	nd
MI Signalling	MI	5.04	-0.0258	nd
MI Signalling	MI	5.08	-0.0223	nd
MI Signalling	MI	5.16	-0.0088	nd
MI Signalling	MI	5.24	-0.0075	nd
MI Signalling	MI	5.28	-0.0127	nd
MI Signalling	MI	5.56	-0.0053	nd
	U	5.72	-0.0069	-0.0320
Prostanoid Signalling	PGF1	5.76	-0.0785	nd
Prostanoid Signalling	PGF1	5.80	-0.0335	nd
	U	5.84	-0.0085	nd

Table A3.2 continued. Significant metabolites and pathways extracted for the action of F14 on the uterus by ¹H-NMR

Pathway	Metabolome	Shift (ppm)	p[1]Tissues	p[1]Fluids
	U		-0.0085	nd
Endocannabinoid Signalling	AEA	5.88	-0.0083	nd
	U	5.96	-0.0067	nd
Catecholamine Synthesis	Tyrosine	6.16	-0.0081	nd
Catecholamine Synthesis	Tyrosine	6.28	nd	-0.0187
Catecholamine Synthesis	Tyrosine	6.36	nd	-0.0123
Catecholamine Synthesis	Tyrosine	6.40	-0.0081	nd
Catecholamine Synthesis	Tyrosine	6.44	-0.0073	nd
Catecholamine Synthesis	Tyrosine	6.48	-0.0073	nd
Catecholamine Synthesis	Tyrosine	6.52	-0.0065	nd
Catecholamine Synthesis	Tyrosine	6.60	nd	0.0134
Catecholamine Synthesis	Tyrosine	6.88	-0.0063	nd
Catecholamine Synthesis	Tyrosine	6.92	-0.0109	nd
Catecholamine Synthesis	Tyrosine	6.96	-0.0097	nd
Catecholamine Synthesis	Tyrosine	7.00	-0.0074	nd
AA metabolism	Histidine	7.08	nd	-0.0291
	U	7.24	-0.0101	
	U	7.76		-0.0095
	U	7.80	-0.0072	nd
	U	7.88	-0.0069	-0.0107
Purine Metabolism	Adenine	8.00	nd	-0.0132
Purine Metabolism	Adenine	8.08	-0.0073	-0.0148
	U		-0.0085	nd
Purine Metabolism	Adenine	8.16	-0.0055	nd
Purine Metabolism	Adenine	8.68	nd	-0.0100
	U	9.16	0.0249	nd
	U	9.28	-0.0060	nd
		9.40		
		9.76	-0.0067	
	U	9.84	-0.0086	-0.0170

Table A3.3 Significant metabolites and pathways extracted for the action of F4-31 on the uterus.

GABA =gamma aminobutyric acid; **NA** = nucleic acid; **aa** = amino acid; **TCA** = tricarboxylic acid cycle; **cAMP** = cyclic adenosine monophosphate; **MI** = myoinositol; **PC** = phosphatidylcholine; **PS**= phosphatidylserine; **PGF1**= prostaglandinF1; **PHE** = phenylalanine; **PE**= phosphatidylethanolamine; **AEA** = anandamide; **U** = unknown; **DAG** = diacylglycerol; **ATP** = adenosinetriphosphate; **AA** = arachidonic acid; **NA** = nucleic acid; **ERK** = extracellular signal regulated kinase; **RhoA** = Ras homolog gene family, member A, **mTOR** = mammalian target of rapamycin; **NAA** = N-acetylaspartate **ATP** = Adenosine triphosphate; **nd** = not detected

Pathways	Metabolome	Chemical Shift (ppm)	p[1]Tissues	p[1]Fluids
	U	0.04	nd	-0.0369
	U	0.52	-0.0297	nd
Lipid Metabolism	Lipid	0.68	nd	-0.1019
DAG Signalling	DAG	0.72	nd	-0.1308
DAG Signalling	DAG	0.76	nd	-0.1731
Leucine Metabolism	Leucine	0.80	nd	-0.2088
Endocannabinoid Signalling	AEA	0.88	0.0780	nd
aa Metabolism	Valine	1.04	-0.0907	nd
	U	1.08	-0.0862	-0.0183
	U	1.12	nd	-0.0345
	U	1.16	-0.1259	-0.0314
	U	1.20	-0.1734	-0.1954
Endocannabinoid Signalling	AEA	1.24	nd	-0.0469
RhoA/mTOR Signalling	Threonine	1.32	0.0631	nd
Endocannabinoid Signalling	AEA	1.40	nd	-0.1207
Endocannabinoid Signalling	AEA	1.44	nd	-0.1376
	U	1.48	nd	-0.1718
aa Metabolism	Alanine	1.52	nd	-0.2748
ERK1/2 Signalling	NAA	2.00	-0.1297	nd
Glutamate Signalling	NAG	2.04	-0.1373	nd
DAG Signalling	DAG	2.08	-0.1153	nd
Glutamate Signalling	Glutamate	2.16	0.0313	nd
Glutamate Signalling	Glutamate	2.20	0.0403	nd
	Acetoacetate	2.24	0.0324	nd
TCAcycle/Energy production	Pyruvate	2.32	-0.1418	nd

Table A3.3 continued. Significant metabolites and pathways extracted for the action of F4-31 on the uterus by ¹H-NMR

Pathway	Metabolome	Shift (ppm)	p[1]Tissues	p[1]Fluids
TCA cycle/Energy production	Pyruvate	2.36	-0.1013	nd
Glutamate Signalling	Glutamate	2.44	nd	0.0429
	U	2.56	0.0417	nd
	U	2.60	0.3332	nd
ERK1/2 Signalling	Aspartate	2.64	0.2028	nd
ERK1/2 Signalling	NAA	2.68	0.1535	nd
Glutamate Signalling	NAG	2.72	nd	0.0552
	U	2.76	0.0448	0.0361
	U	2.88	nd	-0.1814
	U	2.92	0.0420	-0.2505
	U	2.96	nd	-0.0702
GABA Signalling	GABA	3.00	nd	0.0699
Catecholamine Synthesis	Tyrosine	3.04	nd	-0.3466
	U	3.08	nd	-0.3244
	Creatine	3.12	nd	-0.2578
Endocannabinoid Signalling	PE	3.16	nd	-0.1964
aa Metabolism	Taurine	3.24	nd	-0.0280
NA Metabolism	Betaine	3.40	nd	-0.1451
	U	3.44	nd	-0.1849
MI Signalling	MI	3.60	nd	-0.2344
	U	3.68	nd	-0.0197
aa Metabolism	AA	3.80	nd	-0.0324
Energy production	ATP	4.24	nd	-0.1075
Energy production	ATP	4.28	-0.3187	-0.2665
RhoA/mTOR Signalling	Threonine	4.32	-0.2460	-0.0358
NA Metabolism	Nucleotide Sugars	4.40	nd	0.0764
	U	4.56	-0.1637	nd
	U	4.60	-0.1844	0.0301
	U	4.64	-0.2034	nd
MI Signalling	MI	5.04	nd	-0.0509

Table A3.3 continued. Significant metabolites and pathways extracted for the action of F4-31 on the uterus by ¹H-NMR

Pathway	Metabolome	Shift (ppm)	p[1]Tissues	p[1]Fluids
MI Signalling	MI	5.08	nd	-0.0189
Endocannabinoid Signalling	AEA	5.36	nd	-0.0200
cAMP Signalling	AMP	5.40	0.0540	nd
	U	5.44	0.0361	nd
MI Signalling	MI	5.56	0.0181	nd
Prostanoid Signalling g	PGF ₁	5.76	nd	-0.0826
Endocannabinoid Signalling	AEA	5.88	nd	-0.0378
cAMP Signalling	Adenosine	5.92	0.0393	nd
Catecholamine Synthesis	Tyrosine	6.00	0.0201	nd
Catecholamine Synthesis	Tyrosine	6.20	0.0169	nd
Catecholamine Synthesis	Tyrosine	6.24	0.0271	nd
Catecholamine Synthesis	Tyrosine	6.36	0.0437	nd
Catecholamine Synthesis	Tyrosine	6.76	nd	-0.0262
Catecholamine Synthesis	Tyrosine	6.80	-0.0318	nd
aa Metabolism	Glutamine	7.16	0.0200	nd
aa Metabolism	Glutamine	7.52	0.0176	nd
	U	7.56	-0.0325	nd
	U	7.64	0.0161	nd
	U	7.68	0.0201	nd
Purine Metabolism	Adenine	8.08	nd	nd
	U	8.80	nd	-0.0217
	Amines	9.00	0.0340	
	Amines	9.40	nd	0.0289
	Amines	9.48	0.0343	nd
	Amines	9.68	0.0331	nd
	Amines	9.72	-0.0075	nd

Table A3.4 Significant metabolites and pathways extracted for the action of F6.17 on the uterus

GABA =gamma aminobutyric acid; NA = nucleic acid; aa = amino acid; TCA = tricarboxylic acid cycle; cAMP = cyclic adenosine monophosphate; MI = myoinositol; PC = phosphatidylcholine; PS= phosphatidylserine; PGF1= prostaglandinF1; PHE = phenylalanine; PE= phosphatidylethanolamine; AEA = anandamide; U = unknown; DAG = diacylglycerol; ATP = adenosinetriphosphate; ERK = extracellular signal regulated kinase; RhoA = Ras homolog gene family, member A, mTOR = mammalian target of rapamycin; NAA = N-acetylaspartate; ATP = Adenosine triphosphate; NAG = N-acetylglutamate; AA = arachidonic acid; nd= not detected

Pathway	Metabolome	Chemical Shift		
		(ppm)	p[1]Tissues	p[1]Fluids
DAG Signalling	DAG	0.84	nd	0.0395
Endocannabinoid Signalling	AEA	0.88	nd	0.0258
Prostanoid Signalling	AA	0.96	-0.0368	-0.0482
Prostanoid Signalling	AA	1.00	-0.0378	-0.0658
Prostanoid Signalling	AA	1.04	-0.0361	-0.0658
Prostanoid Signalling	AA	1.08	-0.0367	nd
	U	1.12	-0.3300	-0.0269
	Hydrxybutyrate	1.24	nd	0.0421
Endocannabinoid Signalling	AEA	1.28	nd	0.0343
RhoA/Rho-kinase/ mTOR Signalling	Threonine	1.32	0.2523	nd
	U	1.48	nd	-0.1143
	U	1.52	nd	-0.1794
AA metabolism	Lysine	1.56	nd	-0.3586
DAG Signalling	DAG	1.60	nd	-0.3338
DAG Signalling	DAG	1.64	nd	-0.1475
Endocannabinoid Signalling	AEA	1.72	nd	0.0786
Endocannabinoid Signalling	AEA	1.76	nd	0.1103
	U	1.80	0.0535	0.0971
	U	1.84	nd	0.0913
GABA/Glutamate metabolism	Glutamate	1.88	nd	0.0819
	U	1.92	0.0351	0.0625
	U	1.96	nd	0.0670
ERK1/2 Signalling	NAA	2.00	nd	0.1327
GABA/Glutamate metabolism	NAG	2.04	nd	0.0839
DAG Signalling	DAG	2.08	-0.0236	-0.0448
GABA/Glutamate metabolism	Glutamine	2.12	0.0959	0.1067
GABA/Glutamate metabolism	Glutamine	2.16	nd	-0.0320
GABA/Glutamate metabolism	Glutamine	2.20	nd	-0.0380
TCA Cycle	Acetoacetate	2.24	nd	-0.0468

Table A3.4 continued. Significant metabolites and pathways extracted for the action of F6.17 on the uterus by ¹H-NMR

Pathway	Metabolome	Shift (ppm)	p[1]Tissues	p[1]Fluids
GABA/Glutamate metabolism	GABA	2.28	nd	-0.0580
GABA/Glutamate metabolism	GABA	2.32	nd	-0.0656
TCA Cycle	Pyruvate	2.36	nd	-0.0746
GABA/Glutamate metabolism	Succinate	2.40	0.0405	nd
	U	2.44	0.0508	nd
ERK1/2 Signalling	NAA	2.48	0.0312	nd
ERK1/2 Signalling	NAG	2.52	0.0313	nd
	U	2.56	nd	0.4855
	U	2.60	nd	0.1652
ERK1/2 Signalling	Aspartate	2.64	nd	0.1027
ERK1/2 Signalling	NAA	2.68	0.0792	nd
ERK1/2 Signalling	Aspartate	2.80	nd	-0.0553
Endocannabinoid Signalling	AEA	2.84	nd	-0.0874
	U	2.88	nd	-0.1690
	U	2.92	nd	-0.1548
	U	2.96	-0.0296	
GABA/Glutamate metabolism	GABA	3.00	nd	-0.1127
Histamine Signalling	Histamine	3.04	nd	-0.2621
Endocannabinoid Signalling	PE	3.16	nd	-0.1444
	U	3.20	nd	-0.1243
	U	3.24	nd	-0.1075
	U	3.28	nd	-0.0898
	U	3.32	nd	-0.0699
Endocannabinoid Signalling	AEA	3.40	nd	-0.1539
Endocannabinoid Signalling	AEA	3.44	0.3265	nd
Gluconeogenesis/Glycolysis	Glucose	3.52	0.0478	nd
MI Signalling	MI	3.60	nd	-0.2436
	U	3.76	nd	0.0405
aa metabolism	aa	3.80	nd	-0.0500
Endocannabinoid Signalling	Serine	3.84	nd	-0.0631
	U	3.88	nd	-0.0657
Catecholamine Synthesis	Tyrosine	3.92	-0.0328	-0.0665
Catecholamine Synthesis	PHE	3.96	-0.0546	-0.0616
	U	4.00	nd	-0.0589
	U	4.08	-0.0526	-0.0500
Lipid Metabolism	TG	4.12	-0.0694	-0.0412
Lipid Metabolism	TG	4.16	-0.0962	-0.0270

Table A3.4 continued. Significant metabolites and pathways extracted for the action of F6.17 on the uterus by ¹H-NMR

Pathway	Metabolome	Shift (ppm)	p[1]Tissues	p[1]Fluids
Energy production	ATP	4.20	-0.1287	-0.0297
Energy production	ATP	4.24	-0.1922	-0.1150
Energy production	ATP	4.28	-0.2531	-0.1326
RhoA/Rho-kinase/ mTOR Signalling	Threonine	4.32	-0.2249	nd
RhoA/Rho-kinase mTOR Signalling	Threonine	4.36	-0.2186	-0.0670
RhoA/Rho-kinase/ mTOR Signalling	Threonine	4.40	-0.2180	-0.0636
NA Metabolism	Nucleotide sugars	4.44	-0.2011	-0.0580
NA Metabolism	Nucleotide sugars	4.48	-0.1826	-0.0496
NA Metabolism	Nucleotide sugars	4.52	-0.1773	-0.0420
	U	4.56	-0.1712	-0.0299
	U	4.60	-0.1668	nd
	U	4.64	-0.1609	nd
	U	4.68	-0.1556	-0.0261
	U	4.72	-0.1363	nd
	U	4.76	-0.0996	nd
	U	4.80	-0.0760	-0.0412
	U	4.84	-0.0659	-0.0451
	U	4.88	-0.0580	-0.0774
MI Signalling	MI	4.92	-0.0492	nd
MI Signalling	MI	4.96	-0.0384	nd
MI Signalling	MI	5.00	-0.0316	nd
MI Signalling	MI	5.04	nd	-0.0412
MI Signalling	MI	5.08	nd	-0.0380
MI Signalling	MI	5.12	nd	-0.0380
MI Signalling	MI	5.16	nd	-0.0369
MI Signalling	MI	5.20	nd	-0.0334
MI Signalling	MI	5.24	nd	-0.0290
MI Signalling	MI	5.28	-0.0158	-0.0227
Endocannabinoid Signalling	AEA	5.32	nd	-0.0157
Prostanoid Signalling	PGF ₁	5.76	0.0691	nd
Catecholamine Synthesis	Tyrosine	6.00	0.0309	nd
Catecholamine Synthesis	Tyrosine	6.72	nd	-0.0079
	U	7.04	-0.0264	nd
	U	7.12	-0.0097	nd
	U	7.20	nd	0.0404
	U	7.24	nd	0.1070
	U	7.28	nd	0.2860

Table A3.4 continued. Significant metabolites and pathways extracted for the action of F6.17 on the uterus by ¹H-NMR

Pathway	Metabolome	Shift (ppm)	p[1]Tissues	p[1]Fluids
Catecholamine Synthesis	PHE	7.32	nd	0.0983
	U	7.40	-0.0853	nd
	U	7.44	-0.0465	nd
	U	8.20	-0.0326	nd
	U	9.84	-0.0321	nd

Table A3.5 Significant metabolites and pathways extracted for the action of F28 on the uterus.

GABA =gamma aminobutyric acid; **NA** = nucleic acid; **aa** = amino acid; **TCA** = tricarboxylic acid cycle; **cAMP** = cyclic adenosine monophosphate; **MI** = myoinositol; **PC** = phosphatidylcholine; **PS**= phosphatidylserine; **PGF1**= prostaglandinF1; **PHE** = phenylalanine; **PE**= phosphatidylethanolamine; **AEA** = anandamide; **U** = unknown; **DAG** = diacylglycerol; **ATP** = adenosinetriphosphate; **ERK** = extracellular signal regulated kinase; **RhoA** = Ras homolog gene family, member A, **mTOR** = mammalian target of rapamycin; **NAA** = N-acetylaspartate; **ATP** = Adenosine triphosphate; **NAG** = N-acetylglutamate; **AA** = arachidonic acid; **TG** = Triacylglycerol; **nd** = not detected

Pathway	Metabolome	Chemical Shift (ppm)	p[1]Tissues	p[1]Fluids
	U	0.04	nd	-0.0362
Lipid Metabolism	Lipid	0.68	nd	-0.0881
DAG Signalling	DAG	0.72	nd	-0.1160
DAG Signalling	DAG	0.76	nd	-0.1526
DAG Signalling	DAG	0.80	-0.1327	-0.2046
DAG Signalling	DAG	0.84	-0.0386	nd
Endocannabinoid Signalling	AEA	0.88	-0.0511	nd
Prostanoid Signalling	AA	0.92	-0.0382	nd
Prostanoid Signalling	AA	0.96	-0.0387	nd
Prostanoid Signalling	AA	1.00	-0.0332	nd
Prostanoid Signalling	AA	1.04	-0.0332	nd
Prostanoid Signalling	AA	1.08	-0.0380	-0.1250
	U	1.12	-0.0367	-0.0294

Table A3.5 continued. Significant metabolites and pathways extracted for the action of **F28** on the uterus by ¹H-NMR

Pathway	Metabolome	Shift (ppm)	p[1]Tissues	p[1]Fluids
	U	1.16	-0.0268	-0.1451
	U	1.20		-0.1621
	HB	1.24	-0.0743	-0.2319
Endocannabinoid Signalling	AEA	1.28	0.3334	nd
RhoA/Rho-kinase/ mTOR Signalling	Threonine	1.32	-0.0366	nd
Endocannabinoid Signalling	AEA	1.36	-0.0278	nd
	AEA	1.40	-0.0238	nd
	AEA	1.44	-0.1494	nd
	U	1.48	-0.0235	nd
aa metabolism	Lysine	1.56	-0.0205	nd
	U	1.68	nd	0.2822
Endocannabinoid Signalling	AEA	1.72	nd	0.2316
	U	1.96	0.0549	nd
ERK1/2 Signalling	NAA	2.00	0.1137	nd
GABA/Glutamate Signalling	NAG	2.04	0.1575	nd
DAG Signalling	DAG	2.08	0.1401	-0.0462
GABA/Glutamate Signalling	Glutamine	2.12	0.0875	nd
GABA/Glutamate Signalling	GABA	2.28	0.0536	nd
GABA/Glutamate Signalling	GABA	2.32	0.1235	nd
GABA/Glutamate Signalling	Succinate	2.40	0.0333	nd
	U	2.44	0.0370	nd
ERK1/2 Signalling	NAA	2.48	0.0290	nd
GABA/Glutamate Signalling	NAG	2.52	-0.3268	-0.3940
	U	2.56	nd	0.0548
	U	2.60	0.0700	
	Aspartate	2.64	nd	0.3735
ERK1/2 Signalling	NAA	2.68	nd	0.1428
GABA/Glutamate Signalling	NAG	2.72	nd	0.1011
		2.76	0.0355	nd
	Aspartate	2.80	0.0620	nd
Endocannabinoid Signalling	AEA	2.84	0.0549	nd
	U	2.88	0.0345	nd
	U	2.92	nd	-0.2009
Catecholamine Synthesis	Tyrosine	3.04	nd	-0.2871
	U	3.08	nd	-0.2222

Table A3.5 continued. Significant metabolites and pathways extracted for the action of **F28** on the uterus by ¹H-NMR

Pathway	Metabolome	Shift (ppm)	p[1]Tissues	p[1]Fluids
	Creatine	3.12	nd	-0.1920
	U	3.24	0.0716	nd
	U	3.28	0.0825	nd
NA metabolism	Betaine	3.36	nd	0.0322
NA metabolism	Betaine	3.40	nd	-0.1446
	U	3.48	nd	-0.1290
Gluconeogenesis/Glycolysis	Glucose	3.52	nd	0.2800
Gluconeogenesis/Glycolysis	Glucose	3.56	nd	0.1231
MI Signalling	MI	3.60	-0.0345	nd
Catecholamine Synthesis	PHE	3.96	-0.0426	nd
	U	4.08	0.0309	nd
	TG	4.12	-0.0592	nd
	TG	4.16	-0.0813	nd
Energy production	ATP	4.20	-0.1084	nd
Energy production	ATP	4.24	nd	-0.0833
Energy production	ATP	4.28	-0.2162	-0.1936
RhoA/Rho-kinase/ mTOR Signalling	Threonine	4.32	0.0789	nd
RhoA/Rho-kinase/ mTOR Signalling	Threonine	4.36	0.0570	0.2020
RhoA/Rho-kinase/ mTOR Signalling	Threonine	4.40	0.0364	nd
NA metabolism	Nucleotide sugars	4.44	0.0225	nd
NA metabolism	Nucleotide sugars	4.48	-0.1544	nd
NA metabolism	Nucleotide sugars	4.52	-0.1501	nd
	U	4.56	-0.1451	nd
	U	4.60	-0.1413	nd
	U	4.64	-0.1361	nd
	U	4.72	-0.1153	nd
	U	4.76	-0.0845	nd
	U	4.80	-0.0650	nd
	U	4.84	-0.0568	nd
	U	4.88	-0.0490	nd
	U	4.92	-0.0429	-0.2113
MI Signalling	MI	5.20	0.0302	nd
cAMP Signalling	Adenosine	5.36	0.1111	nd
cAMP Signalling	Adenosine	5.40	0.1165	nd
cAMP Signalling	Adenosine	5.44	0.0871	nd
cAMP Signalling	Adenosine	5.48	0.0568	nd
	U	7.36	nd	0.0819

APPENDIX 4

Significantly Regulated Metabolites in **OT** and **RIT**- treated Tissues as detected by ¹H-NMR

Table A4.1 Summary of Differentially Expressed Metabolites in OTTP and OTFP								
Abbreviations: DAG =diacyl glycerol,; PC= phosphatidylcholine; PE= phosphoethanolamine; PS= phosphatidylserine; PG = phosphoglycerol; TG=triacylglycerol; m/z = mass to charge; Rt = Retention time; FC = fold change; PV = p value. A positive FC value indicates a relatively higher metabolite concentration in the treated groups, while a negative value is indicative of a relatively lower concentration in the treated; nd = not detected								
Rt (min)	ID	m/z	Adduct	Metabolic Pathway	Tissue		Fluid	
					FC	PV	FC	PV
1.28	Glutamate	148.0606	[M+H] ⁺	TCA cycle; Glutamate Metabolism	-6.241	0.347	nd	nd
1.29	GABA (γ-amino butyric acid)	104.0708	[M+H] ⁺	Ligand-receptor Interaction;	5.847	0.124	2.952	0.409
1.37	α-heptenoic acid	170.1175	[M+ACN+H] ⁺		426.553	0.374	nd	nd
1.53	cysteinyl-tyrosine	143.0486	[M+2H] ²⁺	Tyrosine metabolism	1.395	0.144	nd	nd
1.69	6-deoxy-D-glucose	147.0659	[M+H-2H ₂ O] ⁺	Glycolysis/ Gluconeogenesis	nd	nd	3.129	0.087
1.73	Glucosamine	180.0873	[M+H] ⁺	Amino sugar and nucleotide sugar metabolism	nd	nd	14.554	0.382
1.73	γ-hexenoic acid	115.0755	[M+H] ⁺		nd	nd	-7.998	0.086
1.75	Myo-inositol	163.0608	[M+H-H ₂ O] ⁺	Phosphatidyl-inositol signalling	nd	nd	1.980	0.251

Rt (min)	ID	m/z	Adduct	Metabolic Pathway	Tissue		Fluid	
					FC	PV	FC	PV
1.77	4Z,7-Octadienoic Acid	163.0729	[M+Na] ⁺		- 407.149	0.375	nd	nd
1.78	Isoleucine	132.1023	[M+H] ⁺	Pyridine Synthesis/ Valine, leucine and isoleucine biosynthesis	nd	nd	-16.709	0.189
1.80	Niacinamide	123.0554	[M+H] ⁺	Nicotine and Nicotinamide Metabolism	2.858	0.005	nd	nd
1.80	PC(3:0/3:0)	124.0590	[M+3H] ³⁺	Glycerophospho- lipid Metabolism	2.871	0.015	nd	nd
1.83	3-keto valeric acid	117.0551	[M+H] ⁺	Cell Signalling	nd	nd	2.704	0.110
1.83	1,6-Anhydro-β-D- glucose	204.0873	[M+ACN+H] ⁺	Glycolysis/ Gluconeogenesis	nd	nd	2.953	0.141
1.84	3-Hexenedioic Acid	127.0394	[M+H-H ₂ O] ⁺	Lipid Metabolism/ Cell Signalling	nd	nd	2.371	0.298
1.85	2-oxo-4-hydroxy- hexanoic acid	129.0550	[M+H] ⁺	Lipid Metabolism/ Cell Signalling	nd	nd	5.927	0.069
1.85	3-O-Methyl-myo- inositol	159.0658	[M+H-2H ₂ O] ⁺	Phosphatidyl- inositol signalling system	nd	nd	5.929	0.103
1.87	Glycolaldehyde	102.0551	[M+ACN+H] ⁺		-15.680	0.369	nd	nd
1.88	D-Ribose	115.0395	[M+H-2H ₂ O] ⁺	Pentose phosphate pathway	nd	nd	5.060	0.127

Rt (min)	ID	m/z	Adduct	Metabolic Pathway	Tissue		Fluid	
					FC	PV	FC	PV
1.90	myo-Inositol	145.0501	[M+H-2H ₂ O] ⁺	Phosphatidyl- inositol signalling system	nd	nd	1.993	0.421
1.95	Methylsuccinic acid	174.0767	[M+ACN+H] ⁺	Energy production	nd	nd	5.440	0.095
2.05	2-Methyl-Hexanoic Acid	163.1329	[M+CH ₃ OH+H] ⁺		239.180	0.374	nd	nd
2.20	Betaine aldehyde	102.0914	[M+H] ⁺	Glycine, serine and threonine metabolism	-1.332	0.695	3.506	0.190
6.77	N-methyl arachidonoyl amine	340.2595	[M+Na] ⁺	Cell Signalling	nd	nd	-5.007	0.265
7.32	N-methyl arachidonoyl amine	340.2593	[M+Na] ⁺	Cell Signalling	-2.337	0.316	-1.700	0.636
7.32	norleucine	340.2593	[M+H-H ₂ O] ⁺	Pyridine Synthesis/ Valine, leucine and isoleucine biosynthesis	-2.337	0.316	-1.700	0.636
8.56	DAG(22:5)	679.5118	[M+H-2H ₂ O] ⁺	Second messenger/ Cell Signalling	-5.989	0.241	-1.264	0.839
12.17	3-methyl-nonanoic acid	214.1801	[M+ACN+H] ⁺		-3.527	0.076	-3.527	0.076
17.63	2-keto palmitic acid	288.2531	[M+NH ₄] ⁺	LipidMetabolism			-82.668	0.184

Rt (min)	ID	m/z	Adduct	Metabolic Pathway	Tissue		Fluid	
					FC	PV	FC	PV
18.85	N-arachidonoyl amine	300.2684	[M+H-2H ₂ O] ⁺	Cell Signalling	8.514	0.056	nd	nd
18.93	LysoPE(0:0/22:6)	526.2933	[M+H] ⁺	Glycerophospho- lipid Metabolism	2.163	0.147	nd	nd
18.94	Glycerophospho-N- Arachidonoyl Ethanolamine	502.2931	[M+H] ⁺	Cell Signalling	5.906	0.239	nd	nd
18.99	Glycerophospho-N- Arachidonoyl Ethanolamine	502.2931	[M+H] ⁺	Cell Signalling	2.256	0.153	nd	nd
19.03	Sphingosine	300.2897	[M+H] ⁺	Sphingolipid metabolism	2.213	0.096	1.678	0.175
19.11	PC(20:4)	544.3403	[M+H] ⁺	Glycerophospho- lipid Metabolism	2.034	0.147	nd	nd
19.40	PE(10:0/11:0)[U]	520.3403	[M+H-2H ₂ O] ⁺	Glycerophospho- lipid Metabolism	nd	nd	- 252.938	0.192
20.34	PC(O-14:0/2:0)	496.3401		Glycerophospho- lipid Metabolism	2.261	0.120	nd	nd
20.79	Glycerophospho-N- Palmitoyl Ethanolamine	454.2931	[M+H] ⁺	Lipid Metabolism/ Cell Signalling	2.007	0.112	nd	nd
20.89	PC(O-14:0/2:0)	496.3399	[M+H] ⁺	Glycerophospho- lipid Metabolism	nd	nd	-71.773	0.216
20.96	Glycerophospho-N- Oleoyl Ethanolamine	480.3089	[M+H] ⁺	Lipid Metabolism/ Cell Signalling	2.318	0.144	nd	nd
20.99	PC(18:3)	518.3220	[M+H] ⁺	Glycerophospho- lipid Metabolism	2.158	0.010	nd	nd
21.71	PC(O-16:1(11Z)/2:0)	522.3559	[M+H] ⁺	Glycerophospho- lipid Metabolism	2.150	0.149	nd	nd

Rt (min)	ID	m/z	Adduct	Metabolic Pathway	Tissue		Fluid	
					FC	PV	FC	PV
21.78	PE(P-16:0/0:0)	438.2981	[M+H] ⁺	Glycerophospho- lipid Metabolism	2.867	0.084	-2.749	0.142
21.84	PC(O-15:0/O-1:0)[U]	482.3607	[M+H] ⁺	Glycerophospho- lipid Metabolism	2.175	0.106	nd	nd
24.27	PG(16:0/0:0)[U]	526.3144	[M+ACN+H] ⁺	Glycerophospho- lipid Metabolism	1.919	0.189	nd	nd
24.52	PC(O-14:0/16:0)	736.5204	[M+2Na-H] ⁺	Glycerophospho- lipid Metabolism	nd	nd	-4.210	0.289
24.86	PE(18:0/0:0)	482.3244	[M+H] ⁺	Glycerophospho- lipid Metabolism	2.037	0.116	nd	nd
25.13	LysoPC(20:3)	546.3531	[M+H] ⁺	Glycerophospho- lipid Metabolism	2.381	0.836	nd	nd
25.17	PC(2:0/O-16:0)[U]	524.3714	[M+H] ⁺	Glycerophospho- lipid Metabolism	1.981	0.115	nd	nd
25.18	PC(2:0/O-16:0)[U]	524.3714	[M+H] ⁺	Glycerophospho- lipid Metabolism	1.865	0.261	nd	nd
25.31	PC(2:0/O-16:0)[U]	524.3714	[M+H] ⁺	Glycerophospho- lipid Metabolism	nd	nd	- 113.092	0.085
25.81	PC(16:0/20:4)	782.5687	[M+H] ⁺	Glycerophospho- lipid Metabolism	nd	nd	3.163	0.104
26.01	Vitamin D3	467.3328	[M+H] ⁺	Steroid Biosynthesis	2.985	0.136	nd	nd
26.01	PC(P-15:0/0:0)	466.3294	[M+H] ⁺	Glycerophospho- lipid Metabolism	3.037	0.074	-1.427	0.450
26.09	PE(O-18:0/16:0)[U]	750.5359	[M+2Na-H] ⁺	Glycerophospho- lipid Metabolism	nd	nd	-3.937	0.287
26.22	Dihydroxyvitamin D3	545.3850	[M+H] ⁺	Steroid Biosynthesis	nd	nd	-4.637	0.255

Rt (min)	ID	m/z	Adduct	Metabolic Pathway	Tissue		Fluid	
					FC	PV	FC	PV
28.07	PC(O-14:0/18:0)	764.5515	[M+2Na-H] ⁺	Glycerophospho- lipid Metabolism	nd	nd	-3.088	0.327
28.21	PC(16:0/20:1(11Z))[U]	788.6161	[M+H] ⁺	Glycerophospho- lipid Metabolism	6.609	0.091	1.729	0.169
29.19	PG(17:0/17:0)[U]	783.5722	[M+CH ₃ OH+H] ⁺	Glycerophospho- lipid Metabolism	nd	nd	2.496	0.188
29.31	Oleamide	282.2791	[M+H] ⁺	Lipid Metabolism/ Cell Signalling	2.691	0.001	2.085	0.489
29.81	PC(16:0/20:4)	782.5693	[M+H] ⁺	Glycerophospho- lipid Metabolism	3.634	0.393	nd	nd
34.52	N-Adenylyl-L- phenylalanine	536.1659	[M+ACN+H] ⁺	cAMP biosynthesis	nd	nd	-3.606	0.297
36.25	TG(16:1(9Z)/20:0/20:0) [iso3]	470.4207	[M+H+Na] ⁺	Lipid Metabolism/ Cell Signalling	nd	nd	-74.773	0.187
36.49	PS(13:0/12:0)	701.4100	[M+ACN+Na] ⁺		4.016	0.304	nd	nd
36.59	Archaetidylglycerol- myo-inositol	909.7162	[M+H] ⁺	Phosphatidyl- inositol signalling system	12.203	0.089	nd	nd
39.65	Valeric acid	158.1175	[M+ACN+H] ⁺	Cell Signalling	2.450	0.836	-1.067	0.954
41.18	6-Deoxy-D-Glucose	165.0758	[M+H] ⁺	Glycolysis/ Gluconeogenesis	13.999	0.161	1.259	0.754
44.23	L-2,4-diaminobutyric acid	119.0816	[M+H] ⁺	Ligand-receptor Interaction; Lipid Metabolism	6.871	0.300	1.183	0.811

Table A4.2 Summary of Differentially Regulated Metabolites in **RITTP** and **RITFP** as detected by ¹H-NMR

Rt (min)	ID	m/z	Adduct	Metabolic Pathway	Tissue		Fluid	
					FC	PV	FC	PV
1.19	Choline	104.1071	[M+H] ⁺	Glycerophospho- lipid Metabolism	6.900	0.229	-3.908	0.656
1.24	N-Acetyl-D- glucosamine	244.0794	[M+Na] ⁺	Amino sugar and nucleotide sugar metabolism	nd	nd	6.358	0.110
1.29	3,5-Dichloro-L-tyrosine	213.9828	[M+H-2H ₂ O] ⁺	Tyrosine metabolism	-3.264	0.005	nd	nd
1.29	Creatine	132.0768	[M+H] ⁺	Glycine, serine and threonine metabolism	2.258	0.033	nd	nd
1.30	α-D-Glucose	203.0529	[M+Na] ⁺	Glycolysis / Nucleotide synthesis	nd	nd	3.512	0.061
1.40	10-hydroxy- tetradecanoic acid	145.0913	[M+2Na] ²⁺		-12.102	0.146	nd	nd

Rt (min)	ID	m/z	Adduct	Metabolic Pathway	Tissue		Fluid	
					FC	PV	FC	PV
1.40	(RS)-4-Methyl-gamma-aminobutyric acid	118.0864	[M+H] ⁺	Cell Signalling	nd	nd	-55.947	0.071
1.41	Hydroxyprolyl-Tyrosine	148.0681	[M+2H] ²⁺	Tyrosine metabolism	nd	nd	12.886	0.188
1.64	7-Methylguanine	166.0731	[M+H] ⁺	Purine/Pyrimidine metabolism	nd	nd	-36.386	0.061
1.68	4-Methylaminobutyrate	150.1126	[M+CH ₃ OH+H] ⁺	Cell Signalling	10.959	0.059	nd	nd
1.75	myo-Inositol	163.0607	[M+H-2H ₂ O] ⁺	Phosphatidyl-inositol signalling system	-13.582	0.154	nd	nd
1.81	<i>p</i> -Coumaroyl 3-hydroxytyrosine	308.0915	[M+H-2H ₂ O] ⁺	Tyrosine metabolism	1.304	0.746	nd	nd
1.82	Niacinamide	123.0554	[M+H] ⁺	Nicotinate and nicotinamide metabolism	4.691	0.041	nd	nd
1.82	4-Methoxytyramine	168.1020	[M+H] ⁺	Tyrosine metabolism	nd	nd	-28.431	0.004

Rt (min)	ID	m/z	Adduct	Metabolic Pathway	Tissue		Fluid	
					FC	PV	FC	PV
1.83	Creatinine	114.0662	[M+H] ⁺	Arginine and Proline Metabolism	28.854	0.153	nd	nd
1.84	Isoleucine	132.1019	[M+H] ⁺	Pyridine Synthesis/ Valine, leucine and isoleucine biosynthesis	1.624	0.225	-43.227	0.068
2.02	6-O-beta-D- Xylopyranosyl-D- glucose	105.0424	[M+3H] ³⁺	Glycolysis/ Nucleotide synthesis	1.025	0.922	3.720	0.120
2.13	Betaine aldehyde	102.0915	[M+H] ⁺	Glycine, serine and threonine metabolism	1.103	0.710	3.191	0.044
2.13	Betaine aldehyde	102.0914	[M+H] ⁺	Glycine, serine and threonine metabolism	1.179	0.140	-2.318	0.071
2.31	L-Adrenaline	166.0864	[M+H-H ₂ O] ⁺	Ligand-receptor interaction/	1.435	0.465	nd	nd

Rt (min)	ID	m/z	Adduct	Metabolic Pathway	Tissue		Fluid	
					FC	PV	FC	PV
4.38	<i>Ritodrine</i>	288.1594	[M+H] ⁺		nd	nd	3847.849	0.044
5.76	2-methyl-hexanoic acid	172.1333	[M+ACN+H] ⁺	Fatty Acid Metabolism	1.594	0.017	nd	nd
7.46	PA(17:1)	701.4935	[M+H-2H ₂ O] ⁺		nd	nd	-396.931	0.080
7.48	norleucine	340.2593	[M+H-H ₂ O] ⁺	Pyridine Synthesis/ Valine, leucine and isoleucine biosynthesis	nd	nd	-735.820	0.062
7.48	N-methyl arachidonoyl amine	340.2593	[M+Na] ⁺	Cell Signalling	nd	nd	-735.820	0.062
8.14	N-(5-hydroxy-pentyl) arachidonoyl amine	453.3438	[M+ACN+Na] ⁺	Cell Signalling	nd	nd	-1104.975	0.058
12.09	DAG(22:5)	679.5119	[M+H-2H ₂ O] ⁺	Second messenger/ Cell Signalling	nd	nd	- 24582.825	0.058
12.85	10-hydroxy- tetradecanoic acid	262.2377	[M+NH ₄] ⁺	Lipid Metabolism;	240.514	0.181		

Rt (min)	ID	m/z	Adduct	Metabolic Pathway	Tissue		Fluid	
					FC	PV	FC	PV
15.44	12R-hydroxy-octadecanoic acid	318.3004	[M+NH ₄] ⁺	Lipid Metabolism; Signal transduction	243.488	0.179	nd	nd
15.59	15,16-dihydroxy-octadecanoic acid	334.2951	[M+NH ₄] ⁺	Lipid Metabolism; Signal transduction	185.367	0.179	nd	nd
16.93	Myristaldehyde	230.2479	[M+NH ₄] ⁺	Lipid Metabolism	nd	nd	-25.402	0.062
17.70	2S-amino-tridecanoic acid	230.2114	[M+H] ⁺		nd	nd	-287.547	0.058
17.72	2-keto palmitic acid	288.2531	[M+NH ₄] ⁺	Lipid Metabolism	nd	nd	-172.505	0.058
18.94	Glycerophospho-N-arachidonoyl ethanolamine	502.2931	[M+H] ⁺	Cell Signalling	5.906	0.239	nd	nd
19.42	Glycerophospho-N-arachidonoyl ethanolamine	502.2931	[M+H] ⁺	Cell Signalling	2.479	0.325	nd	nd
19.51	PC(18:2(2E,4E)/0:0)	520.3403	[M+H] ⁺	Glycerophospho-lipid Metabolism	nd	nd	-451.904	0.066

Rt (min)	ID	m/z	Adduct	Metabolic Pathway	Tissue		Fluid	
					FC	PV	FC	PV
19.86	Palmitaldehyde	258.2791	[M+NH ₄] ⁺	Sphingolipid Metabolism	nd	nd	-32.455	0.059
20.34	PC(O-14:0/2:0)	496.3400	[M+H] ⁺	Glycerophospho- lipid Metabolism	2.108	1.000	nd	nd
21.31	Sphingosine	300.2897	[M+H] ⁺	Sphingolipid metabolism; Signal Transduction	2.525	0.133	nd	nd
21.50	Glycerophospho-N- Oleoyl Ethanolamine	480.3087	[M+H] ⁺	Glycerophospho- lipid Metabolism	2.422	0.331	nd	nd
21.72	PC(O-16:1(11Z)/2:0)	522.3558	[M+H] ⁺	Glycerophospho- lipid Metabolism	nd	nd	-55.707	0.069
21.76	1-Hexadecyl Lysophosphatidic Acid	438.2981	[M+ACN+H] ⁺	Diacylglycerol biosynthesis	3.027	0.177	nd	nd
22.11	Isopentenyladenosine- 5'-diphosphate	528.1259	[M+CH ₃ OH+H] ⁺		5.174	0.253	nd	nd
22.75	DAG(14:1(9Z)/14:1 (9Z)/0:0)	553.3826	[M+2Na-H] ⁺	Second messenger/ Cell Signalling	nd	nd	-2397.808	0.058

Rt (min)	ID	m/z	Adduct	Metabolic Pathway	Tissue		Fluid	
					FC	PV	FC	PV
23.38	N-(2'-(4-benzenesulfonamide)-ethyl) arachidonoyl amine	487.2973	[M+H] ⁺	Cell Signalling	nd	nd	-67.352	0.058
23.95	PS(17:1(9Z)/22:2(13Z, 16Z))	869.6022	[M+ACN+H] ⁺		nd	nd	-2298.827	0.058
24.18	PE(18:0/20:4)	825.5760	[M+ACN+H] ⁺		nd	nd	-1626.688	0.058
24.78	PG(O-18:0/0:0)	516.3639	[M+NH ₄] ⁺	Ligand-receptor interaction/ Cell Signalling	nd	nd	-1008.694	0.073
24.80	PE(18:4)	737.5237	[M+ACN+H] ⁺		nd	nd	-1547.763	0.058
24.84	PE(18:0/0:0)	482.3243	[M+H] ⁺	Glycerophospholipid Metabolism	2.175	0.238	nd	nd
25.18	PC(2:0/O-16:0)[U]	524.3714	[M+H] ⁺	Glycerophospholipid Metabolism	1.865	0.261	nd	nd
25.31	PC(2:0/O-16:0)[U]	524.3714	[M+H] ⁺	Glycerophospholipid Metabolism	nd	nd	-113.092	0.085

Rt (min)	ID	m/z	Adduct	Metabolic Pathway	Tissue		Fluid	
					FC	PV	FC	PV
25.72	28-Glucopyranosyl-3-methyloleanolic acid	633.4373	[M+H] ⁺	-	nd	nd	-76.973	0.060
25.83	PS(O-16:0/22:4(7Z,10Z,13Z,16Z))	839.5915	[M+ACN+H] ⁺		nd	nd	-244.520	0.058
26.10	1-Octadecyl Lysophosphatidic Acid	466.3294	[M+ACN+H] ⁺	Diacylglycerol biosynthesis	2.880	0.137	nd	nd
26.35	13-beta-D-Glucosyloxydocosanoate	560.4161	[M+ACN+H] ⁺		nd	nd	-442.764	0.044
26.46	PE(20:4)	750.5430	[M+H] ⁺		nd	nd	-54.010	0.044
26.67	Dihydroxyvitamin D3	545.3851	[M+H] ⁺	Steroid Biosynthesis	nd	nd	-34.181	0.061
26.80	PG(17:0/14:1(9Z))	707.5133	[M+H-2H ₂ O] ⁺		nd	nd	-56.296	0.062
26.99	PE(16:0/17:0)[U]	706.5383	[M+H] ⁺		nd	nd	-57.554	0.060
27.08	PA(17:0/22:2(13Z,16Z))	707.5415	[M+H-2H ₂ O] ⁺		nd	nd	-29.598	0.066
27.20	PI(P-20:0/21:0)	984.6828	[M+ACN+Na] ⁺		nd	nd	-46.978	0.060

Rt (min)	ID	m/z	Adduct	Metabolic Pathway	Tissue		Fluid	
					FC	PV	FC	PV
27.75	PS(19:1(9Z)/22:2(13Z, 16Z))	897.6334	[M+ACN+H] ⁺		nd	nd	-31.950	0.061
28.42	PA(17:1)	782.5695	[M+ACN+H] ⁺	Glycerophospho- lipid metabolism	-3.544	0.223	nd	nd
28.76	2Z-octadecenoic acid	283.2626		Lipid Metabolism; Signal transduction	11.769	0.211	nd	nd
28.91	Palmitic amide	256.2634	[M+H] ⁺	Lipid Metabolism; Signal transduction	3.679	0.220	nd	nd
29.20	DAG(20:4)	677.5028	[M+NH ₄] ⁺		nd	nd	-31.767	0.061
29.48	PC(16:0/20:3(11E,14E, 17E))[U]	784.5846	[M+H] ⁺	Glycerophospho- lipid metabolism; Cell Signalling	nd	nd	35.026	0.175
29.51	Linoleic acid	313.2737	[M+CH ₃ OH+H] ⁺	Lipid Metabolism; Signal transduction	nd	nd	5.541	0.046

Rt (min)	ID	m/z	Adduct	Metabolic Pathway	Tissue		Fluid	
					FC	PV	FC	PV
29.51	DAG(20:5)	734.5695	[M+ACN+H] ⁺		1.454	0.199	5.901	0.322
29.54	Oleamide	282.2791	[M+H] ⁺	Lipid Metabolism; Signal transduction	5.242	0.210	nd	nd
29.54	PC(14:0/18:1(11Z))	732.5551	[M+H] ⁺	Glycerophospho- lipid metabolism; Cell Signalling	nd	nd	47.071	0.156
29.54	PC(P-18:0/18:1(9Z))	813.6475	[M+H] ⁺	Glycerophospho- lipid metabolism; Cell Signalling	nd	nd	7.032	0.053
29.61	MG(0:0/16:0/0:0)	331.2842	[M+H] ⁺	Lipid Metabolism; Signal transduction	nd	nd	5.643	0.036
29.98	PE(18:0/20:4(5Z,8Z, 11Z,14Z))[U]	768.5544	[M+H] ⁺	Glycerophospho- lipid metabolism; Cell Signalling	nd	nd	43.689	0.153

Rt (min)	ID	m/z	Adduct	Metabolic Pathway	Tissue		Fluid	
					FC	PV	FC	PV
30.04	PC(16:0/20:4(5Z,8Z, 11Z, 14Z))	782.5698	[M+H] ⁺	Glycerophospho- lipid metabolism; Cell Signalling	nd	nd	15.263	0.079
30.04	PA(21:0/22:6(4Z,7Z, 10Z, 13Z,16Z,19Z))	808.5854	[M+H] ⁺	Glycerophospho- lipid metabolism	nd	nd	12.986	0.116
30.13	PC(18:4)	779.5709	[M+ACN+H] ⁺		nd	nd	-17.568	0.063
30.68	8-hexadecenoylglycerol	691.5187	[M+H-2H ₂ O] ⁺		nd	nd	-22.348	0.062
33.30	Sphinganine	284.2947	[M+H-H ₂ O] ⁺	Sphingolipid metabolism; Signal Transduction	5.247	0.216	nd	nd
35.04	N-Adenylyl-L- Phenylalanine	536.1659	[M+ACN+H] ⁺	cAMP biosynthesis	nd	nd	- 15508.470	0.058
35.08	3-Pent-2-Enediol-CoA	1003.2454	[M+ACN+H] ⁺		nd	nd	130.197	0.183
36.68	PE(16:0/22:6)	764.5209	[M+H] ⁺	Glycerophospho- lipid metabolism; Cell Signalling	3.265	0.213	nd	nd
37.13	PS(12:0/18:2(9Z,12Z))	686.4394	[M+H-H ₂ O] ⁺	Glycerophospho- lipid metabolism	nd	nd	2.271	0.105

Rt (min)	ID	m/z	Adduct	Metabolic Pathway	Tissue		Fluid	
					FC	PV	FC	PV
39.10	PGF1 α	179.1354	[M+2H] ²⁺	Signal Transduction	nd	nd	-17.764	0.201
39.12	2,3-Dinor-6-keto-PGF1a	171.1017	[M+2H] ²⁺	Signal Transduction	-2.109	0.079	-3.241	0.077
39.57	D-Glyceraldehyde-3- Phosphate	171.0060	[M+H] ⁺	Glycolysis / Gluconeogenesis; Pentose phosphate pathway	-21.483	0.171	nd	nd
40.41	L-Tyrosine	110.0201	[M+2H+Na] ³⁺	Tyrosine metabolism	nd	nd	4.078	0.091
42.21	Homoserine lactone	102.0551	[M+H] ⁺	Signal Transduction	-16.117	0.172	-20.235	0.068
42.58	9-oxo-2,4,5,7- decatetraenoic acid	179.0702	[M+H] ⁺	Lipid Metabolism	nd	nd	-9.447	0.183
44.27	3R-methyl-undecanoic acid	101.0962	[M+2H] ²⁺		nd	nd	-40.059	0.192
44.59	3-Oxo-3- ureidopropanoate	111.0203	[M+H-H ₂ O] ⁺	Pyrimidine metabolism	1.506	0.395	nd	nd